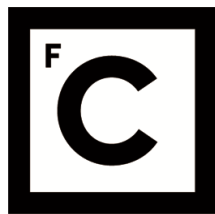


UNIVERSIDADE DE LISBOA
FACULDADE DE CIÊNCIAS



Ciências
ULisboa

**Different approaches to the development and use of carbon
materials for water treatment purposes**

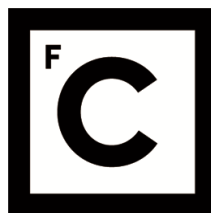
Doutoramento em Química
Especialidade em Química Tecnológica

Susana Cristina Roque Marques

Tese orientada por:
Professora Doutora Ana Paula Carvalho
Doutor Ricardo Dias

Documento especialmente elaborado para a obtenção do grau de doutor

2017



**Ciências
ULisboa**

**Different approaches to the development and use of carbon
materials for water treatment purposes**

Doutoramento em Química
Especialidade em Química Tecnológica

Susana Cristina Roque Marques

Tese orientada por:
Professora Doutora Ana Paula Carvalho
Doutor Ricardo Dias

Júri:

Presidente:

- Doutora Ana Maria Jara Ponces da Costa Freire, Professora catedrática da Faculdade de Ciências da Universidade de Lisboa

Vogais:

- Doutor Alain Celzard, *Enseignant-chercheur, Laboratoire de Recherche en Science des Matériaux do Institut Jean Lamour da Université de Lorraine (França)*
- Doutora Ângela Maria Pereira Martins Nunes, Professora adjunta do Instituto Superior de Engenharia de Lisboa do Instituto Politécnico de Lisboa
- Doutora Ana Paula Baptista de Carvalho, Professora auxiliar da Faculdade de Ciências da Universidade de Lisboa (orientadora)
- Doutora Ana Sofia Dias Mestre Homem, Professora auxiliar convidada da Faculdade de Ciências da Universidade de Lisboa
- Doutora Carla Maria Duarte Nunes, Investigadora FCT “nível desenvolvimento”, equiparação a Investigador Principal da carreira de investigação científica da Faculdade de Ciências da Universidade de Lisboa

Documento especialmente elaborado para a obtenção do grau de doutor

Fundação para a Ciência e Tecnologia (FTC) no âmbito de Bolsa individual de doutoramento
(SFRH/BD/91767/2012)

“Tudo o que é bom dura o tempo
necessário para ser inesquecível”

Fernando Pessoa

To my family and to all the people
that passed through my life and
became unforgettable

Acknowledgments

As I end my PhD thesis I would like to acknowledge Fundação para a Ciência e Tecnologia for their financial support through a PhD grant (SFRH/BD/91767/2012) that allowed me to develop my research, and to participate in several scientific meetings where I presented part of the work reported in this thesis. I also thank Faculdade de Ciências da Universidade de Lisboa (FCUL) and Biosystems & Integrative Sciences Institute (BioISI) where the majority of my work was developed, more specifically to Centro de Química e Bioquímica (CQB) for providing the installations and technical resources necessary to my thesis.

I greatly acknowledge my coordinator Ana Paula Carvalho for completely raising me in this scientific field, and for guiding me throughout this thesis. Her dedication was completely unvaluable to the development of this research, and I am truly grateful for her faith and trust. On a personal level, our “living together”, eight hours *per day* for almost five years, made me feel completely “at home” during this period of my life. Thank you so much.

I thank my co-coordinator Ricardo Dias for having accepted to orientate, and share his expertise with me throughout the biological experiments of my thesis.

A warming thank you to Institute Jean Lamour (Université de Lorraine, CNRS7198) for receiving me in internship, and personally to Professors Vanessa Fierro and Alain Celzard for accepting me in their research group during this period, and for all their support when I was in Epinal, and later in Portugal. I also thank Philippe Gadonneix, Clara Delgado, and Angela Sánchez for helping me during my work at the institute, and for their friendship.

I acknowledge Doctor Miguel Machuqueiro for carrying out the molecular modelling studies that contributed so much to the discussion of the adsorption results

I thank Professors Andreja Žgajnar and Marjan Marinsek for their partnership, and for providing the precursor materials for activated carbons preparation and reagent tiamulin. I also thank to Doctors Jossano Marcuzzo and Mauricio Baldan for providing the activated carbon cloth and for all their knowledge and work during my thesis.

I am very grateful to all my colleagues at Grupo de Adsorção e Materiais Adsorventes for being a part of my life everyday, for these last five years. I thank especially Doctor Ana Sofia Mestre, my office roommate, for her support and counseling during the writing of this thesis.

A big thank you to my family who believed in me, and supported me unconditionally throughout this thesis, with a lot of patience.

To everybody in Institute Jean Lamour a great thank you for receiving me so well, for all your work and personal support, and your friendship (and French classes on Sundays). You made my stay in Epinal unforgettable.

To my friend Teresa thank you for your friendship, and for always believing in me, professionally and personally. I will never forget when you printed my scholarship contract and came to me with it rolled in a pink ribbon and a congratulations card. For me that was the beginning of my PhD.

To Rosana, Tiago and Fadhil for their friendship, support, and company in our night and weekend shifts at the laboratory, thank you so much.

A thank you to all the people I met in this period of my life, in the French, dance, and programming classes, for your friendship and for teaching me so much.

At last, I am very grateful to my Seb for showing me the meaning of partnership, love and friendship.

Resumo

O trabalho que se apresenta nesta tese consistiu na preparação de materiais porosos e na sua aplicação em processos de adsorção de compostos orgânicos em fase aquosa e adesão bacteriana.

Após a introdução teórica (Capítulos II a VI), os resultados que se apresentam no Capítulo VII correspondem ao estudo centrado na preparação de carvões activados a partir de um carbonizado de casca de macieira por activação química com carbonato e hidróxido de potássio, sob diferentes condições experimentais. A metodologia empregue permitiu obter materiais com um elevado rendimento global de preparação e reduzir o conteúdo em compostos voláteis do precursor. Os carvões activados sintetizados com carbonato e hidróxido de potássio apresentam uma porosidade bastante desenvolvida, com volumes microporosos e áreas superficiais específicas elevadas (valores até $1920 \text{ m}^2 \text{ g}^{-1}$ e $2445 \text{ m}^2 \text{ g}^{-1}$, respectivamente). O impacto da activação na morfologia dos carvões foi avaliada por microscopia electrónica de varrimento e verificou-se que a activação mais severa com KOH levou a um maior consumo da matriz carbonácea e homogeneização de tamanho de partícula comparativamente com a activação com carbonato. No que se refere ao estudo do desempenho destes materiais na adsorção dos compostos farmacêuticos atenolol e hidrogenofumarato de tiamulina foi comparável ao das amostras comerciais testadas. Os carvões com maior capacidade de adsorção foram as amostras activadas com KOH, que permitiram capacidades de adsorção de 556 mg g^{-1} de atenolol e aproximadamente 250 mg g^{-1} de tiamulina. O volume de supermicroporos revelou ser importante para a adsorção do atenolol e algum impacto da química superficial dos carvões no processo foi observado. A adsorção do antibiótico tiamulina decorreu também nos supermicroporos dos sólidos e o volume mesoporoso do carvão NS facilitou a sua difusão.

No Capítulo VIII investigou-se o desempenho de carvões activados de diferentes morfologias na adsorção de dois poluentes orgânicos, e avaliou-se a influência da morfologia em processos de regeneração por tratamento térmico.

O feltro de carvão activado foi caracterizado em termos de textura, morfologia e química superficial, juntamente com amostras comerciais nas formas granular e em pó. O feltro de carvão apresenta uma estrutura aberta composta por fibras de largo diâmetro. A porosidade deste sólido mostrou ser composta maioritariamente por supermicroporos facilmente acessíveis à superfície das fibras do material.

Os carvões foram testados em ensaios de adsorção em fase líquida para remoção de paracetamol e de ácido clofíbrico. A difusão destas espécies foi facilitada no feltro por os seus microporos estarem à superfície da matriz, e no carvão NS devido ao elevado volume de mesoporos. Ambos os poluentes foram eficientemente adsorvidos pelos sólidos até quantidades máximas adsorvidas de 323 mg g^{-1} e 568 mg g^{-1} de paracetamol e ácido clofíbrico, respectivamente.

Foram efectuados estudos de regeneração por tratamento térmico em ensaios cíclicos de saturação-regeneração. As condições de regeneração mais moderadas (aquecimento a $400 \text{ }^\circ\text{C}$ durante 1 h) foram mais eficazes na recuperação da porosidade das amostras. O tratamento de regeneração foi mais eficaz no caso do feltro e carvão granular, que retiveram alguma porosidade e aproximadamente 50 % da capacidade inicial de adsorção após o seu segundo reuso.

No que refere ao estudo da adesão bacteriana de células *Escherichia coli* em carvões activados, os resultados do Capítulo IX revelam que o carvão em pó teve claramente um melhor desempenho removendo até 4log de células por cm³ de suspensão após 48 h de contacto. O mecanismo de adesão neste sólido parece ocorrer em duas etapas: uma adesão inicial favorecida por interacções electrostáticas atractivas, e imobilização de células bacterianas devido à formação de aglomerados carvão-célula-célula-carvão. Não ocorreu adesão de microorganismos na amostra oxidada, o que sugere que o estabelecimento de interacções iniciais repulsivas foi o suficiente para evitar colonização da amostra. A formação das estruturas célula + carvão mostrou-se mais difícil quando as partículas de carvão se encontravam saturadas com cafeína.

Por último, no estudo apresentado no Capítulo X, caracterizaram-se polímeros de tanino obtidos a partir de casca de árvore mimosa, tendo sido também avaliadas as potencialidades dos materiais como adsorventes de diversos compostos orgânicos em fase aquosa.

O uso de maiores quantidades de surfactante promoveu a formação de mesoporos mais largos e menor conteúdo fenólico. Uma das amostras foi lavada com uma solução de ácido clorídrico, e o tratamento causou um ligeiro alargamento dos mesoporos com alguma perda de volume poroso, e sem perda de conteúdo fenólico.

Foi realizado um estudo detalhado da adsorção do corante azul de metileno em fase aquosa, e seguidamente os materiais foram testados relativamente à remoção de um conjunto de compostos farmacêuticos e um plasticizante, muito consumidos a nível mundial. As duas amostras testadas mostram propriedades adsorventes removendo até uma quantidade máxima de 152 mg g⁻¹ de poluente, em condições de equilíbrio. O bom desempenho dos polímeros foi atribuído em grande extensão ao carácter aromático dos materiais. As espécies moleculares de menor volume molar, e com menor espessura foram adsorvidas em maiores quantidades sugerindo um empacotamento das espécies nos mesoporos dos polímeros.

Abstract

The work presented in this thesis consisted in the preparation of porous materials and in their application in adsorption processes of organic compounds in aqueous phase, and bacteria adhesion.

After the theoretical introduction (Chapters II to VI), the results presented in Chapter VII correspond to the study centred in the preparation of activated carbons from an apple tree branches char by chemical activation with potassium carbonate and hydroxide, under different experimental conditions. The employed methodology allowed to obtain materials with a high global preparation yield and to reduce the volatile content of the precursor. The activated carbons synthesized with potassium carbonate and hydroxide present a highly developed porosity, with high micropore volumes and specific surface areas (values up to $1920 \text{ cm}^3 \text{ g}^{-1}$ and $2445 \text{ cm}^3 \text{ g}^{-1}$, respectively). The impact of activation on the morphology of the carbons was evaluated by scanning electron microscopy and it was observed that the more severe activation with KOH led to a higher consumption of the carbonaceous matrix and an homogenization of the particle size, in comparison to the activation with carbonate. The performance of the materials in the adsorption of the pharmaceutical compounds atenolol and tiamulin hydrogen fumarate was comparable and better than that of the commercial samples tested. The carbons with higher adsorption capacity were the KOH activated samples, which allowed for the removal of 556 mg g^{-1} of atenolol and of approximately 250 mg g^{-1} of tiamulin, in equilibrium conditions. The supermicropores volume was important for atenolol adsorption and some impact of the carbons's surface chemistry on the process was observed. The adsorption of the antibiotic tiamulin also occurred on the supermicropores of the solids and the mesopore volume of carbon NS facilitated its diffusion.

In Chapter VIII the performance of activated carbons with different morphologies in the adsorption of two organic pollutants was assessed, and the role of morphology in thermal treatment regeneration processes was evaluated.

The activated carbon cloth was characterized in terms of texture, morphology and surface chemistry, together with commercial samples in the granular and powdered forms. The carbon felt presents an open structure composed by fibres of high diameter. The porosity of this solid revealed to be mostly composed by supermicropores easily accessible at the surface of the material fibres.

The carbons were tested in liquid phase adsorption experiments for the removal of paracetamol and clofibric acid. The diffusion of these species was facilitated in the cloth because the micropores are at the matrix surface, and in carbon NS due to the high mesopore volume. Both pollutants were efficiently adsorbed by the solids up to maximum adsorbed quantities of 323 mg g^{-1} and 568 mg g^{-1} of paracetamol and clofibric acid, respectively.

Regeneration by thermal treatment was studied in cyclic saturation-regeneration assays. The more moderate conditions of regeneration (heating at $400 \text{ }^\circ\text{C}$ during 1 h) were more efficient in recovering the porosity of the samples. The regeneration treatment was more efficient in the case of the cloth and granular carbon that retained some porosity and approximately 50 % of the initial adsorption capacity up to the third reuse.

In regards to the study of bacteria adhesion of *Escherichia coli* cells in activated carbons, the results in Chapter IX reveal that the powdered carbon had a clear better performance removing up to 4log of cells per cm³ of suspension after 48 h of contact time. The adhesion mechanism in this solid seems to occur in two stages: an initial adhesion favoured by attractive electrostatic interactions, and immobilization of bacteria cells due to the formation of carbon-cell-cell-carbon agglomerates. No adhesion of microorganisms occurred on the oxidized sample, suggesting that the establishment of initial repulsive interactions was sufficient to avoid colonization of the sample. The formation of cell + carbon structures was more difficult when the carbon particles were saturated with caffeine.

At last, in the study reported in Chapter X, tannin polymers obtained from Mimosa tree bark were characterized, and the potential of the materials as adsorbents of several organic compounds in aqueous phase was evaluated.

The use of higher surfactant amounts promoted the formation of wider mesopores and lower phenolic content. One of the samples was washed with a hydrochloric acid solution, and the treatment caused a slight widening of the mesopores with some porous volume loss, and without loss in phenolic content.

A detailed study of methylene blue adsorption in aqueous phase was performed, and then the materials were tested for the removal of a set of pharmaceutical compounds and a plasticizer, highly consumed worldwide. The two tested samples showed adsorbent properties removing up to a maximum amount of 152 mg g⁻¹ of pollutant, in equilibrium conditions. The good performance of the polymers was attributed at a great extent to the aromatic character of the materials. The molecular species with smaller molar volume, and with lower width were adsorbed in higher amounts suggesting a packing of the species in the polymers mesopores.

Index

Acknowledgments	v
Resumo	vii
Abstract	ix
Index	xi
Tables index	xix
Figures index	xxv
Abbreviations glossary	xxxiii
Symbols glossary	xxxvii
Chapter I – Contextualization	1
Chapter II – Objectives	5
Chapter III – Porous materials	8
III.1. Activated carbons.....	10
III.1.1. Historical perspective.....	10
III.1.2. Activated carbons structure.....	11
III.1.2.1. Physical structure.....	11
III.1.2.2. Chemical structure.....	12
III.1.3. Types of activated carbons.....	14
III.1.4. Preparation of activated carbons.....	16
III.1.5. Regeneration.....	20
III.1.6. Applications of activated carbons.....	24
III.2. Tannins.....	25
III.2.1. Definitions and extraction.....	25
III.2.2. Structure, classification and polymerization.....	25
III.2.3. High Internal Phase Emulsion (HIPE).....	28
III.2.3.1. Polymer synthesis by High Internal Phase Emulsion (polyHIPE).....	29

Chapter IV – Techniques for porous materials characterization.....	31
IV.1. Characterization of porous structure.....	33
IV.1.1. Adsorption of gases and vapors.....	33
IV.1.1.1. Types of adsorption.....	34
IV.1.1.2. Adsorption isotherms classification.....	34
IV.1.1.3. Methods for adsorption isotherms analysis.....	39
IV.1.2. Mercury intrusion porosimetry (MIP).....	44
IV.1.3. Density	47
IV.2. Chemical characterization	48
IV.2.1. Elemental analysis and ash content.....	48
IV.2.2. pH at the point of zero charge (pH_{PZC}) and at the isoelectric point (pH_{IEP}).....	49
IV.2.3. Fourier Transform Infrared Spectroscopy (FTIR).....	51
IV.2.4. Thermogravimetric Analysis (TGA).....	53
IV.2.5. Scanning Electron Microscopy (SEM).....	54
IV.2.6. X-ray Diffraction (XRD).....	56
IV.2.7. X-ray Photoelectron Spectroscopy (XPS).....	57
IV.2.8. Contact angle measurements.....	58
Chapter V – Liquid phase adsorption.....	60
V.1. Adsorption kinetics.....	64
V.1.1. Pseudo-first order kinetic model.....	65
V.1.2. Pseudo-second order kinetic model.....	66
V.2. Equilibrium adsorption.....	67
V.2.1. Langmuir isotherm.....	68
V.2.2. Freundlich isotherm.....	69
V.3. Activated carbons for water treatment purposes.....	70

V.3.1. Aquatic environment contamination by pharmaceutical compounds.....	73
V.3.2. Pollutant compounds studied.....	74
V.3.2.1. Analgesics/anti-inflammatories.....	74
V.3.2.2. Antibiotics.....	76
V.3.2.3. β -blockers.....	76
V.3.2.4. Cholesterol regulators.....	76
V.3.2.5. Blood-lipid regulators.....	77
V.3.2.6. Anti-acid medication.....	77
V.3.2.7. Stimulant.....	77
V.3.2.8. Plasticizers.....	78
Chapter VI – Adhesion of faecal coliform bacteria on activated carbons.....	79
VI.1. Faecal coliform bacteria in the environment.....	81
VI.2. <i>Escherichia coli</i>	82
VI.2.1. <i>Escherichia coli</i> , a biological drinking water indicator.....	82
VI.3. Bacteria adhesion.....	83
VI.3.1. <i>E coli</i> cell and role of surface structures in adhesion to abiotic surfaces...85	
Chapter VII – Wood-based activated carbons for adsorption of pharmaceuticals from aqueous solution.....	87
VII.1. Experimental procedure.....	89
VII.1.1. Preparation and characterization of activated carbons.....	89
VII.1.2. Material's characterization techniques, liquid phase adsorption, molecular modelling and desorption experiments.....	89
VII.2. Results and discussion.....	90
VII.2.1. Optimization of the activation conditions.....	90
VII.2.2. Characterization of the adsorbents.....	92
VII.2.3. Lab-made carbons as adsorbents for atenolol.....	99

VII.2.4. Atenolol thermal desorption.....	102
VII.2.5. Adsorption of tiamulin hydrogen fumarate.....	107
VII.3. Partial conclusions.....	113
Chapter VIII – Pharmaceuticals removal by activated carbons: Role of morphology on cyclic thermal regeneration	115
VIII.1. Experimental procedure.....	117
VIII.1.1. Materials.....	117
VIII.1.2. Material's characterization techniques, and liquid phase adsorption and thermal regeneration experiments.....	117
VIII.2. Results and discussion.....	118
VIII.2.1. Characterization of the adsorbents.....	118
VIII.2.2. Adsorption of paracetamol and clofibric acid.....	124
VIII.2.3. Role of morphology on thermal cyclic regeneration of paracetamol-exhausted carbons.....	129
VIII.3. Partial conclusions.....	134
Chapter IX – <i>Escherichia coli</i> immobilization on activated carbons: Impact of immobilization conditions and role of morphology.....	135
IX.1. Experimental procedure.....	137
IX.1.1. Preparation and characterization of activated carbons.....	137
IX.1.2. Immobilization experiments.....	138
IX.2. Results and discussion.....	139
IX.3. Partial conclusions.....	146
Chapter X – Tannin-based materials for water remediation: Adsorption mechanism and removal of Pharmaceutical and Personal Care Products (PPCPs) from aqueous phase.....	148
X.1. Experimental procedure.....	150
X.1.1. Preparation of the tannin-based powders.....	150
X.1.2. Material's characterization techniques and liquid phase adsorption.....	150

X.2. Results and discussion.....	151
X.2.1. Characterization of the adsorbents.....	151
X.2.2. Adsorption of methylene blue.....	156
X.2.3. Adsorption of Pharmaceutical Compounds and Personal Care Products (PPCPs).....	158
X.3. Partial conclusions.....	163
Chapter XI. Final conclusions.....	164
Chapter XII. Bibliographic references.....	168
Appendix A. Experimental procedures.....	I
A.1. Development of porous materials.....	III
A.1.1. Preparation of the apple tree branches biochar.....	III
A.1.2. Preparation of wood biochar derived activated carbons by chemical activation.....	III
A.1.3. Preparation of the activated carbon cloth (ACC).....	IV
A.1.4. Preparation of of tannin-based monoliths powders.....	IV
A.2. Characterization techniques.....	V
A.2.1. N ₂ adsorption at -196 °C.....	V
A2.2. CO ₂ adsorption at 0 °C	V
A.2.3. Water vapor adsorption at 20 °C.....	VI
A.2.4. Mercury intrusion.....	VI
A.2.5. Scanning Electron Microscopy (SEM).....	VI
A.2.6. X-ray Photoelectron Spectroscopy (XPS).....	VI
A.2.7. X-ray Powder Diffraction (XRD).....	VII
A.2.8. pH at the point of zero charge (pH _{PZC}).....	VII
A.2.9. Contact angle measurements.....	VIII
A.2.10. Phenolic groups content determination.....	VIII
A.2.11. Elemental analysis.....	IX

A.2.12. Determination of volatile matter content.....	IX
A.2.13. Determination of ash content.....	IX
A.2.14. Density measurements.....	X
A.2.15. Fourier transform infrared spectroscopy (FTIR).....	X
A.2.16. Thermogravimetric analysis (TGA).....	X
A.2.17. Cyclic thermal regeneration treatments.....	XI
A.3. Liquid phase experiments.....	XI
A.3.1. Pollutants studied.....	XI
A.3.2. Aqueous phase adsorption.....	XIII
A.3.3. Bacteria immobilization assays.....	XV
A.3.3.1. Strain and culture conditions.....	XV
A.3.3.2. Immobilization of <i>E. coli</i> onto the carbon materials.....	XV
A.3.3.3. Quantification of <i>E. coli</i> and caffeine.....	XV
A.3.3.4. Optical and phase-contrast microscopy.....	XVI
A.4. Appendix A references.....	XVI
Appendix B. Experimental results.....	XVIII
B.1. N ₂ adsorption at -196 °C.....	XX
B.2. CO ₂ adsorption at 0 °C.....	XXVIII
B.3. Mercury porosimetry.....	XXXI
B.4. Liquid phase adsorption.....	XXXV
Appendix C. National and international scientific conferences.....	XXXVII
Appendix D. Publications in international journals with scientific arbitrage.....	LXXIV

Tables index

Table III.1. Examples of industrial application of activated carbons, in liquid and gaseous phases.....	24
Table IV.1. Different properties of physical and chemical adsorption.....	34
Table IV.2. Examples of IR absorption bands and corresponding assignments.....	53
Table V.1. Parameters affecting the extension of adsorption in solution.....	63
Table VII.1. Materials prepared and commercial adsorbents studied in Chapter VII and detailed information regarding their preparation and/or provenance.....	89
Table VII.2. Experimental procedures of the characterization techniques employed in Chapter VII, liquid phase adsorption, molecular modelling and desorption experiments.....	90
Table VII.3. Lab-made samples, corresponding preparation yield, and volatile content.....	91
Table VII.4. Nanotextural properties of the lab-made carbons and corresponding pH_{PZC} values.....	95
Table VII.5. Pseudo-second order parameters for atenolol adsorption onto the studied samples at 30 °C.....	100
Table VII.6. Fitting parameters of atenolol equilibrium data to the Langmuir and Freundlich models, coefficient of correlation, and chi-square test analysis.....	101
Table VII.7. Percentage of final weight of atenolol and pristine carbons.....	104
Table VII.8. Percentage of final weight of atenolol-exhausted carbons and corresponding DTG peaks.....	106
Table VII.9. Activation energy of desorption, pre-exponential factor, and correspondent correlation coefficients.....	107
Table VII.10. Pseudo-second order parameters for fumaric acid and tiamulin hydrogen fumarate adsorption onto the studied samples at 30 °C.....	108
Table VIII.1. Activated carbons studied in Chapter VIII and information regarding their preparation and/or provenance.....	117
Table VIII.2. Experimental procedures of the characterization techniques employed in Chapter VIII, and liquid phase adsorption and regeneration experiments performed.....	118
Table VIII.3. Nanotextural properties of the lab-made carbons.....	119
Table VIII.4. XPS atomic percentages for samples ACC, NS and GAC.....	122
Table VIII.5. Pseudo-second order pharmaceutical compounds adsorption parameters for the studied carbon samples at 30 °C.....	125
Table VIII.6. Molecular structure, chemical properties, and dimensions of the pollutants paracetamol and clofibric acid.....	126

Table VIII.7. Fitting parameters of paracetamol and clofibrac acid equilibrium data to the Langmuir and Freundlich models, coefficient of correlation, and chi-square test analysis.....	128
Table VIII.8. Nanotextural properties of the fresh activated carbons, samples heated at 400 °C and 600 °C and obtained after the 3 rd re-use.....	133
Table IX.1. Activated carbons studied in Chapter IX and information regarding their preparation and/or provenance.....	137
Table IX.2. Parameters studied in the <i>E. coli</i> 's removal by activated carbons assays, and the corresponding experimental conditions used.....	138
Table X.1. Experimental procedures of the characterization techniques employed in Chapter X.....	150
Table X.2. Experimental procedures of the liquid phase adsorption experiments.....	151
Table X.3. Elemental analysis and pH _{PZC} values of <i>Mimosa</i> bark of the tannin-based powders.....	152
Table X.4. Total phenol content of the materials, obtained by the Folin-Ciocalteu method.....	153
Table X.5. Pseudo-second order parameters for the methylene blue adsorption onto the studied adsorbents, at 30 °C.....	157
Table A.1. Experimental conditions used for the calibration plot of tannic acid.....	IX
Table A.2. Compounds studied, their abbreviation, reagents brand, solution preparation information and solution pH.....	XI
Table A.3. Chemical properties of the pharmaceutical compounds studied.....	XII
Table A.4. Wavelengths used for the quantification of the compounds by UV-Vis spectroscopy.....	XIV
Table B.1. N ₂ adsorption and desorption data, at– 196 °C, of carbon CA(1:3/700/2)....	XX
Table B.2. N ₂ adsorption and desorption data, at– 196 °C, of carbon CA(1:3/800/1)....	XX
Table B.3. N ₂ adsorption and desorption data, at– 196 °C, of carbon CA(1:3/800/2)....	XX
Table B.4. N ₂ adsorption and desorption data, at– 196 °C, of carbon CA(1:3/800/3)....	XXI
Table B.5. N ₂ adsorption and desorption data, at– 196 °C, of carbon CA(1:3/800/4)....	XXI
Table B.6. N ₂ adsorption and desorption data, at– 196 °C, of carbon CA(1:4/800/1)....	XXI
Table B.7. N ₂ adsorption and desorption data, at– 196 °C, of carbon CA(1:4/800/2)....	XXII
Table B.8. N ₂ adsorption and desorption data, at– 196 °C, of carbon CA(1:4/800/4)....	XXII
Table B.9. N ₂ adsorption and desorption data, at– 196 °C, of carbon HA(1:3/800/1)....	XXII
Table B.10. N ₂ adsorption and desorption data, at– 196 °C, of carbon HA(1:3/800/2).....	XXIII
Table B.11. N ₂ adsorption and desorption data, at– 196 °C, of carbon HA(1:3/800/3).....	XXIII

Table B.12. N ₂ adsorption and desorption data, at– 196 °C, of carbon HA(1:3/800/4).....	XXIII
Table B.13. N ₂ adsorption and desorption data, at– 196 °C, of carbon NS.....	XXIV
Table B.14. N ₂ adsorption and desorption data, at– 196 °C, of carbon CP.....	XXIV
Table B.15. N ₂ adsorption and desorption data, at– 196 °C, of carbon ACC.....	XXIV
Table B.16. N ₂ adsorption and desorption data, at– 196 °C, of carbon VP.....	XXV
Table B.17. N ₂ adsorption and desorption data, at– 196 °C, of carbon GAC830.....	XXV
Table B.18. N ₂ adsorption and desorption data, at– 196 °C, of carbon GACm.....	XXV
Table B.19. N ₂ adsorption and desorption data, at– 196 °C, of carbon NSox.....	XXVI
Table B.20. N ₂ adsorption and desorption data, at– 196 °C, of carbon ACCsat/600.....	XXVI
Table B.21. N ₂ adsorption and desorption data, at– 196 °C, of carbon ACC/400.....	XXVI
Table B.22. N ₂ adsorption and desorption data, at– 196 °C, of carbon GAC/400.....	XXVII
Table B.23. N ₂ adsorption and desorption data, at– 196 °C, of carbon GAC/600.....	XXVII
Table B.24. N ₂ adsorption and desorption data, at– 196 °C, of carbon GACsat/400.....	XXVII
Table B.25. N ₂ adsorption and desorption data, at– 196 °C, of carbon GACsat/600.....	XXVIII
Table B.26. CO ₂ adsorption data, at 0 °C, of carbon CA(1:3/700/2).....	XXVIII
Table B.27. CO ₂ adsorption data, at 0 °C, of carbon CA(1:3/800/1).....	XXVIII
Table B.28. CO ₂ adsorption data, at 0 °C, of carbon CA(1:3/800/2).....	XXIX
Table B.29. CO ₂ adsorption data, at 0 °C, of carbon CA(1:3/800/4).....	XXIX
Table B.30. CO ₂ adsorption data, at 0 °C, of carbon CA(1:4/800/1).....	XXIX
Table B.31. CO ₂ adsorption data, at 0 °C, of carbon HA(1:3/800/1).....	XXX
Table B.32. CO ₂ adsorption data, at 0 °C, of carbon HA(1:3/800/2).....	XXX
Table B.33. Mercury porosimetry data of 2M sample.....	XXXI
Table B.34. Mercury porosimetry data of 5M sample.....	XXXII
Table B.35. Mercury porosimetry data of 8M sample.....	XXXIII
Table B.36. Mercury porosimetry data of 5AM sample.....	XXXIV
Table B.37. Kinetic data of paracetamol adsorption, at 30 °C, on the carbons.....	XXXV
Table B.38. Kinetic data of clofibric acid adsorption, at 30 °C, on the carbons.....	XXXV
Table B.39. Kinetic data of atenolol adsorption, at 30 °C, on the commercial carbons.....	XXXV
Table B.40. Kinetic data of atenolol adsorption, at 30 °C, on the lab-made carbons.....	XXXV
Table B.41. Kinetic data of tiamulin hydrogen fumarate adsorption, at 30 °C, on the commercial carbons.....	XXXVI

Table B.42. Kinetic data of tiamulin hydrogen fumarate adsorption, at 30 °C, on the lab-made carbons.....	XXXVI
Table B.43. Kinetic data of methylene blue, at 30 °C, on the tannin-based powders.....	XXXVI
Table B.44. Equilibrium data of paracetamol adsorption, at 30 °C, on the commercial carbons.....	XXXVI
Table B.45. Equilibrium data of clofibric acid adsorption, at 30 °C, on the carbons.....	XXXVII
Table B.46. Equilibrium data of tiamulin hydrogen fumarate adsorption, at 30 °C, on the commercial carbons.....	XXXVII
Table B.47. Equilibrium data of tiamulin hydrogen fumarate adsorption, at 30 °C, on the lab-made carbons.....	XXXVII

Figures index

Figure III.1. Illustration of charcoal and activated carbons uses and manufacture, throughout history.....	10
Figure III.2. Schematic representation of activated carbon microstructure and porous structure.....	11
Figure III.3. Examples of oxygen and nitrogen functional groups possibly present at the surface of the activated carbons.....	13
Figure III.4. Increase of activated carbon hydrophilic character (introduction of oxygenated groups) can cause blockage of the micropores due to water adsorption.....	13
Figure III.5. Different morphologies of activated carbon.....	15
Figure III.6. Scheme of the porosity location in a granular activated carbon and an activated carbon fibre.....	16
Figure III.7. General procedure for the production of activated carbons.....	16
Figure III.8. General experimental procedure for preparing activated carbons by chemical activation.....	19
Figure III.9. Schematic representation of the basic regeneration techniques available for the recovery of spent adsorbents.....	21
Figure III.10. Tannin classification and examples of structures.....	26
Figure III.11. Possible monoflavonoids structures, depending on the number of hydroxyl groups of A and B rings.....	26
Figure III.12. Possible linkages between catechin units, in condensed tannins.....	27
Figure III.13. Example of reaction between a tannin and an intermediate species formed by hexamine decomposition.....	28
Figure III.14. Illustration of tannin-based polymers preparation procedures.....	29
Figure IV.1. Illustration of adsorption process.....	33
Figure IV.2. IUPAC classification of physical adsorption isotherms.....	35
Figure IV.3. Types of isotherms usually obtained with activated carbons.....	36
Figure IV.4. Illustration of capillary condensation phenomenon in slit-shaped pores.....	37
Figure IV.5. Illustration of adsorption and desorption in bottle-shaped pores.....	38
Figure IV.6. IUPAC classification of the different types of hysteresis cycles.....	38
Figure IV.7. Representations of t or α_s curves for different types of adsorbents.....	43
Figure IV.8. Adsorption isotherms of microporous adsorbents and correspondent α_s theoretical curves.....	44
Figure IV.9. Illustration of mercury entering a cylindrical pore under increasing pressure and mercury powder penetrometer.....	45

Figure IV.10. Illustration of intrusion-extrusion mercury cycles and description of the different mechanism stages.....	46
Figure IV.11. Representation of the intrusion volume derivative as function of pore diameter.....	47
Figure IV.12. Representation of the volumes considered for the absolute, apparent and global densities.....	47
Figure IV.13. Macroscopic representation of the amphoteric behaviour of an activated carbon surface chemistry.....	49
Figure IV.14. Energy levels and possible energy absorption transitions and infrared spectra divided in constituent regions.....	51
Figure IV.15. Schematic illustration of TG and DTG curves profile.....	54
Figure IV.16. Schematic illustration of a scanning electron microscope and its several components.....	55
Figure IV.17. Representation of Bragg's law.....	57
Figure IV.18. Schematic representation of an X-ray photoelectron spectrometer.....	58
Figure IV.19. Contact angle measurement: goniometer and sessile drop measurement schematics.....	59
Figure V.1. Illustration of the several stages of adsorption process in liquid phase.....	65
Figure V.2. Adsorption isotherms more frequently obtained for the adsorption of diluted aqueous solutions in carbonaceous materials.....	67
Figure V.3. Schematic layout of a WWTP from Huntsville, Unites States.....	70
Figure V.4. Schematic diagrams of WWTPs where activated carbon are used.....	71
Figure V.5. Schematic representation of the main methodologies employed in drinking water treatment plants and indication of the stages where activated carbon can be employed.....	72
Figure VI.1. Conceptual diagram of bacteria spreading throughout the environment...	81
Figure VI.2. Example of <i>Escherichia coli</i> cells.....	82
Figure VI.3. Development stages of biofilm formation.....	83
Figure VI.4. Simplified interaction model between activated carbon, microorganism and contaminant, in a water treatment scenario.....	84
Figure VI.5. <i>Escherichia coli</i> cellular structures.....	85
Figure VII.1. Comparison graphics to evaluate the impact of activation temperature and that of biochar fraction on K_2CO_3 activated samples preparation yield and volatile content.....	91

Figure VII.2. Comparison graphics to evaluate the impact of the impregnation proportion and of the activating agent used on the preparation yield and volatile content of the carbons.....	92
Figure VII.3. Nitrogen adsorption-desorption isotherms at -196 °C of the carbons activated with K ₂ CO ₃ and KOH, as well as the commercial samples studied.....	93
Figure VII.4. CO ₂ adsorption isotherms, at 0 °C, of the lab-made samples and commercial carbons.....	96
Figure VII.5. Micropore size distribution, obtained from the CO ₂ adsorption data, of the K ₂ CO ₃ activated carbons and KOH activated and commercial carbons.....	97
Figure VII.6. SEM micrographs of the lab-made carbons.....	98
Figure VII.7. Kinetic results for the adsorption of atenolol in the activated carbons, at 30 °C.....	99
Figure VII.8. Molecular structure of atenolol species and corresponding dimensions, and pKa value. Illustration of atenolol access to the micropores.....	100
Figure VII.9. Atenolol adsorption isotherms of the mentioned carbons, at 30 °C.....	101
Figure VII.10. Thermogram of atenolol and corresponding DTG curve.....	103
Figure VII.11. Thermograms of the pristine adsorbents and corresponding DTG curves.....	103
Figure VII.12. Thermograms of the atenolol-exhausted adsorbents, at 5, 10 and 20/K min.....	104
Figure VII.13. DTG profiles of the pristine and atenolol-exhausted carbons at heating rates of 5, 10 and 20 K min ⁻¹	105
Figure VII.14. Kinetic results for the adsorption of fumaric acid and tiamulin hydrogen fumarate in the mentioned carbons, at 30 °C.....	108
Figure VII.15. Correlation between the initial adsorption velocity, and the sum of the meso and supermicropores volumes of the mentioned carbons.....	109
Figure VII.16. Molecular structure of tiamulin and corresponding dimensions, and pKa value. Illustration of tiamulin access to the micropores.....	109
Figure VII.17. Kinetic results for the adsorption of atenolol and tiamulin hydrogen fumarate in the mentioned carbons, at 30 °C.....	110
Figure VII.18. Equilibrium adsorption isotherms of fumaric acid and tiamulin hydrogen fumarate, on the lab-made carbons, at 30 °C.....	111
Figure VII.19. Correlation between the difference in maximum uptake values obtained for FA and THF adsorption, and the volume of meso and supermicropore of the materials.....	113

Figure VIII.1. Nitrogen adsorption-desorption isotherms at -196 °C of the mentioned samples.....	118
Figure VIII.2. CO ₂ adsorption isotherms at 0 °C of the mentioned carbons.....	120
Figure VIII.3. Micropore size distributions of the mentioned samples obtained from the CO ₂ adsorption data, at 0 °C.....	120
Figure VIII.4. SEM micrographs of the ACC surface and a cross-section and longitudinal surfaces.....	121
Figure VIII.5. XPS survey spectra for the mentioned samples.....	122
Figure VIII.6. Deconvoluted high-resolution C 1s and O 1s XPS spectra for the mentioned samples.....	123
Figure VIII.7. X-ray diffraction patterns of the ashes of the carbons GAC and NS.....	124
Figure VIII.8. Kinetic results of paracetamol and clofibric acid adsorption, at 30 °C for the carbon samples.....	124
Figure VIII.9. Correlation between the critical dimensions of the pollutants species in solution and the micropore size distribution of the carbons, previously presented in Figure VIII.3	127
Figure VIII.10. Adsorption isotherms of paracetamol and clofibric acid onto the mentioned carbons, at 30 °C.....	127
Figure VIII.11. Thermograms of the raw and exhausted carbons and corresponding DTG curves.....	130
Figure VIII.12. Thermogram of paracetamol.....	130
Figure VIII.13. Nitrogen adsorption-desorption isotherms at -196 °C of samples heated in the absence of adsorbate, and samples obtained after the 3 rd regeneration cycle at the temperature indicated.....	132
Figure VIII.14. Regeneration efficiency of samples ACC, NS and GAC, for consecutive re-uses after regeneration by thermal treatment at 400 °C and 600 °C for 1 h.....	133
Figure IX.1. <i>E. coli</i> removal, in STD water, by the mentioned carbons, after 24 and 48 h.....	139
Figure IX.2. <i>E. coli</i> removal, in STD water, by the mentioned carbons.....	139
Figure IX.3. <i>E. coli</i> removal after 24 and 48 h, by the powder, cloth and granular carbons, in STD water.....	140
Figure IX.4. Impact of solution chemical composition on <i>E. coli</i> removal from solution by 10 mg, 50 mg and 150 mg of NS.....	141
Figure IX.5. Effect of presence of caffeine on <i>E. coli</i> cells removal.....	143
Figure IX.6. Effect of carbon dosage on cellular suspensions of approximately 8log cells/ml solution; 6log cells/ml solution and 5log cells/ml solution.....	144

Figure IX.7. Comparison of the removal efficiencies achieved by each carbon amount in the cellular suspensions.....	144
Figure IX.8. Optical microscopy of NS carbon in cellular suspensions standardized at $8 \log \text{ cells cm}^{-3}$, viewed with amplifications of 40, 400 and 1000x.....	145
Figure IX.9. Frames obtained with an amplification of 1000x of a carbon aggregate formed after 30 min of contact between cellular suspension and carbon. .	146
Figure X.1. Mercury porosimetry: intrusion isotherms and pore diameter distributions of the tannin-based powders.....	151
Figure X.2. Sorption isotherms of water on the mentioned samples.....	153
Figure X.3. Water contact angle measurements at the surface of the dried monoliths pellets.....	153
Figure X.4. FTIR spectra of the tannin powders.....	154
Figure X.5. Thermogravimetric analysis of the tannin powders.....	155
Figure X.6. Comparison of TG of activated carbons studied in Chapter VII and VIII with the tannin-based polymers.....	155
Figure X.7. Kinetic data of MB adsorption.....	156
Figure X.8. Correlation between the phenolic group content of the samples and the initial adsorption rate and MB amount adsorbed after 4 h of contact time.....	157
Figure X.9. Equilibrium isotherms of MB adsorption.....	158
Figure X.10. Uptake results for the mentioned PPCPs by samples 5M and 5AM, at $30 \text{ }^{\circ}\text{C}$ after 8 h of contact time.....	159
Figure X.11. Correlation between molar volume of the PPCPs species and 5M uptakes and the thickness of the pollutants and 5AM results.....	159
Figure X.12. FTIR spectra of the studied compounds, and of the pristine and spent 5M samples.....	160
Figure X.13. Atenolol, paracetamol and ibuprofen uptake values for the mentioned samples.....	162
Figure A.1. Preparation of the biochar.....	III
Figure A.2. Representation of the activated carbons preparation stages.....	III
Figure A.3. Scheme of the automatic apparatus ASAP 2010.....	V
Figure A.4. Conventional volumetric installation used to perform the CO_2 adsorption experiments.....	V
Figure A.5. Schematic representation of pH_{PZC} measurement procedures.....	VIII
Figure A.6. Heating regime for ash content determination.....	X
Figure A.7. Representation of the experimental procedure adopted for liquid phase adsorption experiments.....	XIV

Figure A.8. Representation of the experimental procedure adopted for the bacteria immobilization experiments.....XV

Figure A.9. Representation of the experimental procedure adopted for the quantification of cell concentration remaining in solution.....XVI

Abbreviations glossary

AC	Activated Carbon
ACC	Activated Carbon Cloth
ACF	Activated Carbon Fibre
ACM	Activated Carbon Monolith
ACS	Activated Carbon Sheet
AT	Atenolol
ATORV	Atorvastatin
BAC	Biological Activated Carbon
BDDT	Brunauer, Deming, Deming and Teller
BET	Brunauer, Emmet and Teller
BPA	Bisphenol A
CAF	Caffeine
CFU	Colony-forming units
CLOF	Clofibric acid
DCF	Diclofenac
DTG	Thermogram derivative
DR	Dubin-Radushkevich
<i>E. coli</i>	<i>Escherichia coli</i>
EDS	Energy-dispersive Spectroscopy
EPA	Environmental Protection Agency
ESVAC	European Surveillance of Veterinary Antimicrobial Consumption
ETA	Equivalents of Tannic Acid
F	Freundlich
FA	Fumaric acid
FDA	Food and Drug Administration
FT	Fourier Transform
FTIR	Fourier Transform Infrared spectroscopy
GAC	Granular Activated Carbon
H	High-affinity
HIPE	High Internal Phase Emulsion
IBP	Ibuprofen
IEP	Isoelectric Point
IR	Infrared
ISO	International Organization for Standardization
IUPAC	International Union for Pure and Applied Chemistry
L	Langmuir

LPS	Lipopolysaccharides
MB	Methylene Blue
MBR	Membrane filtration
NOM	Natural Organic Matter
NSAID	Nonsteroidal anti-inflammatory
PAC	Powder Activated Carbon
PARA	Paracetamol
PolyHIPE	Polymerized High Internal Phase Emulsion
PPCPs	Pharmaceutical and Personal Care Products
PZC	Point of Zero Charge
RAN	Ranitidine
S	Sigmoid
SEM	Scanning Electron Microscopy
SOC	Synthetic Organic Chemical
TC	Tetracycline hydrochloride
TG	Thermogram
TGA	Thermogravimetric Analysis
THF	Tiamulin hydrogen fumarate
T&O	Taste and odour
VC	Volatile content
WHO	World Health Organization
WWI	World War I
WWTP	Wastewater treatment plant
XPS	X-ray Photoelectron Spectroscopy
XRD	X-ray Diffraction

Symbols glossary

A	Adsorption potential	42
A	Pre-exponential Arrhenius factor	106
A_{BET}	Specific surface area determined by the BET method	39
$a_{\text{m}}(\text{N}_2)$	Average area occupied by nitrogen (adsorbate) molecule in the monolayer	40
b	Interception at the plot origin	40
B	Constant independent of the temperature and characteristic of the adsorbent porous structure, obtained by the DR equation	41
C_0	Initial solute concentration	107
C_{BET}	BET constant	40
C_e	Solute concentration at equilibrium	68
C_t	Solute concentration at time t	107
D	Pore diameter	46
d	Interplanar spacing of a crystal, according to Bragg's law	56
E_0	Characteristic energy of adsorption, determined by the DR equation	41
E_{des}	Activation energy of desorption	106
ΔG	Variation of Gibbs free energy	33
h	Initial adsorption rate, determined by the pseudo-second order kinetic equation	66
ΔH	Variation of enthalpy	33
k_1	Pseudo-first order rate constant	66
k_2	Pseudo-second order rate constant	66
K_{F}	Freundlich constant	69
K_{L}	Langmuir constant	68
L_0	Mean pore width	41
m	Plot slope	40
M_{w}	Molecular weight	126
N	Avogadro constant	40
n	Order of reflection, according to Bragg's law	56
n	Freundlich exponent	69
n^{ads}	Adsorbed amount at pressure p	33
n_{m}	Amount adsorbed on the monolayer	40
P	Applied pressure	33
p	Equilibrium pressure of the adsorptive at the experiment temperature	40
p^0	Saturation pressure of the adsorptive at the experiment temperature	33
pH_{IEP}	pH at the isoelectric point	49

pH_{PZC}	pH at the point of zero charge	49
pK_a	Acidic constant	63
p/p^0	Relative pressure of the adsorptive at the experiment temperature	33
q_e	Amount of solute adsorbed in equilibrium	66
$q_{e, \text{calc}}$	Amount of solute adsorbed calculated by the pseudo-second order kinetic model	99
$q_{e, \text{exp}}$	Amount of solute adsorbed experimentally obtained	99
q_m	Monolayer adsorption capacity	68
q_t	Amount of solute adsorbed at time t	66
R	Ideal gas constant	37
r	Meniscus radius formed in capillary condensation	37
R^2	Determination coefficient	101
RE	Regeneration efficiency	133
r_K	Kelvin radius	37
ΔS	Variation of entropy	33
$t_{1/2}$	Half-life time obtained by the pseudo-second order kinetic equation	66
T	Temperature	33
T_A	Temperature value close to room temperature in TGA	54
T_B	Temperature at which weight loss starts to occur in TGA	54
T_C	Temperature after which the sample mass remains constant in TGA	54
T_D	Temperature at which a higher weight change occurs in TGA	54
V	Molar volume in Kelvin equation	37
V_{meso}	Mesopore volume	94
V_{mol}	Molar volume	159
$V_{\alpha \text{ super}}$	Total supermicropore volume determined by the α_S method	94
V_{total}	Total pore volume (volume adsorbed at $p/p^0 = 0.95$)	94
$V_{\alpha \text{ total}}$	Total micropore volume determined by the α_S method	94
$V_{\alpha \text{ ultra}}$	Total ultramicropore volume determined by the α_S method	94
W_0, V_{DR}	Micropore volume determined by DR equation	41
W^{ads}	Volume occupied by the adsorbed phase	41
W_{final}	Final sample height in TGA	104
B	Affinity coefficient	41
B	TGA heating rate	106
γ	Liquid-vapour interfacial surface tension	37
σ_t	Average thickness of a single monolayer, determined by the t method	43
Θ	Contact angle	46

θ_1	Angle formed by the intersection of the liquid-solid interface and the liquid-vapour interface	59
λ	Radiation wavelength	56
η	Global preparation yield	90
χ^2	Non-linear chi-square analysis	101

Chapter I

Contextualization

Activated carbons are adsorbent materials with a versatile field of applications, due to their structural, surface chemistry properties, and also because they are easily adapted to the requirements of their application. One of the activated carbons most common applications is in water remediation. However, the high production costs of these materials constitute a barrier to their broad application. One solution for this limitation is the use of low-cost precursor materials. In this context, the use of biomass wastes, namely of agricultural and industrial origin have shown great potential as precursors for the preparation of activated carbons, with a developed porosity, and advantageous from an economic point of view (Pap *et al.*, 2017; Kopac *et al.*, 2016; Moloukhia *et al.*, 2016; Yu *et al.*, 2016; Dias *et al.*, 2007; Ioannidou and Zabaniotou, 2007; Menéndez-Díaz and Martín-Gullón, 2006)

Considering aquatic pollution, in the last decades, the detection of numerous compounds belonging to the class of pollutants designated Pharmaceutical and Personal Care Products (PPCPs) has raised a special concern among the scientific community. The reason for this is the fact that the development of medical care, for humans and animals, has led to the production of increasingly more effective pharmaceutical active ingredients such as lipid-regulating drugs, analgesics, antibiotics, antiseptics, hormones, and chemotherapy and beta-blocking heart drugs. Even though regulation rules have been enforced by Food and Drug Administration (FDA) to minimize PPCPs consumption (Aminoshariae and Khan, 2015), in 2014, the worldwide consumption of medicines containing these active ingredients reached around 15 g values *per capita* and, in industrialized countries the value increased to 50-150 g (Yang *et al.*, 2017; Daughton, 2002). After administration, a large amount of these compounds is excreted by the human body partially or completely un-metabolized, resulting in the continuous release of a wide variety of pharmaceutical active ingredients, their metabolites and transformation products into the sanitation systems (Zwiener *et al.*, 2001). Moreover, the detection of PPCPs in sub-therapeutic concentrations in surface and subterranean waters has also raised concerns about the efficiency of the conventional treatments used in wastewater treatment plants (WWTPs). In the particular case of pharmaceutical compounds, their presence has been detected in influents and effluents of WWTPs (García *et al.*, 2014; Afonso-Olivares *et al.*, 2012). Consequently these pollutants are continuously released to the aquatic environment, being detected in lakes and rivers (Azuma *et al.*, 2017; Mandarić *et al.*, 2017; Yang *et al.*, 2017; Lin *et al.*, 2016; Oliveira *et al.*, 2015; Carmona *et al.*, 2014), and reaching drinking water treatment plants (Yang *et al.*, 2017).

Several studies have demonstrated the efficiency of the use of lab-made and commercial activated carbons for the removal of pharmaceutical compounds in aqueous phase, namely the studies developed in the research facility where this PhD thesis was developed (Batista *et al.*, 2016; Galhetas *et al.*, 2015, 2014a, and 2014b; Mestre *et al.*, 2016, 2015, 2014a, 2014b, 2012, 2011). Taking into account the production costs of activated carbons, the use of adsorbents prepared from low-cost materials, such as wood bark, that allow to obtain activated carbons with adequate properties to adsorption, is a fundamental and important theme of investigation for their sustainable application in water treatment.

Bacteria adhesion is deeply considered in the scenario of water treatment where activated carbons are applied in the granular (in columns) and powder (in a batch reactor) forms, in several stages of the water treatment process. This phenomenon can have positive and/or negative impact on water treatment depending of the purpose the

solids application. One example is the so-called biological activated carbon (BAC) that is prepared by controlled colonization of activated carbons, usually in the granular morphology. The use of BAC allows for an increase of the carbon life time, in comparison to the use of pristine material, by converting a portion of the recalcitrant organics into biodegradable matter (Korotta-Gamage SM and Sathasivan, 2017 Westphalen *et al.*, 2016; Bautista-Toledo *et al.*, 2014; Rivera-Utrilla *et al.*, 2013). The microorganisms adhered at the carbon surface can also change the surface charge of the material, for example, to a more negative global charge enhancing the adsorption capacity towards positively charged species, such as, heavy metals.

On the other hand, spontaneous and long-term colonization of activated carbon during water treatment can prevent the adsorbent from removing the targeted pollutants from water, enabling its effectiveness.

Bacteria colonization of activated carbons has been reported in the literature, but the studies published are focused almost exclusively on granular solids (Qin *et al.*, 2016; Borges, *et al.*, 2016; Islam *et al.*, 2016). In this context, besides evaluating the carbons adsorptive properties, an understanding of the material behaviour in a biologic environment is crucial prior to application for water remediation.

Tannins are polyphenolic biomolecules that occur naturally in vegetable tissues of many species of the Plant Kingdom, where their biological role is related to protection against fungi infections, insects predation, animal herbivory and perhaps even regulation of plant growth (Gross *et al.*, 2012; Khanbabaee and van Ree, 2001).

Tannin-based polymer materials prepared by high internal phase emulsions, designated PolyHIPEs (Polymerized High Internal Phase Emulsions) are nowadays applied in numerous fields of material science, for example, for thermal insulation (Kovačič *et al.*, 2012), molecular storage applications (Cooper *et al.*, 2009), and for solid phase synthesis (Sadeghi and Moghbeli, 2012). These materials have also been used in biological and biomedical applications, namely as potential substrates for tissue engineering (Wang *et al.*, 2016), and in other fields, such as, electrochemical sensing (Zhao *et al.*, 2007).

The textural and chemical properties of these materials also make them good candidates as adsorbent materials. Their application in water decontamination is furthermore supported from an economic point of view given the easiness and cost efficiency of the PolyHIPEs materials preparation. However, in the literature few studies have been reported exploring this thematic, and even fewer have investigated the underlying mechanism of the pollutants retention in the polymers (Sieniawska and Baj, 2017; Sánchez-Martín *et al.*, 2013a and 2013b).

Chapter II

Objectives

The research developed in this PhD thesis has as main objective a deep insight into the adsorption mechanism of several pharmaceutical and personal care compounds onto porous materials, which is of paramount importance to improve, water treatment purposes technologies. This process was approached from different perspectives, namely the preparation of activated carbons from a biochar from apple tree branches. The prepared solids proved to have potential to be used as adsorbents for atenolol adsorption and good results were also obtained in competitive adsorption conditions, in the case of tiamulin hydrogen fumarate medicine. The mechanism of atenolol thermal desorption from the solids was assessed and the chemical nature of the carbons revealed to be of great importance. The role of morphology on the adsorption of paracetamol and clofibrac acid compounds, and cyclic thermal regeneration of paracetamol-exhausted samples were also evaluated. Other innovative perspective considered was the potential of ACs to immobilize/remove bacteria cells from solution and a complete study on the key role parameters and mechanism of immobilizations was performed. Results demonstrated a novel mechanism of immobilization onto the powder carbon consisting in the formation of agglomerates carbon-cell-cell-carbon. Finally, the adsorption mechanism of methylene blue onto tannin-based polymers was studied and screening adsorption experiments were carried out with a set of pharmaceutical compounds and personal care products, chosen by their high consumption and frequent detection in water decontamination.

Chapter III

Porous materials

III. 1. Activated carbons

III.1.1. Historical perspective

The exact first use of charcoal is not known, however, one of the oldest references to the use of charcoal for medicinal purposes was found in an Egyptian papyrus dating from 1550 B.C., where curiously the black pigment used to draw the illustration was also charcoal (see **Figure III.1 (a)**). The Egyptians also used it to fabricate bronze, adsorb odours, cure intestinal problems, fabricate beer, as pigment for makeup purposes, and even to preserve the corpses before proceeding to the embalming (Cooney, 2016; Çeçen, 2011; Ménendez-Díaz and Martín-Gullón, 2006; Dinsley, 2005).

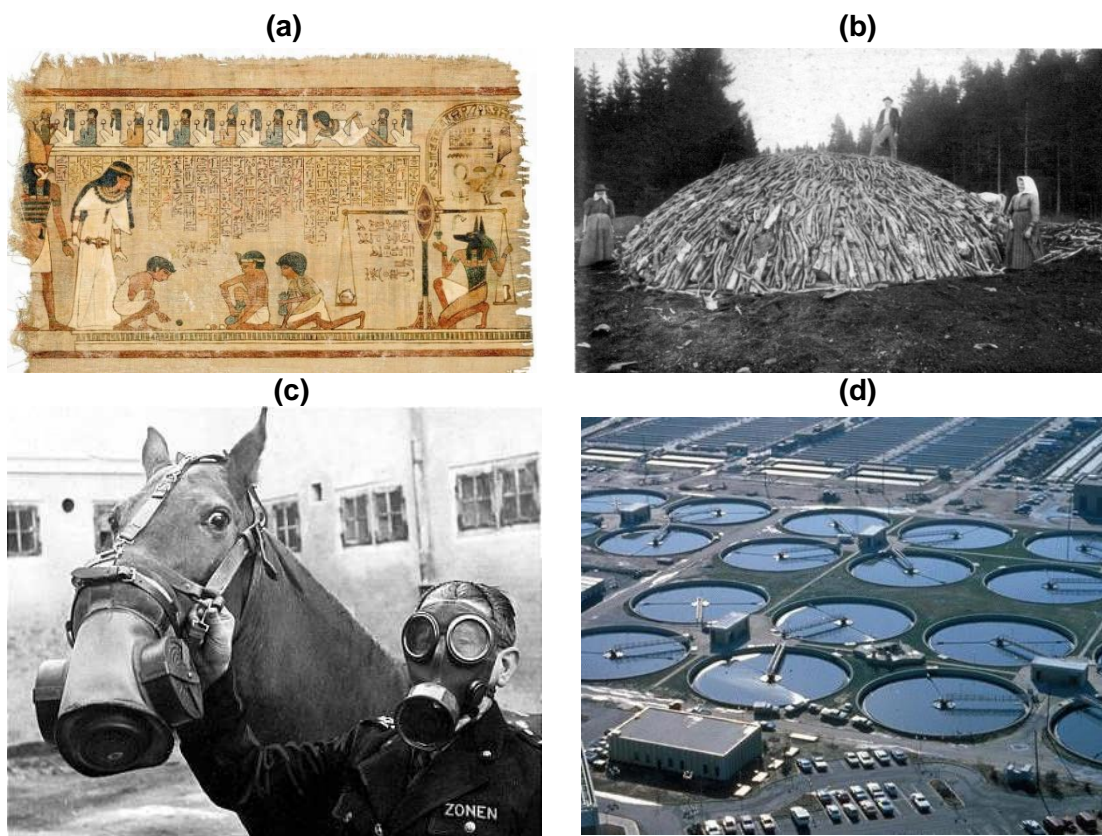


Figure III.1. Illustration of charcoal and activated carbons uses and manufacture, throughout history: (a) Egyptian papyrus; (b) Charcoal kiln; (c) Gas mask in WWI; (d) water treatment plant.

Another interesting fact about charcoal, is the method by which it has been produced. For example, in the 19th century, the charcoal production was made in a conical pile of logs with a fire shaft inside where the fire was set using, typically, wood chips. These structures, called kilns, were then covered with grass, moss and earth to reduce the flow of oxygen to a minimum (**Figure III.1 (b)**).

The first application of activated carbon in the industrial sector took place in England in 1794, when it was used as a decolorizing agent in the sugar production industry (Ménendez-Díaz and Martín-Gullón, 2006). In the early 1900s, as the potential of these materials was becoming known, the first patent concerning activated carbons production was granted to Raphael von Ostrejko (<http://speicyte.wixsite.com/raphael-von-ostrejko>). At this time, the first plant to produce activated carbons (ACs) industrially was built in Ratibor in the German Empire, now Raciborz (Poland) (Bandosz, 2016).

Many other plants then emerged to produce activated carbons primarily for decolorization.

During World War I (WWI), activated carbon was used in gas masks for protection against hazardous gases and vapours (see **Figure III.1 (c)**), which boosted the application of these adsorbents in several fields.

Nowadays, activated carbons are applied in an enormous variety of fields, such as water (see **Figure III.1 (d)**) and air treatment industry (Sulyman *et al.*, 2017; Shammay *et al.*, 2016; Westphalen *et al.*, 2016), petrochemical industry (Przepiórski, 2006; Lin *et al.*, 2001), chemicals and gas purification (Brea *et al.*, 2017), and even food and beverage industries (Martínez-Romero *et al.*, 2007). Activated carbons have for a long time been used in filters for protection equipment, namely gas masks, and even at present they have a key role in this field. ACs are also employed in other areas, such as, the metallurgy industry, for the recovery of metals, and in medicine, for wound care and in the maintenance of several medicinal products and consumables (Przepiórski, 2006).

III.1.2. Activated carbons structure

The high performance of the activated carbons in adsorption applications can be attributed to its physical and chemical properties, so the characterization of these materials is of paramount importance to understand their behaviour as adsorbents.

Activated carbons are characterized by an extensive pore network, formed essentially by graphitic layers interconnected in a complex and disorganized structure. Besides their highly developed porosity, these materials also present, at their surface, various functional groups resulting in a very rich surface chemistry, determinant to their interaction with the surrounding environment.

III.1.2.1. Physical structure

In terms of structure, activated carbons are composed by carbon atoms linked in condensed hexagonal aromatic rings, which constitute the so-called graphitic layers (see **Figure III.2 (a)**). These layers are interconnected by van der Waals forces and are disposed in a disorganized way, highly more disorganized than the graphite structure (Biscoe and Warren, 1964). Due to this randomised disposition of the graphitic layers, a high amount of interstices appear on the structure of the activated carbons (see **Figure III.2 (a)**), which may be occupied by disorganized carbonaceous matter, and also by inorganic matter (ash) originated from the starting material used as precursor.

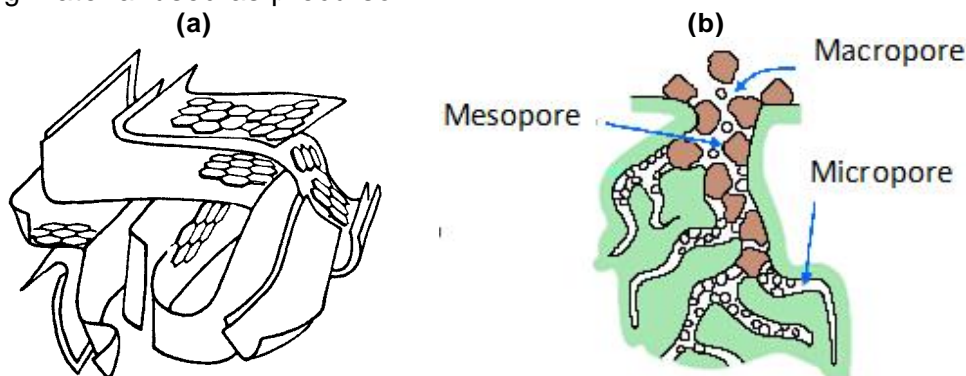


Figure III.2. Schematic representation of activated carbon **(a)** microstructure (adapted from Rodríguez-Reinoso and Sepulveda-Escribano, 2001) and **(b)** porous structure.

During the activation process the disorganized carbonaceous matter and some carbon atoms from the graphitic layers are removed, leading to the development of pores (see **Figure III.2 (b)**).

In porous materials, pores with different forms are considered and the way their dimension is defined is related to their shape. For example, in the case of slit shape pores, the dimension is considered in terms of width, *i.e.*, the distance between its two opposite walls, while in cylindrical pores the width is defined in terms of diameter (Menéndez-Díaz and Martín-Gullón, 2006; Dabrowski, 2001). In the case of activated carbons, the pores are commonly assumed to have a slit shape and thus, they can be classified in respect to their width.

According to the *International Union for Pure and Applied Chemistry* (IUPAC) (Thommes *et al.*, 2015) pores can be classified in:

Macropores: width higher than 50 nm.

Mesopores: width between 2 and 50 nm.

Micropores: width smaller than 50 nm.

Micropores can be further divided in supermicropores (widths between 0.7 nm and 2 nm) and ultramicropores (widths smaller than 0.7 nm).

Pore dimensions influences the adsorption process in different ways because, first of all, the micropores, which are located in the interior of the material particles, are where the adsorption takes place. Thus, the micropore volume of an activated carbon deeply influences its adsorption capacity. On the other hand, the mesopores, also called “transition pores” affect the rate of adsorption process since they connect the wider pores (macropores), located at the external surface, with the micropores (internal pores). At last, the macropores are considered transport pores because they allow the adsorbate to have access to the more internal narrow pores.

As the access to the adsorption sites in the micropores is ruled by the presence and dimension of the wider pores, each application requires a material with a specific pore size distribution, which depends greatly of the experimental conditions used during activation, as well as the properties of the starting material used (Marsh and Rodríguez-Reinoso, 2006).

Carbons with similar textural characteristics can, however, have different adsorption performances, if they have different surface chemistry properties. The functional groups present at the carbon surface have, in fact, an extremely important role in the interaction between the material and the adsorbate. Thus, it is the combination of both chemical and textural properties of the activated carbons that dictates its behaviour in a specific adsorption process (Menéndez-Díaz and Martín-Gullón, 2006).

III.1.2.2. Chemical structure

Activated carbons have a very rich surface chemistry, composed by functional groups due to the presence of heteroatoms, such as, oxygen, hydrogen and nitrogen. The functionalities, commonly existing at the surface of the ACs, are presented in **Figure III.3**.

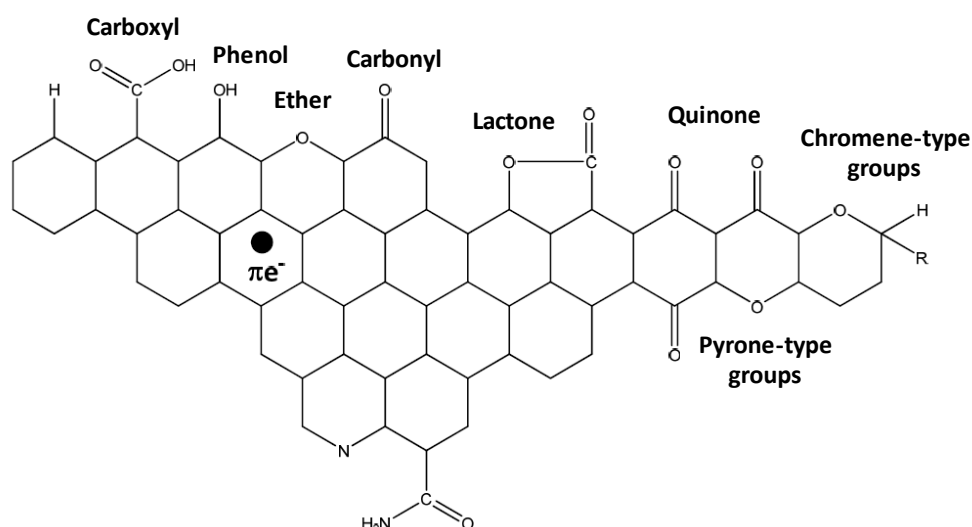


Figure III.3. Examples of oxygen and nitrogen functional groups possibly present at the surface of the activated carbons (adapted from Menéndez-Díaz and Martín-Gullón, 2006).

The oxygen functionalities are the most common and abundant surface groups, largely influencing the chemical properties of the material. These groups may be formed during the preparation of the AC, in the activation, or can be introduced through oxidising treatments (Menéndez-Díaz and Martín-Gullón, 2006). Nitrogen groups, besides being introduced during the production of the material, can also result from the treatment of ACs with different compounds such as ammonia, melanin or urea.

Despite the fact that the area occupied by surface groups represents a small fraction of the total surface area of the ACs, small variations in its chemical nature can affect the adsorption capacity of the material. Two properties, clearly related to the nature of the surface chemical groups are the hydrophobic/hydrophilic character of the carbon and obviously its acid/basic nature. Although the ACs are generally hydrophobic, the introduction of polar oxygenated groups causes the increase of the AC hydrophilicity due to the formation of hydrogen bonds between the oxygen functionalities at the surface of the carbon and water molecules which, after being adsorbed can continue to establish interactions to other water molecules, forming agglomerates of water molecules at the surface of the carbon. This effect may have a positive or negative impact, depending of the intended application because, a high hydrophilicity may facilitate the impregnation of the material in solution but, in adsorption from aqueous solutions, the presence of water molecules agglomerates can block the access of the adsorbate to the micropores, decreasing the adsorption capacity of the carbon (see **Figure III.4**).

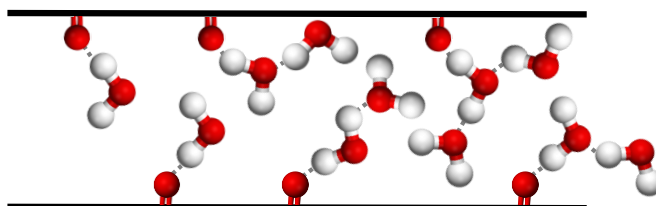


Figure III.4. Increase of AC hydrophilic character (introduction of oxygenated groups) can cause blockage of the micropores due to water adsorption (adapted from Menéndez-Díaz and Martín-Gullón, 2006).

Regarding the acid-base character, carbons are normally amphoteric materials, *i.e.*, they have both acidic and basic surface groups. Thus, when the activated carbon is immersed in water, charges will be generated at the surface of the carbon due to the dissociation of the acidic functional groups and/or the adsorption of ions from solution (basic functionalities). The negative surface charge is a consequence of the dissociation of carboxyl and hydroxyl groups, whereas the positive charge (in carbons without nitrogen groups), can be attributed to groups like chromene and pyrone, or to the regions inside the graphitic layers, rich in π electrons, which will act as Lewis bases. Depending on whether the acidic or the basic groups are predominant, the net surface charge will be, negative or positive, respectively. As a consequence, the pH of the water where the material is suspended will become lower or higher than 7 (Bandosz and Ania, 2006).

Lastly, the content in inorganic matter (ashes) existent in the precursor may block the porosity of the carbon and adsorb water, due to its hydrophilic character, reducing the adsorbate retention capacity (Linares-Solano *et al.*, 2000).

III.1.3. Types of activated carbons

Due to the numerous applications of the activated carbons, addressed in section III.1.6, these materials are used under different morphologies (see **Figure III.5**).

Powder activated carbons (PACs) have particle dimensions inferior to 100 μm , being the most common sizes between 15 and 25 μm (Bansal *et al.*, 1988). This type of carbon has high external surface areas and is nowadays used, for example, in the treatment of industrial and municipal wastewater, in food and pharmaceutical industry, and also for energy storage. PACs smaller particle size allows them to be used for liquid phase adsorption, when the solute has diffusion hindrance in transport pores (mesopores) towards the adsorption sites (micropores). In this case, using an adsorbent with a more accessible microporosity is preferable (Menéndez-Díaz and Martín-Gullón, 2006).

Granular activated carbons (GACs) have particle dimensions superior to 100 μm (Bansal *et al.*, 1988) and, according to Marsh and Rodríguez-Reinoso, 2006, inferior to 1 mm. Other authors consider that GAC particles size can reach 5 mm (Menéndez-Díaz and Martín-Gullón, 2006). GACs are prepared from hard precursor materials, which are broken and activated to produce the activated carbon. The pellet form is prepared by mixing an activated carbon, preferably in the powder form, with a binder. The mixture is shaped to the desired form (*i.e.* cylindrical shape) and then subjected to thermal treatment.

The higher particle size of GAC results in low external surface area. These carbons are applied as adsorbents in liquid and gas phase, in water treatment, gas purification, in air filtration and in gas masks. The advantage of using GAC in comparison to PAC is the possibility to regenerate or reactivate the exhausted granular materials, allowing its reuse.

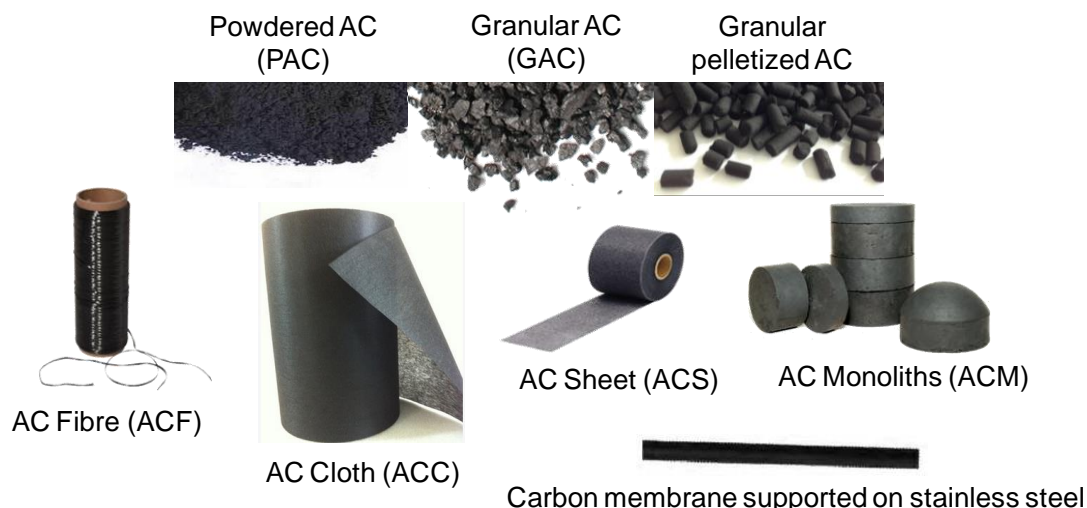


Figure III.5. Different morphologies of activated carbon.

Activated carbon monoliths (ACM) are prepared in a similar way as GAC pellets, but in this case the carbon binder mixture is shaped into a monolith form. The shape of monolith allows to surpass many of the limitations of using ACs in the powder and granular morphologies in gas or liquid streams. Actually, when monoliths are used in adsorption columns, problems of pressure drop in the system or the appearance of channels in the carbon bed are reduced (Plaza-Recobert *et al.*, 2017). Monoliths are also used for gas storage and separation, in order to reduce the inter-particle spaces and optimize the adsorption capacity of the activated carbon (Menéndez-Díaz and Martín-Gullón, 2006).

Carbon membranes supported on stainless steel are commonly used for molecular gases separation, because they are able to separate different gases according to their different molecular sizes. Carbon membranes are considered molecular sieves because they present good shape selectivity for planar molecules, high hydrophobicity, heat resistance and high corrosion resistance (Saufi and Ismail, 2004). Examples of mixture of gases that can be separated using these materials are N_2/O_2 from atmospheric air, H_2/C_xH_y from light hydrocarbon mixtures, or CO_2/CH_4 from biogas (Menéndez-Díaz and Martín-Gullón, 2006). Among the existing carbon membranes, two types can be differentiated: the molecular sieves which separate gases according to their molecular dimensions, and the adsorbent membranes where the gases separation occurs as a consequence of their textural and chemical surface properties.

Activated carbon fibres (ACFs) began being developed in the 1980s using steam activation. Nowadays, these materials are prepared by carbonization and thermal activation of the precursor fibres, under oxidizing atmosphere, at temperatures between 700 and 1000 °C (Lee *et al.*, 2014).

These materials have all the advantages of the conventional forms of activated carbon, such as, high surface area and adsorption capacity, together with a uniform pore size distribution, consisting almost exclusively of micropores. These properties made ACFs suitable materials to be used in a variety of applications, such as, adsorption in liquid phase (for example, heavy metal removal) (Rusova *et al.*, 2016; Liu, 2007; Mays, 1999), biomedical applications (Park and Jang, 2003; Mays, 1999), refrigeration (Attan *et al.*, 2011; Hamamoto *et al.*, 2006) and catalysis (Yang *et al.*, 2015; Yanzong, *et al.*, 2008). Although the cloth form of

activated carbon is considered expensive, it presents several advantages, in comparison to the traditional morphologies mentioned previously. These are high contact efficiency, very low charge loss, high adsorption rate, allied with high flexibility and ease to handle (Radovic and Reinoso, 1997). The sheet and cloth morphologies also have the advantage of higher mechanical strength, in comparison to the ACFs. In liquid phase adsorption, the better performance of these materials is justified by the fact that, while with GACs, and even PACs, the adsorbates have to diffuse through the macro and mesopores network to reach the adsorption sites in the micropores, in this type of materials, the porosity is almost exclusively composed by micropores, located at the external surface area of the solid (Menéndez-Díaz and Martín-Gullón, 2006) (see **Figure III.6**). Consequently, as opposed to the diffusion limitations that may occur for some adsorbates in granular and powdered carbons, no hindrances to diffusion occur in ACF, ACS and ACC morphologies.

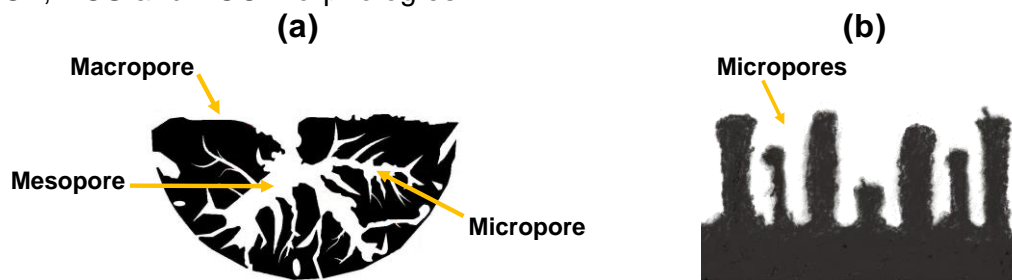


Figure III.6. Scheme of the porosity location in (a) a granular activated carbon and (b) an activated carbon fibre (adapted from Menéndez-Díaz and Martín-Gullón, 2006).

III.1.4. Preparation of activated carbons

The preparation of activated carbons generally encloses the experimental steps represented in **Figure III.7**.

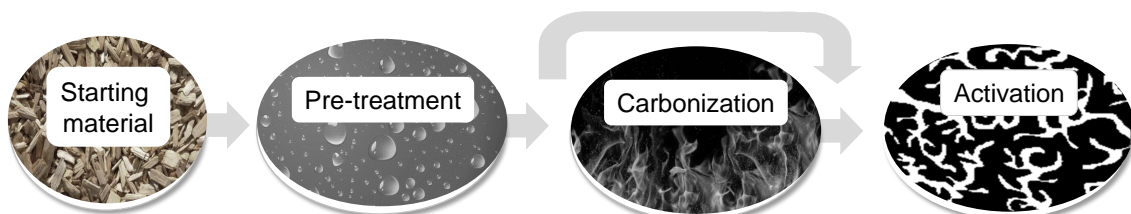


Figure III.7. General procedure for the production of activated carbons.

Starting material

Activated carbons can be manufactured from a wide variety of raw materials, with the predominant requirement of being rich in carbon (Bansal, *et al.*, 1988). Other properties, like hardness, ash content and trace impurities, also play an important role because they end up in the final product and can affect the final properties of the AC. In this context, it is important that the precursor has a low ash content because the inorganic matter present in the material can have a negative effect in its application in liquid phase adsorption and can also decrease the adsorption capacity of the carbon because this parameter is measured by mass of porous material (the ashes are non-porous). Conversely, ashes rich in iron, calcium and alkaline compounds, when present in the precursor material, can have a catalytic effect during the physical activation process leading to the production of carbons with a wider porosity.

The more attractive materials for AC development are the low-cost ones (preferably wastes), since the preparation yields are usually low, reaching values as low as 5 to 10 % (Menéndez-Díaz and Martín-Gullón, 2006). Several reviews published in the literature have listed examples of low-cost precursors used in the development of ACs (Dias *et al.*, 2007; Ioannidou and Zabaniotou, 2007).

These adsorbents can be prepared from mineral and vegetable carbons, turf (Sani, 2011), wood residues (Zhang and Zhang, 2014), fruit stones (Pap *et al.*, 2017), walnut (Yu *et al.*, 2016) and coconut shells (Moloukhia *et al.*, 2016), fruit pits (Erabee *et al.*, 2017), cork (Mestre *et al.*, 2014b), sisal (Mestre *et al.*, 2011) and bituminous coal (Kopac *et al.*, 2016).

A key element, especially when using biomass waste, is also the homogeneity and constancy of the precursor, to ensure the reproducibility and quality of the final adsorbent.

Agricultural wastes have proven to be promising precursors for the development of ACs due to their availability and low price. Also, these raw materials lead to activated carbons with high adsorption capacity and in some cases also with considerable mechanic strength and low ash content (Ioannidou and Zabaniotou, 2007). This is especially true in the case of activated carbons made from coconut shells commercialized, for example, by Cabot-Norit company - granular carbons GCN 48, GCN 612 G and GCN 816 G (company site <http://www.cabotcorp.com/solutions/products-plus/activated-carbon/granulated>).

Pre-treatment

There are several treatments that can take place prior to the activation process, such as homogenization, washing and impurities removal. In this sense, washing with water or sieving, in the case of visible solid impurities are the first steps of the pre-treatment process. After making sure that the material is homogeneous, if a specific particle size is required, the material can be grounded and sieved to obtained particles with the desired dimensions.

In the case of materials with high content of mineral matter, decreasing it is important, prior to its use, and this can be achieved by treating the starting material with acid, followed by an exhaustive washing with water.

When the precursor is a coke, the sample is pre-oxidized, which consists in exposing the material to the atmospheric air, during long periods of time, at moderate temperatures (180-300 °C). This will allow the stabilization of the matrix by creating cross-links in its structure, preventing the appearance of a fluid phase during its heating (Menéndez-Díaz and Martín-Gullón, 2006).

Carbonization

Carbonization consists in heating the material under inert atmosphere (commonly nitrogen), with the objective of devolatilizing the material and enriching the matrix in carbon. The removal of heterogeneous elements namely, hydrogen and oxygen, originates a skeleton made essentially of carbon, designated char, with a rudimentary porous structure. The material is, in this way, enriched in carbon and with a higher level of aromaticity than the starting solid. The increase in aromaticity is accompanied by the development of an incipient porosity because many functional groups and bridged chains, existent in the starting material, are volatilised during carbonization, leading to empty spaces, the pores. The carbonization step is not always performed, depending on the properties of the precursor, as well as, the activation conditions chosen for the

preparation of the activated carbon, as it is explained in more detail in the next paragraphs.

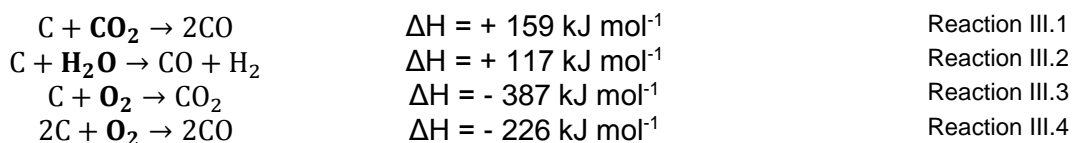
Activation

The porosity of the char obtained after carbonization is not sufficiently developed for the majority of applications, being necessary to perform a further activation step. The activation is responsible by a considerable development of porosity, as well as, by the introduction of functional groups at the activated carbon surface. In this context, the solid (precursor or char) can be activated by two methods: thermal (or physical) or chemical activation.

Thermal activation

This method is characterized by resorting to gases, at temperatures between 800 and 1000 °C, and by usually requiring a previous carbonization of the material. The activation is made under flow of oxidizing gases (for example, CO₂, water vapour or O₂) that react selectively with the atoms of carbon what results in the development of porosity.

Activation with CO₂ and water vapour (Reactions III.1 and III.2) are endothermic processes (positive values of enthalpy) and, for that reason, easy to control, as opposed to activation with molecular oxygen (Reactions III.3 and III.4) where the activation is of exothermic nature and thus hard to control (Marsh and Rodríguez-Reinoso, 2006).



Chemical activation

In chemical activation, the AC precursor (previously carbonized or not) is placed in contact with the activating agent and then heated, under inert atmosphere, at temperatures between 400 and 900 °C. The final material is exhaustively washed to remove any activating agent existent in excess amount, as well as reaction products.

The impregnation step can be made by two different methodologies; impregnation in solution or by physical mixture in the solid state (see **Figure III.8**). The first method consists in dispersing a chosen amount of solid in a saturated solution of the activating agent (in the amount necessary to obtain the desired solid/activating agent ratio) and then drying to obtain the impregnated material. In the second case, the precursor is mixed with the activating agent, in the solid state and grounded to ensure the homogeneity of the final mixture, which is then heated at the desired temperature, under inert atmosphere (for example N₂), during the desired time. The resulting material is then thoroughly washed and dried.

Both impregnation processes are usually made at ambient temperature.

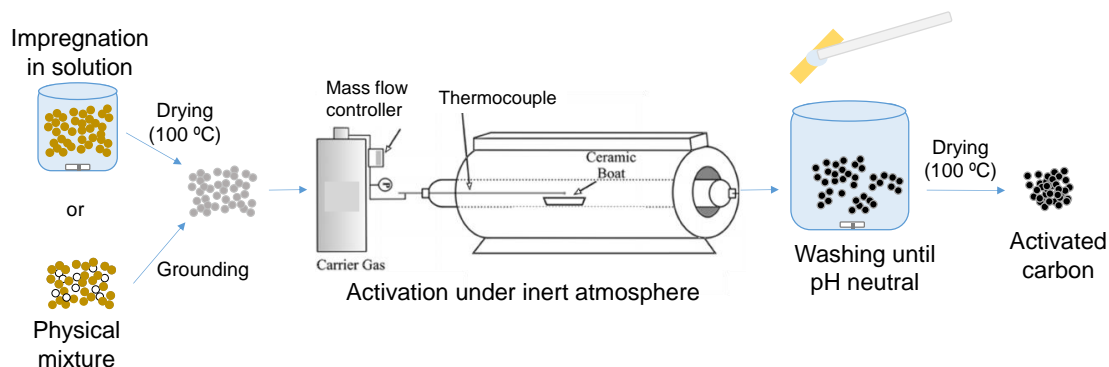
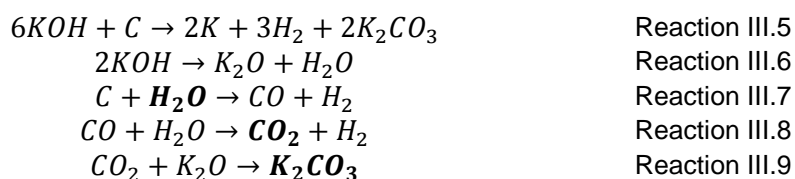


Figure III.8. General experimental procedure for preparing ACs by chemical activation.

The most commonly used activating agents are ZnCl_2 , H_3PO_4 , KOH and K_2CO_3 . The first two reagents allow to obtain activated carbons with high preparation yields (up to 40 %), but their recovery efficiencies at the end of the process are very small. Also, the use of these compounds presents problems of corrosion and pollution related with environmental contamination by zinc residues and eutrophication by phosphorus compounds. Because of this, the costs associated with these reagents have become very high due to the necessity of complying with the environmental regulations. For this reason, the use of other activating agents, KOH and NaOH , has been considered for the development of activated carbons by chemical activation.

Carbons activated with alkaline hydroxides were first commercialized in the 80's by the company Anderson Development Company (Menéndez-Díaz and Martín-Gullón, 2006). Since then, the use of these compounds as activating agents has been extensively explored by the scientific community for the development of activated carbons with high apparent surface areas and developed porosity (Boyjoo, *et al.*, 2017; Elmouwahidi *et al.*, 2017; Laksaci *et al.*, 2017; Ma, 2017; Mestre *et al.*, 2014b, Foo and Hameed, 2012a; Wang and Kaskel, 2012; Król *et al.*, 2011).

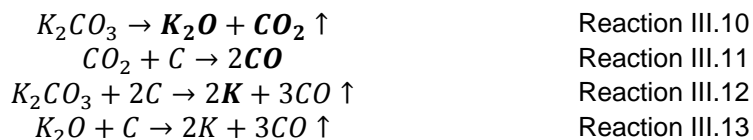
Regarding activation with KOH , its mechanism can be traduced by Reaction III.5, where the carbon atoms of the carbonaceous matrix are oxidised by KOH and the activating agent is reduced from K^+ to metallic K , which remains intercalated in the matrix structure. The metallic potassium formed is removed, during the final washing stage of the preparation procedure, unblocking the microporosity of the final activated carbon. According to the literature (Wang and Kaskel, 2012) several other reactions occur during activation with KOH , at relatively low temperatures ($\approx 400\text{ }^\circ\text{C}$). Some of the compounds formed, such as, H_2O and CO_2 , are commonly used as activating agents in physical activation and, consequently, even though the main reaction III.5 requires higher temperatures, around $600\text{ }^\circ\text{C}$, the secondary reactional system (Reactions III.6 to III.8) leads to the consumption of the carbonaceous matrix at lower temperatures, close to $400\text{ }^\circ\text{C}$. Another by-product formed is K_2CO_3 (Reaction III.9) which will decompose at temperatures between 700 and $800\text{ }^\circ\text{C}$, resulting in the formation of metallic K , which remains inserted in the matrix structure (Reaction III.12, presented ahead).



The use of hydroxides of alkaline metals has, however, some disadvantages, namely related to some corrosion problems, which can be overcome by the use of alkaline

carbonates (K_2CO_3 e Na_2CO_3). These compounds also lead to activated carbons with high surface areas, while having a less harmful impact on the environment. For example, the potential of K_2CO_3 in the preparation of activated carbons, from several precursors has been extensively demonstrated in the literature (Gurten *et al.*, 2012; Mestre *et al.*, 2010, 2011, 2014a; Tsubouchi *et al.*, 2016; Zhang *et al.*, 2016). In fact, an extensive analysis of the potential of K_2CO_3 for the preparation of activated carbons was also made in this PhD work, where the impact of several experimental conditions (temperature and duration of activation and biomass/ K_2CO_3 ratio) on the activation of apple tree branches char have been explored (study presented in Chapter VII).

The activation mechanism of K_2CO_3 involves the chemical transformations, corresponding to the Reactions III.10 to III.13, which occur between 700 and 800 °C (Wang and Kaskel, 2012; Addoun *et al.*, 2002). The CO_2 and K_2O released in K_2CO_3 decomposition (Reaction III.10) will consume the solid matrix, releasing CO and developing porosity (Reactions III.11 and III.13). The direct reaction of potassium carbonate with the solid matrix, described in Reaction III.12, is almost consensually accepted. However, the study developed by Mims and Pabst (Mims and Pabst, 1983) demonstrated that, when in contact with the carbon matrix, K_2CO_3 decomposes releasing CO_2 and forming C-O- K^+ complexes, very reactive and that can be considered as a kind of K^+ species with a high capacity for dispersion. The presence of C-O- K^+ complexes was demonstrated by ^{13}C NMR of samples obtained after surface methylation.



In inert atmosphere, the species K_2CO_3 and K_2O , from the carbonate decomposition, are reduced by the carbon, at temperatures between 700 and 800 °C, according to Reactions III.12 and III.13. The consumption of carbon atoms in these reaction creates the porosity of the final carbon (Reactions III.12 and III.13) (Addoun *et al.*, 2002; Mims and Pabst, 1983).

III.1.5. Regeneration

The industrial adsorption processes rely on the adsorptive properties of materials, which in the case of water treatment, are powder and granular activated carbons. According to Belyaeva *et al.* (Belyaeva *et al.*, 2009 cited in Omorogie *et al.*, 2014) it was estimated that in 2017, the global production of activated carbon would be 2.3 million metric tons. The annual consumption per capita of active carbon is 0.5 kg in Japan, 0.4 kg in the United States, 0.2 kg in Europe, and 0.03 kg in the rest of the world (Gogate and Pandit, 2004, cited by Omorogie *et al.*, 2014).

As the adsorption process progresses, the pores of the activated carbon become filled with adsorbate molecules and its adsorption capacity decreases up to the limit of complete saturation, when they fail to adsorb the targeted pollutants. After saturation the activated carbons can be disposed of as solid waste in a landfill or incinerated. However, the disposable of hazardous wastes in landfills is becoming increasingly unacceptable due to growing concerns about the effect of pollutants on the environment (Zanella *et al.*, 2014). On the other hand, the replacement of the spent adsorbent by new material is an expensive option due to the high costs associated to the material production.

With the purpose of decreasing the operational costs of adsorption processes, prevent further environmental contaminations from the disposal/incineration of the exhausted solid, and also aiming to a more sustainable society, the regeneration (and/or reactivation) of these materials, for continuous re-uses, has become an important issue both from academic and industrial perspectives, as well as from an economic point of view (Zanella *et al.*, 2014). Regeneration of powder activated carbons has proven to be difficult to achieve because the commercial processes available cause significant losses of adsorption capacity. For this reason, GACs are usually the only ones considered suitable for regeneration (Menéndez-Díaz and Martín-Gullón, 2006).

The regeneration of adsorbent materials, that is, the removal of the adsorbed compounds in order to recover their original adsorption capacity, can be achieved via two distinct routes: desorption or decomposition (see **Figure III.9**) (Omorogie *et al.*, 2014; Zanella *et al.*, 2014). The first consists in desorption of the adsorbed compounds, requiring only their mass transport from one phase (the adsorbed phase at AC surface) to another, usually the gas phase. The desorption-based regeneration methods can be classified in thermal or non-thermal procedures. The second route addresses regeneration based on decomposition of the pollutants adsorbed on the AC, involving reactions with the possibility of complete mineralization of the pollutants (Zanella *et al.*, 2014).

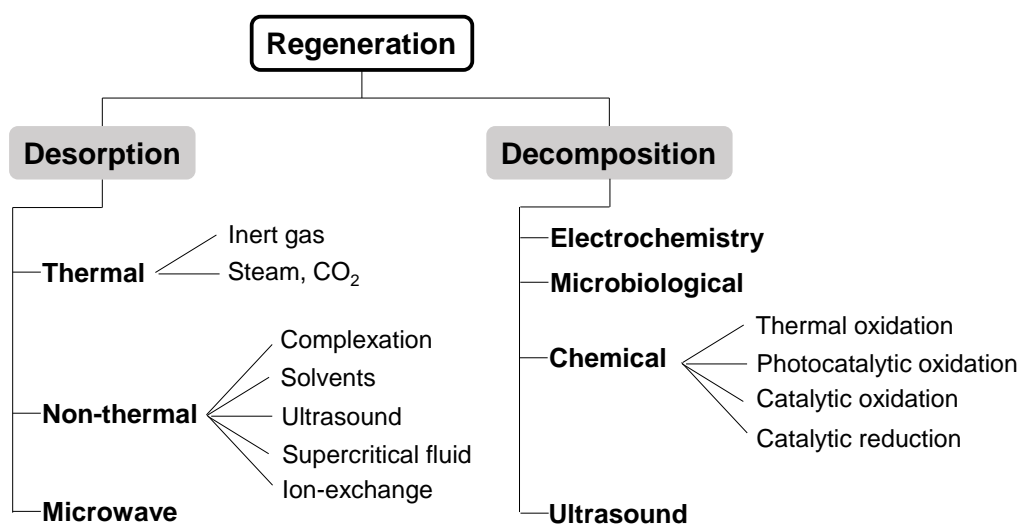


Figure III.9. Schematic representation of the basic regeneration techniques available for the recovery of spent adsorbents (adapted from Zanella *et al.*, 2014).

Several regeneration methodologies, based on desorption and decomposition have been extensively explored by the scientific community, such as thermal regeneration (Radic *et al.*, 2017; Batista *et al.*, 2016; Watanabe *et al.*, 2016; Ledesma *et al.*, 2014a and 2014b; Cazetta *et al.*, 2013; Berenguer *et al.*, 2010) microwave-induced regeneration (Caliskan *et al.*, 2016; Nor *et al.*, 2016; Foo and Hameed, 2012b and 2009), solvent extraction (Li *et al.*, 2016; Ma *et al.*, 2016; Salvador *et al.*, 2015; Zhou *et al.*, 2015; Cooney *et al.*, 1983), advanced oxidation and reduction processes (Benhamed *et al.*, 2016; Kim *et al.*, 2015; Salvador *et al.*, 2015; Julcour-Lebigue *et al.*, 2012) and microbial degradation (Aguayo-Villarreal *et al.*, 2016; Kew *et al.*, 2016; Oh *et al.*, 2016; Salvador *et al.*, 2015).

The selection of an appropriate regeneration process greatly depends on several factors such as, types of adsorbate (toxicity, ignitable, corrosion and radioactive properties), types of adsorption (physical adsorption or chemisorption), costs of regeneration and conditions of processing. Some of the methodologies presented will be

approached in more detail, especially the thermal-based regenerated methodology, which was the methodology applied in this PhD work.

Thermal regeneration methodologies are based on energy driven processes and generally follow three steps: i) adsorbent drying at around 105 °C; ii) high-temperature desorption heating (500-900 °C) under inert atmosphere, and iii) residual adsorbate gasification by an oxidizing agent (CO₂ or steam), usually at 800 °C. The heating under inert atmosphere (stage ii) involves partial cracking and polymerization of the adsorbed molecules. The last stage aims to remove the coke residue formed in the porous structure of the adsorbent in the previous stage and the recovery and reactivation of porous structure of the adsorbent. This final step may not be performed, depending on the exhausted material and operational conditions of the thermal treatment step. An important point that has to be noted is that, in thermal regeneration the thermal behaviour of an adsorbent has to be properly understood because subjecting the material to very high temperatures, above their thermal stability, will result in the loss of its properties. This assessment is performed by thermogravimetric analysis (TGA), which allows to select the operational conditions necessary to regeneration (Zanella *et al.*, 2014).

Thermal regeneration has some disadvantages, such as high energy costs and the fact that, as consequence of the process, the activated carbon loses in general, some adsorption capacity and 5 to 15 % of its initial mass (Roberts *et al.*, 2005). Nonetheless, this methodology is the unique regeneration technology used at industrial level (<http://www.cabotcorp.com/solutions/products-plus/activated-carbon/reactivation-services>), and several other studies have been published reporting its use (Radic *et al.*, 2017; Batista *et al.*, 2016; Watanabe *et al.*, 2016; Ledesma *et al.*, 2014a and 2014b; Cazetta *et al.*, 2013; Román *et al.*, 2013; Berenguer *et al.*, 2010; Pastrana-Martínez *et al.*, 2009; Sabio *et al.*, 2004).

The remaining regeneration technologies presented in **Figure III.9** have still some limitations that need to be overcome, and for this reason their implementation is not as well developed as thermal regeneration. For example, the regeneration with water vapour is a variant of the thermal regeneration, requiring a lower operational temperature. The main limitation of this process resides in the necessity of using additional processes, such as the vapour removal or distillation, to recover the desorbed compounds and avoid obtaining a contaminated effluent (Menéndez-Díaz and Martín-Gullón, 2006).

The regeneration based on the use of solvents is an expensive technology, due to the high cost of the solvents as well as due to the necessity of a final stage to recover them, usually by distillation or precipitation (Menéndez-Díaz and Martín-Gullón, 2006).

Regeneration with supercritical fluids uses carbon dioxide (critical temperature and pressure of 31 °C and 73 bar, respectively) and water (critical temperature and pressure of 374 °C and 220 bar, respectively). This technology may present some problems of corrosion of the equipment used, and so it requires the use of installations capable of operating under extreme conditions (Menéndez-Díaz and Martín-Gullón, 2006).

Microwave-assisted regeneration is a method that relies in electromagnetic energy which is converted into heat by mutual interaction between the electric field, component of the wave, with the polar or charged compounds (Omorogie *et al.*, 2014).

A clear distinction between microwave devices and conventional heating systems is the mode of heat generation. Thermal regeneration is performed conventionally in rotary

kilns on vertical furnaces. Hence, the source of heat is situated outside the adsorbent bed, being the heating made through convection and/or conduction, creating a temperature gradient in the adsorbent bed, and even in the adsorbent particles, until steady state conditions are reached. In contrast, the microwave device supplies microwave irradiation directly to the adsorbent bed (Jones *et al.*, 2002) with the transfer of heat energy being readily transformed into heat inside the adsorbent particles by dipole rotation and/or ionic conduction (Bradshaw *et al.*, 1998).

In recent years this technology has been extensively explored by many researchers as a potential regeneration for activated carbons (Wu *et al.*, 2017; Yang *et al.*, 2017; Nor *et al.*, 2016; Qu *et al.*, 2016; Foo and Hameed, 2012b and 2009; Ania *et al.*, 2004). A microwave-based regeneration has some advantages, in comparison with thermal regeneration, since it allows a fast application, with a precise control of temperature, it requires small operational areas and low energy, and it has proven to be efficient in recovering the initial adsorption capacity of the regenerated products. But this technique also suffers some disadvantages such as the fact that chlorinated products and nitrogenous organic compounds retained on the adsorbents produce HCl, CO₂ and N₂ gases when these adsorbents are regenerated by microwaves (Omorogie *et al.* 2014).

Microbiological regeneration of exhausted ACs occurs as the result of microbial oxidation that leads to degradation/removal of the compounds retained by the solid (Oh *et al.*, 2016; Bautista-Toledo *et al.*, 2014; Omorogie *et al.* 2014; Zanella *et al.*, 2014; Menéndez-Días and Martín-Gullón, 2006). Adsorption and biodegradation can occur simultaneously and the regeneration efficiency strongly depends on several factors such as the presence of mineral compounds (for example, nitrogen, phosphorus or sulfur compounds) for metabolism of adsorbate, optimum conditions for microorganism activity, adsorption mechanism of the adsorbate, biodegradability of adsorbate, adsorbent particle size and morphology, adsorbent porosity and nature, desorption kinetics, concentration gradient of adsorbate and adsorbent saturation, biomass concentration, dissolved oxygen, type of microorganism, molecular structure of organic pollutants, and structural characteristics of the adsorbent (Omorogie *et al.*, 2014; Aktas and Cecen, 2007; Witthuhn *et al.*, 2006 and 2005; Yang *et al.*, 2003; Benzing, 1993). The main limitations of this process reside in the need of a minucious control of the conditions of temperature, pH and solution concentration to maintain the colony of microorganisms alive. Besides this, the reactional times of this technology are usually very long (Omorogie *et al.*, 2014).

Chemical Regeneration is a process that implies the reaction of the exhausted activated carbon with a regeneration agent, promoting the reaction that will result in the desorption of the adsorbate species. In some cases, the regeneration agent can remain adsorbed on the carbon. An example of this type of process is the use of acids at high temperatures for the removal of heavy metals from saturated carbons. The treatment with chemical agents can affect the structure of the carbon causing alteration in its porosity and its efficiency depends on the existence of an additional step for the recuperation of the extracting agent (Menéndez-Días and Martín-Gullón, 2006). The application of the technology is then limited to situations where it exists the risk of ignition or decomposition of the adsorbate (Menéndez-Días and Martín-Gullón, 2006).

III.1.6. Applications of activated carbons

As mentioned in the beginning of this chapter, ACs have been used in several application throughout its history and, as their properties became more and more known, the fields of applications became more diverse.

Nowadays, activated carbons are applied in numerous fields, such as, water and air treatment industry, petrochemical industry, chemical and gas purification and even food and beverage industries (Brea *et al.*, 2017; Sulyman *et al.*, 2017; Shammay *et al.*, 2016; Westphalen *et al.*, 2016; Rivera-Utrilla *et al.*, 2013; Karanfil, 2006; Przepiórski, 2006; Rivera-Utrilla *et al.*, 2003; Lin *et al.*, 2001).

Among the most common applications of activated carbons are those related to the environmental remediation field due to the crescent need to preserve and remediate the environment from the impact of industrialization. This scenario led to a very marked growing of activated carbons consumption for water and gas treatment purposes (Przepiórski, 2006). Examples of industrial application of activated carbons, in liquid and gaseous phases, are given in **Table III.1**.

Table III.1. Examples of industrial application of activated carbons, in liquid and gaseous phases (Przepiórski, 2006).

Liquid phase adsorption	
Potable water treatment	Removal of dissolved organic matter, control of taste and odour, lead, chlorine, colour.
Food industry	Decolourization of liquid sugars (glucose, maltose).
Soda and beer	Removal of chlorine from potable water, after disinfection with chlorine
Pharmaceutical industry	Purification and separation of antibiotics, vitamins, hormones, etc.
Semi-conductors	Production of ultra-high purity water.
Petrochemical	Removal of oil and hydrocarbon contaminations from recycled steam condensate for boiler feed water.
Groundwater	Reduction of total organic halogens and adsorbable organic halogens in industrial reserves of contaminated groundwater.
Industrial wastewater	Effluent treatment to meet the environmental legislation.
Swimming pools	Removal of residual ozone and control of chloramine levels.
Gas phase adsorption	
Solvent recovery	Control of vapour emissions and recovery of organic solvents.
Carbon dioxide	Purification of carbon dioxide from fermentation processes.
Industrial respirators	Adsorption of organic vapours and inorganic gases.
Waste disposal	Removal of heavy metals and dioxins from flue gas of waste incineration.
Cigarettes	Removal of some harmful substances (nicotine and tar).
Air conditioning	Removal of contaminants from air, ventilation, and air conditioning.
Semi-conductors	Production of ultra-high purity air.
Toxic gas removal	Purification of industrial off-gases.
Fridge deodorizers	Removal of general food odours.

Since the studies developed in this thesis were focused on the use of activated carbon materials for wastewater treatment purposes, more specifically for the removal of micro-

pollutants and immobilization of bacteria, these applications will be approached in more detail in Chapters V and VI.

III. 2. Tannins

III.2.1. Definitions and extraction

Based on the classical Bate-Smith definition, tannins are a group of plant secondary metabolites that have the ability to tan or convert animal skin into leather. These compounds are classified as being water soluble phenolics with a molar mass between 300 and 3000 Da, and with the ability to precipitate alkaloids, gelatins, and other proteins. This definition, however, excluded more recently identified larger molecular compounds with masses up to 2000 Da, with similar structures (Sieniawska and Baj, 2017).

These compounds occur naturally in the vegetable tissues of many species of the Plant Kingdom and they can be located in almost every part of the plant, such as, in the bark, wood, leaves, fruit, roots, and seed (Gross *et al.*, 2012; Haslam, 1989). Because higher concentrations of these compounds are normally found in sick plants, it is believed that their biological role is related to protection against fungi infections, insects predation, animal herbivory and perhaps even regulation of plant growth (Khanbabaee and van Ree, 2001). High concentrations of tannins can be found dispersed throughout quebracho tree* (*Schinopsis balansae*), and in the wood barks of Mimosa tree bark (*Acacia mollissima*) and pine (*Pinus radiata*) (Haslam, 1989).

Plant preparation and extraction processes will have a great influence on tannin extract composition. Phenolic compounds can be extracted from fresh, frozen or dried plants and the extraction method to be employed is influenced by the chemical nature of the substance, sample particle size, and also by the presence of interfering substances (Domínguez-Rodríguez *et al.*, 2017; Mojzer *et al.*, 2016). The procedures conventionally used are usually based on solvents (Galan *et al.*, 2017; Machado *et al.*, 2017) however, more advanced extraction techniques have been developed, such as, extraction assisted by microwave (Galan *et al.*, 2017) and ultrasound (Machado *et al.*, 2017), and supercritical fluid extraction (Ameer *et al.*, 2017).

III.2.2. Structure, classification and polymerization

The classical division of tannins was based on their resistance degree, to hydrolysis in the presence of hot water or the enzymes tannases. As a result, tannins were grouped as hydrolysable (Gallotannins and Ellagitannins) or non-hydrolysable (condensed) tannins (Sieniawska and Baj, 2017). However, as several new tannin compounds began to be discovered, this classification was no longer adequate. Nowadays, tannins are categorized according to their structural characteristics into four major groups: Gallotannins, Ellagitannins, and Complex and Condensed Tannins (see **Figure III.10**) (Sieniawska and Baj, 2017; Khanbabaee and Ree, 2001).

*quebracho name derives from *quiebrahacha* meaning “axe-braker”, and it is used to describe hard wood tree species.

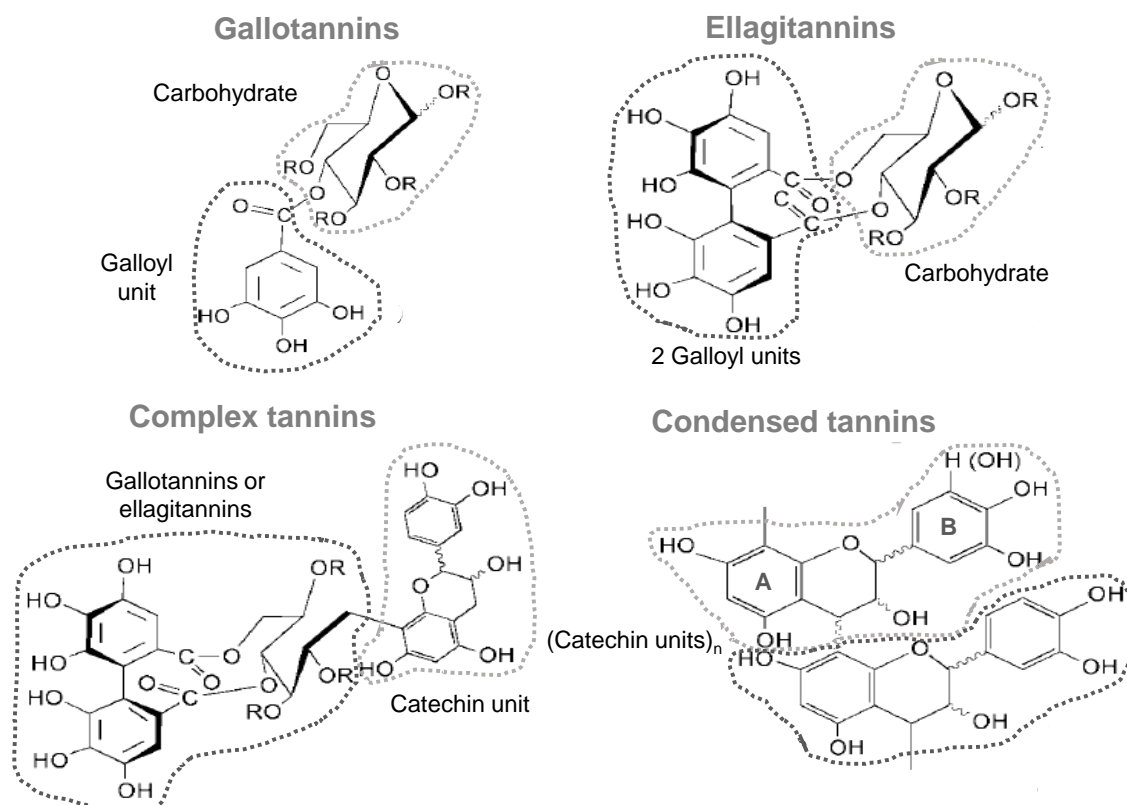


Figure III.10. Tannin classification and examples of structures (adapted from Khanbabaee and van Ree, 2001).

Gallotannins have the simplest chemical structure of tannin compounds with a carbohydrate, usually D-glucose, partly or fully substituted with galloyl units. In the case of partial substitution the remaining hydroxyl groups may be unsubstituted or substituted with various other residues.

Ellagitannins are by far the largest group of known tannins, with more than 500 natural products characterized so far. These tannins present a similar structure to gallotannins but with, at least, two galloyl units coupled with a carbohydrate.

Complex tannins are built up from a gallotannin or ellagitannin unit and a catechin moiety.

Condensed (or polyflavonoid) tannins are formed by the successive C-C linking of catechin (or monoflavonoid) units, the building blocks, with a degree of polymerization, as low as two, but being able to reach values higher than fifty. Each catechin structure is composed by a heterocycle ring linking two phenolic rings, the A and B rings. B ring will have a different reactivity than A ring, when they have different amount of hydroxyl groups. These various configurations generate two possibilities for each ring and four possible structures, shown in **Figure III.11**.



Figure III.11. Possible monoflavonoids structures, depending on the number of hydroxyl groups of A and B rings.

According to the type of tannins considered, the different catechin units are present in different proportions. Mimosa tannin, the material used in this thesis, is composed predominantly by 50 to 70% of type prorobinetinidin and 15 to 25% of type profisetinidin (Pasch *et al.*, 2001).

The nature of the rings will affect the linkage established between the units. Thus, the monoflavonoids can be linked by C4-C8 or C4-C6 linkages (see **Figure III.12**) which will naturally have an impact on the pore network of the oligomer. Furthermore, both the amount of phenolic groups and porous structure will influence the reactivity of the condensed tannin. For this reason, knowing the composition of the tannin polymers is crucial to predict how the tannins will react, and to assess their potential applications. Generally, the degree of polymerization of condensed tannins is around 4-5. Mimosa tannins consist of 2 to 11 units, with an average of 4 to 5 degrees of polymerization (Meikleham *et al.*, 1994).

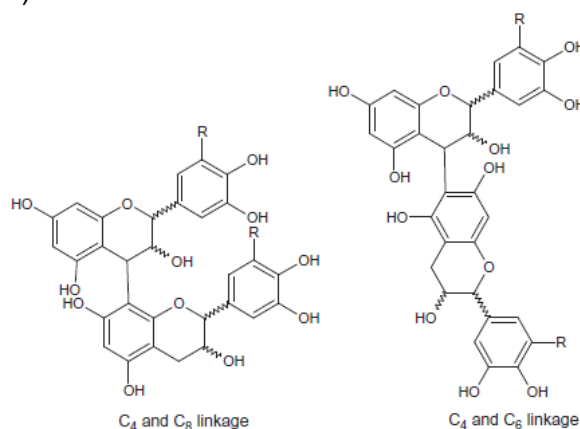


Figure III.12. Possible linkages between catechin units, in condensed tannins (Sieniawska and Baj, 2017).

The polymers studied in this thesis were prepared through reaction of condensed Mimosa tannins and the cross-linking hexamine. Hexamine is a heterocyclic organic compound that decomposes under acidic conditions into formaldehyde and trimethylamine (Kamoun *et al.*, 2003). When this reagent reacts with highly reactive species, such as, tannins polyflavonoids (**Figure III.13**), it does not produce a formaldehyde bond because the reaction rate that occurs with the intermediates is greater than that of the decomposition. So, instead, a variety of intermediates that derivate in imines and amino-imino methylene bases are formed. These species are highly reactive and unstable reacting with tannin and forming amino-methylene bridges (Pichelin *et al.*, 2006). Thus, two tannin units become connected by one benzylamine bridge.

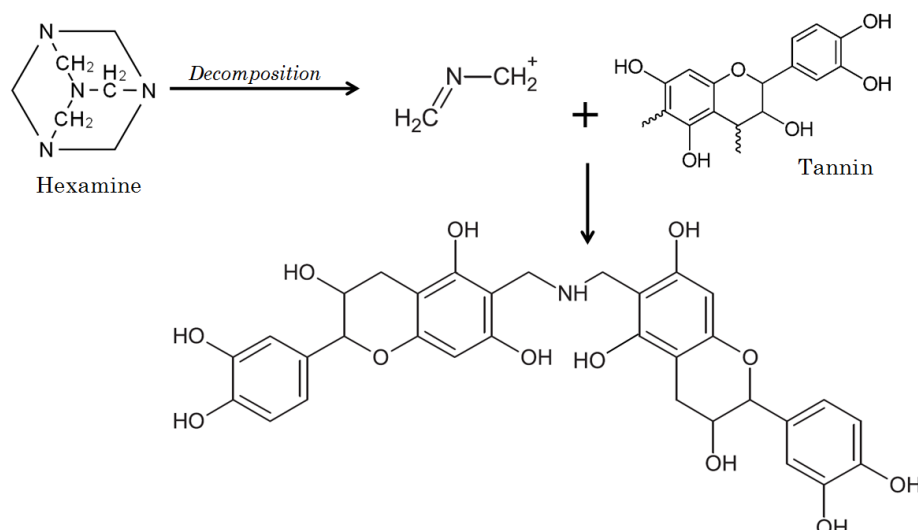


Figure III.13. Example of reaction between a tannin and an intermediate species formed by hexamine decomposition (Pichelin *et al.*, 1999).

The pH conditions of the reaction medium can influence not only hexamine decomposition but also the reactions pathways between tannin and hexamine (Peña *et al.*, 2009). Hexamine decomposition occurs easily at acid pH (Walker, 1964) and, in these conditions tannin and hexamine will react instantaneously forming a gel. On the other hand, at basic pH, hexamine decomposition will be faster than the reaction with tannin, forming formaldehyde. Also, at high pH, deprotonation of hydroxyl groups of the flavonoid molecule will occur more easily (Peña *et al.*, 2009, Walker, 1964).

III.2.3. High Internal Phase Emulsion (HIPE)

A High Internal Phase Emulsion (HIPE) requires the presence of two immiscible liquids. The volume of one of the liquids will be much higher than that of the other, at a maximum proportion of around 74 %. One of the liquids is commonly water (or aqueous solution) whereas the nature of the organic or oil phase can vary considerably (Cameron and Sherrington 1996).

Considering a much higher volume of organic/oil phase than water, this phase is named internal or dispersed phase and water is designated continuous phase. Because a HIPE is highly unstable, a surfactant is necessary to stabilize the emulsion. When centrifugation is made, the dispersed phase droplets can be forced into contact with each other whereas the continuous phase is forced out of the emulsion, forming a separate phase (process referred to as “creaming”) (Cameron and Sherrington, 1996).

HIPEs have been known and used for many years (Lissant, 1974) and, at the present moment, these emulsions present several usages, such as, for petroleum gels production, recovery of oil from tar and oil sands, as detergents, and as potential agricultural sprays. Highly concentrated emulsions are also evident in everyday applications namely, mayonnaise in which a large volume of vegetable oil is emulsified in a small amount of vinegar, and in many cosmetic products (gels and creams) (Cameron, 2005). Nevertheless one of the most important applications of HIPEs is their ability to be used as template systems for the synthesis of a range of polymeric porous materials (Delgado-Sánchez *et al.*, 2016; Grishechko *et al.*, 2016; Braghiroli *et al.*, 2014; Basso *et al.*, 2013; Szczurek *et al.*, 2013; Cameron, 2005).

III.2.3.1. Polymer synthesis by High Internal Phase Emulsion (HIPE)

In this PhD thesis, tannin-based polymers prepared by HIPEs were studied and, for this reason, the synthesis mechanism according to three methodologies, reported by Szczurek *et al.*, (Szczurek *et al.*, 2013) will be presented in more detail in the paragraphs below.

Polymer materials can be prepared by emulsion if one or both phases contain monomeric species (Cameron and Sherrington, 1996). The underlying mechanism consists in the incorporation of the dispersed phase in the polymer structure during polymerization (see **Figure III.14**).

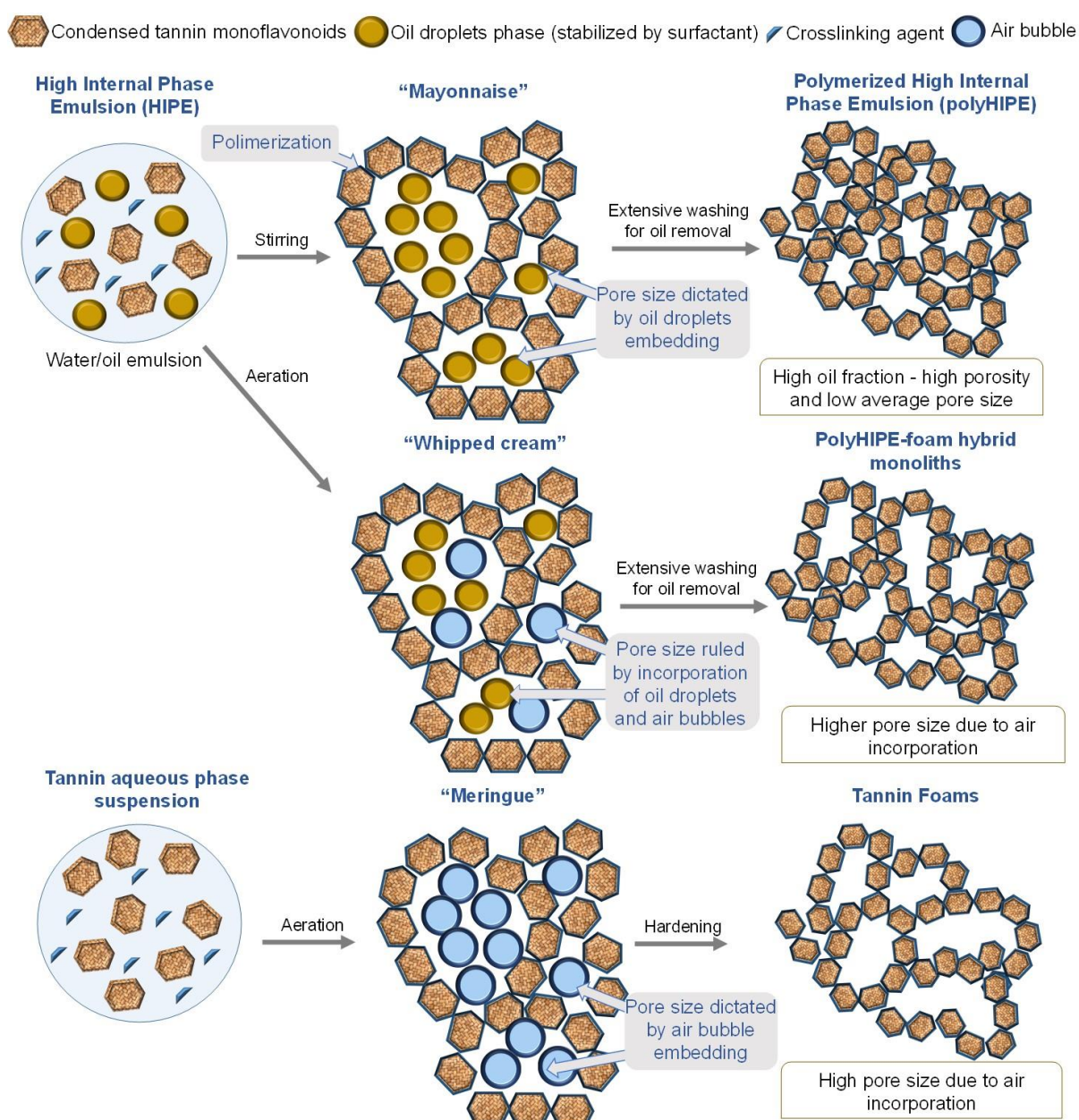


Figure III.14. Illustration of tannin-based polymers preparation procedures (scheme not on scale).

HIPE mixture consists in the monomeric species, crosslinking agent and surfactant dispersed in an emulsion water/oil. In the first example, by stirring, the oil droplets become embedded in the surface of the polymer, conditioning the size of the pores

formed (“mayonnaise” emulsion). Polymerized High Internal Phase Emulsions (polyHIPEs) are characterized by a spherical open porous structure composed by meso and macropores. Since the emulsion is stabilized by the surfactant, higher amounts of this component promote a homogeneous dispersion of the oil throughout the polymer. Consequently, when higher surfactant amounts are used, a more developed porosity is obtained and lower pore sizes are formed.

If the starting water/oil emulsion is vigorously whipped, the aeration of the mixture will occur and a “whipped cream” emulsion is obtained. The air bubbles formed also contribute to pore development and the intensity of the stirring will determine the additional amount of porosity created. A wider pore size distribution, with narrower and wider pores, will be obtained due to the incorporation of both oil droplets and air bubbles.

Tannin foams result solely from the aeration of the aqueous dispersion of tannin monoflavonoids with the crosslinking reagent and surfactant. The pores formed result only from the embedding of air bubbles (in a “meringue” emulsion) and so, these materials present extremely high pore sizes.

PolyHIPEs are nowadays applied in numerous fields of material science, for example, they are considered good candidates for thermal insulation (Kovačič *et al.*, 2012), for molecular storage applications (Cooper *et al.*, 2009), and for solid phase synthesis (Sadeghi and Moghbeli, 2012). These materials have also been used in biological and biomedical applications, namely as potential substrates for tissue engineering (Wang *et al.*, 2016), and in other fields, such as, electrochemical sensing (Zhao *et al.*, 2007).

In this PhD thesis, the application of three polyHIPEs for water treatment was assessed (see **Chapter XI**) for the removal of several pharmaceutical compounds, the plasticizer bisphenol A, and methylene blue dye.

Chapter IV

Techniques for porous
materials characterization

IV. 1. Characterization of porous structure

Porosity corresponds to the ratio between the total pore volume and the apparent volume of a particle or powder (Rouquerol *et al.*, 1999) and, as it was mentioned in Chapter III, pores can be classified in micro, meso and mesopores, according to their dimensions (Thommes *et al.*, 2015).

The adsorption of gases and vapours is the more common technique used to assess the micro and mesoporosity of solids, through isotherms analysis. In this sense, the adsorption isotherm ($n^{\text{ads}} = f(p/p^0)_T$) corresponds to the representation of the adsorbed amount of gas/vapour (n^{ads} in mmol g^{-1}) as function of the relative pressure (p/p^0) of the adsorptive, at constant temperature, being p^0 the saturation pressure of the adsorptive (Rouquerol *et al.*, 1999).

IV.1.1. Adsorption of gases and vapors

In general, adsorption is defined as the enrichment of molecules, atoms or ions in the vicinity of an interface, in comparison to the bulk (see **Figure IV.1**) (Thommes *et al.*, 2015). Depending on the physical state of the components (solid, liquid or gaseous), different adsorption systems can be considered, namely, liquid–gas, liquid–liquid, solid–liquid or solid–gas. On an industrial scale, the more common adsorption systems are the ones with an interface solid–gas or solid–liquid. In these cases, the species to be adsorbed in the fluid phase (the bulk), are named adsorptives, and after adsorption are designated adsorbate. The solid where the adsorption takes place is denominated adsorbent.

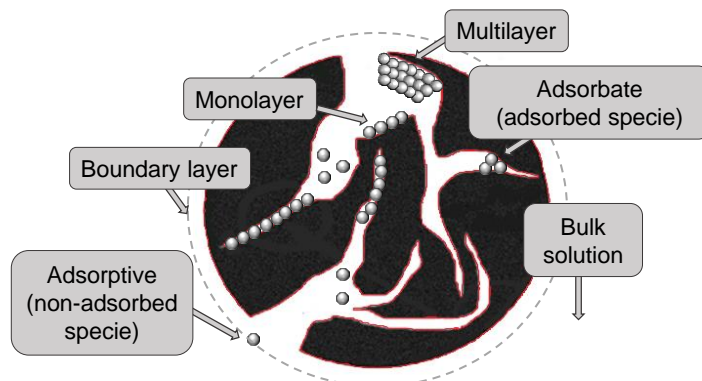


Figure IV.1. Illustration of adsorption process (adapted from Tran *et al.*, 2017).

Depending on the type of adsorption (chemical or physical), discussed ahead in topic IV.1.1.1., the adsorbate can form a single layer at the surface of the solid, designated monolayer, or successive layers (multilayers).

Adsorption is a spontaneous process and, as such, at constant temperature (T), the variation of Gibbs free energy (ΔG) is negative. On the other hand, during adsorption the species dispersed in solution are retained, in an organized way, at the surface of the solid and, because of that, the variation in entropy (ΔS) is also negative. So, attending to the variation in Gibbs energy definition, translated by Equation IV.1, it can be concluded that the enthalpy variation (ΔH) should also be negative, indicating that the adsorption processes are exothermal, which can be explained by the fact that, during adsorption, forces of attraction are established between the adsorbate and the solid and, as consequence, heat is released. Consequently, this process is disfavored by temperature.

$$\Delta G = \Delta H - T\Delta S$$

Equation IV.1

IV.1.1.1. Types of adsorption

Adsorption results from interactions established between the adsorbate and the adsorbent. These interactions can be van der Waals forces of attraction, which are weak forces, or chemical bonds, which are strong forces. The type of forces established during adsorption will affect several aspects of the adsorption process such as specificity, the energy involved, the way adsorption occurs (mono or multilayer). Depending of its properties, this process can be distinguished in physical adsorption (physisorption) or chemical adsorption (chemisorption) (Rouquerol *et al.*, 1999). The criteria used for this classification are presented on **Table IV.1**.

Table IV.1. Different properties of physical and chemical adsorption (Rouquerol *et al.*, 1999).

	Physical adsorption	Chemical adsorption
Specificity	Low degree of specificity (always occurs between gas-solid)	Specific to the adsorption system <ul style="list-style-type: none"> ○ Depends on the adsorbate-adsorbent affinity ○ Occurs in specific sites (adsorption sites).
Adsorption equilibrium	Thermodynamic equilibrium reached quickly (no activation energy required)	Slow process (requires activation energy)
Desorbed species	After desorption, the molecules maintain their identity.	The molecule may react or dissociate, losing its original identity.
Adsorption energy	Adsorption energy in the same order of magnitude as the condensation energy of the adsorptive. When it occurs in narrow pores, the adsorption energy increases.	Adsorption energy comparable to the energy of a chemical reaction.
Adsorbate layer	Multi-layers can be formed at high relative pressures.	Adsorption occurs only in adsorption sites resulting in the formation of a monolayer.

IV.1.1.2. Adsorption isotherms classification

The interpretation of adsorption isotherms is a very helpful tool to understand the textural properties of the materials studied. This analysis consists in relating the configuration (shape) of the isotherm obtained to the porous characteristics of the material. For this purpose, a first classification of adsorption isotherms was proposed in 1940 by Brunauer, Deming, Deming and Teller, known as BDDT classification (Brunauer *et al.*, 1940). This classification considered the existence of five types of isotherms and it was complemented, in 1985 (Sing *et al.*, 1985) with a sixth type of isotherm, completing the IUPAC (International Union of Pure and Applied Chemistry) classification. At last, in 2015, IUPAC refined the original IUPAC classification of 1985 (Thommes *et al.*, 2015) by including sub-categories (see **Figure IV.2**), and a more detailed classification of the hysteresis loops associated to each type of curve (**Figure IV.6**).

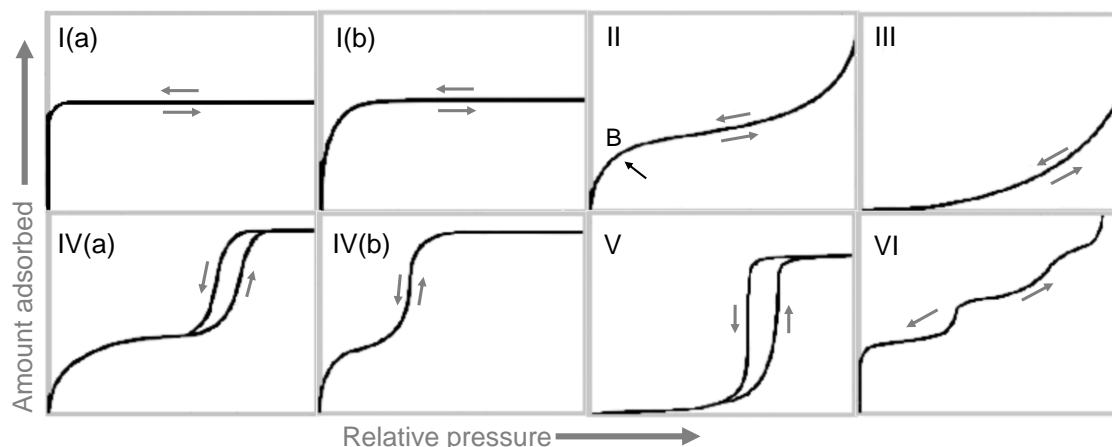


Figure IV.2. IUPAC classification of physical adsorption isotherms (adapted from Thommes *et al.*, 2015).

Type I isotherm is also designated Langmuir isotherm and is characteristic of physical and chemical adsorption on essentially microporous solids. This type of isotherm is concave towards the p/p^0 axis and the amount adsorbed reaches a limiting value, represented by a horizontal plateau over a wide range of pressure values. This limiting uptake (monolayer adsorption) is governed by the filling of the accessible micropore volume. The curvature of the knee located at low relative pressure values can allow to draw conclusions about the microporosity of the material. Thus, when a material has almost exclusively narrower micropores, their filling occurs at lower p/p^0 values and the isotherm obtained is of **type I(a)**. **Type I(b)** isotherm is obtained with materials having wider micropore size distributions and possibly narrow mesopores (width up to 2.5 nm) (Thommes *et al.*, 2015). When this type of isotherm is obtained the saturation plateau corresponds to the formation of a monolayer.

Type II isotherms represent the physisorption of most gases on non-porous or macroporous adsorbents. This isotherm presents an inflexion (point B) at low relative pressure, followed by a continuous increase of uptake up to $p/p^0 = 1$. This shape is the result of an adsorption process that consists in the formation of a monolayer, whose complete filling is indicated by point B, after which multilayers start to be formed (Gregg and Sing, 1982). A more gradual curvature, that is, a less distinctive point B, indicates an overlap of the monolayer coverage and the onset of multilayer adsorption. The thickness of the adsorbed multilayer generally appears to increase without limit up to $p/p^0 = 1$ (Thommes *et al.*, 2015).

Type III isotherm represents an adsorption system where the interactions between the adsorbate molecules are stronger than their interactions with the solid and, as consequence, the molecules initially adsorbed at the surface of the solid will favour the adsorption of more molecules (cooperative adsorption). In this isotherm there is no point B because the adsorption of molecules in higher layers begins before the initial monolayer is completely filled. This curve is always convex towards the pressure axis, indicating less energetic interactions adsorbent-adsorbate than in the case of type II isotherm.

In the low pressure region, the configuration of **type IV** isotherms is similar to that of type II curves. However, in the high pressure range, the curves are quite distinct, with a saturation plateau observed in the case of type IV isotherms. This type of curves are typical of mesoporous adsorbents where the adsorption in the mesopores is determined by the adsorbent-adsorbate interactions and also by the interactions between the molecules in the condensed state. In this case, the initial monolayer-multilayer

adsorption on the mesopores walls, which takes the same path as the corresponding part of a type II isotherm, is followed by capillary condensation in the pores. A typical feature of type IV isotherms is a final saturation plateau, of variable length (sometimes reduced to a mere inflexion point). In contrast to type II isotherm, the amount adsorbed remains constant at the saturation pressure ($p/p^0 = 1$). The main difference between **type IV(a)** and **IV(b)** isotherms is a hysteresis loop, defined below in the text, parallel or not to the adsorption branch. In the case of type IV(a) curve, the pore width and/or shape can make the desorption of the adsorbate more difficult and, for this reason, in the region where the hysteresis loop is observed, at a given p/p^0 value the amount adsorbed in the desorption branch is higher than that in the adsorption branch. On the contrary, the type IV(b) isotherm is completely reversible presenting coincident adsorption-desorption branches.

Type V isotherms are usually obtained with micro and mesoporous materials, where there are relatively weak adsorbent-adsorbate interactions, presenting, at low p/p^0 range, a shape similar to that of type III curve. At higher pressures, molecular clustering is followed by pore filling, represented by a horizontal plateau.

The **type VI** isotherm is unusual and represents a layer-by-layer adsorption on a highly uniform non-porous surface. Each step represents a layer formed at a specific p/p^0 range, and with a specific capacity (step height). It is a cooperative adsorption mechanism, where the filling of each layer favours the formation of the next one, due to lateral interactions between the molecules in the adsorbed phase and in the bulk. Amongst the best examples of type VI isotherms are those obtained with argon or krypton at low temperature on graphitised carbon blacks (Rouquerol *et al.*, 1999; Thommes *et al.*, 2015).

In the particular case of activated carbons, the adsorption isotherms can have the configurations illustrated on **Figure IV.3**. The classification of these three types of isotherms was originally presented by Rodríguez-Reinoso and Sepúlveda-Escribano in 2001. Curves a and b were considered in the recent IUPAC classification as isotherms type I(a) and I(b).

The **type a** isotherm is typical of a microporous carbon composed by narrow micropores with similar widths. The adsorption capacity of the material corresponds to the filling of the microporous volume, which is complete at very low relative pressures (accentuated knee followed by a very well defined plateau over a wide range of pressure values).

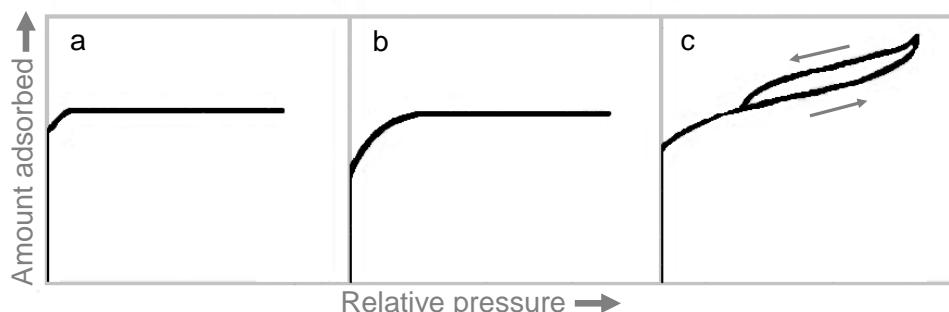


Figure IV.3. Types of isotherms usually obtained with activated carbons (Rodríguez-Reinoso and Sepúlveda-Escribano, 2001).

The **type b** isotherm has a similar configuration to isotherm previously presented, but in this case a more rounded knee is observed corresponding to the presence of a wider micropore size distribution. The plateau indicates, such as in the case of isotherm type a, the almost or complete absence of a mesopore network on the material.

The **type c** isotherm is characteristic of carbons with a wide micropore size distribution, associated to the presence of some mesoporosity. Thus, no saturation plateau is reached, and instead there is a deviation to linearity at higher relative pressure values (Rodríguez-Reinoso and Sepúlveda-Escribano, 2001).

In the case of mesoporous materials, sometimes the isotherms can present a hysteresis cycle, as it was previously mentioned in the case of type IV(a) and V isotherms. This phenomenon very often occurs in the case of activated carbons. As mentioned before, a hysteresis loop results from the fact that desorption of the adsorbate occurs at lower relative pressures than its adsorption, causing a deviation of the desorption branch, in comparison to the adsorption curve. The analysis of this phenomenon has become an integrated part of the analysis of physical adsorption isotherms (for example, of nitrogen, carbon dioxide and water vapour adsorption), and it is normally attributed to thermodynamic effects, related to the meta-stability of the adsorption and desorption regions of the experimental isotherm, namely with phenomenon of capillary condensation and evaporation on the mesopores which do not occur at the same relative pressure. In more detail, during adsorption in the pores (**Figure IV.4 (a)**) there is a high number of van der Waals forces of attraction between the gas particles. Eventually adsorption occurs on the walls of the pores (**Figure IV.4 (b)**) and, as more particles enter the porous network, adsorption in multilayers occurs (**Figure IV.4 (c)**) leading to the formation of a meniscus, due to, condensation of the gas to the liquid (**Figure IV.4 (d)**).

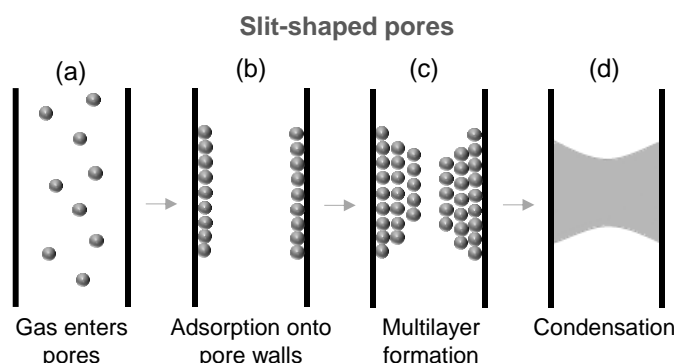


Figure IV.4. Illustration of capillary condensation phenomenon in slit-shaped pores.

The different pressures experienced by the two phases of a meniscus of radius r and with liquid-vapour interfacial surface tension, γ , was considered by Laplace equation. Several derivations were made taking into account the different radius values of both sides of the meniscus and replacing the mechanical pressure parameter for the relative pressure, p/p^0 , for an ideal gas. As a consequence, the Kelvin equation was obtained (see Equation IV.2). This equation relates p/p^0 to the meniscus radius, designated Kelvin radius, r_K , considering the molar volume of the liquid, v , the ideal gas constant, R , and the absolute temperature, T (Fisher and Israelachvili, 1981; Thomson, 1872).

$$\ln\left(\frac{p}{p^0}\right) = \frac{2\gamma v}{r_K RT} \quad \text{Equation IV.2}$$

For this reason, one of the applications of this model can be the calculation of pore size distributions of pores materials from their experimental adsorption isotherms (Lordgooei *et al.*, 2001; Nguyen and Do, 2000).

The hysteresis phenomenon is more pronounced in the case of bottle-shaped pores (**Figure IV.5**).

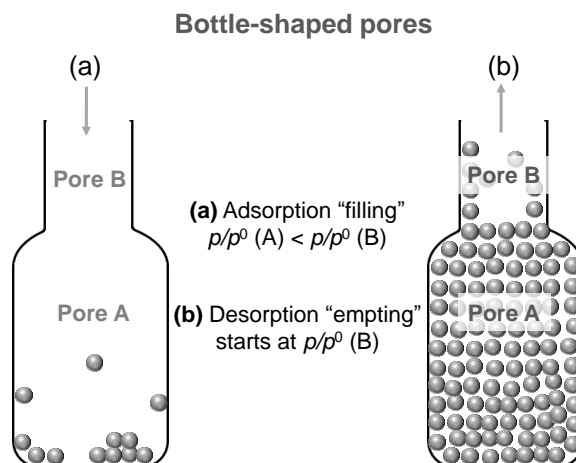


Figure IV.5. Illustration of adsorption and desorption in bottle-shaped pores.

In bottle-shaped pores the inner part (represented by pore A) is connected to the exterior through pores with smaller width (pore B) (**Figure IV.5 (a)**). During adsorption the first pores to be filled are those represented by pore A, but in desorption the first pores to be emptied are those represented by pore B (**Figure IV.5 (b)**). The different radius values of pores A and B will then result in different p/p^0 values at which the condensation/evaporation phenomena occurs (Choma and Jaroniec, 2006).

According to the IUPAC recommendations, the hysteresis cycles can be classified in five categories, represented in **Figure IV.6** (Thommes *et al.*, 2015).

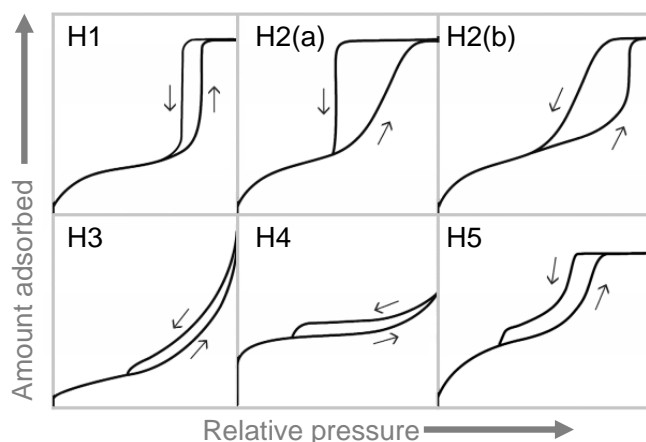


Figure IV.6. IUPAC classification of the different types of hysteresis cycles (adapted from Thommes *et al.*, 2015).

H1-type cycle presents parallel and practically vertical branches (Choma and Jaroniec, 2006). This type of hysteresis is characteristic of materials which exhibit a narrow range of uniform mesopores. This type of hysteresis is a sign of delayed condensation on the adsorption branch and it has also been found in networks of ink-bottle pores where the width of the neck size distribution is similar to the width of the pore/cavity size distribution.

H2(a)-type cycle has a triangular shape and a desorption branch in plateau. This configuration is observed in many porous inorganic oxides being, in a simplified way, attributed to effects of connectivity between pores (Liu *et al.*, 1993), which results many times in the presence of pores with narrow widths (pores with a bottle shape), leading to

pore-blocking. The **type H2(b)** loop is also associated with pore blocking, but the size distribution of the neck widths of the pores is now much larger.

H3-type cycle is characteristic of materials with isotherms without a plateau at relative pressures close to saturation. The adsorption branch resembles Type II isotherm and it has been reported in materials made by particles agglomerates with slit shaped pores.

H4-type cycle has parallel and practically horizontal branches and its occurrence is associated to adsorption-desorption in narrow pores in a slit shape. This type of hysteresis is commonly reported in the case of activated carbons (Choma and Jaroniec, 2006).

H5-type cycle has a distinctive form associated with pore structures with open and partially blocked mesopores.

IV.1.1.3. Methods for adsorption isotherms analysis

Beyond the analysis of the configuration of the isotherms, their interpretation should be made also from a quantitative approach in order to allow for the comparison of different materials. The characterization of carbons texture requires the determination of the specific surface area, the volume of the various existent types of porosity, as well as, the pore size distribution. This quantitative analysis was essential throughout this work in order to compare textural properties of several materials and to interpret their performance as adsorbents for the removal of pollutants in aqueous phase. In this context, several methods used for the quantitative analysis of adsorption isotherms will be described in the following paragraphs.

Brunauer, Emmet and Teller (BET) method

The first step for the characterization of activated carbons adsorptive properties usually consists in determining the specific surface area and the porous volume of the material. The BET method (Brunauer *et al.*, 1940) was proposed in 1940 and has been the most used methodology for the analysis of adsorption isotherms, namely for the determination of the specific surface area, designated A_{BET} (m^2g^{-1}). This model was developed for multilayer adsorption in non-porous solids, based on physical adsorption and so, considering van der Waals attractive forces. Among the assumptions of this model are the following:

- i) the existence of a surface energetically homogeneous, where all the adsorption sites are equivalent;
- ii) that all layers, above the first one, have adsorption heats with similar value and coincident to the condensation heat.

The application of this model to the analysis of isotherms of porous solids, especially microporous solids, must be done carefully because the adsorption potential created inside the micropores is much higher than what would be observed on a completely flat surface, leading to a considerable increase of the adsorbed amounts calculated (Gregg and Sing, 1982). For this reason, in the case of microporous solids, it is advised the use of the designation “apparent specific area”, to the specific surface values assessed using this model. Actually, these values may not represent the surface area of the solids, but the equivalent area of a non-porous surface, in the conditions defined by the BET model (Sing *et al.*, 1985; Rouquerol *et al.*, 1994). It should also be mentioned the importance of the gas or vapour used in the adsorption, especially in the case of microporous materials because the existence of pores with dimensions smaller than those of the adsorbate will prevent the access to all the surface of the solid. That way, the

measurements made with the same material, but using different molecules, may not be comparable.

Despite the limitations presented, this method is, with no doubt, the most used methodology to characterize the texture of porous solids due to the mathematic easiness of the equation. The gas used to estimate the A_{BET} values is normally nitrogen, at its ebullition temperature (-196 °C), due to the easiness to obtain this reagent with a high degree of purity and due to the fact that, experimentally is easy to reach and maintain the desired temperature, by using a cryogenic bath of liquid nitrogen. Additionally, the small dimension of the nitrogen molecule and its chemical inertia contribute to be the most used adsorbate for this end. The application of the BET equation for nitrogen adsorption isotherms analysis was reviewed by Sing, 2001.

There are different forms to represent the linear form of the BET equation but the most used is:

$$\frac{p/p^0}{n^{ads}(1-(p/p^0))} = \frac{1}{n_m C_{BET}} + \frac{C_{BET}-1}{n_m C_{BET}} (p/p^0) \quad \text{where } C_{BET} = e^{\frac{E_1-E_L}{RT}} \quad \text{Equation IV.3}$$

where p and p^0 are, respectively, the equilibrium and saturation pressures at the temperature at which the assay is performed (-196 °C); n^{ads} represents the adsorbed amount at the pressure p ; n_m is the adsorbed amount on the monolayer and C_{BET} is the BET constant (where E_1-E_L is the liquid molar adsorption energy); R is the perfect gases constant, and T is the temperature (Rouquerol *et al.*, 1999). The application of this equation to the experimental data, represented in the form $(p/p^0)/[n^{ads}(1-p/p^0)]$ versus p/p^0 (highlighted in equation IV.3 in bold), allows the determination of the number of moles adsorbed on the monolayer (n_m), through the slope (m) and interception at the origin (b) of the straight line adjusted in a restricted range of relative pressures, by applying the following equation:

$$n_m = \frac{1}{m+b} \quad \text{Equation IV.4}$$

In the case of non-porous materials, the linearity of the graphic $(p/p^0)/[n^{ads}(1-p/p^0)]$ versus p/p^0 occurs in the relative pressure range between 0.05 and 0.35. However, in the case of porous materials the p/p^0 range is more limited, which can be selected following the methodology reported in ISO 9277.

The area occupied by a monolayer at the surface of a solid relates to the amount adsorbed at the monolayer, n_m , by:

$$A_{BET} = N \times n_m \times a_m(N_2) \quad \text{Equation IV.5}$$

where N is the Avogadro constant; n_m is the monolayer capacity and $a_m(N_2)$ is the average area occupied by an adsorbate molecule on the monolayer (in the case of nitrogen $a_m = 16.2 \times 10^{-12} \text{ m}^2$) (Gregg and Sing, 1982).

Dubinin-Radushkevich equation

The Dubinin-Radushkevich equation can be used to assess the micropore volume of porous materials. In this sense, the present section will present a brief description of the assumptions in the base of this equation and the conclusions that it allows to draw.

The basic principles of the Dubinin-Radushkevich model follow the Polanyi potential theory. According to this theory, the adsorption phenomenon in the micropores corresponds to the filling of the porous volume, and not to the formation of layers. This

way, due to the proximity of the micropore walls, the adsorbed molecules will suffer the influence of two potential fields, coming from each of the walls.

The Dubinin-Radushkevich equation (designated DR equation) was proposed in 1947 and it occupies a central position on the theory of volume filling of micropores (Choma and Jaroniec, 2006). Usually, the DR equation is applied in its linear form:

$$\log W^{ads} = \log W_0 - B \left(\frac{T}{\beta} \right)^2 \log^2(p/p^0) \quad \text{where } B = 5.403 (R/E_0)^2 \quad \text{Equation IV.6}$$

where W^{ads} represents the volume occupied by the adsorbed phase; W_0 is the micropore volume (also designated V_{DR}); B is a constant independent of the temperature and characteristic of the porous structure of the adsorbent; E_0 is the characteristic energy; T is the temperature at which the process occurs, β corresponds to a constant designated by coefficient of affinity and, at last, p and p^0 are, respectively, the equilibrium and saturation pressures. The coefficient of affinity (β) of each adsorbate is defined against a standard vapour, benzene, for which it was established that $\beta = 1$. In the case of nitrogen and carbon dioxide, β has the value of 0.33 and 0.36, respectively (Gregg and Sing, 1982). Considering equation IV.6, the graphical representation of $\log W^{ads}$ vs $\log^2(p/p^0)$ will be a straight line, which intercept corresponds to $\log W_0$. From the slope of the line, E_0 can be deduced, which is a parameter related with the mean pore width, L_0 , through empirical equations. An example of this type of equations is the relation proposed by Dubinin and Stoeckli in 1980:

$$L_0 = \frac{13.028 - 1.53 \times 10^{-5} E_0^{3.5}}{E_0} \quad \text{Equation IV.7}$$

The linearity of the graphic representation of DR equation is observed only for low relative pressure values, deviating from linearity in the case of solids not exclusively microporous. The deviations become more accentuated with the progressive increase of the relative pressure values. In several cases, the positive deviation is related with a loss of the rectangular character of the adsorption isotherm, due to the presence the wider micropores, where the adsorption follows a cooperative mechanism. The existence of two types of micropores in the solid, in different range dimensions, has been pointed out as the justification for the deviation from linearity that occurs equally due to the presence of mesopores (Rodríguez-Reinoso and Sepúlveda-Escribano, 2001).

A deeper characterization of carbon's textural characteristics can be achieved by complementing the N_2 adsorption data with CO_2 isotherms. The results obtained with this latter molecule has proven to be extremely important for the characterization of the micropore network of activated carbons materials. In fact, when CO_2 assays are made (i) the problems of the diffusional effects associated with nitrogen adsorption are avoided; (ii) the characterization of the volume of the narrow and wide micropores is achieved; (iii) it gives information about the energy of the surfaces which adsorb at low relative pressures or concentrations (Marsh and Rodríguez-Reinoso, 2006). For these reasons, all the carbons studied in this PhD thesis were characterized by N_2 and CO_2 adsorption.

When, for a given carbon, one compares the micropore volume obtained by applying DR equation to the nitrogen adsorption isotherm at $-196^\circ C$, $V_{DR}(N_2)$ with the microporous volume obtained by applying this same equation to the carbon dioxide isotherm, at $0^\circ C$, $V_{DR}(CO_2)$, three different results can be obtained (Rodríguez-Reinoso, 1986):

- i. $V_{DR}(N_2) < V_{DR}(CO_2)$ – This situation occurs when the microporosity is very narrow and can be attributed to the difficulty in reaching equilibrium in the adsorption of nitrogen molecules at the low temperature at which the process occurs;

- ii. $V_{DR}(N_2) \approx V_{DR}(CO_2)$ – This case is observed in carbons with intermediate activations. The DR plots are practically linear throughout a vast range of relative pressures. Despite that, a positive deviation can occur for nitrogen adsorption at high relative pressures. The characteristic curves of both adsorbates ($\log W$ vs A^2 being A the adsorption potential $A = -RT \ln(p/p^0)$) can be fitted to the same straight line. The carbons that present this behaviour have relatively narrow microporosities, but sufficiently wide so that no diffusional hindrances occurs for nitrogen at -196 °C:
- iii. $V_{DR}(N_2) < V_{DR}(CO_2)$ – These results are observed for carbons with high degrees of activation. When it is not possible to obtain results for nitrogen adsorption at -196 °C at low relative pressures ($p/p^0 = 0.01$), the extrapolation of the characteristic curve for N_2 at -196 °C and for CO_2 at 0 °C is not coincident. Thus, the range of relative pressures used for the application of DR equation is not the same and, consequently, the microporous volume obtained with nitrogen is higher than the used obtained with carbon dioxide. These carbons have a very wide microporosity and the nitrogen adsorption at -196 °C occurs in micropores of higher dimensions than the micropores where the CO_2 adsorption occurs at 0 °C and, due to the different range of relative pressures used.

The uncertainty resulting from the limit of the DR equation application to the adsorption data of nitrogen at -196 °C in carbons with a wider pore size distribution suggests the use of other complementary approaches for the analysis of adsorption isotherms, namely α_s method.

The α_s and t methods

The analysis of the adsorption isotherms can also be made using empirical methods, such as the α_s and t methods. These methods compare the adsorption isotherm of a given adsorbate on a porous solid, with a reference isotherm of the same adsorbate in a non-porous reference material, with a similar composition to the studied material (Rouquerol *et al.*, 1999; Gregg and Sing, 1982).

By applying the α_s method, the experimental results are confronted with the reference curve, in the form of α_s vs p/p^0 , being α_s defined by:

$$\alpha_s = n^{ads}/n_{0.4} \quad \text{Equation IV.8}$$

where n^{ads} and $n_{0.4}$ are the adsorbed amounts at, respectively, a given relative pressure and at $p/p^0 = 0.4$ (see **Figure IV.7**). The relative pressure 0.4 was chosen because it is considered that the filling of the micropores and the formation of the monolayer occurs at pressure values lower than 0.4. Besides, in a great number of cases, the isotherm is relatively horizontal in a range of relative pressures close to this value. Also, this method considers that the adsorption on the micropores is complete before the adsorption on the remaining porous surface of the solid. In this sense, depending on the porous structure of the solid, considerable adsorption occurs, over a wide range of relative pressures, on micro or mesopores. Like with other methods, the application of α_s method and, the analysis of the obtained results should be done carefully (Marsh and Rodríguez-Reinoso, 2006).

In the application of t method, the reference isotherm is expressed in the form t vs p/p^0 , where t is the statistic thickness of the adsorbed film, given by:

$$t = (n^{ads}/n_m)\sigma_t \quad \text{Equation IV.9}$$

where n^{ads} is the amount adsorbed at a given value of p/p^0 , n_m is the monolayer capacity and σ_t is the average thickness of a single molecular layer. Because t deriving from n^{ads}/n_m , this method has the limitation of depending on the determination of the monolayer capacity of the reference material (Rouquerol *et al.*, 1999; Gregg and Sing, 1982).

Comparing t and α_s methods, the α_s method has some advantages, namely the fact that it is not restricted to the use of nitrogen as adsorbate, and different solids can be used as reference materials to build the α_s curve.

Figure IV.7 presents schematic representations of t or α_s curves for different types of adsorbents.

When the sample analysed differs from the reference sample, in terms of surface area and not in terms of porosity, than the α_s curve will be a straight line passing through the axis origin (**Figure IV. 7 (a)**). However, if the test sample has meso or micropores, deviations to linearity will be observed (Gregg and Sing, 1982) (remaining correlation lines presented in the figure).

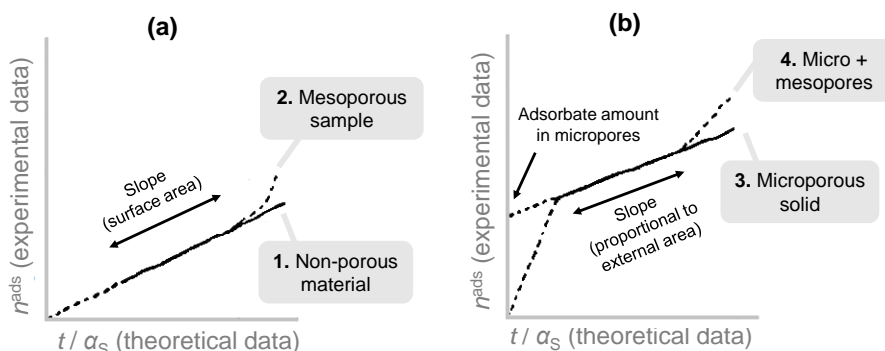


Figure IV.7. Representations of t or α_s curves for different types of adsorbents (adapted from Marsh and Rodríguez-Reinoso, 2006).

When the sample has an essentially mesoporous nature line 2 of Figure IV.6 (a) is obtained, with interception at the axis origin but with a positive deviation at higher values, attributed to capillary condensation in the mesopores. Lines 3 and 4 shown in **Figure IV.7 (b)** are characteristic of a microporous solid and of a material with micro and mesopores, respectively. The deviations observed at low values indicate that the adsorbent has micropores that are filled at very low pressure values.

In the case of samples with no micropores, represented in the lines of Figure IV.6 (a), the surface area can be estimated from the line slope. When micropores are present (**Figure IV.7 (b)**), the slope of the linear section (continuous line) is proportional to the external area of the adsorbent, and back-extrapolation allows to obtain the amount of adsorbate retained in the micropores. This amount, when converted in liquid volume, through the density of the adsorbate in liquid phase, allows to estimate the micropore volume of the sample.

Activated carbons frequently present α_s graphics with two linear sections, such as represented in the curves of **Figure IV.8**. Considering that there are no complications associated with distinct surface chemical structures, the difference between the forms presented by the α_s curves, can be attributed to effects of primary and secondary filling mechanisms of the micropores. The first section normally occurs at $\alpha_s < 1$ ($p/p^0 < 0.4$) and corresponds to the adsorption in wider micropores, as soon as the narrow micropores are filled, at lower relative pressures ($p/p^0 < 0.01$ (Carrott and Sing, 1988)). The slope of this section helps to obtain the surface area of this type of porosity and the interception allows to determine the volume of the narrower micropores.

In **Figure IV.8 (a)**, the configuration 1 is due to the distortion of the isotherm in the monolayer region, which is associated with the reinforced interactions adsorbent-adsorbate in the pores with molecular dimensions (primary filling of the micropores). The section 2 that can be extrapolated up to the origin is, evidently due to a false range of adsorption monolayer on the walls of the wider micropores (Rouquerol *et al.*, 1999). The second linear zone, at higher α_s values ($\alpha_s > 1$), corresponds to multilayer adsorption in the external area; the slope of this section gives the external surface area and from its interception one can obtain the total microporous volume. This analysis allows for a semi-quantitative estimate of the micropore size distribution if one considers that: (i) the pores are rigid and do not suffer any distortion through the physical adsorption measurements and (ii) the narrow (ultra) and wider (super) micropores present the dimensions previously mentioned.

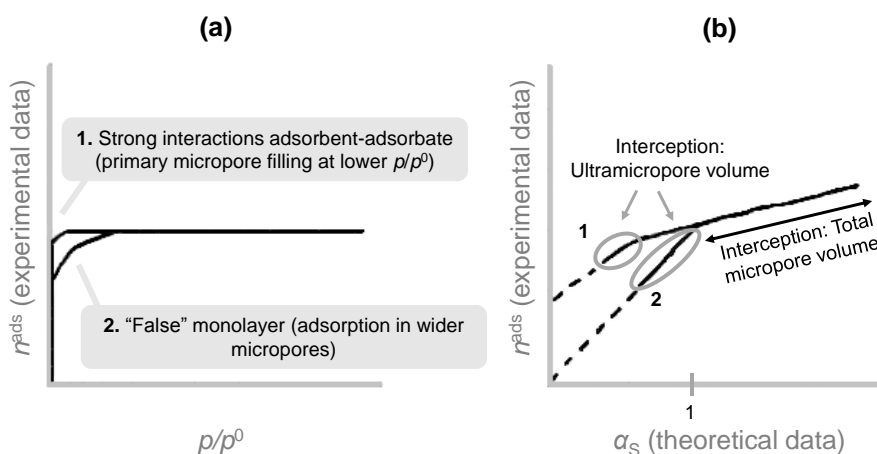


Figure IV.8. (a) Adsorption isotherms of microporous adsorbents and (b) correspondent α_s theoretical curves (adapted from Rouquerol *et al.*, 1999).

The analysis of CO_2 adsorption isotherms by α_s method has proven to be extremely important for the characterization of the micropore network of activated carbons materials. When this analysis is used as complementary to the analysis of N_2 adsorption isotherms it allows a deep characterization of the adsorbents and of the activation process because (i) it avoids the problems of the diffusional effects associated with nitrogen adsorption; (ii) it allows for the characterization of the volume of the narrow and wide micropores; (iii) it characterizes the mesoporosity and (iv) it gives information about the energy of the surfaces which adsorb at low relative pressures or concentrations (Marsh and Rodríguez- Reinoso, 2006). For these reasons, these two techniques have always been used together to characterize the adsorbents studied in this thesis.

IV.1.2. Mercury Intrusion Porosimetry (MIP)

Mercury intrusion porosimetry (MIP) is a generally accepted and widely employed method for textural analysis of macroporous materials, being considered by IUPAC as, at present, the standard method for macroporous samples analysis (*i.e.* pores with diameters higher than 50 nm) (Rouquerol *et al.*, 2012). In fact, this technique is also sensitive to mesopores, being able to analyse a wide range of mesopore-macropore widths (routinely from 0.003 to 400 μm).

In addition, mercury porosimetry may prove to be useful for surface area and particle size distribution determination and also to assess the tortuosity, permeability, fractal dimension, and compressibility of porous materials. Furthermore, it may provide information relating to pore shape, network effects, and skeletal and bulk densities

(Friess *et al.*, 2010). From its numerous applications, the most common one is the use of mercury intrusion to assess materials pore size distribution, which was reported in the International Standard ISO 15901-1, in 2016 (ISO 15901-1, 2016).

The basis for this methodology was first proposed by Washburn in 1921 (Washburn, 1921) that suggested that it would be possible to obtain the pore diameter distribution of porous materials from pressure-volume data by penetrating the material with mercury. As mercury behaves as a non-wetting fluid, at a porous material surface it does not penetrate spontaneously in the fissures of these materials unless pressure is applied.

The instrument used to perform this technique, known as porosimeter, has a pressurized chamber, to force mercury to intrude into the voids of a porous substrate (see **Figure IV.9 (a)**). As pressure is applied, mercury fills the larger pores first. In theory, as pressure increases, the filling proceeds to progressively smaller pores.

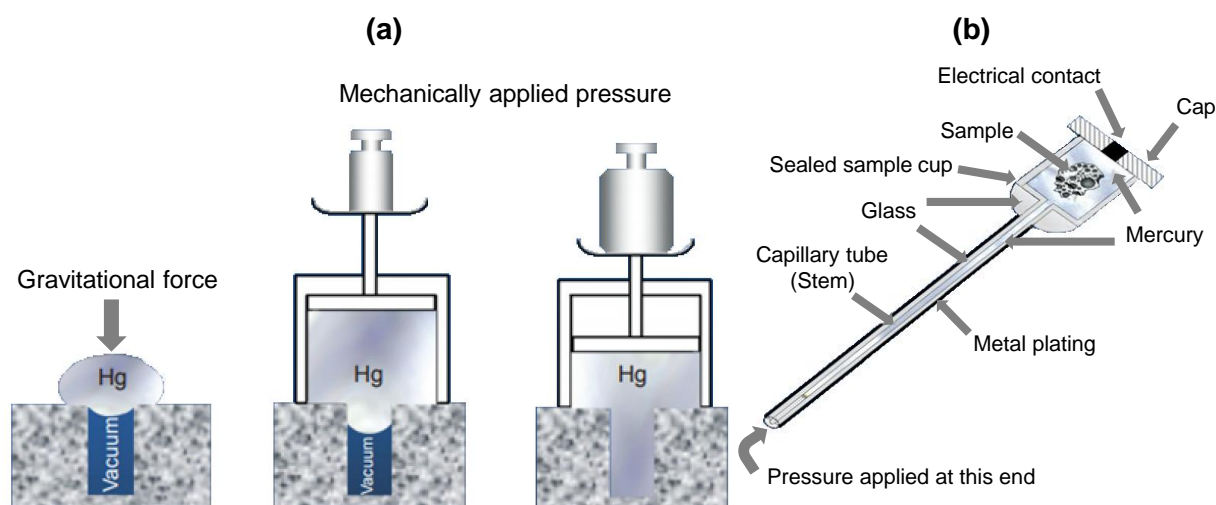


Figure IV.9. Illustration of (a) mercury entering a cylindrical pore under increasing pressure and (b) Mercury powder penetrometer (http://www.micromeritics.com/Repository/Files/MercuryPorosemityTheory_poster.pdf).

Mercury intrusion is performed in two parts, the “low pressure” and “high pressure” analysis, performed in the ranges 0.001-0.24 MPa and 0.24 – 414 MPa, respectively (Giesche, 2002). Two different pressure transducers are used, for better resolution within each range of analysis. Prior to analysis the sample is evacuated to remove air and residual moisture from the pore network. The sample is placed inside the penetrometer (**Figure IV.9. (b)** illustrates a penetrometer for powder analysis), which consists in a sample cell (cup) made of glass, which is connected to a capillary tube where the volume of mercury intruded into the material is measured, as described in the following paragraphs. With the system under vacuum, the mercury is supplied and slowly increasing the overall applied pressure allows mercury to penetrate the largest pores in the sample or any void spaces between the material particles. At pressures around 0.24 MPa, the penetrometer’s weight (with the mercury saturated sample) is determined, which allows to calculate the sample’s bulk density (using corresponding blank-runs as reference). The penetrometer is again introduced in the porosimeter and the second analysis phase, at higher pressures, is performed (Giesche, 2006; Giesche, 2002).

The volume of mercury entering the pore structure is measured continuously through changes in capacitance between a metal plating of the glass capillary and the length of mercury column in the stem (Giesche, 2006).

The intrusion data obtained by this method is analysed by the modified Young-Laplace equation, more commonly referred to as the Washburn equation (Equation IV.10), which assumes that the material pores are cylindrical-shaped (Washburn, 1921).

This equation correlates the applied pressure values, p , to pore diameters, D , using physical properties (surface tension, γ , and contact angle, θ) of the non-wetting liquid used, which, in this case, is mercury. As pressure continuously increases the pore size distribution of a sample's pore network can be obtained.

$$D = -\left(\frac{1}{p}\right) 4\gamma \cos \theta \quad \text{Equation IV.10}$$

The surface tension of mercury (0.485 N m^{-1}) and the contact angle of mercury can be measured for the material studied however, in most cases and out of convenience, researchers often consider a fixed value of 130° or 140° . The volume of mercury entering the pore network at a given pressure value (experimentally determined) is designated "cumulative intrusion volume" because it corresponds to the total volume of pores with diameter D (Rouquerol *et al.*, 2012).

An intrusion-extrusion mercury isotherm, illustrated in **Figure IV.10**, can be obtained by plotting the cumulative intruded volume as function of the applied pressure. This curve can be divided in different parts, associated to the intrusion and extrusion mechanism.

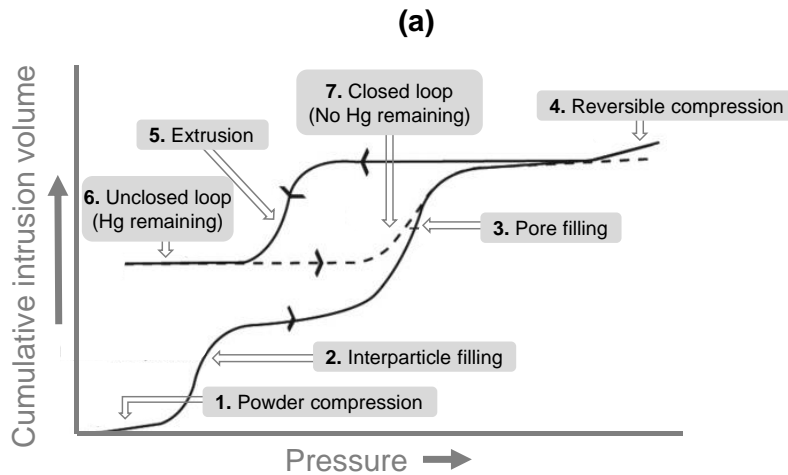


Figure IV.10. Illustration of intrusion-extrusion mercury cycles and description of the different mechanism stages (adapted from Rouquerol *et al.*, 2012).

Initially, as the mercury is introduced in the sample cup of the penetrometer, the solid particles rearrange, that is, compress (1) and the mercury starts to fill the interparticle voids (2). The mercury fills the macro and mesopores of the sample (3) and, for some materials a new reversible compression can occur at higher pressures (4). Mercury can then extrude (5) from the saturated sample originating a hysteresis loop which occurs at lower pressure values than intrusion. On the first extrusion cycle, some mercury is usually retained by the sample, thereby preventing the loop from closing (6) If more than one intrusion-extrusion cycle is performed the loop will eventually close (7), showing that there is no further entrapment of mercury.

Analog to gas adsorption characterization, also for mercury porosimetry an understanding of hysteresis is important to pore size analysis. Different mechanisms have been proposed to explain intrusion-extrusion hysteresis (Felipe *et al.*, 2006; Giesche, 2006; Rigby, 2002), and recent studies have reported that thermodynamically, mercury intrusion and the capillary evaporation follow similar pathways (Coasne *et al.*, 2013; Thommes *et al.*, 2008) and even the shape of mercury hysteresis loop often agrees with that of the corresponding gas adsorption loop caused by capillary condensation.

Mercury intrusion data are usually analysed by plotting the derivative of the cumulative intrusion volume as function of the pore diameter (see **Figure IV.11**). This representation shows the pore diameter range of the material studied and the width of the majority of the sample pores, given by the maximum peak of the derivative curve.

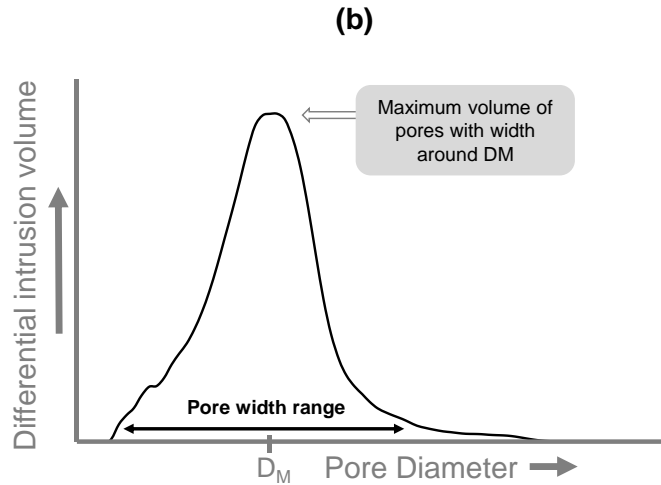


Figure IV.11. Representation of the intrusion volume derivative as function of pore diameter.

This methodology has proven to be an extremely useful characterization technique for porous materials like activated carbons, catalysts, cements, filters or adsorbents, and as new materials are developed, this methodology continues to prove its utility. Examples of this are its use for tannin foams characterization (Sánchez-Martín *et al.*, 2013a and 2013b) as well as the tannin-based monolith powders studied in this PhD thesis, in Chapter XI.

IV.1.3. Density

The density of a substance is defined as the relation between its mass and the volume it occupies. While the mass can be determined with precision, in the case of porous materials, the measurement of the volume has a bigger uncertainty, which is reflected in the density determined.

In the case of ACs, due to their extensive porosity, a large part of these materials consists in porous volume (empty space) and, depending on how the density measurement is performed, the hollow spaces between particles (interparticle spaces) can, or not, be included in the determination. Thus, the density can be, according to IUPAC (Rouquerol, *et al.*, 1994), distinguished in absolute, apparent and global density, as illustrated in **Figure IV.12**.

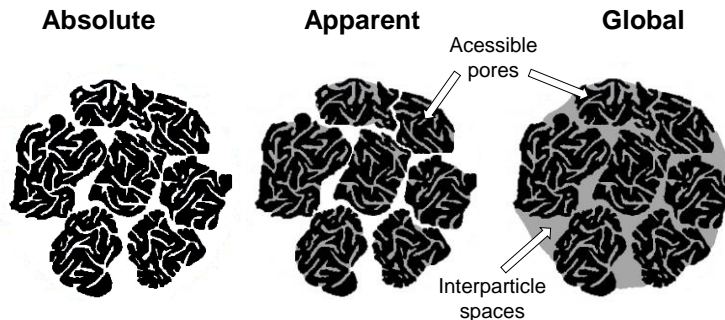


Figure IV.12. Representation of the volumes considered for the absolute, apparent and global densities.

Absolute density: it is also referred to as “true” and “real” density and it excludes the pores and the interparticle spaces of the solid.

Apparent density: it is also referred to as “bulk” density and it includes the pores of the particles but not the interparticle spaces.

Global density: it includes the pores and interparticle spaces.

In this work, the apparent density of the studied materials was assessed and, for this reason, an overall approach of the main factors impacting the collected data will be presented.

The apparent density of a solid should be determined according to recommendations described in the International Standard ISO 697 (ISO, 1981), and depends on the form of its particles, the composition of the substance and the method of storage. Rounded, compact particles will be closer together during the pouring than edged, splintery particles. The density of free flowing powders depends strongly on the influences of external mechanical forces, for example, the pressure exerted on the material (compression). Also, the friability (tendency of a solid to break into smaller pieces under pressure or contact) of powder and granules, as well as their flow or caking (powder's tendency to form lumps or masses rather than flow smoothly) properties, the varying geometry of particles of which it is composed, and the unavoidable compaction resulting from pouring into the measurement container can affect the apparent density value obtained.

IV. 2. Chemical characterization

The potential of both activated carbons and tannin polymers for the removal of pollutants from aqueous phase is influenced by their porous structure as well as by their chemical nature. So, a complete characterization of these materials is crucial to foresee their potentialities as adsorbents in liquid phase, as well as to understand their behaviour. Besides characterizing the material's texture, the chemical characterization is also essential because the physico-chemical properties of porous materials will affect, for example, their electrochemical, catalytic, acid-base, redox, hydrophilic/hydrophobic properties, among others.

The surface characterization of the materials may be made through numerous techniques to obtain information about the composition and concentration of the surface groups of the solids. Amongst many others, infrared spectroscopy, X-ray photoelectron spectroscopy (XPS), determination of the pH at the point of zero charge, contact angle measurement, Boehm titration and potentiometric and thermal analysis are techniques commonly used for this purpose (Bandosz and Ania, 2006). The more appropriate way to obtain a more complete characterization of the surface of these materials is to use complementary techniques and to combine the results obtained.

Next, a brief description of the chemical characterization methods used in this PhD thesis will be presented.

IV.2.1. Elemental analysis and ash content

As was previously mentioned in Chapter III, the activated carbons and tannin-based powders, are materials predominantly composed by carbon, with surface functionalities, resulting from the presence of heteroatoms.

Elemental analysis allows to determine the elemental and sometimes isotopic composition of a given material. This analysis can be made qualitatively, or quantitatively. For the determination of the carbon, hydrogen, nitrogen and sulfur

contents, the dried samples are typically combusted at high temperatures (*i.e.*, around 1200 °C) in a stream of oxygen, and the products of combustion are measured in a single analysis. As a result of the complete combustion, in the presence of excess of oxygen, all of the carbon compounds are converted to carbon dioxide, the hydrogen is converted to water vapour, and sulfur to sulfur dioxide. The nitrogen present in the sample is reduced to N₂ by copper turnings. The oxygen content can be indirectly calculated as the difference between 100 and the total value of the percentage of the other measured components in the material (C, H, S, N). In the present work, elemental analysis was performed to chemically characterize the lab-made polyHIPEs materials, and the *Mimosa* tannin extract, used as precursor (see Chapter XIX).

The ash content of a material can be determined by the complete combustion of the solid, under atmospheric air. The remaining elements constitute the ashes of the solid and its content is determined by a mass percentage. Ash content determination was performed for some of the carbons studied in this PhD thesis.

IV.2.2. pH at the point of zero charge (pH_{PZC}) and at the isoelectric point (pH_{IEP})

Activated carbons have amphoteric properties, and so their surface chemistry consists in a balance between acidic and basic functional groups (see Chapter III) (Bandosz and Ania, 2006). The surface acid/basic properties of an AC depends essentially on its content in heteroatoms and, more specifically, on the presence of surface complexes of oxygen. The presence of these groups will determine the surface charge and hydrophobicity, as well as, the electronic density of the graphitic layers. In this context, when a carbon is immersed in an aqueous solution, a surface charge develops resulting from the surface groups that can dissociate and/or adsorb ions from the solution, depending on the solution pH. The most common functional groups present at the surface of an AC, as well as their behaviour in acidic and basic media are illustrated in **Figure IV.13**. The oxygenated groups, with an acidic character, such as phenolic (ArOH) and carboxylic (ArCOOH) groups, dissociate in a basic pH originating a negative surface charge. The source of the positive surface charge is more uncertain because, in carbons without nitrogen functional groups, this charge can be due to oxygenated groups of basic nature, such as pyrone (ArO) and cromene-type groups or even due to the existence of electron rich regions in between the graphitic layers, which act as Lewis basic centres, accepting protons from the aqueous solution (Marsh and Rodríguez-Reinoso, 2006).

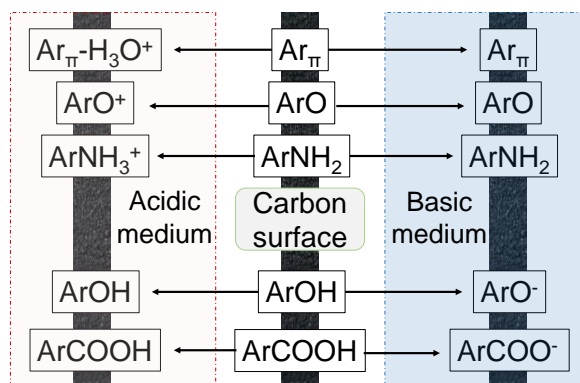


Figure IV.13. Macroscopic representation of the amphoteric behaviour of an AC surface chemistry (adapted from Moreno-Castilla, 2004; Radovic *et al.*, 2000).

The tannin-based polymers present a much simpler surface chemistry than the activated carbons since, in this case, surface functionalities consist mostly in phenolic groups. So, in the case of these materials, their surface chemistry properties will be dictated by the amount of phenolic groups present in the structure, that is, higher phenolic groups amounts will naturally increase the solid acidic nature.

The surface charge can be determined by electro-kinetic methods or by mass titration (Marsh and Rodríguez-Reinoso, 2006). The first technique determines the charge of the more external surface of the particles whereas the second method determines the total surface charge of the material. The pH at which the more external surface charge is null is denominated pH at the isoelectric point, pH_{IEP} . On the other hand, the pH at which the total surface charge is zero is designated pH at the point of zero charge, pH_{PZC} (Bandosz and Ania, 2006; Marsh and Rodríguez-Reinoso, 2006). The knowledge of these two parameters gives a notion of the surface charge distribution of the materials namely, the smaller the difference between these two points, more homogeneous will be the surface charge distribution (Moreno-Castilla, 2004).

pH_{PZC} measurement

The pH_{PZC} measurements are made measuring the final pH of mixtures water-carbon, with different mass percentages below 20 % (Noh and Schwarz, 1989). The suspensions can be prepared independently or result from successive dilutions. When the final pH of the mixture is 7, that is, the pH of water, the material is considered to be neutral, whereas carbons with pH_{PZC} lower or higher than 7 are denominated acidic or basic, respectively. The measurement of pH_{PZC} is also an indicator of the surface oxidation degree, since it allows to detect an increase in acidity or basicity of the surface after modification treatments. For example, an oxidation treatment (introduction of oxygenated acidic groups), results in an increase of the acid character of a carbon (Bandosz and Ania, 2006).

Instead of water, the assays can be made adding an electrolyte, such as, Na^+ , K^+ , NO_3^- or ClO_3^- , to increase the ionic strength of the mixture (Noh and Schwarz, 1989).

Mass titration (Noh and Schwarz, 1989) and potentiometric titration (Lützenkirchen *et al.*, 2012) are the most used methods to determine the pH_{PZC} values. The biggest advantage of mass titration, in comparison to the potentiometric, is the fact that, in the last case, at least three different concentration levels of electrolytes are necessary which end up being adsorbed, thus affecting the pH_{PZC} measurements.

In the present work, pH_{PZC} values were assessed for all the activated carbons studied by mass titration, following the experimental procedure presented in topic A.2.5 of the Appendix Chapter.

pH_{IEP} measurement

The isoelectric point of an amphoteric substance can be defined as the hydrogen ion activity of a solution or suspension in which the ampholyte shows no migration in an electric field (Hitchcock, 1931).

pH_{IEP} can be experimentally determined by immersing the sample or specimen in an electrolyte solutions with different pH values. The ions in solution will neutralize the surface charges of the powder and, depending on the solution pH, the resulting particle may present positive, negative or neutral net charge. If the particle in solution remains positive or negatively charged, this means that the concentration of negative or positive ions in solution, respectively, is not enough to completely counterbalance the surface charge of the solid. Consequently, when applying an electrical field across the dispersion, the sample will migrate towards the electrode of opposite charge because

the electrostatic energy solid-ions (named zeta potential) is different from zero. The electrolyte solution pH at which no particle migration is observed (zeta potential equal to zero) corresponds to pH_{IEP} (Pergante and Cologna, 2017; Llorente *et al.*, 2014).

In this work, the pH_{IEP} value of tannin-based polymers was determined as a complement to pH_{PZC} .

IV.2.3. Fourier Transform Infrared Spectroscopy (FTIR)

Infrared (IR) spectroscopy, also named vibrational spectroscopy, is one of the most important analytic technique available today because it can be used practically in any sample, in any state (liquid, solid, gas) and in a variety of forms, such as, pastes, powders, films, fibres, and surfaces (Stuart, 2004). Because of its versatility this technique can be applied in a high number of fields, including biological, industrial and environmental applications, to gather information about organic and inorganic compounds, polymers, and biological samples, among many others (Jiang *et al.*, 2017; Kakoi *et al.*, 2017; Nenadis and Tsimidou, 2017; Paschalis *et al.*, 2017; Prati *et al.*, 2016; Wielogorska *et al.*, 2017).

This technique relies in the interaction of heteronuclear molecules with infrared radiation (Stuart, 2004). To understand the process, it is necessary to have in mind that any atom or molecule presents quantized discrete energy levels, such as the ones illustrated in **Figure IV.14 (a)**. When a molecule interacts with radiation, a quantum of energy is either emitted or absorbed.

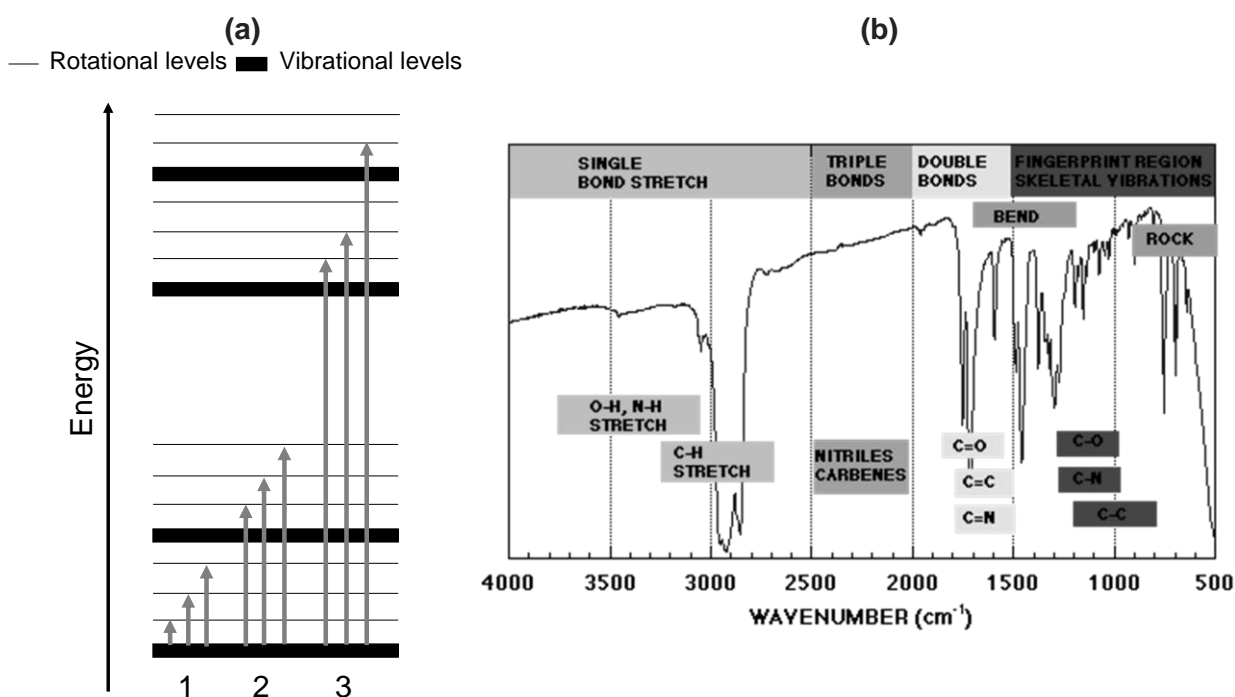


Figure IV.14. (a) Energy levels and possible energy absorption transitions (1-pure rotational transitions; 2-rotational-vibrational transitions; 3-rotational-vibrational-electronic transitions)(adapted from https://chem.libretexts.org/Core/Physical_and_Theoretical_Chemistry/Spectroscopy/Vibrational_Spectroscopy/Infrared_Spectroscopy/Infrared%3A_Theory); (b) Infrared spectra divided in constituent regions (adapted from <http://www.chm.bris.ac.uk/webprojects1997/RogerEC/welcome.htm>)

When a molecular system interacts with radiation, an amount of energy proportional to the radiation is absorbed, and different energetic transitions can occur. The first example (phenomenon 1) represents a transition to a higher rotational energy level, *i.e.*, a rotational transition. Transition 2 occurs when quantized energy is absorbed, leading

to an increased vibrational energy level. The third phenomenon involves electrons being raised to a higher internal energy level (phenomenon 3).

Infrared radiation is able to cause rotational-vibrational transitions in molecules with a small energy difference between rotational and vibrational states. A criterion for IR absorption is a net change in dipole moment in a heteronuclear molecule as it vibrates or rotates (Stuart, 2004). Using H-Cl bond as an example, the charge distribution between hydrogen and chloride is not evenly distributed since chloride is more electronegative than hydrogen and has a higher electron density. Thus HCl is a polar molecule with a high dipole moment. The dipole moment is determined by the magnitude of the charge difference and the distance between the two centres of charge. As the molecule vibrates, there is a fluctuation in its dipole moment; and radiation with a specific frequency will be absorbed. A dipole moment change can also be caused by the rotation of asymmetric molecules around their centres, which permits interaction with the radiation field (Smith, 1999)

IR spectra, illustrated in **Figure IV.14 (b)**, can be obtained by registering the amount of radiation emitted by the sample (transmittance, in %) as function of the wavenumber (cm^{-1}) of the radiation. As absorption occurs, transmittance percentage decreases and a peak will appear that can be correlated directly to bonds within the compound. Because each heteronuclear bond may vibrate in several different ways (stretching or bending), individual bonds may absorb at more than one IR frequency. Stretching absorptions usually produce stronger peaks than bending, however the weaker bending absorptions can be useful in differentiating similar types of bonds (*e.g.* aromatic substitution). It is also important to note that symmetric vibrations do not cause absorption of IR radiation. The infrared spectrum is usually divided into three regions; the near-, mid- and far-infrared, named for their relation to the visible spectrum. The higher energy near-IR, between 14000 and 4000 cm^{-1} , excites overtone or harmonic vibrations. The mid-infrared, approximately $4000\text{--}400 \text{ cm}^{-1}$ may be used to study the fundamental vibrations and associated rotational-vibrational structure. This is the range used when plotting IR spectra (Smith, 1999)

Over time the types and locations of IR absorptions produced by a wide variety of chemical bonds in various chemical environments have been recorded (see **Table IV.2**). Therefore, IR spectra provide a molecular fingerprint that can be used for the identification of samples. The absorption data can be quickly referenced through tables of IR absorption ranges and compared to the spectrum under consideration (Bandosz and Ania, 2006). As a general rule, the most important factors determining where a chemical bond will absorb are the bond order and the types of atoms joined by the bond. Conjugation and nearby atoms shift the frequency to a lesser degree. So, the same or similar functional groups in different molecules will typically absorb within the same, specific frequency ranges.

Table IV.2. Examples of IR absorption bands and corresponding assignments (Bandosz and Ania, 2006)

Group or functionality	Assignment regions (cm ⁻¹)		
	1000-1500	1500-2050	2050-3700
C-O stretch of ethers	1000-1300		
Ether bridge between rings	1230-1250		
Cyclic ethers containing COCOC groups	1025-1141		
Alcohols	1049-1276		3200-3640
Phenolic groups:			
C-O stretch	1000-1220		
O-H bend/stretch	1160-1200		2500-3620
Carbonates; carboxyl-carbonates	1000-1500	1590-1600	
Aromatic C=C stretching		1585-1600	
Quinones		1550-1680	
Carboxylic acids	1120-1200	1665-1760	2500-3300
Lactones	1160-1370	1675-1790	
Anhydrides	980-1300	1740-1880	
Ketenes (C=C=O)			2080-2200
C-H stretch			2600-3000

For a higher resolution, the radiation signal (raw data) can be translated into a spectrum through Fourier transform (FT) which is a mathematical process that decomposes the signal received into specific frequencies, its sinusoid components, and then sums them up to provide the final spectrum with a high resolution. Fourier analysis provides an improvement of signal-to-noise ratio, higher energy throughput, greater accuracy of the frequency scale, and the capacity for versatile data manipulation.

Infrared spectroscopy was used during the development of this work for characterization for pristine and spent tannin-based polymers (Chapter XI).

IV.2.4. Thermogravimetric analysis (TGA)

Thermogravimetric analysis (TGA) is a thermal analysis method in which the mass changes of the samples are measured as a function of increasing temperature (under constant heating rate), or as a function of time (at constant temperature and/or constant mass loss) (Kett and Price, 2016). This technique is generally used for the study of materials that undergo mass loss when subjected to a heating regime, due to reactions of decomposition, oxidation, reductions, and desorption, among others. The decomposition, thermal stability and respective kinetics can be analysed under a variety of operational conditions (sample mass, volume, physical form, nature and pressure of the atmosphere and scanning rate), which can influence greatly the recordings.

The instrument used for thermogravimetry is a programmed precision balance designated thermobalance. Results are displayed as a plot of mass loss vs temperature or time and are known as thermogravimetric (TG) curves. **Figure IV.15** represents a TG curve profile for a previously dried material and its correspondent derivative (DTG).

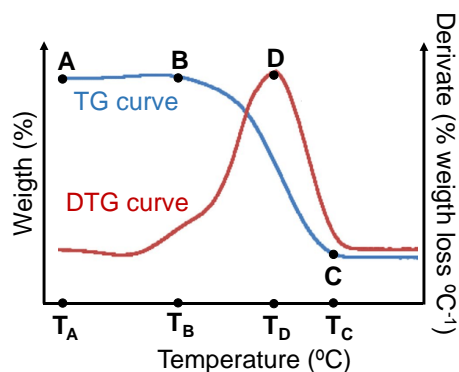


Figure IV.15. Schematic illustration of TG (blue line) and DTG (red line) curves profile.

The TG curve presents an initial plateau (from point A to B), at values closer to room temperature (T_A), where no decomposition of the matrix occurs. However, some mass loss can be observed at this temperature range for highly hydrophilic samples even though a previous drying step is made. At a given temperature (T_B), weight loss starts to occur (point B) as consequence of thermal reactions in the matrix of the solid. This decomposition continues to occur (from point B to point C) until a given temperature (T_C) after which the mass of the sample remains constant. In order to pinpoint the temperature(s) at which higher mass loss reaction(s) occur(s), the TG data is usually analysed by plotting the derivative of the TG curve (DTG, units of % weight loss $^{\circ}\text{C}^{-1}$), represented by the red line in **Figure IV.15**. This curve measures the successive variations of mass as function of the temperature allowing to identify the exact temperature (T_D) at which a higher weight change is detected (point D). This analysis is, for example, very useful for purposes of thermal regeneration where a porous solid exhausted with a given pollutant is subjected to a thermal treatment at a given temperature, to promote desorption of the adsorbate. DTG analysis becomes thus essential to identify the minimum temperature (T_D) necessary to regenerate the exhausted material.

This methodology has applications in numerous fields to promote desorption reactions (Batista *et al.*, 2016; Ledesma *et al.*, 2014a; Fortunová *et al.*, 2011), to assess thermal stability of materials (Li *et al.*, 2017; Cao and Mu, 2014), as integrant part of their characterization (Saboya *et al.*, 2017; Lin *et al.*, 2017), for compositional analysis (Dweck *et al.*, 2017; Carrier *et al.*, 2011), to simulate industrial processes (Plis *et al.*, 2016; Liang *et al.*, 2015), and to perform kinetic (Al-Salem *et al.*, 2017; Nishikawa *et al.*, 2017) and corrosion (Hari *et al.*, 2017, Liu *et al.*, 2015) studies.

Thermogravimetry analysis proved to be an essential tool to study atenolol desorption mechanism from lab-made ACs prepared from apple tree branches char residues (see Chapter VII) and it also allowed to assess the adequate thermal regeneration conditions for paracetamol-exhausted activated carbons (study presented in Chapter VIII).

IV.2.5. Scanning Electron Microscopy (SEM)

Scanning Electron Microscopy (SEM) is an analytical method that consists in bombarding a given sample with a beam of high-energy electrons. The electrons interact with electrons of the samples exciting them and producing various signals that give information about the sample's topography, morphology, chemical composition and crystallography (Reichelt, 2007).

The general structure of a scanning electron microscope is presented in **Figure IV.16**. This apparatus is composed by the microscope column that focuses the electron beam

towards the sample, electronic components that permit the optimization of the experimental conditions used to obtain the micrograph, and the computational components, that is the interface program where the image is acquired, processed and stored (Goldstein *et al.*, 2012; Reichelt, 2007).

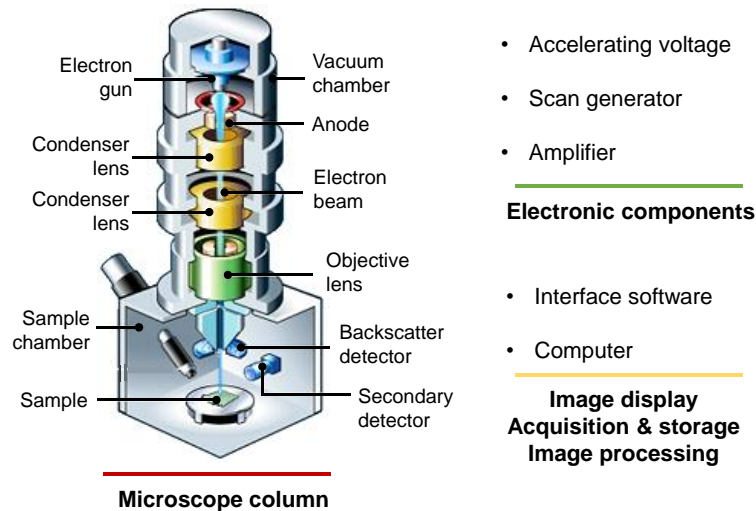


Figure IV.16. Schematic illustration of a scanning electron microscope and its several components (adapted from Amin, 2012)

The electro gun creates a fine and controlled electron beam which is emitted from the cathode and accelerated by a voltage of 0.5-30 kV between the cathode and anode to decrease the cross section of the beam. Even so, after passing through the anode, the diameter of the beam is still too large to produce a sharp image. Therefore, its diameter is demagnified by the condenser lenses and one objective lens and focused on the sample's surface.

The objective lens has a variable relatively long focal length that allows a large working distance which ensures that the various signals generated by the electrons resulting from the interaction between the beam and the sample can be collected by detectors located lateral above the specimen with sufficient efficiency.

The microscope column and sample chamber are kept under vacuum because if the column was in a gas filled environment, electrons would be scattered by gas molecules affecting the beam's intensity and stability. Also, other gas molecules coming from the sample or the microscope itself could form compounds and condense upon the sample. This would lower the contrast and obscure detail in the image.

As the electron beam reaches the sample elastic and/or inelastic interactions can occur. In the first case, the trajectory of the incident electrons (named primary electrons) will change but their energy remains the same whereas, in inelastic interactions the primary electrons trajectory will change and part of their energy will be transferred to the sample. This energy loss can be used to generate low-energy secondary electrons, X-radiation characteristic of the sample's elements, and Auger electrons, resultant of the interaction between the primary electrons and electrons in the inner orbitals of the surface material atoms. The electrons from elastic interactions are diffused from deeper layers (around 1 μm from the surface), and are collected by the backscatter detector. The secondary electrons result from interactions at lower depths and so originate high resolution images. These particles are more efficiently collected and so the total signal generated results mainly from the detection of secondary electrons. Higher number of electrons is emitted by the more prominent zones and thus the amount of secondary

electrons emitted by each area point, together with their direction, provides information about the material topography. Scanning the surface with the electron beam will then result in a tridimensional image (SEM micrograph) (Reichelt, 2007).

The beam deflection coils are controlled by a scan generator and scan the electron probe across the sample. Simultaneously, the scan generator controls the deflection coil system of a monitor. The amplifier allows to control the intensity of the signals received in order to perfect the quality of the image. Modern apparatus use a PC to control the electron beam, to select the signals, and to record, as well as, to store the digital image. In that case the electronic components are replaced by an interactive program running on the PC (Goldstein *et al.*, 2012; Reichelt, 2007).

The scanning electron microscopy is now a well-established method for the characterization of surfaces in many different fields, such as materials (activated carbons, metals, alloys, ceramics, glasses) and surface sciences (Zhao, *et al.*, 2017; Nantaphol *et al.*, 2017; Ma *et al.*, 2017; Batista *et al.*, 2016), semiconductor research and industry (Thongjamroon *et al.*, 2017; Susanto *et al.*, 2017), life sciences (Moraes *et al.*, 2017; Zhang *et al.*, 2017) and miscellaneous sciences such as polymer and food research (Kazemi *et al.*, 2017; Szkoda *et al.*, 2017), minerology (Aliyu *et al.*, 2017; Oberthur *et al.*, 2017), geology (Aliyu *et al.*, 2017; Kallel *et al.*, 2017), the oil industry (Subrati *et al.*, 2017; Valbe *et al.*, 2017), and archaeology (Solazzo, 2017; VanValkenburgh *et al.*, 2017).

This technique was used to assess the impact of different activation conditions during the development of activated carbons from apple tree branches in Chapter VII. It also proved to be very useful for the study of the role of morphology on cyclic thermal regeneration treatments (reported in Chapter VIII) and in the immobilization of *Escherichia coli* cells (Chapter IX).

IV.2.6. X-ray Diffraction (XRD)

X-ray diffraction is an analytical technique based on the fact that crystalline substances act as three-dimensional diffraction grating for X-ray wavelengths, similar to the spacing of planes in a crystal lattice.

X-rays are generated by a cathode ray tube, filtered to produce monochromatic radiation, directed toward the sample. The interaction of the incident ray with the sample produces constructive interference and a diffracted ray when Bragg's Law conditions are observed (see **Figure IV.17**) (Bertin, 2012; Jenkins and Snyder, 1996).

Considering the X-ray 2, incident on the second crystallographic plane, the X-ray wave must travel a distance ABC farther than the wave reflected from the top plane. Similarly, the wave reflecting from the third plane must travel the distance DEF further. Thus, all waves reflecting from planes below the surface will be phase retarded with respect to the first wave, causing interference. Plane geometry shows that when the distance ABC is exactly equal to one wavelength, λ , the distance DEF will equal 2λ (the proportion of the distance 2 is named "order" of reflection and designated **n**) and the reflection from all planes at any depth in the crystal will emerge in phase, producing the constructive interference known as diffraction (Jenkins and Snyder, 1996).

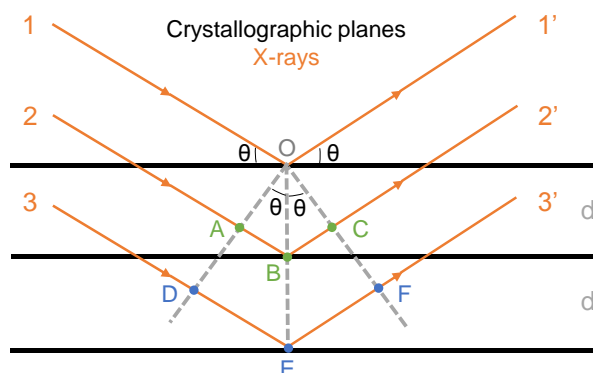


Figure IV.17. Representation of Bragg's law. The incident and reflecting X-rays are designated by 1 to 3 and 1' to 3', respectively. d is the distance between the crystallographic planes and θ is the incident angle of the X-rays (adapted from Jenkins and Snyder, 1996).

Considering the OAB triangle:

$$AB = d \sin \theta \quad \text{Equation IV.11}$$

Taking into account that, for interference to occur ABC must equal λ , the Bragg equation will be given by:

$$n\lambda = 2d \sin \theta \quad \text{Equation IV.12}$$

In X-ray diffraction (XRD) the interplanar spacing, d , of a crystal is used for identification and characterization purposes. In this case, the wavelength, λ , of the incident X-ray is known and so experimentally it is the incident angle (θ) at which constructive interference occurs that is recorded. Solving Bragg's equation gives the d -spacing between the crystal lattice planes of atoms that produce the constructive interference. A given unknown crystal is expected to have many rational planes of atoms in its structure; therefore, the collection of "reflections" of all the planes can be used to uniquely identify an unknown crystal. Typically, the identification is achieved by comparing d -spacings with standard reference patterns (Bertin, 2012; Jenkins and Snyder, 1996).

The X-ray diffractogram of the lab-made carbons ashes was obtained, as well as, that of medicine atenolol to elucidate about the racemic nature of this commercial compound within the scope of atenolol thermal desorption mechanism assessment in the carbons synthesized (see Chapter VII).

IV.2.7. X-ray Photoelectron Spectroscopy (XPS)

This technique relies in exciting a samples surface to cause the emission of photoelectrons (photoelectric effect). The binding energy and quantity of the electrons emitted, allows to identify the element studied.

The XPS instrumentation, illustrated in **Figure IV.18**, possesses an X-ray source where electrons are produced by a heated filament and are then accelerated by high voltage to impact a metal anode. The interaction of these electrons with the anode material results in the emission of characteristic X-rays which are focused on the sample. Aluminium and magnesium are two commonly used anodes for XPS analysis, although occasionally other anode materials such as titanium or chromium may be used for specific applications. An X-ray beam of a specific wavelength is generated. As the X-ray beam reaches the sample, energy is transferred from the beam to the sample, causing it to emit electrons (photoelectric effect). The photoelectrons reach the analyser that will separate them according to their kinetic energy. The detector, with an electron multiplier,

counts the photoelectrons (as discrete events) as they emerge from the analyser. From the binding energy and intensity of a photoelectron peak, a XPS spectrum can be obtained, characteristic of the element analysed (Connors and Banerjee, 1995).

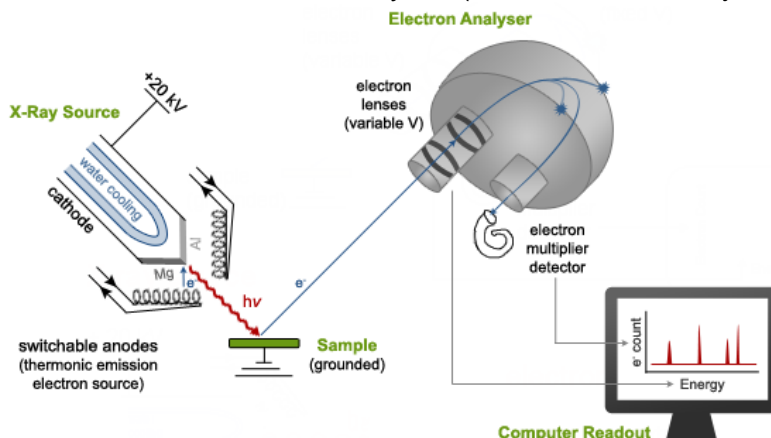


Figure IV.18. Schematic representation of an X-ray photoelectron spectrometer (<http://faculty.chem.queensu.ca/people/faculty/horton/research.html>).

XPS is the most widely used surface analysis technique because it can be applied to a broad range of materials and provides valuable quantitative and chemical state information from the surface of the material being studied. The information XPS provides about surface layers or thin film structures is important for many industrial and research applications where surface or thin film composition plays a critical role in performance including: nanomaterials (Sadri *et al.*, 2017), photovoltaics (Constantini *et al.*, 2017; Prabhu *et al.*, 2017), catalysis (Qin *et al.*, 2017, Liu *et al.*, 2017), corrosion (Boonserm *et al.*, 2017; Yi *et al.*, 2017), adhesion (Mugica-Vidal *et al.*, 2017; Yin *et al.*, 2017), development of magnetic materials (Zhou *et al.*, 2017; Wu *et al.*, 2017), and thin film coatings (Wang *et al.*, 2017; Taha *et al.*, 2017) used for numerous applications.

In this PhD thesis, this technique was used to complement the chemical characterization of several ACs surface (study presented in Chapter VIII).

IV.2.8. Contact angle measurements

Wetting properties play an important role in many industrial processes, such as oil recovery, lubrication, surface coating, printing, and spray quenching (AfzaliTabar *et al.*, 2017; Bhatt *et al.*, 2017; Mazzola and Bruno, 2017; Thokchom *et al.*, 2017). In recent years, there has been an increasing interest in the study of superhydrophobic surfaces, due to their potential applications in, for example, self-cleaning, nanofluidics, and electrowetting (Jain *et al.*, 2017; Rifai *et al.*, 2017, Gopalan and Kandlikar, 2014). Wettability studies usually involve the measurement of contact angles as the primary data, which indicates the degree of wetting when a solid and liquid interact. Two different types of contact angles can be measured, static and dynamic contact angles. The static contact angle is more commonly used because it is relatively easy to be measured. The procedures used to quantify the static contact angle mainly include sessile drop method (drop placed at the sample surface), and pendant drop method (drop pending from the needle) (Gu *et al.*, 2016).

The equipment used for contact angle measurement (**Figure IV.19 (a)**), named goniometer, consists nowadays on a horizontal stage to place the sample (liquid or solid), a motor-driven syringe to form a liquid drop and control the addition rate, an illumination source, and a telescope. A camera is nowadays used to take photographs of the drop

profile so as to measure the contact angle. The use of relatively high magnifications enables a detailed examination of the intersection profile (Yuan and Lee, 2013).

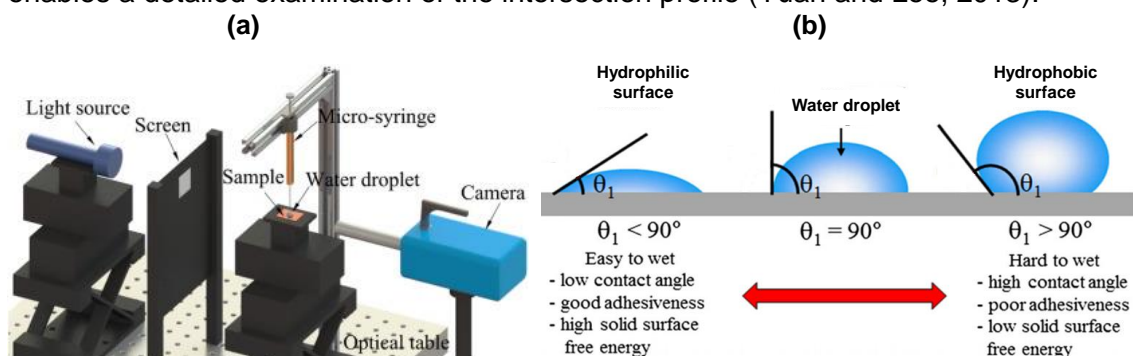


Figure IV.19. Contact angle measurement: (a) goniometer (Gu *et al.*, 2012) and (b) sessile drop measurement schematics (adapted from Lim and Kim, 2015).

As the liquid drop rests on a horizontal solid surface (**Figure IV.19 (b)**) that is, according to the sessile drop method, the contact angle is defined as the angle formed by the intersection of the liquid-solid interface and the liquid-vapour interface (represented by θ_1), geometrically acquired by applying a tangent line from the contact point along the liquid-vapour interface in the droplet profile. A small contact angle is observed when the liquid spreads on the surface, while a large contact angle is observed when the liquid beads on the surface. More specifically, a contact angle less than 90° indicates that wetting of the surface is favourable, and the fluid will spread over a large area on the surface; while contact angles greater than 90° generally means that wetting of the surface is unfavourable so the fluid will minimize its contact with the surface and form a compact liquid droplet.

The most common contact angle measurements are performed with water, to assess the hydrophilicity/hydrophobicity of a sample.

In this PhD thesis contact angle measurements of sessile water drops were made to assess the hydrophilicity of tannin-based polymers (study presented in Chapter XI).

Chapter V

Liquid phase adsorption

As already mentioned in Chapter IV, adsorption is defined as the increase of fluid density in the vicinity of a solid-solute or solid-gas interface. However adsorption from solution, for example aqueous solutions, is considered to be a much more complex process than the previously discussed gaseous phase adsorption because, in solution the adsorbate is diluted in a solvent. Thus, on the contrary to what happens in gas phase adsorption, where only interactions adsorbent-adsorbate are considered, in solution the interactions established between adsorbate-solvent, adsorbent-solvent and adsorbate-adsorbate have an impact on the adsorption process and have to be taken into account in the interpretation of the experimental data obtained.

The higher complexity of aqueous phase adsorption, in comparison to gas phase, distinguishes this process essentially because (Moreno-Castilla, 2008; Lyklema, 1995):

- i. Adsorption from solution is considered an exchange process, that is, solute adsorption can result from the attraction of the molecules towards the solid surface, but it can also be attributed to low affinity of the adsorbate towards its solvent (ex: adsorption in aqueous solution of hydrophobic molecules in hydrophobic adsorbents);
- ii. The isotherms may be non-linear due to lateral interactions established between the adsorbed molecules, but also due to the fact that the solution is not ideal;
- iii. Multilayer adsorption is less common than in gas phase adsorption since shielding forces are stronger in the condensed fluids.

The extension and properties of adsorption from solution processes are influenced by several factors related to the characteristics of the adsorbent and targeted compound, as well as the properties of the solution. A summary of these factors and their impact on the adsorption process are presented in **Table V.1**.

When considering adsorption of binary or multicomponents mixtures, besides the listed factors, it is also necessary to take into account (Al-Duri, 1995):

- i. Lateral interactions between the solute species at the adsorbent surface (Romanielo *et al.*, 2015)
- ii. Competition of the adsorbates for the active sites of the adsorbent (competitive adsorption). This competition will be affected by the compounds diffusion rate inside the particles, as well as their retention capacity when they are alone in solution. In general, the compound with higher retention capacity when it is alone in solution will also have a priority adsorption in an equimolar binary mixture of two adsorbates (Sotelo *et al.*, 2014; Sulaymon and Ahmed, 2008).
- iii. Molecular sieving effect due to the difference in adsorbates molecular sizes (Al-Malack and Dauda, 2017; Pelekan and Snoeyink, 1998)
- iv. Type of interactions adsorbent-adsorbates. For example, a specie chemically (irreversibly) adsorbed on some active sites will limit the access of other species present in solution, thus affecting equilibrium of the overall system (Al-Malack and Dauda, 2017).

Table V.1. Parameters affecting the extension of adsorption in solution (LeCloirec and Faur, 2006; Marsh and Rodríguez-Reinoso, 2006; Moreno-Castilla, 2004).

Adsorbent		Impact on adsorption in solution	
Apparent surface area		Adsorption capacity tends to increase with A_{BET} .	
Pore size distribution		The pore diameter of micropores (< 2 nm) and mesopores (2-50 nm) rules the adsorption of molecules of low and high molecular weight, respectively.	
Surface chemistry		Impact related to oxygenated complexes, which determine the surface charge and hydrophobicity of the carbon. Besides conditioning the pH_{PZC} , they also affect the electronic density of the graphitic layers (Coughlin and Ezra, 1968), influencing the dispersive interactions between the carbon surface and the adsorbate molecule. It can have an impact on the retention capacity of the adsorbent as a function of the ionization degree of the adsorbate (Bean <i>et al.</i> , 1964).	
Inorganic matter		It can block porosity and preferably adsorb water due to its hydrophilic character, reducing adsorbate uptake.	
Adsorbate		Impact on adsorption in solution	
Solubility		Higher affinity between adsorbate and solvent (high solubility) causes the decrease of adsorption capacity (Lundelius, 1920).	
Molecular size		Molecular weight and size of the adsorbate control its accessibility to the adsorbent pores.	
Polarity		Conditions adsorbate solubility and the type of interactions with the adsorbent.	
pKa ¹		Controls the adsorptive dissociation and it is related to the solution pH. It determined the adsorbate species present in solution at different pHs and, consequently, its solubility and polarity, influencing the interaction with the adsorbent.	
Substituent groups ²		The substituent groups of aromatic compounds can favour the interaction with other polar groups of the adsorbent. They can also remove or donate electrons to the ring affecting the dispersive interactions between the adsorbate ring and the carbon graphitic layers.	
Solvent		Impact on adsorption in solution	
pH		It is a very important factor because it affects the adsorbent surface net charge and the adsorptive when it is ionisable. It controls the electrostatic interactions between the adsorbent and the adsorbate.	
Ionic strength		It controls the attractive or repulsive electrostatic interactions which can be reduced by increasing the solution ionic strength due to the shielding effect of the surface charge produced by the added salt.	
Temperature		An increase in temperature generally results in a decrease in adsorption capacity (adsorption is exothermic). However, the adsorption enthalpies in liquid phase are usually very low and their variation with temperature are very small. It has also been reported a higher paracetamol adsorption with the increase of temperature, due to the change of adsorptive structure or due to diffusional restrictions connected to the molecule size, which decrease with a temperature increase (Terzyk <i>et al.</i> , 2003). More recent studies demonstrated that an increase of paracetamol adsorption capacity with temperature is linked with a non-continuous micropore size distribution centred at pore widths close to the critical dimensions of the planar form of the molecule (Galhetas <i>et al.</i> , 2015).	

¹in the case of electrolytes; ²in the case of aromatic compounds.

To study a given adsorption process it is necessary to assess the solid adsorption behaviour in kinetic and equilibrium conditions (Moreno-Castilla, 2008). Liquid phase adsorption studies generally include kinetic assays, important to evaluate, for example, the adsorption rate of the studied system and the contact time necessary for the system to reach equilibrium. The equilibrium data are obtained from adsorption isotherms and allow to evaluate the adsorption capacity of the adsorbent to retain the targeted molecule. This data is usually used to distinguish materials with the purpose of choosing

the most appropriate samples for a given application. All the equations derived from gas adsorption in monolayer are considered valid for liquid phase adsorption and some of these equations, such as Langmuir and Dubinin-Astakhov models, are used to determine the adsorption capacity of activated carbons in liquid phase (Mestre *et al.*, 2016; Mestre *et al.*, 2010).

Activated carbons are nowadays successfully applied as adsorbents for the removal of a great variety of pollutants in aqueous solutions, as was previously mentioned in Chapter III. These materials have indeed a great importance in advanced processes for water treatment, namely those that conjugate adsorption with, for example, micro and nanofiltration (Rodríguez *et al.*, 2016). Considering the strong role of ACs in this field, numerous scientific studies were, and are, being developed concerning adsorption of several pollutants onto activated carbons (Bjorklund and Li, 2017; Haro *et al.*, 2017; Krishnaiah *et al.*, 2017; Lemraski *et al.*, 2017; Ma *et al.*, 2017; Rodríguez *et al.*, 2017; Sulyman *et al.*, 2017; Anisuzzaman *et al.*, 2016; Pap *et al.*, 2016; Rusova *et al.*, 2016; Shu *et al.*, 2016; Mestre *et al.*, 2014a; Mestre *et al.*, 2011).

Due to the complexity of adsorption in solution, to understand the underlying mechanism of a given system can turn out to be very difficult due to the several factors impacting this process, listed in **Table V.1**. For this reason, a deep characterization of the texture and surface chemistry of the solids is necessary as well as a careful analysis kinetic and equilibrium adsorption data. Examples of this type of studies are the works reported by Al-Ghouti *et al.*, 2017; Bahamon *et al.*, 2017; Mestre *et al.*, 2014a; Sun *et al.*, 2014 and Yu and Luo, 2014.

V. 1. Adsorption kinetics

Due to the surface character of the adsorption process, the more used adsorbent materials are porous solids with highly developed surface areas. However, before the adsorption at the material's surface can occur, the adsorbate must first reach the outer surface of the particles and migrate towards the adsorption sites. In more detail, the adsorption process includes the three following steps (see **Figure V.1**) (Álvarez, 2009):

- i. External transport of the adsorptive species from solution bulk to the external surface of the adsorbent particles (**Figure V.1 (i)**);
- ii. Intraparticule diffusion from the external surface of the adsorbent to the active adsorption sites (**Figure V.1 (ii)**);
- iii. Adsorption at the surface of the internal pores of the adsorbent (**Figure V.1 (iii)**).

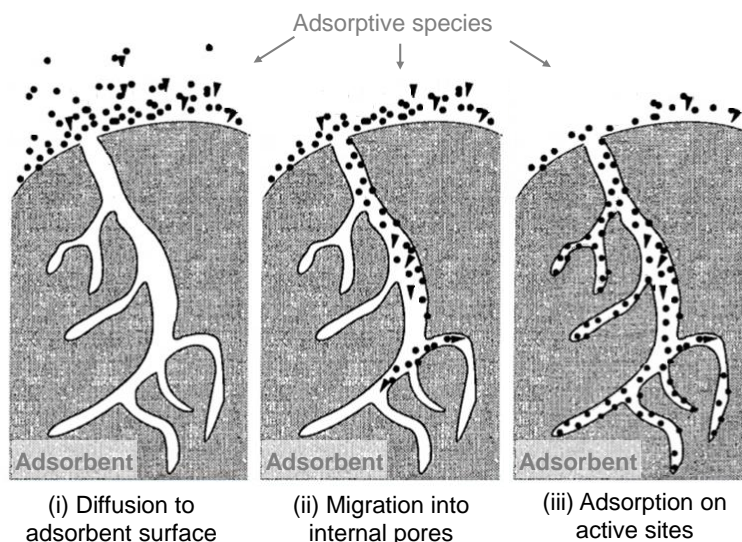


Figure V.1. Illustration of the several stages of adsorption process in liquid phase (adapted from <https://www.slideshare.net/VivekKumar36/adsorption-regenerationvivek-kumarneeri>).

From a kinetic point of view, the adsorption stage is the fastest of all, being assumed that equilibrium is reached instantaneously, and that the amount of adsorbate at the surface of the pores is in equilibrium with the solute species present in solution. Due to this, one can assume that the external transport and/or intraparticle diffusion are the limiting factors to adsorption and, consequently, responsible by the global rate of the process.

The transport inside the particles (**Figure V.1 (ii)**) is generally considered a diffusional process. This process can be distinguished in two types of mechanisms (Álvarez, 2009): normal molecular diffusion through the fluid that reaches the interior of the pores (pore diffusion), and surface diffusion which consists in the migration of the adsorbate throughout the pore walls without occurring a complete desorption, *i.e.*, the adsorbate specie suffers the influence of the surface potential without being retained until it reached the active site.

The objective of studying the process kinetics is to determine the adsorption rate of the solute onto the solid. Assessing this rate gives an idea of the contact time necessary to reach adsorption equilibrium. So, this assessment is extremely important for the purpose of designing adsorption systems (Ho, 2006). The solute uptaken during the kinetic experiments is influenced by several factors such as the initial solution concentration and pH, reaction temperature, particle size and amount of adsorbent and the solute nature (Largitte and Pasquier, 2016). Kinetic data can be analysed by several methods reported in the literature (Largitte and Pasquier, 2016; Qiu *et al.*, 2009; Ho, 2006; Azizian, 2004; Ho and McKay, 1998; Weber and Moris, 1963). Next, the kinetic models considered for the analysis of the kinetic data obtained in this thesis will be presented.

V.1.1. Pseudo-first order kinetic model

The pseudo-first order model was proposed in 1898 by Lagergren to interpret the adsorption of oxalic and malonic acids on carbon (Lagergren, 1898). This is the first known model that describes the adsorption rate as function of the adsorption capacity (Ho, 2006) and it has been, in the last decades, amply applied for the adsorption of pollutants in aqueous phase (Ho, 2004).

The adsorption rate, according to the Lagergren equation model, is defined by the following expression (Lagergren, 1898):

$$\frac{dq_t}{dt} = k_1(q_e - q_t) \quad \text{Equation V.1}$$

where k_1 is the pseudo-first order rate constant (h^{-1}), q_e and q_t correspond to the amount of solute adsorbed (mg g^{-1}) in equilibrium and at time t , respectively. Integrating Equation V.1 for the limit conditions $q_t = 0$ ($t = 0$) and $q_t = q_t$ ($t = t$) and rearranging it to a linear form, the following equation is obtained:

$$\ln(q_e - q_t) = \ln(q_e) - k_1 t \quad \text{Equation V.2}$$

Following this equation, the pseudo-first order rate constant, k_1 , can be directly obtained through the slope of the linear representation of $\ln(q_e - q_t)$ vs t , and the amount of adsorbed solute at equilibrium, q_e , will be calculated from the interception value with $\ln(q_e - q_t)$ axis.

V.1.2. Pseudo-second order kinetic model

The pseudo-second order kinetic model was proposed by Ho and McKay (1998) and, just as the pseudo-first order equation it includes the term “pseudo” because it is a kinetic equation based on the adsorption capacity of solids (Ho, 2006). In this model, the total adsorption rate is proportional to the square of the difference ($q_e - q_t$). Thus, a pseudo-second order kinetics can be expressed by the following equation:

$$\frac{dq_t}{dt} = k_2(q_e - q_t)^2 \quad \text{Equation V.3}$$

where k_2 is the pseudo-second order rate constant ($\text{g mg}^{-1} \text{h}^{-1}$), q_e and q_t correspond the amount of solute adsorbed, in equilibrium and in time t , respectively. Integrating Equation V.3 for the limit conditions $q_t = 0$ ($t = 0$) and $q_t = q_t$ ($t = t$) and rearranging it to a linear form, the following equation is obtained:

$$\frac{t}{q_t} = \frac{1}{k_2 q_e^2} + \left(\frac{q}{q_e}\right) t \quad \text{Equation V.4}$$

The q_e and k_2 values can be estimated, respectively, by the slope and interception values of the plot (t/q_t) vs t . The product $k_2 q_e^2$ represents the initial adsorption rate and, in this work, it will be designated by h . The time required for the adsorbent to uptake half of the adsorbate amount that will be retained at equilibrium is designated half-life time, $t_{1/2}$. This parameter is often used to measure the adsorption rate and is calculated by the following equation:

$$t_{1/2} = \frac{1}{k_2 q_e} \quad \text{Equation V.5}$$

which can be obtained by rearranging Equation V.4, considering $t = t_{1/2}$ and $q_t = q_e/2$.

The study performed by Ho and McKay (1999), in 12 systems where adsorbents and bioadsorbents were used to treat aqueous effluents with dyes and metallic organic ions reveals that, while the pseudo-first order model only shows a good fitting to the experimental data obtained in the initial adsorption period of time, the second-pseudo order equation presents better correlations for all the systems studied in the time period considered, that is, until equilibrium was reached.

The pseudo-second order equation has been successfully applied to the adsorption of metallic ions, dyes, herbicides, oils and other organic substances in aqueous solution (Batista *et al.*, 2016; Dastkhon *et al.*, 2017; Li *et al.*, 2017; Marques *et al.*, 2017; Pap *et al.*, 2017; Wei *et al.*, 2016). The use of this model has the advantage of not requiring to

know the experimental adsorption capacity in equilibrium because this parameter can be determined by the application of the method.

V. 2. Equilibrium adsorption

During the adsorption process an increase of solute concentration at the solid surface occurs, with the consequent decrease of its concentration in solution. The smaller the difference between solute concentration, in solution and adsorbed, the smaller will be the adsorption rate, until the equilibrium is reached. This equilibrium is dynamic and characteristic of each adsorbent/adsorbate system. Generally, the adsorbed amount increases with the increase of solute concentration in the liquid phase and the distribution of adsorbate between the two phases represents the adsorption equilibrium. This equilibrium is usually represented by the amount of solute adsorbed by unit mass of adsorbent as function of the solute concentration in solution, at equilibrium. When this type of studies are performed at constant temperature, these representations are denominated equilibrium adsorption isotherms, or simply adsorption isotherms.

The adsorption isotherms are normally obtained with the purpose of estimating the adsorption capacity of adsorbents towards a given compound. As previously mentioned, together with the adsorption kinetic data, the equilibrium results are used to differentiate the activated carbons and to choose the most adequate for a given application. The shape of the isotherms is the first tool used to diagnose the nature of a specific adsorption phenomenon. There are several types of adsorption isotherms in solution, however the five representations presented in **Figure V.2** are the most commonly obtained for activated carbons. A more detailed analysis of the isotherms configuration can be made according to the classification system proposed by Giles (Giles 1974a and 1974b), which takes into account the initial part of the curve, as well as the configuration at higher concentration values.

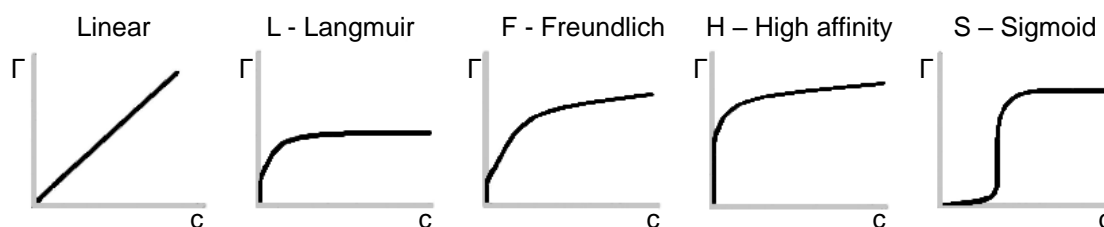


Figure V.2. Adsorption isotherms more frequently obtained for the adsorption of diluted aqueous solutions in carbonaceous materials (Moreno-Castilla, 2004). Γ represents the amount adsorbed and c the equilibrium concentration.

The **linear adsorption isotherms** are uncommon in activated carbons, however they can be found in the initial part of all the isotherms obtained for homogeneous surfaces.

The **Langmuir isotherm** (L) occurs frequently and it is concave towards the x-axis. As the liquid phase concentration increases, the adsorbed amount also increases, slower and slower until it reaches a plateau, that is, the saturation limit. This type of isotherm has been obtained, for example, in several studies performed by the research group where this PhD thesis was developed concerning pharmaceutical compounds adsorption in commercial and lab-made activated carbons (Mestre *et al.*, 2015; Mestre *et al.*, 2014a and 2014b).

The **Freundlich isotherm** (F) is characteristic of heterogeneous surfaces and is probably among the most obtained in liquid phase adsorption, especially with activated carbons (Mestre *et al.*, 2016). This type of isotherms has a less concave curvature than

L-type isotherms, showing that the amount adsorbed increases continuously but no saturation plateau is achieved for high solute concentrations.

High affinity isotherm (H) present an initial inclination very accentuated (practically vertical), followed by a pseudo-plateau. When compared to the L-type isotherm, no big differences can be found between these two types (Lyklema, 1995). H-type curve is a special case of the Langmuir isotherm where the solute has so high affinity towards the solid phase that, in diluted solutions, it is completely adsorbed not being detected in solution.

The **sigmoidal type isotherm (S)** has a concavity directed towards the y-axis being the adsorption favoured as the solute concentration increases in the liquid phase. The configuration of this isotherm strongly indicates the existence of lateral interactions between the solute molecules (Denoyel *et al.*, 2008). The IUPAC classification for the gas phase isotherms presents a similar interpretation for this type of configuration relating it to phenomena involving interactions between the adsorbate molecules (cooperative adsorption) (West *et al.*, 1952), such as capillary condensation or multilayer adsorption (Choma and Jaroniec, 2006; Rouquerol *et al.*, 1999). This type of isotherms is obtained when a moderate attraction exists between the adsorbate and adsorbent and there is a strong competition between the solute and the solvent for the adsorption sites.

Besides the analysis of the isotherms configuration, it is common to resort to theoretical models to obtain parameters that allow for the analysis of the experimental results. These models can be: (i) thermodynamic obtained by applying theoretical adsorption models to the thermodynamic properties of the adsorbent or (ii) semi-empirical models which result from the fitting of the experimental data to several functions.

Langmuir (Langmuir, 1918), Freundlich (Freundlich, 1906), Redlich-Peterson (Redlich and Peterson, 1959), Temkin (Temkin and Pyzhev 1940), Toth (Jossens *et al.*, 1978) and Dubinin-Astakhov equations (Furmaniak *et al.*, 2011) are among the most commonly used models for the treatment of adsorption isotherms of mono-component in liquid phase.

In the next paragraphs the models employed for the analysis of the adsorption isotherms obtained in this thesis will be addressed in more detail.

V.2.1. Langmuir isotherm

The Langmuir model assumes the formation of a monolayer over the homogeneous surface of the adsorbent, which corresponds to the appearance of a plateau (Langmuir, 1918). The underlying theory of this model is based on four assumptions (Ruthven, 1984; Langmuir, 1918):

- (1) The molecules are adsorbed in a fixed number of well-defined adsorption sites (specific adsorption);
- (2) Each site is only able to adsorb one molecule;
- (3) All the adsorption sites are energetically equivalent;
- (4) There are no interactions between the molecules adsorbed in close sites.

The mathematical expression that describes this model is the following:

$$q_e = \frac{q_m K_L C_e}{1 + K_L C_e} \quad \text{Equation V.6}$$

where K_L and q_m are, respectively, the Langmuir constant ($\text{dm}^3 \text{g}^{-1}$) and the monolayer adsorption capacity (mg g^{-1}), C_e and q_e are the solute concentration at equilibrium and the amount of adsorbed at equilibrium (mg g^{-1}), respectively. The Langmuir constant (K_L) is related to the free energy or total adsorption enthalpy ($K_L \propto e^{-\Delta H/RT}$) (Mohan *et al.*, 2005)

and it can be understood as a measure of the affinity between the adsorbate and the adsorbent.

The constants K_L and q_m are normally determined through the linearization of equation V.6:

$$\frac{C_e}{q_e} = \frac{1}{K_L q_m} + \frac{1}{q_m} C_e \quad \text{Equation V.7}$$

From the graphic representation of C_e/q_e vs C_e , it is possible to determine the monolayer adsorption capacity (q_m) value through the slope ($1/q_m$) and K_L value is obtained from the intercept to the C_e/q_e axis ($1/(K_L q_m)$).

With the decrease of C_e , the product $K_L C_e$ of Equation V.6, decreases to values lower than 1 and, consequently, $q_e = q_m K_L C_e$, which is analogue to Henry's Law. Thus, the linearization presented in Equation V.7 is adequate essentially to high concentration ranges.

V.2.2. Freundlich isotherm

The Freundlich isotherm is an empirical model developed to take into account the fact that the material's surface is not homogeneous, contrary to the assumptions of Langmuir (Freundlich and Heller, 1939). According to this equation, the increase in free adsorption energy causes an exponential decrease of the number of adsorption sites and, besides that, this model assumes that the interaction force between the adsorbate molecules is not negligible (Montgomery, 1985). The Freundlich expression (Equation V.8) is an exponential equation that assumes that, with an increase of the adsorbate concentration in solution, an increase of the adsorbate concentration at the adsorbent surface is also observed.

$$q_e = K_F (C_e)^{1/n} \quad \text{Equation V.8}$$

In this equation K_F and n are, respectively, Freundlich constant ($\text{mg}^{1-1/n} (\text{dm}^3)^{1/n} \text{g}^{-1}$) and exponent, being obtained through the linear regression of the representation $\ln(q_e)$ vs $\ln(C_e)$ (Equation V.9), where q_e is the solute uptake at equilibrium (mg g^{-1}) and C_e is the equilibrium concentration in solution (mg dm^{-3}).

$$\ln(q_e) = \ln(K_F) + \frac{1}{n} \ln(C_e) \quad \text{Equation V.9}$$

The values of K_F and $1/n$ are characteristic of the system adsorbent-adsorbate and depend on the temperature. The Freundlich constant is related to the adsorption capacity and the value of the exponent $1/n$ reflects the process energetic (Mohan *et al.*, 2005), or the heterogeneity of the adsorbent surface. A value of $1/n < 1$ indicates a favourable adsorption whereas, when $1/n > 1$ the adsorption is unfavourable (LeCloirec and Faur, 2006). The closer the $1/n$ exponent is to 0, the higher the surface heterogeneity will be, which will be reflected on the isotherm.

The Freundlich isotherm was the first to be applied in solid-liquid systems with good results, being recommended because of its simplicity. The equation that describes this type of curve is adequate for very heterogeneous surfaces and it frequently presents good fittings to experimental results in a restricted range of concentration values (Juang *et al.*, 1996). However, the basis for the original assumptions of this equation are not completely valid (Montgomery, 1985), reason why the equation is used only as an empirical model for the fitting of the experimental data. When the concentrations become close to zero and only a small surface coverage is observed, this equation does not translates itself in a linear isotherm (Henry's Law) what, in theory, would be possible.

Generally, it is observed that, when a good fitting of the experimental data is obtained at moderate and high concentrations, a less favourable adjust is observed for the adsorption data obtained at low concentrations (Jossens *et al.*, 1978).

V. 3. Activated carbons for water treatment processes

Water is a crucial resource for multiple human activities, such as, domestic uses, agriculture, and industry.

As the result of high water consumption, high volumes of residual wastewater are originated containing large amounts of anthropogenic compounds, such as, pharmaceutical and personal care products (PPCPs), pesticides or even hormones (Rodriguez *et al.*, 2017). These residual waters (sewage and other wastewater) are treated in Wastewater Treatment Plants (WWTPs) that have the purpose of processing and releasing them back into the environment with a safe quality to humans, fish and plants.

Figure V.3 illustrates the general layout of a WWTP facility and the treatment stages it usually combines.

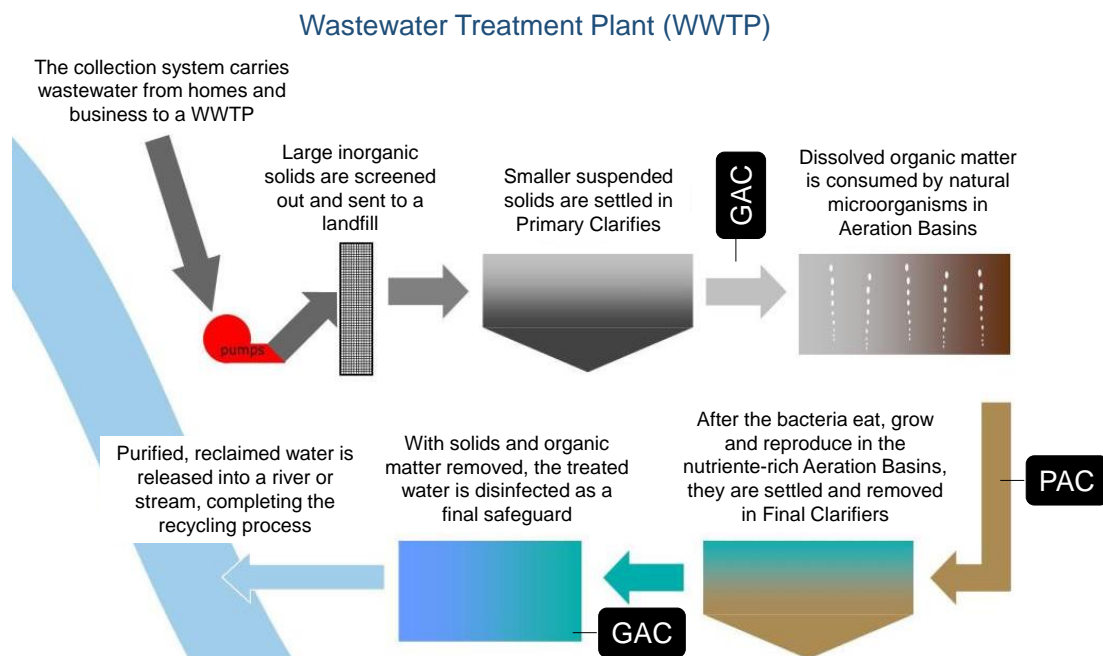


Figure V.3. Schematic layout of a WWTP from Huntsville, Unites States (adapted from <https://www.huntsvilleal.gov/environment/water/water-pollution-control-information/wastewater-collection-treatment/> and Przepiórski, 2006).

Conventionally, a WWTPs facility comprises four treatment stages (Batt *et al.*, 2006; Crites and Tchobanoglous, 1998).

- i. A **preliminary treatment** to remove large inorganic solids (trash), which are disposed in a landfill.
- ii. The **primary treatment** where the sewage is temporarily held in a basin where heavy solids will settle to the bottom while oil, grease and lighter solids float to the surface. The settled and floating materials are removed and the remaining liquid is subjected to secondary treatment.

- iii. The **secondary treatment** removes dissolved and suspended biological matter. This treatment is usually performed by indigenous, waterborne microorganisms in a controlled habitat that are later removed through membrane (MBR) filtration. The treated effluent may be discharged or subjected to a tertiary treatment.
- iv. **Tertiary treatment** consists mainly in the disinfection of the water prior to its discharge into the aquatic environment. The recycled water can also be reused, for example, for irrigation.

However, the described processes are not able to completely remove certain pollutants such as, for example, pharmaceutical and personal care products present in vestigial amounts (García *et al.*, 2014; Afonso-Olivares *et al.*, 2012). Consequently, these pollutants are continuously released into the aquatic environment reaching drinking water treatment plants (Yang *et al.*, 2017). In the context of this serious scenario, additional treatment technologies have been considered to improve removal efficiencies of several micropollutants (Rúa-Gómez *et al.*, 2012). In fact, activated carbons are usually implemented as an end-of-pipe technology or added to an existing technology in a WWTP. Although GAC columns are commonly used in the final processing stages (tertiary treatment), they can also be positioned in early steps of the plants, especially when highly polluted influents are considered (**Figure V.4a**). Another possibility is the addition of PAC to the ultrafiltration membrane module of MBR systems (**Figure V.4b**).

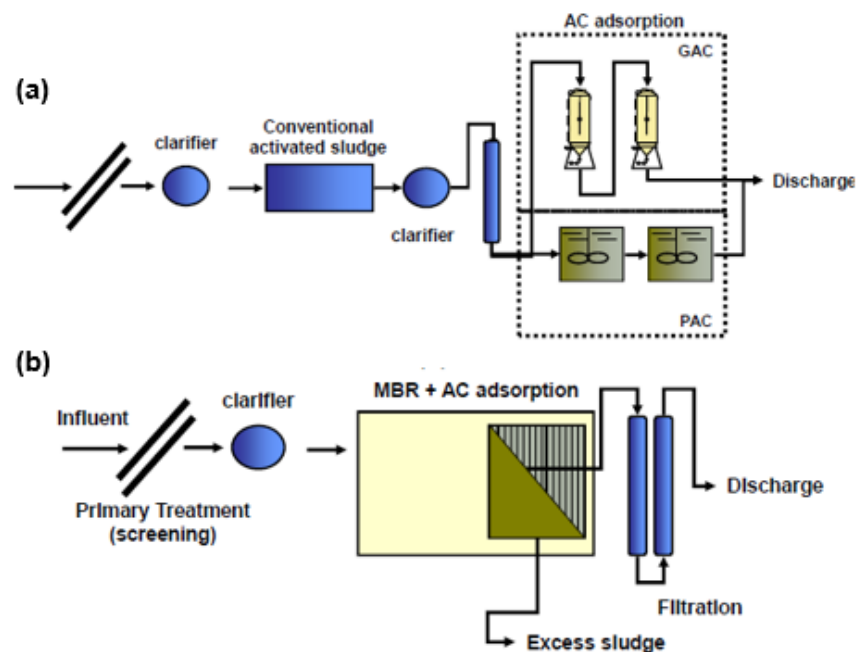


Figure V.4. Schematic diagrams of WWTPs where activated carbon are used; **(a)** filtration by GAC columns as a post-treatment in tertiary treatment and **(b)** AC addition to MBR system (adapted from Carvalho *et al.*, 2013).

In drinking water treatment plants, the concern for water quality is focused on the removal/degradation of organic matter, microorganisms, heavy metals and other priority pollutants. These facilities are thus projected to achieve this goal, making use of methodologies like coagulation, flocculation, sedimentation and filtration. **Figure V.5** illustrates an example of a water treatment plant layout, and the main processes employed.

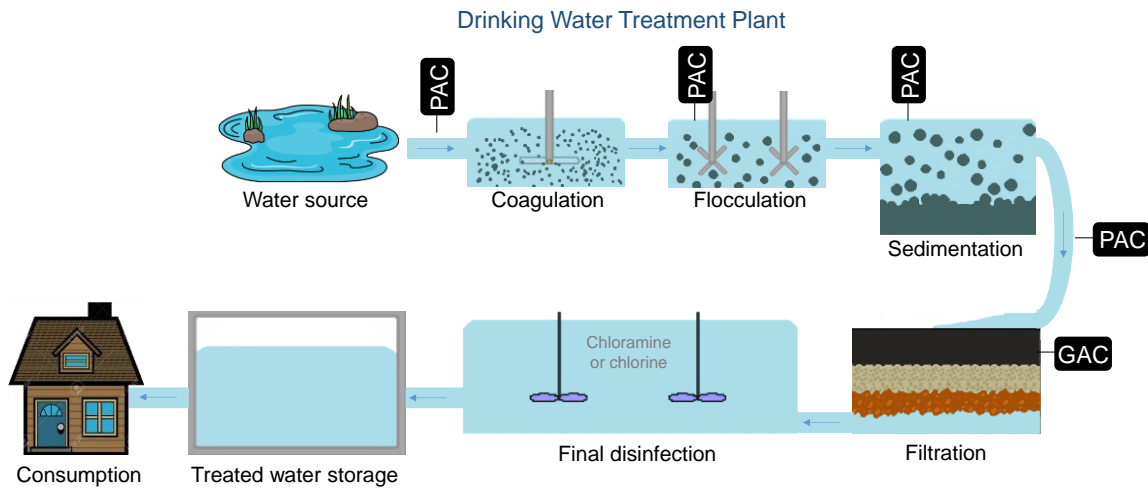


Figure V.5. Schematic representation of the main methodologies employed in drinking water treatment plants and indication of the stages where activated carbon can be employed (adapted from Karanfil, 2006).

Firstly, chemicals positively charged are added to the water with the purpose of neutralizing the negative charge of dirt and other dissolved particles in the water (coagulation) and, consequently larger particles, called floc are formed (flocculation). These particles tend to settle due to their weight (sedimentation) and the clear water will be located at the top of the reservoir. This clear portion will be filtered with several materials (filtration), like sand, gravel and activated carbon, of different pore sizes in order to remove dissolved particles, such as dust, parasites, bacteria, viruses and some priority chemicals. The final step consists usually in a disinfection (for example, chlorination), in order to kill any remaining parasites, bacteria and viruses, and to protect water from germs when it is piped to be consumed (Yang *et al.*, 2017; Stackelberg *et al.*, 2004; Zwiener *et al.*, 2001).

Activated carbons, in powdered or granular forms, are commonly used in drinking water treatment for the adsorption of several pollutants, as was previously mentioned in Chapter III. These materials can be used for removing taste and odour (T&O) compounds, synthetic organic chemicals (SOCs), and dissolved natural organic matter (NOM) from water. PACs can be applied at various locations in a treatment system, whereas GAC is employed in fixed-beds, such as, granular media filters or post filters. Even though the particle size does not affect the adsorption capacity of the materials, it does have a great impact on adsorption kinetics. The greatest challenge for effectively applying activated carbon adsorption technologies in drinking water treatment is to accurately understand the impacts of "system heterogeneity" on the adsorption process. The organic and inorganic chemical composition of natural waters may vary substantially from source to source affecting, for example, its hardness. In fact, it has been reported in the literature that water hardness decreases ACs adsorption capacity, as consequence of competitive adsorption or salting effect (Mestre *et al.*, 2016; Couto *et al.*, 2015; Martínez *et al.*, 2010; Pastrana-Martínez *et al.*, 2010).

The location(s) where activated carbons are applied in a treatment plant and changes in water media composition (*e.g.*, addition of various chemicals, especially oxidants, and acid/bases for pH adjustment) for different treatment objectives can have impact on the performance of activated carbon. Each of these factors must be properly evaluated in determining the use of activated carbon in a practical application (Karanfil, 2006). The objective of the activated carbon application in a particular water treatment plant determines the process design and operation; multiple objectives cannot, in most cases, be simultaneously optimized (Karanfil, 2006). Whenever the composition and concentration of the water contaminants have considerable variables, it is recommended

the use of powder carbon. When the water contamination is more or less constant, the use of granular carbons is favoured in adsorption columns placed, generally, after filtration and before oxidation/disinfection (National Research Council, 1980). The growing concerns about the quality of drinking water have maintained and will maintain, a certain level of demand for activated carbons, especially in countries where the treatment of residual waters by activated carbons is mandatory for purposes of reuse.

When activated carbons are employed in drinking water treatment plants, in adsorption columns (GACs) or in suspension in a batch reactor (PACs), the material is in contact with effluent for long periods of time (months) and bacteria present in the aquatic environment can colonize the solid. This inconvenient may be overcome by modifying the operational conditions of the system, so that the bacteria adherent to the filter can become useful, eliminating natural organic matter by oxidation, forming carbon dioxide, or to decomposing it in compounds of lower molecular weight (Graham, 1999). However, even though adjustments can be made to overcome bacteria colonization in a water treatment plant, spontaneous and long-term colonization of activated carbon filters can be extremely dangerous, leading to the development of multi-resistant bacteria, which can detach from the solid surface and contaminate the treated effluent of the water treatment plant. For this reason, in order to take advantage of bacteria adhesion of activated carbons, a different approach can be made. This consisted in the preparation of biological activated carbons (BACs) by controlled colonization of activated carbons (almost always in the granular form), prior to their application. The use of BACs allows for an increase of the carbon-bed life by converting a portion of the recalcitrant organics into biodegradable organics by preozonation (Westphalen *et al.*, 2016; Bautista-Toledo *et al.*, 2014; Rivera-Utrilla *et al.*, 2003). The microorganisms attached to the solid then convert the biodegradable portion to biomass, carbon dioxide, and waste products before the pollutants can occupy adsorption sites of the AC. Furthermore, the biofilm formed on the solid can change the net surface charge of the material, for example, to a more negative value, enhancing its adsorption capacity against some positively charged species, such as most of the heavy metals (Abd Rahman *et al.*, 2014; Vargas *et al.*, 2012; Rivera-Utrilla *et al.*, 2003; Rivera-Utrilla *et al.*, 2001).

V.3.1. Aquatic environment contamination by pharmaceutical compounds

The development of medical care as led to the production of increasingly more effective pharmaceutical active ingredients such as lipid-regulating drugs, analgesics, antibiotics, antiseptics, hormones, and chemotherapy and beta-blocking heart drugs. Even though regulation rules have been enforced by Food and Drug Administration (FDA) to minimize PPCPs consumption (Aminoshariae and Khan, 2015), in 2014, the worldwide consumption of medicines containing these active ingredients reached values *per capita* around 15 g and, in industrialized countries the value increased to 50-150 g (Yang *et al.*, 2017; Daughton, 2002).

After administration, a large amount of these compounds is excreted by the human body partially or completely un-metabolized, resulting in the continuous release of a wide variety of pharmaceutical active ingredients, their metabolites and transformation products into the sanitation systems (Zwiener *et al.*, 2001).

In the veterinary medicine, the use of pharmaceutical compounds has become an integral part of the growing livestock industry, with the main objectives of preventing and treating infectious diseases (*e.g.* antibiotics), manage animal reproduction (*e.g.* steroids)

and growing (e.g. hormonal growth implants), and control parasites (e.g. insecticides) and non-infectious diseases (e.g. nutritional supplements). The exaggerated administration of medicines in animals, followed by their excretion has led to the continuous and high contamination of the soil and water streams. Among these medicines, the every-day use of antibiotics, has become of special concern due to its impact in human health. In this context, the project European Surveillance of Veterinary Antimicrobial Consumption (ESVAC), aims to gather data concerning the administration of veterinary antimicrobial agents in different animal species in 29 European countries. The report on sales and use of veterinary antibiotics from 2011 to 2014 shows that, in Portugal alone, 190.5 tons of antibiotics active ingredients were sold in 2014 (ESVAC Report, 2014).

Whether the contaminated streams are of medical, industrial, agricultural, or household origin, when they reach wastewater treatment plants (WWTPs), conventional processes are ineffective in their complete decontamination. As a result pharmaceutical compounds are continuously introduced and detected in natural and even in drinking waters (Azuma *et al.*, 2017; Mandaric *et al.*, 2017; Yang *et al.*, 2017; Lin *et al.*, 2016; Oliveira *et al.*, 2015; Carmona *et al.*, 2014). This situation is especially dangerous to human and animal health because medicines have exceptionally high biological activity and, even in residual concentrations synergistic effects may occur (García *et al.*, 2014).

In the last decades, the European legislation stated new strategic approaches regarding pharmaceutical substances in surface and groundwater (European Parliament and Council 2015) considering also that the adverse effects could be magnified due to the simultaneous presence of many of such substances even if at low concentrations (Directives 2015/1787/EU, 2015/495/EU, 2014/80/EU, 2013/39/EU, 2009/90/EC, 2008/105/EC and 2000/60/EC). The urgent need to prevent further contamination of the aquatic system has led to the necessity to implement advanced water treatment technologies, such as membrane filtration, advanced oxidation processes and UV irradiation, to ensure the removal of this class of pollutants, which is composed by numerous compounds present in residual amounts (Rodríguez *et al.*, 2017; Yang *et al.*, 2017; Tabe *et al.*, 2016; Roccaro *et al.*, 2013; Zhou and Smith, 2002). Adsorption onto activated carbons is also considered one of the best methods available for the removal of different trace contaminants (Kim *et al.*, 2007).

V.3.2. Pollutant compounds studied

The studies developed in this thesis evaluated the removal of several micropollutants from aqueous phase by carbon materials. The compounds studied were chosen due to their documented presence in the aquatic environment, to their high impact on human and animal health, as well as, their high consumption. A group of 11 contaminants was considered, including analgesic/anti-inflammatories (paracetamol, diclofenac and ibuprofen), antibiotics (tetracycline hydrochloride and tiamulin hydrogen fumarate), β -blockers (atenolol), cholesterol regulators (atorvastatin), antacid (ranitidine), stimulant (caffeine) and a plasticizer (bisphenol A).

V.3.2.1. Analgesic/anti-inflammatories

Paracetamol (PARA), also known as acetaminophen (chemical structure presented in **Table VIII.5**), is an analgesic and antipyretic used to treat fever, headaches, and other minor pains (Wu *et al.*, 2012). This analgesic is one of the most consumed pharmaceuticals worldwide, besides being also a co-ingredient in other pharmaceutical

products. In fact, concerns regarding the excessive consumption of this drug have been raised and harder regulating rules have been enforced by FDA in order to limit its consumption (Aminoshariae and Khan, 2015). Approximately 58 to 68 % of the consumed paracetamol is expelled by the human body reaching the sewage system. This scenario, together with the relatively high water solubility of this compound, contribute for it to be detected in numerous water bodies throughout the years, in the range of $\mu\text{g L}^{-1}$ and, in some cases, ng L^{-1} (Ali *et al.*, 2017; Yang *et al.*, 2017; Carvalho *et al.*, 2012). In fact there are reports of paracetamol detection in rivers (Azuma *et al.*, 2017; Lopes *et al.*, 2016), surface and groundwater (Balakrishna *et al.*, 2017; Paíga and Delerue-Matos, 2016; Lin *et al.*, 2015; Spongberg *et al.*, 2011), and even in drinking water (Tabe *et al.*, 2016; Fram and Belitz, 2011).

During wastewater treatment, the efficiency in removing paracetamol can reach at least 80 %, in the case of hospital effluents treatment plants and around 86 % in municipal water treatment plants (Xiao *et al.*, 2013). However, during chlorination, paracetamol can be transformed in compounds which may possess greater risk to humans and ecosystems than the pristine compound (Cao *et al.*, 2016). The incomplete removal, together with transformation products formed during water treatment, lead to the continuous introduction of paracetamol and its metabolites and transformation compounds in the aquatic environment (Yang *et al.*, 2017; Oliveira *et al.*, 2015; Leung *et al.*, 2012; Wu *et al.*, 2012).

Diclofenac and ibuprofen are two non-steroidal anti-inflammatory drugs, commonly detected in water bodies.

Diclofenac (DCF) (chemical structure presented in **Table XI.1**) is used to reduce inflammation and to relieve pain in arthritis, or acute injury (Verlichi and Zambello, 2012b) being highly consumed worldwide. According to Zhang *et al.* (Zhang *et al.*, 2008) the annual world consumption of diclofenac reaches 940 tons. In addition, of the orally administrated dose, between 65 and 70 % is excreted in urine as the parent compound or metabolites (Vieno and Sillanpää, 2014; Zhang *et al.*, 2008) plus the amount excreted if the pharmaceutical is administered in the dermal form (Zhang *et al.*, 2008).

The consequential problematic release of this pharmaceutical into the environment made diclofenac one of the three compounds included in the first European Union (EU) Watchlist, in 2013 (Directive 2013/39/EU), in response to the EU growing concern about the need to protect Europe's aquatic environment from contamination by pharmaceutical active compounds. The main pollution sources by DCF are considered to be effluents and sludge from hospital and pharmaceutical manufacturing facilities which can contain high concentrations of this compound (reported an average concentration of 395 ng L^{-1} and a maximum value of 3000 ng L^{-1} , respectively) (Verlichi and Zambello, 2012b; Kümmerer, 2009; Fent *et al.*, 2006).

Ibuprofen (IBP) (chemical structure presented in **Table XI.1**) is a nonsteroidal anti-inflammatory (NSAID), analgesic and antipyretic drug widely used in the treatment of rheumatic disorders, pain and fever. This compounds is one of the most consumed medicines all over the world (Mestre *et al.*, 2007). As an example, the 2004 consumption of ibuprofen in Switzerland was 25 tons (Tambosi *et al.*, 2010).

This compound is commonly detected in several water bodies, having been detected in surface water at a mean concentration of 244 ng L^{-1} (Wang *et al.*, 2017a), in wastewater effluents, at a mean concentration of 1119 ng L^{-1} (Wang *et al.*, 2017a) and at 1.813 ng L^{-1} in the case of hospital effluents, in 2012 (Verlichi and Zambello, 2012b).

V.3.2.2. Antibiotics

Tetracycline hydrochloride (TC) (chemical structure presented in Appendix A.3.1, respectively) belongs to the antibiotic family of tetracyclines and, due to its broad-spectrum antimicrobial activity, it has been widely used to treat several diseases, such as, rickettsiosis, mycoplasma infection and chlamydia infection (Hopkins and Blaney, 2014; Huang *et al.*, 2011). TC is the second most consumed antibiotic worldwide, which has led to the contamination of the aquatic and soil environment, threatening human health and causing the development of drug-resistant bacteria (Borghini and Palma, 2014; Martins *et al.*, 2014). The study developed by Haro *et al.* (Haro *et al.*, 2016) revealed presence of this antibiotic in wastewater, showing the inefficiency of the WWTPs processes in the complete removal of this pollutant. Concentrations ranging from 0.1 ng L⁻¹ to 65.6 ng L⁻¹ and between 0.09 ng L⁻¹ and 3.8 ng L⁻¹ were detected in influent and effluent samples, respectively.

Tiamulin hydrogen fumarate (THF), commercially referred to as solely tiamulin (chemical structure presented in **Figure VII.14**), is a bacteriostatic agent, active against Gram-positive and Gram-negative microorganisms. This compound has been used in veterinary medicine for a considerable period, for the treatment, control, and prophylaxis of dysentery, pneumoniae, and mycoplasma diseases (Wilberts *et al.*, 2014; Taylor, 1980). A field study in ecological and wastewater treatment processes in Eastern China published by Dong *et al.* (2016) revealed that tiamulin was detected in all the influent samples analysed, in concentrations between 0.05 and 4.0 ng L⁻¹, and persisted in 90 % of the treated effluents, with maximum concentrations of 2.1 ng L⁻¹.

V.3.2.3. β -blockers

Atenolol (AT) (chemical structure presented in **Figure VII.10**) is one of the most consumed β -blocker medicines, used for the treatment of disorders, such as hypertension, angina and arrhythmias (Borchard, 1998). This compound is not fully metabolized by the human body being excreted, around 90 %, unaltered through urine (Khetan and Collins, 2007; Jones *et al.*, 2002), which raises a lot of concern due to its potential ecotoxicity as it can affect cardiac rhythm, generate abnormalities or reduce mobility of fish 's spermatozoids (Cleuvers, 2005). Its high consumption and excretion make this compound to be widely detected in hospital sewage and WWTPs effluent in concentrations ranging from 0.78 $\mu\text{g L}^{-1}$ to 6.6 $\mu\text{g L}^{-1}$ (Papageorgioua *et al.*, 2016; Subedi and Kannan, 2015; Santos *et al.*, 2013; Verlicchi *et al.*, 2012) and even in river water (83 ng L⁻¹) (Alder *et al.*, 2010).

In the literature, atenolol adsorption studies are not very common and most of them are quite recent. An example is the study developed by Haro *et al.* (Haro *et al.*, 2017) focused on atenolol adsorption by granular activated carbon. Maximum removal amount of approximately 18 mg g⁻¹ at equilibrium conditions is reported.

V.3.2.4. Cholesterol regulators

Atorvastatin (ATORV) (chemical structure presented in Appendix A.3.1) is a cholesterol-lowering pharmaceutical. It is the main ingredient of the most sold medicine in the history of pharmaceuticals, Lipitor, sold heavily in the United States and India. Less than 5% of a dose of atorvastatin is recovered in urine following oral administration. Consequently, this compounds is present in sewage and surface water, as well as in hospital effluents (Verlicchi *et al.*, 2012a; Verlicchi and Zambello, 2012b; Ternes, 1998).

Atorvastatin was detected at an average concentration of 395 ng L⁻¹ in WWTPs effluent from two sewage treatment plants in India (Subedi *et al.*, 2017) and, according to Verlichi and Zambello (Verlichi and Zambello, 2012b), it can be found in hospital effluents at an average concentration of 212 ng L⁻¹.

V.3.2.5. Blood-lipid regulators

Clofibrac acid (CLOF) (chemical structure presented in **Table VIII.5**) is the metabolite and active principle of several blood lipid regulators, being considered a potential endocrine disruptor, because it interferes with the synthesis of cholesterol (Khetan and Collins, 2007; Heberer, 2002). The first data regarding the detection of this pollutant were reported in the 70's when it was found in raw and treated wastewater at concentrations up to 2 µg dm⁻³ (Hignite and Azamoff, 1977; Garrison *et al.*, 1976). In 1993, this chemical was detected in groundwater in the Berlin area and, a year later, its presence was confirmed in ground, river and even in tap water (Stan *et al.*, 1994).

This compound is considered one of the most persistent drug residue in the environment (Khetan and Collins, 2007; Heberer, 2002), due to its recalcitrant behaviour (Gao and Deshusses, 2011; Onesios *et al.*, 2009; Matamoros *et al.*, 2008; Ternes *et al.*, 2002; Ternes, 1998) and high continuous consumption, leading to its widespread presence in WWTPs influents and effluents. In the literature, there are reports of clofibrac acid concentrations as high as hundreds of nanograms per liter in surface and ground water (Soulet *et al.*, 2002; Buser *et al.*, 1998; Ternes, 1998; Heberer and Stan, 1997) and, even more worrying, in tap water (Heberer, 2002; Zuccato *et al.*, 2000; Heberer and Stan, 1997).

V.3.2.6. Anti-acid medication

Ranitidine (RAN) (chemical structure presented in Appendix A.3.1) belongs to the histamine-2 blockers group and it is an anti-acid medicine, used to decrease the amount of stomach acidity. Because of this, it is used in the treatment of several diseases, such as ulcers, Zollinger-Ellison syndrome and gastroesophageal reflux (Kostich *et al.*, 2014; Batt *et al.*, 2008). This drug has been detected in wastewaters and hospital effluents at average concentrations of 120 ng L⁻¹ (Kostich *et al.*, 2014) and 2.34 ng L⁻¹ (Verlichi and Zambello, 2012b), respectively.

V.3.2.7. Stimulant

Caffeine (CAF) (chemical structure presented in Appendix A.3.1) is a pharmaceutical compound that acts as a cardiac, cerebral and respiratory stimulant, and can be considered as a psychoactive drug (Gros *et al.*, 2017). It has diuretic action and it increases the analgesic effect of several medicines, and so it appears in the formulation of many medicines. In addition to its therapeutic use, caffeine is present in numerous beverages and foods, being the most consumed stimulant worldwide (Engebretsen and Harris, 2001). Its extremely high availability has caused serious health problems, including development problems in fetus, due to the ingestion of caffeine by pregnant women (Galéra *et al.*, 2015).

More alarming is even the proven contamination of water sources by this compound, largely attributed to the inefficient caffeine removal by the current water treatment processes employed. This was demonstrated by Gago-Ferrero *et al.* (Gago-Ferrero *et al.*, 2017) that attributed the concentration of 460 ng L⁻¹ of caffeine in river water to

caffeine incomplete removal by the local wastewater treatment facility. This observation is further supported by other scientific studies, namely Gros *et al.* (Gros *et al.*, 2017), that detected caffeine in wastewater samples at a mean concentration value of $31.9 \mu\text{g L}^{-1}$. In the United States, this micropollutant has also been detected in sewage at maximum concentrations of $320 \mu\text{g L}^{-1}$ (Conn *et al.*, 2006).

V.3.2.8. Plasticizers

Bisphenol A (BPA) (chemical structure presented in Appendix A.3.1) is a highly produced plasticizer compound used for the production of polycarbonate and epoxy resins, unsaturated polyester-styrene resins and flame retardants. BPA-based plastics have been used to make a variety of consumer goods, including baby and water bottles, sports equipment, medical devices, dental fillings, and sealants (Geens *et al.* 2012). BPA-containing epoxy resins are used in the inner linings of food and beverage cans (Geens *et al.* 2012). Over 8 billion pounds (equivalent to approximately 3.6 billion kg) are manufactured annually and applied worldwide (Liu *et al.*, 2017; Liao and Kannan, 2014). The high consumption of BPA results inevitably in its release into the aquatic environment where it can cause many adverse health effects in aquatic organisms and humans (Liu *et al.*, 2017; Wang *et al.*, 2017b; Lu *et al.*, 2015).

This compound has been detected in several water bodies, as is the case of Taihu lake, in China, where BPA was detected at a concentration of 3360 ng L^{-1} (Wang *et al.*, 2017b) and in WWTPs effluents at a maximum concentration of $237 \mu\text{g L}^{-1}$ (Kasprzyk-Hordern *et al.*, 2009).

Chapter VI

Adhesion of faecal coliform
bacteria on activated carbons

V 1. Faecal coliform bacteria in the environment

Coliform bacteria are a group of microorganisms that inhabits human and livestock intestinal tract (faecal coliform bacteria). Since they can survive in the environment, faecal bacteria can spread throughout the environment through faecal contamination. Rochelle-Newall *et al.* (2015) has reported the spreading of faecal coliform bacteria throughout the aquatic system, focusing on the more favourable weather conditions of tropical environments to bacteria spreading. Extrapolating this overview to more temperate weather conditions (see **Figure VI.1**), the main source of the spreading is defecation of the host species (humans and livestock). In humans faeces alone, it is reported the presence of approximately a 7.6 log of viable cells (colony-forming units, CFU) *per g* of faeces (Cabral, 2010), that is $10^{7.6}$ cells. As bacteria reach the soil surface, erosion and washoff can transfer the microorganisms to the water stream. From here bottom sediments can become contaminated and the aquatic environment as well.

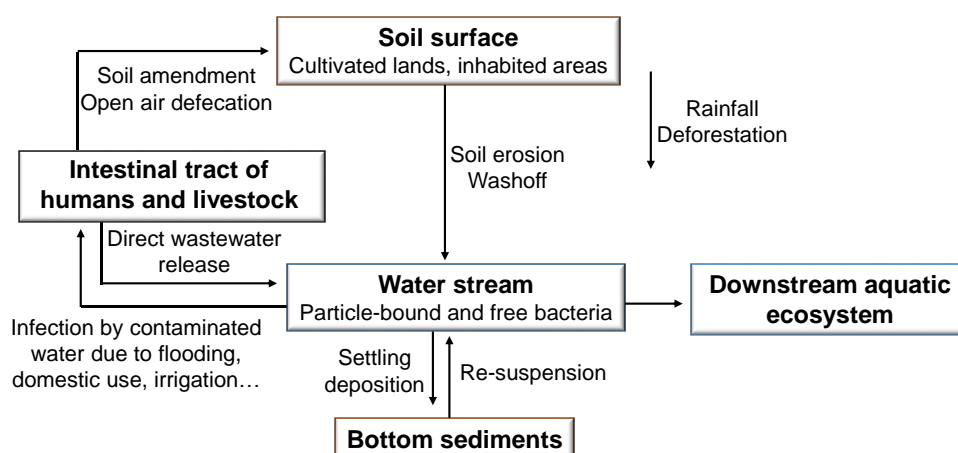


Figure VI.1. Conceptual diagram of bacteria spreading throughout the environment (adapted from Rochelle-Newall *et al.*, 2015).

Faecal coliform bacteria are considered indicators of the hygiene state of water distribution systems, and so, after water disinfection in wastewater treatment facilities, (see diagram presented in **Figure V.3**), before water distribution, these microorganisms should be absent and thus, their presence indicates an inadequate water treatment and the potential presence of pathogenic agents (Environmental fact sheet, 2003; Francy *et al.*, 1993). Ideally, indicator bacteria should be present in the intestinal tract of the same animal as the pathogens, should be present only in contaminated samples and not in uncontaminated ones, should have similar survival patterns as pathogens outside the host, should not be able to grow and proliferate in the environment, should be easily detectable, be of low risk to the person conducting the analyses and, ideally, should be relatively cheap to use (Ishii and Sadowsky, 2008; Ferguson and Signoretto, 2011).

Even though a clean and treated water supply to each house may be considered the norm in Europe and North America, in developing countries, access to both clean water and sanitation are not the rule, and waterborne infections are common. Two and a half billion people have no access to improved sanitation, and more than 1.5 million children die each year from diarrheal diseases (Fenwick, 2006). According to the World Health Organization (WHO), the mortality of water associated diseases exceeds 5 million people per year. From these, more than 50% are microbial intestinal infections. In general terms, the greatest microbial risks are associated with ingestion of water that is contaminated with human or animal faeces. Acute microbial diarrheal diseases are a major public

health problem in developing countries. Children under five, primarily in Asian and African countries, are the most affected by microbial diseases transmitted through water (Seas *et al.*, 2000). Microbial waterborne diseases also affect developed countries. In the USA, it has been estimated that each year 560,000 people suffer from severe waterborne diseases, and 7.1 million suffer from mild to moderate infections, resulting in estimated 12,000 deaths a year (Medema *et al.*, 2003).

VI. 2. *Escherichia coli*

Escherichia coli (**Figure VI.2**) is the microorganism more representative of the faecal coliform bacteria group. It was firstly identified in 1885 by a german bacteriologist named Theodor Escherich, which initially designated it *Bacterium coli*, being later altered to *Escherichia coli* (*E. coli*), in his honour.



Figure VI.2. Example of *Escherichia coli* cells (<http://www.infectionlandscapes.org/2011/10/escherichia-coli.html>).

This bacterium typically colonizes the gastrointestinal tract of human infants within a few hours after birth and coexists with its human host for decades, usually with mutual benefit. This microorganism also inhabits the gastrointestinal tract of livestock.

E. coli has become a model for studying many essential cellular processes, and due to its well established genetics and completed genome sequence, more is now known about *E. coli* than about any other living organism.

V.2.1. *Escherichia coli*, a biological drinking water indicator

E. coli generally does not survive well outside of the intestinal tract, its presence in environmental samples, food, or water usually indicates recent faecal contamination or poor sanitation practices in food-processing facilities (Odonkor and Ampofo, 2013; Feng *et al.*, 2002; Edberg *et al.*, 2000) The population of *E. coli* in these samples is influenced by the extent of faecal pollution, lack of hygienic practices, and storage conditions (Krieg and Holt, 1984). The mere presence of this bacteria in food or water does not indicate directly that pathogenic microorganisms are in the sample, but it does indicate that there is a heightened risk of the presence of other faecal-borne bacteria and viruses, many of which, such as *Salmonella spp.* or *hepatitis A virus*, are pathogenic (Feng *et al.*, 2002).

This bacteria is considered a more specific indicator of faecal contamination than the faecal coliforms group because the more general test for faecal coliforms also detects thermo-tolerant non-faecal coliform bacteria. The *E. coli* test recommended by the United States Environmental Protection Agency (EPA) confirms presumptive faecal coliforms by testing for the lack of an enzyme which is selective for the *E. coli* organism. This test separates *E. coli* from non-faecal thermos-tolerant coliforms.

Even though the use of this bacteria as indicator has been well-established, it still presents some limitations, such as, difficulties to determine the pathogenicity (or not) of the *E. coli* detected, and the fact that *E. coli* is not a single species (Eckner, 1998).

Despite these limitations, studies have shown that this microorganism is a much better indicator of disease risk than faecal coliform (EPA, 1986) and EPA has therefore recommended that *E. coli* be used as a criteria for classifying waters for fresh water contact recreation.

VI. 3. Bacteria adhesion

Bacteria population can exist freely in a solution, being designated planktonic population, and as a unit adhered to a surface, which can lead to the formation of a biofilm (Garrett *et al.*, 2008).

In the aquatic system, the first recorded observation of bacteria adhesion/biofilm comes from a 1933 paper by Henrici in which he states “it is quite evident that for the most part, water bacteria are not free floating organisms, but grow upon submerged surfaces” (Henrici, 1933).

A common model for the formation of a differentiated and mature bacterial biofilm has been proposed and cited by several articles focused on the study of this topic (Davey and O’Toole, 2000; Donlan, 2002; Dunne, 2002; Stoodley, *et al.*, 2002). The mechanism is reported to occur through at least five developmental stages, (represented in **Figure V.3**): **1.** An initial reversible attachment of planktonic bacteria that approach the solid surface by fluid stream or through motility (bacteria adhesion); **2.** Production of extracellular polymers and/or by specific adhesins located on pili and fimbriae, which interact with the surface; **3.** Early development of biofilm architecture; **4.** Development of microcolonies into a mature biofilm. Architectures with pedestal-like structures, water channels and pores are formed, in which bacteria develop specific patterns of growth and a different physiology and metabolism from planktonic cells. Literature has pointed out the existence of water-filled channels separating the microcolonies, compared to a circulatory system (Costerton *et al.*, 1995); **5.** Dispersion of cells from the biofilm into the surrounding environment and return to the planktonic state (Meireles *et al.*, 2015; Houdt and Michiels, 2005).

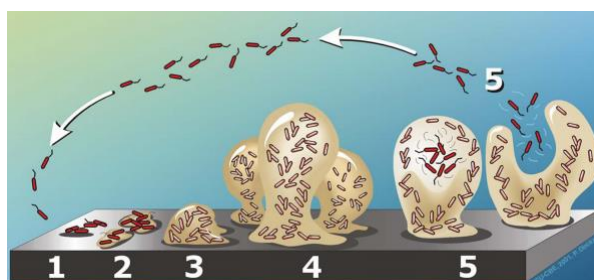


Figure VI.3. Development stages of biofilm formation (Stoodley *et al.*, 2002; Houdt and Michiels, 2005). 1. Bacteria adhesion; 2. Production of extracellular polymers; 3. Early development of biofilm architecture; 4. Development of a mature biofilm; 5. Dispersion of cells and return to the planktonic state.

For bacteria, the advantages of bacteria adhesion are numerous, namely, protection from disinfectants and development of resistance (Rizzo *et al.*, 2013; Davies, 2003), and dynamic environments (Chen *et al.*, 1998). This phenomenon has been observed in many industrial and domestic domains and, in some cases, its formation has been considered detrimental, causing heavy costs in cleaning and maintenance. Examples of such industries include the maritime (Doghri *et al.*, 2015), dairy (Somers *et al.*, 2001), food (Adetunji *et al.*, 2014), water systems (Liu *et al.*, 2014), oil (Lenhart *et al.*, 2014), paper (Torres *et al.*, 2012), opticians (Szczotka-Flynn *et al.*, 2009), dentistry (Hojo *et al.*, 2009) and hospitals (Soto-Giron *et al.*, 2016).

Bacteria adhesion is deeply considered in the scenario of water treatment where activated carbons are applied in the granular (in columns) and powder (in a batch reactor) forms in several stages of the water treatment plant, as mentioned in more detailed in Chapter V.

Activated carbons are considered to be optimum for bacteria adhesion, in part due to: (1) the adsorptive properties of the carbon, which enrich nutrient and oxygen concentrations and remove disinfectant compounds; (2) the porous surface of the carbon particles, which provides a protective environment from fluid shear forces; (3) the presence of a variety of functional groups on the carbon surface, which enhances microbial attachment; and (4) neutralization of stressor compounds (Rivera-Utrilla *et al.*, 2001). This phenomenon can be viewed from a positive or negative perspective, depending on whether bacteria adhesion is intended or not to occur, that is, in a scenario of controlled colonization or contamination, respectively (see **Figure V.4**).

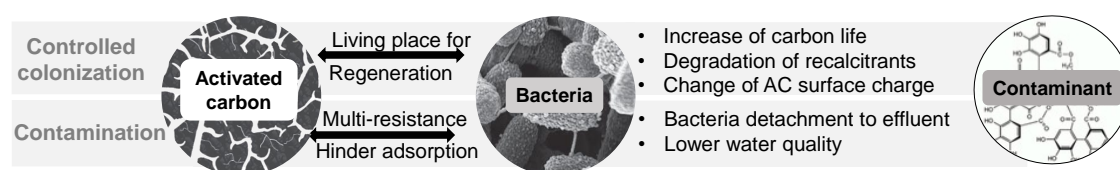


Figure VI.4. Simplified interaction model between activated carbon, microorganism and contaminant, in a water treatment scenario.

One positive example of the advantages of this occurrence is, for example, the so-called biological activated carbon (BAC), which consists in the controlled colonization of activated carbon (almost always granular carbons) prior to the application of the material. The use of BAC in water treatment plants allows for an increase of the carbon-bed life, in comparison to pristine adsorbent, by converting a portion of the recalcitrant organics to biodegradable compounds by preozonation (Korotta-Gamage SM and Sathasivan, 2017 Westphalen *et al.*, 2016; Bautista-Toledo *et al.*, 2014; Rivera-Utrilla *et al.*, 2013). The microorganisms attached to the solid then convert the biodegradable portion of pollutants to biomass, carbon dioxide, and waste products before the pollutants can occupy adsorption sites on the material. Furthermore, the bacteria adhered at the AC surface can change the net surface charge of the material, for example, to a global more negative value, enhancing its adsorption capacity against some positively charged pollutant species, such as most of the heavy metals (Sukumar *et al.*, 2014; Rivera-Utrilla *et al.*, 2001).

Spontaneous and long-term contamination of activated carbon filters during water treatment can occur preventing the activated carbon from removing the targeted micropollutants, by blocking the access of the pollutants to the porosity of the material. Another possible scenario can be even more concerning, that is, the development of antibiotic multi-resistant bacteria, which can then detach from the solid surface, and contaminate the treated effluent of water treatment plants. In any case, a profound understanding of the behaviour of the ACs on a biological environment has become crucial prior to its use in water treatment.

Studies concerning the bacterial colonization of activated carbons have been reported in the literature (Qin *et al.*, 2016; Borges, *et al.*, 2016; Islam *et al.*, 2016), but they are focused almost exclusively on granular carbons. However, as new forms of activated carbons are being developed and become available for adsorption applications, the assessment of their performances needs to include, both the adsorption capacity towards the targeted pollutants and their biological behaviour.

VI.3.1. *E. coli* cell and role of surface structures in adhesion to abiotic surfaces

E. coli is a prokaryotic (no membrane-bound nucleus) and gram-negative cell, with a bacillus shape (around 2.5 μm of diameter and 5 μm of length) (see **Figure VI.5**).

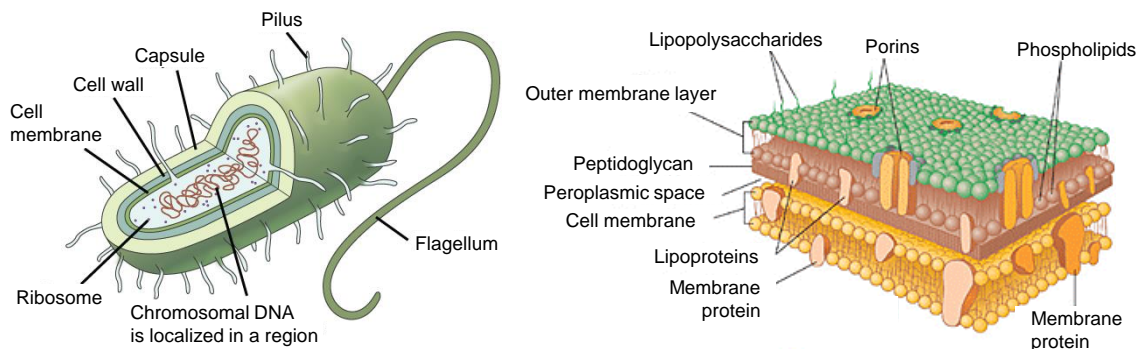


Figure VI.5. *Escherichia coli* cellular structures (adapted from: (left image) <https://www.khanacademy.org/science/biology/structure-of-a-cell/prokaryotic-and-eukaryotic-cells/a/prokaryotic-cells> and (right image) <http://slideplayer.com/slide/4452677/>).

The cellular DNA of this microorganism is not bound by a membrane, like in eukaryotic cells, instead it is located in the cytoplasm, together with ribosomes.

The flagella is responsible for the mobility of this organism and chemotaxis (its movement in response to a chemical stimulus). Studies have shown that cell motility is critical for the initiation of *E. coli* biofilm formation (Pratt and Kolter, 1998), because it promotes initial cell-to-surface contact. It is because of this that, in the case of pathogenic bacteria, mobility has even been considered a virulence factor in the colonization of host organisms or target organs (Houdt and Michiels, 2005). Also, mobility may promote the spread (dispersal) of growing bacteria along an abiotic surface (Jackson *et al.*, 2002).

Fimbriae and pilli are rod-shaped surface appendages, composed by proteins, and have different roles in the cell. Fimbriae are thin and shorter than pilli, presenting, in several *E. coli* strains the dimensions of 7 nm (width) x 1 μm (long) (Type 1 fimbriae) (Klemm and Krogfelt, 1994). Also, a bacteria cells has a much higher amount of fimbriae at its external surface than pilli (300-400 fimbriae vs 3-5 pilli *per cell*). Fimbriae are involved in cell-to-surface attachment, being named “attachment pilli” and it has been defended in the literature that physical interactions between Type 1 fimbriae and a solid surface lead to structural changes in the outer membrane of attached cells, reflected by a reduction in the level of outer membrane proteins (Otto *et al.*, 2001). Pilli are involved in cell-to-cell contact during bacteria conjugation (reproduction), being designated as “sex-pilli”. These organelles can also be involved in bacteria adhesion, more specifically in biofilm maturation.

The cell wall of *Escherichia coli*, a gram-negative bacteria, is composed by three components: the cell membrane, the periplasmic space and an outer membrane located above a thin peptidoglycan layer. For adhesion, besides the external organelles mentioned before, it is essentially the biomolecules present on their outer membrane that influence the adhesion of the bacteria to surfaces. The external surface of the outer membrane contains lipopolysaccharides (LPS) which present a net negative charge, at neutral pH, due to the exposure of the carboxylic and phosphoryl groups, which become ionized (Abu-Lail and Camesano, 2003). For this reason, the external surface of *E. coli* cell becomes negatively charged at a neutral pH, justifying the acidic pH_{PZC} associated with this bacteria of approximately 3.0 (van Loosdrecht *et al.*, 1987a and 1987b; van

Loosdrecht *et al.*, 1990). Because the cellular surface is in direct contact with the external environment, the charged groups are able to interact with the ions or molecules charged in the external medium. As a result, positively charged particles, for example metal cations, can be electrostatically attracted to the cellular surface (Langley and Beveridge, 1999). Studies suggest that the existence of LPS at the cellular surface tends to turn the cell surface more hydrophilic and vice-versa and that, these components can suffer alterations depending on the external environment (Palmer *et al.*, 2007).

The charge of the bacteria surface varies according to the species and it is influenced by the properties of the growth medium, such as pH and ionic strength, bacteria age and surface structure. The level of dissociation of the carboxyl, amino and phosphate groups of the cellular wall is not solely determined by pH but also by the concentration of the electrolyte solution (Hong and Brown, 2008). The magnitude of the electrostatic interactions decreases with the increase of the ionic strength due to the shielding of the surface charges. The electrostatic interactions lose their influence when there is a strong ionic strength.

When a bacteria cell comes close to a substrate surface, interactions begin to develop resultant from the ionic atmosphere that surrounds both cell and substrate surfaces. The intensity of that forces depends of the electric potential of the surfaces, the ionic strength and the dielectric constant of the surrounding medium and also of the distance between bacteria and substrate (Sheng *et al.*, 2008).

The importance of the hydrophobic character of the cells surface to adhesion is explained by the establishment of an effective adhesion between two surfaces in aqueous medium, the water film that separates them has to be removed and the hydrophobicity of the surfaces contributes to the easiness of that removal. Thus, the interface bacteria-liquid and the interface adhesion-liquid will have to be replaced by the interface bacteria- adhesion surface. According to the thermodynamic theory, adhesion only occurs if the process leads to a decrease of the net global energy (van Loosdrecht *et al.*, 1990).

Chapter VII

Wood bark-based activated
carbons for adsorption of
pharmaceuticals from aqueous
solution

The study presented in the present section, was focused on activated carbons prepared from apple tree branches char by chemical activation. The impact of different operational conditions in the textural, morphological and chemical properties of the materials was evaluated. To test adsorption characteristics of the lab-made adsorbents they were applied in the removal of a β -blocker medicine, atenolol, and a veterinary antibiotic, tiamulin hydrogen fumarate, from aqueous solution.

This research was developed in partnership with the University of Ljubljana, in Slovenia, in collaboration with Doctors Andreja Gotvajn and Marjan Marinšek. A manuscript has been submitted to Chemical Engineering Journal, with the title “Apple tree branches derived activated carbons for the removal of beta-blocker atenolol“, presented in Appendix D.

VII. 1. Experimental procedure

VII.1.1. Preparation and characterization of activated carbons

A char of apple tree branches was used as precursor of the activated carbons. In parallel with the materials developed in the laboratory, two commercial carbons, NS and CP, were studied (experimental procedures presented in **Table VII.1**).

Table VII.1. Materials prepared and commercial adsorbents studied and detailed information regarding their preparation and/or provenance.

Lab-made	Preparation
Biochar	Prepared in the University of Ljubljana, according to the specifications presented in Appendix A1.1 and supplied in two size fractions lower and higher than 100 μm .
Activated carbons	Synthesized by chemical activation with KOH and K_2CO_3 (see Appendix A1.2) from biochar with two particle sizes under different biochar:activating agent mass ratios, and temperature and duration of activation. Initially, screening experiments were made to understand the impact of each parameter in some properties, namely the preparation yield and volatile content, of the activated carbons.
Commercial	Information
NS	Norit activated carbon, with the commercial name SAE SUPER. This powder solid is composed of 97 % (mass ratio) by particles with dimensions inferior to 0.15 mm.
CP	Powdered carbon commercialized by ChiemiVall under the designation CCP 900.

The biochar will be designated by A, followed by the numbers 1 or 2, depending on whether the particle size is lower or higher than 100 μm .

The materials will be named according to the expression: CA or HA followed by 1 or 2 and (impregnation ratio/temperature of activation ($^{\circ}\text{C}$)/ duration of activation (h)), where C and H stand for K_2CO_3 or KOH activation, respectively. An example of this nomenclature is CA2(1:3/800/1).

The activated carbons subjected to full characterization and aqueous phase adsorption experiments were all prepared with biochar A2 and, for this reason after the discussion presented in section VIII.2.1, the designation of biochar fraction (1 or 2) was removed from the samples' name.

VII.1.2. Material's characterization techniques, liquid phase adsorption, molecular modeling and desorption experiments

Table VII.2 presents the techniques used for the textural, chemical and morphological characterization. Also, the adsorptive potential of the lab-made ACs was assessed for atenolol (abbreviated AT) and tiamulin hydrogen fumarate (THF). Furthermore, the fumaric acid compound (named FA), present in THF medicine was also included in this study. Thermogravimetric studies were performed on atenolol exhausted samples to obtain information about the interaction mechanism between atenolol and the adsorbents.

Detailed information regarding reagents, solution preparation and molecular properties of the pollutants species are presented in Appendix A.31.

Table VII.2. Experimental procedures of the characterization techniques employed, liquid phase adsorption, molecular modelling and desorption experiments.

Characterization	Technique	Appendix A
Texture	N ₂ adsorption at – 196 °C	2.1
	CO ₂ adsorption at 0°C	2.2
Surface chemistry	pH at the point of zero charge (pH _{PZC}) determination	2.8
Morphology	Scanning Electron Microscopy (SEM)	2.5
Liquid phase adsorption	Experiment	Procedure
Atenolol, tiamulin hydrogen fumarate and fumaric acid adsorption	Adsorption kinetics and equilibrium assays	3.2
Desorption mechanism	Experiment	Procedure
Atenolol desorption from lab-made ACs	Thermogravimetry studies	2.16

Molecular modelling of atenolol, and tiamulin hydrogen fumarate were determined by Doctor Miguel Machuqueiro, in Faculdade de Ciências da Universidade de Lisboa. The molecular dimensions were estimated starting by building initial structures in Avogadro (<http://avogadro.cc>) and the geometries were optimized with GAUSSIAN 09 software package (Frisch *et al.*, 2009) using the B3LYP functional (Becke, 1993; Lee *et al.*, 1988) and the 6-31+G** basis set. All calculations were done using a SMD water model (Marenich *et al.*, 2009). Frequency calculations were performed to confirm the absence of imaginary frequencies for the obtained minima. The torsions around the rotatable bonds were explored without success to identify alternatives to the most extended conformations

VII. 2. Results and discussion

VII.2.1. Optimization of the activation conditions

The impact of several activation conditions on the ACs preparation yield was assessed. Moreover, due to the high volatile content of the biochar (49 %), this study also had as objective to decrease significantly the volatile content of the ACs to prevent any limitations in the characterization of the solids by N₂ and CO₂ adsorption, and also allow the use of the materials for water decontamination purposes.

The synthesized samples are presented in **Table VII.3**, alongside with their corresponding global yields, η , and volatile content, VC.

Table VII.3. Samples prepared, corresponding activation yield, η , and volatile content, VC.

	η^a (%)	VC (%)		η^a (%)	VC (%)
A	-	49	CA2(1:3/900/1)	3	-
			CA2(1:3/900/2)	3	-
CA1(1:1/700/1)	59	-	CA2(1:4/800/1)	49	14
CA1(1:1/800/1)	61	-	CA2(1:4/800/2)	49	-
CA1(1:3/800/1)	57	40	CA2(1:4/800/4)	42	-
CA2(1:3/700/2)	51	-	HA2(1:3/800/1)	46	16
CA2(1:3/700/3)	59	-	HA2(1:3/800/2)	38	-
CA2(1:1/800/1)	48	40	HA2(1:3/800/3)	33	-
CA2(1:3/800/1)	40	12	HA2(1:3/800/4)	22	-
CA2(1:3/800/2)	42	-			
CA2(1:3/800/3)	38	-			
CA2(1:3/800/4)	22	-			

^aActivation yield, defined as: g of activated carbon *per* 1 g of biochar.

The activation methodology employed allowed to obtain carbons with preparation yields, higher than approximately 40 %, with exception of the materials synthesized at 900 °C and during 4 h of treatment.

No effect of activation temperature in the preparation yield was observed when increasing the temperature from 700 to 800 °C, in the case of K₂CO₃ activated biochar A1 (see **Figure VIII.1** – left side graphic). However, when smaller particles (biochar A2) are activated with 1:3 proportion, a clear impact of temperature on η values is observed. A more significant η decrease ($\Delta\eta$ of -37 and -48 percentage points) occurs when increasing temperature from 800 to 900 °C. The use of the highest activation temperature (900 °C) proved not to be advantageous for ACs preparation, because it caused an almost complete destruction of the carbonaceous matrix, even for 1 h treatments (η of almost 3%).

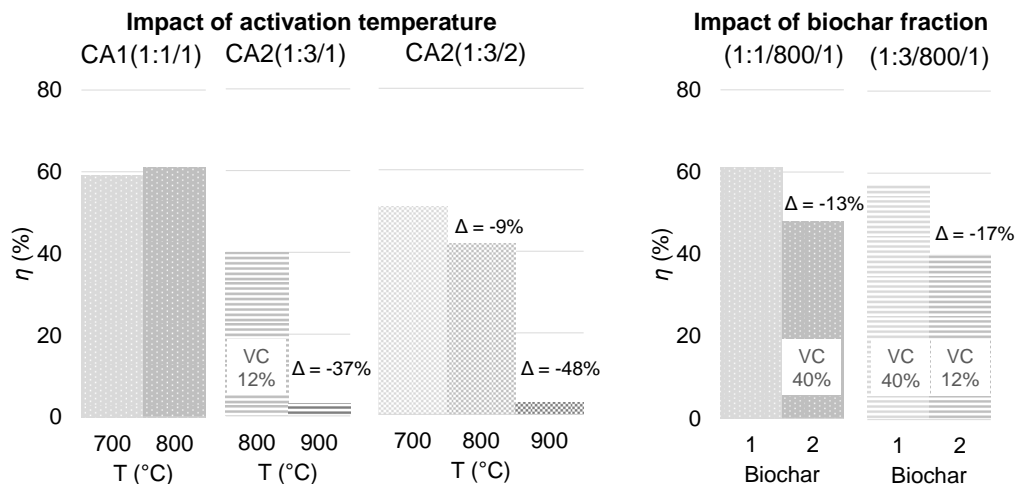


Figure VII.1. Comparison graphics to evaluate the impact of activation temperature (left side graphic) and that of biochar fraction (right side graphic) on K₂CO₃ activated samples preparation yield and volatile content.

Regarding the particle size of the biochar, the impact of this parameter can be evaluated by comparing samples activated with carbonate, as presented in the right side graphic of **Figure VII.1**. Lower yields were obtained when using the biochar A2, with smaller particle size. In comparison with the samples prepared from A1, a decrease of 13 and 17 percentage points was observed when 1:1 and 1:3 ratios were used, respectively. This result can be attributed to a more efficient activation of smaller biochar particles, which caused also a more significant decrease of the volatile content, reaching

only 12 % (sample CA2(1:3/800/1)). This allowed us to conclude that the use of fraction A1 was not advantageous for the preparation of ACs and, for this reason, the study proceeded only with biochar A2.

The use of different biochar:activating agent proportions (see **Figure VII.2**) allowed to assess which proportion was more efficient in decreasing the VC of the biochar, while maintaining a preparation yield high enough to ensure the production of considerable amount of material. When performing 1, 2 and 4 h long treatments, the use of 1:3 ratio seems to be sufficient to decrease the VC down to 12 %. On the other hand, the fact that higher yields are consistently obtained with 1:4 proportion, suggests an excessive activating agent amount, less efficiently distributed throughout the sample.

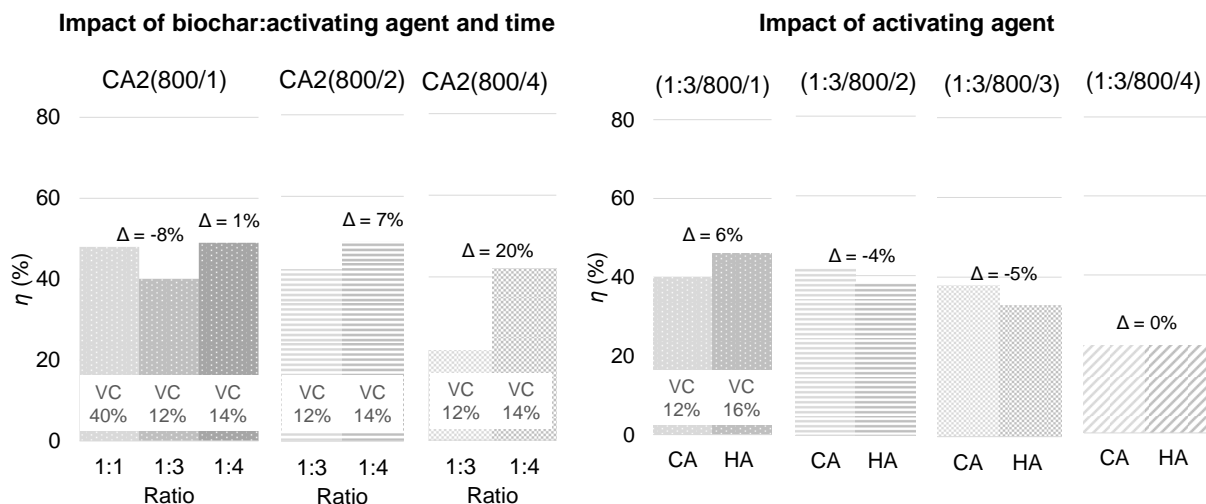


Figure VII.2. Comparison graphics to evaluate the impact of the impregnation proportion and of the activating agent used on the preparation yield and volatile content (VC) of the carbons.

Regarding the activating agent used, it is possible to compare the preparation yields, and volatile content of the set of samples prepared with a 1:3 proportion, at 800 °C during 1 to 4 h. Under the same experimental conditions, both K_2CO_3 and KOH led to samples with similar η , ranging from 46 to 22 %. In what concerns the VC, regardless the K_2CO_3 activation conditions, a sample with 12 % of VC was obtained, and in KOH activated carbon the VC accounts for 16 % of the sample weight.

A set of experimental conditions proved to be more advantageous for the preparation of activated carbons: the use of A2 biochar fraction, and 1 to 4 h long treatments, at 800 °C, with both K_2CO_3 and KOH. In the case of carbonate, considering its softer activation of the matrix, the preparation of carbons with 1:4 was also considered advantageous. The carbons prepared under these conditions were prepared in higher quantities with the purpose of a deeper characterization and to be used in aqueous phase adsorption experiments.

Because the samples chosen to proceed the study were prepared with the same biochar particle size (< 100 μm), the designation of biochar fraction (1 or 2) was removed from the name of the samples.

VII.2.2. Characterization of the adsorbents

The N_2 adsorption-desorption isotherms, at -196 °C presented in **Figure VII.3**, show that all carbons present type I isotherms according to IUPAC classification (Thommes *et al.*, 2015), characteristic of essentially microporous structures. At low relative pressure values a not very pronounced, rectangular character is observed, suggesting a wide micropore size distribution. The widening of the initial knee is evident for all the samples

prepared with KOH, and also for samples activated with K_2CO_3 for longer periods of time. For higher relative pressures a plateau is observed in all the cases, demonstrating that no significant mesopore network or external surface area is present.

The use of KOH as activating agent, in the 1:3 proportion, promotes a more extensive development of porosity and, in the conditions used, increasing the duration of the treatment up to 3 h seems to have a positive effect in the activation process. The use of a 4 h long activation step proved not to be advantageous, leading to a carbon with textural properties similar to those of sample HA(1:3/800/3), as demonstrated by their coincident nitrogen adsorption isotherms, and obtained with a lower preparation yield (22 % vs 33 % for 3 h).

The use of K_2CO_3 , also with a 1:3 proportion, also led to an increase of porosity development when activations were made up to 3 h. Like with what was observed with KOH, no gain (texture or yield) was obtained with 4 h long treatments.

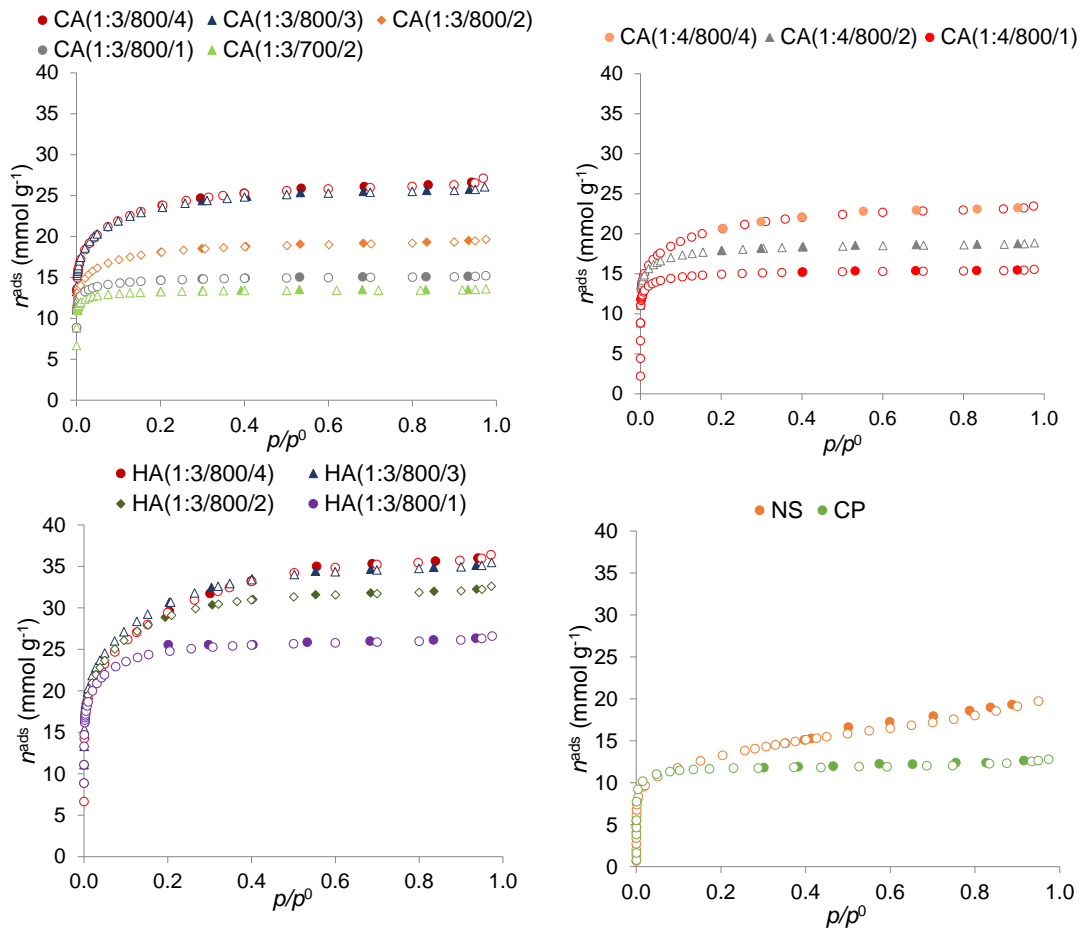


Figure VII.3. Nitrogen adsorption-desorption isotherms at $-196\text{ }^\circ\text{C}$ of the carbons activated with K_2CO_3 and KOH, as well as the commercial samples studied.

The temperature used in K_2CO_3 activation seems to have an important impact in developing porosity. Thus, considering samples CA(1:3/700/2) and CA(1:3/800/2), increasing the temperature from 700 to 800 $^\circ\text{C}$ lead to a more pronounced porosity development, as demonstrated by the higher adsorption capacity of sample CA(1:3/800/2). Also, the less pronounced rectangular character of the isotherm of this sample suggests a more significant presence of wider micropores.

The isotherms of samples K_2CO_3 activated with 1:3 and 1:4 proportions show that the latter ratio does not have a visible effect in the porosity of the carbons treated during 1 and 2 h. Actually, regardless the ratio char: K_2CO_3 considered, the carbons obtained

present similar isotherms in terms of configuration and amount of nitrogen adsorbed to the samples produced using a proportion of 1:3. Considering 4 h of activation, the use of a 1:4 proportion leads to the formation of a carbon with lower adsorption capacity than the sample CA(1:3/800/2), revealing the consumption of the carbonaceous matrix when the higher proportion is used.

The commercial carbons have nitrogen isotherms that distinguish themselves from the lab-made carbons, both in terms of configuration and nitrogen uptake. Regarding carbon CP, its isotherm has a very marked rectangular character at low relative pressures, followed by a horizontal plateau over a wide range of pressure values (type I). A lower nitrogen uptake than that of the other samples is observed, and the isotherm configuration shows that this carbon has an essentially microporous nature. On the contrary, the configuration of NS isotherm suggests the presence of a micro and mesopore network, being classified as a type I+IV isotherm (Thommes *et al.* 2015), presenting a very pronounced upward deviation in the range of high relative pressure, denoting a well developed mesopore structure.

The N₂ adsorption data were analysed by the BET equation (Gregg and Sing, 1982), following the recommendations of the international norm ISO 9277, allowing to calculate the apparent surface area, A_{BET} , of the carbons. The microporosity of the samples was analysed applying the α_s method (Rouquerol, *et al.*, 1999), taking as reference the isotherm reported in reference (Rodríguez-Reinoso and Martín-Martínez, 1987). This method allowed the determination of the total micropore volume, $V_{\alpha \text{ total}}$, the specific volumes of ultra, $V_{\alpha \text{ ultra}}$, and supermicropores, $V_{\alpha \text{ super}}$. The results obtained, as well as the meso, V_{meso} , and total, V_{total} , pore volumes, and the pH_{PZC} values are presented in **Table VII.4**.

The values obtained show that the activation with KOH produced carbons with very high values of A_{BET} , up to 2445 m² g⁻¹. The use of K₂CO₃ allowed to achieve somewhat lower values reaching 1920 m² g⁻¹. On the other hand, the textural parameters reveal that, in both cases, the more significant porosity development occurs for activation times up to 3 h, and that the micropore volume of the samples corresponds to 91 % to 98 % of the total pore volume, confirming the fundamental microporous nature of the samples.

A more detailed analysis of the textural parameters of KOH activated carbons allows to conclude that the duration of the treatment has a profound impact on the composition of the micropore network, leading to the progressive widening of the pores. In fact, the increase of the treatment duration from 1 to 2 h lead to a null $V_{\alpha \text{ ultra}}$, and the increase of $V_{\alpha \text{ super}}$ from 0.76 to 1.06 cm³ g⁻¹, pointing out the conversion of ultramicropores into supermicropores. Longer treatments resulted in further enlargement of the supermicropores leading to the development of some mesoporosity.

Table VII.4. Nanotextural properties of the lab-made carbons and corresponding pH_{PZC} values.

	A_{BET} ($m^2 g^{-1}$)	V_{total}^a ($cm^3 g^{-1}$)	V_{meso}^b ($cm^3 g^{-1}$)	α_s method ^c			pH_{PZC}
				$V_{\alpha total}$ ($cm^3 g^{-1}$)	$V_{\alpha ultra}$ ($cm^3 g^{-1}$)	$V_{\alpha super}$ ($cm^3 g^{-1}$)	
Lab-made							
KOH							
HA(1:3/800/1)	2029	0.93	0.05	0.88	0.12	0.76	6.0
HA(1:3/800/2)	2345	1.14	0.08	1.06	0.00	1.06	7.2
HA(1:3/800/3)	2445	1.24	0.08	1.16	0.00	1.16	7.0
HA(1:3/800/4)	2355	1.27	0.08	1.19	0.00	1.19	-
K₂CO₃							
CA(1:3/700/2)	1057	0.48	0.02	0.46	0.31	0.15	-
CA(1:3/800/1)	1169	0.53	0.01	0.52	0.27	0.25	5.4
CA(1:3/800/2)	1455	0.69	0.06	0.64	0.15	0.49	5.5
CA(1:3/800/3)	1900	0.91	0.08	0.83	0.09	0.74	5.6
CA(1:3/800/4)	1920	0.95	0.09	0.86	0.05	0.81	5.6
CA(1:4/800/1)	1195	0.54	0.01	0.53	0.27	0.26	5.0
CA(1:4/800/2)	1446	0.66	0.03	0.63	0.28	0.35	4.5
CA(1:4/800/4)	1672	0.82	0.05	0.77	0.06	0.71	-
Commercial							
CP ^d	907	0.43	0.03	0.40	0.16	0.24	10.3
NS ^d	1065	0.70	0.30	0.40	0.02	0.38	8.4

^a N_2 volume adsorbed at $p/p^0 = 9.95$; ^b $V_{meso} = V_{total} - V_{\alpha total}$; ^c α_s method was applied using as reference the isotherm presented in Rodríguez-Reinoso and Martín-Martínez, 1987, ^dvalues reported in Mestre *et al.*, 2015.

In the case of K_2CO_3 activation, besides the influence of the chemical agent amount and treatment duration, the effect of temperature was also evaluated. Confronting the characteristics of samples CA(1:3/700/2) and CA(1:3/800/2), it is noticeable that the higher temperature, 800 °C, leads to a more pronounced development of porosity (higher A_{BET} and $V_{\alpha total}$), in line with the previous discussion regarding the isotherms configuration. The increase of temperature also results in a different micropore network composition since while in sample CA(1:3/700/2) the narrow microporosity corresponds to 67 % of the total micropore volume, for sample CA(1:3/800/2) this percentage only reaches 23 %.

The influence of the treatment duration was evaluated considering char: K_2CO_3 ratios of 1:3 and 1:4. In any case, longer calcinations favoured the porosity development associated to micropore broadening. However, on the contrary of what was observed for KOH activated samples, the use of K_2CO_3 always allowed the presence of ultramicropores, even though that, in the conditions tested, the relative amount of $V_{\alpha ultra}$ decreases down to 6% of the total micropore volume. This was the expected behaviour considering the different mechanism of KOH and K_2CO_3 activation, that according to the literature (Wang and Kaskel, 2012) are more extensive at different temperature ranges: the reactions of K_2CO_3 with the carbon matrix start at temperatures around 700-800 °C, while in the case of KOH they begin at a much lower temperature, *i.e.*, between 400 and 600 °C.

Somewhat unexpected, the use of a larger amount of K_2CO_3 did not enhance porosity development. This result may be explained considering that when a larger amount of K_2CO_3 is used we are preventing a homogeneous dispersion of the compound within the char matrix, which will result in the formation of clusters. This hypothesis allows

to explain the higher preparation yields observed for the carbons prepared with 1:4 (char: K_2CO_3) ratio, since a fraction of the activating agent would not be in direct contact with the char matrix, and then it cannot react to create porosity. The matrix consumption would then be prevented, resulting in higher preparation yields.

The two commercial carbons, used as benchmark for the liquid phase assays, present a less developed porosity than the lab-made carbons, with lower values of A_{BET} and pore volumes. These samples differ in terms of meso and microporosity being CP an essentially microporous carbon, with similar volumes of ultra and supermicropores, whereas NS has a significant mesopore volume ($0.30 \text{ cm}^3 \text{ g}^{-1}$) and a microporous network composed mainly by wider micropores.

Regarding the surface chemistry, the choice of activating agent seems to have some impact on the nature of the activated carbons. Thus, considering the samples prepared using a 1:3 proportion, at $800 \text{ }^\circ\text{C}$ for 1 to 4 h, it is possible to verify that the activation with KOH leads to the production of samples with a neutral surface chemistry ($\text{pH}_{PZC} \sim 7.0$), while the carbons prepared with K_2CO_3 are more acidic, with pH_{PZC} values of approximately 5.5 units.

In order to further characterize the lab-made materials and to complement the data obtained from N_2 adsorption, CO_2 adsorption at $0 \text{ }^\circ\text{C}$ was made. This characterization method also allows a deeper insight into how the preparation conditions affected the microporosity of the samples. With this objective, a set of samples was selected.

The CO_2 adsorption isotherms are presented in **Figure VII.4** and reveal that all carbons have isotherms type I + IV, suggestive of a wider micropore structure, which is in accordance with the N_2 textural parameters, which show the presence of high volumes of supermicropores in all the materials. Higher CO_2 uptakes are observed for the lab-made carbons.

Material CA(1:3/700/2) isotherm has a subtle rectangular character, which may be attributed to the higher narrow micropore volume ($V_{\alpha \text{ ultra}} = 0.31 \text{ cm}^3 \text{ g}^{-1}$), in comparison to the other carbons. The widening of the microporosity caused by increasing the duration and proportion of K_2CO_3 activation can be assessed with samples CA(1:3/800/1) and CA(1:3/800/2) and CA(1:4/800/1). Regarding the activation with KOH, the effect of this activating agent as well as the duration of treatment on the microporosity was evaluated considering samples HA(1:3/800/1) and HA(1:3/800/2).

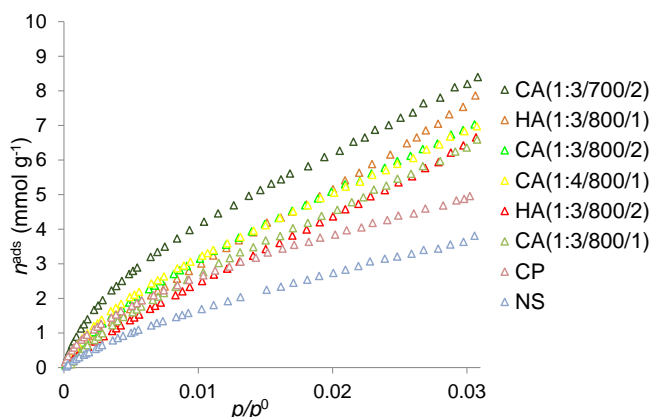


Figure VII.4. CO_2 adsorption isotherms, at $0 \text{ }^\circ\text{C}$, of the lab-made samples and commercial carbons.

When analysing the CO_2 uptake of the lab-made carbons, especially the ones with narrower micropores, a discrepancy between their higher CO_2 uptake and the $V_{\alpha \text{ ultra}}$ values, determined by N_2 adsorption is observed. This can be explained by the fact that

the equilibrium adsorption of N_2 may be more difficult to achieve in microporous samples with narrower micropores. In this sense, CA(1:3/700/2) shows a higher uptake of CO_2 at low and high relative pressures, because even though it presents the lowest value of micropore volume ($V_{\alpha \text{ total}} = 0.46 \text{ cm}^3 \text{ g}^{-1}$), its microporosity is greatly composed by ultramicropores ($V_{\alpha \text{ ultra}} = 0.31 \text{ cm}^3 \text{ g}^{-1}$) which may not be all accessible to N_2 adsorption. The same type of discrepancy is observed for samples HA(1:3/800/1) and HA(1:3/800/2), ($V_{\alpha \text{ total}}$ of 0.88 and $1.06 \text{ cm}^3 \text{ g}^{-1}$, respectively), where the sample with higher volume of narrow micropores, sample HA(1:3/800/1), presents higher CO_2 uptake than the carbon with only supermicropores (HA(1:3/800/1) - $n^{\text{ads}} \approx 8 \text{ mmol g}^{-1}$ vs HA(1:3/800/2) - $n^{\text{ads}} \approx 7 \text{ mmol g}^{-1}$). Still, these results support the conclusions made by N_2 adsorption, showing that the increase of the activation time causes the widening of the microporosity.

The micropore size distributions of the carbons (**Figure VII.5 (a) and (b)**) reveal that all the samples present bimodal distributions in accordance with the analysis of the N_2 adsorption data that revealed the presence of both narrow and wider micropores. The maximum in the region of narrow micropores is centered at 0.52 nm for KOH treated samples, and 0.60 nm for K_2CO_3 activated samples. In the case of carbons CP and NS the maximum is centred at, respectively, 0.60 and 0.70 nm.

The severe activation conditions related with KOH use, led to solids with a wide microporosity, that is, with higher supermicropore volumes in comparison to that of ultramicropores.

The carbonate activated carbons, with exception of CA(1:3/800/2), have narrow micropores with widths between 0.43 and 0.78 nm and supermicropores wider than 1.30 nm. The sample CA(1:3/800/2) has a slightly broader pore size distribution with ultra and supermicropores with diameters values up to 0.87 nm and higher than 1.13 nm, respectively.

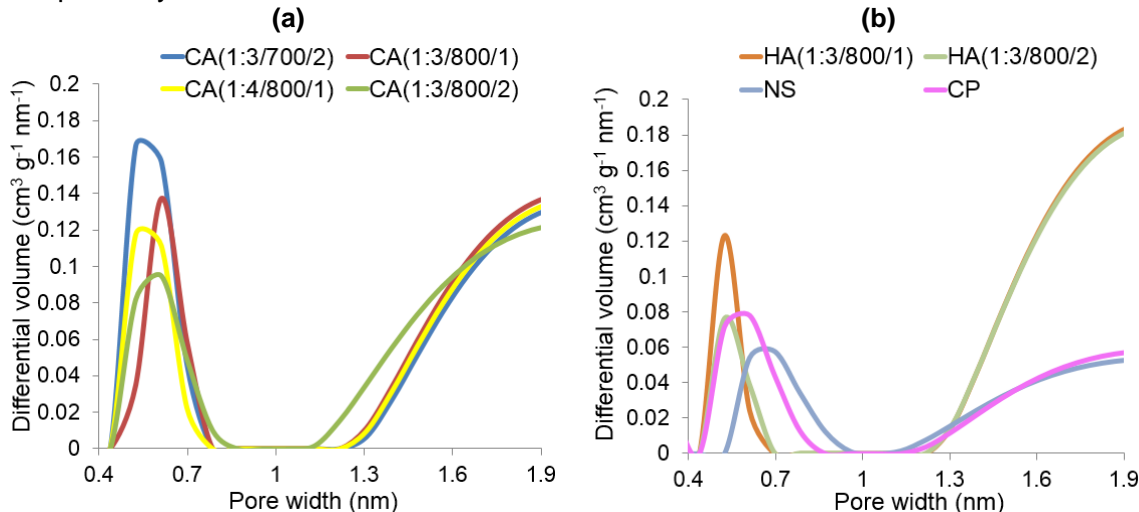


Figure VII.5. Micropore size distribution, obtained from the CO_2 adsorption data, of the (a) K_2CO_3 activated carbons and (b) KOH activated and commercial carbons.

The increase of temperature to 800 °C caused the widening of CA(1:3/700/1) micropores (decrease of $V_{\alpha \text{ ultra}}$ and increase of $V_{\alpha \text{ super}}$). Activation treatments of 2 h also caused the widening of the micropore network of K_2CO_3 and KOH activated solids.

Commercial carbons have smaller micropore volumes than the lab-made carbons.

The pH_{PZC} values of lab-made samples (**Table VIII.4**) seem to indicate that the choice of activating agent have impact on the surface chemistry properties of the carbons. KOH activation led to neutral or slightly acid carbons whereas samples activated with K_2CO_3

present more acidic nature with pH_{PZC} values around 5.5 units. Both commercial carbons are basic, with pH_{PZC} values of 10.3 and 8.4 for CP and NS, respectively.

The morphology of the biochar used as precursor, and samples CA(1:3/800/1) and HA(1:3/800/1) was studied by scanning electron microscopy (SEM). The micrographs presented in **Figure VII.6** allow to shed light on the impact of the activation conditions on the morphology of the carbons.

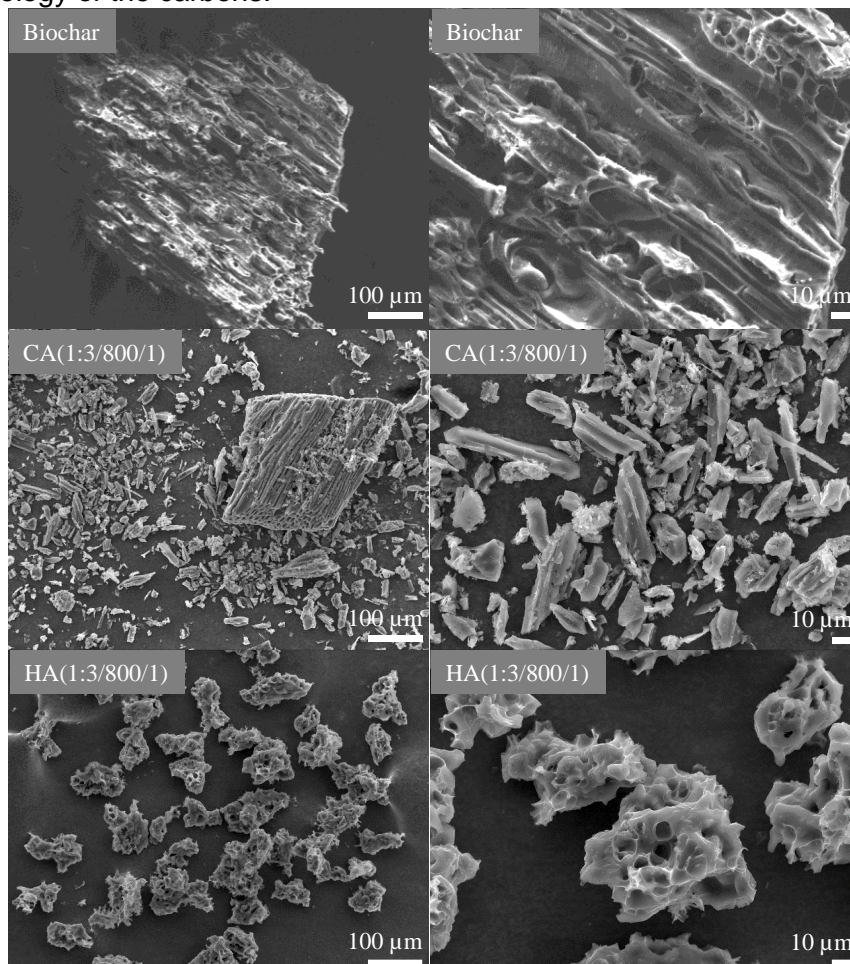


Figure VII.6. SEM micrographs of the mentioned carbons.

The biochar micrographs reveal the characteristic features of a wood-derived material (Zhang and Zhang, 2014), *i.e.*, elongated fibrous shape particles, with a capillary structure and pores which are observed in more detail in the higher amplification micrograph (image on the right side). As expected, the K_2CO_3 activation allowed to maintain some of the morphological characteristics of the precursor, which are especially evident in the larger particles. From the less magnified image of sample CA(1:3/800/1) it is also possible to conclude about the particle size heterogeneity resulting from this activation process. Activation with KOH caused a much more extensive destruction of the biochar structure, leading to a more homogeneous particle size distribution. The particles have rounded shape and present a completely different topography in comparison to the precursor. The EDS analysis revealed that no potassium remaining from the activation procedure was detected in the carbons since only C and O could be quantified.

VII.2.3. Lab-made carbons as adsorbents for atenolol

As a proof of concept four lab-made samples were tested as adsorbents of a pharmaceutical compound - atenolol - through kinetic and equilibrium assays. For comparison purposes, commercial carbons CP and NS were studied in parallel.

The kinetic curves (**Figure VIII.7**) show that the concentration of atenolol in solution presents a marked decay in the first 30 min of contact time, after which the adsorption continues slowly until equilibrium is attained, at 6 h. The experimental points corresponding to 24 h of contact time (data not shown) proved that, in fact, after 6h the equilibrium was attained.

The kinetic data suggest better performances by the lab-made carbons in comparison to the commercial adsorbents, especially in the case of samples CA(1:3/800/2), HA(1:3/800/1) and HA(1:3/800/2). These results are considered highly positive taking into account the high solubility of atenolol in water at 30 °C (17.9 g dm⁻³), that is, the high affinity of the compound towards its solvent.

So, the high removal values achieved suggest a high affinity of atenolol towards the materials, independent of the basic/acidic nature of the carbons, which was able to counterbalance the affinity of the pollutant towards the water.

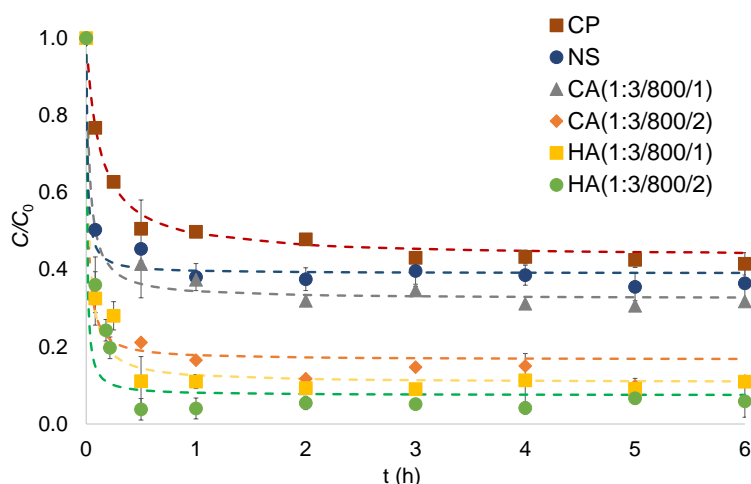


Figure VII.7. Kinetic results for the adsorption of atenolol in the mentioned carbons, at 30 °C. Symbols correspond to experimental data and lines represent the fitting to the pseudo-second order kinetic equation (6 mg of carbon/20 cm³ of pollutant solution 120 mg dm⁻³). Error bars are also included.

The kinetic data were fitted to the pseudo-first and pseudo-second order kinetic models (Ho, 2006). The pseudo-second order model leads to better fittings of the experimental results, as demonstrated by the high R² values quoted in **Table VII.5**. The good adjust of the data to this model is also confirmed comparing the calculated and experimental uptake values ($q_{e \text{ calc}}$ and $q_{e \text{ exp}}$, respectively). The initial adsorption rate, h , and half-life time, $t_{1/2}$, values quoted in **Table VII.5** show that the performance of the lab-made carbons compares favourably with that of the best commercial sample tested, that is, carbon NS.

Table VII.5. Pseudo-second order parameters for atenolol adsorption onto the studied samples at 30 °C: k_2 is the pseudo-second order rate constant; h is the initial adsorption rate; $t_{1/2}$ is the half-life time; $q_{e \text{ calc}}$, $q_{e \text{ exp}}$ and $C_{e \text{ calc}}$ are, respectively, the pharmaceutical compounds uptake and that remaining in solution at equilibrium, both calculated by the pseudo-second order kinetic model.

	$k_2 \times 10^{-4}$ ($\text{g mg}^{-1}\text{min}^{-1}$)	h ($\text{mg g}^{-1}\text{min}^{-1}$)	$t_{1/2}$ (min)	$q_{e \text{ calc}}$ (mg g^{-1})	$q_{e \text{ exp}}$ (mg g^{-1})	$C_{e \text{ calc}}$ (mg dm^{-3})	Re(%)	R^2
CP	5	26	9	227	237	52	57	0.996
NS	60	357	0.7	244	251	47	61	0.999
CA(1:3/800/1)	20	149	1.8	271	272	39	68	0.991
CA(1:3/800/2)	35	385	0.9	350	375	20	83	0.999
HA(1:3/800/1)	21	270	1.3	357	363	13	89	0.999
HA(1:3/800/2)	61	833	0.4	370	374	9	93	0.999

Considering the textural characteristics of the samples we have to conclude that in the case of atenolol, and as it was already observed for other small molecules (Galhetas *et al.*, 2014a and 2014b; Batista *et al.*, 2016), the presence of a developed mesoporosity is not the determinant factor that controls the adsorption kinetics. Actually, the behaviour of carbon NS, the only sample in this set presenting a significant mesopore volume ($V_{\text{meso}} = 0.30 \text{ g cm}^{-3}$), is not different from those of other carbons that have much smaller, or even almost absent, mesoporosity. In previous studies, this behaviour was justified considering that once the materials have a considerable volume of larger micropores, the diffusion of, for example caffeine, that has a critical dimension of 0.45 nm (Galhetas *et al.*, 2014b), towards the adsorption active site is ruled by this type of porosity. To verify if this hypothesis is also correct in the case of atenolol, the molecular dimensions of this compound were estimated within the collaboration with Doctor Machuqueiro of the Inorganic and Theoretical Group of CQB. Atenolol molecular structure and dimensions are presented in **Figure VII.8**, together with the pKa value.

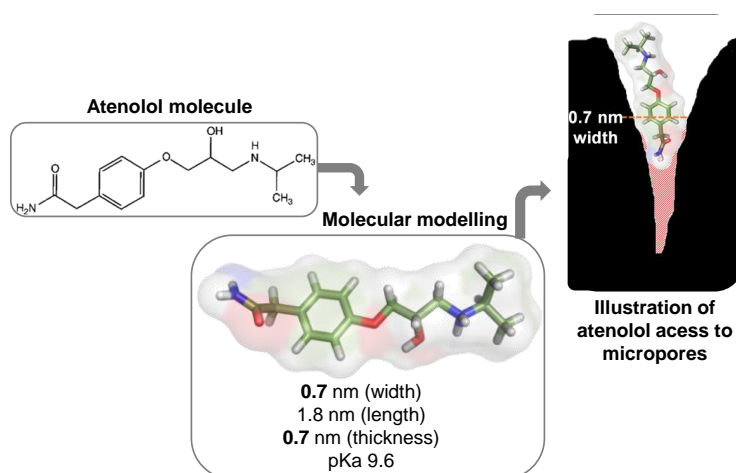


Figure VII.8. Molecular structure of atenolol species and corresponding dimensions (critical dimension highlighted in bold), and pKa value. Illustration of atenolol access to the micropores.

The results obtained show that the critical dimension of atenolol is 0.7 nm thus, no hindrance for its diffusion in the larger microporosity could be expected.

In the conditions used to make the kinetic assays all the carbons attained removal efficiencies higher than around 60 %. However it must be noted that the highest removals were obtained with synthesized samples that, with the exception of sample CA(1:3/800/1), reached values around 90 %.

The equilibrium adsorption isotherms of atenolol, displayed in **Figure VII.9**, show a very steep initial rise up to adsorbed amounts ranging from 100 to 300 mg dm⁻³. These features reveal a high affinity of the molecule towards the surface of the carbons, and allow to classify the isotherms as L-type curves (Giles *et al.*, 1974a; Lyklema, 1995). The initial knee is followed, in the majority of the cases, by a horizontal plateau for C_e values higher than 40 – 60 mg dm⁻³. In the case of samples activated with KOH this plateau is less defined resembling this part of the curves to a Freundlich isotherm.

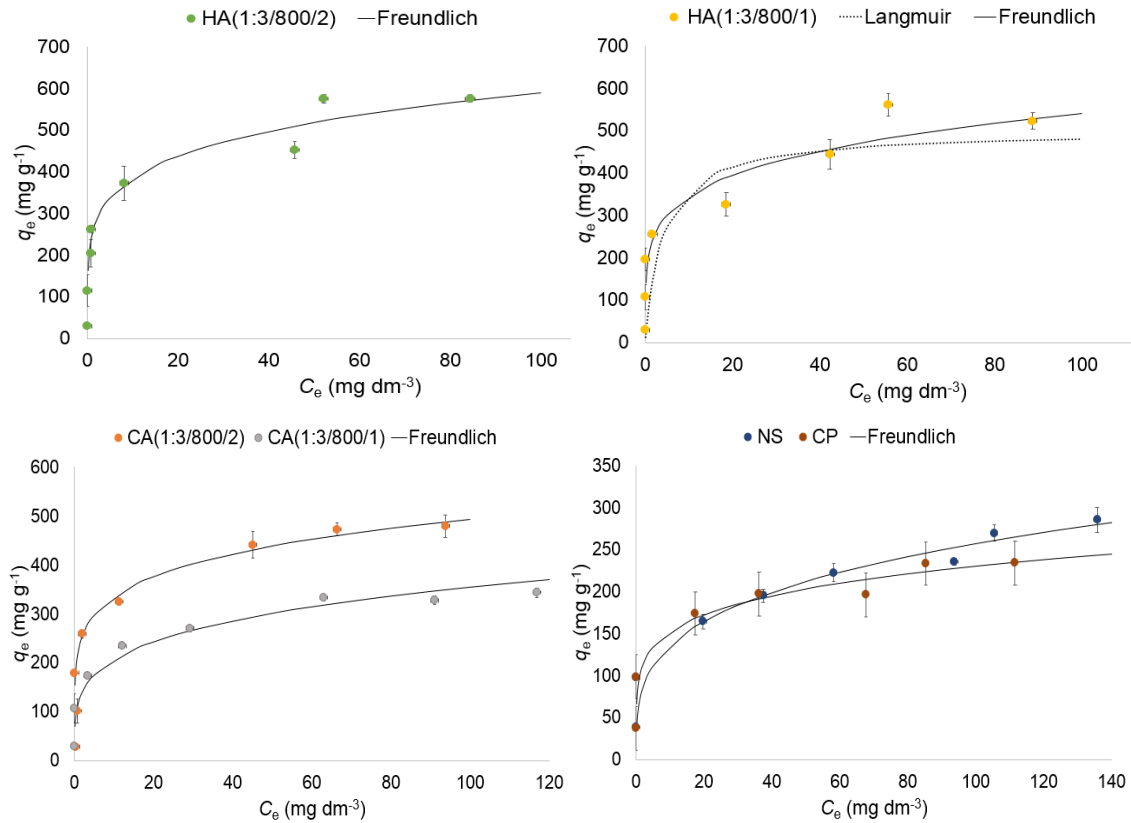


Figure VII.9. Atenolol adsorption isotherms of the mentioned carbons, at 30 °C. Symbols correspond to the experimental data, whereas lines represent the fitting to Langmuir and Freundlich models. Error bars are included.

The equilibrium data was fitted to the linear forms of Langmuir (Langmuir, 1918) and Freundlich (Freundlich, 1918) models and the resulting parameters, as well as the corresponding determination coefficients, R², and non-linear chi-square analysis, χ^2 , are presented in **Table VII.6**.

Table VII.6. Fitting parameters of atenolol equilibrium data to the Langmuir and Freundlich models, coefficient of determination, R², and chi-square test analysis, χ^2 .

	Langmuir				Freundlich			
	q _m (mg g ⁻¹)	K _L (dm ³ mg ⁻¹)	R ²	χ^2	1/n	K _F (mg ^{1-1/n} (dm ³) ^{1/n} g ⁻¹)	R ²	χ^2
CA(1:3/800/1)	344.8	0.319	0.996	11.5	0.077	212.3	0.813	30.3
CA(1:3/800/2)	500.0	0.238	0.998	10.7	0.176	208.4	0.692	55.9
HA(1:3/800/1)	526.3	0.404	0.979	63.2	0.077	324.4	0.719	76.8
HA(1:3/800/2)	555.6	0.529	0.984	41.1	0.125	290.6	0.859	52.4
NS	285.7	0.116	0.973	18.4	0.076	165.9	0.843	13.2
CP	243.9	0.202	0.988	7.41	0.073	157.8	0.842	7.20

In line with the analysis of the isotherms configuration, a better fitting of Langmuir model were obtained with higher values of the correlation coefficient, R^2 , and smaller or identical χ^2 values of those obtained for the adjust of Freundlich equation. As expected, the highest χ^2 values were obtained for the KOH activated carbons since, in this case, the initial part of the isotherms is clearly a Langmuir curve but no horizontal plateau is defined for higher equilibrium concentrations.

The values of the monolayer adsorption capacities, q_m , follow the trend HA(1:3/800/2) > HA(1:3/800/1) > CA(1:3/800/2) > CA(1:3/800/1) > NS > CP. Considering that, as previously discussed, the critical dimension of atenolol (0.7 nm) prevents its access to the narrow microporosity it can only be retained in the supermicropores. In fact, the values of $V_{\alpha \text{ super}}$, assessed from N_2 adsorption, present practically the same tendency. The exception is sample CA(1:3/800/1) that should present a lower monolayer capacity than sample NS with a $V_{\alpha \text{ super}}$ of $0.38 \text{ cm}^3 \text{ g}^{-1}$, in comparison to $0.25 \text{ cm}^3 \text{ g}^{-1}$ of the lab-made sample. These results point out that texture by itself does not explain all the results obtained, demonstrating that the surface chemistry must have an impact on atenolol adsorption process.

Actually, in solution, atenolol molecule (pKa 9.6) will have a positive charge due to the protonation of the amine group, resulting in the increase of the amount of OH^- species in solution, causing the solution pH to be basic (pH 8.2). On the other hand, having NS a pH_{PZC} of 8.4, its net surface charge will be neutral, but CA(1:3/800/1), with a pH_{PZC} of 5.5, will present a negative net surface charge. Thus, in the case of NS the texture should be a key factor ruling the adsorption process, whereas in sample CA(1:3/800/1) the high density of surface negatively charge will also favour the interaction with atenolol molecule. The importance of the contribution of the carbon's surface chemistry to the adsorptive properties of the materials is highlighted when considering that CA(1:3/800/2) has a comparable performance to the KOH activated carbons, with more than double of its $V_{\alpha \text{ super}}$. These results support the conclusion that, even though the surface chemistry of the KOH activated samples favours the interaction with atenolol, their higher pH_{PZC} (between 6 and 7), is enough to affect their adsorption capacity. This observation is further validated by the similar results obtained with KOH activated samples, with different supermicropore volumes.

VII.2.4. Atenolol thermal desorption

Thermal desorption experiments allowed to study the pollutant desorption from the adsorbents and so indirectly to understand the type of interactions established between adsorbate and adsorbent. This study was performed by thermogravimetric analysis of the atenolol-exhausted carbons, under different heating rates (5, 10 and 20 K min^{-1}). The thermal decomposition of atenolol and degradation of the pristine materials was also assessed, at a heating treatment rate of 20 K min^{-1} . For purposes of calculations temperature will be expressed in Kelvin (K).

Thermal degradation of atenolol and that of the pristine adsorbents, at the highest heating rate (20 K min^{-1}), was studied by thermogravimetric analysis (**Figure VII.10**, **Figure VII.11** and **Table VII.7**).

Atenolol seems to be easily degraded by temperature, losing around 85 % of its initial mass, as shown by its TG curve (**Figure VII.10 (a)** and **Table VII.7**).

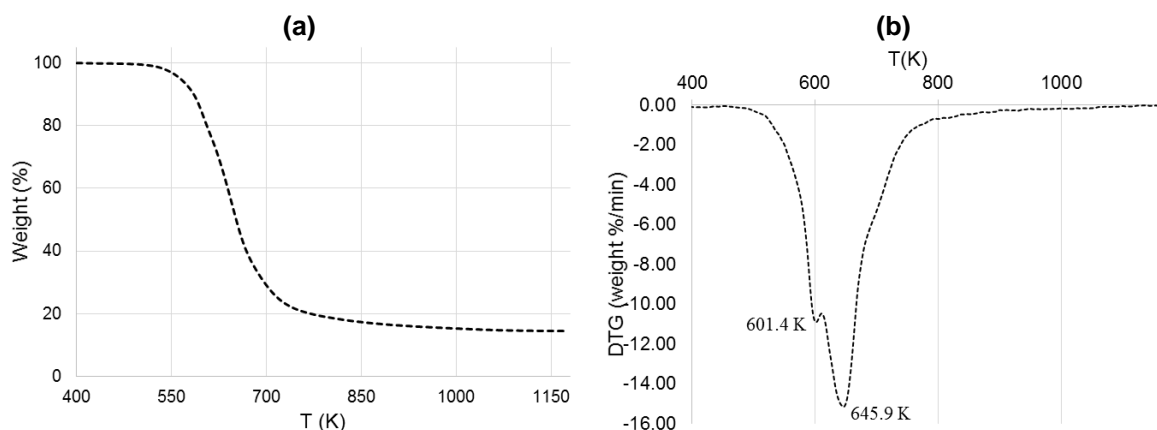


Figure VII.10. (a) Thermogram of atenolol and (b) corresponding DTG curve.

The decomposition seems to occur at two specific temperatures, 601.4 and 645.9 K, leading to marked weight loss peaks in its DTG curve (**Figure VII.10(b)**). Considering the known polymorphism of several pharmaceutical compounds (Lee, 2014) and specifically, the reported existence of atenolol as a racemic mixture (de Castro *et al.*, 2007), atenolol reagent was analysed by X-ray diffraction spectroscopy and the diffractogram was confronted with the published data. The analysis confirmed the existence of atenolol's two forms and the thermogravimetric analysis was made taking this into account. In fact, the results obtained seem to support the existence of two forms of atenolol in the solid state. The prominent polymorph seems to be the most thermally stable, as pointed out by a higher mass loss at 645.9 K.

The pristine materials present low thermal degradation retaining between 72 and 93 % of their initial mass (TG curves in **Figure VII.11** and final weight values in **Table VII.7**).

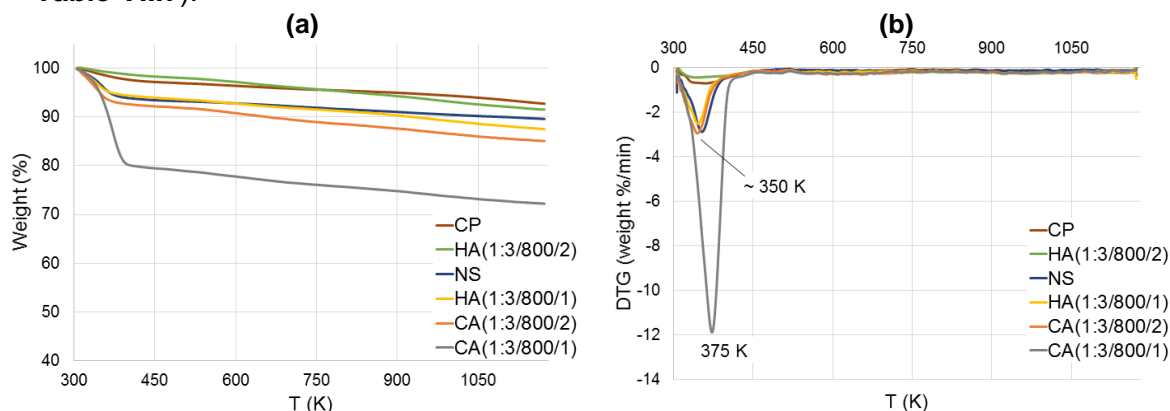


Figure VII.11. (a) Thermograms of the pristine adsorbents and (b) corresponding DTG curves.

The carbons less tolerant to temperature were the K_2CO_3 activated carbons which can be attributed to the higher acidic character of these samples, in comparison to the KOH activated and commercial carbons (neutral and basic nature, respectively).

As expected, the exhausted samples (**Figure VII.12**) present higher weight losses than the pristine materials. Comparing the final masses of fresh and spent materials, higher 20 to 35 % weight decays are observed for the latter (see values corresponding to the assays made with 20 K min^{-1} rate in **Table VII.7**).

Table VII.7. Percentage of final weight (W_{final}) of atenolol and pristine carbons (assays at 20 K min^{-1}).

	W_{final} (%)
Atenolol	14.4
CA(1:3/800/1)	72.2
CA(1:3/800/2)	85.1
HA(1:3/800/1)	87.5
HA(1:3/800/2)	91.5
CP	92.8
NS	89.6

In accordance with the classical temperature programmed desorption theory (Redhead, 1962; Cvetanovic and Amenomiya, 1967), the increase of the heating rate causes higher weight losses and a shift of the DTG profiles to higher temperatures. This shift is interpreted considering that, at higher heating temperatures, the decomposition/desorption occurs at higher temperature, due to the fact that the heat transfer is not as effective as it is when lower heating rates are used. For this reason, the DTG profiles of the spent carbons will be analysed considering the curves obtained at the intermediate heating rate of 10 K min^{-1} , with lower limitations of heat transfer inside the samples and adequate definition for the interpretation of the results.

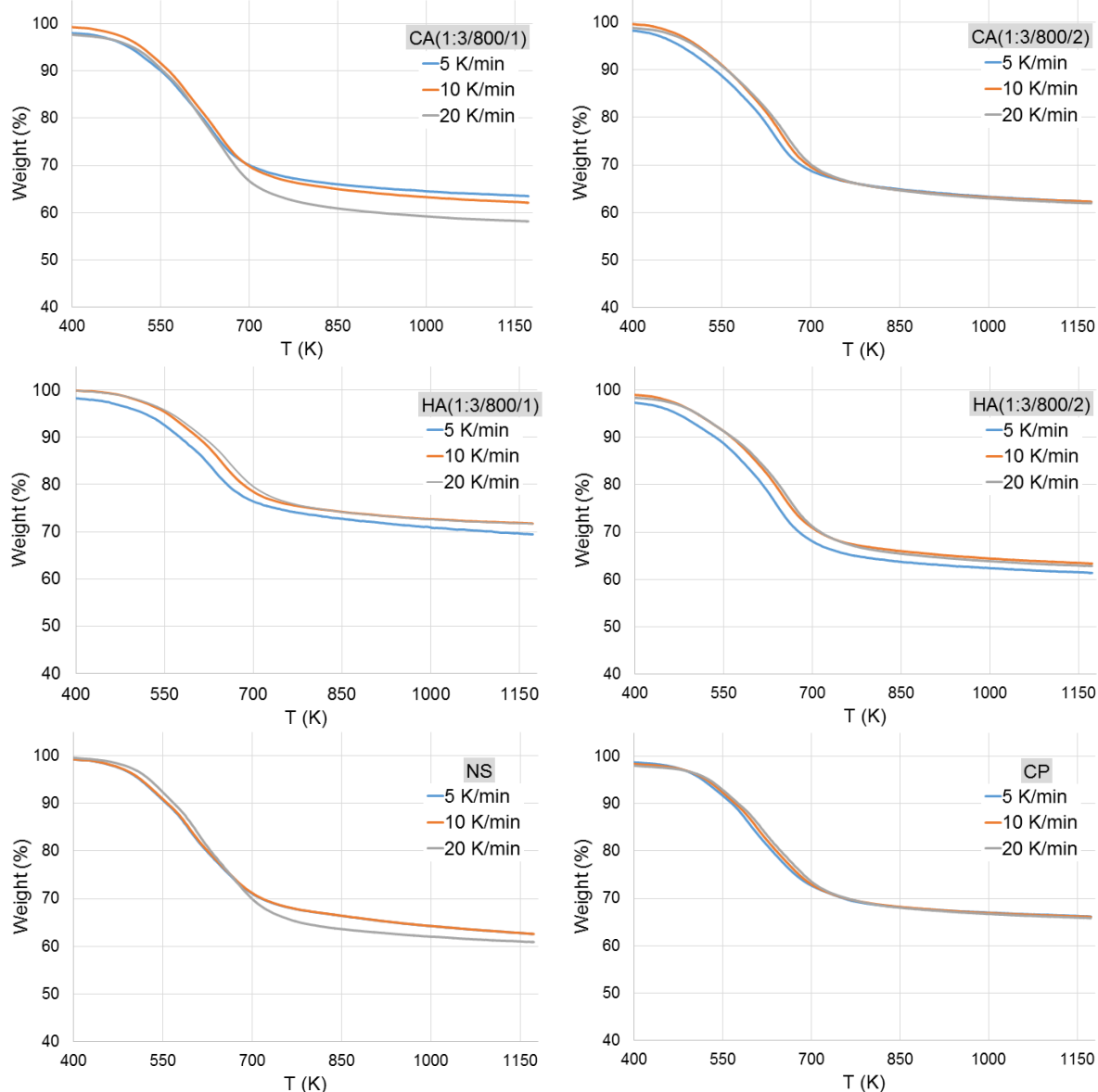


Figure VII.12. Thermograms of the atenolol-exhausted adsorbents, at 5, 10 and 20 K min^{-1} .

The DTG curves, shown in **Figure VII.13**, confirm these findings showing an initial subtle peak of desorption/decomposition, followed by two more prominent weight losses at higher temperature. In all the samples, accentuated weight losses occur in three temperature ranges, 539 – 556 K, 591-609 K and 641-655 K, presented in **Table VII.8** as peak I, II and III, respectively.

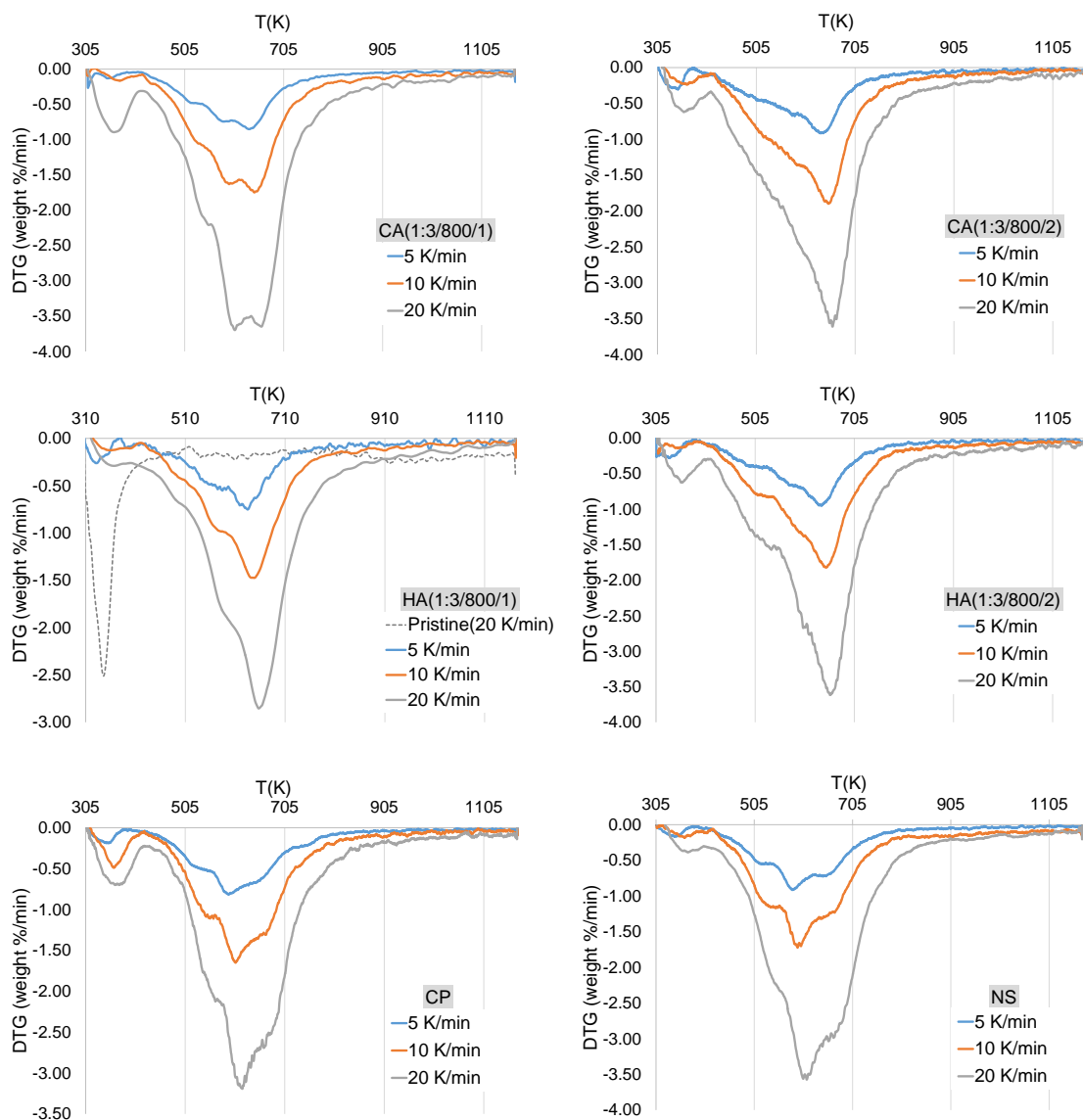


Figure VII.13. DTG profiles of the pristine and atenolol-exhausted carbons at heating rates of 5, 10 and 20 K min⁻¹.

The first mass loss peak, in the lowest temperature range and less distinctive, can be caused by desorption of atenolol molecules weakly adsorbed onto the surface of the activated carbon materials. The two other peaks can be attributed to atenolol thermal decomposition. When atenolol is adsorbed onto activated carbon surface its thermal decomposition, in some cases, occurs at temperatures slightly higher in comparison to pure atenolol thermal decomposition. Such effect is partially explained with slower heat transfer toward active sites of adsorption (*i.e.* inside pores) of the activated carbons. In the case of the lab-made carbons atenolol's decomposition profile seems to be maintained, whereas when the basic commercial samples are used, an inverted profile is observed. It seems that, with exception of sample CA(1:3/1073/1), in the lab-made

materials (with acidic and neutral pH_{PZC} values) the adsorption of the more stable form of atenolol is favoured, whereas in CP and NS (basic carbons) is the less stable form that is predominantly adsorbed. Sample CA(1:3/1073/1) has a clearly different DTG profile, which demonstrates that it has distinct surface adsorption properties allowing it to interact with both atenolol species which may explain the unexpected high adsorption capacity presented by this sample, as discussed in the previous section. These findings clearly demonstrate that the surface chemistry of the carbons interacts differently with the two forms of atenolol and, consequently determines which of the two possible species will be predominantly adsorbed.

Table VII.8. Percentage of final weight (W_{final}) of atenolol-exhausted carbons and corresponding DTG peaks. Heating rates (β) of 5, 10 and 20 $K\ min^{-1}$.

	β ($K\ min^{-1}$)	W_{final} (%)	T(K)		
			Peak I	Peak II	Peak III
CA(1:3/800/1)	5	64	525	585	636
	10	62	539	597	645
	20	58	550	609	660
CA(1:3/800/2)	5	62	520	583	635
	10	62	529	597	650
	20	62	546	607	659
HA(1:3/800/1)	5	69	514	583	632
	10	72	529	592	646
	20	72	537	608	658
HA(1:3/800/2)	5	61	516	584	634
	10	63	530	602	648
	20	62	541	611	659
CP	5	66	541	593	640
	10	66	557	606	655
	20	66	568	623	665
NS	5	62	531	585	631
	10	63	546	596	641
	20	61	558	613	654

The desorption activation energy, E_{des} , and the pre-exponential Arrhenius factor, A , can be calculated from the DTG maximum peak temperature, T , at a heating rate β , according to a first-order desorption process given by the linear equation:

$$\ln\left(\frac{T^2}{\beta}\right) = \frac{E_{des}}{R}\left(\frac{1}{T}\right) + \ln\left(\frac{E_{des}}{AR}\right) \quad \text{Equation VII.1}$$

From the first-order atenolol desorption parameters, given in **Table VII.9**, relatively low E_{des} and A values are calculated for peak I desorption process. These E_{des} and A values are similar for all investigated materials, supporting the conclusion that, at this temperature range, the release of weakly adsorbed atenolol species occurs. Contrary, E_{des} and A values determined for peaks II and III clearly distinguish the materials. As expected, stronger interactions of atenolol with the acidic K_2CO_3 -activated carbons are demonstrated through higher E_{des} and A values, compared to the neutral KOH-activated materials and the basic commercial solids.

Table VII.9. Activation energy of desorption, E_{des} , pre-exponential factor, A , and correspondent correlation coefficients, R^2 .

	E_{des} (kJ mol ⁻¹)	A (s ⁻¹)	R^2
CA(1:3/800/1)			
Peak I	121.9	3.5×10^8	0.9889
Peak II	161.3	7.1×10^{10}	0.9996
Peak III	189.2	1.0×10^{12}	0.9857
CA(1:3/800/2)			
Peak I	118.2	2.1×10^8	0.9683
Peak II	161.0	7.1×10^{10}	0.9927
Peak III	192.2	1.0×10^{12}	0.9800
HA(1:3/800/1)			
Peak I	123.4	9.2×10^8	0.9551
Peak II	147.0	4.3×10^9	0.9751
Peak III	177.0	1.2×10^{11}	0.9980
HA(1:3/800/2)			
Peak I	118.6	2.6×10^8	0.9931
Peak II	135.7	3.1×10^8	0.9548
Peak III	185.2	4.8×10^{11}	0.9974
CP			
Peak I	121.6	1.3×10^8	0.9909
Peak II	129.2	5.4×10^7	0.9973
Peak III	175.9	5.8×10^{10}	0.9759
NS			
Peak I	116.0	6.2×10^7	0.9878
Peak II	134.4	2.5×10^8	0.9901
Peak III	191.3	2.1×10^{12}	0.9981

VII.2.5. Adsorption of tiamulin hydrogen fumarate

The potential of the materials as adsorbents for the veterinary antibiotic tiamulin hydrogen fumarate (designated THF) was evaluated through kinetic and equilibrium adsorption studies in liquid phase. Due to the dual composition of this pharmaceutical (tiamulin + hydrogen fumarate), the role of the fumaric acid component in the adsorption of THF started to be investigated. In this sense, kinetic assays on carbons CA(1:3/800/2) and HA(1:3/800/2) were already performed, as well as, equilibrium studies in all the materials. It must be stressed that in this topic some experimental work is still needed, as well as, a deeper analysis of the data. One opted to present the results already obtained since, even brief analysis allows to withdraw some interesting conclusions regarding the influence of the texture.

Kinetic adsorption

The kinetic experiments performed with fumaric acid (**Figure VII.14 (a)**) reveal that this compound was almost equally removed by both materials, which were able to adsorb around 35 % of the initial concentration present in solution. All the kinetic curves are practically coincident and reveal a fast decrease of C/C_0 in the first 30 min, after which adsorption equilibrium is reached after 4 h (confirmed after 17 h of contact time).

Concerning tiamulin hydrogen fumarate, a clear distinction between the solids is observed (**Figure VII.14 (b)**). The materials adsorbed between 20 % (CP) and 50 % (NS) of THF initial concentration. The curves show a similar profile to those of FA, with a marked decay in C/C_0 values in the first 30 min, with equilibrium being reached after 4 h of contact time. Once again, such as, in the case of fumaric acid no major impact of the carbons surface chemistry seems to be observed (basic carbons CP and NS presenting the highest and lowest C/C_0 values, respectively).

Comparing the data of CA(1:3/800/2) and HA(1:3/800/2) for FA and THF adsorption, in kinetic conditions, a similar C/C_0 decay of, approximately 35 %, was achieved with CA(1:3/800/2) carbon, while in the case of HA(1:3/800/2) a higher decay for THF (50 %) was achieved.

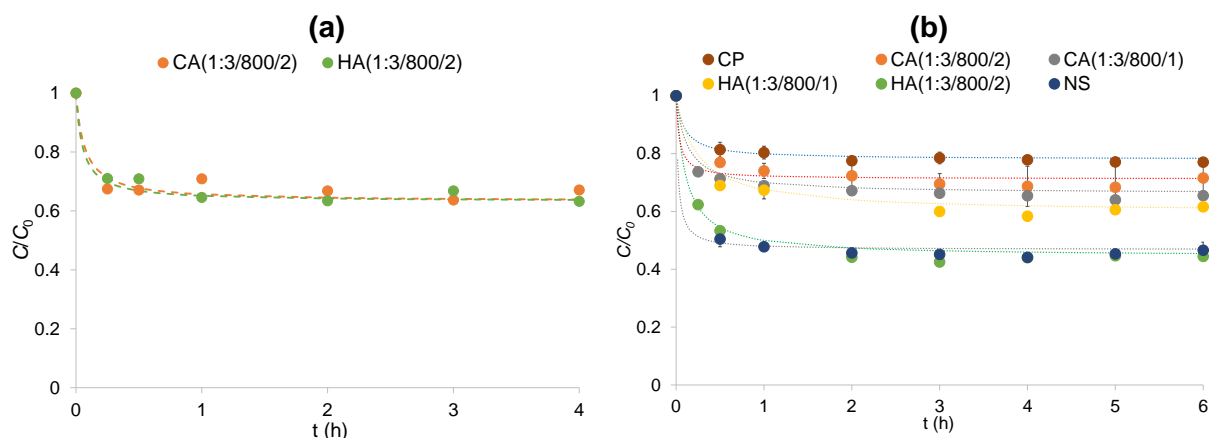


Figure VII.14. Kinetic results for the adsorption of (a) fumaric acid and (b) tiamulin hydrogen fumarate in the mentioned carbons, at 30 °C. Symbols correspond to experimental data and lines represent the fitting to the pseudo-second order kinetic equation (6 mg of carbon/20 cm³ of pollutant solution 120 mg dm⁻³). Error bars are included.

The experimental data was fitted to the pseudo-first and second kinetic order models. Such as occurred in the case of atenolol better fittings were obtained for the pseudo-second order kinetic equation (higher R² and similar $q_{e\text{ calc}}$ and $q_{e\text{ exp}}$ values) (Table VII.10).

Regarding FA kinetic parameters, they confirm the decays observed in the curves analysis, with Re(%) values of 36 %, and q_e values of 143 mg g⁻¹. Results show kinetic parameters quite similar although the samples have different porous characteristics, namely different $V_{\alpha\text{ super}}$. This suggests that, as was previously reported for caffeine molecule, also in the case of fumaric acid no hindrance to diffusion in the wide micropore network is observed. Considering the similar kinetic parameters obtained for the acidic (CA(1:3/800/2)) and neutral (HA(1:3/800/2)) samples, we can admit that the surface chemistry of the solids does not have a great impact on the adsorption process. This may be attributed to the low solubility of fumaric acid in water, around 500 mg dm⁻³ at 27 °C (Ortiz *et al.*, 2017), which favours the adsorption by the carbons.

Different adsorptive behaviours are observed in the case of THF adsorption, in terms of process rate and q_e values achieved. The solids adsorbed between 20 % (CP) and 54 % (HA(1:3/800/2)) of THF initial concentration, corresponding to q_e values between approximately 81 and 219 mg g⁻¹.

Table VII.10. Pseudo-second order parameters for fumaric acid tiamulin hydrogen fumarate adsorption onto the studied samples at 30 °C: k_2 is the pseudo-second order rate constant; h is the initial adsorption rate; $t_{1/2}$ is the half-life time; $q_{e\text{ calc}}$, $q_{e\text{ exp}}$ and $C_{e\text{ calc}}$ are, respectively, the pharmaceutical compounds uptake and that remaining in solution at equilibrium, both calculated by the pseudo-second order kinetic model.

	$k_2 \times 10^{-4}$ (g mg ⁻¹ min ⁻¹)	h (mg g ⁻¹ min ⁻¹)	$t_{1/2}$ (min)	$q_{e\text{ calc}}$ (mg g ⁻¹)	$q_{e\text{ exp}}$ (mg g ⁻¹)	$C_{e\text{ calc}}$ (mg dm ⁻³)	Re(%)	R ²
FA								
CA(1:3/800/2)	22	46	3	145	143	76	36	0.996
HA(1:3/800/2)	16	45	3	147	143	76	36	0.995
THF								
CP	28	18	5	79	81	97	20	0.999
NS	82	303	0.6	192	198	62	48	0.999
CA(1:3/800/1)	12	22	6	133	133	80	33	0.999
CA(1:3/800/2)	11	16	8	121	121	84	30	0.998
HA(1:3/800/1)	5	12	13	156	158	73	39	0.996
HA(1:3/800/2)	23	110	2	217	219	55	54	0.999

The higher h values obtained for samples NS and HA(1:3/800/2) point out that the presence of a developed mesopore network allied with a high supermicropore volume may play an important role in the adsorption rate of THF. This association is illustrated in **Figure VII.15** which shows that, in the materials with almost no mesopores, the volume of supermicropores does not have a direct impact on the adsorption rate. For example, considering that sample CA(1:3/800/2), has twice of the supermicropores volume of samples CP and CA(1:3/800/1) does not show an increase in h values. The same is observed when comparing CA(1:3/800/2) and HA(1:3/800/1). The only considerable increase in initial adsorption is observed for sample HA(1:3/800/2), with higher meso and supermicropores volumes. NS carbon stands out because it has a supermicropores of only $0.38 \text{ cm}^3 \text{ g}^{-1}$ but presents a very developed mesopore network ($V_{\text{meso}} = 0.30 \text{ cm}^3 \text{ g}^{-1}$), which, as expected as a major impact on the h parameter values.

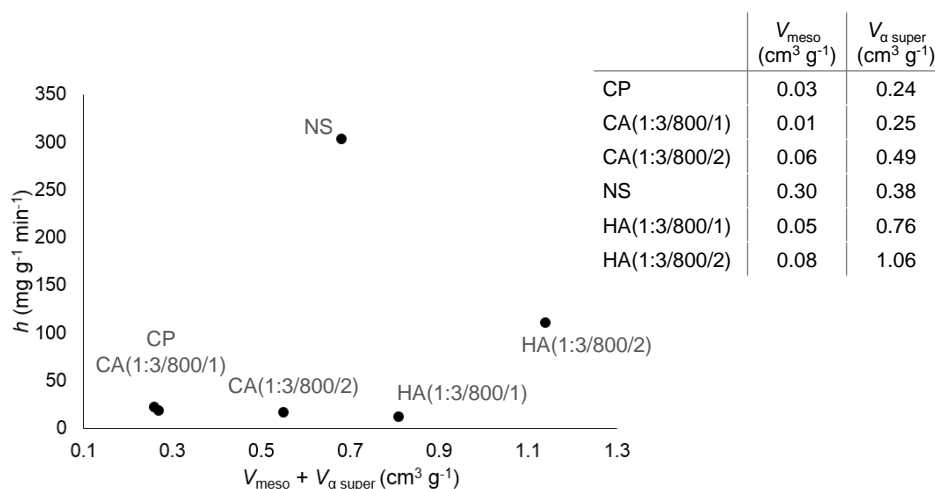


Figure VII.15. Correlation between the initial adsorption velocity, h , and the sum of the meso and supermicropores volumes of the mentioned carbons. The V_{meso} and $V_{\alpha \text{ super}}$ values obtained by N_2 adsorption at $196 \text{ }^\circ\text{C}$ (see **Table VI.3**) are also presented.

Because no direct correlation between h values and $V_{\alpha \text{ super}}$ was observed, a deeper analysis of these results may require the assessment of tiamulin hydrogen fumarate species critical dimensions.

Tiamulin is a large molecule presenting a critical dimension of 1.9 or 1.2 nm, (see **Figure VII.16**) depending on how its adsorption occurs on the micropores. This scenario suggests no access to the ultramicropores, and to a fraction of the wider micropores.

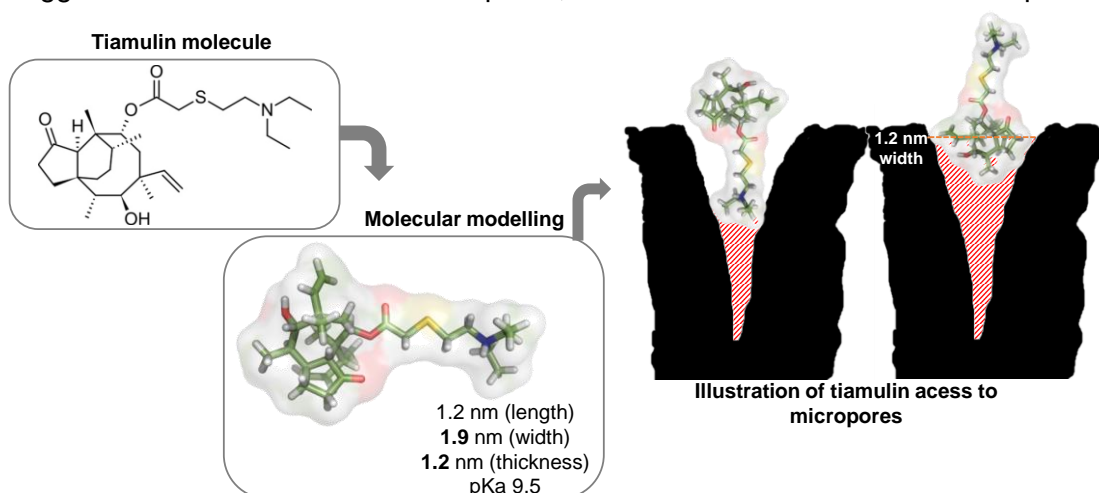


Figure VII.16. Molecular structure of tiamulin and corresponding dimensions (critical dimension highlighted in bold), and pKa value. Illustration of tiamulin access to the micropores.

The significantly higher dimension of this species, as well as its critical dimension justify the major impact of a developed mesopore network, as well as the presence of supermicropores wider than 1.2 nm.

Comparing the kinetic data of THF adsorption with that obtained for atenolol, in the previous topic, very different results were obtained (see **Figure VII.17**).

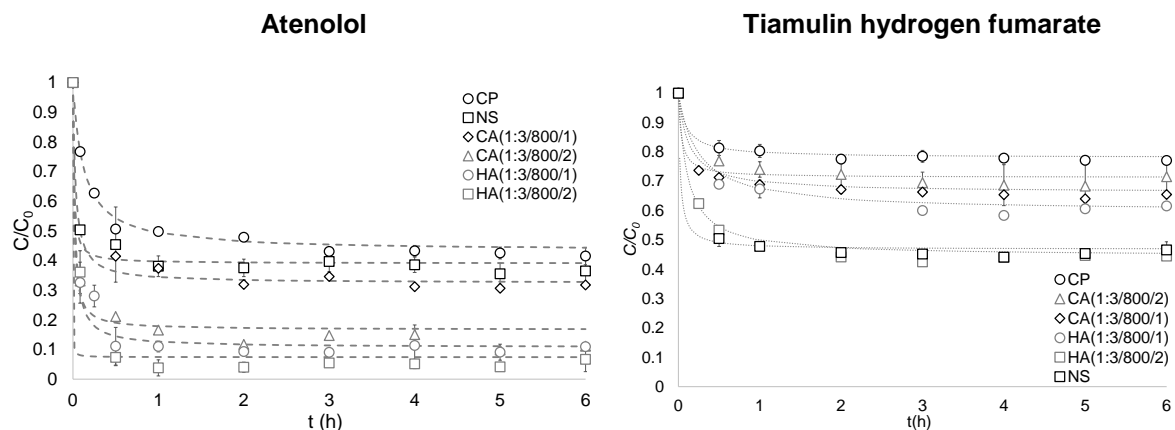


Figure VII.17. Kinetic results for the adsorption of atenolol and tiamulin hydrogen fumarate in the mentioned carbons, at 30 °C.

The results show that atenolol is clearly more removed from solution than THF, which may be correlated with THF's higher solubility in water at 30 °C (solubility determined for atenolol is 17.9 g dm⁻³ and 65.3 g dm⁻³ for tiamulin), suggesting that this compound has a higher affinity towards the solvent water than atenolol.

A marked decay in solution concentration occurs in the first 30 min of contact time, after which the adsorption process proceeds slowly until equilibrium is attained, at 6 h (except for CP carbon) in the case of atenolol and more quickly at 4 h in for THF. The configuration of the kinetic curves, as well as the h and $t_{1/2}$ values of atenolol and THF adsorption systems (**Table VII.5** and **Table VII.10**) indicate a fast adsorption of the pollutants, especially in the case of atenolol for which the initial decay in C/C_0 values corresponds to the adsorption of a higher amount of pollutant than in the case of tiamulin.

Regarding the amount adsorbed, all the adsorbents were efficient in removing atenolol from solution (removals of approximately 60 % and higher), and the synthesized materials revealed similar and better performances than the commercial samples. In the case of THF, 20 to 60 % of the initial concentration was adsorbed, and the synthesized solids adsorption performance was comprised in this range of values.

Atenolol species critical dimensions (0.70 nm) does not allow its adsorption into the ultramicropores volume of the adsorbents, and consequently the solids performances present the same trend as the supermicropores volume of the carbons. In the case of the tiamulin species, with higher dimensions, and a critical dimension of 1.20 nm, both supermicropores and mesopore volume seem to have an important role on the adsorption kinetics.

Equilibrium adsorption studies were performed in parallel with fumaric acid, and tiamulin hydrogen fumarate. The resulting isotherms are shown in **Figure VII.18**.

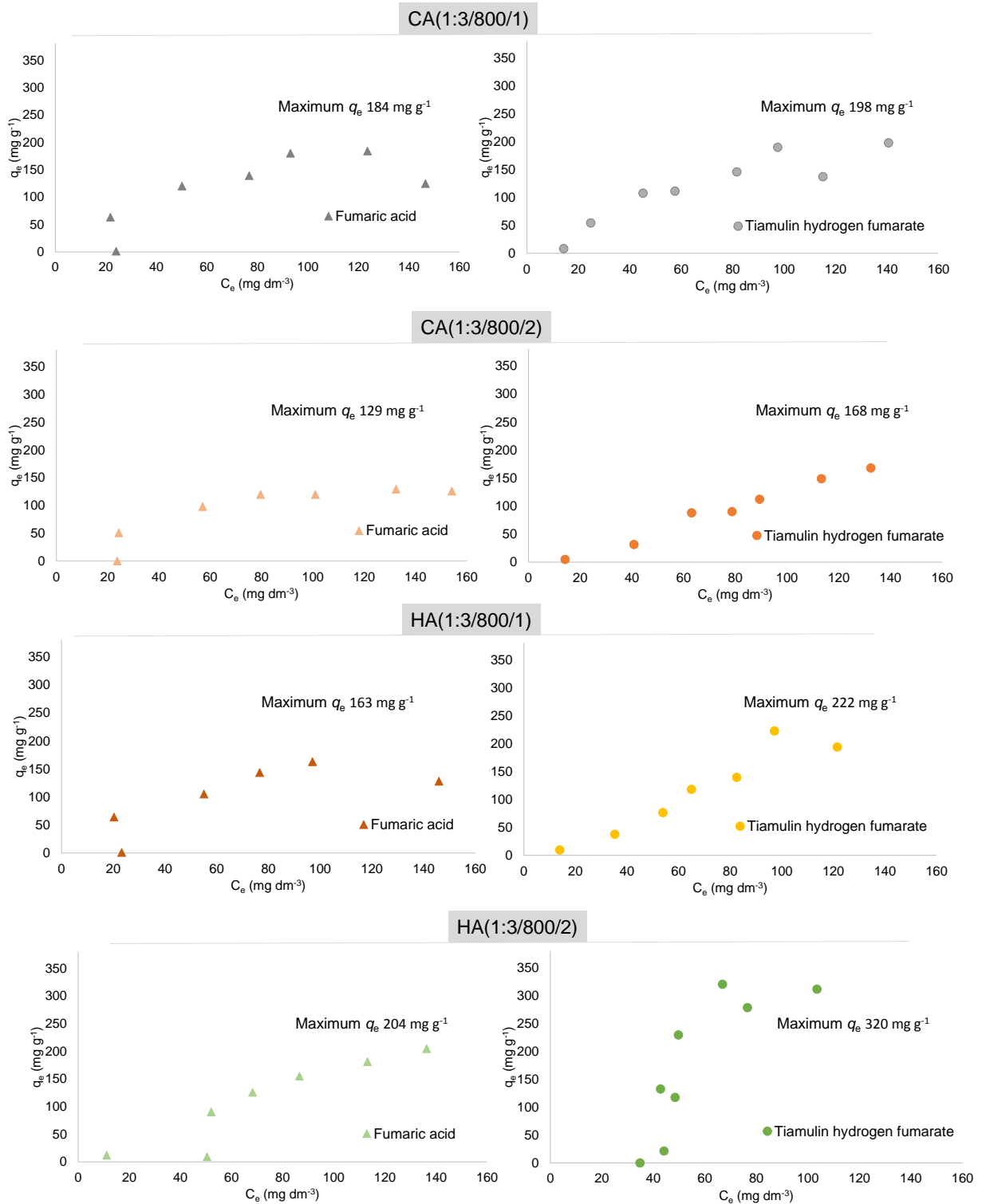


Figure VII.18. Equilibrium adsorption isotherms of fumaric acid (left side) and tiamulin hydrogen fumarate (right side) on the mentioned lab-made carbons, at 30 °C.

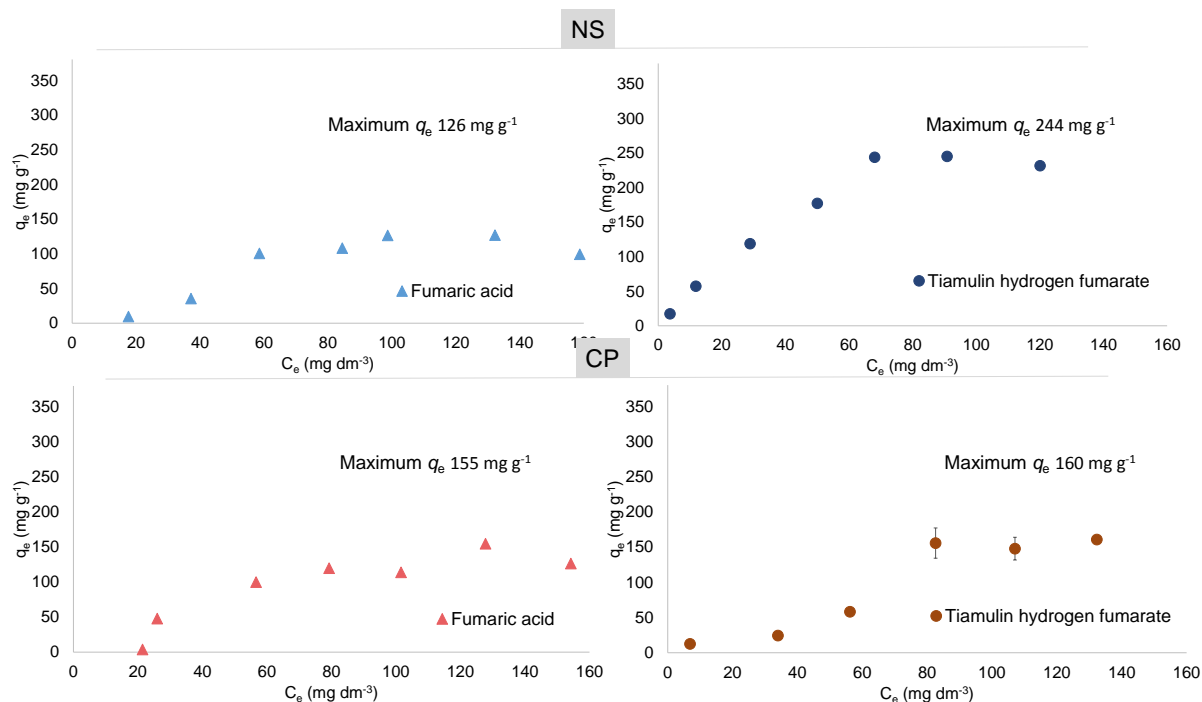


Figure VII.18.(continued) Equilibrium adsorption isotherms of fumaric acid (left side) and tiamulin hydrogen fumarate (right side) on the mentioned commercial carbons, at 30 °C.

The adsorption isotherms obtained for FA and THF present an unusual configuration.

The curves obtained with fumaric acid, present a very pronounced knee at C_e values of approximately 20 mg dm⁻³, except in the case of HA(1:3/800/2), where it occurs at approximately 40 mg dm⁻³. This behaviour is quite similar to that reported in the literature in the case of clofibric acid (Mestre *et al.*, 2010). So, we can hypothesize that also in this case the solvation energies of the protonated and deprotonated species can justify the underlying adsorption mechanism of these isotherms. If so the energy value associated with the solvation of the dissociated specie would be lower, and the fact that this is the predominant specie in solution (pKa of FA is 3.6, and solution pH is 2.6) will justify the cooperative adsorption process. Theoretical calculations are planned.

Regarding THF, all the isotherms present an S type configuration except NS. The shape of the curves suggests a complex adsorption mechanism that can eventually come from a lower affinity of tiamulin specie towards the carbon surface, and so it is the fumarate interaction that boosts the adsorption resulting in curves with configurations identical to those obtained when only fumarate is present in solution. The different shape obtained in the case of NS can point out the impact of the mesopore volume of the sample allied with also an important volume of the wider micropores. These conditions will most probably favour the adsorption of the larger tiamulin specie.

Higher maximum uptake values were achieved for THF, between 160 and 320 mg g⁻¹, in comparison to those obtained in the case of FA, which are between 126 and 204 mg g⁻¹. These results make sense considering that THF uptake values correspond to both fumarate and tiamulin species adsorption. In fact the difference in uptake, Δq_e , is in line with $V_{meso} + V_{\alpha super}$ of the carbons (see **Figure VII.19**) suggesting that, as it was mentioned before, the adsorption of tiamulin specie seems to depend on the presence of a wide network of pores due to the large molecular dimensions in comparison of what can be expected in the case of fumarate.

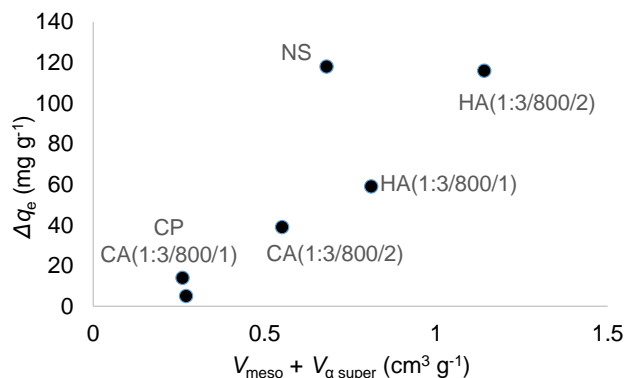


Figure VII.19. Correlation between the difference in maximum uptake values obtained for FA and THF adsorption, and the volume of meso and supermicropore of the materials.

The result of sample NS evidence an important role of the mesopore volume on THF adsorption that can be compensated when a high volume of very large micropores is present as is the case of sample HA(1:3/800/2). When the textural characteristics of the samples conjugate with not very high volumes of wide micropores and almost negligible mesopore networks, there are practically no differences of the maximum uptake of FA and THF.

VII. 3. Partial conclusions

The activation methodology employed allowed to prepare materials with good global activation yield values between 22 % and 61 %. The best compromise between biochar volatile content decrease and preparation yield was achieved for the carbons activated at 800 °C during 1 to 2 h, and synthesized with a ratio biochar:activating agent of 1:3.

Nanotextural characterization of the carbons revealed that the activation with KOH and K_2CO_3 produced carbons with an essentially microporous nature and with very high A_{BET} values, up to 2472 $\text{m}^2 \text{ g}^{-1}$ and 1963 $\text{cm}^3 \text{ g}^{-1}$, respectively. A more significant development of porosity was achieved with treatments at 800 °C during 1 h up to 3 h, with the micropore volume of the samples corresponding to 91% to 98% of the total pore volume. The increase of the heat treatment duration caused the progressive widening of the pores, leading to high supermicropores volumes, and eventually an increase in mesopore volume. The choice of the activating agent seems to have had an impact on the surface chemistry of the solids, having led to materials with acidic (K_2CO_3 activated samples) and neutral (KOH activated carbons) nature.

The impact of the activation conditions on the morphology of the carbons was assessed by scanning electron microscopy. The less severe K_2CO_3 activation conditions allowed to maintain some of the fibrous features of the biochar whereas activation with KOH caused a more extensive destruction of the precursor structure, also leading to a more homogeneous particle size distribution, in comparison with K_2CO_3 .

Four lab-made carbons were tested as adsorbents for atenolol, tiamulin hydrogen fumarate, and fumaric acid, together with two commercial activated carbons.

The kinetic results revealed fast adsorption processes for both pollutants and good performances of the lab-made samples, with maximum removal values of 60 % and 54 % for atenolol and tiamulin. The supermicropore volume of the carbons played an important role in atenolol and tiamulin adsorption kinetics and, in the case of tiamulin, the diffusion of this big species was facilitated by the high mesopore volume of NS.

The solids were able to adsorb up to 300 mg g^{-1} of atenolol, in equilibrium conditions, and the isotherms configuration (L-type) pointed out a high affinity of atenolol species towards the carbons surface. The high monolayer adsorption capacities achieved were

attributed to the supermicropores volume of the solids, and also favoured by the acidic surface of the K_2CO_3 activated samples.

Thermogravimetric studies were carried out with atenolol, and the pristine and atenolol-saturated samples, with the objective of studying the desorption mechanism and to understand the type of interactions established between adsorbate and adsorbent. In all the samples more prominent weight losses seem to occur at three temperature ranges. The first loss, at lower temperature, was attributed to atenolol desorption from the matrix, and atenolol decomposition occurred at higher temperatures. Two weight loss peaks, in the DTG curves, were observed due to the two forms of atenolol existent in the reagent (racemic mixture).

Adsorption of tiamulin hydrogen fumarate medicine was investigated, and the role of the fumarate component started to be assessed.

The kinetic results showed that tiamulin hydrogen fumarate was efficiently removed by the tested samples (concentration decay up to 60 %) and coincident curves leading to a decay of almost 35 % of fumaric acid initial concentration were obtained with NS, CA(1:3/800/2) and HA(1:3/800/2) carbons.

Equilibrium adsorption experiments revealed that fumaric acid adsorption follows a cooperative adsorption mechanism, which seems to occur in the case of THF in almost all the samples. The presence of a wide network of pores seems to be important for the removal of THF.

Chapter VIII

Pharmaceuticals removal by
activated carbons: Role of
morphology on cyclic thermal
regeneration

The work reported in this chapter was focused on the study of the role of carbons morphology (granular, powdered and cloth forms) in cyclic thermal regeneration-saturation processes. For this purpose, the potential of the materials for the adsorption of paracetamol and clofibrac acid was evaluated and consecutive regeneration-saturation cycles were performed on paracetamol-exhausted samples. The studies consisted in morphology, porosity and surface chemistry characterization of the materials, followed by kinetic and equilibrium adsorption assays in liquid phase.

This research was developed in partnership with the Instituto Nacional de Pesquisas Espaciais in Brazil, in collaboration with Doctor Jossano Marcuzzo, and the resulting work gave rise to the article “Pharmaceuticals removal by activated carbons: Role of morphology on cyclic thermal regeneration”, published in *Chemical Engineering Journal* (<https://doi.org/10.1016/j.cej.2017.03.101>). Also, results from this chapter were presented in 6 national and 5 international congress meetings (see Appendix C: Publications in National and International conferences).

VIII. 1. Experimental procedure

VIII.1.1. Materials

Four activated carbons, of cloth, powder and granular morphologies were studied. The activated carbon cloth, named ACC, was prepared in Brazil, whereas the remaining materials were of commercial origin (see **Table VIII.1**).

Table VIII.1. Activated carbons studied and information regarding their preparation and/or provenance.

Morphology	Activated carbon	Information
Cloth	Activated Carbon Cloth (ACC)	Prepared in Brazil, following the experimental procedure presented in Appendix A1.3.
Powder	NS	Commercialized by Norit, with the designation of SAE SUPER. This adsorbent is composed of 97 % (mass ratio) by particles with dimensions inferior to 0.15 mm.
	VP	Made available by ChemiVall, under the designation V Plus. This adsorbent was obtained from pine wood by water vapour activation, and 90 % of the sample is composed by particles smaller than 44 µm.
Granular	GAC	Commercialized by Norit, with the name GAC830. This material is prepared from coal by water vapour activation, and it comprises at 88 % particles with dimensions between 0.60 mm and 2.36 mm. Among the information made available at Norit’s site, GAC830 is particularly referenced for purposes of thermal regeneration (http://www.cabotcorp.com/solutions/products-plus/activated-carbon/granulated)

The paracetamol exhausted carbons analysed by thermogravimetric analysis will be named Carbonexh, and the regenerated samples will have the designation of Carbonexh/thermal treatment temperature (°C). Examples of these nomenclatures are ACCexh and ACCexh/600.

VIII.1.2. Material’s characterization techniques, and liquid phase adsorption and thermal regeneration experiments

Table VIII.2 lists the characterization techniques, and liquid phase adsorption and regeneration experiments performed, and the respective experimental procedures, presented in Appendix A: Experimental procedures.

Table VIII.2. Experimental procedures of the characterization techniques employed, and liquid phase adsorption and regeneration experiments performed.

Characterization	Technique	Appendix A
Texture	N ₂ adsorption at – 196 °C	2.1
	CO ₂ adsorption at 0 °C	2.2
Morphology	Scanning Electron Microscopy (SEM)	2.5
Surface chemistry	pH at the point of zero charge (pH _{PZC}) determination	2.8
	X-ray Photoelectron Spectroscopy (XPS)	2.6
Ash content	Determination: Heating regime	2.13
	Analysis: X-ray Diffraction (XRD)	2.7
Thermal stability	Thermogravimetry analysis	2.16
Liquid phase adsorption	Experiment	Appendix A
Paracetamol and clofibrac acid adsorption	Adsorption kinetics and equilibrium assays	3.2
Regeneration treatment	Experiment	Appendix A
Cyclic thermal treatment	Consecutive regeneration-saturation cycles of paracetamol-exhausted samples	2.17

Information regarding reagents, solution preparation and molecular properties of the pollutants specie are presented in Appendix A.3.1.

NS carbon characterization by N₂ and CO₂ adsorption, and pH_{PZC} value were previously presented in Chapter VII, but being this sample a typical carbon used for water treatment purposes, it was also used in this study for comparison purposes.

VIII. 2. Results and discussion

VIII.2.1. Characterization of the adsorbents

The nitrogen adsorption-desorption isotherms, at –196 °C (**Figure VIII.1**) have distinctive profiles, revealing that the adsorbents have distinct textural properties. In the case of the sample ACC, the isotherm shows a gradual approach to the saturation plateau, which is only reached at relative pressure values higher than 0.5. This does not allow its classification as a type I isotherm (Thommes *et al.*, 2015) and suggests a wider pore size distribution in the range of supermicropores as well as narrow mesopores.

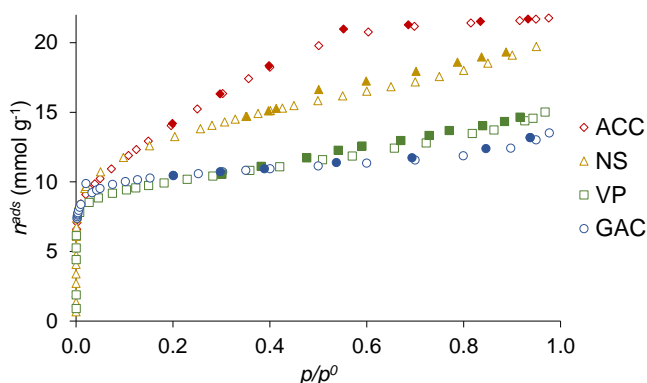


Figure VIII.1. Nitrogen adsorption-desorption isotherms at -196 °C of the mentioned samples (closed symbols are desorption points).

With respect to the commercial activated carbons, their isotherms configuration indicates the presence of a micro and mesopore network and so, in these cases, the isotherms are of type I + IV, according to the IUPAC classification reported in Thommes *et al.*, 2015. The curves present an upward deviation at high relative pressures, more

pronounced for carbon NS, indicating a more developed mesoporous system. Also, the higher amount of N₂ adsorbed by this sample clearly indicates a more developed porosity than that present in the other commercial adsorbents. All the commercial carbons have small hysteresis loops, which in all cases can be classified as type H4.

From the N₂ adsorption data, the nanotextural properties of the activated carbons were determined and the results obtained are presented in **Table VIII.3**.

Table VIII.3. Nanotextural properties of the lab-made carbons.

	A_{BET} ($\text{m}^2 \text{g}^{-1}$)	$V_{\text{total}}^{\text{a}}$ ($\text{cm}^3 \text{g}^{-1}$)	$V_{\text{meso}}^{\text{b}}$ ($\text{cm}^3 \text{g}^{-1}$)	$\alpha\text{s method}^{\text{c}}$		
				$V_{\alpha \text{ total}}$ ($\text{cm}^3 \text{g}^{-1}$)	$V_{\alpha \text{ ultra}}$ ($\text{cm}^3 \text{g}^{-1}$)	$V_{\alpha \text{ super}}$ ($\text{cm}^3 \text{g}^{-1}$)
ACC	1136	0.76	0.03	0.73	0.00	0.73
NS ^d	1065	0.70	0.30	0.40	0.02	0.38
VP ^e	758	0.43	0.13	0.30	0.15	0.15
GAC ^d	838	0.47	0.13	0.34	0.09	0.25

^aN₂ volume adsorbed at $p/p^0 = 0.95$; ^b $V_{\text{meso}} = V_{\text{total}} - V_{\alpha \text{ total}}$; ^c $\alpha\text{s method}$ applied using as reference the isotherm presented in Rodríguez-Reinoso and Martín-Martínez, 1987; ^dvalues presented in Mestre *et al.*, 2012; ^evalues reported in Mestre *et al.*, 2010.

The textural parameters show that all the carbons present high apparent surface areas, which in the case of ACC and NS are close to 1100 m² g⁻¹. Also, in accordance with the isotherms, all the adsorbents have a well-developed micropore network ($V_{\alpha \text{ total}}$ ranging from 0.30 cm³ g⁻¹ to 0.73 cm³ g⁻¹) and, with exception of carbon ACC, all the samples present relevant mesopore volumes (between 0.13 and 0.30 cm³ g⁻¹). The more mesoporous sample is NS for which the V_{meso} value (0.30 cm³ g⁻¹) corresponds to 44% of the total pore volume. Regarding microporosity, all the samples have a micropore network composed mainly by supermicropores, with exception of sample VP, which presents equal volumes of narrow and wider micropores ($V_{\alpha \text{ ultra}} = V_{\alpha \text{ super}}$). In sample ACC the microporosity is only composed by supermicropores, while in carbons NS and GAC, $V_{\alpha \text{ super}}$ corresponds to 95 and 73 % of the total micropore volume, respectively.

The microporosity characterization of the carbons was complemented by CO₂ adsorption at 0 °C being the resulting isotherms presented in **Figure VIII.2**.

The isotherms configuration clearly distinguishes the sample with cloth morphology from the powder and granular carbons. Thus, while the commercial samples have type I isotherms, in the case of ACC the adsorption curve can be clearly divided in two stages, being the change observed at p/p^0 values around 0.02 (see **Figure VIII.1**). In the case of the curve obtained for N₂ adsorption, two stages are also visible and allow to differentiate the micro and mesoporosity and, in the case of CO₂ isotherm profile, it allows to distinguish between the narrow and wide microporosity. Thus, the small slope of the first plateau, at low p/p^0 values, and the significantly low amount of CO₂ adsorbed ($n^{\text{ads}} < 1 \text{ mmol g}^{-1}$) highlights the almost absence of ultramicropores. On the contrary, the sudden increase in adsorption, at relative pressure values higher than 0.02, reveals a high volume of wide micropores.

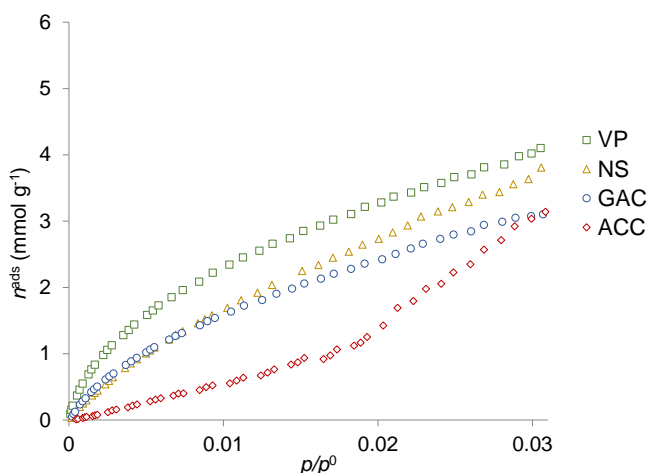


Figure VIII.2. CO₂ adsorption isotherms at 0 °C of the mentioned carbons.

The isotherms of the commercial samples present continuous CO₂ uptake. NS and GAC have coincident isotherms, at relative pressures lower than approximately 0.01 confirming the similar ultramicropore volumes shown by N₂ adsorption. VP isotherm has higher CO₂ uptakes at lower p/p^0 values, which is in line with $V_{\alpha \text{ ultra}}$ (0.15 cm³ g⁻¹) determined by N₂ adsorption. The isotherm of NS presents a marked increase in CO₂ adsorption at higher pressure values, which is in accordance with its higher V_{super} value with GAC.

From the CO₂ adsorption data, the micropore size distributions (**Figure VIII.3**) were obtained, using the methodology presented in Pinto *et al.*, 2010. These results corroborate the previous discussion of the textural parameters obtained from the analysis of N₂ adsorption data, showing that the micropore network of the commercial carbons present both narrow and wider micropores, *i.e.*, in all the cases a broad bimodal distribution was obtained. ACC carbon's microporosity, on the other hand, is exclusively composed by wide supermicropores, which is also in accordance with the N₂ adsorption characterization.

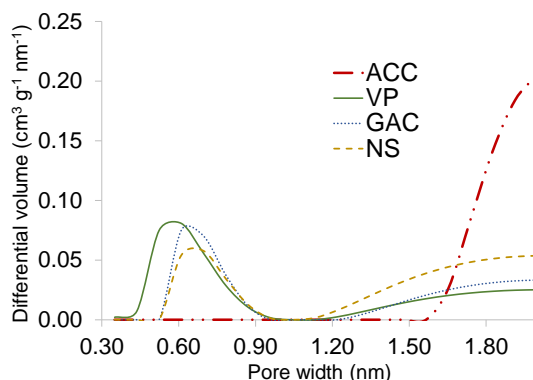


Figure VIII.3. Micropore size distributions of the mentioned samples obtained from the CO₂ adsorption data, at 0 °C.

NS and GAC samples have narrow micropores within the same width range, between 0.52 and 0.96 nm, whereas VP carbon has also narrower ultramicropores but with widths starting at 0.44 nm. Thus, for the commercial carbons the maximum in the region of narrow micropores are located at 0.70, 0.65 and 0.59 nm, for NS, GAC and VP, respectively. Considering only the volumes determined for pores narrower than 0.7 nm (ultramicropores), the CO₂ adsorption corroborates the nanotextural parameters determined by N₂ adsorption, at -196 °C (see **Table VIII.1**), pointing out a higher

ultramicropores volume in VP carbon, followed by GAC and NS. The wider micropores of these carbons present widths always higher than 1.20 nm and, overall, their corresponding volumes follow the same trend as $V_{\alpha \text{ super}}$ (NS > GAC > VP).

Sample ACC has a very distinctive microporosity, composed exclusively by supermicropores wider than 1.60 nm, which corresponds to the highest volume assessed by the CO₂ adsorption, also in line with the highest $V_{\alpha \text{ total}}$ and $V_{\alpha \text{ super}}$ values assessed by N₂ adsorption data.

In any case no pores between 0.96 and 1.13 nm are present.

Morphological characterization, by SEM, was made only for sample ACC. The SEM micrograph shown in **Figure VIII.4** shows the typical structure of a carbon cloth, as it was expected for a material produced from PAN cloth composed by yarns, aggregated in a somewhat disorganized disposition (see **Figure VIII.4(a)**). The yarns of the cloth have smooth cross section and longitudinal surfaces, and a bean shape with an average diameter of 21 μm (**Figure VIII.4(b)** and **(c)**).

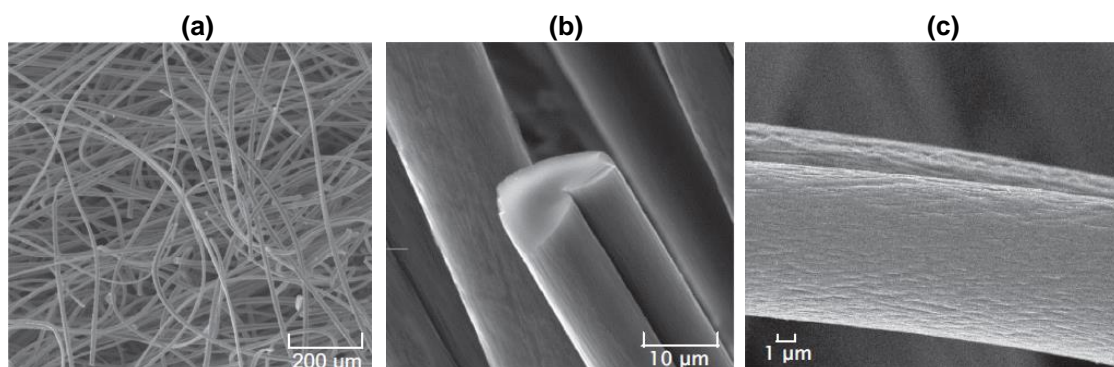


Figure VIII.4. SEM micrographs of the **(a)** ACC surface and **(b)** a cross-section and **(c)** longitudinal surfaces.

These micrographs allow to conclude that the microporosity of ACC can be easily accessed because it is located at the surface of the yarns widely separated due to the “open” structure of the cloth morphology. This observation suggests a very easy diffusion of adsorbate species towards the adsorption sites of the material.

The results of the pH_{PZC} determination show that all the carbons are basic solids, characterized by similar pH_{PZC} values: ACC – 9.0; NS – 8.4; VP – 9.8 and GAC – 8.9.

The surface functionalities of the carbons were characterized by X-ray Photoelectron Spectroscopy (XPS). The survey spectra, displayed in **Figure VIII.5** show that carbon and oxygen are the main elements detected in all the samples. Very small peaks are also noticed in the region between 100 and 200 eV, assigned to the presence of Si and Al, in trace amounts.

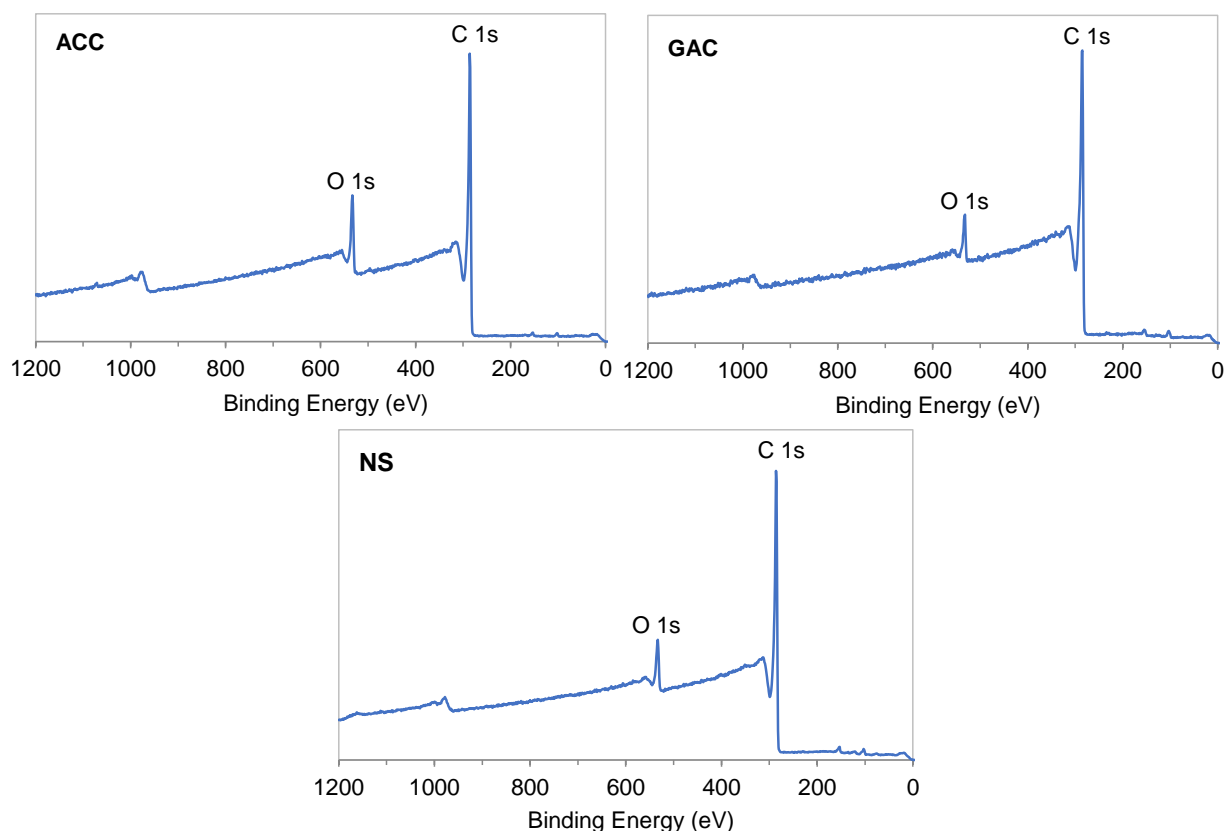


Figure VIII.5. XPS survey spectra for the mentioned samples.

The surface atomic percentages of carbon and oxygen obtained from the survey spectra are displayed in **Table VIII.4** showing that, as expected, carbon is the major component of the samples. Despite these three samples present pH_{PZC} values in a relative narrow range (8.4-9.0), the amount of oxygen quantified by XPS is comprised between 5.2 and 9.0 atomic %, and the higher oxygen percentage was obtained for the more basic carbon, sample ACC, pointing out that the outer surface of this carbon particles may present mainly oxygen basic groups.

Table VIII.4. XPS atomic percentages for samples ACC, NS and GAC.

	Atomic %	
	C 1s	O 1s
ACC	91.0	9.0
NS	93.2	6.8
GAC	94.8	5.2

All high-resolution C 1s spectra, presented in **Figure VIII.6 (left side)** have asymmetric tailing for high binding energy values, which is attributed to the intrinsic asymmetry of the graphitic peak, and to the contribution of oxygen surface complexes (Moreno-Castilla *et al.*, 2000). The spectra were deconvoluted considering the peaks of the carbon skeleton and of the oxygen functionalities usually reported in the literature for this type of materials at binding energies around: 284.6-285.1 eV, a main peak assigned to graphitic carbon (sp^2) (peak 1); 286.3-287.0 eV, attributed to alcohol or ether groups (single C-O bond) (peak 2); 287.5-288.1 eV assigned to carbonyl and/or quinone groups (C=O) (peak 3); 289.3-290.0 eV, related to carboxyl or ester groups (COO) (peak 4); and 291.2-292.1 eV, ascribed to shake-up satellite peaks due to π - π^* transitions in aromatic rings (peak 5) (Moreno-Castilla *et al.*, 2000; Biniak *et al.*, 1997; Bandosz and Ania, 2006).

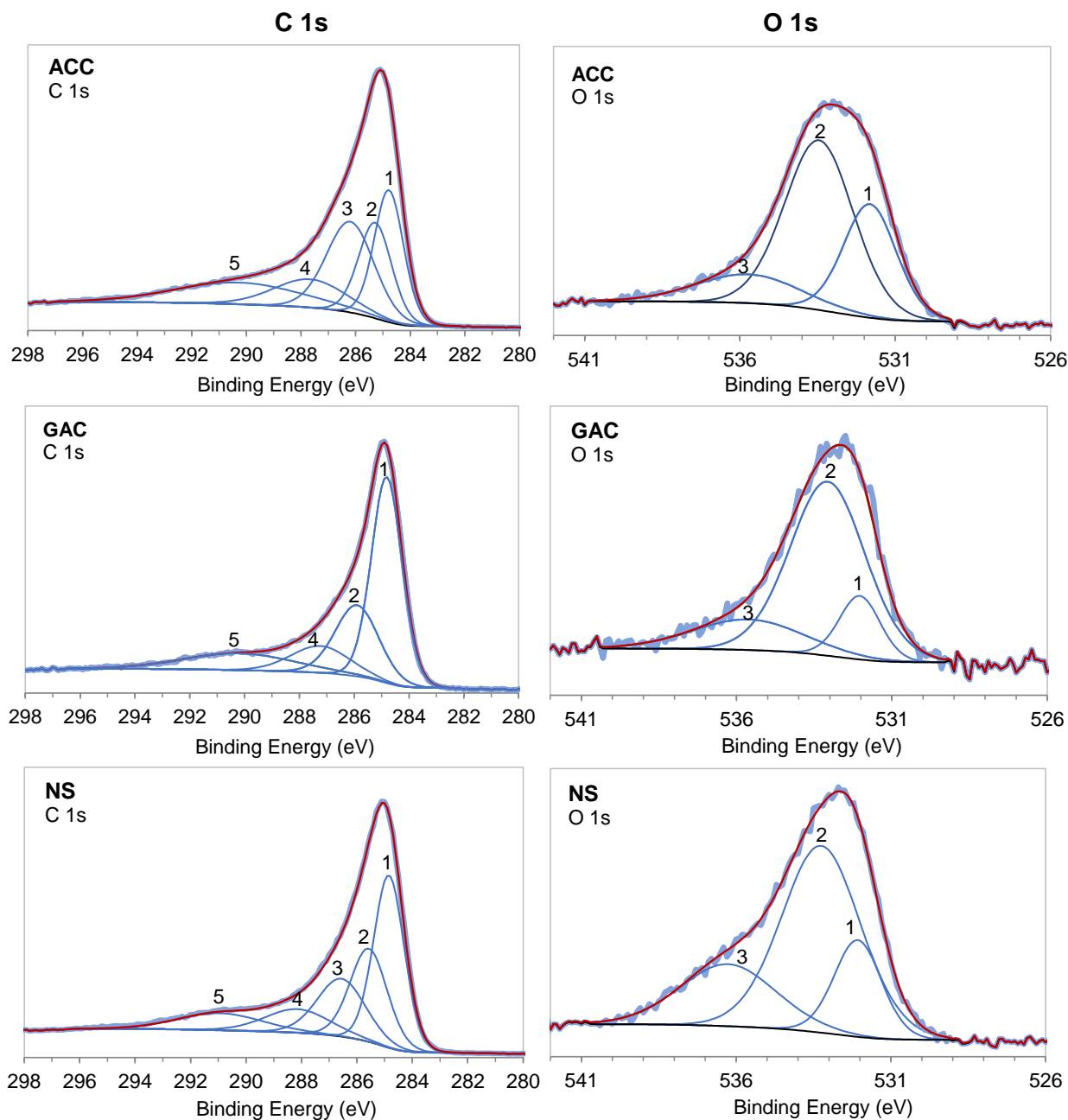


Figure VIII.6. Deconvoluted high-resolution C 1s (left) and O 1s (right) XPS spectra for the mentioned samples.

The high-resolution O 1s spectra (**Figure VIII.6 (right side)**) were fitted considering three peaks which are commonly reported in the range of 503.4-530.8 eV (C=O groups) (peak 1), 532.4-533.1 eV (C-O bond in C-OH and/or C-O-C groups) (peak 2), and 534.8-535.6 eV (quimisorbed oxygen and/or water) (peak 3) (Biniak *et al.*, 1997).

The deconvolution of the C 1s spectra reveal differences in the chemistry of the outer surface of the carbon particles. In the spectra of carbons NS and ACC the deconvolution reflected the presence of all the expected five peaks, while in the case of the granular material the fitting revealed the presence of only four peaks, showing the absence of C=O related to carbonyl and/or quinone functionalities. The deconvolution of the O 1s spectra showed the presence of the three peaks attributed to C=O, C-O and chemisorbed oxygen and/or water. In line with the findings of the C 1s spectra for GAC

sample, the amount of C=O functionalities are considerably smaller than those estimated for the other two samples.

The results of the ash content determination revealed that carbon ACC is an almost ash free material since the mineral matter is only 0.2 % (wt/wt). For GAC and NS the ash content is 6.9 % and 14.0 % (wt/wt), respectively. Further characterization of the NS and GAC ashes was made by X-ray diffraction. The diffractograms (**Figure VIII.7**) show that, in both cases, SiO₂ is the major crystalline structure present, as demonstrated by the most intense peaks of quartz (ICCD-33-1161) and cristobalite (ICCD-39-1425) at around 26 and 21 °2θ, respectively (Powder Diffraction File Alphanumeric Index). These findings are in line with the XPS survey spectra where trace amounts of Si were detected.

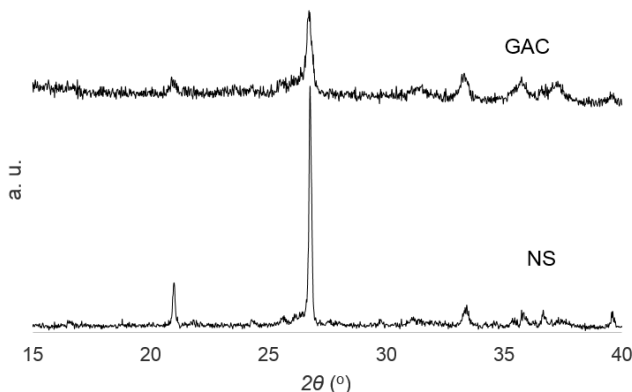


Figure VIII.7. X-ray diffraction patterns of the ashes of the carbons GAC and NS.

VIII.2.2. Adsorption of paracetamol and clofibrac acid

The results of paracetamol and clofibrac acid kinetic assays (**Figure VIII.8**) show similar trends in terms of the performances achieved, that is, ACC and NS were the most efficient adsorbents uptaking higher pollutant amounts, and more rapidly than samples VP and GAC. In the experimental conditions used, the removal reached 50 % in the case of paracetamol (**Figure VIII.8 (a)**), and 80 % when clofibrac acid (**Figure VIII.8 (b)**) was used.

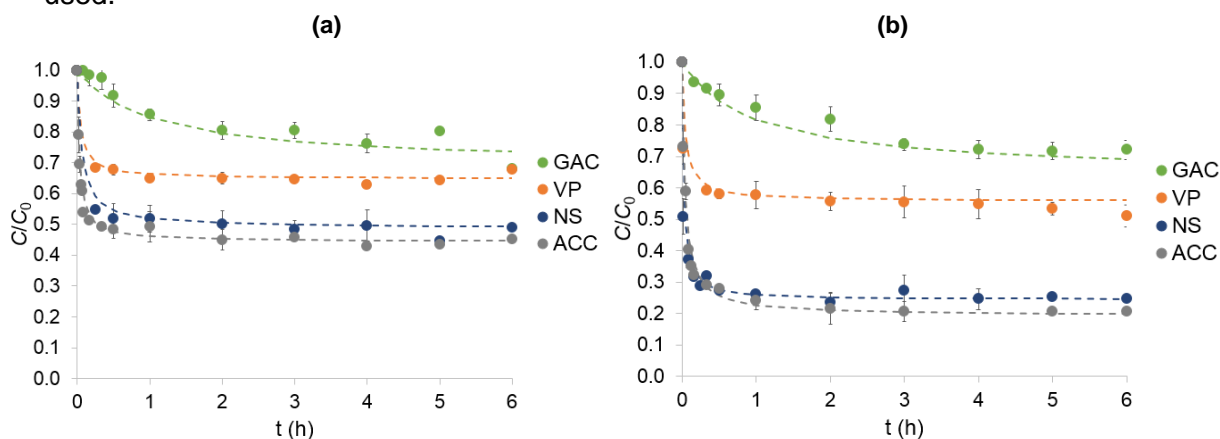


Figure VIII.8. Kinetic results of (a) paracetamol and (b) clofibrac acid adsorption, at 30 °C for the carbon samples. Lines show the fitting to pseudo-second order kinetic model.

The adsorption kinetic curves obtained for GAC show that, in comparison with the other carbons, in this case, a much slower approach to equilibrium is observed, which is in line with the granular morphology of this sample. Actually, regardless the pollutant, equilibrium is reached after 6 h of contact time, which was confirmed by the removal achieved after 24 h.

The adsorption onto the powdered (NS and VP) and cloth (ACC) carbons resulted in kinetic curves with similar profiles, revealing a fast adsorption process. The curves show a very marked decay in the first 5 min, after what the adsorption proceeds more slowly towards equilibrium which was attained after 1 h, in the case of paracetamol, and 2 h when clofibric acid was tested.

Considering the textural characteristics of these samples, namely the fact that all have high volumes of wider micropores ($V_{\alpha \text{ super}}$ in **Table VIII.3**), according to the literature this was the expected behaviour. Actually, in previous studies developed in the research group where this study was developed (Batista *et al.*, 2016; Galhetas *et al.*, 2014a and 2014b) it was concluded that, when the samples present important volumes of supermicropores (*i.e.* pores with widths between 0.7 and 2 nm), the presence of a mesopore network does not have an impact on the diffusion of species with small critical dimensions, as is the case of paracetamol and clofibric acid. In fact, according to the values reported in the literature, the critical dimensions of paracetamol monomer and dimer forms are 0.46 and 0.66 nm, respectively (Galhetas *et al.*, 2014a), and the critical dimensions of clofibric acid is 0.70 nm (Mestre *et al.*, 2016) (see **Table VIII.6**). Therefore, no constraints should occur to the adsorption of these molecules in the supermicropore network of the samples.

The kinetic data were fitted to the pseudo-first order kinetic model (Ho, 2006) but the coefficients of determination, R^2 , were very unfavourable reaching maximum values of 0.8141 and 0.8221 for paracetamol and clofibric acid adsorption data, respectively. The pseudo-second order model (Ho, 2006) leads to better fittings of the experimental results, with high R^2 values and similar calculated and experimental uptake values ($q_{e \text{ calc}}$ and $q_{e \text{ exp}}$, respectively), as reported in **Table VIII.5**.

Table VIII.5. Pseudo-second order pharmaceutical compounds adsorption parameters for the studied carbon samples at 30 °C.

	$k_2 \times 10^{-4}$ ($\text{g mg}^{-1}\text{min}^{-1}$)	h ($\text{mg g}^{-1}\text{min}^{-1}$)	$t_{1/2}$ (min)	$q_{e \text{ calc}}$ (mg g^{-1})	$q_{e \text{ exp}}$ (mg g^{-1})	$C_{e \text{ calc}}$ (mg dm^{-3})	Re(%)	R^2
Paracetamol								
ACC	26	130	1.7	222	218	53	56	0.999
NS	40	179	1.2	217	225	52	48	0.999
VP	40	102	1.7	169	170	69	36	0.999
GAC	1	2	61	132	143	81	33	0.870
Clofibric acid								
ACC	12	137	2.4	333	314	20	83	0.999
NS	23	222	1.4	313	304	26	76	0.999
VP	2	72	2.7	196	186	61	54	0.995
GAC	2	3	39	115	113	86	30	0.992

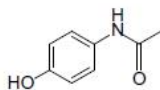
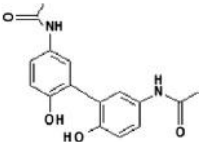
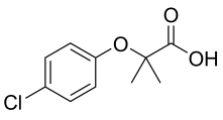
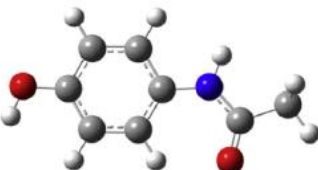

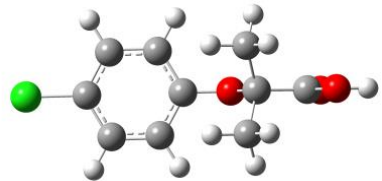
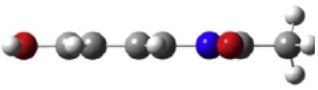

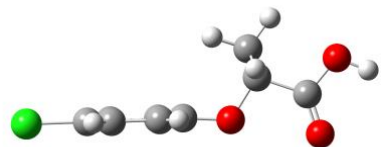
The values of initial rate, h , corroborate the analysis of the kinetic curves configuration since they show that the adsorption of both compounds is a faster process when ACC, NS and VP carbons were used. Actually, in the case of these samples the initial adsorption rate values are two orders of magnitude higher than those obtained for the granular sample (GAC).

The uptake values at equilibrium show that, with exception of carbon GAC, clofibric acid is always more efficiently removed than paracetamol what may be explained considering the solubility of the compounds, that, as it was previously mentioned in the introduction chapter, is a key factor ruling the adsorption process. The values reported in the literature (Mestre *et al.*, 2014b) are 17390 mg dm^{-3} and 755 mg dm^{-3} for paracetamol and clofibric acid, respectively. Thus, the lower affinity of clofibric acid

towards the solvent, will favour the interaction with the carbon surface and, consequently its removal.

A detailed comprehension of the pollutants molecular structure, chemical properties, and critical dimensions is essential to have an insight into the adsorption mechanism. In fact, the inclusion of this topic has proven its usefulness in previous studies conducted in the research group where this thesis was developed (Batista *et al.*, 2016; Mestre *et al.*, 2016; Mestre *et al.*, 2014a and 2014b). For this reason, and like it was done when rationalizing the liquid phase results on Chapter VII, in the following paragraphs the impact of the properties of paracetamol and clofibric acid species in solution (**Table VIII.6**) on the adsorption mechanism will be discussed.

Table VIII.6. Molecular structure, chemical properties (molecular weight - M_w and acidic constant - pK_a), and dimensions of the mentioned pollutants. The critical dimensions of each species are highlighted in bold.

Paracetamol ^a		Clofibric acid ^b
Monomer	Dimer	
		
$M_w = 151.2 \text{ g mol}^{-1}$ $pK_a = 9.7$	$M_w = 303.3 \text{ g mol}^{-1}$ $pK_a = 9.7$	$M_w = 214.6 \text{ g mol}^{-1}$ $pK_a = 3.6$
		
		
1.19 nm (length) x 0.75 nm (width) x 0.46 nm (thickness)	1.58 nm (length) x 1.19 nm (width) x 0.66 nm (thickness)	1.22 nm (length) x 0.72 nm (width) x 0.70 nm (thickness)

^aMolecular dimensions published in Galhetas *et al.*, 2014a; ^bmolecular dimensions reported in Mestre *et al.*, 2016.

Before starting the analysis of the molecular modelling data, it is important to point out that, at dissolution pH (pH ~ 5), that is, the conditions used in this study, paracetamol may form a dimer, as firstly reported by Nematollahi *et al.* (Nematollahi *et al.* 2009). The presence of even more complex agglomerated species was more recently demonstrated in Galhetas *et al.*, 2014a.

All the pollutants present small dimensions and due to the usual slit shape of pores of activated carbons, the critical dimension for adsorption is the section perpendicular to the length that in paracetamol monomer and dimer corresponds to 0.46 and 0.66 nm, respectively and for clofibric acid is 0.70 nm. So, no hindrance is expected to occur for the adsorption of these species in the supermicropores (wider than 0.7 nm) of the carbons. However, the access of the pollutants to the ultramicroporous volume of the carbons will be limited and, depending on the micropore size distribution of the carbons, the molecular dimensions can have an impact on the adsorptive properties of the materials. The only exception to this is sample ACC which is exclusively composed by supermicropores.

Figure VIII.9 illustrates the micropore size distributions of the carbons, previously presented in **Figure VIII.3**, and where the critical dimensions of the pollutant species are indicated.

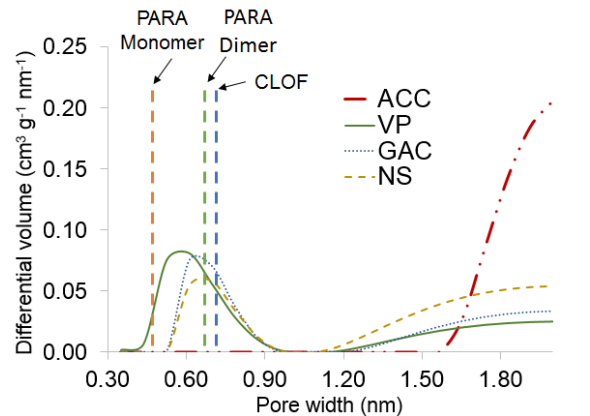


Figure VIII.9. Correlation between the critical dimensions of the pollutants species in solution and the micropore size distribution of the carbons, previously presented in **Figure VIII.3**. PARA – Paracetamol and CLOF – Clofibrac acid.

The monomeric form of paracetamol has the smallest thickness (0.46 nm) and so, it will have access to the total micropore volume, with exception of a small portion of the ultramicropores of carbon VP. Paracetamol dimer has more than double of the thickness of the monomer (0.66 vs 0.46 nm) and, consequently will not have access to the majority of the ultramicropores. Finally, clofibrac acid (thickness of 0.7 nm) will have no access to the ultramicroporous volume of the carbons.

The equilibrium adsorption data for both compounds at 30 °C (see **Figure VIII.10**) show that, for all the carbons, clofibrac acid (**Figure VIII.10(b)**) is more efficiently adsorbed than paracetamol, most certainly due to its lower solubility that increases the adsorption potential and consequently the partition of the clofibrac acid towards the adsorbed phase.

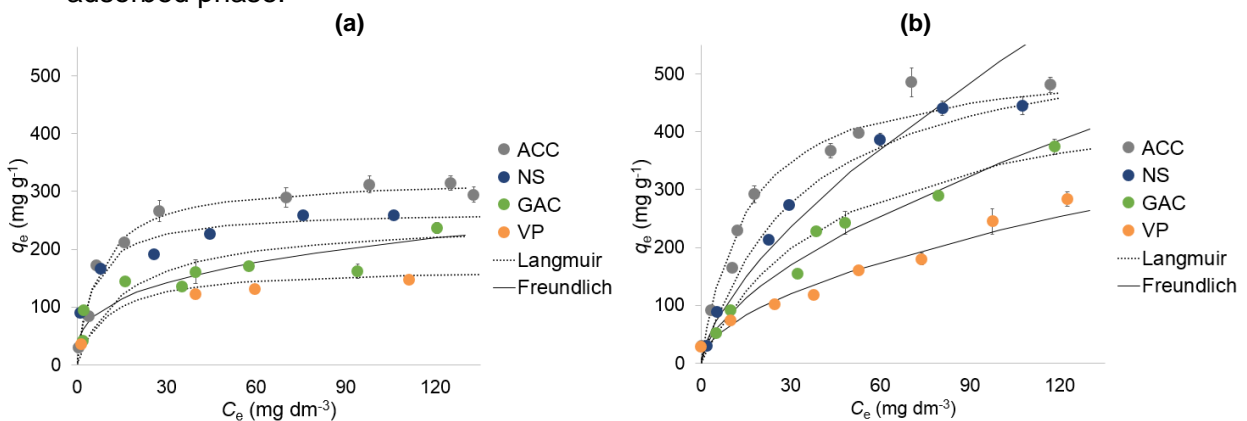


Figure VIII.10. Adsorption isotherms of (a) paracetamol and (b) clofibrac acid onto the mentioned carbons, at 30 °C. Symbols correspond to the experimental data, whereas lines represent the fitting to Langmuir and Freundlich models. Error bars are included.

Considering the liquid phase isotherms classification for diluted solutions, originally proposed by Giles *et al.* (Giles *et al.*, 1974a) and further simplified by Lyklema (Lyklema, 1995), the curves obtained for paracetamol adsorption can be classified as type L, presenting a relatively well defined initial rise of the paracetamol uptake followed by a horizontal plateau for equilibrium concentrations, C_e , higher than $\sim 40\text{ mg dm}^{-3}$.

Due to the relatively high amount of ashes presented by all carbons but ACC sample, to disclose any possible influence of the mineral matter on the performance of the carbons as adsorbents for paracetamol from aqueous phase, the ashes obtained after total consumption of the GAC and NS carbons fractions were assayed as adsorbents. No removal was observed after 24 h of contact time so, even though these results cannot be directly compared with the effect of the mineral matter when distributed in the bulk, they point out that by itself the ash has a negligible contribution to the performance of the carbons as adsorbents.

In the case of clofibric acid adsorption, the isotherms classification is more difficult, since while the data obtained with carbon ACC can be classified as a type L curve, the data obtained with carbon VP is a type F isotherm, due to its less accentuated concavity towards the concentration axis. The curves obtained with samples NS and GAC seem to be a mix of L and F type isotherms. Thus, although an important increase of the clofibric acid uptake is observed up to C_e values around 40-60 mg dm⁻³ – characteristic of L-type curves – afterwards the amount of clofibric acid uptake continues to increase, but more steadily, resembling the curve of a Freundlich isotherm.

Taking into account the correlations shown in **Figure VIII.9**, one could expect clofibric acid to be less adsorbed than paracetamol. However, the equilibrium experiments showed higher q_e values for clofibric acid than for paracetamol, which were attributed to the less favourable interactions between clofibric acid and water solvent (lower solubility). Furthermore, considering the acidic constants of the pollutants, it is also important to have in mind that, at dissolution pH, paracetamol is in neutral form (pH≈5; pKa 9.7) and in clofibric acid solution the neutral and deprotonated forms coexist (pH≈3; pKa 3.6).

The experimental results were fitted to the linear forms of Langmuir and Freundlich models (**Table VIII.7**) (Langmuir, 1918; Freundlich, 1906).

As it was expected from the analysis of the isotherms configuration, paracetamol equilibrium data is better described by the Langmuir model, *i.e.*, higher R^2 and smaller χ^2 values in comparison with those obtained for the fitting to the Freundlich equation. Also in the case of clofibric acid adsorption, the fitting results corroborate the discussion of the isotherms configuration, showing that the adsorption process onto ACC and VP carbons is clearly best described by Langmuir and Freundlich equations, respectively. For the other two carbons, NS and GAC, the fitting results indicate a good adjustment to both models, since identical R^2 and χ^2 values are obtained.

Table VIII.7. Fitting parameters of the equilibrium data to the Langmuir and Freundlich models, coefficient of determination, R^2 , and chi-square test analysis, χ^2 . Best fitting for each system is indicated in bold.

	Langmuir				Freundlich			
	q_m (mg g ⁻¹)	K_L (dm ³ mg ⁻¹)	R^2	χ^2	$1/n$	K_F (mg ^{1-1/n} (dm ³) ^{1/n} g ⁻¹)	R^2	χ^2
Paracetamol								
ACC	322.6	0.137	0.996	6.0	0.295	80.9	0.810	55.6
NS ^a	267.7	0.180	0.997	5.3	0.350	56.4	0.862	47.0
VP ^a	169.5	0.097	0.993	4.2	0.239	46.0	0.868	9.3
GAC	250.0	0.062	0.969	18.2	0.311	49.4	0.850	33.8
Clofibric acid								
ACC	526.3	0.056	0.992	19.7	0.448	63.8	0.929	30.3
NS	567.5	0.028	0.991	20.0	0.659	25.0	0.976	14.0
VP	321.3	0.026	0.785	31.3	0.536	19.5	0.957	9.3
GAC	500.0	0.022	0.986	14.5	0.592	22.7	0.983	14.6

^aData published in Galhetas *et al.*, 2014a.

Considering the paracetamol monolayer capacity, the activated carbons can be ordered ACC > NS > GAC > VP, which coincides with the trend of the total micropore volume of the samples. This type of correlation was observed in previous studies, namely some developed in the laboratory where this work was made (Galhetas, 2014a and 2014b). In the mentioned studies the direct correlation between q_m and micropore volume was interpreted considering the dimensions of the paracetamol species which can access both the narrow and wider micropores. However, if we take into account that the micropore volume of the carbon cloth sample, ACC is roughly twice the values presented by the other carbons we could expect a much higher value for paracetamol monolayer capacity. This result is most probably due to the fact that the micropore network of this sample presents only pores larger than 1.7 nm (see **Figure VIII.3**) which results in an inefficient filling of the porosity, leading to the waste of some pore volume, even if we consider that paracetamol dimer is the specie present in the monolayer.

The rationalization of the clofibric acid results implies a different approach because for the majority of the samples the underlying mechanism of the Freundlich model cannot be disregarded. Thus, the comparison of the carbons performance will be made considering the amount adsorbed at C_e around 120 mg dm^{-3} . The values reveal a trend similar to the one observed for paracetamol monolayer capacities. However due to the critical dimension of this molecule (0.70 nm) we have to consider that the textural parameter ruling the clofibric acid adsorption mechanism is the volume of the supermicropores, $V_{\alpha \text{ super}}$.

The different behaviour of clofibric acid, reflected in the F-type isotherms may be related to the fact that in the experimental conditions tested, *i.e.* pH 3, equal fractions of undissociated (neutral) and dissociated (negative) forms of clofibric acid are present (pKa 3.6). At this pH the carbons have a net positively charged surface ($\text{pH} < \text{pH}_{\text{PZC}}$), so it could be expected a high affinity of the deprotonated specie towards the surface. However, despite no hindrance to the access of this specie to the pore network is expected, as demonstrated in the literature, due to its higher solvation energy the interaction with the carbons surface is shielded (Mestre *et al.*, 2010). Moreover, a recent study evaluating the influence of water hardness on the adsorption of clofibric acid onto activated carbons at pH 3 and 8 (Mestre *et al.*, 2016) reported F-type isotherms and higher adsorption capacities at pH 3. Therefore, it can be admitted that in the experimental conditions used in the present study the adsorption process must rely mainly on the interactions of the undissociated clofibric molecules with the carbon surface which are of dispersive nature and may allow multilayer adsorption. The steady approach to the saturation can then be rationalized considering that the amount of species that can more effectively interact with the carbon is only a fraction of the total clofibric acid concentration, which is dependent of the equilibrium between undissociated and dissociated clofibric acid species. In fact, once the first undissociated species are adsorbed the equilibrium is shifted towards this specie, leading to a progressive increase of the uptake.

VIII.2.3. Role of morphology on thermal cyclic regeneration of paracetamol-exhausted carbons

The regeneration assays were made considering only samples ACC, NS and GAC and paracetamol was selected as target compound. The experimental conditions for the thermal regeneration studies were defined after thermogravimetry studies.

The thermograms (TGs), displayed in **Figure VIII.11(a)** show that the raw NS and GAC materials have negligible weight loss, while carbon cloth ACC loses 10 % of its weight when heat treated under N₂ up to 900 °C. The exhausted samples present similar weight loss profiles with weight loss ranging from 14 % (GACexh) to 22 % (NSexh).

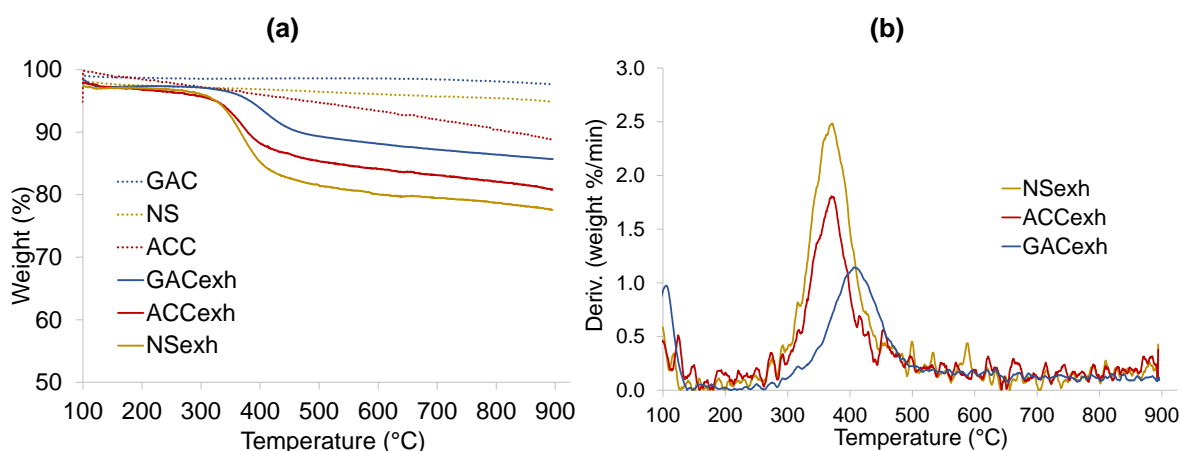


Figure VIII.11. (a) Thermograms of the raw and exhausted carbons and (b) corresponding DTG curves.

The differential thermogravimetric (DTG) curves (**Figure VIII.11 (b)**) show that the most important weight loss occurs between 300 and 500 °C, and in the case of NS and ACC carbons the maximum is centred at 375 °C and 366 °C, respectively, while for the granular sample it occurs at 411 °C. Comparing the TG profiles of the exhausted samples with those of paracetamol and raw carbons (see **Figure VIII.11 (a)** and **Figure VIII.12**), it is possible to attribute the weight loss of the exhausted samples mainly to the removal/degradation of the adsorbed paracetamol, since the thermogram of paracetamol reveals an almost complete weight loss in the temperature range between 300 and 400 °C. The slightly higher temperature needed to remove/degrade paracetamol adsorbed onto sample GAC (411 °C versus 366 and 375 °C for ACC and NS, respectively) seems to be linked to the granular morphology of the material. In fact, in the case of the granular particles heat distribution along the particles may be distinct than that occurring in materials with smaller particles sizes (NS), or fibre-like morphologies (ACC) where the microporosity is readily available. Specific interactions could also explain the higher temperature needed in the case of GAC but equilibrium adsorption data revealed the opposite trend. The adsorption affinity value (K_L , **Table VIII.7**) of GAC for paracetamol is one order of magnitude lower than the values of the carbons NS and ACC indicating a weaker interaction between carbon surface and adsorbed paracetamol.

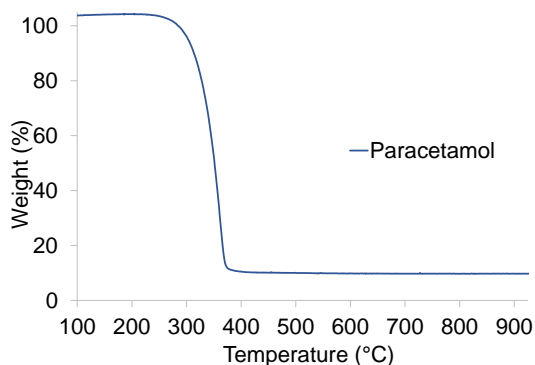


Figure VIII.12. Thermogram of paracetamol.

These results are similar to those reported by Ania *et al.* (Ania *et al.*, 2005), for carbons exhausted with salicylic acid, being the presence of a single peak at around 300 °C assigned to the degradation of physically adsorbed compound. In the same study, the authors also tested phenol saturated carbons for which the DTG presented two peaks, being the one at lower temperature assigned to phenol physically adsorbed, and the one at higher temperature attributed to the degradation of chemically adsorbed specie. The study developed by Ledesma *et al.* (Ledesma *et al.*, 2014a) with carbons saturated with *p*-nitrophenol proved that, also in this case the desorption mechanism is a two-step process. So, according to the results reported in the literature, the paracetamol adsorption onto the carbons tested in the present study seems to follow a physisorption mechanism.

The fact that, in the case of sample GAC, the most important weight loss occurs at higher temperature than that of ACC and NS carbons may be explained in terms of samples morphology, porosity and surface chemistry. Actually, in the case of GAC it can be admitted that the temperature distribution inside the granular particles is not uniform. So, for molecules adsorbed in the inner part of the granules a higher temperature must be applied. On the other hand, as reported in the literature (Ledesma *et al.*, 2014b; Ferro-García *et al.*, 1993), in carbons with wide pore size distributions, desorption of the adsorbate may require lower temperatures. So, the behaviour of carbon NS may be linked to its developed mesopore network, associated to a high volume of wider micropores (see **Table VIII.3**). In the case of sample ACC, we can also admit that desorption is facilitated because the micropores of this carbon are connected to the surface. Additionally, the small particle size of NS favours the diffusion of the desorbed molecules towards the gas phase in comparison with what is expected to occur in the case of the granular sample. The surface chemistry may also justify the slightly distinct surface interactions of GAC with paracetamol since the C 1s XPS spectra reveals that, on the contrary of NS and ACC, in sample GAC no carbonyl or quinone groups were identified.

According to the thermogravimetric results, the regeneration experiments were made at 400 and 600 °C, for 1 h. To evaluate the impact of the heating regimes on the carbons texture, the samples were submitted to the experimental conditions chosen for the regeneration assays in the absence of paracetamol and the N₂ adsorption isotherms of the final samples are presented in **Figure VIII.13**, on the left.

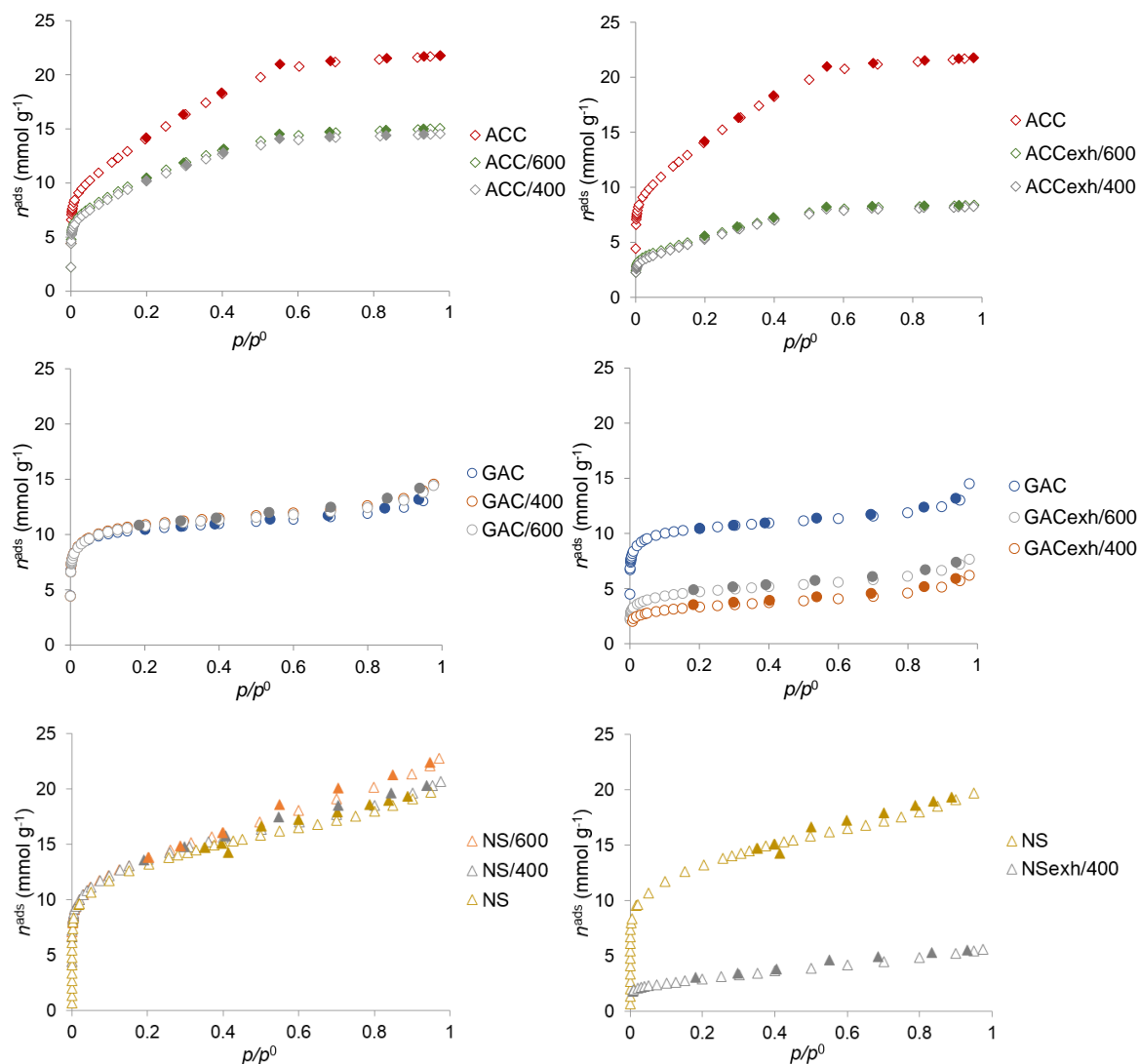


Figure VIII.13. Nitrogen adsorption-desorption isotherms at $-196\text{ }^{\circ}\text{C}$ of **(left)** samples heated in the absence of adsorbate, and **(right)** samples obtained after the 3rd regeneration cycle at the temperature indicated. Closed symbols are desorption points.

The results show that the curves of the treated samples maintain the configuration of the starting material, and only in the case of carbon ACC there is a decrease of the adsorption capacity, most certainly related to the 10 % weight loss observed in ACC thermogravimetric profile (**Figure VIII.11**). In the case of sample GAC the isotherms of the fresh and heated samples are coincident, and for NS the heating regime causes only a slightly increase in mesopore volume, especially when a higher temperature is used.

The textural parameters presented in **Table VIII.8** allow us to quantify the impact of the heating treatment on the carbon's texture. Regarding the cloth carbon, ACC, the heat treatment leads to an important loss of apparent surface area and supermicropore volume. Compared to the initial values, and regardless the temperature used, the A_{BET} decreases around 25 percents, and $V_{\alpha\text{ super}}$ about 32 percents. On the contrary, the heating has no significant impact on GAC texture, and slight positive effect in the case of the sample NS. The results show that, regardless the temperature, the A_{BET} values of the NS treated samples are quite close to the value of the pristine carbon. The heating treatment only affects the mesopore volume that, in comparison to the value presented by NS carbon increases a maximum of 27 percentage points, when 600 $^{\circ}\text{C}$ were used.

Table VIII.8. Nanotextural properties of the fresh activated carbons, samples heated at 400 °C and 600 °C and obtained after the 3rd re-use.

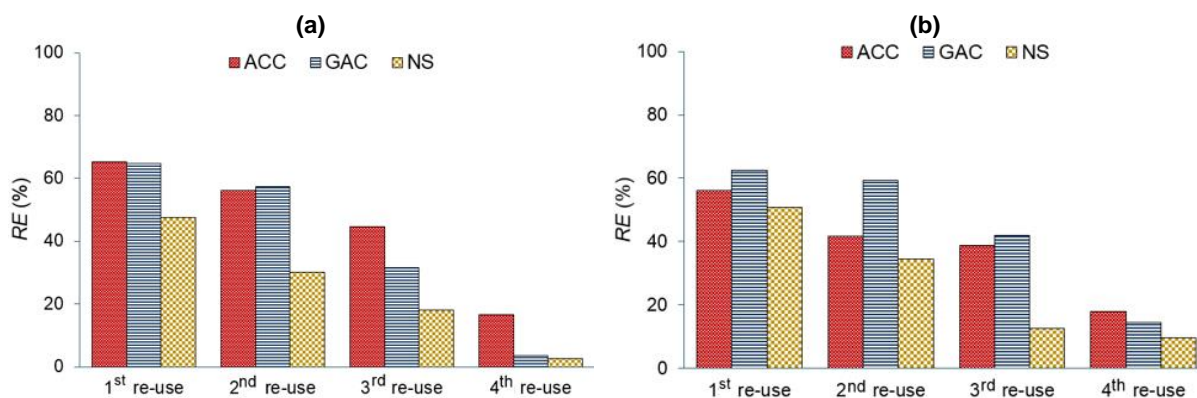
	A_{BET} ($m^2 g^{-1}$)	V_{total}^a ($cm^3 g^{-1}$)	V_{meso}^b ($cm^3 g^{-1}$)	α_S method ^c		
				$V_{\alpha total}$ ($cm^3 g^{-1}$)	$V_{\alpha ultra}$ ($cm^3 g^{-1}$)	$V_{\alpha super}$ ($cm^3 g^{-1}$)
ACC	1136	0.76	0.03	0.73	0.00	0.73
ACC/400	828	0.51	0.03	0.48	0.00	0.48
ACC/600	851	0.53	0.03	0.50	0.00	0.50
ACCexh/400	435	0.29	0.02	0.27	0.00	0.27
ACCexh/600	449	0.29	0.01	0.28	0.00	0.28
GAC	838	0.47	0.13	0.34	0.09	0.25
GAC/400	848	0.51	0.17	0.34	0.09	0.25
GAC/600	840	0.50	0.16	0.34	0.08	0.26
GACexh/400	166	0.22	0.14	0.08	0.00	0.08
GACexh/600	321	0.27	0.13	0.14	0.00	0.14
NS ^d	1065	0.70	0.30	0.40	0.02	0.38
NS/400	1083	0.72	0.33	0.39	0.01	0.38
NS/600	1088	0.80	0.41	0.39	0.01	0.38
NSexh/400	185	0.20	0.12	0.08	0.00	0.38

^aN₂ volume adsorbed at $p/p^0 = 0.95$; ^b $V_{meso} = V_{total} - V_{\alpha total}$; ^c α_S method applied using as reference the isotherm presented in Rodriguez-Reinoso and Martin-Martinez, 1987, ^dvalues presented in Mestre *et al.*, 2012.

The regeneration efficiency, $RE(\%)$, defined in Equation VIII.1, was assessed in terms of the paracetamol adsorption capacity retained by the recovered carbons, compared to the value presented by the fresh sample.

$$RE(\%) = \frac{q_i}{q_0} \times 100 \quad \text{Equation VIII.1}$$

The results obtained (**Figure VIII.14**) show that, as expected, the $RE(\%)$ values decrease gradually with the consecutive re-uses of the carbons, being this effect more accentuated after the 3rd re-use. On the other hand, the influence of the regeneration temperature on the carbon's performance seems to be dependent of the type of carbon used. The results obtained with ACC sample show that the use of milder conditions (400 °C) allows to recover somewhat higher paracetamol adsorption capacities. In these conditions, it is possible to apply two saturation-regeneration cycles maintaining 56% of ACC initial paracetamol capacity. Having in mind that, as it was previously discussed, the heating temperature by itself has a significant effect on this carbon texture, the decrease of the $RE(\%)$ values may result from the combination of the temperature impact on the texture and of a partial blocking of the porosity due to incomplete removal of paracetamol. The loss of ACC porosity is demonstrated by the textural parameters of the samples obtained after the 3rd re-use upon regeneration at 400 and 600 °C.


Figure VIII.14. Regeneration efficiency ($RE(\%)$) of samples ACC, NS and GAC, for consecutive re-uses after regeneration by thermal treatment at (a) 400 °C and (b) 600 °C for 1 h.

The values estimated from the analysis of the N₂ isotherms (see **Figure VIII.13** (right)), presented in **Table VIII.8**, reveal that the regenerated ACC carbon retains around 40% of the A_{BET} and $V_{\alpha_{\text{super}}}$ values presented by the fresh sample. Regarding the thermal regeneration of the granular carbon, our experiments were able to restore 58% of initial paracetamol adsorption capacity after two saturation-regeneration cycles at both temperatures. In this case, the decrease of the $RE(\%)$ may be attributed to the progressive obstruction of the porosity, since the textural characterization of samples heated at 400 and 600 °C in the absence of paracetamol did not reveal any significant loss of porosity. The N₂ adsorption results of the GAC regenerated samples (**Figure VIII.13** (right) and **Table VIII.8**) support this conclusion since there is a significant decrease of A_{BET} and micropore volume, especially in the case of the sample submitted to heat treatment at 400 °C. The relatively better results in the 3rd and 4th re-use cycles when the treatments were performed at 600 °C may be also linked to the fact that, as demonstrated by the DTG analysis, paracetamol removal from this carbon requires a higher temperature than in the case of the other samples. The less efficient regeneration was achieved with the powdered sample NS which, according to the results obtained, only presents $RE(\%)$ values around 50% after a single regeneration. Further re-uses of this carbon lead to a much accentuated decrease of paracetamol uptake. This behaviour is most likely due to the retention of paracetamol on the porosity which, as proved by the data presented in **Table VIII.8** for sample NSexh/400, obtained after 3 re-uses, leads to a drastic decrease of all the textural parameters.

VIII. 3. Partial conclusions

The removal of paracetamol and clofibric acid by powdered, granular and cloth activated carbons was evaluated by kinetic and equilibrium assays. The kinetic results showed that, for small molecules as those tested, the diffusion towards the adsorption active sites is ruled by the volume of wider micropores. Equilibrium data revealed different underlying adsorption mechanisms for the two target molecules. Paracetamol adsorption follows a Langmuir mechanism in all the carbons, while in the case of clofibric acid a more complex mechanism seems to be involved, which was attributed to the nature of the species present in solution. At high equilibrium concentrations, clofibric acid is always adsorbed in much larger amounts.

The regeneration through thermal treatment proved to be a valid strategy to recover the porosity of the paracetamol exhausted samples, especially at the lowest temperature tested (400 °C). The impact of the carbons' morphology was also demonstrated, differentiating positively the granular and cloth samples which could be re-used at least twice keeping adsorption capacities higher than 50%.

Lastly, the overall results show the potentialities of carbon cloth to compete with traditional morphologies since it presented adsorption performances identical, or even better, than powdered samples, and behaved equally well as granular samples when submitted to thermal regeneration. Thus aiming to a more sustainable society where the regeneration of spent carbons must become a rule, carbon cloth is an excellent option to the presently used granular morphology.

Chapter IX

Escherichia coli immobilization
on activated carbons: Impact of
immobilization conditions and
role of morphology

The research presented in this chapter was developed in the Microbiology and Biotechnology Lab, Centre of Biodiversity, Functional & Integrative Genomics, under supervision of my co-coordinator Doctor Ricardo Dias.

Activated carbons ability to remove *Escherichia coli* from aqueous solution was assessed, and the impact of several factors on the materials performance was evaluated. Furthermore, *E.coli* immobilization mechanism on a powdered activated carbon was investigated.

The results gave rise to a manuscript entitled “*E. coli* immobilization on activated carbons: Impact of operational conditions and role of morphology” presented in Appendix C.

IX. 1. Experimental procedure

IX.1.1. Preparation and characterization of activated carbons

Two commercial carbons were considered, one in the granular form, GAC, and the other one in the powder morphology, NS (see **Table IX.1**). From the sample, two other solids were prepared, by grounding and oxidation, that is, solids GACm and NSox, respectively. The potential of the activated carbon cloth ACC for bacteria removal from solution was also evaluated.

Table IX.1. Activated carbons studied and information regarding their preparation and/or provenance.

	Material	Information
Commercial	Granular Activated Carbon, GAC	Commercialized by Norit, with the name GAC830. This material is prepared from coal by water vapour activation, and it comprises 88 % of particles with dimensions between 0.60 mm and 2.36 mm. Among the information made available at Norit’s site, GAC830 is particularly referenced for purposes of thermal regeneration (http://www.cabotcorp.com/solutions/products-plus/activated-carbon/granulated).
	Powdered activated carbon, NS	Adsorbent commercialized by Norit, with the designation SAE SUPER. This powder solid is composed of 97 % (mass ratio) by particles with dimensions inferior to 0.15 mm.
Lab-made	Activated Carbon Cloth, ACC	Prepared in Instituto Nacional de Pesquisas Espaciais, in Brazil, following the experimental procedure presented in Appendix A1.3.
	Grounded GAC, GACm	Sample was obtained, by grounding and sieving the carbon GAC in order to obtain the fraction of particles between 0.420 and 0.297 mm.
	Oxidized NS, NSox	Prepared according to the experimental procedure presented by Mestre <i>et al.</i> , 2012. 1 g of NS was suspended in 10 cm ³ of HNO ₃ (Sigma-Aldrich, 65 %), and heated until boiling temperature, under stirring. The treated carbon was successively washed with distilled water until negative test for nitrate ions. For this test some drops of a solution of diphenylamine (Merck) in sulfuric acid (Merck 96 %) were added to the washing water. To finish the carbon was dried at 100 °C.

The characterization of the solids has been previously made, and so ACC textural, chemical and morphological characterization data was previously presented in Chapter VIII, and the textural properties of the carbons NS, NSox and GAC, as well as their pH_{PZC} value and ash content have been previously reported in published articles made by the research group where this PhD thesis was developed (Mestre *et al.*, 2012). Furthermore, the characterization of sample GACm, through the mentioned techniques, was previously made during my master thesis entitled “Remoção de poluentes em solução aquosa por carvões ativados” (Marques, 2011). Still, the characterization

results of the samples will be presented in this chapter for purposes of discussion of the results.

IX.1.2. Immobilization experiments

Studies regarding bacteria immobilization on activated carbons were made, following the experimental procedure presented in Appendix A.3.3.2. All the experiments were carried out at least three times to ensure data reproducibility.

The impact of several experimental parameters was assessed, including the influence of the activated carbons properties (texture, morphology, particle size and surface chemistry), and the adhesion medium (chemical composition and cellular concentration/mass carbon ratio) on *Escherichia coli* removal from solution (see **Table IX.2**). In an effort to approximate these experiments to real conditions, the impact of the presence of caffeine, a biological marker for faecal contamination, on bacteria immobilization was also taken into account.

Table IX.2. Parameters studied in the *E. coli*'s removal by activated carbons assays, and the corresponding experimental conditions used. Viability and contamination controls performed.

	Carbon		Solvent	Cellular density	Experiments
	Sample	mg per 10 mL solution			
Particle size	GAC GACm NS	150 mg	STD water	8log	Kinetics (up to 48 h)
Surface chemistry	NS NSox				
Medium chemical composition	GAC GACm NS	10,50, 150 mg	STD water NaCl 0.5 % PBS		
Presence of caffeine		150 mg	Caffeine solution (180 mg dm ⁻³)		
Carbon dosage vs inoculum density	NS	1.5, 15, 50, 100, 150 mg		5log 6log 8log	
Morphology/porosity	ACC NS GAC	150 mg	STD water	8log	
Viability and contamination control					
Cellular viability	The suspension of cells in the solvent studied was monitored in parallel with each immobilization experiment.				
Contamination control	The solids were kept in suspension in the sterilized solvent and monitored in parallel with each immobilization experiment. This control was used to prevent the use of contaminated solid, and to monitor possible contaminations coming from the sampling procedure.				

Detailed information concerning the studied *Escherichia coli* strain, culture conditions, and the immobilization experiments procedure are presented in Appendix A3.3.1, as well as information regarding caffeine.

The number of *E. coli* viable cells (colony-forming units – CFU) present in solution after contact with the carbon material was quantified by serial dilution plating method. When the bacteria suspension was prepared using caffeine solution as solvent, caffeine concentration in solution during the assays was determined by UV-Vis

spectrophotometry. The experimental procedures adopted for bacteria and caffeine quantification are presented in Appendix A.3.3.3.

Suspensions of NS carbon in cellular medium were analysed by optical and phase-contrast microscopy (Appendix A3.3.4).

IX. 2. Results and discussion

The removal of *Escherichia coli* cells from solution by activated carbons was studied by different approaches, to evaluate the influence of several experimental parameters on this process.

In order to evaluate the impact of the carbons particle size on *E.coli* removal from aqueous solution, a granular (GAC) and powdered (NS) activated carbons were considered. The solids present basic nature (pH_{PZC} GAC – 8.9 and NS – 8.4) and maximum particle sizes of 0.42 and 0.15 mm. **Figure IX.1** presents the results of the assays made with 10, 50 and 150 mg, after 27 and 48 h of contact time.

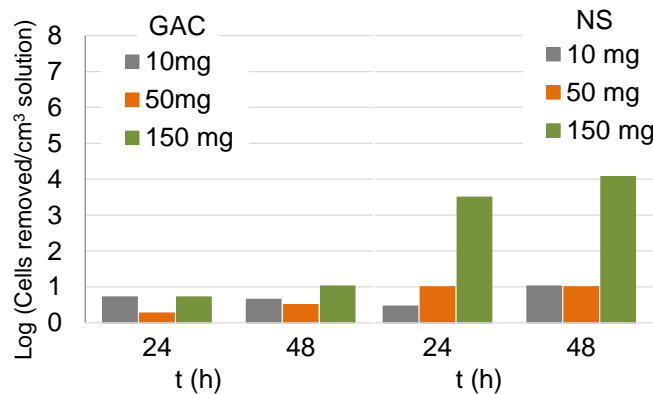


Figure IX.1. *E. coli* removal, in STD water, by the mentioned carbons after 24 and 48 h.

The best performance was achieved with 150 mg of NS carbon that was able to remove a maximum value of 4log of cells after 48 h, in comparison to 1log of cells removed by GAC sample. Most of the bacteria adhesion occurred in the first 24 h, followed by the additional removal of less than 1log of cells from solution. Further studies on this topic were carried out through kinetic experiments with 15 mg of carbons, and included the grounded sample GACm (see **Figure IX.2**), of intermediate size.

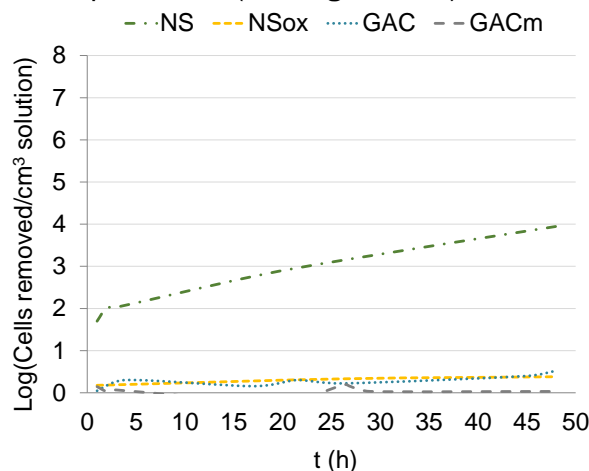


Figure IX.2. *E. coli* removal, in STD water, by the mentioned carbons. No loss of cell viability was detected in STD water during the duration of the experiment. No contamination of the adsorbents was detected either.

The results show that bacteria removal only occurred in the case of the powder sample, NS, which was able to immobilize up to 4log of cells *per* cm³ of solution after 48 h of contact time.

According to studies reported in the literature that point out that an initial adhesion phenomenon is consequence of electrostatic interactions established between the cell wall (charged negatively) and the carbons surface, one could expect a higher removal of cells by samples GAC and GACm, of basic nature (charged positively at the water pH). The fact that the samples removed 0.5log of cells cm⁻³ and less can be explained by their lower external surface (higher particle size). Also, NS solid presents a high content of ashes (13 %), in comparison to that of GAC and GACm (6 %). The presence of metallic oxides in NS matrix may indirectly favour bacteria adhesion due to the formation of hydrogen bonds between water chemisorbed on the oxide surface and the bacterial surface polyssacharides (Jucker *et al.*, 1997).

To evaluate the impact of the surface chemistry on the samples colonization, the oxidized sample NSox, with a pH_{PZC} of 3.7 was tested. No significant cell adhesion occurred in NSox (removal of 0.5log of cells cm⁻³), since both the carbon and bacteria cell will present a negatively charged surface in solution. Thus, even though favourable initial interactions cell wall-carbon surface may not be sufficient to ensure adhesion on carbons with high particle size, repulsive forces between *E. coli* cells and NSox surface were enough to prevent colonization of this solid with a high contact surface available for adhesion. This suggests that the establishment of favourable electrostatic forces between bacteria cell wall and carbon surface is a crucial first step to the immobilization process.

These experiments were continued to explore the role of morphology on *E.coli* adhesion, and so equilibrium experiments were carried out with cloth (ACC), granular (GAC), and powder (NS) samples. The removals achieved after 24 and 48 h are presented in **Figure IX.3**.

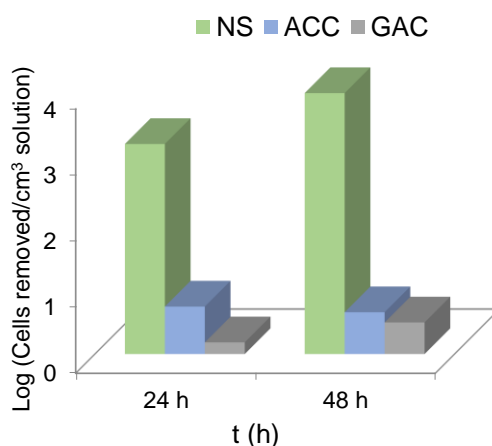


Figure IX.3. *E. coli* removal after 24 and 48 h, by the powder, cloth and granular carbons, in STD water.

Since the porosity of the carbons is inaccessible to the bacteria, and the surface chemistry of the adsorbents is similar (pH_{PZC} NS – 8.4; ACC – 9.0; GAC – 8.9), the assays of immobilization, performed under equilibrium conditions, allowed to infer about the influence of the activated carbons morphology in *E. coli* removal. The results prove NS to be again the most effective material, followed by ACC and GAC samples. ACC reached its maximum performance (removal of only 1log of cells) during the first 24 h. In the case of the granular morphology, GAC carbon seems to immobilize cells in a more progressive way, reaching a removal of approximately 0.5log after 48 h.

One could expect better results from the cloth morphology taking into account the texture of this solid, analysed previously by SEM in Chapter VIII (**Figure VIII.4**). This sample is composed by yarns of cylindrical shape, with average diameter of 20 μm , distanced by an average distance higher than 100 μm . Considering *E. coli* cells dimensions (length of 1-3 μm and diameter of 0.5-1 μm), the structure of the cloth carbon seems to be favourable to the immobilization of cells, by having a readily accessible surface to bacteria adhesion. Moreover, the large diameter of the cloth yarns would allow for the establishment of interactions cell-carbon cloth. However, the performance of this morphology suggests, on the contrary, that the open structure of the solid has a negative impact of the colonization, possibly because the number of interactions bacteria-carbon (necessary to adhesion) would occur in a significantly lower number than the interactions bacteria-bacteria.

The high performance exhibited by NS made it a probe material for the further studies. In this context, the effect of media composition and amount of carbon on *E. coli* immobilization were studied. For this, 10, 50 and 150 mg of NS were dispersed in an *E. coli* suspension (initial concentration 8log cells cm^{-3}) prepared in STD water, NaCl 0.9% and phosphate buffer solutions (PBS). As expected, the increase of carbon amount favoured bacteria removal from solution (**Figure IX.4**).

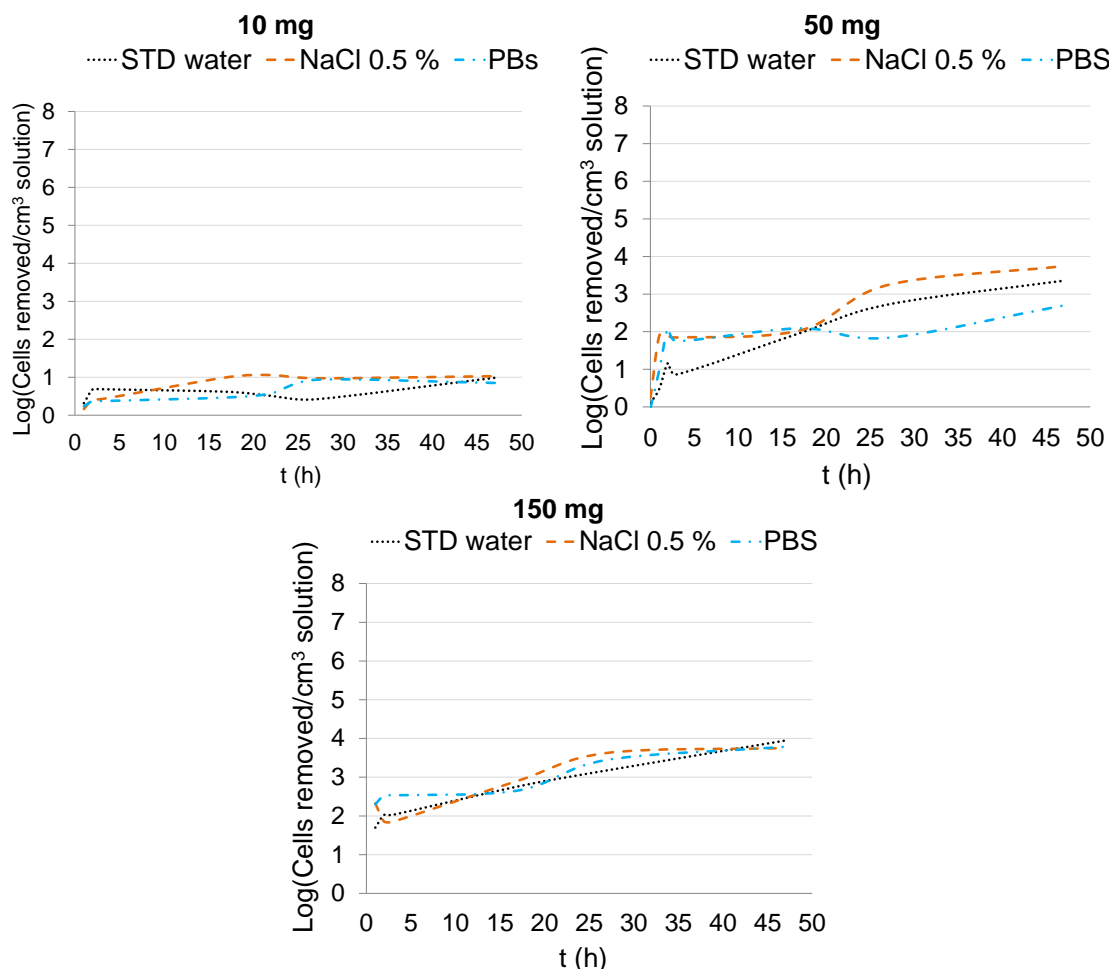


Figure IX.4. Impact of solution chemical composition on *E. coli* removal from solution by 10 mg, 50 mg, and 150 mg of NS.

Regardless the media, the assays using 10 mg led to a maximum removal of 1log of cells cm^{-3} in the first hours of contact time. When 50 mg were tested, the profile of the

removal kinetic curves seem to indicate the occurrence of a two-step immobilization process, more evident in NaCl 0.9 % and PBS than in water. In these systems, a 2log removal of cells occurred after approximately 20 h of contact time, leading to removals of 4log cells cm⁻³ (NaCl 0.9 %), and 3.5log cells cm⁻³ (PBS) after 48 h. In water, the immobilization occurred continuously and a final removal of 3log cells cm⁻³ was achieved. At last, the use 150 mg of NS allowed to obtain similar results in all the solvents tested, with a final removal of 4log of cells per cm³ of solution.

As mentioned above, the impact of the solvent on adhesion is more visible in the data obtained with 50 mg of carbon, and show that initial bacteria adhesion was more favoured in solvents NaCl 0.9 % and PBS, than in STD water. This can be explained by the fact that, as it was mentioned in the Introduction (Chapter VI), the external surface of *E. coli*'s cell wall contains lipopolysaccharides with carboxyl and phosphoryl groups that become ionized at the solutions pH. As a result, sodium cations present in the solvents can be electrostatically attracted to the cellular surface, decreasing the hydrophobicity of the bacteria cell wall. The same occurs to the activated carbon surface, which becomes more hydrophobic in a solution of high ionic strength. The increase in hydrophobicity of the cell wall and solid surface is important to the adhesion phenomenon because it prevents the formation of a water layer at the surface of both bacteria cells and AC's surface, and so the interface *E.coli* - water molecules and NS surface – water molecules will be more easily replaced by the adhesion interface *E.coli*'s external wall – NS surface.

As the adhesion process progresses the more complex composition of PBS solvent (Na₂HPO₄, NaH₂PO₄ and NaCl) may have a shielding effect on the carbons particles and bacteria cells preventing the occurrence of a second stage of immobilization. On the other hand, considering that NaCl 0.9% seems to promote bacteria adhesion, one could expect a higher increase in removal when using 150 mg of carbons. However, on the contrary, similar removal efficiencies were observed.

Immobilization studies, in the presence of caffeine were carried out to investigate the impact of this pollutant on bacteria adhesion on NS carbons. Furthermore, since several studies have reported that the presence of micropollutants, namely metal ions, may promote bacteria immobilization (Rivera-Utrilla *et al.*, 2003; Rivera-Utrilla *et al.*, 2001), NSox sample was also considered in this study. **Figure IX.5** presents the results obtained in caffeine solution, and compares them to the results obtained in STD water, previously presented in **Figure IX.2**. No loss of cell viability was detected in caffeine solution during the duration of the experiment.

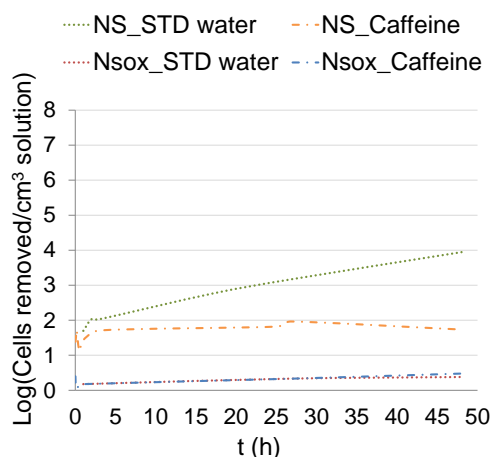


Figure IX.5. Effect of presence of caffeine on *E. coli* cells removal. No loss of cell viability was detected in caffeine solution and STD water during the duration of the experiment.

The results show that caffeine has a clear negative effect on bacteria adhesion onto NS, and no impact on the performance of NSox.

NS removed approximately 2log of cells in the first 1 h of contact time. In STD water, adhesion continued to occur leading to a maximum 4log removal, whereas in caffeine solution no further removal occurred after the initial adhesion.

One possible explanation for the impact of caffeine on NS results could be that caffeine species (positively charged) could decrease the amount of electrostatic interactions between cell wall and carbon surface. However, caffeine was never detected in solution during experiment. The same scenario was observed in the case of the oxidised sample NSox. The cellular concentration of the suspension prepared in caffeine solution remained constant throughout the experiment pointing out no degradation of caffeine compound by the microorganisms. So, one can infer that caffeine was quickly adsorbed by both adsorbents, not remaining in contact with carbon surface and/or cell wall. These findings suggest that, the lower performance of NS was due to the saturation of the carbon particles with caffeine prior to bacteria colonization.

Kinetic experiments were carried out to evaluate different scenarios of amount of carbon vs inoculum density, that is, cellular concentration. The results obtained are illustrated in **Figure IX.6** and clearly point out the importance of this study, revealing an effect of the mass of adsorbent on bacteria removal and, on the other hand, the impact of cellular concentration on the performance of the material.

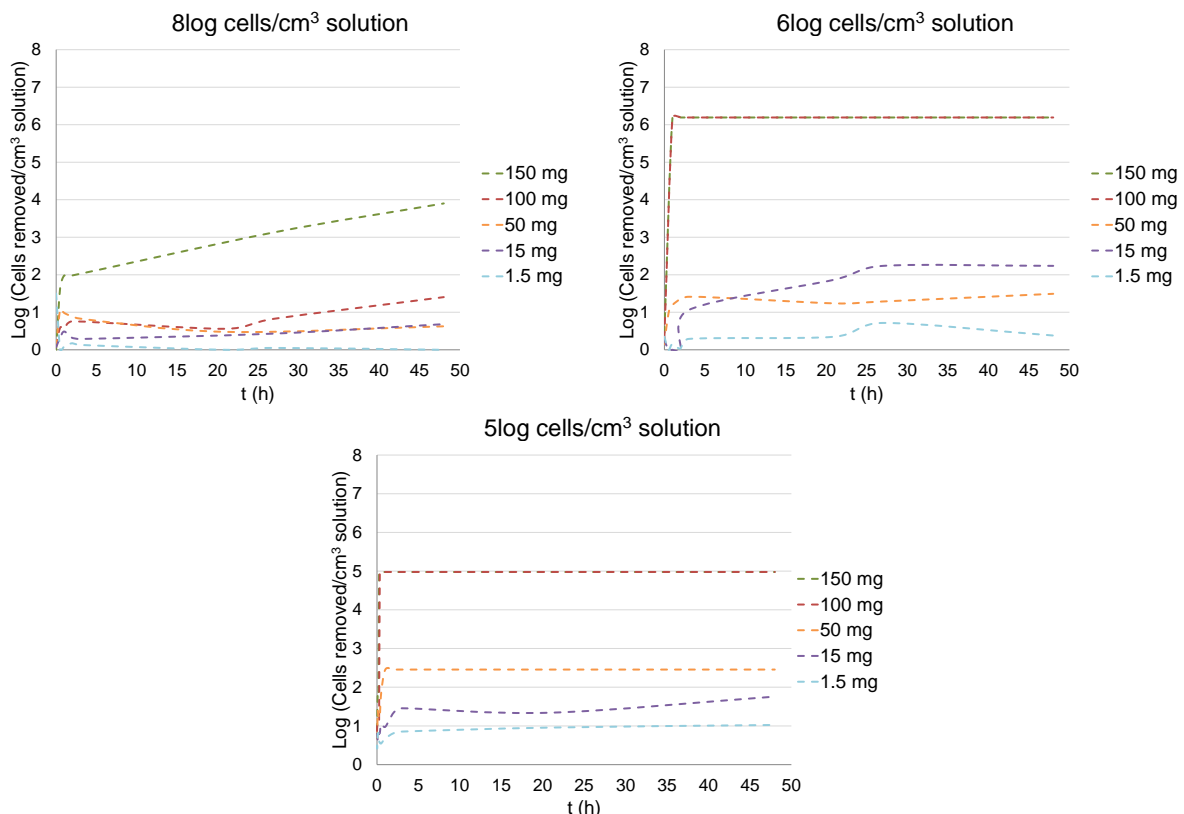


Figure IX.6. Effect of carbon dosage on cellular suspensions of approximately 8log cells cm⁻³ solution 6log cells cm⁻³ solution and 5log cells cm⁻³ solution.

NS has proved to be very efficient in removing *E. coli*'s cells from solution. All the tested amounts were able to remove cells from solution, except when 1.5 mg of NS were used in the 8log cells cm⁻³ suspension.

The results demonstrate that higher amounts of carbon led to higher removal efficiencies, with exception of 50 and 1.5 mg in the 6log cells cm^{-3} cellular suspension.

The results concerning the use of 150 mg of NS in the most concentrated suspension have been previously discussed, and have shown an initial adhesion of 2log in the first hour, followed by a gradual immobilization of cells up to 4log. The use of 100 mg allowed to immobilize only approximately 1.5 log of cells cm^{-3} , less than half of the number of cells immobilized by 150 mg, and the lower amounts removed less than 1log of cells.

In the suspension of 6log cells cm^{-3} total removal was achieved with 150 and 100 mg of NS. In this system, 1.5 mg were able to remove cells than the amount of 50 mg, which clearly suggests that bacteria removal is the result of an equilibrium between cellular concentration and amount of carbon.

The results obtained in the less concentrated suspension show a complete removal with 150 and 100 mg of NS, and a mass effect is observed for the remaining quantities tested, that is, higher amount immobilized higher number of cells.

The results obtained point out that NS removed a higher number of cells in less concentrated suspensions. To better understand this phenomenon, the removal efficiencies of each amount are compared in the next figure (**Figure IX.7**).

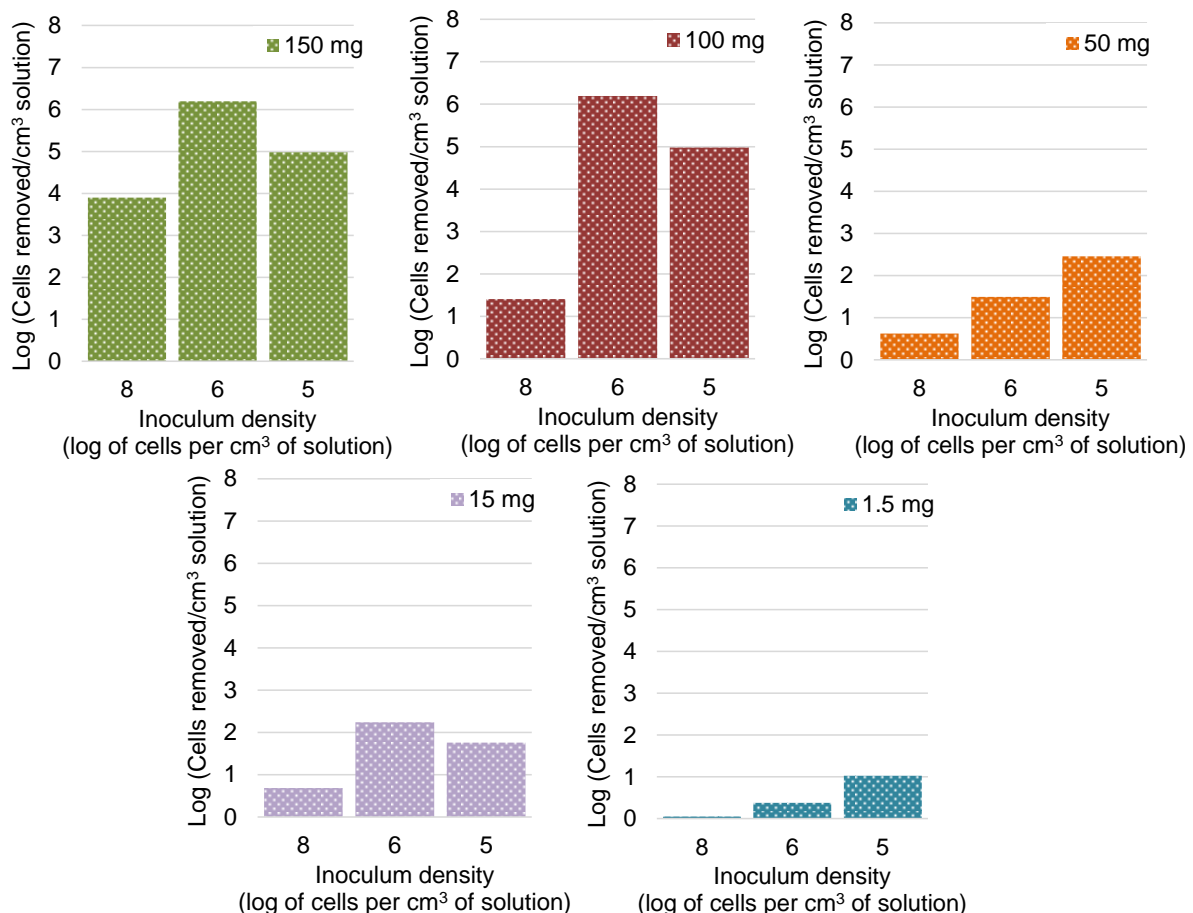


Figure IX.7. Comparison of the removal efficiencies achieved by each NS amount in the cellular suspensions.

The results show that best removals were achieved with 150 and 100 mg of NS in the intermediate concentration tested. In a more or less concentrated cellular medium, a decrease in performance was observed for these amounts, and for 1.5 mg. On the

contrary, 50 mg and 1.5 mg presented better results in the less concentrated suspensions.

These results clearly evidence that there is no direct correlation between NS mass and removal efficiency. In fact, one could expect that, when a higher number of cells is present (case of $8 \log \text{ cells cm}^{-3}$ suspension), higher number of interactions between cell wall and carbon surface should occur, especially considering a powder carbon easily dispersed by the suspension. On the other hand, better performances were expected to occur in the less concentrated inoculum, since the cellular suspension consisted in a small volume of 10 cm^3 and the materials dispersion throughout this volume was adequately promoted. The data obtained clearly suggest an adhesion mechanism based not only on the coating of NS particles surface.

Studies regarding the impact of inoculum density and carbon amount on bacteria adhesion was not found in the literature during the development of this work.

In order to better understand the underlying mechanism, responsible by the good performance presented by NS carbon, the dispersion of different amounts of this carbon in cellular suspension was analysed by optical microscopy (**Figure IX.8**).

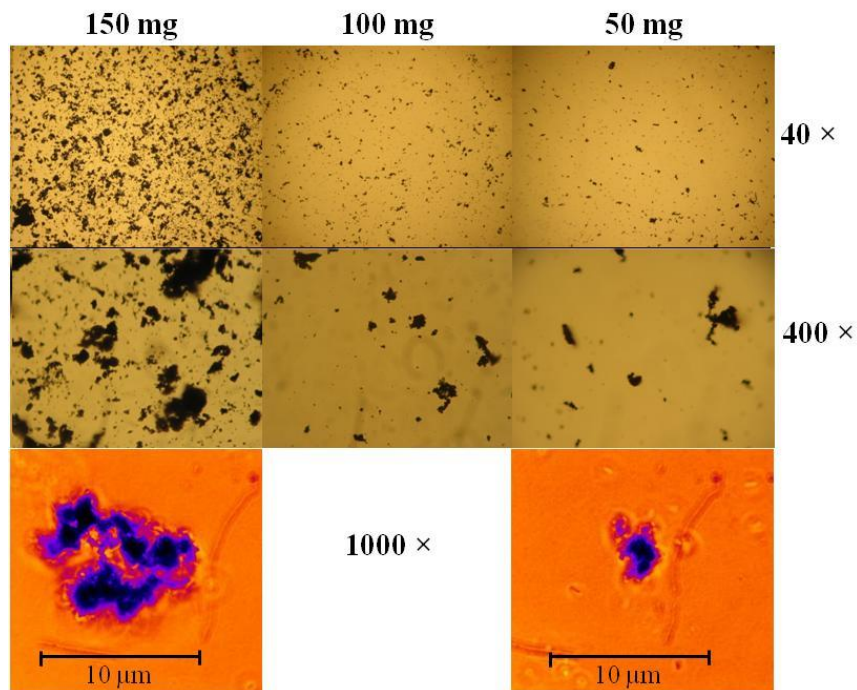


Figure IX.8. Optical microscopy of NS carbon in cellular suspensions standardized at $8 \log \text{ cells cm}^{-3}$, viewed with amplifications of 40, 400 and 1000x.

The images obtained at amplifications of 40, 400x show a good dispersion of this carbon in cellular suspension ($8 \log \text{ cells cm}^{-3}$ of solution) and suggest the formation of agglomerates carbon-cell-cell-carbon, possibly due to electrostatic interactions between NS superficial groups and *E. coli* cell, besides the ones attached only to the carbon. This phenomenon seems to be favoured by higher amounts of NS, which form agglomerates of higher volume, entrapping higher number of cells. Thus, despite ACC structure having a very accessible surface area, with high distance between yarns, *E. coli* immobilization is more efficient in the powder carbon, where electrostatic interactions carbon-bacteria seem to be favoured and complemented by the formation of agglomerates carbon-cell-cell-carbon. In order to see the actual formation of these 3D structures, a cellular suspension, in contact with NS carbon after 30 min, was observed by electronic microscopy and the assembling mechanism of the agglomerates recorded. The frames

captured (**Figure IX.9**) show that the formation of these protection structures is a consequence, not only, of the stirring, but also due to the “dragging” of powder carbon particles by the bacteria in a coordinated effort – the bacteria coating the carbon particle are attracted towards the close carbon agglomerate, and the cells make an effort of moving towards this structure, as can be seen by their orientation towards it.

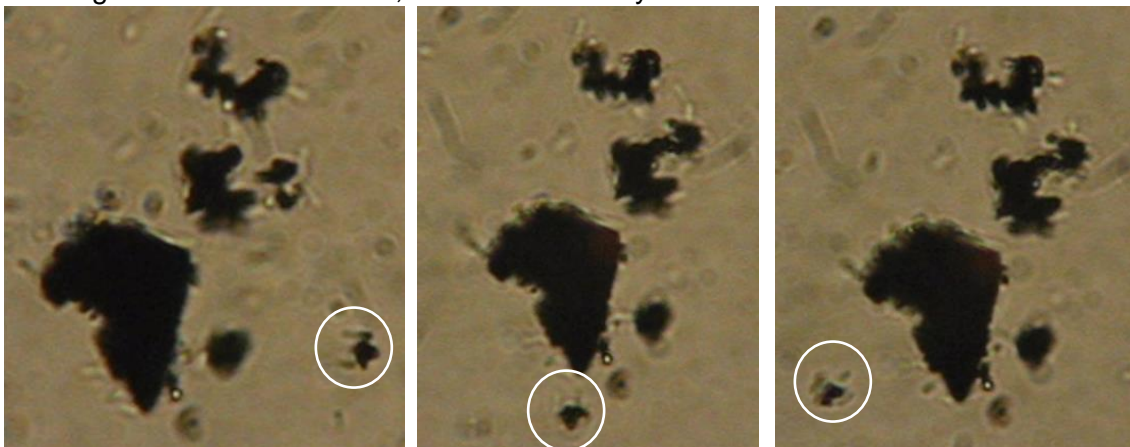


Figure IX.9. Frames obtained with an amplification of 1000x of a carbon aggregate formed after 30 min of contact between cellular suspension and carbon. One bacteria-carbon particle is evidenced by the white circle.

This “capture” of the immobilization mechanism of *E. coli* cells on NS also helps to explain the less efficient immobilization of cells onto the carbon saturated with caffeine. One can hypothesize that the “heavier” exhausted particles are more difficult to dislocate in solution by the cells, limiting the formation of the agglomerates and, consequently affecting negatively the immobilization (and removal) of cells from solution.

IX. 3. Partial conclusions

The removal of *E. coli* cells from solution by activated carbons was studied by different approaches, and the influence of several experimental parameters was evaluated.

Significant bacteria removal was only possible in the carbon with smaller particle size, NS, and 4log of cells cm^{-3} were removed after 48 h of contact time. The results were attributed also to the basic nature of the carbon (pH_{PZC} of 8.4) and high ash content (13 %).

No adhesion of cells occurred on the oxidized sample NSox, with a negatively charged surface, pointing out that the repulsive forces between cell-carbon surfaces were enough to prevent colonization of the solid. Higher NS amounts removed higher number of cells, especially when the solvent NaCl 0.9 %, with a higher ionic strength was used.

The profiles of the kinetic curves obtained with 150 mg of NS suggest at least two stages in the bacteria immobilization mechanism: an initial adhesion of cells on NS surface, formed quickly in the first 1 h, and attributed to the initial favourable interactions cell wall-carbon surface, followed by a second slower mechanism of adhesion of cells.

NS was more efficient removing cells from less concentrated bacteria suspensions (6log and 4log cells/ml of solution), reaching removal efficiencies of 100 % when 150 mg of carbon were used.

Caffeine had a clear negative effect on bacteria immobilization onto NS material, causing a 2log less removal of cells. Moreover, tests with NSox demonstrated that, no change in this sample surface nature occurred as consequence of the presence of caffeine (positively charged, at the solution pH). The negative impact of caffeine was attributed to the saturation of the carbon particles prior to bacteria adhesion.

The cloth morphology proved not to be very efficient in removing cells, pointing out that its structure, with a high distance between yarns did not promoted the establishment of a high number of interactions bacteria-carbon.

NS carbon dispersion in cellular suspensions was investigated by optical microscopy, and the experiments revealed that *E. coli* immobilization on NS sample occurs due to electrostatic interactions carbon-bacteria, and also due to the formation of agglomerates carbon-cell-cell-carbon that allow for the “entrapment” of a higher number of cells. These protection structures are formed, not only, due to the stirring of the suspension but also due to the “dragging” of the powder particles by the bacteria in a coordinated effort. The saturation of the carbon particles prior to bacteria colonization makes the formation of these structure more difficult, and affects negatively the removals achieved.

Chapter X

Tannin-based materials for water remediation: Adsorption mechanism and removal of Pharmaceutical and Personal Care Products (PPCPs) from aqueous phase

The work presented in this chapter was a multi-step study that, in a first stage aimed to understand the impact of different amounts of surfactant on the porosity of the prepared tannin-based powders and, consequently, on the content and availability of the phenolic groups of the matrix. Then, the thermal-assisted hydrolysis of one of the polymers was performed with hydrochloric acid and the resulting impact on the textural and chemical properties was evaluated. On a second stage, the potential of the lab-made samples to retain methylene blue dye from aqueous solution was assessed. The liquid phase experiments were further complemented by screening retention assays, with two of the powders, for several of the most consumed worldwide pharmaceuticals.

This study was performed during a three month internship in Institut Jean Lamour, UMR Université de Lorraine CNRS7198 (Epinal, France) under the supervision of Research Director Vanessa Fierro.

X. 1. Experimental procedure

X.1.1. Preparation of the tannin-based powders

The samples studied were designated according to (wt% surfactant)M. The sample obtained after treatment with hydrochloric acid treatment was designated 5AM.

The powder materials 2M, 5M and 8M were previously prepared in Université de Lorraine and supplied for the development of this study. 5AM sample was prepared during the development of this study. The experimental procedures are presented in Appendix A1.4.

X.1.2. Material's characterization techniques and liquid phase adsorption

Textural and chemical characterization of the polymers was performed through several techniques (see **Table X.1**), namely mercury porosimetry, water vapour adsorption, and elemental analysis, among many others. The materials thermal stability was also assessed through thermogravimetric analysis.

Table X.1. Experimental procedures of the characterization techniques employed.

Characterization	Technique	Appendix A
Texture	Mercury intrusion	2.4
	Skeletal density determination	2.14
	Water vapour adsorption	2.3
Chemical	pH at the point of zero charge (pH _{PZC}) determination	2.8
	Elemental analysis	2.11
	Phenolic group content determination	2.10
	Contact angle measurement	2.9
	Water vapour adsorption	2.3
	Fourier Transform Infrared spectroscopy (FTIR)	2.15
Thermal stability	Thermogravimetric analysis (TG)	2.16

The potential of the solids as adsorbents in aqueous phase was evaluated through kinetic and equilibrium adsorption experiments with a numerous set of pollutant compounds (**Table X.2**).

Detailed information regarding reagents, solutions preparation and molecular properties of the pollutants is presented in Appendix A.3.1.

Table X.2. Experimental procedures of the liquid phase adsorption experiments.

Liquid phase adsorption	Experiment	Procedure
Methylene blue (MB)	Kinetic and equilibrium adsorption experiments with 2M, 5M and 8M samples	3.2
Bisphenol A (BPA) Diclofenac (DCF) Ibuprofen (IBU) Atenolol (AT) Atorvastatin (ATORV) Tetracycline (TC) Paracetamol (PARA) Ranitidine (RAN)	Equilibrium adsorption points with 5M and 5AM samples	3.2

Detailed information regarding reagents, solutions preparation and molecular properties of the pollutants is presented in Appendix A3.1.

X. 2. Results and discussion

The impact of the different formulations on the texture, chemical and physical properties of the samples was evaluated through different techniques in order to better understand the mechanism of preparation of this type of materials, as well as to determine the best material to proceed into the liquid phase adsorption experiments.

X.2.1. Characterization of the adsorbents

The porous structure of the samples was characterized by mercury porosimetry. The mercury isotherms obtained, as well as the pore diameter distribution evaluated by the Washburn method (Washburn, 1921) are presented in **Figure X.1**.

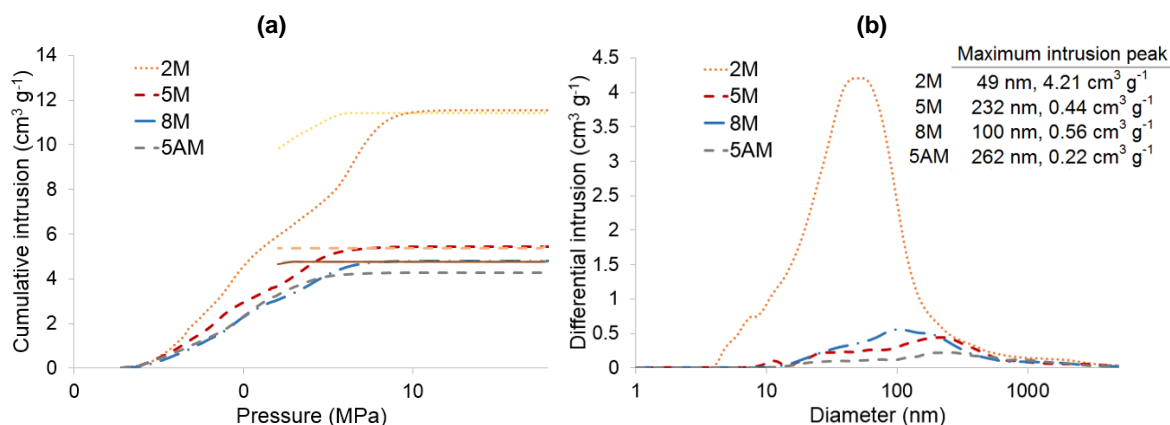


Figure X.1. Mercury porosimetry: **(a)** intrusion isotherms and **(b)** pore diameter distributions of the tannin-based powders.

The materials present intrusion curves with similar configurations (**Figure X.1 (a)**), with an increasing volume of mercury intrusion at lower pressure values, followed by a saturation plateau. The increase in surfactant amount from 2 to 5 wt % caused a significant loss in porosity (less amount of mercury intruded), and the widening of the pores (saturation reached at lower pressure values). On the other hand, the further increase to 8 wt %, seems to have almost no effect on the material's porosity. In comparison to 5M, sample 5AM presents a slightly smaller pore volume, and a widening of the pores seems to have occurred due to hydrolysis.

The pore diameter distributions of the materials (**Figure X.1 (b)**) confirm the meso, and essentially macropore nature of the solids, with pores size between 4.2 nm and 10 μm in the case of sample 2M, and between approximately 12 nm and 10 μm for 5M,

8M and 5AM solids. Sample 2M distinguishes itself by having a larger volume of narrower pores, with a maximum differential intrusion peak at 49 μm . The increase of surfactant amount to 5 and 8 % led to wider pores and, possibly as a consequence, the volume of pores 12 nm to 10 μm wide is lower.

Treatment of sample 5M with hydrochloric acid does not seem to have a significant impact on the pore size distribution but a slight decrease in pore volume is observed.

Skeletal density is also a textural indicator and so, density measurements of the pristine materials were made. The solids are not very dense materials, as density values of 1.64, 1.28 and 1.32 g cm^{-3} were obtained in the case of 2M, 5M and 8M, respectively. These materials are, in fact, much less dense than activated carbons (densities commonly around 2.1 g cm^{-3} (Elsayed *et al.*, 2017) and activated carbon fibres (2.2 g cm^{-3}) (Kunowsky *et al.*, 2013).

Chemical characterization of the solids by elemental analysis and pH_{PZC} determination (results presented in **Table X.3**) show that the chemical composition and surface chemistry of the materials are similar, with exception of powder 2M.

Table X.3. Elemental analysis (wt %) and pH_{PZC} values of *Mimosa* bark of the mentioned samples.

	Elemental analysis (wt %)					pH_{PZC}
	C	H	N	O	S	
<i>Mimosa</i>	55.29	5.04	0.23	39.44	0.00	-
2M	53.72	5.44	2.72	37.89	0.23	5.4
5M	61.35	7.60	1.63	29.36	0.06	5.5
8M	62.50	7.88	1.56	28.05	0.01	5.6
5AM	59.70	7.33	1.50	31.34	0.13	5.6

As it was expected, the predominant element of the tannin polymers is carbon (content higher than 50 wt.%), followed by oxygen (contents higher than 28 wt.%). In regards to the oxygen content, which is linked to the presence of phenolic groups, results follow the trend 2M > 5AM > 5M \approx 8M with small differences in percentage between the samples (higher difference is between 2M and 5AM). Nitrogen, oxygen, and sulfur contents are also detected in higher percentage in solid 2M.

One could expect a decrease of the *Mimosa* bark nitrogen content during polycondensation reaction, however the contrary is observed. The nitrogen quantified in the powders can be attributed to the crosslinking agent hexamine that allows for the connection of tannin units by a benzylamine bridge. The same logic can be used to explain the materials's sulfur content which may come from the polycondensation catalyst used, *p*-TSA.

Considering the polymers chemical structure, previously presented in the introductory chapter III (**Figure III.10**), the oxygen content can be translated in phenolic groups, acidic in nature. The pH_{PZC} values confirm this and show that the differences in oxygen content do not seem to have a significant impact in the samples acidity (similar pH_{PZC} values).

Water adsorption experiments were performed to characterize the materials texture and to assess the hydrophilic/hydrophobic nature of the solids. The isotherms presented in **Figure X.2** show that all the curves have similar sigmoid profiles, being classified as type II isotherms (Delgado-Sánchez *et al.*, 2016; Thommes *et al.*, 2015), characteristic of water adsorption on hydrophobic surfaces. In this sense, the curves present a small shoulder at low relative pressures and a sharp increase of water uptake at high relative pressures, as well as, a significant hysteresis cycle.

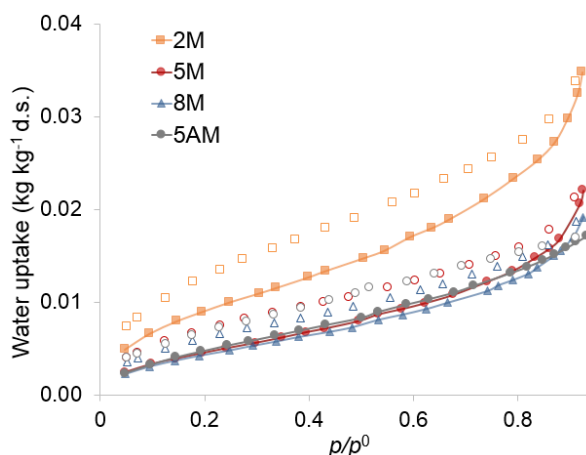


Figure X.2. Sorption isotherms of water on the mentioned samples.

The water adsorption data confirm the predominant hydrophobic nature of the materials, revealing low water uptake values for all the samples. The adsorption capacities of the solids are similar, with exception of sample 2M, which is obviously more hydrophilic.

Hydrophobicity/hydrophilicity studies were complemented by contact angle measurements, being the results shown in **Figure X.3**. The samples tested have a hydrophobic nature, in line with water adsorption results, with contact angles between 120° and 140°, and revealing that 2M has a more hydrophilic surface nature, followed by 5M and 8M.

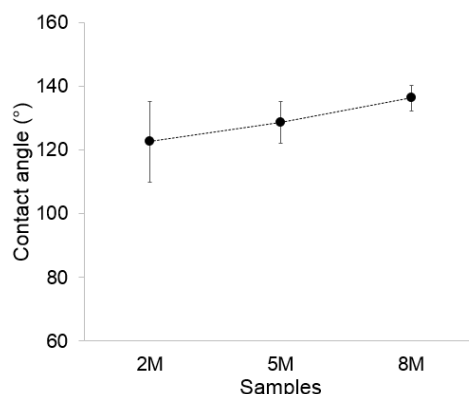


Figure X.3. Water contact angle measurements at the surface of the dried monoliths pellets. Mean deviation values are presented.

The phenolic group content of the materials was quantified by the Folin-Ciocalteu method (**Table X.4**). This technique allowed to determine the amount (g) of tannic acid equivalents present in 100 g of sample by complexation of the phenolic groups with the Folin-Ciocalteu reagent.

Table X.4. Total phenol content of the materials, obtained by the Folin-Ciocalteu method. Results are expressed in g of equivalents of tannic acid (ETA) *per* 100 g of sample.

Total polyphenol content in g (ETA) <i>per</i> 100 g sample	
2M	0.157
5M	0.012
8M	0.003
5AM	0.017

The results show that sample 2M presents higher phenolic content, one to two orders of magnitude higher than the other samples. As the surfactant concentration increases,

the phenolic groups content decrease one order of magnitude, and also, treatment with HCl did not have an impact of the phenolic content.

Besides the characterization techniques presented previously, all the samples were further characterized by Fourier Transform Infrared spectroscopy (FTIR), and the resulting spectra are presented in **Figure X.4**.

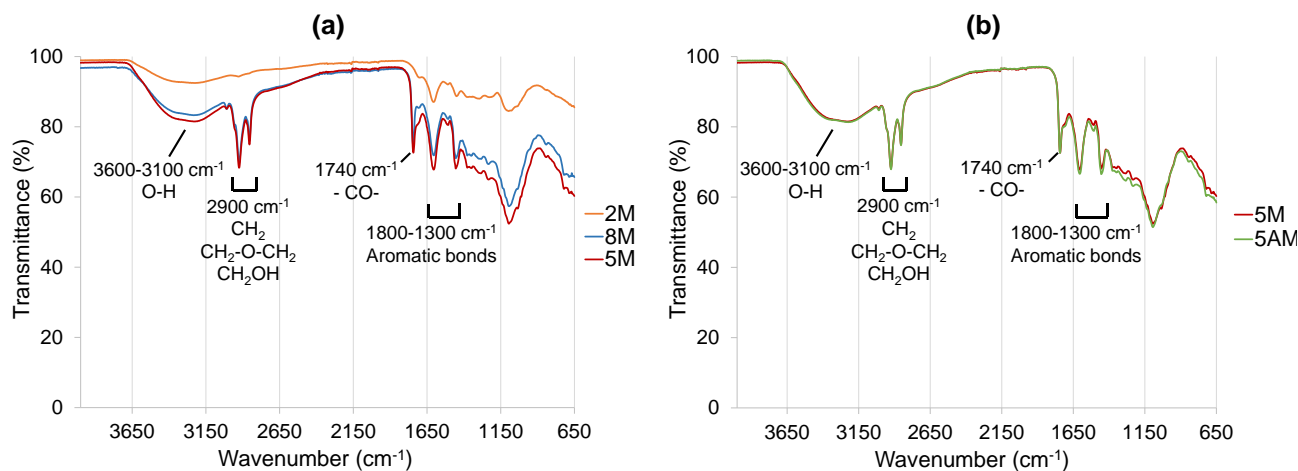


Figure X.4. FTIR spectra of the mentioned samples.

Considering the non-modified samples (**Figure X.4 (a)**), the spectrum of 2M stands out by presenting less marked bands in comparison to the other samples. Considering the broad band in the range of 3600-3100 cm^{-1} representative of O-H stretching, we can consider that these results are in contradiction to the phenolic groups content and water adsorption data. This discrepancy points out some surface chemistry heterogeneity of 2M sample. This hypothesis is corroborated by the contact angles measurements, which were obtained with a higher mean deviation error in the case of this sample.

FTIR spectra present two regions which are easily linked to the structure of the tannin polymers, that is, the zone 3600 cm^{-1} to 3100 cm^{-1} and 1800 cm^{-1} to 1300 cm^{-1} . As mentioned above, the first is attributed to the phenolic groups at the surface of the polymers, and the second represents the aromatic structure of the samples (1620-1450 cm^{-1} – aromatic C=C bonds stretching, 1370 cm^{-1} – aromatic CH₂ groups).

The bands at around 2900 cm^{-1} are attributed to the presence of methylene (-CH₂-), dimethylene ether (-CH₂-O-CH₂-) and methylol (-CH₂OH) groups, more pronounced in samples 5M and 8M. The peak at around 1740 cm^{-1} represents carbonyl groups, most likely in the form of quinones, justifying the red-brown colours of the tannin-based resins, and again much more pronounced in samples 5M and 8M. At 1100 cm^{-1} a strong peak occurs, indicative of aromatic C-H bending (Tondi, 2017).

Finally, the treatment with hydrochloric acid does not seem to have any impact on the surface chemistry of the polymer, as comprovod by the completely coincident FTIR spectra of samples 5M and 5AM (see (**Figure X.4 (b)**)).

Thermal stability is one of the most important properties to consider prior industrial use of any material. In this sense, besides characterization of the texture, chemical composition, surface chemistry and density, thermogravimetric studies of the materials were also performed.

The obtained TG curves (**Figure X.5 (a)**) have similar profiles, with a single prominent weight loss, attributed to polysaccharide decomposition. After this marked decay, the weight remains constant (stable horizontal plateau), in a more evident way in the case of powders 5M and 8M.

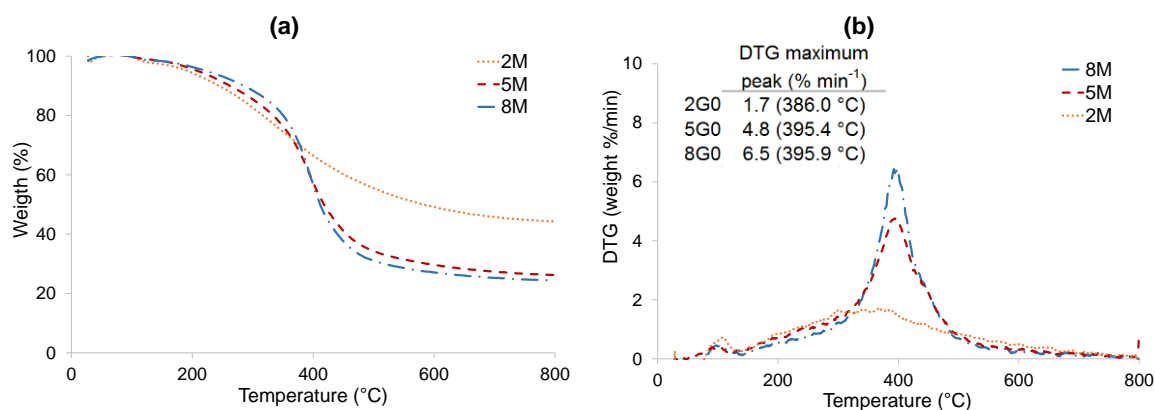


Figure X.5. Thermogravimetric analysis, (a) TG and (b) DTG of the mentioned samples.

The different properties of 2M, revealed by the results previously discussed, were also shown by the thermal degradability behaviour which was different from the other samples, both in terms of decomposition onset, as well as total weight loss. Thus, in the case of sample 2M polysaccharide decomposition is significantly lower (weight loss 19 % lower) but, on the other hand, occurs at lower temperature in comparison to the other two samples (386 °C vs 396 °C) (**Figure X.5 (b)**). Theoretically, polysaccharide decomposition should be favoured by the presence of phenolic groups in the structure however, one must consider, not only the chemical properties of these materials, but also their texture. So, in sample 2M, the decomposition of the more accessible phenolic groups may begin at lower temperatures but, on the other hand, the structure of this material is more resistant to high temperatures than the remaining tannins with a wider porosity.

The materials present decomposition onsets at temperatures significantly higher than those reported in the literature concerning condensed tannins extracted from *Radiata* pine bark, which start to decompose at around 180 °C (Gaugler and Grigsby, 2009). This can result from the different oligomeric structures of *Mimosa* bark and *Radiata* pine bark tannins. *Mimosa* bark tannins consist mainly in prorobinetidin units C4-C6 linked (see Chapter III), whereas *Radiata* pine bark tannins are predominantly formed by C8-C4 linkages. The resulting structure will thus be different with different pore size distributions, and consequently different phenolic groups availability.

Tannin-based polymers show very different thermal decomposition than that of the activated carbons studied in Chapters VII and VIII (see **Figure X.6**).

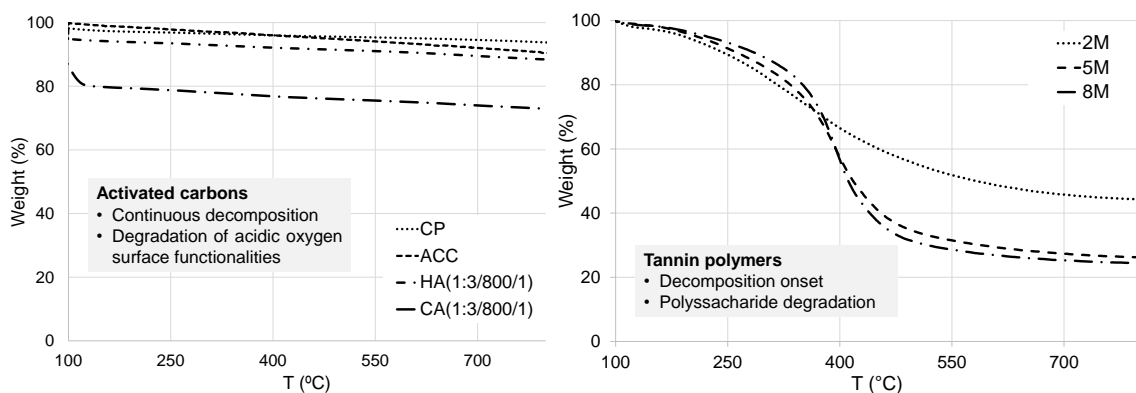


Figure X.6. Comparison of TG of activated carbons studied in Chapter VII and VIII with the tannin-based polymers.

The TG curves of activated carbons show that these solids decompose continuously, as the temperature increases. This degradation occurs due to the decomposition of acidic oxygen functionalities at the carbons's surface, and for this reason lower final weight of approximately 70 % is observed for CA(1:3/800/1), with pH_{PZC} of 5.4, followed by HA(1:3/800/1), ACC, and CP (pH_{PZC} values of 6.0, 9.0 and 10.3, respectively). Tannin-based polymers, on the other hand, do not present a continuous decomposition behaviour. Instead, they tend to maintain around 80 % of their initial weight up to temperatures of 396 °C (lower in the case of powder 2M), after what a rapid decomposition occurs. This extensive and fast degradation, attributed to polyssacharide degradation, points out the thermal instability of these materials. This thermal behaviour can be explained by the fact that their decomposition is directly linked to the presence of phenolic groups, whereas in the case of ACs, a much more complex surface chemistry is present. Also, the wider pore network of the polymers (meso and macropores) allows for a faster thermal degradation than in the case of activated carbons, with an essentially microporous network.

X.2.2. Adsorption of methylene blue

The adsorptive potential of the materials was evaluated, considering the methylene blue (MB) dye as probe molecule. Both kinetic and equilibrium experiments were performed to assess both adsorption rate and mechanism.

The MB kinetic curves presented in **Figure X.7** demonstrate that the adsorption occurs very rapidly, reaching equilibrium after only 1 h (confirmed by 24 h contact time assays).

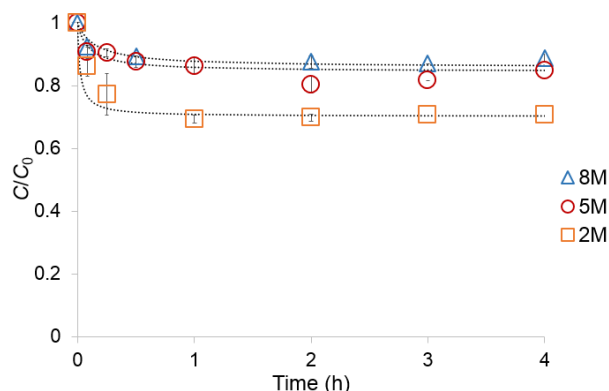


Figure X.7. Kinetic data of MB adsorption (6 mg material with 20 cm³ of 120 mg dm⁻³ solution). Symbols represent the experimental data, whereas lines correspond to the fitting to the pseudo-second order kinetic equation. Error bars are included.

To a more detailed discussion of the results, the experimental data were analysed considering the pseudo-first and pseudo-second order kinetic models (Ho,2006). The pseudo-second order model led to better fittings, with higher R^2 values and similar calculated and experimental uptake values ($q_{e \text{ calc}}$ and $q_{e \text{ exp}}$, respectively) (see **Table X.5**).

Table X.5. Pseudo-second order parameters for the MB adsorption onto the studied adsorbents, at 30 °C. k_2 is the pseudo-second order rate constant; h is the initial adsorption rate; $t_{1/2}$ is the half-life time; $q_{e \text{ calc}}$ and $C_{e \text{ calc}}$ are, respectively, the MB uptake and the concentration remaining in solution at equilibrium, both calculated by the pseudo-second order kinetic model, and $q_{e \text{ exp}}$ the experimental uptake value. R^2 is the coefficient of determination.

	Samples		
	2M	5M	8M
$k_2 \times 10^{-4}$ (g mg ⁻¹ min ⁻¹)	59	28	19
h (mg g ⁻¹ min ⁻¹)	83	11	6
$t_{1/2}$ (min)	1.4	5.7	9.3
$q_{e \text{ calc}}$ (mg g ⁻¹)	119	62	56
$q_{e \text{ exp}}$ (mg g ⁻¹)	119	61	55
$C_{e \text{ calc}}$ (mg dm ⁻³)	84	101	103
R^2	0.999	0.998	0.990

The initial adsorption rate, h , and half-life time, $t_{1/2}$, reveal that adsorption is faster in the case of solid 2M, followed by 5M and 8M. In terms of amount adsorbed, in these experimental conditions, the material 2M was able to remove practically twice the amount of the MB removed by 5M and 8M, after 4 h of contact time.

Considering the dimensions of MB (1.7 nm (length), 0.76 nm (width), 0.33 nm (thickness) (Arias *et al.*, 1999) and the very wide pores of all the polymers, no diffusion limitations are expected to occur. Even though the wideness of the pores should not influence the process rate, MB adsorption on 2M should theoretically be slower (narrower pores) than in 5M and 8M. On the other hand, besides porosity the phenolic group content of the polymers may also have an impact on MB adsorption process. To analyse the impact of this parameter, the correlation between the phenolic content of the samples and the h , and $q_{e \text{ exp}}$ values was performed (see **Figure X.8 (a)** and **(b)**).

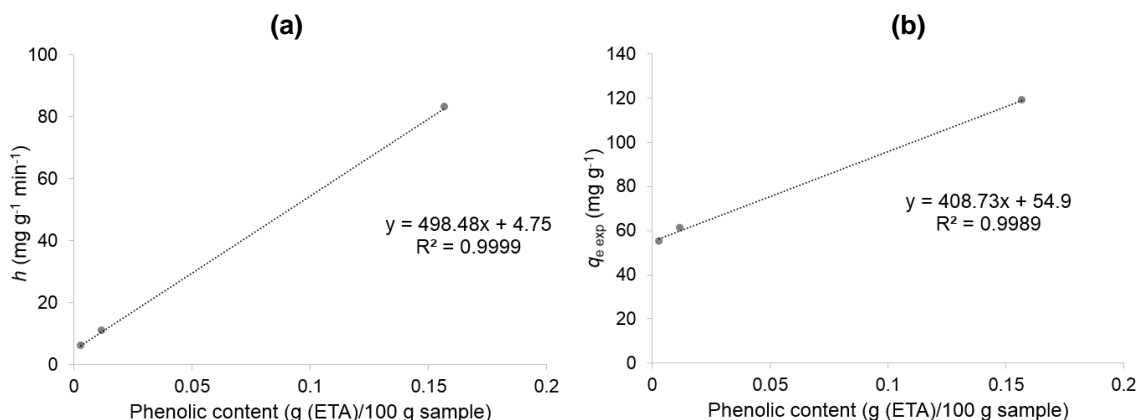


Figure X.8. Correlation between the phenolic group content of the samples and **(a)** the initial adsorption rate, h and **(b)** MB amount adsorbed, $q_{e \text{ exp}}$, after 4 h of contact time.

The results obtained for the three samples show a direct correlation between the adsorption rate and the amount of MB removed after 4 h of contact time with the phenolic group content. The impact on the adsorption rate (**Figure X.8 (a)**) can be explained by the fact that the dissociation of the phenolic groups favour electrostatic attraction between the solids surface and MB species present in solution. Since the amount of phenolic groups is different in each sample, the attractive forces generated between polymer and MB are stronger in 2M sample (0.157 g (ETA)/100g of sample), followed by 5M and 8M (0.012 and 0.003 g (ETA)/100g of sample, respectively). The samples where the initial adsorption rate is higher will consequently have adsorbed higher amount of MB

after 4 h (**Figure X.8 (b)**). For this reason, the MB adsorbed amount, $q_{e \text{ exp}}$, is ruled out by the same effect.

The results obtained compare favourably with data published by Sánchez-Martín *et al.* (Sánchez-Martín *et al.*, 2013b) regarding MB adsorption by *Mimosa* bark tannin-based foams. The authors worked under experimental conditions similar to those used in the present work, and the material was able to adsorb 10 % of MB after one week of contact time. In our work, after only 1 h of contact time, the less efficient material (5M) was able to remove 20 % of MB from solution.

The equilibrium isotherms presented in **Figure X.9** show similar configurations, being classified as L-type isotherms, according to the classification presented in Lyklema, 1995.

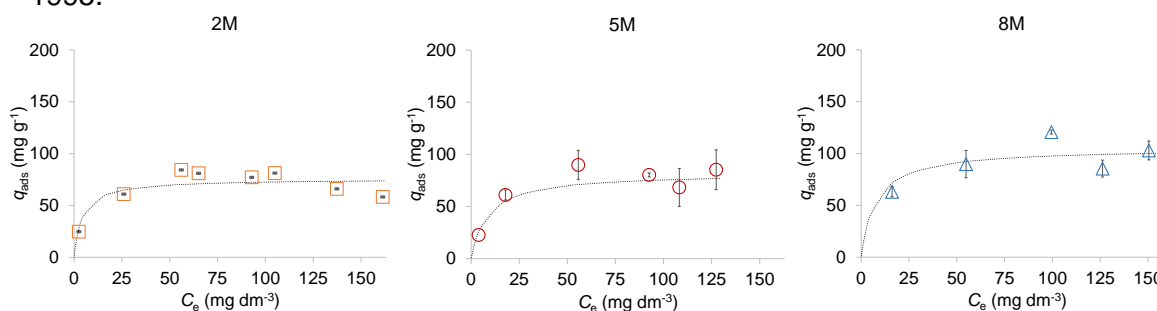


Figure X.9. Equilibrium isotherms of MB adsorption. Symbols represent the experimental data, whereas lines correspond to the fitting to the Langmuir model. Error bars are included.

The MB adsorption capacity ranged between 60 and 100 mg dm^{-3} , being a slight increase in uptake noticed in the case of sample 8M. Having in mind the kinetic results, one could expect a lower performance for this material because of its lower phenolic content. The fact that this is not the case, suggests that the results obtained in these experiments do not rely only in the interactions between MB molecule and the phenolic groups of the polymers. A possible explanation is that the porosity of the samples may also affect the final packing of MB species inside the polymer structure, what will have a direct impact on the maximum adsorption capacity of the materials.

X.2.3. Adsorption of Pharmaceutical Compounds and Personal Care Products (PPCPs)

The assessment of the adsorptive capabilities of 5M and 5AM for several PPCPs species was performed through screening experiments. The results are present in **Figure X.10** and demonstrate the potential of the polymers to retain several pollutants, with uptake values up to 0.67 mol g^{-1} (152 mg g^{-1}).

Considering the possibility that the phenolic groups of the polymers act like adsorption active sites, one could expect a correlation between the net charge of the species in solution (adsorbate and polymer) and the uptake values obtained. However, BPA which is the PPCP presenting the highest uptake value by sample 5M (uptake of 152 mg dm^{-3}), at the solution pH (2.5) is protonated, just like the polymer, and so repulsive interactions should be expected but not verified. On the opposite, ranitidine (pKa value of 2.2) has a negative net charge due to its dissociation in solution (pH 5.7) and, nevertheless it is less removed by 5AM (uptake value of 40 mg dm^{-3}) although the polymer presents a positive or neutral net surface charge. Extrapolating this analysis to the results obtained with 5AM, there seems to be no decisive impact of possible electrostatic interactions between the phenolic groups and the PPCPs species.

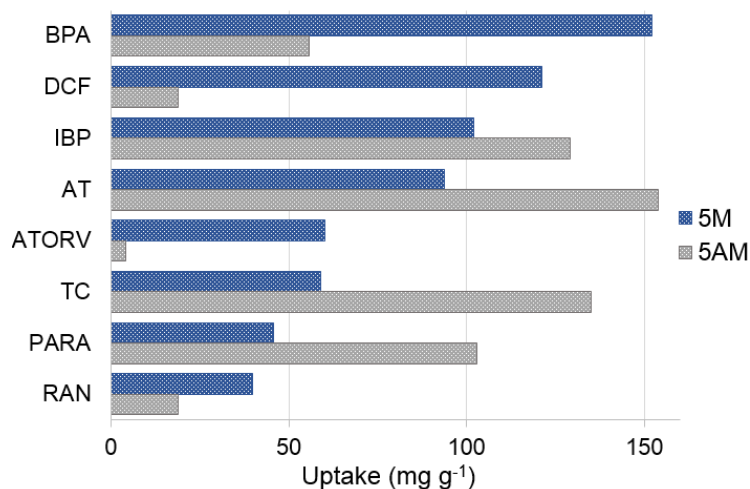


Figure X.10. Uptake results for the mentioned PPCPs by samples 5M and 5AM (5 mg of material, 30 cm³ of pollutant solution (180 mg dm⁻³), at 30 °C after 8 h of contact time.

Regarding the results obtained with 5M, the efficiency of removal by this polymer seems to be strongly connected to the molar volume of the pollutants species (see **Figure X.11 (a)**). The retention of the pollutants seems to be facilitated by smaller V_{mol} and, as the volume of the species increases there is a progressive decay of the uptake achieved from a maximum value of 0.67 mmol g⁻¹, at V_{mol} of 200 cm³ g⁻¹ (BPA), to around 0.15 mmol g⁻¹ when V_{mol} is higher than approximately 270 cm³ mol⁻¹ (TC).

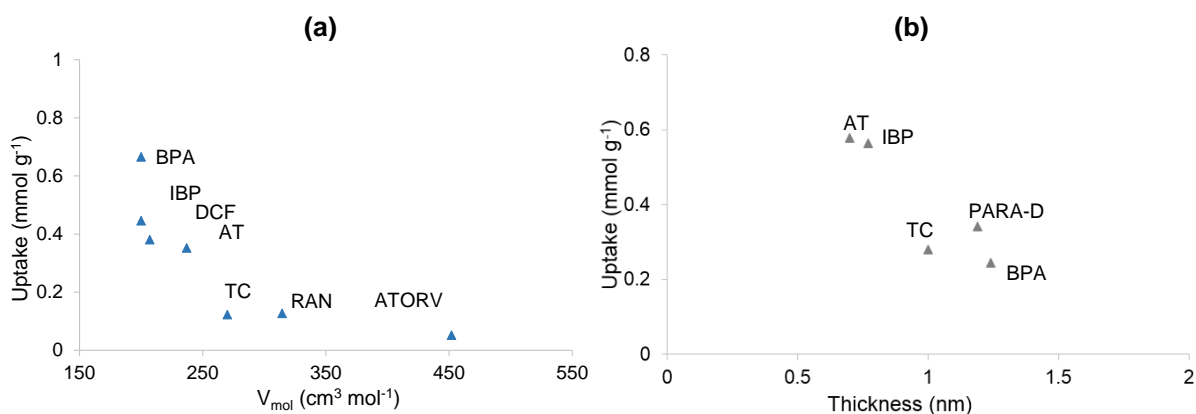


Figure X.11. Correlation between **(a)** molar volume, V_{mol} , of the PPCPs species and **5M** uptakes and **(b)** the thickness of the pollutants and **5AM** results. In the case of paracetamol the results of V_{mol} and thickness concern the dimer form (denominated PARA-D).

Because the volume of the species is much smaller than the pores diameters (wider than 100 nm), any hindrance to the access of the species to the pores can be disregarded. So, the correlation between uptake and V_{mol} can result from multilayer adsorption because, if the adsorption occurred exclusively, or predominantly between the species and the polymer structure, the uptake values would not be so sensitive to the V_{mol} of the species, considering the extremely wide pores diameter. However, the molar volume does not seem to be the only factor impacting the adsorption process because BPA and IBP, with V_{mol} of 200 cm³ mol⁻¹ present different uptake values (0.67 and 0.45 mmol g⁻¹, respectively).

As mentioned above, 5M phenolic content does not seem to have an important role on adsorption otherwise, IBP retention should be higher than that of BPA because ibuprofen was tested in the form of salt (negatively charged in solution). On the other hand, BPA presents one more aromatic ring than IBP which would allow for stronger π - π interactions with the aromatic structure of the polymer.

In the case of 5AM, the removal efficiency of this powder does not seem to be related to the molar volume of the species as the correlation graphic showed no logical association, for example, BPA species, of molar volume $200 \text{ cm}^3 \text{ g}^{-1}$, presents a similar uptake (0.24 mmol g^{-1}) to that of tetracycline of molar volume $270 \text{ cm}^3 \text{ g}^{-1}$ (uptake of 0.28 mmol g^{-1}). On the other hand, when correlating the uptake data with the thickness of the pollutant species, the graphic shown in **Figure X.11 (b)** is obtained. The results seem to suggest that smaller thickness values facilitate a better packing of the species inside 5AM pore volume, which is slightly lower than 5 AM, but with higher pore widths.

In order to shed light into the retention mechanism of the pollutants on 5M solid, these samples were analyzed by FTIR spectroscopy. Figure X.12 shows the FTIR spectra obtained, as well as, the V_{mol} and uptake values (mmol g^{-1}).

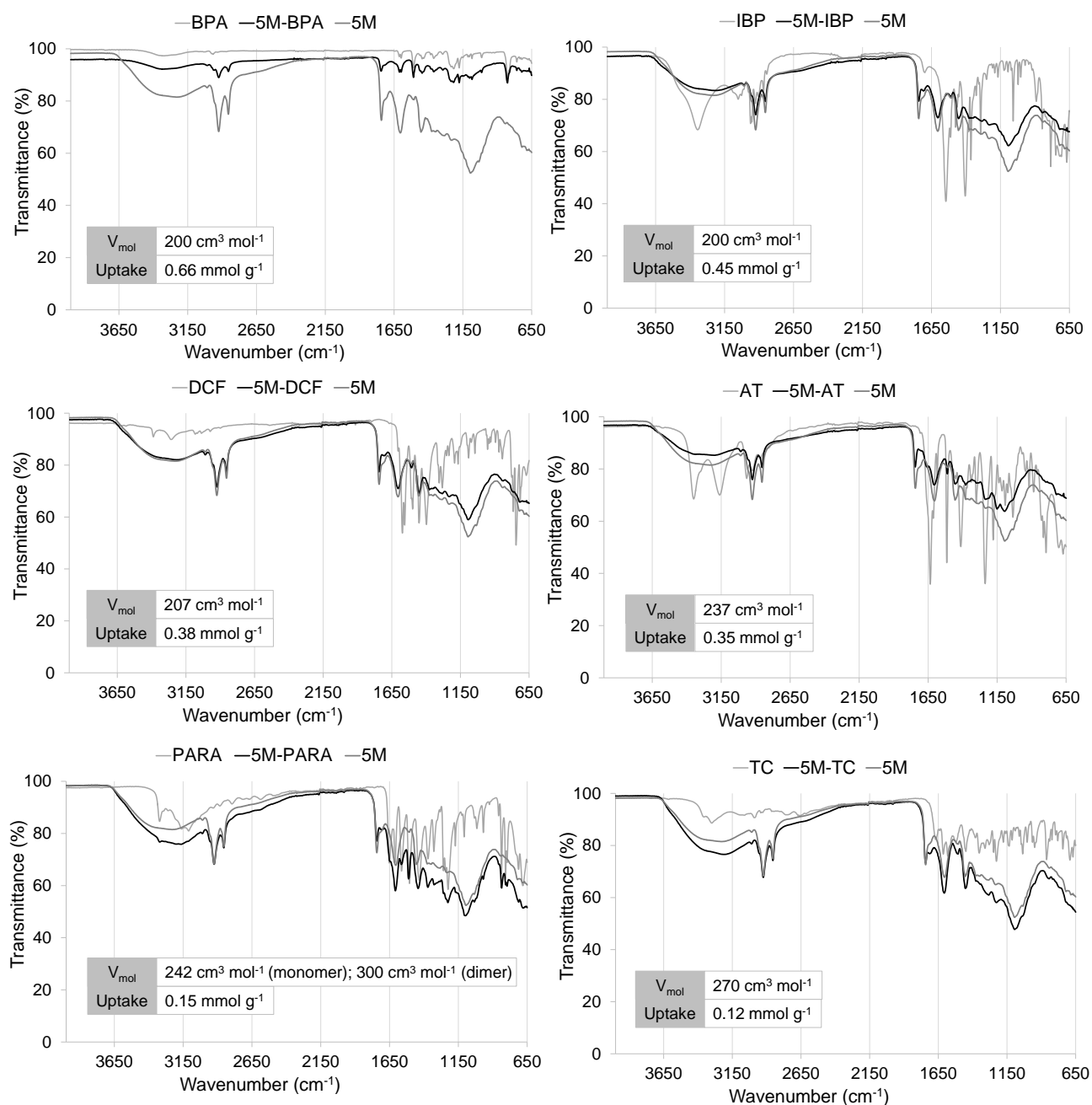


Figure X.12. FTIR spectra of the mentioned compounds, and of the pristine and spent 5M samples. Molar volume, V_{mol} , and uptake values are also presented.

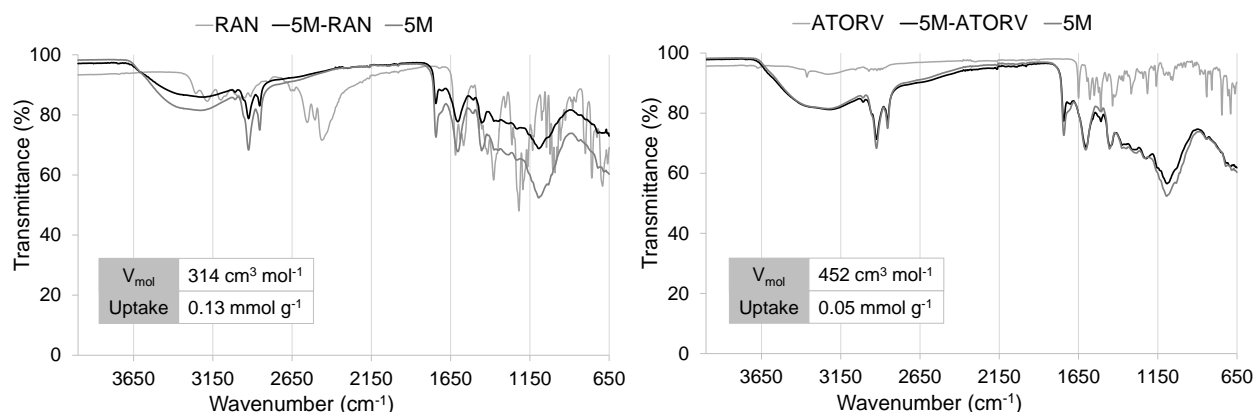


Figure X.12. (continued) FTIR spectra of the mentioned compounds, and of the pristine and spent 5M samples. Molar volume, V_{mol} , and uptake values are also presented.

Considering the pristine and spent 5M spectra, the results can be divided in two groups: systems where adsorption caused a decrease of some peaks intensity in the spent 5M spectrum, preserving the pristine spectrum profile, and systems where adsorption caused an increase of some peaks intensity, possibly with loss of the pristine spectrum profile.

The first scenario is observed for BPA, IBP, DCF, AT and RAN systems, and seems to indicate compound retention inside 5M solid, decreasing some infrared vibrations intensities of the polymer structure, and preventing the compound from being detected. The spectra regions more affected by this decrease will give insight on the type of interactions established between adsorbate and solid, that is, at frequency values between $3650\text{-}2650 \text{ cm}^{-1}$, interactions with the phenolic groups will be assumed and at frequencies lower than 1740 cm^{-1} will point out $\pi\text{-}\pi$ interactions with the aromatic rings of 5M structure.

The second scenario is observed for PARA, ATORV and TC systems, and suggests a less efficient packing of the molecules inside 5M, leading to the detection of some peaks of the compounds spectrum.

The spectra obtained show that species with molar volume lower than $314 \text{ cm}^3 \text{ mol}^{-1}$, that is, BPA, IBP, DCF, AT and RAN, are predominantly retained on the interior of the polymer whereas larger species namely, PARA, ATORV and TC, are less efficiently retained inside the tannin polymer. This analysis is improved considering RAN and TC systems spectra. Even though the two compounds present similar uptake values (0.13 and 0.12 mmol g^{-1}), TC species with a V_{mol} of $483 \text{ cm}^3 \text{ mol}^{-1}$ is detected on the spectrum of the spent sample, whereas no peaks characteristic of RAN, with a V_{mol} of $314 \text{ cm}^3 \text{ mol}^{-1}$ are disclosed on the spent solid spectrum. Also, PARA, with an uptake of 0.15 mmol g^{-1} is even more detected in the spent materials spectra, causing increase of peaks intensity and loss of 5M spectra profile. This can be attributed to a less efficient packing of paracetamol due to the reported existence of both monomer and dimer forms of this compound in solution (Galhetas *et al.*, 2014a).

These findings are in accordance with the correlation between the equilibrium adsorption results and V_{mol} of the species (**Figure X.11 (a)**) implying that higher uptake values are achieved when the pollutants are efficiently packed inside the polymer structure, which occurred in the case of species with molar volume lower than $314 \text{ cm}^3 \text{ mol}^{-1}$. Focusing on this group of compounds, the spectra regions where adsorption led to a decrease in peak intensity can offer insight on the predominant type of interactions established between the adsorbates and the polymer. Adsorption of BPA, AT and RAN species led onto 5M led to a very marked decrease of peak intensity

throughout the spectra suggesting that these pollutants may interact with both the phenolic groups and aromatic rings of the polymer. This is more evidenced in BPA adsorption due to the higher uptake value (0.66 mmol g^{-1}). IBP and DCF seem to predominantly establish π - π interactions with the aromatic rings of 5M structure (peak intensity decrease of aromatic bands). The fact that these compounds are the 2nd and 3rd more removed pollutants, respectively, points out to the importance of the aromatic nature of the tannin polymer for aqueous phase adsorption.

To contextualize the performances of the tannin-based powders 5AM and 5M, the equilibrium adsorption uptakes obtained regarding atenolol, paracetamol and ibuprofen will be compared to those of the lab-made and commercial activated carbons studied in this thesis under the same experimental conditions (see **Figure X.13**). Data published in the literature was also taken into account for this analysis.

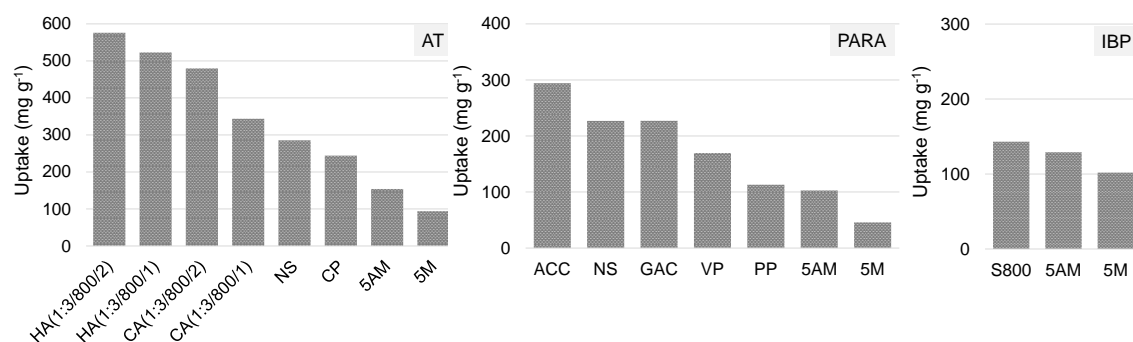


Figure X.13. Atenolol (AT), paracetamol (PARA) and ibuprofen (IBP) uptake values for the mentioned samples. Experiments performed by addition of 30 cm^3 of pollutant solution (180 mg dm^{-3}) to 5 mg of sample. AT-CP carbon and PARA-PP sample data was published in Cabrita *et al.*, 2010; PARA-NS and PARA-VP uptakes reported in Galhetas *et al.*, 2014a; IBP-S800 value reported in Mestre *et al.*, 2014b.

Considering atenolol adsorption, better performances were achieved with the apple tree branches char lab-made ACs (data presented in Chapter VII), with uptake values ranging from 344 mg g^{-1} up to 576 mg g^{-1} . The commercial adsorbents allowed to remove between 244 mg g^{-1} (CP) and 286 mg g^{-1} (NS). At last, the tannin powders removed between 94 mg g^{-1} and 154 mg g^{-1} . To understand the data it is necessary to take into account the different properties and, consequently the different adsorption mechanisms on the ACs and tannin-based polymers. Atenolol adsorption onto the ACs proved to be ruled by the supermicropores volume and (complex) surface chemistry of the materials. Of course, the significantly high surface area of the solids (high amount of pollutant-carbon contact), higher uptake values were achieved. On the other hand, atenolol retention by the polymers seems to rely predominantly on the packing of the molecules inside the mesopores by interactions with phenolic groups and/or aromatic rings of the polymers.

Better performances of ACs were also obtained for paracetamol adsorption especially in the case of ACC cloth carbon. Even though this material adsorbed 294 mg g^{-1} of paracetamol, higher uptake values were expected. In Chapter VI this result was attributed to the wideness of ACC micropores (wider than 1.7 nm). Thus, it is easy to extrapolate this logic to samples 5AM and 5M, composed mainly by meso and macropores wider than 12 nm. Still, sample 5AM presents a similar performance to PP carbon reported in Cabrita *et al.*, (Cabrita *et al.*, 2010).

Finally, ibuprofen adsorption data show comparable uptake values, between 102 mg g^{-1} and 143 mg g^{-1} , for all the materials mentioned. Mestre *et al.*, (Mestre *et al.*, 2014b) reported that ibuprofen adsorption was favored in S800 micropores with widths between 0.72 and 1.40 nm. The good performance of the tannin powders was justified

in previous paragraphs by the combination of an efficient packing inside the polymers structure, ruled by V_{mol} and thickness in the case of 5M and 5AM solids, respectively. Furthermore, in the case of 5M sample, this species seems to predominantly establish $\pi - \pi$ interactions with the aromatic rings of the polymer.

The uptake values achieved by 5M and 5AM powders can be considered especially positive taking into account their easier, greener and more cost-efficient method of preparations (high internal phase emulsion), in comparison to that of activated carbons (chemical and physical activations).

X. 3. Partial conclusions

The tannin-based powders are low-density materials with a meso and macropore network composed by pores wider than 4.2 nm, in the case of 2M sample, and 12 nm for 5M, 8M and 5AM solids. The materials present high amount of carbon and oxygen elements, linked to form a complex polyphenolic structure. This is translated into an acidic nature (pH_{PZC} values around 5.5) and a hydrophobic surface (low water vapour adsorption and contact angles higher than 90°). Acidic hydrolysis of 5M lead to a material with similar chemical composition, phenolic content, and pH_{PZC} , and caused a slight widening of the pores.

The adsorptive potential of the samples towards methylene blue dye and a set of PPCPs was evaluated and the retention mechanism onto 5M and 5AM powders was studied. MB adsorption onto 2M, 5M and 8M powders revealed to be a fast process, reaching equilibrium after only 1 h accompanied by uptake values between 55 and 119 mg g^{-1} . Equilibrium results of PPCPs adsorption onto 5M and 5AM yielded adsorption capacities up to 152 mg g^{-1} . For both polymers the adsorption mechanism seems to be related to the molecular species packing inside the porous structure of the solids which was translated in the data correlation to the PPCPs V_{mol} and thickness, in the case of 5M and 5AM, respectively.

Infrared spectroscopic studies revealed a more efficient packing of species with a molar volume lower than $314 \text{ cm}^3 \text{ mol}^{-1}$ and pointed out the importance of the aromatic nature of the solids for PPCPs retention.

The study reported in this chapter evidenced the promising adsorptive properties of tannin-based solids, which accompanied by the easiness and cost-efficiency of their preparation method (high internal phase emulsion) demonstrated the potential of these materials as adsorbents for water remediation.

Chapter XI

Final conclusions

The work developed in this PhD thesis allowed a great insight into the adsorption of pharmaceutical compounds onto ACs which is of paramount importance to improve water treatment purposes technologies. This process was approached from different perspectives, namely the preparation of materials from wood wastes which revealed to have potential to be used as adsorbents of atenolol, and even in competitive adsorption conditions, in the case of tiamulin hydrogen fumarate. The mechanism of atenolol thermal desorption was also studied in detail giving insight into the atenolol species present in the adsorbed phase, that seem to be dependent on the chemical nature of the carbon. The role of carbons' morphology on paracetamol adsorption and clofibrac acid, and cyclic thermal regeneration of paracetamol-exhausted samples were also evaluated. Other innovative perspective considered was the potential of ACs to immobilize/remove bacteria cells from solution, and a study on the key role parameters and mechanism of immobilizations was performed. Finally, the adsorption potential of novel materials, tannin-based polymers, was also evaluated for a wide set of pharmaceutical compounds and personal care products, with a major importance in water decontamination.

Regarding the preparation of activated carbons from wood bark char, the experimental conditions tested allowed to design micropore networks appropriate to the final applications. The activating agents chosen proved to have an impact on the porosity development of the activated carbons and the results showed that KOH favoured the formation of a pore network composed essentially by large micropores and mesopores while K_2CO_3 promoted the formation of carbons with a wide micropore size distribution. The materials studied were efficient for adsorbing atenolol and tiamulin hydrogen fumarate. The dual composition of the last pollutant, allowed the simultaneous adsorption of both components, without major impact on the adsorption of the tiamulin species.

Morphology has proven to be a key parameter ruling adsorption in liquid phase. The results obtained demonstrated that the cloth morphology presents similar adsorptive behaviour to the powder sample tested, due to the fact that its micropores are readily accessible at its surface. The paracetamol-saturated materials were efficiently regenerated by cyclic thermal treatment and the best results were achieved for the cloth carbon which has high pore accessibility and mechanical strength, withstanding higher number of reuses.

Regarding bacteria immobilization the studies developed shown that *E. coli* cells were preferably immobilized by the powder sample NS, due to its lower particle size that allowed the formation of cell-carbon-cell-carbon-cell agglomerates which entrapped a higher number of cells in this material. The assays with caffeine solutions revealed that when the carbons particles are saturated with caffeine, the formation of these structures is not so efficient and consequently lower removals are achieved.

The tannin-based polymers also proved to be suitable adsorbents for water treatment, removing high amounts of pharmaceutical and personal care products. These materials are essentially meso and macroporous, and their surface chemistry consists mainly in phenolic groups. The adsorption rate of methylene blue was mainly ruled by the phenolic content of the polymers, whereas in equilibrium, the key factor seems to be the packing of the species inside the structure of the solid. The slight change in porosity caused by the acidic hydrolysis proved to be advantageous because it increased the adsorption of pollutants less efficiently removed by the original polymer.

The several approaches to adsorption presented in this thesis can be further deepened by performing further experiments. Regarding the preparation of activated carbons, reported in Chapter VII, it would be interesting to physically activate the

precursor material apple tree branches char, and to study the impact of the experimental parameters evaluated in chemical activation. The role of morphology on cyclic thermal regeneration (study in Chapter VIII) could be further extended considering other pollutants, for example, clofibrilic acid and atenolol. Another possible idea would be to regenerate the spent materials by microwave treatment and to confront the results with the data obtained by thermal treatment. Concerning bacteria adhesion on activated carbons, the work reported in Chapter IX can be further deepened by studying activated carbon colonization by gram-negative bacteria, and also by complementing the study of the impact of caffeine in the suspension to other relevant water pollutants, increasing both the solution concentration, and the contact time of the pollutant with the carbon and cellular suspension. At last, adsorption kinetics studies can be made for the pollutants evaluated in Chapter X, and the molecular dimensions of the compounds can be determined by molecular modelling. It would be interesting to test powder 2M in liquid phase adsorption to better understand the impact of the mesopore diameter and phenolic group content on the pollutants removal from solution. Also, Fourier transform infrared spectra of the pristine and spent 5AM samples should be obtained, and confronted with the spectra obtained in the case of powder 5M to elucidate the adsorption mechanism onto the materials 5AM.

Chapter XII

Bibliographic references

Abu-Lail NI and Camesano TA, Role of lipopolysaccharides in the adhesion, retention, and transport of *Escherichia coli* JM109, *Environmental Science Technology* 37 (2003) 2173-2183.

Addoun A, Dentzer J, Ehrburger P, Porosity of carbons obtained by chemical activation: effect of the nature of the alkaline carbonates, *Carbon* 40 (2002) 1140 - 1143.

Adetunji VO, Adedeji AO, Kwaga J, Assessment of the contamination potentials of some foodborne bacteria in biofilms for food products, *Medicine* 7 (2014) S232-S237.

Afonso-Olivares C, Sosa-Ferrera Z, Santana-Rodríguez JJ, Analysis of anti-inflammatory, analgesic, stimulant and antidepressant drugs in purified water from wastewater treatment plants using SPE-LC tandem mass spectrometry, *Journal of Environmental Science and Health A* 47 (2012) 887–895.

AfzaliTabar M, Alaei M, Bazmi M, Khojasteh RR, Koolivand-Salooki M, Motiee F, Rashidi AM, Facile and economical preparation method of nanoporous graphene/silica nanohybrid and evaluation of its Pickering emulsion properties for Chemical Enhanced oil Recovery (C-EOR), *Fuel* 206 (2017) 453-466.

Aga DS, O'Connor S, Ensley S, Payero JO, Snow D, Tarkalson D, Determination of the persistence of tetracycline antibiotics and their degradates in manure-amended soil using enzyme-linked immunosorbent assay and liquid chromatography–mass spectrometry, *Journal of Agricultural and Food Chemistry* 53 (2005) 7165–7171.

Aguayo-Villarreal IA, Hernandez-Montoya V, Ramirez-Lopez EM, Bonilla-Petriciolet A, Montes-Moran MA, Effect of surface chemistry of carbons from pine sawdust for the adsorption of acid, basic and reactive dyes and their bioregeneration using *Pseudomonas putida*, *Ecological Engineering* 95 (2016) 112 – 118.

Aktas O and Cecen F, Bioregeneration of activated carbon: A review, *International Biodeterioration & Biodegradation* 59 (2007) 257–272.

Alder AC, Schaffner C, Majewsky M, Fenner K, Fate of β -blocker human pharmaceuticals in surface water: Comparison of measured and simulated concentration in the Glatt Valley Watershed, Switzerland, *Water Research* 44 (2010) 936-948.

Al-Duri B, A review in equilibrium in single and multicomponent liquid adsorption liquid adsorption systems, *Reviews in Chemical Engineering* 11 (1995) 101-143.

Al-Ghouti MA, Al-Degs YS, Issa AA, Al Bakain RZ, Khraisheh MA, Mechanistic and adsorption equilibrium studies of dibenzothiophene-rich-diesel on MnO₂-loaded-activated carbon: Surface characterization, *Environmental Progress & Sustainable energy* 36 (2017) 903-913.

Ali AM, Ronning HT, Alarif W, Kallenborn R, Al-Lihaibi SS, Occurrence of pharmaceuticals and personal care products in effluent-dominated Saudi Arabian coastal waters of the Red Sea, *Chemosphere* 175 (2017) 505-513.

Aliyu MM, Murphy W, Lawrence JA, Collier R, Engineering geological characterization of flints, *Quarterly Journal of Engineering Geology and Hydrogeology* 50 (2017) 133-147.

Al-Malack MH and Dauda M, Competitive adsorption of cadmium and phenol on activated carbon produced from municipal sludge, *Journal of Environmental Chemical Engineering* 5 (2017) 2718-2729.

Al-Salem SM, Sharma BK, Khan AR, Arnold JC, Alston SM, Chandrasekaran SR, Al.Dhafeeri AT, Thermal degradation kinetics of virgin polypropylene (PP) and PP with starch blends exposed to natural weathering, *Industrial & Engineering Chemistry Research* 56 (2017) 5210-5220.

Álvarez MBC, *Depuración de efluentes contaminados por hidrocarburos aromáticos policíclicos mediante carbones ativados: Evaluación del processo de adsorción*, Universidad de Oviedo (2009).

Ameer K, Shahbaz HM, Kwon J-H, Green extraction methods for polyphenols from plant matrices and their by-products: A review, *Comprehensive Reviews in Food Science and Food Safety* 16 (2017) 295-315.

Amin G, White lead printed on paper, Doctoral thesis, Linköping University, Sweden (2012).

Aminoshariae A and Khan A, Acetaminophen: Old Drug, New Issues, *Journal of Endodontics* 41 (2015) 588-593.

Ania CO, Parra JB, Menendez JA, Pis JJ, Microwave-induced regeneration of activated carbons polluted with phenol, A comparison with conventional thermal regeneration, *Carbon* 42 (2004) 1383 – 1387.

Ania CO, Parra JB, Pevida C, Arenillas A, Rubiera F, Pis JJ, Pyrolysis of activated carbons exhausted with organic compounds, *Journal of Analytical and Applied Pyrolysis* 74 (2005) 518-524.

Ania CO, Pelayo JG, Bandosz TJ, Reactive adsorption of penicillin on activated carbons, *Adsorption* 17 (2011) 421-429.

Anisuzzaman SM, Joseph CG, Krishnaiah D, Bono A, Suali E, Abang S, Fai LM, Removal of chlorinated phenol from aqueous media by guava seed (*Psidium guajava*) tailored activated carbon, *Water Resources and Industry* 16 (2016) 29-36.

Arias M, López E, Nuñez A, Runinos D, Soto B, Barral MT, Díaz-Fierros D, Adsorption of methylene blue by rem mud, an oxide-rich byproduct of bauxite refining, in: Berthelin J, Huang PM, Bollag J-M, Andreux F (Eds.), Effect of mineral-organic-microorganism interactions on soil and freshwater environments, *Springer* (1999) 361-365.

Attan D, Alghoul MA, Saha BB, Assadeq J, Sopian K, The role of activated carbon fiber in adsorption cooling cycles, *Renewable and Sustainable Energy Reviews* 15 (2011) 1708 – 1721.

Azizian S, Kinetic models of sorption: a theoretical analysis, *Journal of Colloid and Interface Science* 276 (2004) 47-52.

Azuma T, Ishida M, Hisamatsu K, Yunoki A, Otomo K, Kunitou M, Shimizu M, Hosomaru K, Mikata S, Mino Y, A method for evaluating the pharmaceutical deconjugation potential in river water environments, *Chemosphere* 180 (2017) 476-482.

Bahamon D, Carro L, Guri S, Vega LF, Computational study of ibuprofen removal from water by adsorption in realistic activated carbons, *Journal of Colloid and Interface Science* 498 (2017) 323-334.

- Balakrishna K, Rath A, Praveenkumarreddy Y, Guruge KS, Subedi B, A review of the occurrence of pharmaceuticals and personal care products in Indian water bodies, *Ecotoxicology and Environmental Safety* 137 (2017) 113-120.
- Bandosz TJ and Ania CO, Surface chemistry of activated carbons and its characterization, in: Bandosz TJ (Ed.), *Activated Carbon Surfaces in Environmental Remediation*, Elsevier (2006) 159 - 229.
- Bandosz TJ, Nanoporous Carbons: Looking beyond their perception as adsorbents, catalyst supports an supercapacitors, *The Chemical Record* 16 (2016) 205-218.
- Bansal RC, Donnet J-C, Stoeckli R (Eds.), *Active Carbon*, Marcel Dekker (1988).
- Basso MC, Pizzi A, Celzard A, Influence of formulation on the dynamics of preparation of tannin-based foams, *Industrial Crops and Products* 51 (2013) 396–400.
- Batista MK, Mestre AS, Matos I, Fonseca IM, Carvalho AP, Biodiesel production waste as promising biomass precursor of reusable activated carbons for caffeine removal, *RSC Advances* 6 (2016) 45419-45427.
- Batt AL, Bruce IB, Aga DS, Evaluating the vulnerability of surface waters to antibiotic contamination from varying wastewater treatment plant discharges, *Environmental Pollution* 142 (2006) 295-302.
- Batt AL, Kostich MS, Lazorchak JM, Analysis of ecologically relevant pharmaceuticals in wastewater and surface water using selective solid-phase extraction and UPLC-MS/MS, *Analytical Chemistry* 80 (2008) 5021-5030.
- Bautista-Toledo MI, Rivera-Utrilla J, Mendez-Diaz JD, Sanchez-Polo M, Carrasco-Marin F, Removal of the surfactant sodium dodecylbenzenesulfonate from water by processes based on adsorption/bioadsorption and biodegradation, *Journal of Colloid and Interface Science* 418 (2014) 113-119.
- Bean EL, Campbell SJ, Anspach FR, Zeta potential measurements in the control of coagulation chemical doses, *Journal of American Water Works Association* 56 (1964) 214-224.
- Becke AD, Density-functional thermochemistry. III. The role of exact exchange, *The Journal of Chemical Physics* 98 (1993) 5648-5652.
- Belyaeva OV, Golubeva NS, Krasnova TA, Yakusheva AE, Developing a technology for the regeneration of active coal after pyridine adsorption from wastewater, *Chemistry for Sustainable Development* 17 (2009) 243–247.
- Benhamed I, Barthe L, Kessas R, Julcour C, Delmas H, Effect of transition metal impregnation on oxidative regeneration of activated carbon by catalytic wet air oxidation, *Applied Catalysis B-Environmental* 187 (2016) 228 – 237.
- Benzing TR, *The desorption kinetics of non-ionic organic compounds from hexadecyltrimethylammonium-modified soils and clays*, Michigan State University (1993).
- Berenguer R, Marco-Lozar JP, Quijada C, Cazorla-Amorós D, Morallón E, Comparison among chemical, thermal and electrochemical regeneration of phenol-saturated activated carbon, *Energy Fuels* 24 (2010) 3366 – 3372.

- Bertin EP, Principles and Practice of X-Ray Spectrometric Analysis, *Plenum Press* (2012).
- Bhatt NH, Lily, Raj R, Varshney P, Pati AR, Chouhan D, Kumar A, Munshi B, Mohapatra SS, Enhancement of heat transfer rate of high mass flux spray cooling by ethanol-water and ethanol-tween20-water solution at very high initial surface temperature, *International Journal of Heat and Mass Transfer* 110 (2017) 330–347.
- Biniak S, Szymanski G, Siedlewski J, Swiatkowski A, The characterization of activated carbons with oxygen and nitrogen surface groups, *Carbon* 35 (1997) 1799-1810.
- Biscoe J and Warren GE, An X-ray study of carbon black, *Journal of Applied Physics* 13 (1964) 364-371.
- Bjorklund K and Li LY, Adsorption of organic stormwater pollutants onto activated carbon from sewage sludge, *Journal of Environmental Management* 197 (2017) 490-497.
- Boonserm A, Kruehong C, Seithtanabutara V, Artnaseaw A, Kwakhong P, Photoelectrochemical response and corrosion behaviour of CdS/TiO₂ nanocomposite films in an aerated 0.5 M NaCl solution, *Applied Surface Science* 419 (2017) 933-941.
- Borchard U, Pharmaceutical properties of beta adrenoceptor blocking drugs, *Journal of Clinical and Basic Cardiology* 1 (1998) 5-9.
- Borges RM, Minillo A, Lemos EG, Prado HF, Tangerino EP, Use of granular activated carbon filters associated with microorganisms to remove pharmaceuticals in drinking water treatment, *Engenharia Sanitaria e Ambiental* 21 (2016) 709-720.
- Borghi AA and Palma MS, Tetracycline: production, waste treatment and environmental impact assessment, *Brazilian Journal of Pharmaceutical Sciences* 50 (2014) 25-40.
- Boyjoo Y, Cheng Y, Zhong H, Tian H, Pan J, Pareek VK, Jiang SP, Lamonier J-F, Jaroniec M, Liu J, From waste Coca Cola® to activated carbons with impressive capabilities for CO₂ adsorption and supercapacitors, *Carbon* 116 (2017) 490 – 499.
- Bradshaw SM, van Wyk EJ, Swardt JB, Bradshw SM, De Swardt SMJ, Microwave heating principles and their application to the regeneration of granular activated carbon, *The Journal of the South African Institute of Mining and Metallurgy* 98 (1998) 201-212.
- Braghiroli FL, Fierro V, Izquierdo MT, Parmentier J, Pizzi A, Celzard A, Kinetics of the hydrothermal treatment of tannin for producing carbonaceous microspheres, *Bioresource Technology* 151 (2014) 271–277.
- Brea P, Delgado JA, Águeda VI, Uguina MA, Modeling of breakthrough curves of N₂, CH₄, CO, CO₂ and a SMR type off-gas mixture on a fixed bed of BPL activated carbon, *Separation and Purification Technology* 179 (2017) 61 - 71.
- Brunauer S, Deming LS, Deming WE, Teller E, On a theory of the van der waals adsorption of gases, *Journal of the American Chemical Society* 62 (1940) 1723 - 1732.
- Brunauer S, Emmett PH, Teller E, Adsorption of gases in multimolecular layers, *Journal of the American Chemical Society* 60 (1938) 309-319.
- Buser HR, Muller MD, Theobald N, Occurrence of the pharmaceutical drug clofibric acid and the herbicide mecoprop in various Swiss lakes and in the North Sea, *Environmental Science & Technology* 32 (1998) 188–192.

- Cabral JP, Water Microbiology. Bacterial pathogens and water, *International Journal of Environmental Research and Public Health* 7 (2010) 3657-3703.
- Cabrita I, Ruiz B, Mestre AS, Fonseca IM, Carvalho AP, Ania CO, Removal of an analgesic using activated carbons prepared from urban and industrial residues, *Chemical Engineering Journal* 163 (2010) 249–255.
- Caliskan E, Bermudez JM, Parra JB, Menendez JA, Mahramanlioglu M, Ania CO, Low temperature regeneration of activated carbons using microwaves: reusing conventional wisdom, *Journal of Environmental Management* 102 (2016) 134 – 140.
- Cao F, Zhang MT, Yuan SJ, Feng JW, Wang QQ, Wang W, Hu ZH, Transformation of acetaminophen during water chlorination treatment: kinetics and transformation products identification, *Environmental Science and Pollution Research* 23 (2016) 12303-12311.
- Cao Y, Mu T, Comprehensive investigation on the thermal stability of 66 ionic liquids by thermogravimetric analysis, *Industrial & Engineering Chemistry Research* 53 (2014) 8651-8664.
- Carmona E, Andreu V, Picó Y, Occurrence of acidic pharmaceuticals and personal care products in Turia River Basin: From waste to drinking water, *Science of the Total Environment* 484 (2014) 53-63.
- Carrier M, Loppinet-Serani A, Denux D, Lasnier J-M, Ham-Pichavant F, Cansell F, Aymonier C, Thermogravimetric analysis as a new method to determine the lignocellulosic composition of biomass, *Biomass and Bioenergy* 35 (2011) 298-307.
- Carrott PJ and Sing KS, Assessment of microporosity, in: Kral H, Rouquerol J, Sing K, Unger KK (Eds.), *Characterization of Porous Solids*, Elsevier (1988) 77-87.
- Carvalho AP, Mestre AS, Andrade M, Ania CO, Ibuprofen in the aquatic environment: Occurrence, ecotoxicity and water remediation technologies, in: Carter WC and Brown BR (Eds.), *Ibuprofen: Clinical Pharmacology, Medical Uses and Adverse Effects*, Nova Science Publishers, Inc (2013) 1-84.
- Carvalho AP, Mestre AS, Haro M, Ania CO, Advanced methods for the removal of acetaminophen from water, in: Javaherian A and Latifpour P (Eds.), *Acetaminophen: Properties, Clinical Uses and Adverse Effects*, Nova Science Publishers Inc. (2012) 57-105.
- Cazetta AL, Junior OP, Vargas AM, Silva AP, Zou X, Asefa T, Almeida VC, Thermal regeneration study of high surface area activated carbon obtained from coconut shell: Characterization and application of response surface methodology, *Journal of Analytical and Applied Pyrolysis* 101 (2013) 53 – 60.
- Çeçen F, Water and wastewater treatment: historical perspective of activated carbon adsorption and its integration with biological processes, in: Çeçen F and Aktas O (Eds.), *Activated carbon for Water and Wastewater Treatment: Integration of Adsorption and Biological Treatment*, Wiley-VCH (2011) 1-3.
- Chen MJ, Zhang Z, Bott TR, Direct measurement of the adhesive strength of biofilms in pipes by micromanipulation, *Biotechnology Techniques* 12 (1998) 875-880.

Choma J and Jaroniec M, Characterization of Nanoporous Carbons by Using Gas Adsorption Isotherms, in: Bandosz TJ (Ed.), *Activated Carbon Surfaces in Environmental Remediation*, Elsevier (2006) 107-158.

Cleuvers M, Initial rise assessment for three β -blockers found in the aquatic environment, *Chemosphere* 59 (2005) 199-205.

Cloirec PL and Faur C, Adsorption of organic compounds onto activated carbon - applications in water and air treatments, in: Bandosz TJ (Ed.), *Activated Carbon Surfaces in Environmental Remediation*, New York Ltd (2006) 375-420.

Coasne B, Galarneau A, Pellenq RJ, Renzo F, Adsorption, intrusion and freezing in porous silica: the view from the nanoscale, *Chemical Society Reviews* 42 (2013) 4141-4171.

Conn KE, Barber LB, Brown GK, Siegrist RL, Occurrence and fate of organic contaminants during onsite wastewater treatment, *Environmental Science & Technology* 40 (2006) 7358-7366.

Conners TE and Banerjee S (Eds.), *Surface Analysis of Paper*, CRC Press (1995).

Constantini R, Pincelli T, Cossaro A, Verdini A, Goldoni A, Cichon S, Caputo M, Pedio M, Panaccione G, Silly MG, Morgante A, Dell'Angela M, Time resolved resonant photoemission study of energy level alignment at donor/acceptor interfaces, *Chemical Physics Letters* 683 (2017) 135-139.

Cooney D, *Activated Charcoal: Antidote, Remedy and Health Aid*, TEACH Services Inc. (2016).

Cooney D, Nageri A, Hines A, Solvent regeneration of activated carbon, *Water Research* 17 (1983) 403 - 410.

Cooper AI, Bray CL, Su F, Carter BO, Wang W, Adams DY, Clathrates for gas storage in the presence of emulsion-templated porous support, WO 2009 068912, *Ulive Enterprises Limited* (2009).

Costerton JW, Lewandowski Z, Caldwell DE, Korber DR, Lappin-Scott HM, Microbial biofilms, in: Ornston LN, Ballows A, Greenberg EP, Palo Alto CA (Eds.), *Annual Review of Microbiology*, Annual Reviews Inc 49 (1995) 711-745.

Coughlin RW and Ezra FS, Role of surface acidity in the adsorption of organic pollutant s on the surface of carbon, *Environmental Science & Technology* 2 (1968) 291-297.

Couto OM, Matos I, Fonseca IM, Arroyo PA, Silva EA, Barros MASD, Effect of solution pH and influence of water hardness on caffeine adsorption onto activated carbons, *The Canadian Journal of Chemical Engineering* 93 (2015) 68-77.

Crites R, Tchobanoglous G, *Small and Decentralized Wastewater Management Systems*, WCB McGraw-Hill (1998).

Cvetanovic RJ and Amenomiya Y, Application of a temperature-programmed desorption technique to catalyst studies, in: Eley DD, Pines H, Weisz PB (Eds.), *Advances in Catalysis*, Academic Press (1967) 103-149.

Dabrowski A, Adsorption – from theory to practice, *Advances in Colloid and Interface Science* 93 (2001) 135 - 224.

Dastkhon M, Ghaedi M, Asfaram A, Azqhandi MHA, Purkait MK, Simultaneous removal of dyes onto nanowires adsorbent use of ultrasound assisted adsorption to clean waste water: Chemometrics for modelling and optimization, multicomponent adsorption and kinetic study, *Chemical Engineering Research & Design* 124 (2017) 222-237.

Daughton CG, Environmental stewardship and drugs as pollutants, *Lancet* 360 (2002) 1035-1036.

Davey ME and O'Toole GA, Microbial biofilms: From ecology to molecular genetics, *Microbiology and Molecular Biology Reviews* 64 (2000) 847-867.

de Castro RAE, Canotilho J, Barbosa RM, Silva MR, Beja AM, Paixa JA, Redinha JSE, Conformational isomorphism of organic crystals: Racemic and homochiral atenolol, *Crystal Growth and Design* 7 (2007) 496-500.

Delgado-Sánchez C, Letellier M, Fierro V, Chapuis H, Gérardin C, Pizzi A, Celzard A, Hydrophobisation of tannin-based foams by covalent grafting of silanes, *Industrial Crops and Products* 92 (2016) 116-126.

Denoyel R, Rouquerol F, Rouquerol J, Porous texture and surface characterization from liquid-solid interactions: Immersion calorimetry and adsorption from solution, in: Bottani EJ and Tascón JMD (Eds.), *Adsorption by Carbons*, Elsevier Ltd. (2008) 289-293.

Dias JM, Alvim-Ferraz MCM, Almeida MF, Rivera-Utrilla J, Sánchez-Polo M, Waste materials for activated carbon preparation and its use in aqueous-phase treatment: A review, *Journal of Environmental Management* 85 (2007) 833-846.

Dinsley JD, *CharcoalRemedies.com: The Complete Handbook of Medicinal Charcoal and Its Applications*, Gatekeeper Books (2005).

Directive 2015, 2015/1787/EU of the European Commission amending Annexes II and III to Council Directive 98/83/EC on the quality of water intended for human consumption, *Official Journal of the European Union*, JOC number L 260/6 of 7.10.2015.

Directive 2014, 2014/80/EU of the European Commission amending Annex II to Directive 2006/118/EC on the protection of groundwater against pollution and deterioration, *Official Journal of the European Union*, JOC number L 182/52 of 21.6.2014.

Directive 2013, 2013/39/EU of the European Parliament and of the Council amending Directives 2000/60/EC and 2008/105/EC as regards to priority substances in the field of water policy, *Official Journal of the European Union*, JOC number L 226/1 of 24.8.2013.

Directive 2009, 2009/90/EC of the European Parliament and of the Council concerning technical specifications for chemical analysis and monitoring of water status, *Official Journal of the European Union*, JOC number L 201/36 of 1.8.2009.

Directive 2000, 2000/60/EC of the European Parliament and of the Council establishing a framework for Community action in the field of water policy, *Official Journal of the European Union*, JOC number L 327 of 22.12.2000.

Directive 2015, 2015/495/EU of the European Parliament and of the Council establishing a watch list of substances for Union-wide monitoring in the field of water policy pursuant to Directive 2008/105/EC, *Official Journal of the European Union*, JOC number L 78/40 of 24.3.2015.

Directive **2008**, 2008/105/EC of the European Parliament and of the Council on environmental quality standards in the field of water policy, amending and subsequently repealing Council Directives 82/176/EEC, 83/513/EEC, 84/156/EEC, 84/491/EEC, 86/280/EEC and amending Directive 2000/60/EC, *Official Journal of the European Union*, JOC number L 348/84 of 24.12.2008.

Doghri I, Rodrigues S, Bazire A, Dufour A, Akbar D, Sopena V, Sablé S, Lanneluc I, Marine bacteria from the French Atlantic coast displaying high forming-biofilm abilities and different biofilm 3D architectures, *BMC Microbiology* 15 (**2015**) 231-241.

Domínguez-Rodríguez G, Marina ML, Plaza M, Strategies for the extraction and analysis of non-extractable polyphenols from plants, *Journal of Chromatography A* 1514 (**2017**) 1-15.

Donlan RM, Biofilms: Microbial life on surfaces, *Emerging Infectious Diseases Journal* 8 (**2002**) 881-890.

Dubinin MM and Stoeckli HF, Homogeneous and heterogeneous micropore structures in carbonaceous adsorbents, *Journal of Colloid and Interface Science* 75 (**1980**) 34-42.

Dunne MW Jr., Bacterial adhesion: Seen any good biofilms lately?, *Clinical Microbiology Reviews* 15 (**2002**) 155-166.

Dweck J, Melchert MBM, Cartledge FK, Leonardo RS, Toledo RD, A comparative study of hydration kinetics of different cements by thermogravimetry on calcined mass basis, *Journal of Thermal Analysis and Calorimetry* 128 (**2017**) 1335-1342.

Eckner KF, Comparison of membrane filtration and multiple-tube fermentation by the Colilert and Enterolert methods for detection of waterborne coliform bacteria, *Escherichia coli* and *enterococci* used in drinking and bathing water quality monitoring in Southern Sweden, *Applied Environmental Microbiology* 64 (**1998**) 3079-83.

Edberg SC, Rice EW, Karlin RJ, Allem MJ, *Escherichia coli*: the best biological drinking water indicator for public health protection, *Journal of Applied Microbiology* 88 (**2000**) 106S-116S.

Elmouwahidi A, Bailón-García E, Pérez-Cadenas AF, Maldonado-Hódar FJ, Carrasco-Marín F, Activated carbons from KOH and H₃PO₄-activation of olive residues and its application as supercapacitor electrodes, *Electrochimica Acta* 229 (**2017**) 219 – 228.

Elsayed AM, Askalany AA, Shea AD, Dakkama HJ, Mahmoud S, Al-Dadah R, Kaiyaly W, A state of the art of required techniques for employing activated carbon in renewable energy powered adsorption applications, *Renewable and Sustainable Energy Reviews* 79 (**2017**) 503–519.

Engbretsen KM and Harris CR, Caffeine and related nonprescription sympathomimetics, in: Ford MD, Delaney KA, Ling LJ, Erickson WB (Eds.), *Clinical toxicology*, Saunders Company (**2001**) 310–315.

Environmental fact sheet, Fecal coliform as an indicator organism, *New Hampshire Department of Environmental Services* (**2003**).

Erabee IK, Ahsan A, Daud NN, Idrus S, Shams S, Din MF, Rezanian S, Manufacture of low-cost activated carbon using sago palm bark and date pits by physiochemical activation, *Bioresources* 12 (**2017**) 1916-1923.

ESVAC Sixth Report, Sales of veterinary antimicrobial agents in 29 European countries in 2014 – Trends from 2011 to 2014, *European Medicines Agency* (2014).

Felipe C, Rojas F, Kornhauser I, Thommes M, Zgrablich G, Mechanistic and experimental aspects of the structural characterization of some model and real systems by nitrogen sorption and mercury porosimetry, *Adsorption Science & Technology* 24 (2006) 623-644.

Feng P, Weagant SD, Grant MA, Burkhardt W, Enumeration of *Escherichia coli* and the coliform bacteria, in: US Food & Drug Administration, Bacteriological Analytical Manual, *Center of Food Safety & Applied Nutrition* (2002).

Fent K, Weston AA, Caminada D, Ecotoxicology of human pharmaceuticals, *Aquatic Toxicology* 76 (2006) 122-159.

Fenwick A, Waterborne Diseases—Could they be Consigned to History?, *Science* 313 (2006) 1077–1081.

Ferguson D and Signoretto C, Environmental persistence and naturalization of fecal indicator organisms, in: Hagedorn C, Blanch AR, Harwood VJ (Eds.), *Microbial Source Tracking: Methods, Applications, and Case Studies*, Springer (2011) 379–397.

Ferro-García MA, Utrera-Hidalgo E, Rivera-Utrilla J, Moreno-Castilla C, Regeneration of activated carbons exhausted with chlorphenol, *Carbon* 31 (1993) 857-863.

Fisher LR and Israelachvili JN, Experimental studies on the applicability of the Kelvin equation to highly curved concave menisci, *Journal of Colloid and Interface Science* 80 (1981) 528-541.

Foo KY and Hameed BH, Potential of jackfruit peel as precursor for activated carbon prepared by microwave induced NaOH activation, *Bioresource Technology* 112 (2012a) 143 - 150.

Foo KY and Hameed BH, Microwave-assisted regeneration of activated carbon, *Bioresource Technology* 119 (2012b) 234 – 240.

Foo KY and Hameed BH, Recent developments in the preparation and regeneration of activated carbons by microwaves, *Advanced Colloid Interface Science* 149 (2009) 19 – 27.

Fortunová L', Reháková M, Nagyová S, Dolinská S, Mojumdar SC, Jóna E, Thermochemical study of sorption of pyridine derivatives by copper forms of synthetic and natural zeolites, *Journal of Thermal Analysis and Calorimetry* 104 (2011) 955-962.

Fram MS and Belitz K, Occurrence and concentrations of pharmaceutical compounds in groundwater used for public drinking-water supply in California, *Science of the Total Environment* 409 (2011) 3409-3417.

Francy DS, Donna N, Myers T, Metzker KD, *Escherichia coli* and fecal-coliform bacteria as indicators of recreational water quality, *Water Resources Investigations Report* (1993) number 4083.

Freundlich H and Heller W, The adsorption of cis- and trans-azobenzene, *Journal of the American Chemical Society* 61 (1939) 2228-2230.

Freundlich HMF, Over the adsorption in solution, *Journal of Physical Chemistry* 57 (1906) 385-470.

Friess K, Bartovská L, Pilnáček K, Vopička O, Randová A, Lanč M, Physical Chemistry Characterization of Polymeric Membranes, in: Drioli E, Giorno L, Fontananova E (Eds.), *Comprehensive Membrane Science and Engineering*, Elsevier (2010) 445.

Frisch MJ, Trucks GW, Schlegel HB, Scuseria GE, Robb MA, Cheeseman JR, Scalmani G, Barone V, Mennucci B, Petersson GA, Nakatsuji H, Caricato M, Li X, Hratchian HP, Izmaylov AF, Bloino J, Zheng G, Sonnenberg JL, Hada M, Ehara M, Toyota K, Fukuda R, Hasegawa J, Ishida M, Nakajima T, Honda Y, Kitao O, Nakai H, Vreven T, Montgomery Jr JA, Peralta JE, Ogliaro F, Bearpark M, Heyd JJ, Brothers E, Kudin KN, Staroverov VN, Kobayashi R, Normand J, Raghavachari K, Rendell A, Burant JC, Iyengar SS, Tomasi J, Cossi M, Rega N, Millam JM, Klene M, Knox JE, Cross JB, Bakken V, Adamo C, Jaramillo J, Gomperts R, Stratmann RE, Yazyev O, Austin AJ, Cammi R, Pomelli C, Ochterski JW, Martin RL, Morokuma K, Zakrzewski VG, Voth GA, Salvador P, Dannenberg JJ, Dapprich S, Daniels AD, Farkas Ö, Foresman JB, Ortiz JV, Cioslowski J, Fox DJ, Gaussian 09, *Gaussian, Inc.*, Wallingford CT (2009).

Furmaniak S, Terzyk AP, Gauden PA, Kowalczyk P, Harris PJF, The influence of the carbon surface chemical composition on Dubinin-Astakhov equation parameters calculated from SF(6) adsorption data grand canonical Monte Carlo simulation, *Journal of Physics: Condensed Matter* 23 (2011) 395005.

Gadipelly C, Perez-Gonzalez A, Yadav GD, Ortiz I, Ibanez R, Rathod VK, Marathe KV, Pharmaceutical industry wastewater: review of the technologies for water treatment and reuse, *Industrial & Engineering Chemical Research* 53 (2014) 11571–11592.

Gago-Ferrero P, Gros M, Ahrens L, Wiberg K, Impact on-site, small and large scale wastewater treatment facilities on levels and fate of pharmaceuticals, personal care products, artificial sweeteners, pesticides, and perfluoroalkyl substances in recipient waters, *Science of the Total Environment* 601-602 (2017) 1289-1297.

Galan A-M, Calinescu I, Trifan A, Winkworth-Smith C, Calvo-Carrascal M, Dodds C, Binner E, New insights into the role of selective and volumetric heating during microwave extraction: Investigation of the extraction of polyphenolic compounds from sea buckthorn leaves using microwave-assisted extraction and conventional solvent extraction, *Chemical Engineering and Processing* 116 (2017) 29-39.

Galéra C, Bernard JY, van der Waerden J, Bouvard M-P, Lioret S, Forhan A, De Agostini M, Melchior M, Heude B, Prenatal caffeine exposure and child intelligence quotient at age 5.5 years: The eden mother-child cohort, *Biological Psychiatry* 80 (2015) 720-726.

Galhetas M, Andrade MA, Mestre AS, Kangni-foli E, Vila de Brito MJ, Pinto ML, Lopes H, Carvalho AP, The influence of the textural properties of activated carbons on acetaminophen adsorption at different temperatures, *Physical Chemistry Chemical Physics* 17 (2015) 12340-12349.

Galhetas M, Mestre AS, Pinto ML, Gulyurtlu I, Lopes H, Carvalho AP, Carbon-based materials prepared from pine gasification residues for acetaminophen adsorption, *Chemical Engineering Journal* 240 (2014a) 344-351.

- Galhetas M, Mestre AS, Pinto ML, Gulyurtlu I, Lopes H, Carvalho AP, Chars from gasification of coal and pine activated with K_2CO_3 : acetaminophen and caffeine adsorption from aqueous solutions, *Journal of Colloid Interface Sciences* 433 (2014b) 94-103.
- Gao Y and Deshusses MA, Adsorption of clofibric acid and ketoprofen onto powdered activated carbon: Effect of natural organic matter, *Environmental Technology* 32 (2011) 1719–1727.
- García SA, Pinto GL, Encina PA, Irusta-Mata R, Ecotoxicity and environmental risk assessment of pharmaceuticals and personal care products in aquatic environments and wastewater treatment plants, *Ecotoxicology* 23 (2014) 1517-1533.
- Garrett TR, Bhakoo M, Zhang Z, Bacterial adhesion and biofilms on surfaces, *Progress in Natural Science* 18 (2008) 1049-1056.
- Garrison AW, Pope JD, Allen FR, GC/MS analysis of organic compounds in domestic wastewaters, in: Keith CH (Ed.), Identification and Analysis of Organic Pollutants in Water, *Ann Arbor Science Publishers Inc.* (1976) 517-566.
- Gaugler M and Grigsby WJ, Thermal degradation of condensed tannins from Radiata pine bark, *Journal of Wood Chemistry and Technology* 29 (2009) 305-321.
- Geens T, Aerts D, Berthot C, Bourguignon JP, Goeyens L, Lecomte P, Maghuin-Rogister G, Pironnet AM, Pussemier L, Scippo ML, Van Loco J, Covaci A, A review of dietary and nondietary exposure to bisphenol-A, *Food and Chemical Toxicology* 50 (2012) 3725–3740
- Giesche H, Mercury porosimetry: A general (practical) overview, *Particle & Particle Systems Characterization* 23 (2006) 9-19.
- Giesche H, Mercury porosimetry, in: Schueth F, Sing KSW, Weitkamp J (Eds.), Handbook of Porous Solids, *Wiley-VCH* (2002) 309-351.
- Giles CH, Smith D, Huitson A, A general treatment and classification of the solute adsorption isotherm. I. Theoretical, *Journal of Colloid and Interface Science* 47 (1974a) 755-765.
- Giles CH, D'Silva AP, Easton IA, A general treatment and classification of the solute adsorption isotherm part. II. Experimental interpretation, *Journal of Colloid and Interface Science* 47 (1974b) 766-778.
- Gleick PH, Basic water requirements for human activities: Meeting basic needs, *Water International* 21 (1996) 83-92.
- Gogate PR and Pandit AB, A review of imperative technologies for wastewater treatment II: Hybrid methods, *Advances in Environmental Research* 8 (2004) 553–597.
- Goldstein J, Newbury DE, Echlin E, Joy DC, Romig Jr AD, Lyman CE, Fiori C, Lifshin E, Scanning Electron Microscopy and X-ray Microanalysis: A text for Biologists, Materials Scientists, and Geologists, *Springer Science & Business Media* (2012).
- Gopalan P and Kandlikar SG, Contact line characteristics of liquid–gas interfaces over grooved surfaces, *Microfluidics and Nanofluidics* 16 (2014) 999-1008.

Graham M, Optimization of Powdered Activated Carbon Application for Geosmin and MIB Removal, *America Water Works Association* (1999)

Gregg SJ and Sing KSW, Adsorption, Surface Area and Porosity, *Academic Press Inc.* (1982).

Grishechko LI, Amaral-Labat G, Fierro V, Szczurek A, Kuznetsovbc N, Celzard A, Biosourced, highly porous, carbon xerogel microspheres, *Carbon* 6 (2016) 65698-65708.

Gros M, Blum KM, Jernstedt H, Renman G, Rodríguez-Mozaz S, Haglund P, Andersson PL, Wiberg K, Ahrens L, Screening and prioritization of micropollutants in wastewaters from on-site sewage treatment facilities , *Journal of Hazardous Materials* 328 (2017) 37-45.

Gross GG, Hemingway RW, Yoshida T (Eds.), Plant Polyphenols 2: Chemistry, Biology, Pharmacology, Ecology, *Kluwer Academic/Plenum Publishers*, New York (2012).

Guedidi H, Reinert L, Lévêque JM, Soneda Y, Bellakhal N, Duclaux L, The effects of the surface oxidation of activated carbon, the solution pH and the temperature on adsorption of ibuprofen, *Carbon* 54 (2013) 432-443.

Gu H, Wang C, Gong S, Mei Y, Li H, Ma W, Investigation on contact angle measurement methods and wettability transition of porous surfaces, *Surface & Coatings Technology* 292 (2016) 72-77.

Gurten II, Ozmak M, Yagmur E, Aktas Z, Preparation and characterization of activated carbon from waste tea using K_2CO_3 , *Biomass and Bioenergy* 37 (2012) 73 – 81.

Hamamoto Y, Alam KCA, Saha BB, Koyama S, Akisawa A, Kashiwagi T, Study on adsorption refrigeration cycle utilizing activated carbon fibers. Part 1. Adsorption characteristics, *International Journal of Refrigeration* 29 (2006) 305 – 314.

Hari PR, Arivazhagan N, Rao MN, Pavan AHV, Hot corrosion studies on alloy 617 OCC in the context of its use in advanced ultra-supercritical (A-USC) power plants, *Transactions of the Indian Institute of Metals* 70 (2017) 775-781.

Haro NK, Del Vecchio P, Marcilio NR, Feris LA, Removal of atenolol by adsorption-Study of kinetics and equilibrium, *Journal of Cleaner Production* 154 (2017) 214-219.

Haslam E, Plant Polyphenols: Vegetable Tannins Revisited, *Cambridge Academic Press* (1989).

Heberer T, Occurrence, fate, and removal of pharmaceutical residues in the aquatic environment: a review of recent research data, *Toxicology Letter* 131 (2002) 5–17.

Heberer T and Stan HJ, Determination of clofibric acid and N-(phenylsulfonyl)-sarcosine in sewage, river, and drinking water, *International Journal of Environmental Analytical Chemistry* 67 (1997) 113–124.

Henrici AT, Studies of Freshwater Bacteria: I. A direct microscope technique, *Journal of Bacteriology* 25 (1933) 277-287.

Hignite C and Azamoff DL, Drugs and drug metabolites as environmental contaminants: chlorophenoxyisobutyrate and salicylic acid in sewage treatment effluent, *Life Sciences* 20 (1997) 337-342.

- Hitchcock DI, The isoelectric point of a standard gelatin preparation, *The Journal of General Physiology* 14 (1931) 685-699.
- Hojo K, Nagaoka S, Ohshima T, Bacterial interactions in dental biofilm development, *Journal of Dental Research* 88 (2009) 982-990.
- Hong Y and Brown DG, Electrostatic behaviour of the charge-regulated bacterial cell surface, *Langmuir* 24 (2008) 5003-5009.
- Hopkins ZR and Blaney L, A novel approach to modelling the reaction kinetics of tetracycline antibiotics with aqueous ozone, *Science of the Total Environment* 468-469 (2014) 337-344.
- Houdt RV and Michiels CW, Role of bacterial cell surface structures in *Escherichia coli* biofilm formation, *Research in Microbiology* 156 (2005) 626-633.
- Ho Y-S and McKay G, Kinetic models for the sorption of dye from aqueous solution by wood, *Process Safety and Environmental Protection* 76 (1998) 183-191.
- Ho Y-S and McKay G, Pseudo-second order model for sorption processes, *Process Biochemistry* 34 (1999) 451-465.
- Ho Y-S, Citation review of Lagergren kinetic rate equation on adsorption reactions, *Scientometrics* 59 (2004) 171-177.
- Ho Y-S, Review of second-order models for adsorption systems, *Journal of Hazardous Materials B* 136 (2006) 681-689.
- Huang L, Sun Y, Wang W, Yue Q, Yang T, Comparative study on characterization of activated carbons prepared by microwave and conventional heating methods and application in removal of oxytetracycline (OTC), *Chemical Engineering Journal* 171 (2011) 1446-1453.
- Huang MH, Yang YD, Chen DH, Chen L, Guo HD, Removal mechanism of trace oxytetracycline by aerobic sludge. *Process Safety and Environmental Protection* 90 (2012) 141-146.
- Huang XW, Lv D, Yan L, Zhang GS, Effects of water factors on the effectiveness of EDC adsorption on novel tailored activated carbon, *Water, Air and Soil Pollution* 227 (2016) 398.
- Huggett DB, Khan LA, Foran CM, Determination of beta-adrenergic receptor blocking pharmaceuticals in United States wastewater effluent, *Environmental Pollution* 121 (2003) 199-205.
- Ioannidou O and Zabaniotou A, Agricultural residues as precursors for activated carbon production – A review, *Renewable and Sustainable Energy Reviews* 11 (2007) 1966 – 2005.
- Ishii S and Sadowsky MJ, *Escherichia coli* in the environment: implications for water quality and human health, *Microbes and Environments* 23 (2008) 101-108.
- Islam MS, Zhang Y, McPhedran KN, Liu Y, El-Din MG, Mechanistic investigation of industrial wastewater naphthenic acids removal using granular activated carbon (GAC) biofilm based processes, *Science of the Total Environment* 541 (2016) 238-246

ISO 9277, Determination of the specific surface area of solids by gas adsorption – BET method (2010).

ISO 15901-1, Pore size distribution and porosity of solid materials by mercury porosimetry and gas adsorption – Part 1: Mercury porosimetry (2016).

ISO 697, Surface active agents – Washing powders – Determination of apparent density – Method by measuring the mass of a given volume (1981).

Jackson DW, Suzuki K, Oakford L, Simecka JW, Hart ME, Romeo T, Biofilm formation and dispersal under the influence of the global regulator CsrA of *Escherichia coli*, *Journal of Bacteriology* 184 (2002) 290-301.

Jain V, Hole A, Deshmukh R, Patrikar R, Dynamic capacitive sensing of droplet parameters in a low-cost open EWOD system, *Sensors and Actuators A* 263 (2017) 224--233.

Jenkins R and Snyder RL, Introduction to X-ray Powder Diffraction-Vol 138, Winefordner JD (Ed.), *John Wiley & Sons, INC* (1996).

Jiang T, Kaal J, Liang J, Zhang Y, Wei S, Wang D, Green NW, Composition of dissolved organic matter (DOM) from periodically submerged soils in the Three Gorges Reservoir areas as determined by elemental and optical analysis, infrared spectroscopy, pyrolysis-GC-MS and thermally assisted hydrolysis and methylation, *Science of the Total Environment* 603-604 (2017) 461-471.

Jones DA, Lelyveld TP, Mavrofidis SD, Kingman SW, Miles NJ, Microwave heating applications in environmental engineering – a review, *Resources, Conservation and Recycling* 34 (2002) 75 – 90.

Jones OA, Voulvoulis N, Lester NJ, Aquatic environmental assessment of the top 25 English prescription pharmaceuticals, *Water Research* 36 (2002) 5013-5022.

Jossens L, Prausnitz JM, Fritz W, Schlünder EU, Myers AL, Thermodynamics of multisolite adsorption from dilute aqueous solutions, *Chemical Engineering Science* 33 (1978) 1097-1106.

Juang RS, Wu FC, Tseng RL, Adsorption isotherms of phenolic compounds from aqueous solutions onto activated carbon fibres, *Journal of Chemical & Engineering Data* 41 (1996) 487-492.

Jucker BA, Harms H, Hug SJ, Zehnder AJB, Adsorption of bacterial surface polysaccharides on mineral oxides mediated by hydrogen ions, *Colloids and Surfaces B: Biointerfaces* 9 (1997) 331-343.

Julcour-Lebigue C, Krou NJ, Andriantsiferana C, Wilhelm AM, Delmas H, Assessment and modeling of a sequential process for water treatment-adsorption and batch CWAO regeneration of activated carbon, *Industrial & Engineering Chemistry Research* 51 (2012) 8867 – 8874.

Kakoi B, Kaluli JW, Ndiba P, Thiong'o G, Optimization of Maerua Decumbent bio-coagulant in paint industry wastewater treatment with response surface methodology, *Journal of Cleaner Production* 164 (2017) 1124-1134.

- Kallel M, Zouch F, Antar Z, Bahri A, Elleuch K, Hammer premature wear in mineral crushing process, *Tribology International* 115 (2017) 493-505.
- Kamoun C, Pizzi A, Zanetti M, Upgrading melamine-urea-formaldehyde polycondensation resins with buffering additives. I. The effect of hexamine sulfate and its limits, *Journal of Applied Polymer Science* 90 (2003) 203-214.
- Karanfil T, Activated carbon adsorption on drinking water treatment, in: Bandosz TJ (Ed.), *Activated Carbon Surfaces in Environmental Remediation*, Elsevier (2006) 345-373.
- Kasprzyk-Hordern B, Dinsdale RM, Guwy AJ, The removal of pharmaceuticals, personal care products, endocrine disruptors and illicit drugs during wastewater treatment and its impact on the quality of receiving waters, *Water Research* 43 (2009) 363-380.
- Kazemi E, Dadfarnia S, Shabani AMH, Ranjbar M, Synthesis, characterization, and application of a Zn (II)-imprinted polymer grafted on graphene oxide/magnetic chitosan nanocomposite for selective extraction of zinc ions from different food samples, *Food chemistry* 237 (2017) 921-928.
- Kett VL and Price DM, Thermogravimetry, in: Gaisford S, Kett V, Haines P (Eds.), *Principles of Thermal Analysis and Calorimetry*, Royal Society of Chemistry (2016) 18-46.
- Kew SL, Adnan R, Lim PE, Seng CE, Bioregeneration of cresol-loaded granular activated carbon using immobilized biomass: Effects of operational factors and chemical structure of cresol isomers, *Journal of the Taiwan Institute of Chemical Engineers* 63 (2016) 386 – 395.
- Khanbabaee K and van Ree T, Tannins: Classification and definition, *Natural Products Reports* 18 (2001) 641–649.
- Khetan SK and Collins TJ, Human pharmaceuticals in the aquatic environment: a challenge to green chemistry, *Chemical Reviews* 107 (2007) 2319–2364.
- Kim E, Jung C, Han J, Her N, Park CM, Son A, Yoon Y, Adsorption of selected micropollutants on powdered activated carbon and biochar in the presence of kaolinite, *Desalination and Water Treatment* 57 (2016) 27601-27613.
- Kim JR, Hulling SG, Kan E, Effects of temperature on adsorption and oxidative degradation of bisphenol A in an acid-treated iron-amended granular activated carbon, *Chemical Engineering Journal* 262 (2015) 1260 – 1267.
- Kim SD, Cho J, Kim IS, Vanderford BJ, Snyder SA, Occurrence and removal of pharmaceuticals and endocrine disruptors in South Korean surface, drinking, and waste waters, *Water Research* 41 (2007) 1013-1021.
- Klemm P and Krogfelt KA, in: Klemm P (Ed.), *Fimbriae, adhesion, genetics, biogenesis and vaccines*, CRC Press Inc. (1994) 9-26.
- Kopac T, Sulu E, Toprak A, Effect of KOH treatment on bituminous coal for the effective removal of Basic Blue 41 dye from aqueous solutions, *Desalination and Water Treatment* 57 (2016) 290007-29018.

Korotta-Gamage SM and Sathasivan A, A review: Potential and challenges of biologically activated carbon to remove natural organic matter in drinking water purification process, *Chemosphere* 167 (2017) 120-138.

Kostich MS, Batt AL, Lazorchak JM, Concentrations of prioritized pharmaceuticals in effluents from 50 large wastewater treatment plants in the US and implications for risk estimation, *Environmental Pollution* 184 (2014) 354-359.

Kovačič S, Ferk G, Drofenik M, Krajnc P, Nanocomposite polyHIPEs with magnetic nanoparticles: Preparation and heating effect, *Reactive and Functional Polymers* 72 (2012) 955-961.

Krieg NR and Holt JG (Eds.), Bergey's manual of systematic bacteriology, *Williams & Wilkins* (1984) 408-420.

Krishnaiah D, Joseph CG, Anisuzzaman SM, Daud WMAW, Sundang M, Leow YC, Removal of chlorinated phenol from aqueous solution utilizing activated carbon derived from papaya (*Carica Papaya*) seeds, *Korean Journal of Chemical Engineering* 34 (2017) 1377-1384.

Król M, Gryglewicz G, Machnokowski J, KOH activation of pitch-derived carbonaceous materials – Effect of carbonization degree, *Fuel Processing Technology* 92 (2011) 158 - 165.

Kümmerer K, The presence of pharmaceuticals in the environment due to human use – present knowledge and future challenges, *Journal of Environmental Management* 90 (2009) 2354-23366.

Kunowsky M, Suárez-García F, Linares-Solano A, Adsorbent density impact on gas storage capacities, *Microporous and Mesoporous Materials* 173 (2013) 47–52.

Lagergren S, Zur theorie der sogenannten adsorption gelöster stoffe, *Kungliga Svenska Vetenskapsakad Handlingar* 24 (1898) 1-39.

Laksaci H, Khelifi A, Trari M, Addoun A, Synthesis and characterization of microporous activated carbon from coffee grounds using potassium hydroxides, *Journal of Cleaner Production* 147 (2017) 254 – 262.

Langley S and Beveridge TJ, Effect of O-side-chain-lipopolysaccharide chemistry on metal binding, *Applied Environmental Microbiology* 65 (1999) 489-498.

Langmuir I, The adsorption of gases on plane surfaces of glass, mica and platinum, *Journal of the American Chemical Society* 40 (1918) 1361-1403.

Largitte L and Pasquier R, A review of the kinetics adsorption models and their application to the adsorption of lead by an activated carbon, *Chemical Engineering Research and Design* 109 (2016) 495-504.

Ledesma B, Román S, Álvarez-Murillo A, Sabio E, González JF, Cyclic adsorption/thermal regeneration of activated carbons, *Journal of Analytical and Applied Pyrolysis* 106 (2014a) 112 – 117.

Ledesma B, Román S, Álvarez-Murillo A, Sabio E, González-García CM, Fundamental study on the thermal regeneration stages of exhausted activated carbons: kinetics, *Journal of Thermal Analysis and Calorimetry* 115 (2014b) 537 – 543.

- Lee C, Yang W, Parr RG, Development of the Colle-Salvetti correlation-energy formula into a functional of the electron density, *Physical Review B* 37 (1988) 785-789.
- Lee EH, A practical guide to pharmaceutical polymorph screening & selection, *Asian Journal of Pharmaceutical Sciences* 9 (2014) 163-175.
- Lee T, Ooi, C-H, Othman R, Yeoh F-Y, Activated carbon fiber – The hybrid of carbon fiber and activated carbon, *Reviews on Advanced Materials Science* 36 (2014) 118 - 136.
- Lemraski EG, Sharafinia S, Alimohammadi M, New activated carbon from Persian mesquite grain as an excellent adsorbent, *Physical Chemistry Research* 5 (2017) 81-98.
- Lenhart TR, Duncan KE, Beech IB, Sunner JA, Smith W, Bonifay V, Biri B, Suflita JM, Identification and characterization of microbial biofilm communities associated with corroded oil pipeline surfaces, *Biofouling* 30 (2014) 823-835.
- Leung HW, Minh TB, Murphy MB, Lam JC, So MK, Martin M, Lam KSP, Richardson BJ, Distribution, fate and risk assessment of antibiotics in sewage treatment plants in Hong Kong, South China, *Environment International* 42 (2012) 1-9.
- Liang P, Zhang YQ, Jiang WM, Wei AF, Liu T, Wu JF, Simulation study of Shenmu coal pyrolysis by gas heat carrier based on a moving bed, *Energy & Fuels* 29 (2015) 7727-7733.
- Liao C and Kannan K, A survey of alkylphenols, bisphenols, and triclosan in personal care products from China and the United States, *Archives of Environmental Contamination and Toxicology* 67 (2014) 50-59.
- Li D, Yang M, Hu J, Ren L, Zhang Y, Li K, Determination and fate of oxytetracycline and related compounds in oxytetracycline production wastewater and the receiving river, *Environmental Toxicology and Chemistry* 27 (2008) 80–86
- Lim HB and Kim B-W, Effect of NAPL exposure on the wettability and two-phase flow in a single rock fracture, *Hydrological Processes* 29 (2015) 4919-4931.
- Linares-Solano A, Martín-Gullón I, Lecea CSM, Serrano-Talavera B, Activated carbons from bituminous coal: effect of mineral matter content, *Fuel* 79 (2000) 635-643.
- Lin C-K, Tsai T-Y, Liu J-C, Chen M-C, Enhanced biodegradation of petrochemical wastewater using ozonation and BAC advanced treatment system, *Water Research* 35 (2001) 699 – 704.
- Lin T, Yu SL, Chen W, Occurrence, removal and risk assessment of pharmaceutical and personal care products (PPCPs) in an advanced drinking water treatment plant (ADWTP) around Taihu Lake in China, *Chemosphere* 152 (2016) 1-9.
- Lin XY, Guo WM, Zhang TH, Huang JR, Tong Y, Zhang TL, Syntheses, crystal structures and characterization of nitrogen-rich salts based on bis(1H-tetrazol-5-yl) methanone oxime, *Journal of Molecular Structure* 1141 (2017) 1-5.
- Lin YC, Lai WWP, Tung HH, Lin AYC, Occurrence of pharmaceuticals, hormones, and perfluorinated compounds in groundwater in Taiwan, *Environmental Monitoring and Assessment* 187 (2015) 1-19.
- Lissant KJ (Ed.), Emulsions and emulsion technology - Part 1, *Marcel Dekker Inc.* (1974).

Liu CC, Lu S, Fu YT, Zhang HP, Flammability and the oxidation kinetic of the magnesium alloys AZ31, WE43, and ZE10, *Corrosion Science* 100 (2015) 177-185.

Liu G, Bakker GL, Li S, Vreeburg JH, Verberk JQ, Medema GJ, Liu WT, Van Dijk JC, Pyrosequencing reveals bacterial communities in unchlorinated drinking water distribution system: an integral study of bulk water, suspended solids, loose deposits, and pipe wall biofilm, *Environmental Science Technology* 48 (2014) 5467-5476.

Liu H, Zhan L, Seaton NA, Analysis of Sorption Hysteresis in Mesoporous Solids Using a Pore Network Model, *Journal of Colloid and Interface Science* 156 (1993) 285-293.

Liu P, Liu S, Bian SW, Core-shell-structures Fe₃O₄/Pd@ZIF-8 catalyst with magnetic recyclability and size selectivity for the hydrogenation of alkenes, *Journal of Materials Science* 52 (2017) 12121-12130.

Liu Y, Zhang S, Song N, Guo R, Chen M, Mai D, Yan Z, Han Z, Chen J, Occurrence, distribution and sources of bisphenol analogues in a shallow Chinese freshwater lake (Taihu lake): Implications for ecological and human health risk, *Science of the Total Environment* 599-600 (2017) 1090-1098.

Liu ZS, Control of heavy metals during incineration using activated carbon fibers, *Journal of Hazardous Materials* 142 (2007) 506 – 511.

Li WW, Chen JW, Cong GJ, Tang L, Cui Q, Wang HY, Solvent desulfurization regeneration process and analysis of activated carbon for low-sulfur real diesel, *RSC Advances* 6 (2016) 20258 – 20268.

Li XH, Ma R, Huang FL, Li Y, Adsorption of Naphthenic Acids from Dewaxed Vacuum Gas Oil by Activated Clay: Kinetics, Equilibrium and Thermodynamic Studies, *China Petroleum Processing & Petrochemical Technology* 19(1) (2017) 123-134.

Li Y, Tang LP, Ma XX, Wang XR, Zhou W, Bai DS, Synthesis and characterization of Zn-Ti layered double hydroxide intercalated with cinnamic acid for cosmetic application, *Journal of Physics and Chemistry of Solids* 107 (2017) 62-67.

Llorente I, Fajardo S, Bastidas JM, Applications of electrokinetic phenomena in materials science, *Journal of Solid State Electrochemistry* 18 (2014) 293-307.

Lopes VSA, Riente RR, da Silva AA, Torquillo DF, Carreira RD, Marques MRD, Development of a solid-phase extraction system modified for preconcentration of emerging contaminants in large sample volumes from rivers of the lagoon system in the city of Rio de Janeiro, Brazil, *Marine Pollution Bulletin* 110 (2016) 572-577.

Lordgooei M, Rood MJ, Rostam-Abadi M, New general pore size distribution model by classical thermodynamics application: Activated carbon, *Journal of Environmental Engineering-ASCE* 127 (2001) 281-287.

Lu J, Wu J, Stoffella PJ, Wilson PC, Uptake and distribution of bisphenol A and nonylphenol in vegetable crops irrigated with reclaimed water, *Journal of Hazardous Materials* 283 (2015) 865–870.

Lundelius EF, Adsorption and solubility, *Kolloid Zeitschrift* 26 (1920) 145-151.

Lützenkirchen J, Preočanin T, Kovačević D, Tomišić V, Lövgren L, Kallay N, Potentiometric titrations as a tool for surface charge determination, *Croatica Chemica Acta* 85 (2012) 391-417.

Lyklema J, Solid-liquid interfaces, in: Lyklema J (Ed.), *Fundamentals of Interface and Colloid Science, Academic Press II* (1995).

Ma DH, Chen LJ, Liu R, Removal of novel antiandrogens in biological effluents of domestic wastewater by activated carbon, *Science of the Total Environment* 595 (2017) 702-710.

Machado AP, Pereira AL, Barbero GF, Martínez J, Recovery of anthocyanins from residues of *Rubus fruticosus*, *Vaccinium myrtillus* and *Eugenia brasiliensis* by ultrasound assisted extraction, pressurized liquid extraction and their combination, *Food Chemistry* 231 (2017) 1-10.

Mah TC and O'Toole GA, Mechanisms of biofilm resistance to antimicrobial agents, *TRENDS in Microbiology* 9 (2001) 34-39.

Ma J, Huang BX, Zhao XC, Wang CZ, Zhang HM, Effect of zinc substitution for calcium on the structure, dissolution behavior and apatite formation of CaO-ZnO-SiO₂-P₂O₅ bioceramics, *Materials Letters* 296 (2017) 154-157.

Mandaric L, Diamantini E, Stella E, Cano-Paoli K, Valle-sistac J, Mollins-Delgado D, Bellin A, Chiogna G, Majone B, Diaz-Cruz MS, Contamination sources and distribution patterns of pharmaceuticals and personal care products in Alpine rivers strongly affected by tourism, *Science of the Total Environment* 590 (2017) 484-494.

Marenich AV, Cramer CJ, Truhlar DG, Universal solvation model based on solute electron density and a continuum model of the solvent defined by the bulk dielectric constant and atomic surface tensions, *The Journal of Physical Chemistry B* 113 (2009) 6378-6396.

Marques S, Remoção de poluentes em solução aquosa por carvões activados, Universidade de Lisboa (2011).

Marsh H and Rodríguez-Reinoso F, *Activated Carbon, Elsevier* (2006).

Martínez LMP, Ramón MVL, Cámara MAF, Batch and column adsorption of herbicide fluoxypyr on different types of activated carbons from water with varied degrees of hardness and alkalinity, *Water Research* 44 (2010) 879-885.

Martínez-Romero D, Bailén G, Serrano M, Guillén F, Valverde JM, Zapata P, Castillo S, Valero D, Tools to maintain postharvest fruit and vegetable quality through the inhibition of ethylene action: A review, *Critical Reviews in Food Science and Nutrition* 47 (2007) 543 – 560.

Martins VV, Zanetti MO, Pitondo-Silva A, Stechling EG, Aquatic environments polluted with antibiotics and heavy metals: a human health hazard, *Environmental Science and Pollution Research* 21 (2014) 5873-5878.

Matamoros V, García J, Bayona JM, Organic micropollutant removal in a fullscale surface flow constructed wetland fed with secondary effluent, *Water Research* 42 (2008) 653–660.

Ma XL, Peng H, Zhang X, Regeneration of nitrophenol loaded granular activated carbon and its effect on the surface properties of adsorbent, *Desalination and Water Treatment* 57 (2016) 25494 – 25502.

Ma Y, Comparison of activated carbons prepared from wheat straw via $ZnCl_2$ and KOH activation, *Waste Biomass Valor* 8 (2017) 549 – 559.

Mays TJ, Active carbon fibers in: Burchell TD (Ed.), Carbon Materials for Advanced Technologies, Elsevier Science Ltd (1999) 95 – 118.

Mazzola L and Bruno G, Characterization of ice-phobic surfaces: Improvements on contact angle measurements, *Measurement* 110 (2017) 202-210.

Medema GJ, Payment P, Dufour A, Robertson W, Waite M, Hunter P, Kirby R, Anderson Y, Safe drinking water: an ongoing challenge, in: Assessing Microbial Safety of Drinking Water-Improving Approaches and Method, IWA Publishing (2003) 11–45.

Meikleham N, Pizzi A, Stephanou A, Induced accelerated autocondensation of polyflavonoid tannins for phenolic polycondensates. I. ^{13}C -NMR, ^{29}Si -NMR, X-ray, and polarimetry studies and mechanism, *Journal of Applied Polymer Science* 54 (1994) 1827-1845.

Meireles A, Gonçalves AL, Gomes IB, Simões LC, Methods to study microbial adhesion on abiotic surfaces, *AIMS Bioengineering* 2 (2015) 297-309.

Menéndez-Díaz JA and Martín-Gullón I, Types of carbon adsorbents and their production, in: Bandosz TJ (Ed.), Activated Carbon Surfaces in Environmental Remediation, Elsevier (2006) 1 - 48.

Mestre AS, Bexiga AS, Proença M, Andrade M, Pinto ML, Matos I, Fonseca IM, Carvalho AP, Activated carbons from sisal waste by chemical activation with K_2CO_3 : Kinetics of paracetamol and ibuprofen removal from aqueous solution, *Bioresource Technology* 102 (2011) 8263 – 8260.

Mestre AS, Machuqueiro M, Silva M, Freire R, Fonseca IM, Santos MSCS, Calhorda MJ, Carvalho AP, Influence of activated carbons porous structure on iopamidol adsorption, *Carbon* 77 (2014a) 607 - 615.

Mestre AS, Marques SCR, Carvalho AP, Effect of the alcohol cosolvent in the removal of caffeine by activated carbons, *Industrial & Engineering Chemistry Research* 51 (2012) 9850 – 9857.

Mestre AS, Nabiço A, Figueiredo PL, Pinto ML, Santos MSCS, Fonseca IM, Enhanced clofibrac acid removal by activated carbons: Water hardness as a key parameter, *Chemical Engineering Journal* 286 (2016) 538-548.

Mestre AS, Pinto ML, Pires J, Nogueira JMF, Carvalho AP, Effect of solution pH on the removal of clofibrac acid by cork-based activated carbons, *Carbon* 48 (2010) 972-980.

Mestre AS, Pires J, Nogueira JMF, Carvalho AP, Activated carbons for the adsorption of ibuprofen, *Carbon* 45 (2007) 1979-1988.

Mestre AS, Pires RA, Aroso I, Fernandes EM, Pinto ML, Reis RL, Andrade MA, Pires J, Silva SP, Carvalho AP, Activated carbons prepared from industrial pre-treated cork: Sustainable adsorbents for pharmaceutical compounds removal, *Chemical Engineering Journal* 253 (2014b) 408-417.

Mestre AS, Tyszko E, Andrade MA, Galhetas M, Freire C, Carvalho AP, Sustainable activated carbon prepared from a sucrose-derived hydrochar: remarkable adsorbents for pharmaceutical compounds, *RSC Advances* 5 (2015) 19696-19707.

- Mims CA and Pabst JK, Role of surface salt complexes in alkali-catalysed carbon gasification, *Fuel* 62 (1983) 176-179.
- Mohan D, Singh KP, Sinha S, Gosh D, Removal of pyridine derivatives from aqueous solution by activated carbons developed from agricultural waste materials, *Carbon* 43 (2005) 1680-1693.
- Mojzer EB, Hrnčič MK, Škerget M, Knez Ž, Bren U, Polyphenols: Extraction methods, antioxidative action, bioavailability and anticarcinogenic effects, *Molecules* 21 (2016) 1-38.
- Moloukhia H, Hegazy WS, Abdel-Galil EA, Mahrous SS, Removal of Eu^{3+} , Ce^{3+} , Sr^{2+} , and Cs^+ ions from radioactive waste solutions by modified activated carbon prepared from coconut shells, *Chemistry and Ecology* 32 (2016) 324-345.
- Montgomery JR, Water Treatment: Principles and Design, *John Wiley & Sons, Inc* (1985).
- Moraes SS, Otero LS, Freitas AVL, Natural history and comparative morphology of *Gamelia anableps* (C. Felder & R. Felder) (Lepidoptera: Saturniidae, Hemileucinae), *Neotropical entomology* 46 (2017) 397-408.
- Moreno-Castilla C, Adsorption of organic molecules from aqueous solutions on carbon materials, *Carbon* 42 (2004) 83-94.
- Moreno-Castilla C, Adsorption of organic solutes from dilute aqueous solutions, in: Bottani EJ and Táscon JMD (Eds.), Adsorption by Carbons, *Elsevier Ltd* (2008) 653-678.
- Moreno-Castilla C, Lopez-Ramon MV, Carrasco-Marin F, Changes in surface chemistry of activated carbons by wet oxidation, *Carbon* 38 (2000) 1995-2001.
- Mugica-Vidal R, Alba-Elias F, Sainz-Garcia E, Pantoja-Ruiz M, Atmospheric pressure air plasma treatment of glass substrates for improved silver/glass adhesion in solar mirrors, *Solar energy Materials and Solar Cells* 169 (2017) 287-296.
- Nantaphol S, Watanabe T, Nomura N, Siangproh W, Chailapakul O, Einaga Y, Biometallic Pt-Au nanocatalysts electrochemically deposited on boron-doped diamond electrodes for nanenzymatic glucose detection, *Biosensors & Bioelectronics* 98 (2017) 76-82.
- National Research Council, Drinking water and Health – Volume 2, *The National Academies Press* (1980).
- Nematollahi D, Shayani-Jam H, Alimoradi M, Niroomand S, Electrochemical oxidation of acetaminophen in aqueous solutions: Kinetic evaluation of hydrolysis, hydroxylation and dimerization processes, *Electrochimica Acta* 54 (2009) 7407–7415.
- Nenadis N and Tsimidou MZ, Perspective of vibrational spectroscopy analytical methods in on-field/official control of olives and virgin olive oil, *European Journal of Lipid Science and Technology* 119 (2017) 1-18.
- Nguyen C and Do DD, Pore size distribution of micro-mesoporous adsorbents determined by means of the multilayering and capillary condensation theory, *Adsorption Science and Technology* (2000) 199-203.

Nishikawa K, Ueta Y, Hara D, Yamada S, Koga N, Kinetic characterization of multistep thermal oxidation of carbon/carbon composite in flowing air, *Journal of Thermal Analysis and Calorimetry* 128 (2017) 891-906.

Noh JS and Schwarz JA, Estimation of the point of zero charge of simple oxides by mass titration, *Journal of Colloid and Interface Science* 130 (1989) 157-164.

Nor NM, Sukri MFF, Mohamed AR, Development of high porosity structures of activated carbon via microwave-assisted regeneration for H₂S removal, *Journal of Environmental Chemical Engineering* 4 (2016) 4839 – 4845.

Oberthur T, Melcher F, Weiser TW, Detrital platinum-group minerals and gold in placers of southeastern Samar Island, Philippines, *Canadian Mineralogist* 55 (2017) 45-62.

Ocampo-Pérez R, Leyva-Ramos R, Rivera-Utrilla J, Flores-Cano JV, Sánchez-Polo M, Modeling adsorption rate of tetracyclines on activated carbons from aqueous phase, *Chemical Engineering Research and Design* 104 (2015) 579-588.

Odonkor ST and Ampofo JK, *Escherichia coli* as an indicator of bacteriological quality of water: an overview, *Microbiology Research* 4 (2013) 5-11.

Oh WD, Lim PE, Leong KY, Yong SL, Yin H, Bioregeneration of granular activated carbon loaded with binary mixture of phenol and 4-chlorophenol, *Desalination and Water Treatment* 57 (2016) 20476 – 20482.

Oliveira TS, Murphy M, Mendola N, Wong V, Carlson D, Waring L, Characterization of pharmaceuticals and personal care products in hospital effluent and waste water influent/effluent by direct-injection LC-MS-MS, *Science of the Total Environment* 518 (2015) 459-478.

Omorogie MO, Babalolab JO, Unuabonah EI, Regeneration strategies for spent solid matrices used in adsorption of organic pollutants from surface water: a critical review, *Desalination and Water Treatment* (2014) 1-27.

Onesios KM, Yu JT, Bouwer EJ, Biodegradation and removal of pharmaceuticals and personal care products in treatment systems: a review, *Biodegradation* 20 (2009) 441–466.

Ortiz RW, Benincá C, Cardozo-Filho L, Zanoelo EF, High-pressure acid-catalyzed isomerization and hydration of fumaric acid in a homogeneous nonisothermal batch reactor, *Industrial & Engineering Chemistry Research* 56 (2017) 3873-3879.

Otto K, Norbeck J, Larsson T, Karlsson K-A, Hermansson M, Adhesion of type 1-fimbriated *Escherichia coli* to abiotic surfaces leads to altered composition of outer membrane proteins, *Journal of Bacteriology* 183 (2001) 2445-2453.

Paíga P and Delerue-Matos C, Determination of pharmaceuticals in groundwater collected in five cemeteries' areas (Portugal), *Science of the Total Environment* 569-570 (2016) 16-22.

Palmer J, Flint S, Brooks J, Bacterial cell attachment, the beginning of a biofilm, *Journal of Industrial Microbiology and Biotechnology* 34 (2007) 577-588.

Papageorgioua M, Kosmab C, Lambropoulou D, Seasonal occurrence, removal, mass loading and environmental risk assessment of 55 pharmaceuticals and personal care

products in a municipal wastewater treatment plant in central Greece, *Science of the Total Environment* 543 (2016) 547-569.

Pap S, Knudsen TS, Radonić J, Maletić S, Igić SM, Sekulić MT, Utilization of fruit processing industry waste as green activated carbon for the treatment of heavy metals and chlorophenols contaminated water, *Journal of Cleaner Production* 162 (2017) 958-972.

Pap S, Radonic J, Trifunovic S, Adamovic D, Mihajlovic I, Miloradov MV, Sekulic MT, Evaluation of the adsorption of eco-friendly activated carbon prepared from cherry kernels for the removal of Pb²⁺, Cd²⁺ and Ni²⁺ from aqueous wastes, *Journal of Environmental Management* 184 (2016) 297-306.

Park SJ and Jang YS, Preparation and characterization of activated carbon fibers supported with silver metal for antibacterial behavior, *Journal of Colloid and Interface Science* 261 (2003) 228 – 243.

Paschalis EP, Gamsjaeger S, Klaushofer K, Vibrational spectroscopic techniques to assess bone quality, *Osteoporosis International* 28 (2017) 2275-2291.

Pasch H, Pizzi A, Rode K, MALDI–TOF mass spectrometry of polyflavonoid tannins, *Polymer* 42 (2001) 7531-7539.

Pastrana-Martínez LM, López-Ramón MA, Fontecha-Cámara MA, Moreno-Castilla C, Batch and column adsorption of herbicide fluroxypyr on different types of activated carbons from water with varied degrees of hardness and alkalinity, *Water Research* 44 (2010) 879-885.

Pastrana-Martínez LM, López-Ramón MV, Moreno-Castilla C, Adsorption and thermal desorption of the herbicide fluroxypyr on activated carbon fibers and cloth at different pH values, *Journal of Colloid and Interface Science* 331 (2009) 2–7.

Peña C, De la Caba K, Retegi A, Ocando C, Labidi J, Echeverria JM, Mondragon I, Mimosa and chestnut tannin extracts reacted with hexamine in solution, *Journal of Thermal Analysis and Calorimetry* 96 (2009) 515-521.

Pergante MR and Cologna SM, Isoelectric point separations of peptides and proteins, *Proteomes* 5 (2017) 1-14.

Pichelin F, Kamoun C, Pizzi A, Hexamine hardener behaviour: effects on wood glueing, tannin and other wood adhesives, *Holz Als Roh- und Werkst* 57 (1999) 305-317.

Pichelin F, Nakatani M, Pizzi A, Wieland S, Despres A, Rigolet S, Structural beams from thick wood panels bonded industrially with formaldehyde-free tannin adhesives, *Journal of Natural Products* 56 (2006) 31-36.

Pinto ML, Mestre AS, Carvalho AP, Pires J, Comparison of methods to obtain micropore size distributions of carbonaceous materials from CO₂ adsorption based on the Dubinin-Radushkevich isotherm, *Industrial & Engineering Chemistry Research* 49 (2010) 4726-4730.

Plaza-Recobert M, Trautwein G, Pérez-Cadenas M, Alcañiz-Monge J, Preparation of binderless activated carbon monoliths from cocoa bean husk, *Microporous and Mesoporous Materials* 243 (2017) 28-38.

Plis A, Lasek JA, Zuwaia J, Yu C-C, Iluk A, Combustion performance evaluation of *Posidonia oceanica* using TGA and bubbling fluidized-bed combustor (batch reactor), *Journal of Sustainable Mining* 15 (2016) 181-190.

Powder Diffraction Alphabetic Index, International Center for Diffraction Data (1988).

Prabhu S, Cindrella L, Kwon OJ, Mohanraju K, Superhydrophilic and self-cleaning rGO-TiO₂ composite coatings for indoor and outdoor photovoltaic applications, *Solar Energy Materials and Solar Cells* 169 (2017) 304-312.

Prati S, Sciutto G, Bonacini I, Mazzeo R, New frontiers in application of FTIR microscopy for characterization of cultural heritage materials, *Topics in Current Chemistry (Z)* 374 (2016) 1-32.

Pratt LA and Kolter R, Genetic analysis of *Escherichia coli* biofilm formation: Roles of flagella, motility, chemotaxis and type I pili, *Molecular Microbiology* 30 (1998) 285-293.

Przepiórski J, Activated carbon filters and their industrial applications, in: Bandosz TJ (Ed.), *Activated Carbon Surfaces in Environmental Remediation*, Elsevier (2006) 421-474.

Qin W, Li W-G, Zhang D-Y, Huang X-F, Song Y, Ammonium removal of drinking water at low temperature by activated carbon filter biologically enhanced with heterotrophic nitrifying bacteria, *Environmental Science and Pollution Research* 23 (2016) 4650-4659.

Qin X, Fang SW, Zhao L, Shi PH, Fan JC, Min YL, Xu QJ, Yao WF, Cobalt super-microparticles anchored on nitrogen-doped graphene for aniline oxidation based on sulfate radicals, *Science of the Total Environment* 601 (2017) 99-108.

Qiu H, Lv L, Pan B, Zhang Q, Zhang W, Zhang Q, Critical review in adsorption kinetic models, *Journal of Zhejiang University Science A* 10 (2009) 716-724.

Qi Y, Wu S, Xi F, He S, Fan C, Dai B, Huang J, Gao L, Performance of a coupled micro-electrolysis, anaerobic and aerobic system for oxytetracycline (OTC) production wastewater treatment, *Journal of Chemical Technology and Biotechnology* 91 (2016) 1290-1298.

Qu WW, Hu Q, Zhu Y, Peng JH, Zhang LB, Microwave-assisted regeneration of spent activated carbon containing zinc acetate and its application for removal of congo red, *Desalination and Water Treatment* 57 (2016) 28496 – 28511.

Radic DB, Stanojevic MM, Obradovic MO, Jovovic AM, Thermal analysis of physical and chemical changes occurring during regeneration of activated carbon, *Thermal Science* 21 (2017) 1067 – 1081.

Radovic LR and Reinoso F, Carbon materials in catalysis, in: Thrower PA (Ed.), *Chemistry and Physics of Carbon*, Marcel Dekker Inc.(1997) 243 – 358.

Radovic LR, Moreno-Castilla C, Rivera-Utrilla J, Carbon Materials as Adsorbens on Aqueous Solutions, *Chemistry and Physics of Carbon*, Marcel Dekker Inc.(2000).

Rahman NNN, Shahadat M, Won CA, Omar FM, FTIR study and bioadsorption kinetics of biosorbent for the analysis of metal pollutants, *RSC Advances* 4 (2014) 58156-58163.

- Redhead PA, Thermal desorption of gases, *Vacuum* 12 (1962) 203-211.
- Redlich O and Peterson DL, A useful adsorption isotherm, *Journal of Physical Chemistry* 63 (1959) 1024-1024.
- Reichelt R, Scanning Electron Microscopy, in: Howkes PW and Spence JCH (Eds.), *Science of Microscopy – Volume I*, Springer (2007) 133-272.
- Rifai A, Abu-Dheir N, Khaled M, Al-Aqeeli N, Yilbas BS, Characteristics of oil impregnated hydrophobic glass surfaces in relation to self-cleaning of environmental dust particles, *Solar Energy Materials and Solar Cells* 171 (2017) 8–15.
- Rigby SP, New methodologies in mercury porosimetry, *Studies in Surface Science and Catalysis* 144 (2002) 185-192.
- Rivera-Utrilla J, Bautista-Toledo I, Ferro-García MA, Moreno-Castilla C, Activated carbon surface modifications by adsorption of bacteria and their effect on aqueous lead adsorption, *Journal of Chemical Technology and Biotechnology* 76 (2001) 1209-1215.
- Rivera-Utrilla J, Bautista-Toledo I, Ferro-García MA, Moreno-Castilla C, Bioadsorption of Pb(II), Cd(II), and Cr(VI) on activated carbon from aqueous solutions, *Carbon* 41 (2003) 323-330.
- Rivera-Utrilla J, Gomez-Pachaco CV, Sanchez-Polo M, Lopez-Penalver JJ, Ocampo-Perez, Tetracycline removal from water by adsorption/bioadsorption on activated carbons and sludge-derived adsorbents, *Journal of Environmental Management* 131 (2013) 16-24.
- Rizzo L, Manaia C, Merlin C, Schwartz T, Dagot C, Ploy MC, Michael I, Fatta-Kassinos D, Urban wastewater treatment plants as hotspots for antibiotic resistant bacteria and genes spread into the environment: A review, *Science of the Total Environment* 447 (2013) 345-360.
- Roberts A, Figura M, Thiesen PH, Niemeyer B, Desorption of odor-active compounds by microwaves, ultrasound, and water, *AIChE Journal* 51 (2005) 502–510.
- Roccaro P, Sgroi M, Vagliasindi FGA, Removal of xenobiotic compounds from wastewater for environment protection: treatment processes and costs, *Chemical Engineering Transactions* 32 (2013) 505–510.
- Rochelle-Newall E, Nguyen TMH, Le TPQ, Sengtaheuanghoung O, Ribolzi O, A short review of fecal indicator bacteria in tropical aquatic ecosystems: knowledge gaps and future directions, *Frontiers in Microbiology* 6 (2015) 1-15.
- Rodríguez E, Campinas M, Acero JL, Rosa MJ, Investigating PPCP Removal from Wastewater by Powdered Activated Carbon/Ultrafiltration, *Water, Air and Soil Pollution* 227 (2016) 1-14.
- Rodríguez OM, Peralta-Hernandez JM, Goonetilleke A, Bandala ER, Treatment technologies for emerging contaminants in water: A review, *Chemical Engineering Journal* 323 (2017) 361-380.
- Rodríguez-Reinoso F and Martín-Martínez JM, A standard adsorption isotherm for the characterization of activated carbons, *Journal of Physical Chemistry – US* 91 (1987) 515-516.

Rodríguez-Reinoso F and Sepúlveda-Escribano A, Porous carbons in adsorption and catalysis, in: Nalwa HS (Ed.), Handbook of Surfaces and Interfaces of Materials, *Academic Press* (2001) 309 - 355.

Rodríguez-Reinoso F, Preparation and characterization of activated carbons, in: Figueiredo JL and Moulijn JA (Eds.), Carbon and Coal Gasification: Science and Technology, *Martinus Nijhoff Publishers* (1986) 601-642.

Romanielo LL, Arvelos S, Tavares FW, Rajagopal K, A modified multi-site occupancy model: evaluation of azeotropelike behaviour in adsorption, *Adsorption* 21 (2015) 3-16.

Román S, Ledesma B, Álvarez-Murillo A, González JF, Comparative study on the thermal reactivation of spent adsorbents, *Fuel Processing Technology* 116 (2013) 358 – 365.

Rouquerol F, Rouquerol J, Sing K, Adsorption by powders & porous solids – Principles, methodology and applications, *Academic Press* (1999).

Rouquerol J, Avnir D, Fairbridge CW, Everett DH, Haynes JM, Pernicone N, Ramsay JDF, Sing KSW, Unger KK, Recommendations for the characterization of porous solids, *Pure and Applied Chemistry* 66 (1994) 1739-1758.

Rouquerol J, Baron G, Denoyel R, Giesche H, Groen J, Klobes P, Levitz P, Neimark AV, Rigby S, Skudas R, Sing K, Thommes M, Unger K, Liquid intrusion and alternative methods for the characterization of macroporous materials (IUPAC Technical Report), *Pure and Applied Chemistry* 84 (2012) 107-136.

Rúa-Gómez PC, Guedez AA, Ania CO, Püttmann W, Upgrading of wastewater treatment plants through the use of unconventional treatment technologies: Removal of lidocaine, tramadol, venlafaxine and their metabolites, *Water* 4 (2012) 650-669.

Rusova NV, Astashkina OV, Lysenko AA, Adsorption of heavy metals by activated carbon fibres, *Fibre Chemistry* 47 (2016) 320 – 323.

Ruthven DM, Principles of Adsorption and Adsorption Processes, *John Wiley & Sons Inc* (1984).

Sabio E, González E, González JF, González-García CM, Ramiro A, Gañan J, Thermal regeneration of activated carbon saturated with *p*-nitrophenol, *Carbon* 42 (2004) 2285 – 2293.

Saboya RMA, Cecilia JA, García-Sancho C, Sales AV, Luna FMT, Rodríguez-Castellón E, Cavalcante Jr. CL, Synthesis of biolubricants by the esterification of free fatty acids from castor oil with branched alcohols using cationic exchange resins as catalysts, *Industrial Crops & Products* 104 (2017) 52-61.

Sadeghi S, Moghbeli MR, Synthesis and dispersion of colloidal silver nanoparticles on microcellular polyHIPE support, *Colloids and Surfaces A: Physicochemical and Engineering Aspects* 409 (2012) 42-51.

Sadri R, Hosseini M, Kazi SN, Bagheri S, Zubir N, Solangi KH, Zaharinie T, Badarudin A, A bio-based, facile approach for the preparation of covalently functionalized carbon nanotubes aqueous suspensions and their potential as heat transfer fluids, *Journal of Colloid and Interface Science* 504 (2017) 115-123.

- Salvador F, Martín-Sánchez N, Sánchez-Hernández R, Sánchez-Montero MJ, Regeneration of carbonaceous adsorbents. Part II: Chemical, microbiological and vacuum regeneration, *Microporous and Mesoporous Materials* 202 (**2015**) 277 – 296.
- Sánchez-Martín J, Beltrán-Heredia J, Delgado-Regaña, Rodríguez-González MA, Rubio-Alonso F, Adsorbent tannin foams: New and complementary applications in wastewater treatment, *Chemical Engineering Journal* 228 (**2013a**) 575-582.
- Sánchez-Martín J, Beltrán-Heredia J, Delgado-Regaña, Rodríguez-González MA, Rubio-Alonso F, Optimization of tannin rigid foam as adsorbents for wastewater treatment, *Industrial Crops and Products* 49 (**2013b**) 507-514.
- Sani S, Activated carbon production from turf soil, *Jurnal Teknik Kimia* 5 (**2011**) 400-406.
- Santos LH, Gros M, Rodriguez-Mozaz S, Delerue-Matos C, Pena A, Barcelo D, Montenegro BS, Contribution of hospital effluents to the load of pharmaceuticals in urban wastewaters: identification of ecologically relevant pharmaceuticals, *Science of the Total Environment* 461- 462 (**2013**), 302-316.
- Saufi SM and Ismail AF, Fabrication of carbon membranes for gas separation – a review, *Carbon* 43 (**2004**) 241 – 259.
- Seas C, Alarcon M, Aragon JC, Beneit S, Quiñonez M, Guerra H, Gotuzzo E, Surveillance of Bacterial Pathogens Associated with Acute Diarrhea in Lima, Peru, *International Journal of Infectious Diseases* 4 (**2000**) 96–99.
- Shammy A, Sivret EC, Le-Minh N, Fernandez RL, Evanson I, Stuetz RM, Review of odour abatement in sewer networks, *Journal of Environmental Chemical Engineering* 4 (**2016**) 3866 – 3881.
- Sheng X, Ting YP, Pehkonen SO, The influence of ionic strength, nutrients and pH on bacterial adhesion to metals, *Journal of Colloid and Interface Science* 321 (**2008**) 256-264.
- Shu Y, Li KL, Song JF, Li B, Tang CF, Single and competitive adsorption of Cd(II) and Pb(II) from aqueous solution by activated carbon prepared with *Salix matsudana* Kiodz, *Water Science and Technology* 74 (**2016**) 2751-2761.
- Sieniawska E and Baj T, Tannins, in: McCreath SB and Delgoda R (Eds.), Pharmacognosy: Fundamentals, Applications and Strategies, *Academic Press* (**2017**) 199-232.
- Sing KSW, Everett DH, Haul RAW, Moscou L, Pierotti RA, Rouquérol J, Siemieniowska, IUPAC Reporting physisorption data for gas/solid systems with special reference to the determination of surface area and porosity, *Pure and Applied Chemistry* 57 (**1985**) 603-619.
- Sing K, The use of nitrogen adsorption for the characterization of porous materials, *Colloids and Surfaces A: Physicochemical and Engineering Aspects* 187-188 (**2001**) 3-9.
- Smith B (Ed.), Infrared Spectral Interpretation: A Systematic Approach, *CRC Press* (**1999**).

Solazzo C, Follow-up on the characterization of peptidic markers in hair and fur for the identification of common North American species, *Rapid Communications in Mass Spectrometry* 31 (2017) 1375-1384.

Somers EB, Johnson ME, Wong ACL, Biofilm formation and contamination of cheese by nonstarter lactic acid bacteria in the dairy environment, *Journal of Dairy Science* 84 (2001) 1926-1936.

Sotelo JL, Ovejero G, Rodríguez A, Álvarez S, Galán J, García J, Competitive adsorption studies of caffeine and diclofenac aqueous solutions by activated carbon, *Chemical Engineering Journal* 240 (2014) 443-453.

Soto-Giron MJ, Rodriguez-R LM, Luo C, Elk M, Ryu H, Hoelle J, Santo Domingo JW, Konstantinidis KT, Biofilms on Hospital Shower Hoses: Characterization and Implications for Nosocomial Infections, *Applied and Environmental Microbiology* 82 (2016) 2872-2883.

Soulet B, Tauxe A, Tarradellas J, Analysis of acidic drugs in Swiss wastewaters, *International Journal of Environmental Analytical Chemistry* 266 (2002) 175–189.

Spongberg AL, Witter JD, Acuna J, Vargas J, Murillo M, Umana G, Gómez E, Perez G, Reconnaissance of selected PPCP compounds in Costa Rican surface waters, *Water Research* 45 (2011) 6709-6717.

Stackelberg PE, Furlong ET, Meyer MT, Zaugg SD, Henderson AK, Reissman DB, Persistence of pharmaceutical compounds and other organic wastewater contaminants in a conventional drinking-water treatment plant, *Science of the Total Environment* 329 (2004) 99-113.

Stoodley P, Sauer K, Davies DG, Costerton JW, Biofilms as complex differentiated communities, *Annual Review of Microbiology* 56 (2002) 187-209.

Stuart B (Ed.), *Infrared Spectroscopy: Fundamentals and Applications*, Wiley (2004).

Subedi B and Kannan K, Occurrence and fate of select psychoactive pharmaceuticals and antihypertensives in two wastewater treatment plants in New York State, USA. *Science of the Total Environment* 514 (2015) 273e280.

Subedi B, Balakrishna K, Joshua DI, Kannan K, Mass loading and removal of pharmaceuticals and personal care products including psychoactives, antihypertensives, and antibiotics in two sewage treatment plants in southern India, *Chemosphere* 167 (2017) 429-437.

Subrati A, Mondal S, Ali M, Alhindi A, Ghazi R, Abdala A, Reinalda D, Alhassan S, Developing hydrophobic graphene foam for oil spill cleanup, *Industrial & Engineering Chemistry Research* 56 (2017) 6945-6951.

Sukumar C, Gowthami G, Nitya R, Janaki V, Kamala-Kannan S, Shanthi K, Significance of co-immobilized activated carbon and *Bacillus subtilis* on removal of Cr(VI) from aqueous solutions, *Environmental Earth Sciences* 72 (2014) 839-847.

Sulaymon AH and Ahmed KW, Competitive adsorption of furfural and phenolic compounds onto activated carbon in fixed bed column, *Environmental Science & Technology* 42 (2008) 392-397.

- Sulyman M, Namiesnik J, Gierak A, Low-cost adsorbents derived from agricultural by-products/wastes for enhancing contaminant uptakes from wastewater: A review, *Polish Journal of Environmental Studies* 26 (2017) 479 – 510.
- Sun Y, Yue Q, Gao B, Gao Y, Xu X, Li Q, Wang Y, Adsorption and cosorption of ciprofloxacin and Ni(II) on activated carbon-mechanism study, *Journal of the Taiwan Institute of Chemical Engineers* 45 (2014) 681-688.
- Sun Y, Yue Q, Gao B, Li Q, Huang L, Yao F, Xu X, Preparation of activated carbon derived from cotton linter fibers by fused NaOH activation and its application for oxytetracycline (OTC) adsorption, *Journal of Colloid and Interface Science* 368 (2012) 521–527.
- Sun YY, Yue QY, Gao BY, Wang Y, Gao Y, Li Q, Preparation of highly developed mesoporous activated carbon by $H_4P_2O_7$ activation and its adsorption behaviour of oxytetracycline, *Powder Technology* 249 (2013) 54-62.
- Susanto I, Kan KY, Yu IS, Temperature effects for GaN films grown on 4H-SiC substrate with 4 degrees miscutting orientation by plasma-assisted molecular beam epitaxy, *Journal of Alloys and Compounds* 723 (2017) 21-29.
- Szczotka-Flynn LB, Imamura Y, Chandra J, Yu C, Mukherjee PK, Pearlman E, Ghannoum MA, Increased resistance of contact lens related bacterial biofilms to antimicrobial activity of soft contact lens care solution, *Cornea* 28 (2009) 918-926.
- Szczurek A, Fierro V, Pizzi A, Celzar A, Mayonnaise, whipped cream and meringue, a new carbon cuisine, *Carbon* 58 (2013) 238-251.
- Szkoda M, Rysz J, Ryl J, Lisowska-Oleksiak A, Siuzdak K, Fabrication and photoactivity of organic-inorganic systems based on titania nanotubes and PEDOT containing redox centres formed by different Prussian Blue analogues, *Journal of Alloys and Compounds* 723 (2017) 498-504.
- Tabe S, Pileggi V, Nowierski M, Kleywegt S, Yang P, Occurrence, removal, and environmental impacts of emerging contaminants detected in water and wastewater in Southern Ontario-Part I: occurrence and removal, *Water Practice and Technology* 11 (2016) 298-314.
- Taha H, Henry DJ, Yin CY, Amri A, Zhao XL, Bahri S, Minh CL, Ha NN, Rahman MM, Jiang ZT, Probing the effects of thermal treatment on the electronic structure and mechanical properties of Ti-doped ITO thin films, *Journal of Alloys and Compounds* 721 (2017) 333-346.
- Tambosi JL, Yamanaka LY, Jose HJ, Moreira R, Schröder HF, Recent research data on the removal of pharmaceuticals from sewage treatment plants (STP), *Química Nova* 33 (2010) 411-420.
- Taylor DJ, Tiamulin in the treatment and prophylaxis of experimental swine dysentery, *Veterinary Record* 106 (1980) 526-528.
- Temkin M and Pyzhev V, Kinetics of ammonia synthesis on promoted iron catalysts, *Acta Physicochimica Urss* 12 (1940) 327-356.

Ternes TA, Meisenheimer M, McDowell D, Sacher F, Brauch H-J, HaistGulde B, Preuss G, Wilme U, Zulei-Seibert N, Removal of pharmaceuticals during drinking water treatment, *Environmental Science and Technology* 36 (2002) 3855–3863.

Ternes TA, Occurrence of drugs in German sewage treatment plants and rivers, *Water Research* 32 (1998) 3245–3260.

Terzyk AP, Rychlicki G, Biniak S, Lukaszewicz JP, New correlations between the composition of the surface layer of carbon and its physicochemical properties exposed while paracetamol is adsorbed at different temperatures and pH, *Journal of Colloid and Interface Science* 257 (2003) 13-30.

Thokchom AK, Zhou Q, Kim D-J, Ha D, Kim T, Characterizing self-assembly and deposition behavior of nanoparticles in inkjet-printed evaporating droplets, *Sensors and Actuators B* 252 (2017) 1063–1070.

Thommes M, Kaneko K, Neimark A, Olivier J, Rodríguez-Reinoso F, Rouquerol J, Sing K, Physisorption of gases, with special reference to the evaluation of surface area and pore size distribution (IUPAC Technical Report), *Pure and Applied Chemistry* 87 (2015) 1051-1069.

Thommes M, Skudas R, Unger KK, Lubda D, Textural characterization of native and n-alkyl-bonded silica monoliths by mercury intrusion/extrusion, inverse size exclusion chromatography and nitrogen adsorption, *Journal of Chromatography A* 1191 (2008) 57-66.

Thomson W, On the equilibrium of vapour at a curved surface of liquid, *Proceeding of the Royal Society of Edinburgh* 7 (1872) 63-68.

Thongjamroon S, Ding J, Herng TS, Tang IM, Thongmee S, Dependence of the magnetic properties of the dilute magnetic semiconductor Zn_{1-x}Mn_xO nanorods on their Mn doping levels, *Journal of Magnetism and Magnetic Materials* 439 (2017) 391-396.

Tondi G, Tannin-Based Copolymer Resins: Synthesis and Characterization by Solid State ¹³C NMR and FT-IR Spectroscopy, *Polymers* 9 (2017) 223-239.

Torres CE, Negro C, Fuente E, Blanco A, Enzymatic approaches in paper industry for pulp refining and biofilm control, *Applied Microbiology and Biotechnology* 96 (2012) 327-344.

Tran HN, You S-J, Hosseini-Bandegharaei A, Mistakes and inconsistencies regarding adsorption of contaminants from aqueous solutions: A critical review, *Water Research* 120 (2017) 88 – 116.

Tsubouchi N, Nishio M, Mochizuki Y, Role of nitrogen in pore development in activated carbon prepared by potassium carbonate activation of lignin, *Applied Surface Science* 371 (2016) 301 – 306.

United States Environmental Protection Agency (EPA), Report of task force on guide standard and protocol for testing microbiological water purifiers (1986) 1-29.

Valbe R, Tarkanovskaja M, Maeorg U, Reedo V, Lohmus A, Taaber T, Vlassov S, Lohmus R, Phosphonium-based ionic liquids mixed with stabilized oxide nanoparticles as highly promising lubricating oil additives, *Proceedings of the Estonian Academy of Sciences* 66 (2017) 174-183.

van Loosdrecht MCM, Lyklema J, Norde W, Schraa G, Zehnder AJB, Electrophoretic mobility and hydrophobicity as a measure to predict the initial steps of bacterial adhesion, *Applied Environmental Microbiology* 53 (1987a) 1898-1901.

van Loosdrecht MCM, Lyklema J, Norde W, Schraa G, Zehnder AJB, The role of bacterial wall hydrophobicity in adhesion, *Applied Environmental Microbiology* 53 (1987b) 1893-1897.

van Loosdrecht MCM, Norde W, Lyklema J, Zehnder AJB, Hydrophobic and electrostatic parameters in bacterial adhesion, *Aquatic Sciences* 52 (1990) 103-114.

VanValkenburgh P, Kelloway SJ, Privat KL, Sillar B, Quilter J, Rethinking cultural hybridity and technology transfer: SEM microstructural analysis of lead glazed ceramics from early colonial Peru, *Journal of Archaeological Science* 82 (2017) 17-30.

Vargas C, Brandao PFB, Agreda J, Castillo E; Bioadsorption using compost: an alternative for removal of chromium (VI) from aqueous solutions, *Bioresources* 7 (2012) 2711-2727.

Verlicchi P, Al Aukidy M, Galletti A, Petrovic M, Barcelo D, Hospital effluent: investigation of the concentrations and distribution of pharmaceuticals and environmental risk assessment, *Science of the Total Environment* 430 (2012a) 109-118.

Verlicchi P and Zambello E, Predicted and measured concentrations of pharmaceuticals in hospital effluents. Examination of the strengths and weaknesses of the two approaches through the analysis of a case study, *Science of the Total Environment* 565 (2012b) 82-94.

Vieno N and Sillanpää M, Fate of diclofenac in municipal wastewater treatment plant – A review, *Environment International* 69 (2014) 28-39.

Walker JF (Ed.), Formaldehyde, *American Chemistry Society Monograph Series* (1964).

Wang A-J, Paterson T, Owen R, Sherborne C, Dugan Y, Li J-m, Claeysens F, Photocurable high internal phase emulsions (HIPEs) containing hydroxyapatite for additive manufacture of tissue engineering scaffolds with multi-scale porosity, *Materials Science and Engineering: C* 67 (2016) 51-58.

Wang J and Kaskel S, KOH activation of carbon-based materials for energy storage, *Journal of Materials Chemistry* 22 (2012) 23710 - 23725.

Wang J, He B, Yan D, Hu X, Implementing ecopharmacovigilance (EPV) from a pharmacy perspective: A focus on non-steroidal anti-inflammatory drugs, *Science of the Total Environment* 603-604 (2017a) 772-784.

Wang Q, Chen M, Shan G, Chen P, Cui S, Yi S, Zhu L, Bioaccumulation and biomagnification of emerging bisphenol analogues in aquatic organisms from Taihu lake, China, *Science of the Total Environment* 598 (2017b) 814-820.

Wang WQ, Ji L, Li HX, Zhou HD, Chen JM, Self-organized formation of nano-multilayer structure in the carbon-copper thin film during reactive magnetron sputtering deposition process, *Journal of Alloys and Compounds* 722 (2017) 242-249.

Washburn EW, Note on a method of determining the distribution of pore sizes in a porous material, *Proceedings of the National Academy of Sciences of the United States of America* 7 (1921) 115-116.

Watanabe N, Takemine S, Yamamoto K, Haga Y, Takata M, Residual organic fluorinated compounds from thermal treatment of PFOA, PFHxA, PFOS adsorbed onto granular activated carbon (GAC), *Journal of Material Cycles and Waste Management* 18 (2016) 625 – 630.

Weber WJ and Moris JC, Kinetics of adsorption on carbon from solution, *Journal of Sanitary Engineering Division of American Society of Civil Engineers* 89 (1963) 31-60.

Wei X, Gao N, Li C, Deng J, Zhu Y, Wang Q, Adsorption of bentazon on two kinds of granular activated carbons: equilibrium, kinetic and thermodynamic studies, *Desalination and Water Treatment* (2016) 1-14.

Westphalen APC, Corção G, Benetti AD, Use of biological activated carbon for drinking water treatment, *Water Resources* 21 (2016) 425 – 436.

West W, Carroll BH, Whitcomb DH, The adsorption of sensitizing dyes in photographic emulsions, *The Journal of Physical Chemistry* 56 (1952) 1054-1067.

Wielogorska E, Chevallier O, Black C, Galvin-King P, Delêtre M, Kelleher CT, Haughey SA, Elliott CT, Development of a comprehensive analytical platform for the detection and quantitation of food fraud using a biomarker approach. The oregano adulteration case study, *Food Chemistry* 239 (2017) 32-39.

Wilberts BL, Arruda PH, Warneke HL, Erlandson KR, Hammer JM, Burroughs ER, Cessation of clinical disease and spirochete shedding after tiamulin treatment in pigs experimentally infected with “*Brachyspira hampsonii*”, *Research in Veterinary Science* 97 (2014) 341-347.

Witthuhn B, Klauth P, Klumpp E, Narres HD, Martinius H, Sorption and biodegradation of 2,4-dichlorophenol in the presence of organoclays, *Applied Clay Science* 28 (2005) 55–66.

Witthuhn B, Klauth P, Pernyeszi T, Vereechen H, Klumpp E, Organoclays for aquifer bioremediation: Adsorption of chlorobenzene on organoclays and its degradation by *Rhodococcus* B528, *Water, Air & Soil Pollution* 6 (2006) 317–329.

Wu DJ, Li SJ, Wang N, Microwave regeneration of biological activated carbon, *Journal of Advanced Oxidation Technologies* 20 (2017a).

Wu L, Sui WB, Dong CH, Zhang C, Jiang CJ, One-dimensional BiFeO₃ nanotubes: Preparation, characterization, improved magnetic behaviors, and prospects, *Applied Surface Science* 384 (2017b) 368-375.

Wu S, Zhang L, Chen J, Paracetamol in the environment and its degradation by microorganisms, *Applied Microbiology and Biotechnology* 96 (2012) 875-884.

Xiao H, Song H, Xie H, Huang W, Tan J, Wu J, Transformation of acetaminophen using manganese dioxide – mediated oxidative processes: Reaction rates and pathways, *Journal of Hazardous Materials* 250-251 (2013) 138-146.

Yang L, Zhou Z, Xiao L, Wang X, Chemical and biological regeneration of HDTMA-modified montmorillonite after sorption with phenol, *Environmental Science Technology* 37 (2003) 5057–5061.

Yang S, Xiao T, Zhang J, Chen Y, Li L, Activated carbon fiber as heterogeneous catalyst of peroxydisulfate activation for efficient degradation of Acid Orange 7 in aqueous solution, *Separation and Purification Technology* 143 (2015) 19 – 26.

Yang Y, Ok YS, Kim K-H, Kwon EE, Tsang YF, Occurrences and removal of pharmaceuticals and personal care products (PPCPs) in drinking water and water/sewage treatment plants: A review, *Science of the Total Environment* 596-597 (2017) 303-320.

Yang ZY, Yi HH, Tang XL, Zhao SZ, Yu QJ, Gao FY, Zhou YS, Wang JG, Huang YH, Yang K, Shi YR, Potential demonstrations of “hot spots” presence by adsorption-desorption of toluene vapor onto granular activated carbon using microwave radiation, *Chemical Engineering Journal* 319 (2017) 191 – 199.

Yanzong Z, Jingtang Z, Xianfeng Q, Weizhao, Honggang C, Catalytic effect of activated carbon and activated carbon fiber in non-equilibrium plasma-based water treatment, *Plasma Science and Technology* 10 (2008) 358.

Yin YP, Chen HX, Kuang DL, Song LF, Wang L, Effect of chemical composition of aggregate on interfacial adhesion property between aggregate and asphalt, *Construction and Building Materials* 146 (2017) 231-237.

Yi YM, Weinberg G, Prenzel M, Greiner M, Heumann S, Becker S, Schlogl R, Electrochemical corrosion of a glassy carbon electrode, *Catalysis Today* 295 (2017) 32-40.

Yuan Y and Lee TR, Contact angle and wetting properties, in: Bracco G and Holst B (Eds.), *Surface Science and Techniques*, Springer (2013) 3-34.

Yu L and Luo M, The adsorption mechanism of anionic dyes by Jerusalem artichoke stalk-based mesoporous activated carbon, *Journal of Environmental Chemical Engineering* 2 (2014) 220-229.

Yu Q, Li M, Ji X, Qiu Y, Zhu Y, Leng C, Characterization and methanol adsorption of walnut-shell activated carbon prepared by KOH activation, *Journal of Wuhan University of Technology – Materials Science Edition* 31 (2016) 260-268.

Zanella O, Tessaro IC, Feris LA, Desorption- and decomposition-based techniques for the regeneration of activated carbon, *Chemical Engineering & Technology* 37 (2014) 1447 – 1459.

Zhang J and Zhang W, Preparation and characteristics of activated carbon from wood bark and its use for adsorption of Cu(II), *Materials Science* 20 (2014) 474-478.

Zhang SL, Tao LC, Zhang YL, Wang ZK, Gou GJ, Jiang M, Huang CP, Zhou ZW, The role and mechanism of K₂CO₃ and Fe₃O₄ in the preparation of magnetic peanut shell based activated carbon, *Powder Technology* 295 (2016) 152 – 160.

Zhang X, Shi YL, Wang ZQ, Duan JY, Jiang P, Liu RD, Cui J, Morphological and mitochondrial genomic characterization of eyeworms (*Thelazia callipaeda*) from clinical cases in Central China, *Frontiers in Microbiology* 8 (2017) 1-9.

Zhang Y, Geißen S-U, Gal C, Carbamazepine and diclofenac: Removal in wastewater treatment plants and occurrence in water bodies, *Chemosphere* 73 (2008) 1151-1161.

Zhao C, Danish E, Cameron NR, Katakya R, Emulsion-templated porous materials (PolyHIPEs) for selective ion and molecular recognition and transport: applications in electrochemical sensing, *Journal of Materials Chemistry* 23 (2007) 2446-2453.

Zhao HY, Lu XA, Wang Y, Sun B, Wu XH, Lu HF, Effects of additives on sucrose-derived activated carbon microspheres synthesized by hydrothermal carbonization, *Journal of Materials Science* 52 (2017) 10787-10799.

Zhou C, Gao NY, Li RY, Deng Y, Desorption of bisphenol-A (BPA) and regeneration of BPA-spent granular activated carbon using ultrasonic irradiation and organic solvent extraction, *Desalination and Water Treatment* 54 (2015) 3106 – 3113.

Zhou C, Zhu H, Wang Q, Wang JX, Cheng J, Guo YF, Zhou XJ, Bai RB, Adsorption of mercury(II) with an Fe₃O₄ magnetic polypyrrole-graphene oxide nanocomposite, *RSC Advances* 7 (2017) 18466-18479.

Zhou H, Smith DW, Advanced technologies in water and wastewater treatment, *Journal of Environmental Engineering* 1 (2002) 247-264.

Zuccato E, Calamari D, Natangelo M, Fanelli R, Presence of therapeutic drugs in the environment, *Lancet* 355 (2000) 1789–1790.

Zwiener C, Gremm TJ, Frimmel FH, Pharmaceutical residues in the aquatic environment and their significance for drinking water production, in: Kümmerer K (Ed.), *Pharmaceuticals in the Environment*, Springer (2001) 81-89.

Appendix A

Experimental procedures

A.1. Development of porous materials

A.1.1. Preparation of the apple tree branches biochar

This biochar was prepared in the University of Ljubljana, according to the following specifications.

Branches of approximately 10 cm long, previously dried for 24 h were placed horizontally in a pyrolysis oven (see **Figure A.1 (a, b)**). The oven was ignited using methanol (**Figure A.1(c)**) and, after approximately 30 min, when the branches were carbonized, the pyrolysis process was stopped. After cooling to room temperature the resulting biochar was grounded and sieved, and the fraction of particles with dimensions lower and higher than 200 μm were obtained.

The biochar will be designated by A, followed by the numbers 1 or 2, depending on whether the particle size is lower or higher than 100 μm .

The biochar fractions were used as precursors for the development of activated carbons, as detailed in the following topic.



Figure A.1. Preparation of the biochar – (a) Dry 10 cm long branches, (b) pyrolysis oven with branches placed horizontally, (c) pyrolysis process.

A.1.2. Preparation of wood biochar derived activated carbons by chemical activation

The general procedure for the preparation of the ACs studied in Chapter VII is schematized in **Figure A.2**. The methodology followed for the chemical activation of the apple tree branches biochar included homogenization, impregnation in solution, calcination, and washing steps.

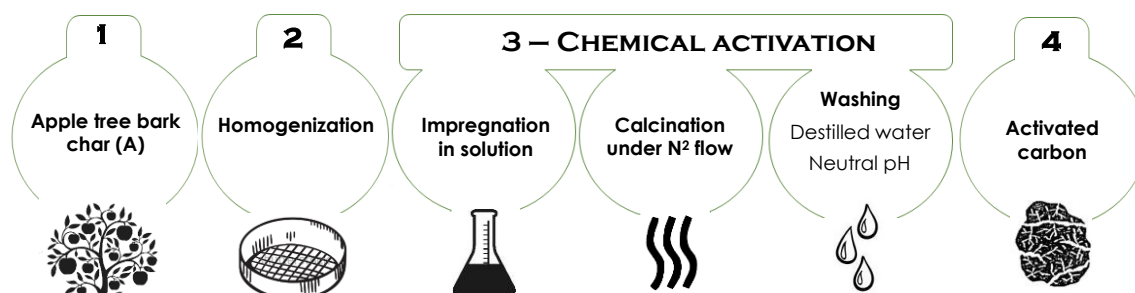


Figure A.2. Representation of the ACs preparation stages.

The biochar, with the desired particle size, was impregnated in solution with the activating agent by stirring for 17 h. The resulting mixture was dried in a ventilated oven at 60 °C. The dried material was placed in a ceramic boat and introduced in a horizontal furnace (Bansted-Thermolyne 21100, Controlador Eurotherm 2116). The activation was made under N_2 flow (5 $\text{cm}^3 \text{s}^{-1}$) with a heating rate of 10 °C min^{-1} until the desired activation temperature, which was maintained for a chosen period of time. After cooling to room temperature under N_2 flow, the carbon was removed from the furnace and washed exhaustively with distilled water until pH around 7.

Firstly, the impact of different preparation conditions on the global preparation yield of the carbons and on the carbon's volatile content was assessed. For this purpose, both A1 and A2 chars were used for the preparation of ACs, using K_2CO_3 (Aldrich, 99 %) and KOH (Panreac) as activating agents, in mass ratios of 1:1, 1:3 and 1:4. Activations at 700, 800 and 900 °C for 1 h to 4 h were made.

A set of operational conditions was chosen for the development of activated carbons for the purposes of characterization and liquid phase adsorption. The samples subjected to full characterization and adsorption experiments were all prepared with biochar A2 and, for this reason, no differentiation of the biochar size fraction will be made after optimization of the activation conditions debated in topic VII.2.1.

The activated carbons were designated following the expression: CA or HA (impregnation ratio/temperature of activation (°C)/ duration of activation (h)), where C and H stand for K_2CO_3 or KOH activation, respectively.

A.1.3. Preparation of the activated carbon cloth (ACC)

The activated carbon cloth, designated ACC, was prepared in Instituto Nacional de Pesquisas Espaciais, in Brazil, from polyacrilonytrile (PAN) textile fibers of 5.0 dtex, following the procedure described in Marcuzzo *et al.*, 2013. Briefly, the textile fibres were submitted to atmospheric thermal oxidation, in an oven that operates between the temperatures of 200 and 300 °C. Then, the oxidized PAN fibres were converted to the cloth form through a standard textile process. The resulting cloth was, at last, carbonized and consecutively activated in the same electric oven. Firstly, the material was carbonized under argon flow at 900 °C during 20 minutes. Afterwards, its activation was made by changing the argon atmosphere to carbon dioxide and by increasing the temperature to 1000 °C that was kept for 50 minutes.

The potential of this material as adsorbent in aqueous phase was assessed, as well as, its regeneration by cyclic thermal treatments (Chapter VIII). ACC performance in bacteria removal was also addressed in Chapter X.

A.1.4. Preparation of of tannin-based monoliths powders

To an aqueous solution of tannin (20 g of *Mimosa* bark tannin in 30 cm³ of distilled water), 0.7 g of *p*-toluenesulphonic acid (pTSA) and 6 drops of antifoam were added. The solution was mechanically stirred with a Teflon-lined blade mixer to ensure homogeneity, and then 1.15 g of surfactant Cremophor ELP was added to the emulsion and stirred again (750 rpm), resulting in a homogeneous brown solution. In a second step, 150 cm³ of sunflower oil were incorporated slowly into the mixture. When half of the oil volume was added, hexamine (1.9 g) was poured into the mixture. The emulsion was placed in sealed glass test tubes and placed in a ventilated oven at 70 °C for 24 h to complete crosslinking. After this time, the hardened blocks were let to cool down to room temperature, cut into cylinders and placed in a Soxhlet extractor for 7 days, during which the oil was thoroughly leached by refluxing acetone. The resulting monoliths were dried at room conditions. To increase the accessibility to the porosity the monoliths were ground and sieved, and the particle size fraction between 100 and 300 µm was chosen to proceed with the studies.

Sample 5AM was prepared treating sample 5M with hydrochloridric acid 0.1 mol dm⁻³ solution (Sigma-Aldrich). A volume of 30 cm³ of HCl was added to 150 mg of powder, and the suspension was stirred at 300 rpm, for 3 h, in a thermostated bath at 25 °C. The final material was washed exhaustively with distilled water until reaching neutral pH, and dried at 60 °C under vacuum (Heraeus-Vacutherm).

A.2. Characterization techniques

A.2.1. N₂ adsorption at -196 °C

The experiments were made using approximately 50 mg of sample, previously degassed at 120 °C for 17 h under vacuum better than 10^{-2} Pa. The assays were made in an automatic apparatus ASAP 2010 (Micromeritics) with the internal operating system illustrated in **Figure A.3**.

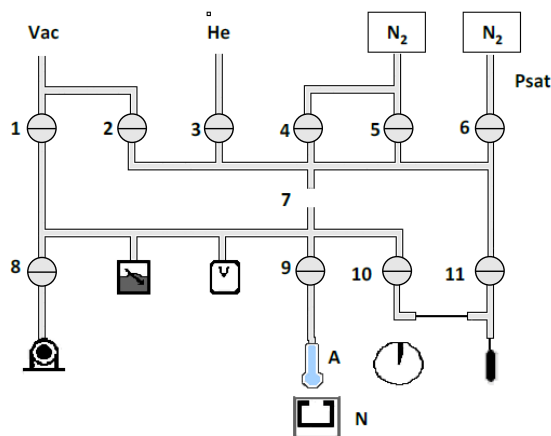


Figure A.3. Scheme of the automatic apparatus ASAP 2010. 1 to 11 - system valves, A – cell with sample, N – liquid nitrogen, Vac – vacuum, He – helium inlet, N₂ – nitrogen inlet, Psat – saturation pressure.

A.2.2. CO₂ adsorption at 0 °C

These experiments were performed using approximately 50 mg of sample, and degassing it at 120 °C for 17 h under vacuum better than 10^{-2} Pa. The CO₂ adsorption, at 0 °C, was done in a conventional volumetric installation where the vacuum was made using a rotatory pump, an oil diffuser pump and a vapour condenser of liquid nitrogen, designated “trap” (installation scheme presented in **Figure A.4**) to achieve a residual vacuum of approximately $1.33 \times 10^{-2} - 1.33 \times 10^{-3}$ Pa. The variations of pressure were measured by a sensor Baratron 310BHS-1000. During the isotherm acquisition, the sample was maintained at 0 °C, by immersion in a bath of ice and water.

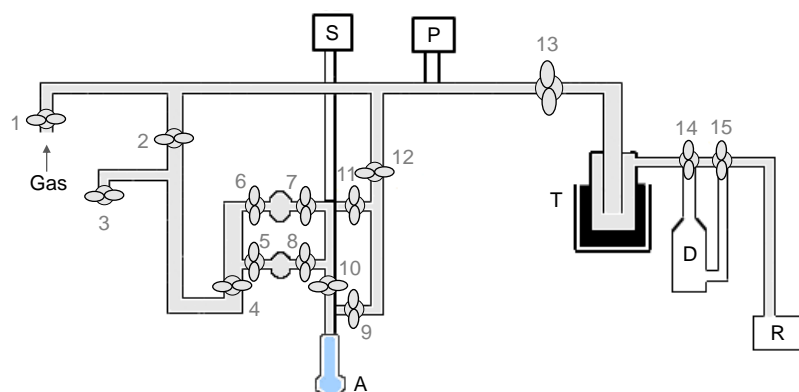


Figure A.4. Conventional volumetric installation used to perform the CO₂ adsorption experiments. A – cell with sample, 2-4 – non-lubricated valves, 1,5-15 – lubricated valves, S – Sensor Baratron, P – Manometer Pirani, T – vapours condenser (“trap”), D, R – diffusional and rotatory pumps.

CO₂ adsorption allowed to characterize the microporosity of the ACs studied in this thesis. The results were essential to deeply discuss the adsorption from aqueous phase results.

A.2.3. Water vapor adsorption at 20 °C

Water vapour adsorption-desorption isotherms were obtained by Research Director Vanessa Fierro, with an automatic adsorption apparatus (3Flex, Micromeritics). Prior to analysis, the samples were outgassed at 40 °C under secondary vacuum, for at least 72 h. The measurements were performed by dosing water vapour at relative pressures (p/p^0) ranging from 0.01 to 0.9 at 20 °C and measuring the water uptake at equilibrium for each value of p/p^0 . Once $p/p^0 = 0.9$ was reached, desorption was monitored, and the corresponding uptake volumes of water at equilibrium were measured in order to obtain the desorption branch of the isotherm. At least 60 points of water uptake vs relative pressure were recorded for each complete isotherm. The equilibrium times were quite long so that the entire process lasted for about ten days.

A.2.4. Mercury intrusion

Mercury intrusion experiments were carried out in order by laboratory chief technician Philippe Gadonneix. This methodology allowed to determine the pore diameters of the samples and the associated volumes, corresponding to pores wider than 3.7 nm. The previously weighted penetrometer (PEN 3CCPOW) was filled with enough powder sample to fill approximately 70 % of the cup volume, and weighted again. The sealed penetrometer was introduced in an AutoPore IV 9500 instrument (Micromeritics). Two-phase measurements were performed: mercury intrusion at low pressures, in the range 0.001 – 0.24 MPa, followed by an intrusion at high-pressure, between 0.24 and 414 MPa. The mass of the intruded sample obtained after the first measurement was considered as an initial value for the second intrusion experiment.

A.2.5. Scanning Electron Microscopy (SEM)

The morphology of the lab-made carbons and that of the activated carbon cloth were analysed by Scanning Electron Microscopy (SEM).

The SEM photographs of the lab-made samples, prepared from apple tree branches char (Chapter VI) were obtained in a field emission gas scanning electron microscope (JEOL mod. 7001F) with an X-ray energy-dispersive system (EDS), using an accelerating voltage of 25 kV.

In the case of sample ACC (Chapter VII) the analysis was performed in Instituto Nacional de Pesquisas Espaciais in Brazil, in an apparatus NovaNanoSEM400, with a 20 kV voltage accelerator.

A.2.6. X-ray Photoelectron Spectroscopy (XPS)

The experiment was carried out in Instituto Nacional de Pesquisas Espaciais, in Brazil, in a Kratos Axis Ultra XPS spectrometer using a monochromatic Al-K α (1486.5 eV) X-ray radiation. The emitted photoelectrons were detected using a hemispherical analyzer and 15 μ m spatial resolution. The vacuum system was maintained at approximately 10⁻⁷ Pa during all the experiments. Survey scans were collected from 0 to 1200 eV with 160 eV pass energy and step size of 1 eV, in order to identify the elements present on the surface of the materials, and a pass energy of 40 eV for high resolution scans on specific atomic peaks (280-300 eV and 525-543 eV). For calibration purposes C 1s band (284.6 eV) was taken as an internal standard. The deconvolution of the XPS spectra was made using Casa XPS software considering a non-linear least square fitting. Before deconvolution a Shirley type background subtraction was made.

This technique was employed to complement the chemical characterization of ACs surface in Chapter VIII.

A.2.7. X-ray Powder Diffraction (XRD)

X-ray powder diffracton (XRD) was performed in a Pan' Analytical PW3050/60X'Pert PRO ($\theta/2\theta$) equipped with X'Pert Data Collector detector software, using a monochromatized CuK α radiation as incident beam, 40 kV-30mA. The diffractograms were obtained at room temperature by continuous scanning in a 2θ range of 15-40° with a step size of 0.017° 2θ and a time per step of 20 s.

This technique was used for the analysis of GAC and NS activated carbons ashes in Chapter VIII.

A.2.8. pH at the point of zero charge (pH_{PZC})

The pH_{PZC} was determined following different procedures, for the different morphologies (powder, granular and cloth forms) of the activated carbons and for the tannin-based polymers. The general experimental protocols adopted are illustrated in **Figure A.5**.

The pH_{PZC} of the powder and granular activated carbons was determined in deionized water (Milli-Q water purification systems), by reverse mass titration, following the procedure described in the literature (Noh and Schwarz, 1989). Suspensions of 2, 4, 6, 8 and 10 % (m/m) were prepared, in sealed glass flasks, and pH measurements were made after 24 h of stirring, at room temperature. The deionized water was previously aired with nitrogen to eliminate any CO₂ present, and the pH measurements were made with a semi-micro electrode of epoxide resin (Symphony, modelo SP70P). The pH_{PZC} of the activated carbons correspond to the pH values of the linear plateau of the graphic of the final *versus* the initial pH values.

The pH_{PZC} of the activated carbon ACC was determined following the procedure reported by Babić *et al.* 1999. Solutions of KNO₃ (0.01 mol dm⁻³), with initial pH ranging from 2 to 12 were prepared mixing different volumes of KOH and HNO₃ (0.1 mol dm⁻³) solutions. A volume of 10 cm³ of solution, was added to 50 mg of ACC, in different vials, that were sealed under N₂ and stirred for 24 h at room temperature. The pH_{PZC} of ACC corresponds to the pH value of the linear plateau of the graphic of the final *versus* the initial pH values. In all cases, the pH measurements were made with a Symphony SP70P pH meter.

To determine the pH_{PZC} of the tannin-based polymers, the experimental procedure was quite similar to that used in the case of ACC but some changes needed to be introduced. Briefly, solutions of NaNO₃ (0.1 mol dm⁻³), with initial pH 2, 6 and 10 were prepared mixing different volumes of NaOH and HNO₃ (0.1 mol dm⁻³) solutions. A volume of 10 cm³ of each of the solutions, was added to 50 mg of solid, in different vials, that were sealed under N₂ and stirred for 24 h. The pH measurements were made with a Symphony SP70P pH meter and the pH_{PZC} of these materials corresponds to the pH value of the linear plateau of the graphic of the final *versus* the initial pH values

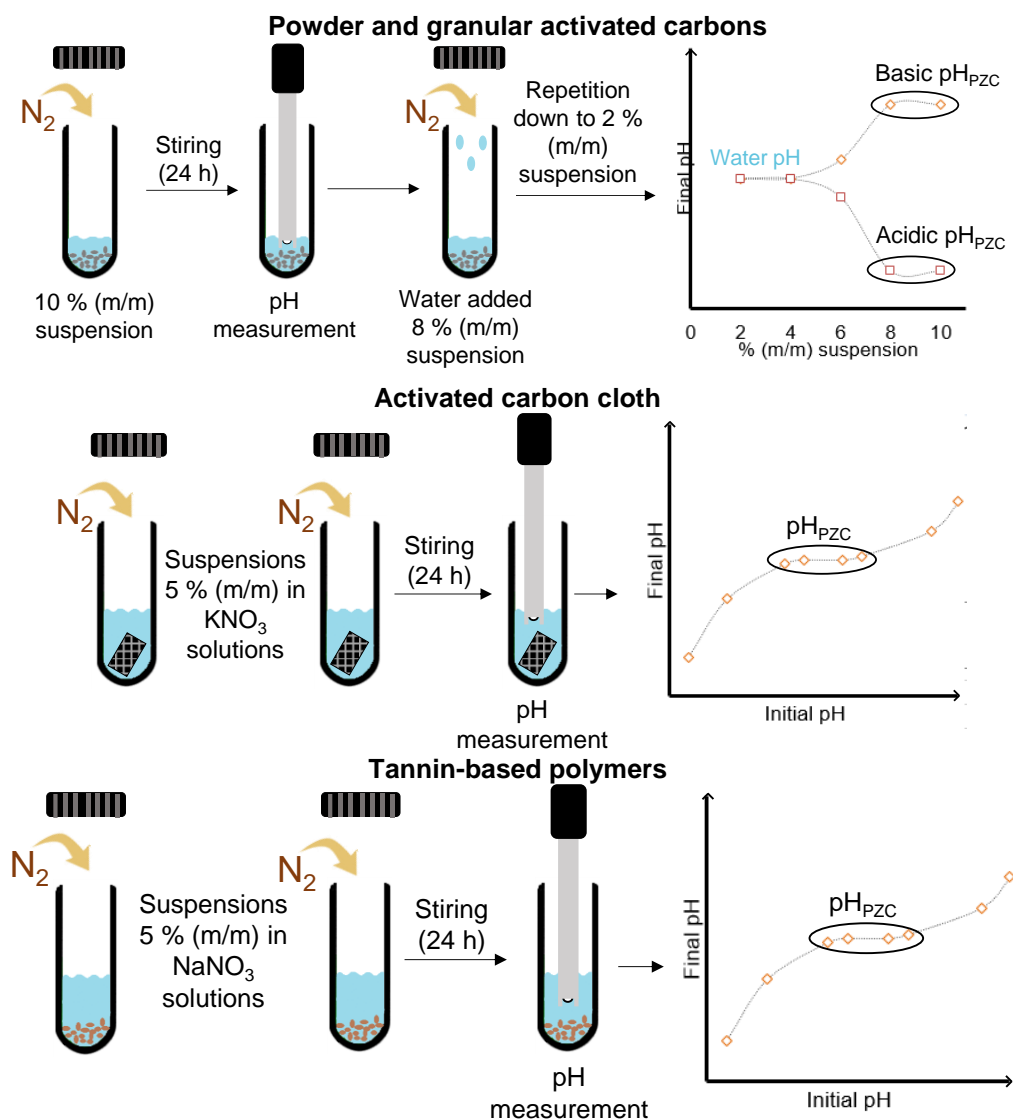


Figure A.5. Schematic representation of pH_{PZC} measurement procedure adopted in this PhD thesis.

A.2.9. Contact angle measurements

Samples hydrophilicity was determined by contact angle measurements by sessile drop method, which consists in using a liquid-solid contact angle analyser (DSA100, Krüss). The experiments consisted in placing 2 μ L droplets of water at the surface of the previously dried samples, in the pellet form, with an automatic drop deposition system. The contact angles were measured using the Krüss software from the droplet images, captured with a digital camera. The measurements were performed on different pellets of each sample and repeated at least ten times. The obtained data were averaged, and the corresponding standard deviation was assessed.

The measurements were carried out by PhD student Clara Delgado-Sanchez.

A.2.10. Phenolic groups content determination

The total content in phenolic groups was determined using the Folin-Ciocalteu method (Singleton and Rossi, 1965) which is based on the oxidation of the phenolic group and reduction of the Folin-Ciocalteu reagent, which consists in a mixture of phosphomolybdate and phosphotungstate, to form a blue chromophore. The concentration of the chromophore in solution after contact with the polymers corresponds to the amount of phenolic groups present at the surface of the solids. The calibration plot

was performed considering tannic acid in representation of the phenolic analyte. The analysis was performed in duplicate by stirring, at 300 rpm, 10 and 20 mg of powder with a solution consisting 2.5 cm³ of the Folin-Ciocalteu reagent, 12.5 cm³ of the sodium carbonate solution and 5 cm³ of distilled water, for 6 h, at room temperature. Absorbance measurements were made at 642 nm and the phenolic content was determined, taking into account a calibration plot previously performed (see **Table A.1**).

Table A.1. Experimental conditions used for the calibration plot of tannic acid.

Tube	Tannic acid solution (0.1 mg dm ⁻³) (cm ³)	Distilled water (cm ³)	Folin-Ciocalteu reagent (cm ³)	Sodium carbonate solution (cm ³)
Blank	0.0	5.0		
T1	0.2	4.8		
T2	0.4	4.6		
T3	0.6	4.4	2.5	12.5
T4	0.8	4.2		
T5	1.0	4.0		
T6	1.2	3.8		

The phenolic groups content was expressed in terms g of equivalents of tannic acid (ETA) per 100 g of sample.

A.2.11. Elemental analysis

Elemental analysis of the tannin-based powders was carried out by laboratory chief technician Philippe Gadonneix, during the intership in University of Lorraine, with a CHONS elemental analyser (Vario EL cube, Elementar) to determine carbon, hydrogen, nitrogen and sulphur contents by combustion of the samples at around 1700 °C in a mixed stream of oxygen and helium, the latter being used as a carrier gas. Oxygen content was quantified by the difference.

A.2.12. Determination of volatile matter content

The volatile matter content is defined by the mass loss of the sample (disregarding the mass loss associated to moisture) when heated under inert atmosphere and well defined heating rate, final temperature and total duration of treatment.

The volatile content measurements were made according to recommendations described in the Derivative D 5832 – 98. Approximately 100 mg of sample, previously dried at 100 °C overnight, in a ceramic boat, was introduced in a horizontal furnace (Thermolyne mod. 21100). The sample was heated, under N₂ flow (10 cm³ s⁻¹), with a heating rate of 15 °C min⁻¹, up to 900 °C and kept at that temperature for 10 min. Considering the mass loss due to the heating regime, the volatile content was calculated.

A.2.13. Determination of ash content

The determination of ash content was made considering the mass of the residue obtained after combustion of the samples under atmospheric air, according to the international norm D 2866 – 94.

Approximately 1 g of samples was placed in a quartz boat and the material was dried in a ventilated oven at 100 °C (Heraeus Instruments, T 6060). The carbon was weighted and the moisture content determined (CEFIC, 1987). Then, the quartz boat with the dried sample was introduced in a tubular furnace and submitted to the heating regime shown in **Figure A.6**, under air atmosphere. The final mass of the material was weighted and the ash content determined. In these assays an analytic balance (Mettler, AE 240), with

a precision of 0.01 mg, and a tubular furnace with a controller Eurotherm 2416 were used.

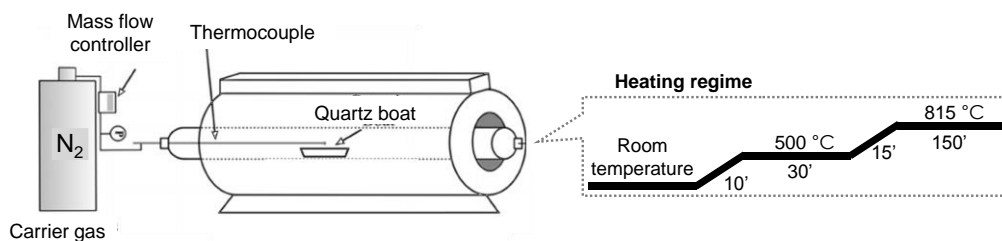


Figure A.6. Heating regime for ash content determination.

A.2.14. Density measurements

Apparent and absolute density measurements were performed by laboratory chief technician Philippe Gadonneix, following the recommendations reported in Conseil Européen des Fédérations de L'Industrie Chimique, in 1986.

The apparent density of the lab-made activated carbons (Chapter VII) was determined as the carbons' mass of a unit volume (1 cm^3). The practical determinations were made filling a volume of 1 cm^3 of a 5 cm^3 measuring cylinder (previously weighted) with dried sample. Consecutive tapping was made and cylinder+sample was weighted. The procedure was repeated at least three times, and a mean density value was obtained.

The absolute (or skeletal) density, ρ_s , of the tannin-based powders (Chapter X) was determined with a helium pycnometer (Accupyc II 1340, Micromeritics) by finely crushing the samples to avoid errors relating to possibly closed porosity, and all the materials were previously dried in vacuum at $85 \text{ }^\circ\text{C}$.

A.2.15. Fourier transform infrared spectroscopy (FTIR)

FTIR spectroscopy studies of pristine and saturated tannin-based powders were carried out with a Brücker Equinox 55 spectrometer by dispersing and pressing approximately 1 mg of the samples grounded. The resulting pellets were analysed in transmission mode from 650 to 4000 cm^{-1} (20 scans at a resolution of 4 cm^{-1}). FTIR spectra was obtained for all the pristine samples, as well as, the saturated powders obtained in the screening experiments.

A.2.16. Thermogravimetric analysis (TGA)

Thermogravimetric analysis was performed to evaluate the thermal stability of several materials (activated carbons and tannin-based polymers), and to assess pollutants thermal degradation (atenolol and paracetamol) for purposes of desorption and regeneration experiments (atenolol and paracetamol-exhausted activated carbons).

Thermogravimetric studies of atenolol desorption and decomposition were performed using $\sim 50 \text{ mg}$ of the sample and a NETZSCH STA 449 F3 set-up with a microbalance having a sensitivity of $\pm 0.1 \text{ g}$ coupled with QMS 403 C system. The experiments were conducted in a constant Ar flow ($50 \text{ cm}^3 \text{ min}^{-1}$) with heating rates, β , of 5, 10 and $20 \text{ }^\circ\text{C min}^{-1}$ up to $900 \text{ }^\circ\text{C}$. Regarding the thermogravimetry analysis performed on paracetamol and paracetamol-exhausted activated carbons (Chapter VII), the experiments were carried out in Instituto Nacional del Carbón (INCAR, Oviedo), on a Setaram Labsys apparatus, under N_2 flow ($30 \text{ cm}^3 \text{ min}^{-1}$) and at a heating rate of $15 \text{ }^\circ\text{C min}^{-1}$ up to $900 \text{ }^\circ\text{C}$. Analysis of the raw carbons was also made in the same experimental conditions. The thermal stability of tannin-based polymers was carried out in a NETZSCH STA 449F3 instrument. The samples were heated from 25 to $800 \text{ }^\circ\text{C}$, in a flow of pure argon at a heating rate of $10 \text{ }^\circ\text{C min}^{-1}$.

A.2.17. Cyclic thermal regeneration treatments

Regeneration assays were performed on paracetamol-exhausted samples obtained by contact with the paracetamol solution (180 mg dm⁻³) using the proportion of approximately 6 mg of carbon/30 cm³ of solution. After equilibrium, the solids were recovered by filtration and dried at 100 °C for 24 h. To perform the thermal regeneration, the samples were placed in a ceramic boat and heated in a horizontal furnace (Thermolyne, model 21100) at 400 and 600 °C for 1 h, under N₂ flow of 5 cm³ s⁻¹ (heating rate of 10 °C min⁻¹). After cool down to room temperature the samples were weighted and re-exhausted using the experimental conditions above mentioned.

The efficiency of each regeneration cycle was quantified by the regeneration efficiency, $RE(\%)$, defined as

$$RE(\%) = \frac{q_i}{q_0} \times 100 \quad \text{Equation A.1}$$

where q_i is the adsorption capacity of the regenerated carbon in a given i^{th} re-use cycle, and q_0 the adsorption capacity of the fresh carbon.

A.3. Liquid phase experiments

A.3.1. Pollutants studied

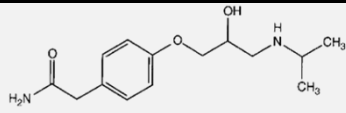
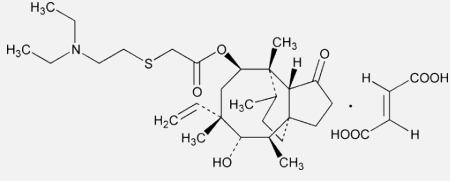
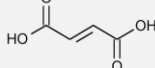
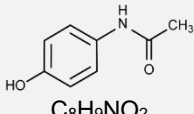
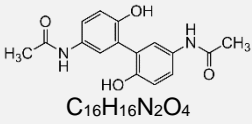
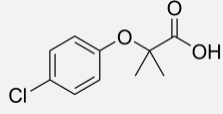
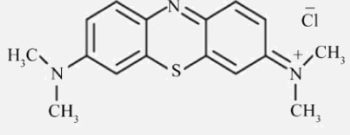
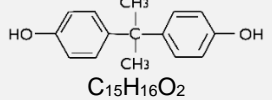
The target compounds tested during the development of this thesis are presented in **Table A.2**, along with their abbreviations, reagent brand, solution preparation and pH information.

Table A.2. Compounds studied, their abbreviation, reagents brand, solution preparation information and solution pH.

Compound (abbreviation)	Reagent	Solution preparation	Solution pH
Atenolol (AT)	Generis		8.2
Tiamulin hydrogen fumarate (THF)	TOKU-E Company		
Fumaric acid (FA)	Sigma-Aldrich		-
Paracetamol (PARA)	Sigma-Aldrich Lot 535764-326	Dissolved in distilled water	5.8
Clofibric acid (CLOF)	Alfa Aesar GmbH & Co., KG Lot G1266B		
Methylene blue (MB)	Fischer Scientific		-
Bisphenol A (BPA)	Sigma-Aldrich CAS 80-05-7	Dissolved in NaOH (VWR Chemicals, CAS. 1310-73-2) and prefaced with distilled water. pH adjusted with HCl (Sigma-Aldrich Lot. 5ZB60070V)	2.4
Diclofenac sodium salt (DCF)	Sigma-Aldrich CAS 15307-79-6		5.5
Ibuprofen sodium salt (IBU)	Sigma-Aldrich CAS. 31121-93-4	Dissolved in distilled water	5.9
Atorvastatin calcium salt (ATORV)	Sigma-Aldrich CAS. 344423-98-9	Aqueous solution with 20 % (wt/wt) of ethanol (Carlo Erba Reagents 96 °C)	5.6
Tetracycline hydrochloride (TC)		Dissolved in aqueous solution with 1% of HCl (Sigma-Aldrich Lot. 5ZB60070V)	2.2
Ranitidine (RAN)	Sigma-Aldrich		6.1
Caffeine (CAF)	Normapur	Dissolved in distilled water	5.2

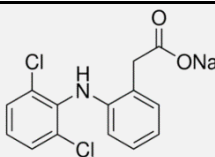
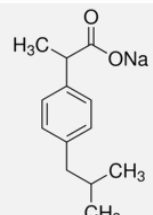
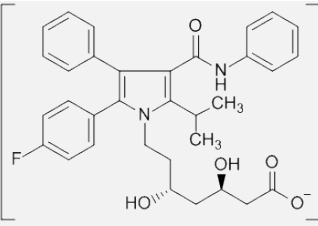
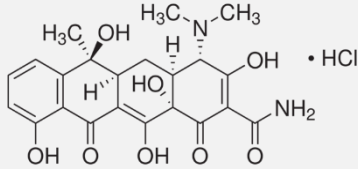
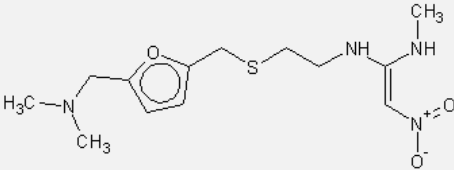
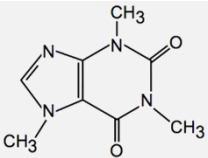
The molecular properties of the studied pollutants are presented in **Table A.3**, together with the molar volume.

Table A.3. Chemical properties of the pharmaceutical compounds studied.

Compound	Properties				
	Structure/Formula	Dimensions	Molecular weight (g mol ⁻¹)	pKa	Molar volume (cm ³ mol ⁻¹)
AT	 C ₁₄ H ₂₂ N ₂ O ₃	0.7 nm (length) 1.8 nm (width) 0.7 nm (thickness)	266.3	9.6 ^a	237 ^b
THF	 C ₃₂ H ₅₁ NO ₈ S	Tiamulin 1.2 nm (length) 1.9 nm (width) 1.2 nm (thickness)	609.8	9.6 ^c	447 ^d
FA	 C ₄ H ₄ O ₄	-	116.1	3.6 ^e	77.4 ^f
PARA	Monomer  C ₈ H ₉ NO ₂	0.75 nm (width) ^g 1.19 nm (length) 0.46 nm (thickness)	151.2	9.9 ^h	121 ⁱ
	Dimer  C ₁₆ H ₁₆ N ₂ O ₄	1.19 nm (width) ^g 1.58 nm (length) 0.66 nm (thickness)	300.3		-
CLOF	 C ₁₀ H ₁₁ ClO ₃	1.22 nm (length) 0.72 nm (width) 0.70 nm (thickness)	214.6	3.5 ^j	-
MB	 C ₁₆ H ₁₈ ClN ₃ S	-	373.9	3.8 ^k	-
BPA	 C ₁₅ H ₁₆ O ₂	0.80 nm (width) 1.29 nm (length) 1.24 nm (thickness)	228.3	9.7 ^l	200 ^m

a - Martínez *et al.*, 2000; b - <http://www.chemspider.com/Chemical-Structure.2162.html>; c - Meimaroglou *et al.*, 2015; d, e, f, i, m - <https://comptox.epa.gov/dashboard/>; g - Galhetas *et al.*, 2014; h - Garcia-Ivers *et al.*, 2017; j - Gao and Deshusses, 2011; k - Kim *et al.*, 2013; l - Sambe *et al.*, 2006.

Table A.3. (continued) Chemical properties of the pharmaceutical compounds studied.

Compound	Properties				Molar volume (cm ³ mol ⁻¹)
	Structure/Formula	Dimensions	Molecular weight (g mol ⁻¹)	pKa	
DCF	 C ₁₄ H ₁₀ Cl ₂ NNaO ₂	-	318.1	4.2 ^h	207 ⁿ
IBP	 C ₁₃ H ₁₇ O ₂ Na	0.72 nm (width) ^o 1.32 nm (length) 0.77 nm (thickness)	228.3	4.9 ^h	200 ^p
ATORV	 (C ₃₃ H ₃₄ FN ₂ O ₅) ₂ Ca	-	1155.4	4.5 ^q	452 ^r
TC	 C ₂₂ H ₂₄ N ₂ O ₈ ·HCl	1.00 nm (width) 1.60 nm (length) 1.00 nm (thickness)	480.9	3.3 ^s 7.8 9.6	270 ^t
RAN	 C ₁₃ H ₂₂ N ₄ O ₃ S	-	314.4	2.2 ^u	265 ^v
CAF	 C ₈ H ₁₀ N ₄ O ₂	0.85 nm (width) ^w 1.06 nm (length) 0.45 nm (thickness)	194.2	10.4 ^g	133 ^x

n, p, r, t, v, x - <https://comptox.epa.gov/dashboard/>; o – Mestre *et al.*, 2007; q – Wu *et al.*, 2000 ; s – Chico *et al.*, 2012; u – Roat *et al.*, 1997 ; w – Batista *et al.*, 2016

A.3.2. Aqueous phase adsorption

The adsorption experiments were performed following the procedure illustrated in **Figure A.7**. The pollutant solution was added to the carbon previously dried overnight at 100 °C (Heraeus Instruments, T 6060). A magnetic stirrer was introduced and the sealed flasks were placed in a thermostatic bath (Eurotherm 2216L) at 30 °C, stirring at 700 rpm (Variomag Multipoint).

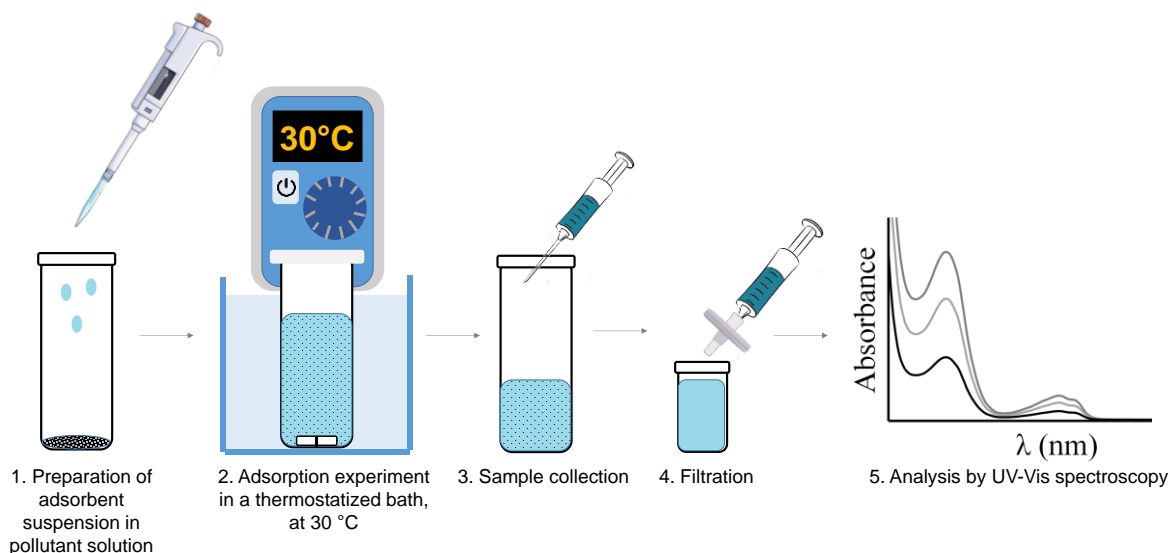


Figure A.7. Representation of the experimental procedure adopted for liquid phase adsorption experiments.

Samples were collected after different contact times, filtrated with a 0.45 μm nylon filter, and analysed by UV-Vis spectrophotometry (Genesys 10S UV-vis Thermo-Scientific), in quartz cells with 5 mm of width. Resorting to the calibration plots, previously made, the remaining concentration of solute was determined and, from this, the amount of adsorbed pollutant was determined, using the following equation:

$$q_t = \frac{(C_0 - C_t)V}{W} \quad \text{Equation A.2}$$

where q_t is the amount of pollutant (mg g^{-1}) adsorbed at time t , C_0 the initial pollutant concentration (mg dm^{-3}), C_t the pollutant concentration at time t , V the volume (dm^3) of solution and W the weight of dried carbon (g).

Blank experiments were performed to ensure that no retention of the pollutants occurred in the laboratory material used (glass vials, magnetic stirrer and filters). All data presented was obtained, at least, in triplicate.

The kinetic experiments were performed by adding 20 cm^3 of pollutant solution, of concentration 120 mg dm^{-3} , to 6 mg of carbon. Samples were collected after different contact times, ranging from 5 min to 24 h, to ensure adsorption equilibrium was reached.

Equilibrium adsorption studies were performed varying the adsorbent dose (around 3-6 mg), solution volume (9-30 cm^3) and adsorbate initial concentration (20-180 mg dm^{-3}). After stirring overnight, the concentration of adsorbate that remained in solution at equilibrium (C_e) was determined, and the uptake was calculated.

The concentration of pollutant remaining in solution was calculated considering the absorbance detected at the compounds maximum absorbance peaks, presented in the following table.

Table A.4. Wavelengths used for the quantification of the mentioned compounds by UV-Vis spectroscopy.

Compound	λ (nm)	Compound	λ (nm)	Compound	λ (nm)	Compound	λ (nm)
AT	224	THF	208	FA	208	PARA	243
CLOF	228	MB	664	BPA	226	DCF	276
IBP	226	ATORV	242	TC	218	RAN	313

A.3.3. Bacteria immobilization assays

A.3.3.1. Strain and culture conditions

The microorganism studied was *E. coli* K12 MG1655, propagated in Lysogeny Broth (LB) medium at 37 °C, overnight and then harvested by centrifugation at 4 °C and 4000 rpm. The cells were washed three times with sterile distilled (STD) water and re-suspended in 20 cm³ of STD water. The cellular suspensions were standardized at approximately 8, 6 and 5 log cells cm⁻³, by UV-Vis spectrophotometry (JascoV560). The absorbance measurements were performed in 1 cm path length plastic cells, at the wavelength of 625 nm. All microbiological procedures were performed in Biohazard class II cabinets.

A.3.3.2. Immobilization of *E. coli* onto the carbon materials

The assays were performed by dispersing the materials in the cellular suspension, in sterilized falcons (see representation in **Figure A.8**). The falcons were sealed, to insure no contact with atmospheric air and maintained stirring horizontally at 200 rpm, in an oven with ventilation at 30 °C.

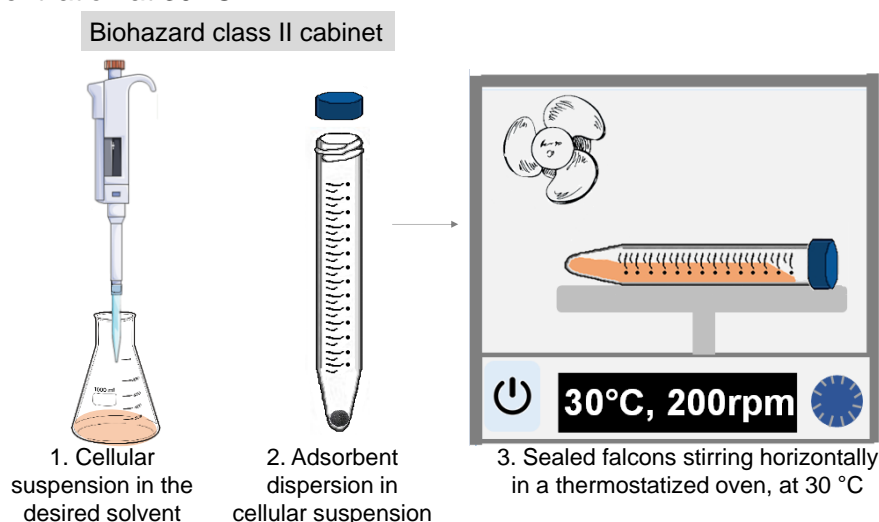


Figure A.8. Representation of the experimental procedure adopted for the bacteria immobilization experiments.

The cellular suspensions were prepared in sterilized (STD) water, NaCl 0.9 % (wt./wt.) solution, PBS phosphate buffer, and caffeine solution.

NaCl 0.9 % (wt./wt.) solution was prepared by dissolving 9 g of NaCl (Ducheja Lt. 007551.06) in 1 dm³ of sterilized water. PBS buffer was obtained by diluting 1.09 g of anhydrous di-sodium hydrogen phosphate (Merck), 0.32 g of sodium di-hydrogen phosphate (Merck), and 9 g of NaCl (Ducheja Lt. 007551.06). Caffeine solutions were also prepared with initial concentrations of 180 mg dm⁻³ (Normapur).

A.3.3.3. Quantification of *E. coli* and caffeine

The number of *E. coli* viable cells (colony-forming units – CFU) present after contact with the carbon material was quantified by serial dilution plating method (see **Figure A.9**). Briefly, an aliquot of final cells suspension was successively diluted with STD water, from 10⁻¹ to 10⁻⁸ cells cm⁻³. A volume of 10 µL of each dilution was inoculated in LB medium supplemented with 1.5 % of Agar and incubated overnight at 37 °C, after what the number of colonies formed was counted. For the calculation of cellular concentration,

the number of bacteria colonies was considered when its value ranged between 3 and 30 colonies *per* dilution.

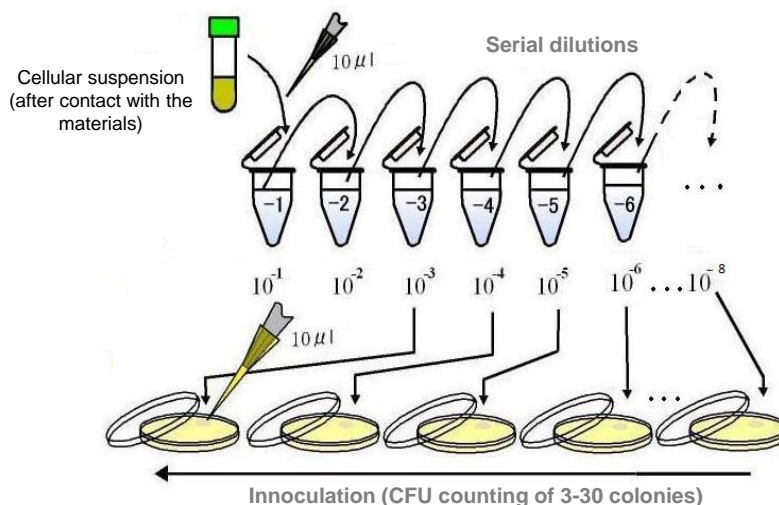


Figure A.9. Representation of the experimental procedure adopted for the quantification of the cell concentration remaining in solution.

From the number of cells remaining in solution, the removal rates (%) of each carbon were calculated, according to the following expression:

$$\text{Removal rate (\%)} = \frac{\log(C_0) - \log(C_t)}{\log(C_0)} \quad \text{Equation A.4}$$

where C_0 is the cellular initial concentration (cells cm^{-3}) and C_t is the cellular concentration at time t (cells cm^{-3}).

Control of cells viability was performed monitoring the suspension of the cells in the solvents used. To discard any possible contamination arising from the adsorbents, the carbons were stirred with the sterile solvents under the experimental conditions used in *E. coli* assays. No bacterial colonies were detected in the liquid phase recovered.

When the immobilization assays were performed in a caffeine solution instead of distilled water, to quantify the amount of caffeine, the final samples were filtrated with a $0.45 \mu\text{m}$ nylon filter. The concentration of caffeine remaining in solution was determined by UV-Vis spectrophotometry at its maximum absorbance wavelength of 273 nm. The adsorbate uptake was calculated according to equation A.2.

A.3.3.4. Optical and phase-contrast microscopy

The carbon NS dispersion in aqueous solution, cell-carbon, and cell-cell interactions were analysed by optical and phase-contrast microscopy (Leica) in cellular suspensions of $8 \log$ cells per cm^3 , using amplifications of 1000 x (optical) and 40, 400 and 1000x (phase-contrast). During this experiment, the immobilization of *E. coli* on NS carbon was recorded in the optical microscope using an amplification of 1000 x.

A.4. Appendix A references

Batista MKS, Mestre AS, Matos I, Fonseca IM, Carvalho AP, Biodiesel production waste as promising biomass precursor of reusable activated carbons for caffeine removal, *RSC Advances* 51 (2016) 1-34.

Chico J, van Holthoon F, Zuidema T, Ion suppression study for tetracyclines in feed, *Chromatography Research International* 2012 (2012) 1-9.

Conseil Européen des Fédérations de l'Industrie Chimique, Test methods for activated carbon (1986).

Gao Y and Deshusses MA, Adsorption of clofibrac acid and ketoprofen onto powdered activated carbon: Effect of natural organic matter, *Environmental Technology* 32 (2011) 1719-1727.

Galhetas M, Mestre AS, Pinto ML, Gulyurtlu I, Lopes H, Carvalho AP, Carbon-based materials prepared from pine gasification residues for acetaminophen adsorption, *Chemical Engineering Journal* 240 (2014) 344-351.

Garcia-Ivars J, Durá-María J, Moscardó-Carreño C, Carbonell-Alcaina C, Alcaina-Miranda M-I, Iborra-Clar M-I, Rejection of trace pharmaceutically active compounds present in municipal wastewaters using ceramic fine ultrafiltration membranes: Effect of feed solution pH and fouling phenomena, *Separation and Purification Technology* 175 (2017) 58–71.

Kim JR, Santiano B, Kim H, Kan E, Heterogeneous oxidation of methylene blue with surface-modified iron-amended activated carbon, *American Journal of Analytical Chemistry* 4 (2013) 115-122.

Martínez V, Maguregui MI, Jiménez RM, Alonso RM, Determination of the pKa values of β -blockers by automated potentiometric titrations, *Journal of Pharmaceutical and Biomedical Analysis* 23 (2000) 459-468.

Meimaroglou S, Vonaparti A, Migias G, Gennimata D, Poulou S, Panderi I, Direct injection human plasma analysis for the quantification of antihypertensive drugs for therapeutic drug monitoring using hydrophilic interaction liquid chromatography/electrospray ionization mass spectrometry, *Journal of Chromatography B* 1004 (2015) 1–9.

Mestre AS, Pires J, Nogueira JMF, Carvalho AP, Activated carbons for the adsorption of ibuprofen, *Carbon* 45 (2007) 1979–1988.

Roat RM, Jerardi MJ, Kopay CB, Heath DC, Clark JA, DeMars JA, Weaver JM, Bezemer E, Reedijk J, Platinum(II) complexes catalyze reactions between platinum(IV) complexes and 9-methylxanthine, *Journal of the Chemical Society, Dalton Transactions* (1997) 3615-3621.

Sambe H, Hoshina K, Hosoya K, Haginaka J, Simultaneous determination of bisphenol A and its halogenated derivatives in river water by combination of isotope imprinting and liquid chromatography–mass spectrometry, *Journal of Chromatography A*, 1134 (2006) 16–23.

Wu X, Whitfield LR, Stewart BH, Atorvastatin transport in the Caco-2 cell model: Contributions of p-glycoprotein and the proton-monocarboxylic Acid co-transporter, *Pharmaceutical Research* 17 (2000) 209-215.

Appendix B

Experimental results

B.1. N₂ adsorption at -196 °C**Table B.1.** N₂ adsorption and desorption data, at– 196 °C, of carbon CA(1:3/700/2).

Adsorption				Desorption	
p/p^0	n^{ads} (mmol g ⁻¹)	p/p^0	n^{ads} (mmol g ⁻¹)	p/p^0	n^{ads} (mmol g ⁻¹)
0.00000	6.661	0.10215	13.037	0.93231	13.538
0.00008	8.875	0.12708	13.111	0.83174	13.501
0.00166	10.983	0.15173	13.168	0.68081	13.509
0.00195	11.080	0.20076	13.249	0.53064	13.516
0.00246	11.214	0.25108	13.307	0.39180	13.435
0.00290	11.306	0.30128	13.348	0.29927	13.383
0.00344	11.403	0.35015	13.377	0.20029	13.283
0.00401	11.489	0.40019	13.398		
0.00501	11.617	0.50032	13.417		
0.00740	11.832	0.61935	13.429		
0.00985	11.989	0.71931	13.435		
0.01974	12.348	0.81915	13.442		
0.02887	12.531	0.91860	13.480		
0.03902	12.666	0.95006	13.528		
0.04982	12.769	0.97506	13.605		
0.07518	12.927				

Table B.2. N₂ adsorption and desorption data, at– 196 °C, of carbon CA(1:3/800/1).

Adsorption				Desorption	
p/p^0	n^{ads} (mmol g ⁻¹)	p/p^0	n^{ads} (mmol g ⁻¹)	p/p^0	n^{ads} (mmol g ⁻¹)
0.00000	8.874	0.10358	14.310	0.93281	15.129
0.00091	11.041	0.12731	14.419	0.83220	15.078
0.00198	11.563	0.15328	14.510	0.68144	15.059
0.00247	11.714	0.20106	14.633	0.53139	15.033
0.00296	11.843	0.25177	14.726	0.40170	14.920
0.00339	11.937	0.30217	14.795	0.29917	14.822
0.00391	12.036	0.35169	14.846	0.20018	14.663
0.00504	12.217	0.40020	14.884		
0.00721	12.476	0.50033	14.933		
0.00998	12.714	0.60002	14.969		
0.02021	13.241	0.70024	14.995		
0.02856	13.494	0.80013	15.017		
0.03847	13.704	0.89987	15.059		
0.04968	13.875	0.94988	15.118		
0.07505	14.129	0.97491	15.206		

Table B.3. N₂ adsorption and desorption data, at– 196 °C, of carbon CA(1:3/800/2).

Adsorption				Desorption	
p/p^0	n^{ads} (mmol g ⁻¹)	p/p^0	n^{ads} (mmol g ⁻¹)	p/p^0	n^{ads} (mmol g ⁻¹)
0.00000	8.868	0.1011	17.171	0.9337	19.506
0.00049	11.085	0.1274	17.491	0.8342	19.315
0.00079	11.514	0.1536	17.737	0.6831	19.180
0.00195	12.383	0.2029	18.074	0.5326	19.064
0.00246	12.611	0.2549	18.324	0.4033	18.794
0.00292	12.766	0.3061	18.504	0.2983	18.525
0.00339	12.917	0.3504	18.626	0.2008	18.107
0.00407	13.101	0.4008	18.735		
0.00497	13.304	0.5013	18.889		
0.00774	13.772	0.6010	19.001		
0.00974	14.026	0.7013	19.092		
0.02020	14.902	0.7998	19.186		
0.02871	15.368	0.8996	19.324		
0.03841	15.774	0.9495	19.478		
0.0497	16.146	0.9750	19.650		
0.0754	16.749				

Table B.4. N₂ adsorption and desorption data, at– 196 °C, of carbon CA(1:3/800/3).

Adsorption				Desorption	
p/p^0	n^{ads} (mmol g ⁻¹)	p/p^0	n^{ads} (mmol g ⁻¹)	p/p^0	n^{ads} (mmol g ⁻¹)
0.00001	8.869	0.07460	21.242	0.93601	25.784
0.00012	11.078	0.09926	21.903	0.83382	25.631
0.00051	13.274	0.12736	22.486	0.68274	25.506
0.00079	13.967	0.15351	22.921	0.53328	25.363
0.00195	15.228	0.20450	23.559	0.40564	24.909
0.00241	15.505	0.25843	24.050	0.29963	24.382
0.00289	15.747	0.31080	24.406	0.20444	23.600
0.00335	15.947	0.35869	24.657		
0.00389	16.148	0.39980	24.828		
0.00485	16.450	0.50055	25.116		
0.00728	17.016	0.59980	25.293		
0.00980	17.449	0.69936	25.410		
0.02003	18.592	0.79947	25.509		
0.03110	19.394	0.89946	25.629		
0.04172	19.980	0.94952	25.750		
0.04908	20.320	0.97210	26.055		

Table B.5. N₂ adsorption and desorption data, at– 196 °C, of carbon CA(1:3/800/4).

Adsorption				Desorption	
p/p^0	n^{ads} (mmol g ⁻¹)	p/p^0	n^{ads} (mmol g ⁻¹)	p/p^0	n^{ads} (mmol g ⁻¹)
0.00005	8.856	0.07483	21.186	0.94095	26.629
0.00017	11.072	0.09833	21.881	0.83747	26.313
0.00064	13.269	0.12724	22.552	0.68518	26.104
0.00078	13.593	0.15335	23.044	0.53506	25.893
0.00194	14.917	0.20554	23.795	0.39941	25.294
0.00241	15.229	0.26118	24.373	0.29541	24.688
0.00291	15.489	0.31449	24.784	0.20394	23.811
0.00344	15.725	0.34867	24.995		
0.00392	15.904	0.40000	25.249		
0.00483	16.194	0.50074	25.592		
0.00716	16.750	0.59951	25.817		
0.00975	17.207	0.69939	25.976		
0.02009	18.386	0.79928	26.115		
0.03049	19.170	0.89901	26.298		
0.04170	19.825	0.94846	26.526		
0.04899	20.181				

Table B.6. N₂ adsorption and desorption data, at– 196 °C, of carbon CA(1:4/800/1).

Adsorption				Desorption	
p/p^0	n^{ads} (mmol g ⁻¹)	p/p^0	n^{ads} (mmol g ⁻¹)	p/p^0	n^{ads} (mmol g ⁻¹)
0.00004	8.864	0.10381	14.620	0.93307	15.478
0.00081	11.037	0.12736	14.732	0.83249	15.416
0.00193	11.681	0.15357	14.827	0.68161	15.391
0.00244	11.852	0.20108	14.951	0.53163	15.359
0.00289	11.979	0.25183	15.044	0.40173	15.243
0.00353	12.128	0.30222	15.112	0.29917	15.148
0.00395	12.212	0.35017	15.162	0.20018	14.989
0.00477	12.350	0.40029	15.202		
0.00770	12.720	0.50034	15.254		
0.00980	12.908	0.60012	15.292		
0.01996	13.471	0.70021	15.322		
0.02887	13.760	0.80019	15.350		
0.03836	13.974	0.89993	15.398		
0.04968	14.159	0.94995	15.465		
0.07506	14.429	0.97504	15.562		

Table B.7. N₂ adsorption and desorption data, at– 196 °C, of carbon CA(1:4/800/2).

Adsorption				Desorption	
p/p^0	n^{ads} (mmol g ⁻¹)	p/p^0	n^{ads} (mmol g ⁻¹)	p/p^0	n^{ads} (mmol g ⁻¹)
0.00000	8.869	0.10370	17.350	0.93436	18.775
0.00018	11.077	0.12789	17.539	0.83375	18.701
0.00171	13.217	0.15463	17.700	0.68289	18.648
0.00194	13.338	0.20187	17.910	0.53193	18.585
0.00244	13.549	0.25341	18.076	0.40289	18.390
0.00290	13.709	0.30427	18.198	0.29829	18.207
0.00349	14.584	0.35034	18.285	0.20056	17.926
0.00384	13.969	0.40061	18.360		
0.00499	14.219	0.50101	18.462		
0.00773	14.646	0.60061	18.532		
0.00961	14.865	0.70085	18.582		
0.02037	15.654	0.80094	18.627		
0.03185	16.140	0.90097	18.690		
0.04100	16.414	0.95109	18.763		
0.04949	16.616	0.97595	18.870		
0.07517	17.042				

Table B.8. N₂ adsorption and desorption data, at– 196 °C, of carbon CA(1:4/800/4).

Adsorption				Desorption	
p/p^0	n^{ads} (mmol g ⁻¹)	p/p^0	n^{ads} (mmol g ⁻¹)	p/p^0	n^{ads} (mmol g ⁻¹)
0.00000	2.213	0.04903	17.591	0.93468	23.249
0.00002	4.426	0.07479	18.434	0.83369	23.097
0.00008	6.640	0.09891	19.035	0.68319	22.958
0.00017	8.852	0.12696	19.587	0.55203	22.819
0.00049	11.052	0.15290	20.004	0.39982	22.103
0.00079	11.827	0.20371	20.644	0.29874	21.511
0.00200	13.090	0.25823	21.159	0.20399	20.684
0.00240	13.324	0.31023	21.544		
0.00293	13.563	0.35844	21.839		
0.00338	13.736	0.39998	22.049		
0.00394	13.924	0.50053	22.428		
0.00496	14.204	0.60007	22.685		
0.00756	14.723	0.69973	22.850		
0.00965	15.038	0.79946	22.969		
0.02031	16.081	0.89905	23.106		
0.03120	16.774	0.94950	23.233		
0.04235	17.315	0.97354	23.452		

Table B.9. N₂ adsorption and desorption data, at– 196 °C, of carbon HA(1:3/800/1).

Adsorption				Desorption	
p/p^0	n^{ads} (mmol g ⁻¹)	p/p^0	n^{ads} (mmol g ⁻¹)	p/p^0	n^{ads} (mmol g ⁻¹)
0.00002	8.870	0.07582	22.912	0.93511	26.339
0.00009	11.083	0.10043	23.524	0.83429	26.135
0.00035	13.290	0.12793	24.008	0.68302	25.998
0.00079	14.684	0.15440	24.346	0.53283	25.862
0.00195	16.159	0.20486	24.783	0.40315	25.557
0.00241	16.470	0.25604	25.069	0.29750	25.276
0.00292	16.757	0.30745	25.267	0.20120	24.798
0.00337	16.971	0.35477	25.403		
0.00390	17.192	0.40000	25.505		
0.00490	17.535	0.50026	25.662		
0.00734	18.171	0.59990	25.775		
0.00986	18.663	0.69978	25.871		
0.02025	19.991	0.79996	25.971		
0.03094	20.881	0.89942	26.126		
0.04198	21.565	0.94941	26.312		
0.04890	21.916	0.97417	26.582		

Table B.10. N₂ adsorption and desorption data, at– 196 °C, of carbon HA(1:3/800/2).

Adsorption				Desorption	
p/p^0	n^{ads} (mmol g ⁻¹)	p/p^0	n^{ads} (mmol g ⁻¹)	p/p^0	n^{ads} (mmol g ⁻¹)
0.00000	8.859	0.07323	25.034	0.93714	32.247
0.00012	11.068	0.09554	26.059	0.83531	32.001
0.00038	13.269	0.12681	27.185	0.68449	31.792
0.00078	14.709	0.15288	27.927	0.55283	31.592
0.00194	16.496	0.20899	29.102	0.40313	31.027
0.00241	16.885	0.26639	29.909	0.30603	30.354
0.00291	17.233	0.32091	30.443	0.19376	28.867
0.00347	17.548	0.36521	30.762		
0.00388	17.749	0.39950	30.949		
0.00478	18.121	0.50049	31.331		
0.00786	19.036	0.60029	31.557		
0.00978	19.460	0.69936	31.714		
0.01951	20.963	0.79982	31.864		
0.02861	21.951	0.90013	32.049		
0.03814	22.794	0.94999	32.237		
0.04956	23.642	0.97240	32.597		

Table B.11. N₂ adsorption and desorption data, at– 196 °C, of carbon HA(1:3/800/3).

Adsorption				Desorption	
p/p^0	n^{ads} (mmol g ⁻¹)	p/p^0	n^{ads} (mmol g ⁻¹)	p/p^0	n^{ads} (mmol g ⁻¹)
0.00008	11.096	0.095272	27.111	0.936117	35.137
0.00030	13.300	0.126216	28.370	0.834742	34.890
0.00079	15.381	0.152154	29.242	0.684421	34.652
0.00192	17.185	0.20708	30.695	0.552543	34.415
0.00243	17.623	0.263978	31.798	0.401041	33.489
0.00288	17.943	0.320116	32.602	0.304135	32.458
0.00346	18.288	0.347901	32.922	0.203447	30.674
0.00390	18.510	0.400171	33.404		
0.00480	18.897	0.501889	34.013		
0.00793	19.862	0.599448	34.356		
0.00974	20.272	0.699137	34.574		
0.01959	21.833	0.799621	34.746		
0.02884	22.853	0.899777	34.949		
0.03812	23.686	0.949501	35.130		
0.049571	24.554	0.972806	35.465		
0.073085	26.005				

Table B.12. N₂ adsorption and desorption data, at– 196 °C, of carbon HA(1:3/800/4).

Adsorption				Desorption	
p/p^0	n^{ads} (mmol g ⁻¹)	p/p^0	n^{ads} (mmol g ⁻¹)	p/p^0	n^{ads} (mmol g ⁻¹)
0.00001	6.649	0.07356	24.683	0.94027	35.989
0.00007	8.862	0.10443	26.175	0.83887	35.633
0.00021	11.073	0.12577	27.047	0.68788	35.313
0.00078	14.245	0.15187	27.986	0.55539	35.005
0.00193	16.164	0.19986	29.427	0.39932	33.248
0.00241	16.586	0.26371	30.952	0.30090	31.731
0.00289	16.918	0.31980	32.008	0.20381	29.591
0.00337	17.202	0.34717	32.450		
0.00394	17.491	0.40007	33.181		
0.00496	17.910	0.50188	34.209		
0.00757	18.689	0.59990	34.849		
0.00957	19.137	0.69911	35.215		
0.01979	20.673	0.79757	35.446		
0.02982	21.706	0.89727	35.714		
0.04099	22.629	0.94926	35.964		
0.04908	23.212	0.97158	36.403		

Table B.13. N₂ adsorption and desorption data, at– 196 °C, of carbon NS.

Adsorption				Desorption	
p/p^0	n^{ads} (mmol g ⁻¹)	p/p^0	n^{ads} (mmol g ⁻¹)	p/p^0	n^{ads} (mmol g ⁻¹)
0.00001	0.677	0.25654	13.824	0.88759	19.329
0.00002	1.356	0.28061	14.063	0.83688	18.972
0.00003	2.034	0.30673	14.309	0.78722	18.596
0.00004	2.716	0.3285	14.507	0.70170	17.942
0.00005	3.396	0.35071	14.701	0.59870	17.246
0.00011	4.075	0.37569	14.913	0.50082	16.636
0.00016	4.753	0.40086	15.118	0.41322	15.278
0.00026	5.428	0.42599	15.303	0.39708	15.107
0.00044	6.099	0.44985	15.483	0.35244	14.706
0.00083	6.758	0.49899	15.836		
0.00158	7.395	0.5502	16.184		
0.00308	7.985	0.60008	16.51		
0.00483	8.355	0.64995	16.837		
0.01802	9.528	0.69993	17.183		
0.02083	9.67	0.74984	17.568		
0.05052	10.719	0.79986	18.012		
0.09769	11.752	0.84991	18.531		
0.15171	12.599	0.90037	19.108		
0.20389	13.255	0.95015	19.726		

Table B.14. N₂ adsorption and desorption data, at– 196 °C, of carbon CP.

Adsorption				Desorption	
p/p^0	n^{ads} (mmol g ⁻¹)	p/p^0	n^{ads} (mmol g ⁻¹)	p/p^0	n^{ads} (mmol g ⁻¹)
0.00039	0.786	0.22961	11.746	0.91553	12.636
0.00039	1.637	0.28816	11.746	0.82645	12.388
0.00053	3.832	0.3725	11.832	0.75474	12.388
0.00039	4.656	0.43605	11.809	0.65237	12.21
0.00039	5.528	0.52645	11.916	0.57434	12.249
0.00079	7.751	0.59237	11.906	0.46513	11.971
0.00395	9.208	0.68645	12.034	0.38233	11.923
0.01513	10.186	0.74737	12.048	0.30123	11.802
0.04776	11.026	0.83434	12.265		
0.07961	11.323	0.87513	12.317		
0.10237	11.463	0.93421	12.541		
0.13500	11.581	0.94961	12.634		
0.17303	11.643	0.97408	12.792		
0.00039	0.786	0.22961	11.746		

Table B.15. N₂ adsorption and desorption data, at– 196 °C, of carbon ACC.

Adsorption				Desorption	
p/p^0	n^{ads} (mmol g ⁻¹)	p/p^0	n^{ads} (mmol g ⁻¹)	p/p^0	n^{ads} (mmol g ⁻¹)
0.00018	4.430	0.10819	11.899	0.93288	21.699
0.00118	6.599	0.12454	12.319	0.83468	21.525
0.00196	7.076	0.14907	12.928	0.68578	21.280
0.00245	7.274	0.19631	14.039	0.55211	20.983
0.00291	7.421	0.25027	15.236	0.39822	18.343
0.00346	7.563	0.30266	16.342	0.29697	16.325
0.00384	7.650	0.35603	17.412	0.19871	14.191
0.00513	7.883	0.39990	18.234		
0.00757	8.201	0.50093	19.781		
0.00983	8.422	0.60306	20.764		
0.02015	9.091	0.69836	21.176		
0.02856	9.474	0.81472	21.411		
0.03860	9.861	0.91567	21.592		
0.04979	10.242	0.94924	21.686		
0.07296	10.940	0.97557	21.772		

Table B.16. N₂ adsorption and desorption data, at– 196 °C, of carbon VP.

Adsorption				Desorption	
p/p^0	n^{ads} (mmol g ⁻¹)	p/p^0	n^{ads} (mmol g ⁻¹)	p/p^0	n^{ads} (mmol g ⁻¹)
0.00039	0.904	0.22947	10.183	0.91618	14.654
0.00026	1.888	0.28224	10.419	0.88421	14.341
0.00039	4.414	0.35868	10.825	0.83921	14.031
0.00039	5.258	0.42026	11.091	0.77000	13.692
0.00066	6.140	0.50882	11.599	0.72842	13.335
0.00763	7.803	0.57000	11.856	0.67039	12.971
0.02697	8.522	0.65697	12.428	0.59013	12.575
0.04579	8.853	0.72263	12.798	0.54092	12.270
0.07513	9.183	0.81763	13.476	0.47605	11.729
0.10408	9.428	0.86250	13.734	0.38205	11.123
0.12329	9.570	0.92618	14.391		
0.14961	9.740	0.94303	14.567		
0.18171	9.923	0.96803	15.015		

Table B.17. N₂ adsorption and desorption data, at– 196 °C, of carbon GAC830.

Adsorption				Desorption	
p/p^0	n^{ads} (mmol g ⁻¹)	p/p^0	n^{ads} (mmol g ⁻¹)	p/p^0	n^{ads} (mmol g ⁻¹)
0.00002	4.494	0.10175	10.023	0.93732	13.183
0.00065	6.709	0.12677	10.161	0.84583	12.391
0.00081	6.849	0.15266	10.276	0.69322	11.735
0.00199	7.382	0.20099	10.445	0.53724	11.391
0.00243	7.503	0.25229	10.595	0.38852	10.950
0.00291	7.614	0.30264	10.727	0.29764	10.738
0.00336	7.699	0.35022	10.839	0.20046	10.469
0.00386	7.785	0.40024	10.949	0.93732	13.183
0.00510	7.957	0.49971	11.147		
0.00725	8.179	0.59978	11.347		
0.00990	8.382	0.69974	11.570		
0.02047	8.886	0.79909	11.873		
0.03270	9.227	0.89715	12.428		
0.04251	9.421	0.94950	13.017		
0.04940	9.531	0.97671	13.513		
0.07525	9.826				

Table B.18. N₂ adsorption and desorption data, at– 196 °C, of carbon GACm.

Adsorption				Desorption	
p/p^0	n^{ads} (mmol g ⁻¹)	p/p^0	n^{ads} (mmol g ⁻¹)	p/p^0	n^{ads} (mmol g ⁻¹)
0.00001	4.499	0.10139	10.928	0.93728	14.436
0.00035	6.726	0.12669	11.090	0.84524	13.540
0.00078	7.315	0.15249	11.220	0.69255	12.809
0.00195	7.922	0.20114	11.410	0.53682	12.429
0.00249	8.063	0.25217	11.572	0.38830	11.951
0.00296	8.198	0.30256	11.715	0.29793	11.724
0.00343	8.296	0.35016	11.836	0.20002	11.427
0.00395	8.391	0.40013	11.956		
0.00486	8.531	0.49981	12.170		
0.00775	8.862	0.59979	12.386		
0.00977	9.030	0.69974	12.632		
0.01961	9.573	0.79926	12.971		
0.02940	9.910	0.49731	13.595		
0.03877	10.147	0.94954	14.260		
0.04976	10.360	0.97675	14.816		
0.07529	10.699				

Table B.19. N₂ adsorption and desorption data, at– 196 °C, of carbon NSox.

Adsorption				Desorption	
p/p^0	n^{ads} (mmol g ⁻¹)	p/p^0	n^{ads} (mmol g ⁻¹)	p/p^0	n^{ads} (mmol g ⁻¹)
0.00012	4.487	0.15130	10.135	0.93537	14.803
0.00369	6.609	0.20147	10.628	0.83797	14.423
0.00392	6.646	0.25558	11.074	0.68979	13.933
0.00515	6.814	0.30696	11.447	0.55199	13.466
0.00734	7.036	0.34997	11.726	0.40100	12.083
0.00984	7.228	0.40008	12.024	0.29444	11.391
0.02025	7.757	0.49924	12.528	0.18659	10.525
0.02887	8.062	0.60002	12.969		
0.03907	8.354	0.69926	13.389		
0.04995	8.616	0.79923	13.859		
0.07461	9.096	0.89957	14.411		
0.09826	9.473	0.95023	14.767		
0.12584	9.843	0.97508	15.026		

Table B.20. N₂ adsorption and desorption data, at– 196 °C, of carbon ACCsat/600.

Adsorption				Desorption	
p/p^0	n^{ads} (mmol g ⁻¹)	p/p^0	n^{ads} (mmol g ⁻¹)	p/p^0	n^{ads} (mmol g ⁻¹)
0.00053	2.267	0.09989	4.513	0.83330	8.332
0.00082	2.439	0.12477	4.745	0.68277	8.287
0.00194	2.772	0.14970	4.977	0.55080	8.222
0.00249	2.861	0.19908	5.431	0.39792	7.263
0.00299	2.935	0.24973	5.896	0.29330	6.425
0.00366	3.005	0.30077	6.340	0.19906	5.589
0.00393	3.033	0.35074	6.750		
0.00524	3.131	0.40101	7.125		
0.00749	3.252	0.50156	7.705		
0.00998	3.351	0.60194	8.052		
0.01949	3.589	0.70106	8.188		
0.02946	3.756	0.81995	8.254		
0.03960	3.896	0.92005	8.316		
0.05016	4.023	0.95172	8.356		
0.07359	4.264	0.97721	8.393		

Table B.21. N₂ adsorption and desorption data, at– 196 °C, of carbon ACC/400.

Adsorption				Desorption	
p/p^0	n^{ads} (mmol g ⁻¹)	p/p^0	n^{ads} (mmol g ⁻¹)	p/p^0	n^{ads} (mmol g ⁻¹)
0.00083	2.255	0.12501	4.529	0.93164	8.205
0.00198	2.568	0.14990	4.774	0.83169	8.152
0.00240	2.632	0.19904	5.255	0.68159	8.085
0.00313	2.721	0.24929	5.735	0.55068	8.012
0.00344	2.752	0.30005	6.196	0.39597	7.104
0.00411	2.809	0.35036	6.618	0.29431	6.261
0.00508	2.877	0.40040	6.991	0.19888	5.376
0.00746	2.998	0.50110	7.556		
0.00999	3.095	0.60086	7.876		
0.01963	3.331	0.69962	8.005		
0.02968	3.497	0.81859	8.079		
0.03977	3.635	0.91846	8.152		
0.05019	3.762	0.95015	8.196		
0.07373	4.013	0.97540	8.236		
0.09993	4.278				

Table B.22. N₂ adsorption and desorption data, at– 196 °C, of carbon GAC/400.

Adsorption				Desorption	
p/p^0	n^{ads} (mmol g ⁻¹)	p/p^0	n^{ads} (mmol g ⁻¹)	p/p^0	n^{ads} (mmol g ⁻¹)
0.00005	4.424	0.10074	10.325	0.93969	14.200
0.00076	6.612	0.12708	10.524	0.85242	13.293
0.00079	6.648	0.15316	10.676	0.70019	12.475
0.00196	7.251	0.20222	10.896	0.53440	12.004
0.00243	7.391	0.25382	11.076	0.39234	11.500
0.00294	7.512	0.30455	11.229	0.29651	11.239
0.00346	7.619	0.35357	11.363	0.18454	10.857
0.00387	7.693	0.40022	11.482		
0.00506	7.869	0.49965	11.714		
0.00762	8.151	0.59967	11.954		
0.00961	8.319	0.69970	12.230		
0.02052	8.904	0.79885	12.608		
0.03170	9.279	0.89660	13.263		
0.04304	9.555	0.94919	13.956		
0.04892	9.672	0.97737	14.555		
0.07559	10.069				

Table B.23. N₂ adsorption and desorption data, at– 196 °C, of carbon GAC/600.

Adsorption				Desorption	
p/p^0	n^{ads} (mmol g ⁻¹)	p/p^0	n^{ads} (mmol g ⁻¹)	p/p^0	n^{ads} (mmol g ⁻¹)
0.00002	4.434	0.10085	10.234	0.93763	14.056
0.00079	6.606	0.12672	10.420	0.84759	13.089
0.00079	6.626	0.15245	10.564	0.69448	12.292
0.00243	7.339	0.20164	10.771	0.53797	11.871
0.00256	7.377	0.25275	10.940	0.38940	11.362
0.00288	7.453	0.30317	11.086		
0.00337	7.549	0.35015	11.210		
0.00386	7.641	0.40023	11.331		
0.00518	7.834	0.49963	11.557		
0.00758	8.096	0.59993	11.792		
0.00993	8.286	0.69971	12.063		
0.02019	8.830	0.79923	12.434		
0.02908	9.137	0.89699	13.098		
0.03894	9.395	0.94928	13.817		
0.04997	9.619	0.97690	14.435		
0.07552	9.985				

Table B.24. N₂ adsorption and desorption data, at– 196 °C, of carbon GACsat/400.

Adsorption				Desorption	
p/p^0	n^{ads} (mmol g ⁻¹)	p/p^0	n^{ads} (mmol g ⁻¹)	p/p^0	n^{ads} (mmol g ⁻¹)
0.00760	2.018	0.25195	3.443	0.93752	5.912
0.01015	2.271	0.30216	3.541	0.84687	5.180
0.01901	2.458	0.35178	3.635	0.69412	4.566
0.03140	2.607	0.40032	3.722	0.53747	4.256
0.04365	2.721	0.49982	3.886	0.40186	3.935
0.04967	2.770	0.59950	4.073	0.29823	3.765
0.07574	2.922	0.70011	4.291	0.18255	3.547
0.09958	3.032	0.79891	4.593		
0.12555	3.129	0.89710	5.138		
0.15079	3.209	0.94942	5.711		
0.20083	3.334	0.97674	6.201		

Table B.25. N₂ adsorption and desorption data, at – 196 °C, of carbon GACsat/600.

Adsorption				Desorption	
p/p^0	n^{ads} (mmol g ⁻¹)	p/p^0	n^{ads} (mmol g ⁻¹)	p/p^0	n^{ads} (mmol g ⁻¹)
0.00002	4.43393	0.10085	10.23368	0.847592	13.088528
0.000792	6.606210	0.12672	10.41985	0.694485	12.292310
0.000793	6.626394	0.15245	10.56365	0.537973	11.870809
0.002429	7.339247	0.20164	10.77131	0.389397	11.361940
0.002561	7.376674	0.25275	10.94016		
0.002884	7.452510	0.30317	11.08604		
0.003369	7.549265	0.35015	11.20970		
0.003865	7.640657	0.40023	11.33144		
0.005177	7.834114	0.49963	11.55741		
0.007585	8.095965	0.59993	11.79171		
0.009930	8.285873	0.69971	12.06304		
0.020187	8.829518	0.79923	12.43378		
0.029081	9.137474	0.89699	13.09787		
0.038940	9.394839	0.94928	13.81652		
0.049974	9.619180	0.97690	14.43452		
0.075522	9.985227	0.93763	14.05555		

B.2. CO₂ adsorption at 0 °C

Table B.26. CO₂ adsorption data, at 0 °C, of carbon CA(1:3/700/2).

Adsorption					
p/p^0	n^{ads} (mmol g ⁻¹)	p/p^0	n^{ads} (mmol g ⁻¹)	p/p^0	n^{ads} (mmol g ⁻¹)
0.00013	0.190	0.00485	2.702	0.01683	5.610
0.00024	0.305	0.00513	2.793	0.01818	5.818
0.00039	0.461	0.00545	2.891	0.01930	6.085
0.00060	0.653	0.00645	3.198	0.02053	6.267
0.00075	0.757	0.00696	3.340	0.02155	6.528
0.00093	0.890	0.00751	3.495	0.02240	6.649
0.00127	1.130	0.00843	3.732	0.02315	6.872
0.00149	1.249	0.00935	3.976	0.02417	7.010
0.00175	1.396	0.01042	4.216	0.02506	7.222
0.00224	1.666	0.01147	4.455	0.02597	7.372
0.00254	1.795	0.01264	4.691	0.02676	7.642
0.00288	1.949	0.01376	4.963	0.02802	7.804
0.00353	2.232	0.01462	5.131	0.02909	8.104
0.00390	2.358	0.01544	5.315	0.03002	8.200
0.00431	2.505	0.01615	5.440	0.03080	8.397

Table B.27. CO₂ adsorption data, at 0 °C, of carbon CA(1:3/800/1).

Adsorption					
p/p^0	n^{ads} (mmol g ⁻¹)	p/p^0	n^{ads} (mmol g ⁻¹)	p/p^0	n^{ads} (mmol g ⁻¹)
0.00016	0.098	0.00493	1.690	0.01697	4.509
0.00025	0.154	0.00519	1.765	0.01805	4.712
0.00038	0.207	0.00547	1.829	0.01903	4.954
0.00064	0.319	0.00649	2.089	0.02003	5.155
0.00078	0.382	0.00697	2.217	0.02092	5.414
0.00096	0.440	0.00750	2.344	0.02197	5.632
0.00135	0.600	0.00841	2.565	0.02293	5.883
0.00157	0.683	0.00930	2.792	0.02429	6.157
0.00182	0.757	0.01022	3.008	0.02552	6.483
0.00226	0.913	0.01111	3.237	0.02625	6.652
0.00249	0.993	0.01209	3.456	0.02694	6.855
0.00276	1.062	0.01302	3.677	0.02785	7.047
0.00355	1.310	0.01410	3.909	0.02868	7.323
0.00394	1.435	0.01510	4.190	0.02971	7.533
0.00439	1.544	0.01613	4.335	0.03063	7.866

Table B.28. CO₂ adsorption data, at 0 °C, of carbon CA(1:3/800/2).

Adsorption					
p/p^0	n^{ads} (mmol g ⁻¹)	p/p^0	n^{ads} (mmol g ⁻¹)	p/p^0	n^{ads} (mmol g ⁻¹)
0.00011	0.063	0.00515	1.963	0.01796	4.692
0.00017	0.106	0.00549	2.050	0.01890	4.889
0.00025	0.159	0.00633	2.267	0.01990	5.082
0.00051	0.312	0.00676	2.370	0.02092	5.299
0.00067	0.402	0.00725	2.496	0.02202	5.388
0.00088	0.507	0.00817	2.705	0.02290	5.611
0.00120	0.640	0.00863	2.813	0.02388	5.776
0.00137	0.717	0.00915	2.934	0.02481	5.969
0.00159	0.806	0.01013	3.146	0.02580	6.118
0.00217	1.023	0.01114	3.375	0.02671	6.316
0.00249	1.144	0.01207	3.552	0.02780	6.474
0.00287	1.276	0.01301	3.753	0.02881	6.733
0.00353	1.487	0.01398	3.937	0.02971	6.863
0.00388	1.599	0.01496	4.146	0.03057	7.030
0.00430	1.720	0.01599	4.325		
0.00486	1.878	0.01700	4.532		

Table B.29. CO₂ adsorption data, at 0 °C, of carbon CA(1:3/800/4).

Adsorption					
p/p^0	n^{ads} (mmol g ⁻¹)	p/p^0	n^{ads} (mmol g ⁻¹)	p/p^0	n^{ads} (mmol g ⁻¹)
0.00020	0.103	0.00492	1.591	0.01726	3.941
0.00032	0.160	0.00524	1.663	0.01805	4.058
0.00046	0.229	0.00558	1.744	0.01878	4.196
0.00074	0.352	0.00647	1.940	0.01969	4.328
0.00090	0.413	0.00691	2.031	0.02052	4.501
0.00109	0.483	0.00737	2.130	0.02193	4.699
0.00139	0.594	0.00836	2.321	0.02318	4.995
0.00156	0.648	0.00933	2.526	0.02408	5.139
0.00175	0.709	0.01036	2.725	0.02490	5.376
0.00223	0.867	0.01135	2.925	0.02592	5.505
0.00249	0.943	0.01238	3.097	0.02683	5.764
0.00278	1.027	0.01335	3.282	0.02777	5.885
0.00351	1.232	0.01447	3.467	0.02861	6.114
0.00388	1.330	0.01553	3.673	0.02978	6.267
0.00429	1.436	0.01649	3.753	0.03082	6.558

Table B.30. CO₂ adsorption data, at 0 °C, of carbon CA(1:4/800/1).

Adsorption					
p/p^0	n^{ads} (mmol g ⁻¹)	p/p^0	n^{ads} (mmol g ⁻¹)	p/p^0	n^{ads} (mmol g ⁻¹)
0.00017	0.153	0.00524	2.106	0.01707	4.516
0.00029	0.233	0.00559	2.192	0.01816	4.692
0.00045	0.342	0.00651	2.433	0.01910	4.902
0.00068	0.504	0.00697	2.525	0.02011	5.055
0.00085	0.579	0.00744	2.634	0.02098	5.229
0.00104	0.671	0.00843	2.869	0.02205	5.371
0.00134	0.837	0.00892	2.951	0.02296	5.568
0.00154	0.905	0.00941	3.060	0.02397	5.706
0.00175	0.991	0.01029	3.236	0.02481	5.889
0.00223	1.198	0.01069	3.308	0.02601	6.057
0.00250	1.281	0.01111	3.400	0.02699	6.304
0.00280	1.386	0.01217	3.591	0.02795	6.451
0.00348	1.632	0.01314	3.776	0.02874	6.679
0.00386	1.728	0.01412	3.958	0.02982	6.830
0.00425	1.841	0.01500	4.113	0.03074	6.975
0.00490	2.038	0.01607	4.329		

Table B.31. CO₂ adsorption data, at 0 °C, of carbon HA(1:3/800/1).

Adsorption					
p/p^0	n^{ads} (mmol g ⁻¹)	p/p^0	n^{ads} (mmol g ⁻¹)	p/p^0	n^{ads} (mmol g ⁻¹)
0.00016	0.102	0.00493	1.644	0.01697	4.201
0.00025	0.159	0.00519	1.715	0.01805	4.375
0.00038	0.212	0.00547	1.773	0.01903	4.597
0.00064	0.325	0.00649	2.013	0.02003	4.773
0.00078	0.388	0.00697	2.132	0.02092	5.018
0.00096	0.444	0.00750	2.248	0.02197	5.209
0.00135	0.603	0.00841	2.450	0.02293	5.442
0.00157	0.685	0.00930	2.660	0.02429	5.682
0.00182	0.755	0.01022	2.855	0.02552	5.986
0.00226	0.907	0.01111	3.067	0.02625	6.139
0.00249	0.986	0.01209	3.263	0.02694	6.332
0.00276	1.050	0.01302	3.466	0.02785	6.501
0.00355	1.288	0.01410	3.672	0.02868	6.769
0.00394	1.407	0.01510	3.936	0.02971	6.953
0.00439	1.507	0.01613	4.047	0.03063	7.279

Table B.32. CO₂ adsorption data, at 0 °C, of carbon HA(1:3/800/2).

Adsorção					
p/p^0	n^{ads} (mmol g ⁻¹)	p/p^0	n^{ads} (mmol g ⁻¹)	p/p^0	n^{ads} (mmol g ⁻¹)
0.00018	0.053	0.00524	1.446	0.01806	3.992
0.00027	0.090	0.00559	1.531	0.01904	4.199
0.00037	0.128	0.00641	1.697	0.02003	4.369
0.00066	0.241	0.00679	1.786	0.02094	4.577
0.00082	0.298	0.00721	1.877	0.02192	4.731
0.00101	0.361	0.00831	2.090	0.02282	4.949
0.00138	0.476	0.00881	2.205	0.02388	5.130
0.00157	0.536	0.00937	2.332	0.02490	5.353
0.00179	0.599	0.01028	2.502	0.02592	5.528
0.00235	0.752	0.01116	2.689	0.02689	5.766
0.00264	0.829	0.01215	2.861	0.02789	5.937
0.00295	0.907	0.01308	3.064	0.02879	6.214
0.00359	1.055	0.01408	3.231	0.02973	6.423
0.00389	1.134	0.01502	3.424	0.03068	6.652
0.00423	1.219	0.01605	3.601		
0.00491	1.369	0.01700	3.815		

B.3. Mercury porosimetry

Table B.33. Mercury porosimetry data of 2M sample.

Intrusion							
P (MPa)	Cumulative intrusion (cm ³ g ⁻¹)	P (MPa)	Cumulative intrusion (cm ³ g ⁻¹)	P (MPa)	Cumulative intrusion (cm ³ g ⁻¹)	P (MPa)	Cumulative intrusion (cm ³ g ⁻¹)
0.00359	0.00000	0.06410	3.58966	1.31946	8.14224	24.94600	11.52146
0.00405	0.02227	0.07203	3.86163	1.48475	8.41711	28.01722	11.52311
0.00452	0.04241	0.08095	4.13201	1.67596	8.73429	31.47879	11.52652
0.00504	0.06733	0.09095	4.38012	1.88543	9.07424	35.37313	11.52652
0.00563	0.09596	0.10226	4.59960	2.11331	9.40085	39.76098	11.52652
0.00630	0.13466	0.11488	4.81167	2.39173	9.73761	44.68845	11.52652
0.00705	0.19086	0.12947	5.01949	2.68632	10.03776	50.21990	11.52652
0.00791	0.25978	0.14550	5.18860	3.02257	10.29518	56.46877	11.52652
0.00884	0.34725	0.16346	5.34977	3.39653	10.53200	63.50654	11.52652
0.00990	0.48509	0.18371	5.50723	3.82748	10.73994	71.40635	11.52652
0.01110	0.60543	0.20669	5.65939	4.30223	10.91359	80.27965	11.52652
0.01247	0.73108	0.23975	5.83291	4.83900	11.04945	90.26049	11.52652
0.01406	0.88536	0.27110	5.98835	5.44029	11.15787	101.48147	11.52652
0.01578	1.08575	0.30977	6.13931	6.11833	11.24365	114.08254	11.52652
0.01774	1.25169	0.34943	6.28049	6.88049	11.30999	128.23594	11.52652
0.01992	1.44202	0.38820	6.42172	7.73752	11.36048	144.24780	11.52652
0.02240	1.75852	0.44572	6.59458	8.69737	11.39898	162.22639	11.52652
0.02516	1.92657	0.50302	6.74592	9.77727	11.42883	182.38680	11.52652
0.02828	2.11213	0.57186	6.90539	10.99038	11.45171	205.03282	11.52652
0.03178	2.28920	0.64654	7.04972	12.35267	11.47015	230.47484	11.52652
0.03573	2.51133	0.72356	7.20489	13.89309	11.48469	259.06449	11.52652
0.04016	2.69370	0.81682	7.36975	15.61564	11.49700	291.12465	11.52652
0.04515	2.89092	0.92497	7.54169	17.54533	11.50322	327.12062	11.52652
0.05074	3.09821	1.03467	7.70659	19.72175	11.51127	367.74746	11.52652
0.05700	3.32883	1.17322	7.91748	22.18990	11.51736	413.33379	11.52652
Extrusion							
Pressure (MPa)	Cumulative intrusion (cm ³ g ⁻¹)	Pressure (MPa)	Cumulative intrusion (cm ³ g ⁻¹)	Pressure (MPa)	Cumulative intrusion (cm ³ g ⁻¹)	Pressure (MPa)	Cumulative intrusion (cm ³ g ⁻¹)
363.90926	11.43017	60.80156	11.43017	10.13197	11.43017	1.70381	11.43017
320.33485	11.43017	53.54003	11.43017	8.91860	11.43017	1.50092	11.39514
281.80911	11.43017	47.09529	11.43017	7.84990	11.43017	1.31750	11.33732
247.99808	11.43017	41.48820	11.43017	6.90800	11.43017	1.16683	11.26676
218.25496	11.43017	36.47384	11.43017	6.07377	11.43017	1.03228	11.17867
192.04710	11.43017	32.10960	11.43017	5.34828	11.43017	0.91406	11.07383
169.04276	11.43017	28.19088	11.43017	4.71152	11.43017	0.80098	10.95194
148.71490	11.43017	24.82339	11.43017	4.14772	11.43017	0.61727	10.71159
130.92016	11.43017	21.83352	11.43017	3.65540	11.43017	0.59960	10.67729
115.19551	11.43017	19.21251	11.43017	3.21654	11.43017	0.49564	10.50842
101.36885	11.43017	16.90381	11.43017	2.82907	11.43017	0.38156	10.25946
89.22034	11.43017	14.87358	11.43017	2.49043	11.43017	0.25784	9.80135
78.49523	11.43017	13.07990	11.43017	2.19706	11.43017		
69.16683	11.43017	11.51224	11.43017	1.93808	11.43017		

Table B.34. Mercury porosimetry data of 5M sample.

Intrusion							
P (MPa)	Cumulative intrusion (cm ³ g ⁻¹)	P (MPa)	Cumulative intrusion (cm ³ g ⁻¹)	P (MPa)	Cumulative intrusion (cm ³ g ⁻¹)	P (MPa)	Cumulative intrusion (cm ³ g ⁻¹)
0.00359	0.00000	0.07202	2.63534	1.48475	5.22833	31.45901	5.43675
0.00405	0.01726	0.08095	2.75196	1.67375	5.26037	35.36077	5.43675
0.00451	0.03138	0.09098	2.86022	1.88284	5.28705	39.76750	5.43675
0.00505	0.05021	0.10228	2.96064	2.11452	5.30926	44.70563	5.43675
0.00563	0.07845	0.11494	3.05896	2.38996	5.33093	50.23194	5.43675
0.00630	0.12970	0.12916	3.15205	2.69090	5.35019	56.47341	5.43675
0.00705	0.20083	0.14515	3.24723	3.02461	5.36434	63.48206	5.43675
0.00790	0.26986	0.16352	3.34974	3.39679	5.37652	71.40569	5.43675
0.00885	0.33890	0.18374	3.44074	3.82365	5.38866	80.28094	5.43675
0.00992	0.44297	0.20669	3.53279	4.30826	5.39875	90.23637	5.43675
0.01111	0.53711	0.20763	3.56656	4.84121	5.40734	101.46848	5.43675
0.01248	0.62602	0.23421	3.61884	5.44616	5.41520	114.07250	5.43675
0.01406	0.73061	0.27088	3.73109	6.11820	5.42184	128.25697	5.43675
0.01578	0.83312	0.30430	3.84484	6.88528	5.42756	144.23837	5.43675
0.01772	0.95236	0.34608	3.97269	7.74065	5.42917	162.23064	5.43675
0.01992	1.07056	0.39095	4.11362	8.69051	5.43223	182.38466	5.43675
0.02238	1.19869	0.44681	4.26552	9.77740	5.43286	205.03218	5.43675
0.02517	1.32159	0.50410	4.40065	10.99208	5.43286	230.47029	5.43675
0.02828	1.43717	0.56770	4.54378	12.35774	5.43339	259.03343	5.43675
0.03180	1.55380	0.64131	4.67807	13.87990	5.43625	291.12368	5.43675
0.03574	1.68611	0.72681	4.80550	15.61932	5.43625	327.11970	5.43675
0.04017	1.83412	0.81640	4.90381	17.54778	5.43675	367.73283	5.43675
0.04515	1.99729	0.92494	5.00096	19.72769	5.43675	413.32751	5.43675
0.05074	2.18034	1.03991	5.07361	22.16725	5.43675		
0.05703	2.35502	1.17127	5.13528	24.93260	5.43675		
0.06410	2.50302	1.32218	5.18919	28.03103	5.43675		
Extrusion							
Pressure (MPa)	Cumulative intrusion (cm ³ g ⁻¹)	Pressure (MPa)	Cumulative intrusion (cm ³ g ⁻¹)	Pressure (MPa)	Cumulative intrusion (cm ³ g ⁻¹)	Pressure (MPa)	Cumulative intrusion (cm ³ g ⁻¹)
363.86253	5.43675	60.81136	5.35549	10.13121	5.35549	1.70428	5.35549
320.28427	5.35549	53.52013	5.35549	8.91455	5.35549	1.50249	5.35549
281.73213	5.35549	47.08605	5.35549	7.85143	5.35549	1.32507	5.35549
247.96121	5.35549	41.45467	5.35549	6.90604	5.35549	1.16986	5.35549
218.20977	5.35549	36.49006	5.35549	6.07809	5.35549	1.03118	5.35549
192.04357	5.35549	32.08993	5.35549	5.34812	5.35549	0.90704	5.35549
168.99746	5.35549	28.21667	5.35549	4.70539	5.35549	0.80004	5.35549
148.73181	5.35549	24.82768	5.35549	4.14929	5.35549	0.62020	5.35549
130.90217	5.35549	21.83622	5.35549	3.64932	5.35549	0.59883	5.35549
115.18654	5.35549	19.22162	5.35549	3.21515	5.35549	0.49317	5.35549
101.39005	5.35549	16.90542	5.35549	2.83270	5.35549	0.38163	5.35549
89.22698	5.35549	14.87047	5.35549	2.48538	5.35549	0.25816	5.35549
78.62220	5.35549	13.08529	5.35549	2.19902	5.35549		
69.14401	5.35549	11.5157	5.35549	1.93126	5.35549		

Table B.35. Mercury porosimetry data of 8M sample.

Intrusion							
P (MPa)	Cumulative intrusion (cm ³ g ⁻¹)	P (MPa)	Cumulative intrusion (cm ³ g ⁻¹)	P (MPa)	Cumulative intrusion (cm ³ g ⁻¹)	P (MPa)	Cumulative intrusion (cm ³ g ⁻¹)
0.00359	0.00000	0.06410	1.74751	1.32002	4.39927	24.93371	4.80047
0.00405	0.01141	0.07205	1.88941	1.48443	4.47136	28.02489	4.80047
0.00452	0.02084	0.08095	2.04074	1.67633	4.53658	31.46671	4.80047
0.00505	0.03175	0.09097	2.18959	1.88575	4.58980	35.37246	4.80047
0.00563	0.04664	0.10228	2.31959	2.12012	4.63038	39.75592	4.80047
0.00630	0.07046	0.11492	2.44313	2.38541	4.66366	44.69449	4.80047
0.00705	0.11412	0.12915	2.55626	2.68449	4.69085	50.24446	4.80047
0.00790	0.17664	0.14553	2.67137	3.02225	4.71416	56.46945	4.80047
0.00884	0.23766	0.16351	2.76713	3.39896	4.73232	63.49159	4.80047
0.00992	0.29175	0.18373	2.85595	3.82993	4.74865	71.39115	4.80047
0.01111	0.35079	0.20666	2.94377	4.30324	4.76161	80.29031	4.80047
0.01248	0.42373	0.23708	3.01182	4.83840	4.77249	90.25900	4.80047
0.01403	0.49964	0.26812	3.10038	5.44118	4.78087	101.47101	4.80047
0.01577	0.57903	0.30795	3.19378	6.12432	4.78770	114.07062	4.80047
0.01774	0.65197	0.34965	3.28439	6.87695	4.79252	128.23868	4.80047
0.01992	0.73036	0.39127	3.36857	7.73998	4.79564	144.24096	4.80047
0.02239	0.82265	0.44297	3.46155	8.69856	4.79838	162.23491	4.80047
0.02517	0.93478	0.50196	3.57235	9.78383	4.79925	182.39012	4.80047
0.02828	1.01814	0.56869	3.68195	10.98937	4.80015	205.03548	4.80047
0.03179	1.10199	0.64588	3.80562	12.35253	4.80036	230.47414	4.80047
0.03574	1.21115	0.72354	3.91776	13.89531	4.80047	259.05972	4.80047
0.04017	1.30592	0.82188	4.03832	15.61604	4.80047	291.14568	4.80047
0.04514	1.39721	0.91851	4.13909	17.55485	4.80047	327.12137	4.80047
0.05075	1.50538	1.04003	4.23350	19.73002	4.80047	367.75864	4.80047
0.05702	1.61255	1.17288	4.32090	22.18229	4.80047	413.35280	4.80047
Extrusion							
Pressure (MPa)	Cumulative intrusion (cm ³ g ⁻¹)	Pressure (MPa)	Cumulative intrusion (cm ³ g ⁻¹)	Pressure (MPa)	Cumulative intrusion (cm ³ g ⁻¹)	Pressure (MPa)	Cumulative intrusion (cm ³ g ⁻¹)
363.89819	4.75183	60.84257	4.75183	10.13411	4.75183	1.70088	4.75183
320.28479	4.75183	53.48486	4.75183	8.91198	4.75183	1.50151	4.75183
281.83615	4.75183	47.15878	4.75183	7.84957	4.75183	1.32659	4.75183
247.99180	4.75183	41.46704	4.75183	6.90327	4.75183	1.16473	4.75183
218.17989	4.75183	36.46006	4.75183	6.08240	4.75183	1.03320	4.75183
192.01206	4.75183	32.08315	4.75183	5.35562	4.75183	0.91345	4.75183
169.06096	4.75183	28.19878	4.75183	4.70835	4.75183	0.79845	4.75183
148.75538	4.75183	24.82798	4.75183	4.14079	4.75183	0.62207	4.75183
130.90337	4.75183	21.84630	4.75183	3.64905	4.75183	0.59751	4.75183
115.19740	4.75183	19.20336	4.75183	3.21606	4.75183	0.49247	4.75183
101.41987	4.75183	16.88979	4.75183	2.83372	4.75183	0.37943	4.75183
89.24016	4.75183	14.87734	4.75183	2.49623	4.75183	0.26047	4.651632
78.59820	4.75183	13.08577	4.75183	2.19975	4.75183		
69.16214	4.75183	11.50915	4.75183	1.93322	4.75183		

Table B.36. Mercury porosimetry data of 5AM sample.

Intrusion							
P (MPa)	Cumulative intrusion (cm ³ g ⁻¹)	P (MPa)	Cumulative intrusion (cm ³ g ⁻¹)	P (MPa)	Cumulative intrusion (cm ³ g ⁻¹)	P (MPa)	Cumulative intrusion (cm ³ g ⁻¹)
0.00356	0.00000	0.06407	1.80347	1.31989	4.18791	24.93896	4.29127
0.00402	0.01838	0.07200	1.94473	1.48721	4.20436	28.02874	4.29127
0.00448	0.03531	0.08091	2.08793	1.66547	4.21363	31.46032	4.29127
0.00500	0.05757	0.09096	2.22677	1.88679	4.22717	35.38408	4.29127
0.00559	0.09337	0.10224	2.36512	2.12010	4.23759	39.74806	4.29127
0.00626	0.14561	0.11490	2.50396	2.38571	4.24708	44.69228	4.29127
0.00702	0.21044	0.12911	2.63990	2.68124	4.25360	50.24662	4.29127
0.00786	0.27623	0.14544	2.78745	3.02413	4.26149	56.45525	4.29127
0.00881	0.33912	0.16342	2.91516	3.39895	4.26624	63.50376	4.29127
0.00989	0.41023	0.18368	3.03852	3.82522	4.27081	71.39716	4.29127
0.01108	0.48328	0.20666	3.15656	4.30180	4.27574	80.27411	4.29127
0.01243	0.55052	0.23921	3.24017	4.83728	4.27916	90.25885	4.29127
0.01401	0.62793	0.26958	3.35719	5.44238	4.28256	101.44767	4.29127
0.01575	0.71210	0.30628	3.46325	6.11890	4.28505	114.07862	4.29127
0.01770	0.78708	0.34605	3.55656	6.88398	4.28719	128.23886	4.29127
0.01988	0.86352	0.39375	3.64708	7.74514	4.28916	144.23873	4.29127
0.02237	0.96898	0.44704	3.72862	8.69763	4.29002	162.22496	4.29127
0.02513	1.04832	0.50692	3.81275	9.77897	4.29066	182.38492	4.29127
0.02826	1.13152	0.56784	3.88384	10.97941	4.29105	205.01479	4.29127
0.03177	1.21667	0.64493	3.95641	12.36368	4.29127	230.44661	4.29127
0.03571	1.30907	0.72740	4.01253	13.88168	4.29127	259.05886	4.29127
0.04014	1.39421	0.81713	4.06326	15.61386	4.29127	291.14057	4.29127
0.04512	1.48564	0.92000	4.10945	17.55157	4.29127	327.11310	4.29127
0.05071	1.58094	1.02943	4.13879	19.73414	4.29127	367.75478	4.29127
0.05699	1.68253	1.16087	4.16292	22.19063	4.29127	413.33618	4.29127
Extrusion							
Pressure (MPa)	Cumulative intrusion (cm ³ g ⁻¹)	Pressure (MPa)	Cumulative intrusion (cm ³ g ⁻¹)	Pressure (MPa)	Cumulative intrusion (cm ³ g ⁻¹)	Pressure (MPa)	Cumulative intrusion (cm ³ g ⁻¹)
363.87759	4.75183	60.80603	4.75183	10.13711	4.75183	1.704843	4.75183
320.31374	4.75183	53.54914	4.75183	8.920604	4.75183	1.503923	4.75183
281.81474	4.75183	47.13399	4.75183	7.854444	4.75183	1.326078	4.75183
247.99237	4.75183	41.45325	4.75183	6.908863	4.75183	1.168407	4.75183
218.21177	4.75183	36.52339	4.75183	6.080239	4.75183	1.033572	4.75183
192.05853	4.75183	32.09165	4.75183	5.358511	4.75183	0.910501	4.75183
168.99145	4.75183	28.22152	4.75183	4.715262	4.75183	0.803906	4.75183
148.72744	4.75183	24.82259	4.75183	4.152151	4.75183	0.619869	4.75183
130.86503	4.75183	21.84158	4.75183	3.648904	4.75183	0.595911	4.75183
115.18209	4.75183	19.19064	4.75183	3.214549	4.75183	0.489019	4.75183
101.37571	4.75183	16.9102	4.75183	2.832076	4.75183	0.377891	4.75183
89.22923	4.75183	14.87565	4.75183	2.488926	4.75183	0.255478	4.651632
78.57528	4.75183	13.08493	4.75183	2.195998	4.75183		
69.13289	4.75183	11.51558	4.75183	1.933703	4.75183		

B.4. Liquid phase adsorption

Table B.37. Kinetic data of paracetamol adsorption, at 30 °C, on the mentioned carbons.

GAC		VP		NS		ACC	
t (h)	C/C ₀	t (h)	C/C ₀	t (h)	C/C ₀	t (h)	C/C ₀
0.00	1.000	0.00	1.000	0.00	1.000	0.00	1.000
0.02	0.997	0.02	0.791	0.02	0.661	0.02	0.791
0.08	0.998	0.03	0.696	0.03	0.579	0.03	0.696
0.17	0.984	0.05	0.629	0.05	0.570	0.05	0.629
0.33	0.977	0.07	0.609	0.07	0.564	0.07	0.609
0.50	0.918	0.08	0.539	0.08	0.535	0.08	0.539
1.00	0.855	0.17	0.514	0.17	0.508	0.17	0.514
2.00	0.805	0.33	0.493	0.33	0.489	0.33	0.493
3.00	0.805	0.50	0.484	0.50	0.486	0.50	0.484
4.00	0.762	1.00	0.492	1.00	0.470	1.00	0.492
		2.00	0.450	2.00	0.456	2.00	0.450
		3.00	0.459	3.00	0.452	3.00	0.459
		4.00	0.427	4.00	0.440	4.00	0.427

Table B.38. Kinetic data of clofibric acid adsorption, at 30 °C, on the mentioned carbons.

GAC		VP		NS		ACC	
t (h)	C/C ₀	t (h)	C/C ₀	t (h)	C/C ₀	t (h)	C/C ₀
0.00	1.000	0.00	1.000	0.00	1.000	0.00	1.000
0.17	0.936	0.02	0.726	0.02	0.508	0.02	0.732
0.33	0.916	0.08	0.609	0.08	0.373	0.05	0.590
0.50	0.896	0.17	0.588	0.17	0.316	0.08	0.405
1.00	0.856	0.25	0.606	0.25	0.289	0.13	0.351
2.00	0.818	0.33	0.591	0.33	0.320	0.17	0.323
3.00	0.738	0.50	0.579	0.50	0.275	0.33	0.291
4.00	0.721	1.00	0.577	1.00	0.262	0.50	0.280
		2.00	0.556	2.00	0.237	1.00	0.242
		3.00	0.555	3.00	0.272	2.00	0.217
		4.00	0.548	4.00	0.246	3.00	0.207

Table B.39. Kinetic data of atenolol adsorption, at 30 °C, on the commercial carbons.

CP		NS	
t (h)	C/C ₀	t (h)	C/C ₀
0.00	1.000	0.00	1.000
0.50	0.506	0.50	0.454
1.00	0.498	1.00	0.381
2.00	0.478	2.00	0.375
3.00	0.431	3.00	0.397
4.00	0.433	4.00	0.386
5.00	0.425	5.00	0.355
6.00	0.415	6.00	0.365
7.00	0.412	7.00	0.348
17.00	0.342	17.00	0.406
24.00	0.342	24.00	0.316

Table B.40. Kinetic data of atenolol adsorption, at 30 °C, on the lab-made carbons.

CA(1:3/800/1)		CA(1:3/800/2)		HA(1:3/800/1)		HA(1:3/800/2)	
t (h)	C/C ₀	t (h)	C/C ₀	t (h)	C/C ₀	t (h)	C/C ₀
0.00	1.000	0.00	1.000	0.00	1.000	0.00	1.000
0.50	0.414	0.50	0.211	0.50	0.111	0.50	0.073
1.00	0.374	1.00	0.165	1.00	0.110	1.00	0.038
2.00	0.319	2.00	0.117	2.00	0.093	2.00	0.040
3.00	0.346	3.00	0.147	3.00	0.090	3.00	0.054
4.00	0.312	4.00	0.150	4.00	0.113	4.00	0.051
5.00	0.306	5.00	0.099	5.00	0.091	5.00	0.041
6.00	0.317	6.00	0.111	6.00	0.109	6.00	0.067
7.00	0.346	7.00	0.122	7.00	0.093	7.00	0.059
17.00	0.292	17.00	0.118	17.00	0.100	17.00	0.072
24.00	0.287	24.00	0.112	24.00	0.066	24.00	0.054

Table B.41. Kinetic data of tiamulin hydrogen fumarate adsorption, at 30 °C, on the commercial carbons.

CP		NS	
t (h)	C/C ₀	t (h)	C/C ₀
0,00	1,000	0,00	1,000
0,50	0,813	0,50	0,505
1,00	0,803	1,00	0,478
2,00	0,775	2,00	0,507
3,00	0,785	3,00	0,452
4,00	0,779	4,00	0,441
5,00	0,771	5,00	0,453
6,00	0,771	6,00	0,466
7,00	0,782	7,00	0,468
17,00	0,753	17,00	0,443
24,00	0,744	24,00	0,432

Table B.42. Kinetic data of tiamulin hydrogen fumarate adsorption, at 30 °C, on the lab-made carbons.

CA(1:3/800/1)		CA(1:3/800/2)		HA(1:3/800/1)		HA(1:3/800/2)	
t (h)	C/C ₀	t (h)	C/C ₀	t (h)	C/C ₀	t (h)	C/C ₀
0.00	1.000	0.00	1.000	0.00	1.000	0.00	1.000
0.50	0.737	0.50	0.769	0.50	0.690	0.25	0.624
1.00	0.713	1.00	0.720	1.00	0.674	0.50	0.533
2.00	0.689	2.00	0.703	2.00	0.721	2.00	0.412
3.00	0.672	3.00	0.655	3.00	0.600	3.00	0.425
4.00	0.663	4.00	0.645	4.00	0.583	4.00	0.440
5.00	0.654	5.00	0.683	5.00	0.606	5.00	0.447
6.00	0.640	6.00	0.687	6.00	0.616	6.00	0.445
7.00	0.655	7.00	0.720	7.00	0.597	7.00	0.445
24.00	0.626	17.00	0.754	17.00	0.594	17.00	0.433
		24.00	0.712	24.00	0.572	24.00	0.445

Table B.43. Kinetic data of methylene blue, at 30 °C, on the tannin-based powders.

2M		5M		8M	
t (h)	C/C ₀	t (h)	C/C ₀	t (h)	C/C ₀
0.00	1.000	0.00	1.000	0.00	1.000
0.08	0.863	0.08	0.908	0.08	0.925
0.25	0.773	0.25	0.905	0.50	0.894
1.00	0.692	0.50	0.877	2.00	0.875
2.00	0.698	1.00	0.863	3.00	0.870
3.00	0.707	2.00	0.803	4.00	0.887
4.00	0.708	3.00	0.816	5.00	0.844
6.00	0.761	4.00	0.847	6.00	0.854
7.00	0.668	5.00	0.860	7.00	0.843
8.00	0.727	6.00	0.829	8.00	0.878
17.00	0.693	7.00	0.828	24.00	0.783
24.00	0.675	8.00	0.833		
		17.00	0.862		
		24.00	0.838		

Table B.44. Equilibrium data of paracetamol adsorption, at 30 °C, on the commercial carbons.

VP		NS		ACC	
C _e (mg g ⁻¹)	q _e (mg g ⁻¹)	C _e (mg g ⁻¹)	q _e (mg g ⁻¹)	C _e (mg g ⁻¹)	q _e (mg g ⁻¹)
1.433	1.433	0.998	90.494	0.600	29.302
39.548	39.548	7.989	166.874	3.941	84.133
59.425	59.425	25.646	190.955	6.350	171.588
111.054	111.054	44.403	226.490	15.716	211.385
198.392	198.392	75.760	258.389	27.521	265.852
266.102	266.102	106.076	258.830	69.989	289.209
436.283	436.283	137.447	253.032	97.918	311.977
				125.062	313.837
				132.780	294.256

Table B.45. Equilibrium data of clofibric acid adsorption, at 30 °C, on the carbons.

VP		NS		ACC	
C_e (mg g ⁻¹)	q_e (mg g ⁻¹)	C_e (mg g ⁻¹)	q_e (mg g ⁻¹)	C_e (mg g ⁻¹)	q_e (mg g ⁻¹)
0.000	28.551	1.852	30.612	0.298	30.265
9.755	74.255	5.362	89.324	3.352	91.302
24.705	102.282	22.657	212.625	10.365	164.882
37.763	118.645	29.422	273.221	12.013	229.889
52.723	160.403	59.854	386.456	17.791	292.070
73.792	180.035	80.683	440.713	52.552	398.349
97.397	244.835	107.465	445.108	116.739	481.090
122.431	283.459			43.304	367.125
				91.948	428.458

Table B.46. Equilibrium data of tiamulin hydrogen fumarate adsorption, at 30 °C, on the commercial carbons.

CP		NS	
C_e (mg g ⁻¹)	q_e (mg g ⁻¹)	C_e (mg g ⁻¹)	q_e (mg g ⁻¹)
0.000	37.125	0.000	38.559
0.000	98.394	0.000	97.551
17.425	174.141	19.722	164.380
36.184	197.122	37.400	195.282
67.667	195.998	58.141	222.526
85.285	233.586	93.703	235.694
111.524	233.921	105.459	269.742
142.337	244.612	135.694	285.493

Table B.47. Equilibrium data of tiamulin hydrogen fumarate adsorption, at 30 °C, on the lab-made carbons.

CA(1:3/800/1)		CA(1:3/800/2)		HA(1:3/800/1)		HA(1:3/800/2)	
C_e (mg g ⁻¹)	q_e (mg g ⁻¹)	C_e (mg g ⁻¹)	q_e (mg g ⁻¹)	C_e (mg g ⁻¹)	q_e (mg g ⁻¹)	C_e (mg g ⁻¹)	q_e (mg g ⁻¹)
0.000	28.273	0.263	28.056	0.000	28.935	0.000	28.834
0.000	106.721	0.797	101.136	0.000	107.045	0.000	114.893
3.338	173.249	0.053	179.350	0.000	196.232	0.779	204.166
12.043	233.995	1.928	258.827	1.641	255.165	0.824	261.899
29.131	270.677	11.267	324.301	18.506	326.154	8.035	372.991
62.965	332.896	45.106	441.064	42.218	444.279	45.676	452.537
90.938	327.338	66.340	472.774	55.629	561.214	52.106	575.874
116.776	343.691	93.673	479.897	88.649	522.895	84.306	575.961

Appendix C

National and international
scientific conferences

Certificado de Participação

Susana Marques participou no CQB Day 2014 que decorreu
a 9 de Julho de 2014 onde apresentou a comunicação em painel

com o título Adsorption of pharmaceutical compounds
onto activated carbon cloth

Pela Comissão organizadora

Ana Paula Carvalho

Ana Paula Carvalho

CQB - Day 2014



ORGANIZADO POR



Universidad de Granada



UNIVERSIDAD DE JAÉN

CERTIFICADO DE ASISTENCIA Y PARTICIPACION

Agustín Francisco Pérez Cadenas, Secretario del Comité Organizador de la XXXIX Reunión Ibérica de Adsorción certifica que:

Roque Marques, Susana Cristina

ha asistido a la mencionada Reunión celebrada en Baeza del 14 al 17 de septiembre de 2014.

Baeza, 17 de Septiembre de 2014

El Presidente

Francisco Carrasco Marín

El Secretario

Agustín F. Pérez Cadenas

DKG CongressPro - Submission

congress@dkg.de

seg 15-12-2014 17:15

Para: Ana Sofia Dias Mestre <asmestre@fc.ul.pt>;

Cc: Ana Paula Baptista de Carvalho <apcarvalho@fc.ul.pt>;

Dear Ms. Dr Ana Sofia Mestre,

you have made a submission for this event:

[Congress]

CARBON 2015

Jul 12, 2015 – Jul 17, 2015, Dresden

<http://www.carbon2015.org>

Title of submission:

Adsorption of pharmaceutical compounds on carbons of different morphologies

Author(s):

MARQUES, Susana C. (Centro de Química e Bioquímica, Faculdade de Ciências, Universidade de Lisboa, 1749-016 Lisboa, Portugal AND Microbiology and Biotechnology Lab, Center for Biodiversity, Functional & Integrative Genomics, Edifício ICAT, Campo Grande 1749-016 Lisboa, Portugal)

MARCUZZO, Jossano S. (Faculdade de Tecnologia do Estado de São Paulo FATEC- Campus São José dos Campos, 12247-014 – São José dos Campos –SP- Brasil)

MESTRE, Ana Sofia (Centro de Química e Bioquímica, Faculdade de Ciências, Universidade de Lisboa, 1749-016 Lisboa, Portugal)

DIAS, Ricardo (Microbiology and Biotechnology Lab, Center for Biodiversity, Functional & Integrative Genomics, Edifício ICAT, Campo Grande 1749-016 Lisboa, Portugal)

ANIA, Conchi O. (ADPOR Group, Instituto Nacional del Carbón, INCAR-CSIC, Apdo.73, 33080, Oviedo, Spain)

CARVALHO, Ana Paula (Centro de Química e Bioquímica, Faculdade de Ciências, Universidade de Lisboa, 1749-016 Lisboa, Portugal)

Presenter:

Ms. Prof. Dr Ana Paula Carvalho

ana.carvalho@fc.ul.pt

Faculdade de Ciências da Universidade de Lisboa

Centro de Química e Bioquímica

Campo Grande

1749-016 Lisboa

Portugal

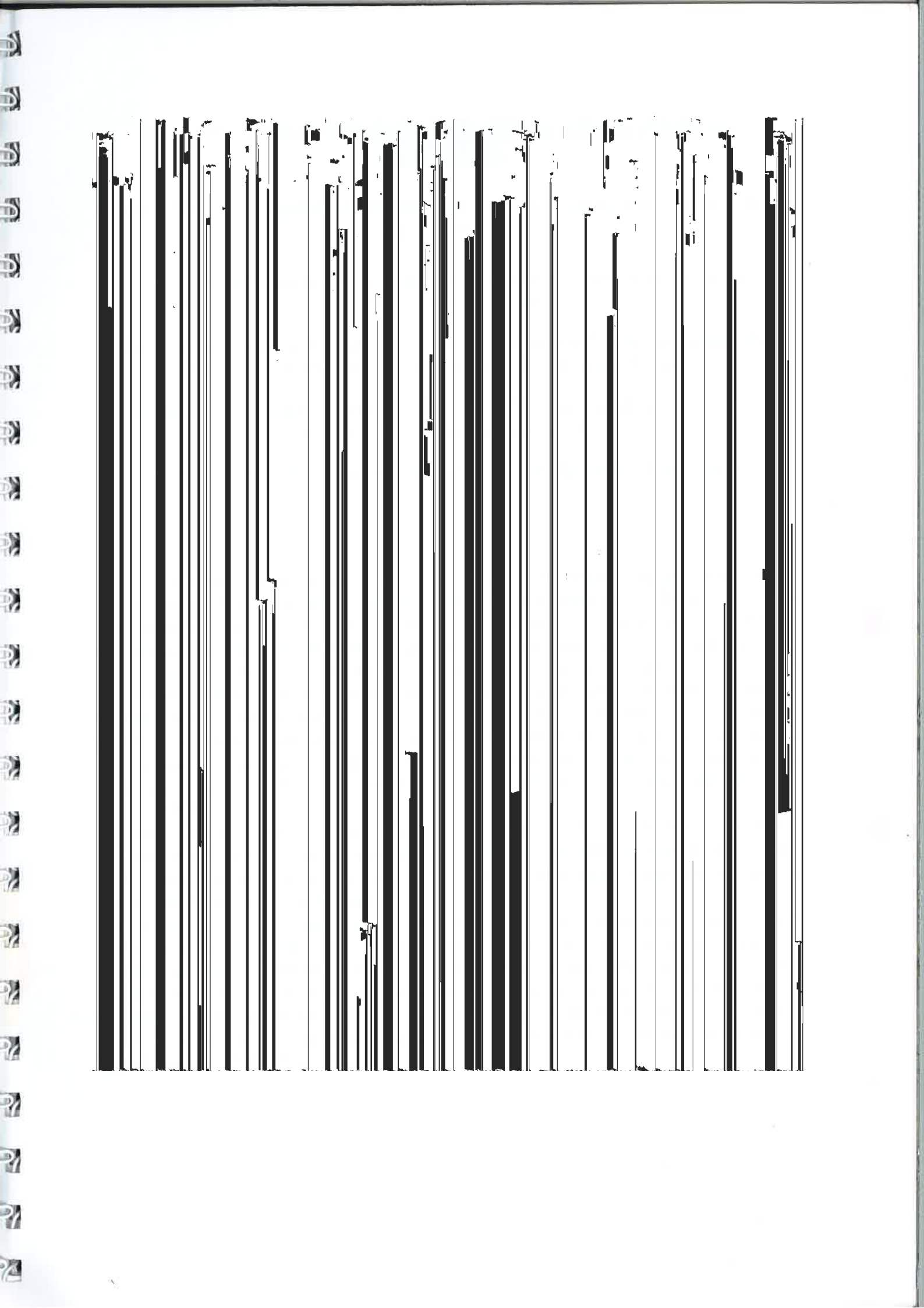
Date and time of submission:

Dec 15, 2014 6:15 PM CET

Sincerely,

Deutsche Keramische Gesellschaft e. V.

(German ceramic society)



Adsorption of pharmaceutical compounds on carbons of different morphologies

MARQUES, Susana C¹; MARCUZZO, Jossano S²; MESTRE, Ana Sofia³; DIAS, Ricardo⁴; ANIA, Conchi O⁵; CARVALHO, Ana Paula³

¹ Centro de Química e Bioquímica, Faculdade de Ciências, Universidade de Lisboa, Portugal; Center for Biodiversity, Functional & Integrative Genomics, Lisboa, Portugal; ² Faculdade de Tecnologia do Estado de São Paulo FATEC, Brasil; ³ Centro de Química e Bioquímica, Faculdade de Ciências, Universidade de Lisboa, Portugal; ⁴ Center for Biodiversity, Functional & Integrative Genomics, Lisboa, Portugal; ⁵ Instituto Nacional del Carbón, Oviedo, Spain

Presenter

Prof. Dr
Carvalho, Ana Paula
ana.carvalho@fc.ul.pt

Organization/Company

Faculdade de Ciências da Universidade de Lisboa
Centro de Química e Bioquímica

Campo Grande
1749-016 Lisboa
Portugal

Subject

Environmental and Medical Applications

Keywords

Activated carbon cloth, regeneration, paracetamol, clofibrac, liquid phase adsorption

Reference key

1 / 70

One of the main environmental problems affecting public health is aquatic environment contamination. Pharmaceutical compounds are considered emergent pollutants that have been detected in all sorts of water streams all over the world. Acetaminophen and clofibrac acid are among the most detected compounds since both are highly consumed medicines continuously introduced in the aquatic media, due to the lack of effectiveness of the conventional water treatment technologies. Advanced wastewater treatments processes, namely those based on adsorption onto activated carbons, can be used to solve this problem. Although these adsorbents are normally employed in granular or powder morphologies, other forms of activated carbons have been developed based on the carbonization and activation of cloths from different polymeric materials, called activated carbon cloths.

The aim of this work was to study the adsorption properties of four activated carbons with different morphologies (powder, granular and cloth) for the removal acetaminophen and clofibrac acid from aqueous solution by kinetic and equilibrium assays. Regeneration cycles at 400 and 600°C were also performed.

The results show that, regarding the adsorption process, the activated carbon cloth performance is comparable only to the powder sample that has a developed mesopore network pointing out the importance of the accessible microporosity present in the cloth. Additionally, cloth morphology has the advantage of, as in the case of granular carbon, allowing thermal regeneration. After three re-use cycles the activated carbon cloth retains ~45% of the adsorption capacity obtained with the fresh sample, while powder sample retains less than 20% of the initial value.



Ciências
ULisboa
Faculdade
de Ciências
da Universidade
de Lisboa

Certificado de Participação

Susana Cristina Roque Marques participou no CQB Day 2015 que decorreu
a 15 de Setembro de 2015 onde apresentou a comunicação em painel
com o título Adsorption of pharmaceutical compounds on
carbons of different morphologies

Comissão Organizadora

Centro
de Química e Bioquímica
FCUL

Ana Paula Carvalho

Ana Paula Carvalho

CQB-Day 2015



RESÚMENES DE LA XIII REUNIÓN DEL GRUPO ESPAÑOL DEL CARBÓN

Este libro contiene los resúmenes de las diferentes contribuciones presentadas en la "XIII Reunión del Grupo Español del Carbón" en Octubre de 2015 en Alicante.

El contenido del libro ha sido organizado en cuatro partes: (i) Conferencias plenarias; (ii) Orales; (iii) Premio GEC a Jóvenes Investigadores; (iv) Pósters. Las distintas comunicaciones se han organizado según las seis temáticas que abarca el congreso: (1) Generación sostenible de energía; (2) Preparación y caracterización de materiales de carbón; (3) Nanomateriales, grafeno y materiales carbonosos avanzados; (4) Aplicaciones en adsorción y catálisis; (5) Aplicaciones en generación y almacenamiento de energía y (6) Aplicaciones medioambientales.

Teniendo en cuenta que los resúmenes que contiene el presente volumen incluyen los últimos avances de los diferentes equipos de investigación vinculados al "Grupo Español del Carbón", este libro constituye un manual muy interesante para profundizar en el carbón y los materiales de carbono, y en especial en todos aquellos aspectos relacionados con sus múltiples aplicaciones, destacándose las energéticas y medioambientales, entre otras.



Libro de resúmenes

XIII REUNIÓN DEL GRUPO ESPAÑOL DEL CARBÓN

XIII Reunión

Grupo Español del Carbón

ALICANTE

2015



grupo español del carbón



Universitat d'Alacant
Universidad de Alicante
Departamento de Química Inorgánica
Instituto Universitario de Materiales

REMOVAL OF OXYTETRACYCLINE CHLORIDE BY POROUS CARBON MATERIALS

S. Marques^{1,2}, A.S. Mestre¹, R. Dias², A.Z. Gotvajn³, A.P. Carvalho¹

¹ Centro de Química e Bioquímica, Faculdade de Ciências, Universidade de Lisboa, 1749-016 Lisboa, Portugal

² Microbiology and Biotechnology Lab, Center for Biodiversity, Functional & Integrative Genomics, Edifício ICAT, Campo Grande 1749-016 Lisboa, Portugal.

³ Faculty of Chemistry and Chemical Technology, University of Ljubljana, Slovenia
scmarques@fc.ul.pt

Key-words: Oxytetracycline chloride, carbon materials, adsorption, wastewater.

Introduction

Wastewater pollution by antibiotics, namely tetracyclines, has proved to be a serious problem due to their difficult degradation/removal and their very dangerous adverse effects. Adsorption onto carbon materials provides a simple and efficient way to eliminate these contaminants. However the major drawbacks for a more extensive use of these adsorbents are a poor economic feasibility and short lifetime, often due to low and expensive regeneration capacities. The search for low-cost adsorbent made from largely available resources is then a valid strategy that continues to attract the scientific community. This methodology can also contribute to solve the problem of waste disposal and recycling.

The aim of this work is to merge these two issues studying the removal of oxytetracycline chloride (OTC) from aqueous solution using commercial and two lab-made carbons prepared from cork and apple tree bark residues.

Experimental

Sample S800 was obtained from pre-treated cork activated with steam at 90 °C, carried by a N₂ flow (8 cm³ s⁻¹), at 800 °C with a heating rate of 10 °C min⁻¹ for 1 h. The carbon was milled and sieved being collected the fraction with particle size lower than 0.297 mm. To prepare sample A800, the char of apple tree bark was impregnated with K₂CO₃ solution in a weight proportion of 1:3, at room temperature. After drying, the sample was activated at 800 °C for 1 h under N₂ flow of 5 cm³ s⁻¹ (heating rate 10 °C min⁻¹). After cooling under N₂ flow, the sample was washed with distilled water until pH 7, dried overnight at 100 °C and stored.

The materials were characterized by N₂ and CO₂ adsorption isotherms at, respectively, -196 and 0 °C, and determination of the pH at the point of zero charge (pH_{PZC}).

Liquid phase kinetic assays were made adding 9 cm³ of OTC solution (120 mg dm⁻³) to 6 mg of carbon, at 30 °C. Samples were collected at different contact times and the quantification of OTC in solution was determined by UV-Vis spectrophotometry. Equilibrium studies were made varying the carbon dose (3.0-6.7 mg), solution volume (9-30 cm³) and adsorbate initial concentration (20-180 mg dm⁻³) considering an equilibrium time of 24 h.

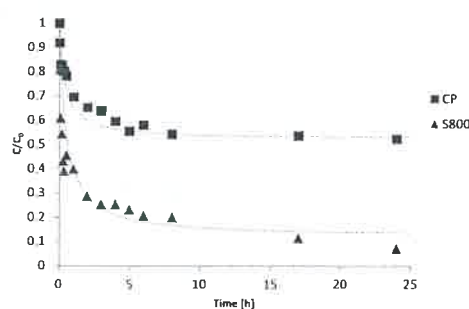
Results and Discussion

Carbons S800 and A800 have well developed porosity (Table 1), comparable to the commercial carbons CP and VP. All but sample A800 are basic carbons, and regarding porous structure the most significant difference is the mesopore volume: almost inexistent in A800 and CP, but reaching almost 50% of the total pore volume in carbon S800.

Table 1. Nanotextural properties and pH_{PZC} of the carbons.

	A_{BET} ($\text{m}^2 \text{g}^{-1}$)	$V_{\text{total}}^{\text{a}}$ ($\text{cm}^3 \text{g}^{-1}$)	$V_{\text{meso}}^{\text{b}}$ ($\text{cm}^3 \text{g}^{-1}$)	α_s method			pH_{PZC}
				$V_{\alpha \text{ total}}$ ($\text{cm}^3 \text{g}^{-1}$)	$V_{\alpha \text{ ultra}}$ ($\text{cm}^3 \text{g}^{-1}$)	$V_{\alpha \text{ super}}$ ($\text{cm}^3 \text{g}^{-1}$)	
CP	907	0.43	0.03	0.40	0.16	0.24	10.3
VP	758	0.43	0.13	0.30	0.15	0.15	9.8
S800	750	0.50	0.22	0.28	0.09	0.19	> 11.3
A800	1169	0.53	0.01	0.52	0.27	0.25	5.5

^a N_2 volume adsorbed at $p/p^0 = 0.95$; ^b $V_{\text{meso}} = V_{\text{total}} - V_{\alpha \text{ total}}$.

**Figure 1.** Kinetic profile of OTC adsorption at 30 °C on the mentioned samples.**Table 2.** Langmuir and Freundlich equations parameters for OTC adsorption by the carbons.

	S800	CP
<i>Langmuir</i>		
q_m (mg g^{-1})	305.2	88.94
K_L ($\text{dm}^3 \text{mg}^{-1}$)	0.095	0.607
R^2	0.986	0.985
<i>Freundlich</i>		
$1/n$	0.271	0.054
K_F ($\text{mg}^{1-1/n} (\text{dm}^3)^{1/n} \text{g}^{-1}$)	78.2	68.2
R^2	0.947	0.238

The results obtained with carbons S800 and CP (Fig. 1 and Table 2) exemplify the performance of these set of carbons for the adsorption of OTC from aqueous solutions. Kinetic results suggest that mesopore volume is the main factor responsible for the removal efficiency of the samples, but other parameter must rule the adsorption rate since despite its high V_{meso} , sample S800 reaches equilibrium only after 24 h against the 8 h required for sample CP. The importance of the mesoporosity for the adsorption of OTC is also demonstrated by equilibrium results (Table 2). In fact, following the sequence of V_{meso} , the monolayer capacity values are $q_m(\text{S800})=3.5q_m(\text{CP})$. Regarding affinity between carbons surface and OTC, the higher K_L value of CP carbon points out that the presence of a large supermicropore network plays an important role in the adsorption. A deeper analysis of the parameters ruling the OTC adsorption mechanism will be made considering the performance of samples VP and A800.

Acknowledgements

The authors thank FCT for the project UID/MULTI/00612/2013 to CQB and for fellowships to SM (SFRH/BD/91767/2012) and ASM (SFRH/BPD/86693/2012). Quimitejo (CP and VP) and Amorim Isolamentos (cork precursor) are also acknowledged for supplying samples.

References

- [1] Bhatnagar A., Sillanpaa M. Utilization of agro-industrial and municipal waste materials as potential adsorbents for water treatment. *Chemical Engineering Journal* 2010;157;277-296.
- [2] Sun Y., Yue Q., Gao B., Wang Y., Gao Y., Li Q. Preparation of highly developed mesoporous activated carbon by $\text{H}_2\text{P}_2\text{O}_7$ activation and its adsorption behavior for oxytetracycline. *Powder Technology* 2014; 249; 54-62.



El Comité Organizador de la
XIII Reunión del Grupo Español del Carbón
celebrada en
Alicante del 18 al 21 Octubre 2015

CERTIFICA

que

SUSANA CRISTINA MARQUES

asistió a la Reunión

Dolores Lozano Castelló

Presidenta

6º CONGRESSO BRASILEIRO DE CARBONO

arbono 2015

24 a 27 de novembro de 2015

Hotel Comfort Suítes Vitória

Vitória - ES



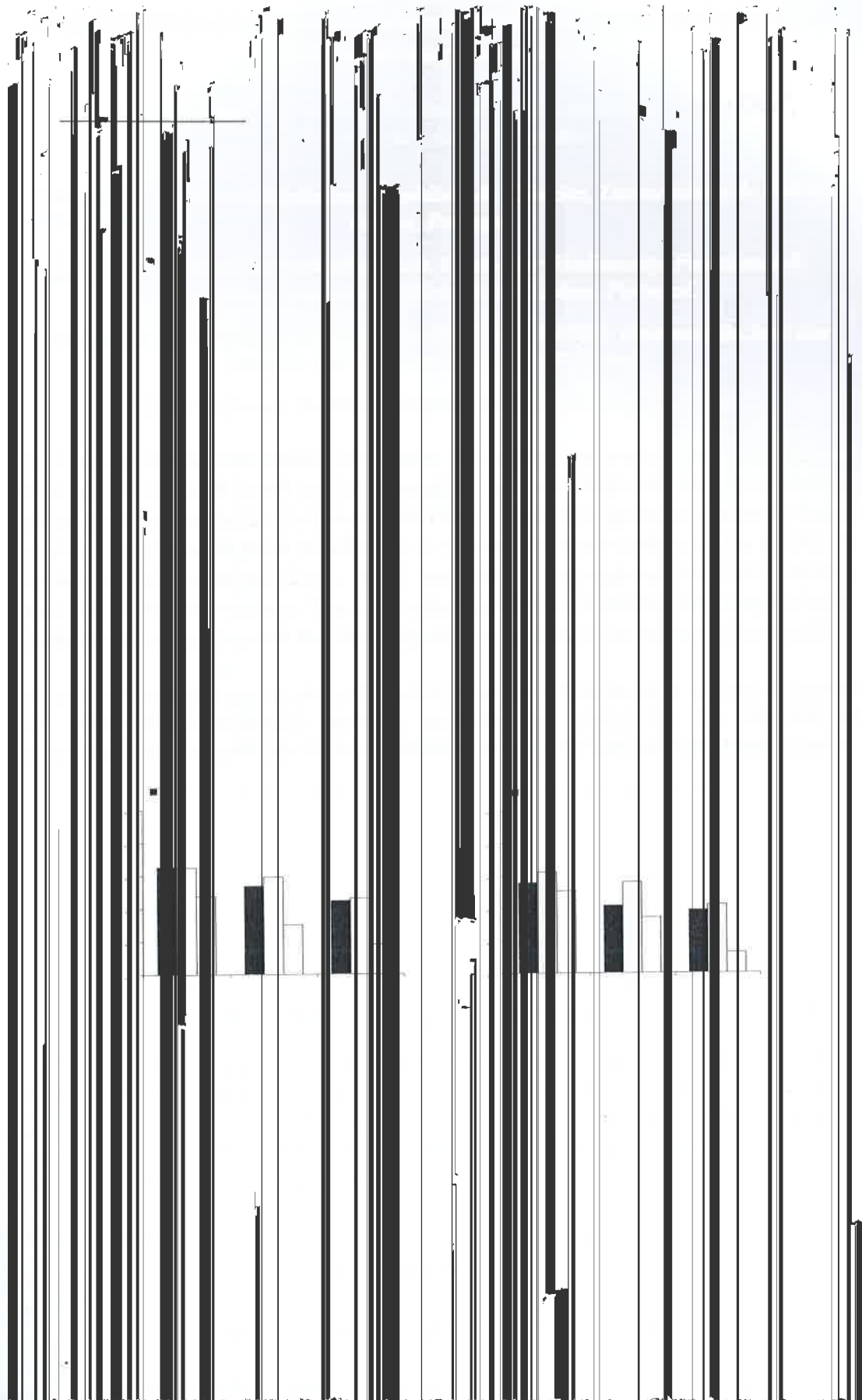
Programação e Resumos

Organização:



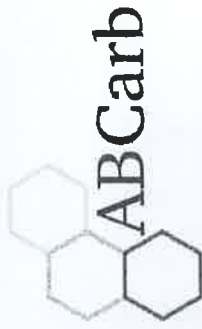
UFES





Carbono
2015

6º Congresso Brasileiro
de Carbono



Certificado

Certificamos que o trabalho

Regeneration of acetaminophen exhausted activated carbons with different morphologies
dos autores

Susana C. Marques, Jossano S. Marcuzzo, Ana S. Mestre, Ricardo Dias,

Conchi O. Ania, Ana P. Carvalho

foi apresentado na forma de pôster no 6º Congresso Brasileiro de Carbono, realizado em Vitória,
Espírito Santo, no período de 24 a 27 de Novembro de 2015.

F. C. Emmerich

Prof. Dr. Francisco G. Emmerich
Comissão Organizadora

Luiz Depine de Castro

Prof. Dr. Luiz Depine de Castro
Presidente da ABCarb

NEW INSIGHTS ON THE IMMOBILIZATION MECHANISM OF *ESCHERICHIA COLI* ONTO ACTIVATED CARBONS

Susana Marques^{1,2}, Marta Pacheco², Jossano Marcuzzo³, Ana S. Mestre¹, Ricardo Dias²,
and Ana P. Carvalho¹

¹*Centro de Química e Bioquímica, Faculdade de Ciências, Universidade de Lisboa,
1749-016 Lisboa, Portugal*

²*Microbiology and Biotechnology Lab, Center for Biodiversity, Functional & Integrative
Genomics, Edifício ICAT, Campo Grande 1749-016 Lisboa, Portugal*

³*Faculdade de Tecnologia do Estado de São Paulo FATEC- Campus São José dos Campos,
12247-014 – São José dos Campos –SP- Brasil*

Adsorption on activated carbons is a well-established method used in water treatment to remove numerous pollutants. Microorganisms present in water can become immobilized in the adsorbent, possibly affecting the adsorption process. As new forms of adsorbents ~~become known~~ are developed, it is important to understand the impact of these materials' properties in the mechanism of bacteria immobilization, to conclude about the possible advantages of using these new materials in water treatment purposes.

In this work, the influence of the adsorbent morphology (granular, powder and cloth), texture and superficial chemistry in the immobilization of *E. coli* cells in aqueous media was investigated.

The results indicate that favorable electrostatic interactions carbon surface-cells is a key factor in bacteria immobilization by activated carbons that must be complemented by its morphology and textural characteristics. Thus using basic carbons, electron microscopy results revealed that powder morphology allows the formation of agglomerates carbon-cell-cell-carbon. In the case of granular and cloth samples the data already obtained suggest that, in an initial stage, individual cells adhere to the external surface of the carbon particles (more efficiently in cloth morphology). Further assays, considering different cellular densities and the simultaneous presence of pharmaceutical compounds in the aqueous medium are being performed.

Adsorption of pharmaceutical compounds onto activated carbon cloth

Susana C. R. Marques^{a,b}, Jossano M. Marcuzzo^c, Ana S. Mestre^a, Ricardo Dias^b, Ana P. Carvalho^a

^a*Centro de Química e Bioquímica, Faculdade de Ciências, Universidade de Lisboa, 1749-016 Lisboa, Portugal.*

^b*Microbiology and Biotechnology Lab, Center for Biodiversity, Functional & Integrative Genomics, Edifício ICAT, Campo Grande 1749-016 Lisboa.*

^c*Faculdade de Tecnologia do Estado de São Paulo FATEC-Campus São José dos Campos, 12247-014 – São José dos Campos – SP – Brasil.*

scrmarques@fc.ul.pt

1. Introduction

Pharmaceuticals are compounds with biological activity, developed to promote human health and well being. Because a considerable amount of these compounds is excreted by our body un-metabolized, a variety of these chemicals, including painkillers, tranquilizers and antibiotics, are finding their way into the environment (Bolong *et al.* 2009; Sauvé & Desrosiers 2014; Taylor & Senac 2014; Rivera-Utrilla *et al.* 2013).

The recent inclusion of some pharmaceutical compounds detected in the aquatic environment in the Watch List of 2013/39/EU directive reveals that this issue, a concern for a long time to the scientific community, is now also calling the attention of legislative authorities.

Among the most detected pharmaceuticals, paracetamol and clofibric acid removal in water treatment has become a priority due to their detection in all sorts of water around the world, their high consumption and possible long-term impact in human health. Paracetamol is one of the most consumed analgesic and antipyretic medicines worldwide, being a major ingredient in numerous cold and flu remedies. Because of its solubility in water, it is frequently detected in the aquatic environment (Carvalho *et al.* 2012, Gómez *et al.* 2007, Gracia-Lor *et al.* 2011). Clofibric acid is the metabolite and active principle of several blood lipid regulators, considered a potential endocrine disruptor and is nowadays regarded as one of the most persistent drug residues in the environment (Khetan & Collins 2007, Heberer 2002). This pollutant was first detected in 1976 in raw and treated sewage waters at concentrations up to $2 \mu\text{g L}^{-1}$, confirmed a year later by its detection in the effluent of a sewage treatment plant in Kansas City, USA (Garrison *et al.* 1976; Hignite & Azamoff 1977). In 1993, the monitorization of ground water for acidic herbicides in the Berlin area, uncovered the presence of this chemical, detected a year later in ground, river and tap water.

Over the last decades, activated carbons (ACs) have been employed in a wide number of applications on an industrial scale, including technologies for the removal of organic pollutants from water (i.e., purification of drinking water and wastewater) (Ania, Parra, *et al.*, 2005; Bolong, Ismail, *et al.*, 2009). Eventually, these adsorbents reach their saturation limit and no longer adsorb the targeted pollutants. In many cases, the saturated carbon would simply be disposed in a landfill or incinerated. However, the incineration of these materials also contributes to air pollution as well as the discarded AC which may leach into the water becoming a secondary source of pollution. Thus, the possibility of

CQB-day 2016

June 28th



Book of Abstracts

CQB-Day 2016

June 28th

Faculdade de Ciências – Universidade de Lisboa



Ciências
ULisboa

Faculdade
de Ciências
da Universidade
de Lisboa

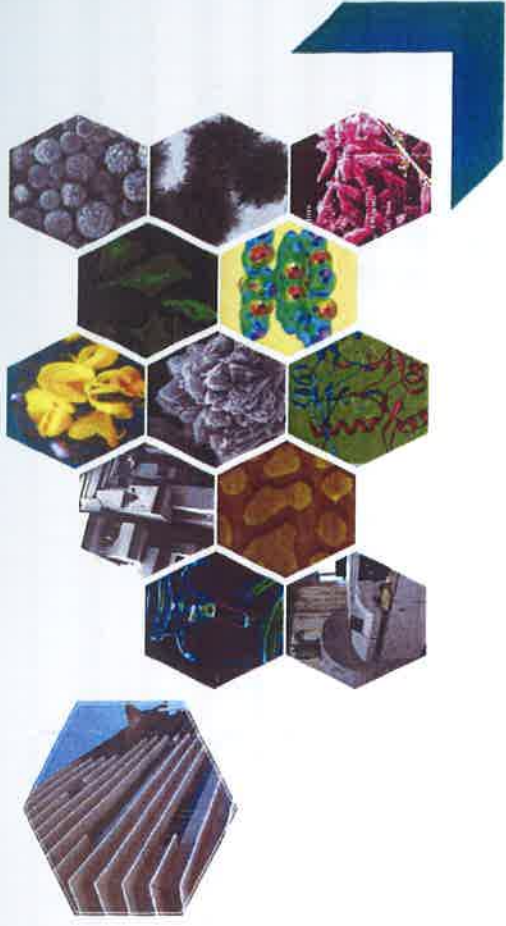


FCT

Fundação para a Ciência e a Tecnologia

INSTITUTO DE CIÊNCIAS DE LISBOA

CQBday
June 28th



Certificado de Participação

Susana Cristina Roque Marques participou no CQB day 2016, onde apresentou a comunicação oral com o título ***New Insights on the Immobilization Mechanism of Escherichia Coli onto Activated Carbons.***

P' Comissão organizadora

Ana Cristina Palmeira Loureiros

Ana Mourato



✓

“Designing” porous networks for water treatment: Removal of atenolol and antibiotics by activated carbons

Susana Marques^{a*}, Stephane Gonçalves^b, Ana S. Mestre^a, Andreja Z. Gotvajn, Ana P. Carvalho^a

^aCentro de Química e Bioquímica, Faculdade de Ciências, Universidade de Lisboa, 1749-016 Lisboa, Portugal

^bUniversité Pierre et Marie Curie – 4 Place Jussieu, 7500 Paris, France

^cFaculty of Chemistry and Chemical Technology, University of Ljubljana, Slovenia

*scmarques@fc.ul.pt

Continuous release of antibiotics into the environment could exert pressure on ecosystem by developing microbial antibiotic resistance leading to public health important issues. These drugs are only partially absorbed by the body, reaching domestic wastewater and, since the conventional wastewater treatment processes are ineffective in removing these compounds, they are continuously introduced in the aquatic system [1-3]. To solve this problem, advanced technologies, such as adsorption onto carbon materials, have been developed. However, high cost restricts the application of these materials, boosting researchers to explore the preparation of carbons from waste materials or renewable sources [4].

The objective of this work was to prepare activated carbons from the char of apple tree bark residues and evaluating the influence of different experimental conditions in the textural properties of the materials. Selected samples were tested as adsorbents of a β -blocker medicine (atenolol), and two antibiotics (tiamulin fumarate and oxytetracycline hydrochloride).

Acknowledgements

The authors thank FCT, Portugal, for financial support to CQB center (Project UID/MULTI/00612/2013) and fellowships to SM (SFRH/BBD/91767/2012) and ASM (SFRH/BPD/86693/2012). Salmon & Cia (Norit) and Quimitejo are also acknowledged by kindly supplying of the commercial carbon samples.

REFERENCES

- [1] A.M. Pereira, L.J. Silva, L.M. Meisel, A. Pena, *J Toxicol Env Health* 78 (2015) 959-975.
- [2] J. L. Sotelo, A. Rodriguez, S. Álvarez, J. Garcia, *Int J Environ Res* 6(4) (2012) 961-968.
- [3] M. Pomorska-Mól, C Kowalski, *J Liq Chromatogr R T* 32 (2009) 1023-1031.
- [4] A.S. Mestre, E. Tyszko, M.A. Andrade, M. Galhetas, C. Freire, A. P. Carvalho, *RSC Adv* 5 (2015) 19696-19707.

Common fundamentals, remarkably versatile applications

CARBON

July
10-15

2016

Program



The World Conference on Carbon

The Penn Stater Conference Center Hotel
State College, Pennsylvania, USA



PennState

S10: Porous Carbons

²University of Bordeaux, France

³Federal University of Parana, Brazi

⁴FGV Cambridge Nanosystems, Cambridge, United Kingdom.

P3-93

DESULFURIZATION ORIENTED SURFACE MOLECULARLY IMPRINTED POLYMERS BASED ON ORDERED MESOPOROUS CARBON NANOSPHERES

Lei Qin^{1,2}, Xiaofeng Zhao^{1,2}, Yongzhen Yang^{1,3}, and Xuguang Liu^{1,2}

¹Key Laboratory of Interface Science and Engineering in Advanced Materials, Ministry of Education, Taiyuan University of Technology, Taiyuan 030024, China

²College of Chemistry and Chemical Engineering, Taiyuan University of Technology, Taiyuan 030024, China

³Research Center of Advanced Materials Science and Technology, Taiyuan University of Technology, Taiyuan 030024, China.

P3-94

MECHANICALLY IMPROVED CARBON FOAM DERIVED FROM MELAMINE FOAM AND ITS APPLICATIONS AS FLEXIBLE ELECTRODE

Ming Liu¹, Liying Zhang¹, Yujie Song², Yushan Tay² and Xiao Hu²

¹Temaasek Laboratories @NTU, Nanyang Technological University, 50 Nanyang Drive, Singapore

²School of Materials Science and Engineering, Nanyang Technological University, 50 Nanyang Avenue, Singapore.

P3-95

NEW INSIGHTS ON THE IMMOBILIZATION MECHANISM OF *ESCHERICHIA COLI* ONTO ACTIVATED CARBONS

Susana Marques^{1,2}, Marta Pacheco², Jossano Marcuzzo³, Ana S. Mestre¹, Ricardo Dias², and Ana P. Carvalho¹

¹Centro de Química e Bioquímica, Faculdade de Ciências, Universidade de Lisboa, 1749-016 Lisboa, Portugal

²Instituto de Biosistemas & Ciências Integrativas, Faculdade de Ciências, Universidade de Lisboa, 1749-016 Lisboa, Portugal

³Faculdade de Tecnologia do Estado de São Paulo FATEC - Campus São José dos Campos, 12247-014 - São José dos Campos, SP Brasil.

P3-96

POROSITY AND MORPHOLOGY TRANSFORMATIONS OF PITTSBURGH No. 8 COAL CHAR IN CO₂ GASIFICATION UNDER PORE DIFFUSION LIMITATION

Bowarnrat Thanasattayaviboon and Jonathan P. Mathews

The Leone Department of Energy and Mineral Engineering, and The EMS Energy Institute, The Pennsylvania State University, United States.

P3-97

TAILORED DESIGN OF 3D HIERARCHICALLY POROUS CARBON FROM METAL- OXOCARBON ANION COORDINATION COMPLEXES

Christian Mbaya Mani, Thomas Berthold, Markus Antonietti, Nina Fechner

Max Planck Institute of Colloids and Interfaces, Department of Colloid Chemistry, Am Mühlenberg 1, 14476 Potsdam, Germany.



Influence of the morphology

Figure 3 illustrates the removal rates of *E. coli* with the cloth, powder and granular carbons. Because the porosity of these carbons is inaccessible to these bacteria, and their surface chemistry is similar, these assays allow to infer about the influence of the activated carbon morphology in *E. coli* removal. The results prove NS to be again the most effective material, followed by the ACC, with removal rates of, respectively, 100 % and approximately 80 %. These carbons allow a much faster removal of *E. coli* than GAC. Since these carbons have similar surface chemistry, the results suggest a significant impact of morphology in this process. The structure of ACC was analyzed by SEM (**Figure 4**), revealing that the sample is composed by yarns of cylindrical shape, with average diameter of 20 μm and the average distance between yarns being higher than a 100 μm .

In order to better understand the underlying mechanism, possibly through immobilization, responsible by the removal rates achieved with NS carbon, the dispersion of different amounts of this carbon in cellular suspension was analyzed by optical microscopy (**Figure 5**). The images obtained at amplifications of 40, 400 \times show a good dispersion of this carbon in cellular suspension (1×10^8 cells/ml of solution) and suggest the formation of agglomerates carbon-cell-cell-carbon, possible due to electrostatic interactions between NS superficial groups and *E. coli* cell wall. The formation of these structures allows the immobilization of a higher number of cells, besides the ones attached only to the carbon. This phenomenon seems to be favored by higher amounts of NS, which form agglomerates of higher volume, entrapping higher number of cells. Thus, despite ACC structure having a very accessible surface area, with high distance between yarns, *E. coli* immobilization is more efficient in the powder carbon, where electrostatic interactions carbon-bacteria seem to be favored and complemented by the formation of agglomerates carbon-cell-cell-carbon.

ACKNOWLEDGMENT

The authors thank FCT, Portugal, for financial support to CQB center (Project UID/MULTI/00612/2013) and fellowships to SM (SFRH/BD/91767/2012) and ASM (SFRH/BPD/86693/2012). Salmon & Cia (Norit) is also acknowledged by kindly supplying of the commercial carbon sample.

REFERENCES

1. T.J. Bandosz (Eds.), *Academic Press*, 2006.
2. Cukierman, A.L. (2013). *ISRN Chem Eng* (DOI: 10.1155/2013/261523)
3. Paruch, A.M. (2011). *Water Sci Technol.* 63, 558-564.
4. Veglio, F. and Beolchini, F. (1997). *Hydrometallurgy* 44, 301-316.
5. Bai, X. *et al.* (2015). *Sci Total Environ* 533, 24-31.
6. Rivera-Utrilla, J., *et al* (2001). *J Chem Technol Biotechnol* 76, 1209-1215.
7. Edberg, S.C., *et al.* (2000). *J Appl Microbiol.* 88(S6), 106-116.
8. Boehm, H.P. (1994). *Carbon* 32(5), 759-769.
9. Mestre, A.S. *et al.* (2007). *Carbon* 45, 1979-1988.
10. Sing, K.S.W., *Pro. Int Symp., 1970.*

Table 1. Nanotextural properties and pH_{PZC} of the carbons.

Carbon	A_{BET} ($m^2 g^{-1}$)	V_{total}^a ($cm^3 g^{-1}$)	V_{meso}^b ($cm^3 g^{-1}$)	V_{micro}^c ($cm^3 g^{-1}$)	pH_{PZC}
ACC	1300	0.59	0.06	0.53	9.0
NS	1065	0.70	0.31	0.40	8.4
NSox	856	0.52	0.22	0.36	3.7
GAC	838	0.47	0.13	0.34	8.9
GACm	917	0.52	0.16	0.36	8.9

^a N_2 volume adsorbed at $p/p^0 = 0.95$; ^b $V_{meso} = V_{total} - V_{micro}$; ^c V_{micro} evaluated by α_S method [10].

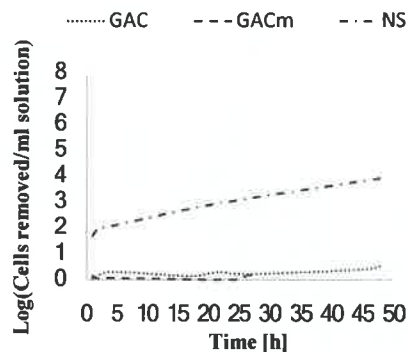


Figure 1. Effect of carbon particle size on *E. coli* removal, in STD water.

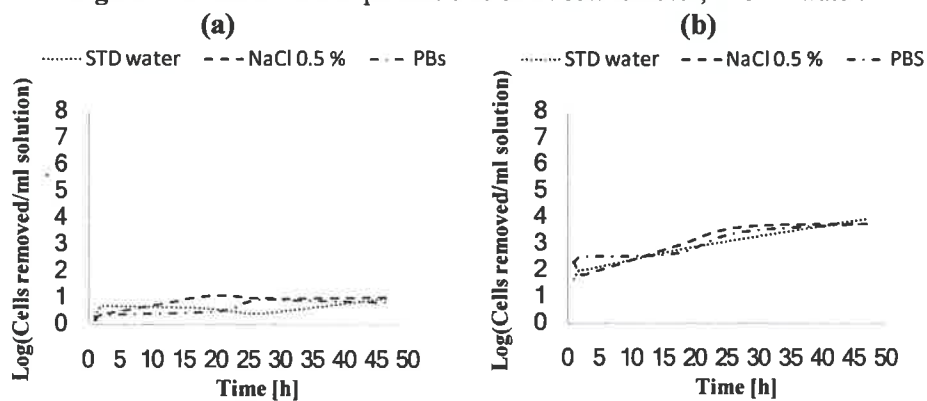


Figure 2. Effect of solution chemical composition impact on *E. coli* removal from solution by (a) 10 mg and (b) 15 mg of NS.

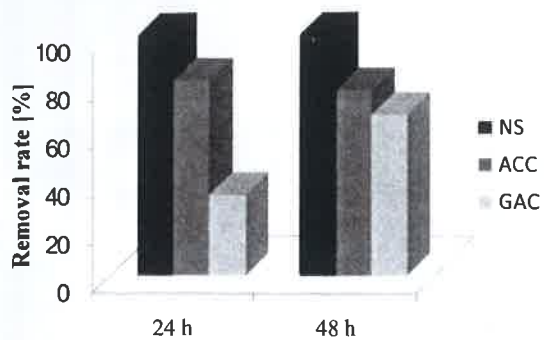


Figure 3. Removal rates (%) after 24 and 48 h, with powder, cloth and granular carbons, in STD water.

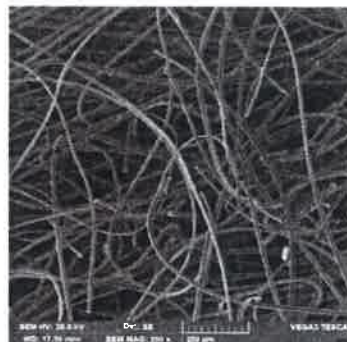


Figure 4. SEM micrograph of ACC carbon with magnification factor of 200x.

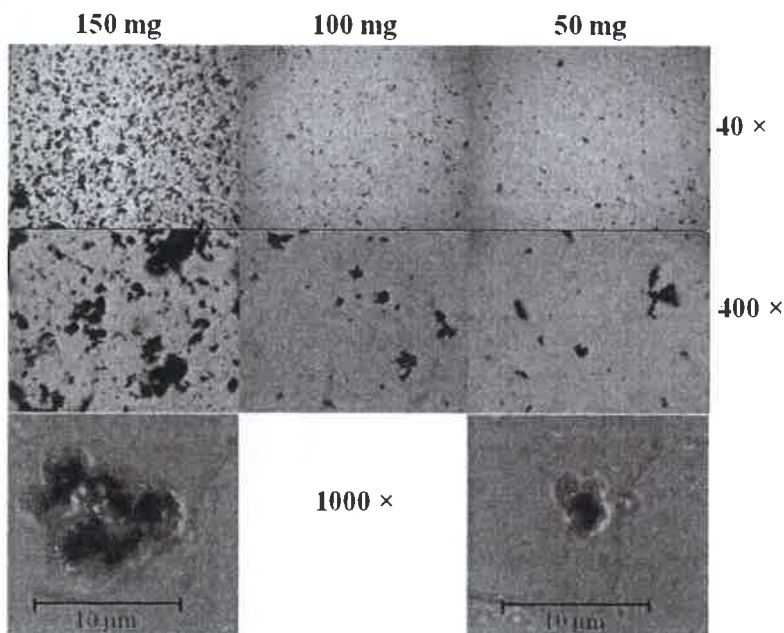


Figure 5. Optical microscopy of NS carbon in cellular suspensions standardized at 1×10^8 cells/ml, viewed with amplifications of 40, 400 and 1000x.



UNIVERSIDADE DE ÉVORA

40^a REUNIÃO IBÉRICA DE ADSORÇÃO

5 a 7 SETEMBRO 2016 | ÉVORA | PORTUGAL



LIVRO DE RESUMOS

- **Surface chemistry** through equilibrium assays with samples NS and NSox (basic and acidic nature, respectively).

The results presented correspond to average values obtained through, at least, two or three experimental assays.

Phase-contrast microscopy

The NS dispersion in aqueous solution, cell-carbon, and cell-cell interactions were analyzed by phase-contrast microscopy (Leica) in cellular suspension 1×10^8 cells/ml using amplifications of 40, 400 and 1000 \times .

RESULTS AND DISCUSSION

Carbons properties

The activated carbons tested present high apparent surface area, A_{BET} , and developed porosity (high value of V_{total}), being the porosity mainly formed by micropores (**Table 1**). All the samples have basic nature, with exception of sample NSox, which as consequence of the oxidation treatment presents a pH_{PZC} of 3.7.

Bacterial removal

Effect of particle size

The results of *E. coli* removal assays, performed onto the carbons GAC, GACm and NS (**Figure 1**), show that bacteria removal is favored in NS carbon. This carbon effectiveness appears to be due to its smallest particle size and high external surface area, since *E. coli* cells dimensions (average length of 2.5 μm and diameter of 1 μm) do not allow them to have access to the carbons' pore network.

Effect of surface chemistry

The role of the carbons' surface chemistry was studied through assays with NS and NSox samples. These carbons are both powder, with the same particle size and similar porosity, but different surface chemistry: NS is a basic carbon (pH_{PZC} value of 8.4) and NSox has acidic nature (pH_{PZC} value of 3.7). Results show that NSox, on the contrary of NS, did not remove any cells from aqueous solution. This may be because, at the aqueous solution pH (approximately 7), NSox has a negatively charged surface, as does *E. coli* cell, a gram-negative bacteria. This shows that favorable electrostatic interactions are a crucial first step to the removal process.

Influence of the solution chemical composition

The assays were made with carbon NS using different amounts in 1×10^8 CFU/ml cellular suspensions of STD water, NaCl 0.5 % and PBS. **Figure 2 (a)** and **(b)** illustrate *E. coli* removal profiles correspondent to the experiments with 10 and 150 mg of carbon, respectively. In both systems, similar results were obtained for all the solvents. After 48 h, 10 mg of NS remove approximately 10 CFU/ml of solution, whereas the highest amount used was able to remove approximately 1×10^2 CFU/ml of solution after 24 h of contact time, in a slow and progressive kinetic process.

✓

40ª REUNIÃO IBÉRICA DE ADSORÇÃO

LIVRO DE RESUMOS

Universidade de Évora

Título: 40ª Reunião Ibérica de Adsorção – Livro de Resumos

Editores: Manuela Ribeiro Carrott e Peter Carrott

Design da Capa: Gabinete de Comunicação da Universidade de Évora

Impressão: Reprografia da Universidade de Évora

Tiragem: 100 exemplares

ISBN: 978-989-8550-34-7

Depósito Legal nº 414298/16

Síntesis y Caracterización de un Polímero Poroso de Coordinación Compuesto por Hierro y Ácido Gálico	25
A. Briz, J.M. Oliva, M.J. Sayagués, S. Calero, A.P. Zaderenko	
Preparation of Activated Carbons from Apple Tree Bark Char for Water Treatment	27
Susana Marques, Ana S. Mestre, Andreja Z. Gotvajn, Ana P. Carvalho	
Equilibrio y Cinética de Adsorción de n-Parafinas de Cadena Larga sobre Zeolita 5A	29
V.I. Águeda, M.A. Uguina, J.A. Delgado, M.T. Holik, D. Aranda, I.D. López, J.J. Lázaro, J. Peláez	
Adsorción de N₂, Ar, O₂, CH₄ e H₂ a 77 K para la Caracterización Textural de Materiales Mesoporosos	31
Jhonny Villarroel-Rocha, Deicy Barrera, Karim Sapag	
Adsorption: the Key in Response Surface Methodology for the Synthesis of Bespoke Carbon Xerogels	33
Natalia Rey-Raap, J. Angel Menéndez, Ana Arenillas	
Zeolites as Sieves for Butene Isomers Separation	35
Ana Martín-Calvo, Sofía Calero	
Preparación de Adsorbentes Carbonosos a partir de Plástico Industrial. Adsorción de Solutos en Disolución	37
Juan Manuel Ladera López, María Alexandre Franco, Carmen Fernández González, Manuel Alfaro Domínguez, Vicente Gómez Serrano	
Hollow Silica Microspheres Functionalized with TEPA for the CO₂ Capture at High Temperature	39
E. Vilarrasa García, J.A. Cecilia, C. García Sancho, R.M.A. Saboya, C.L. Cavalcante Jr., D.C.S. Azevedo, E. Rodríguez Castellón	
Experimental Realization of Single-Column Batch Chromatography with Recycle Lag	41
Abimaelle Silva Chibério, Luís Grossinho Dias da Silva, Snežana Reljić, Rui P.P.L. Ribeiro, Ricardo J.S. Silva, José P.B. Mota	
Physical Activation of Wood Pellets for CO₂ Selective Adsorption	43
J.F. Vivo-Vilches, A.F. Pérez-Cadenas, F.J. Maldonado-Hódar, F. Carrasco-Marín, R.P.V. Faria, A.M. Ribeiro, A.F.P. Ferreira, A.E. Rodrigues	
Enhancement of the Photochemical Conversion Tuning the Surface Chemistry and Structure of Nanoporous Carbons	45
Alicia Gomis-Berenguer, Jesús Iniesta, João C. Lima, Conchi O. Ania	
Chemical Warfare Agents S- and R-Sarin Isomers Adsorption and Separation in Chiral Metal-Organic Frameworks	47
Francisco D. Lahoz-Martín, Ana Martín-Calvo, Sofía Calero	

Preparation of Activated Carbons from Apple Tree Bark Char for Water Treatment

Susana Marques^{a*}, Ana S. Mestre^a, Andreja Z. Gotvajn^b, Ana P. Carvalho^a

^a*Centro de Química e Bioquímica, Faculdade de Ciências, Universidade de Lisboa, 1749-016 Lisboa, Portugal*

^b*Faculty of Chemistry and Chemical Technology, University of Ljubljana, Slovenia*

**scrmarques@fc.ul.pt*

Introduction

Nowadays, an increasing number of pharmaceuticals is used for the treatment and prevention of various diseases. These drugs are only partially absorbed by the body, reaching domestic wastewater and, since the conventional water treatment processes are ineffective in removing these compounds, they are continuously introduced in the aquatic system [1]. To solve this problem, advanced technologies, such as adsorption onto carbon materials, have been developed. However, there are still improvements to be made in order to make their application more economic and efficient [2]. One way to achieve this goal is to produce adsorbents from biomass wastes under optimized conditions to maximize their performance as adsorbents of recalcitrant compounds.

The objective of this work was to prepare activated carbons from the char of apple tree bark residues, evaluating the influence of different experimental conditions in the textural properties of the materials. Selected samples were tested as adsorbents of a β -blocker medicine (atenolol) and a veterinary antibiotic (tiamulin fumarate).

Materials and Methods

The activated carbons were produced by impregnation of apple tree bark char, with K_2CO_3 and KOH solutions in the weight proportions of 1:3, at room temperature. The dried samples were activated at 800 °C for 1, 2, and 3 h under N_2 flow of $5 \text{ cm}^3 \text{ s}^{-1}$ (heating rate $10 \text{ }^\circ\text{C min}^{-1}$), then cooled down under N_2 flow. The samples were finally washed with distilled water until pH 7, dried overnight at 100 °C and stored. The obtained carbon samples are designated by activated agent (C, for K_2CO_3 , and H, for KOH)A800/activation time (h).

The materials were characterized by N_2 (ASAP 2010 from Micromeritics) and CO_2 (conventional volumetric apparatus, equipped with an MKS-Baratron 310BHS-100 pressure sensor) adsorption isotherms at, respectively, -196 and 0 °C. The pH at the point of zero charge (pH_{PZC}) was also determined, using a microelectrode (Symphony SP70P pH Meter) following the reversed mass titration procedure.

The removal efficiency of the pharmaceuticals was studied adding 20 cm^3 of pollutant solution (120 mg dm^{-3}) to 6 mg of carbon (30 °C). Samples were collected after 18 h of contact time, and quantification of remaining solute was made by UV-Vis spectrophotometry. For comparison purposes, powdered commercial carbons used in water treatment were also tested (CP – ChiemiVall CCP 900, NS – Norit NSAE Super).

Results and Discussion

exclusively by micropores. In any case the micropore volume is higher than those presented by the commercial samples but one of the commercial samples has a large mesopore structure that is absent in the lab-made carbons (Table 1).

The samples produced with KOH have A_{BET} values higher than $2000 \text{ m}^2 \text{ g}^{-1}$, being the microporosity mainly (and for longer treatments exclusively) composed by supermicropores. The activation with K_2CO_3 produced carbons with less developed porosity (lower values of A_{BET} and V_{total}). As it was already reported for other precursors [2] this activating agent enables a more controllable development of the porosity than what is observed with KOH, thus allowing to "design" the micropore network of the final samples. Regarding the activation yield is interesting to notice that with exception of sample HA800/1 all the other materials present values around 40 %. The lab-made samples have a pH_{PZC} value of 5.5, whereas the commercial carbons are basic (10.3 and 8.4 for CP and NS, respectively).

Table 1. Nanotextural properties of the lab-made and commercial activated carbons. Activation yield (η) of the lab-made samples also presented.

Sample	A_{BET} ($\text{m}^2 \text{ g}^{-1}$)	$V_{\text{total}}^{\text{a}}$ ($\text{cm}^3 \text{ g}^{-1}$)	$V_{\text{meso}}^{\text{b}}$ ($\text{cm}^3 \text{ g}^{-1}$)	Method α_s			η^{c} (%)
				$V_{\alpha \text{ total}}$ ($\text{cm}^3 \text{ g}^{-1}$)	$V_{\alpha \text{ ultra}}$ ($\text{cm}^3 \text{ g}^{-1}$)	$V_{\alpha \text{ super}}$ ($\text{cm}^3 \text{ g}^{-1}$)	
HA800/1	2029	0.93	0.05	0.88	0.12	0.76	46
HA800/2	2345	1.14	0.08	1.06	0.00	1.06	38
HA800/3	2445	1.24	0.08	1.16	0.00	1.16	22
CA800/1	1169	0.48	0.01	0.52	0.27	0.25	44
CA800/2	1455	0.69	0.06	0.64	0.15	0.49	42
CA800/3	1900	0.91	0.08	0.83	0.09	0.74	38
CP	907	0.43	0.03	0.40	0.16	0.24	-
NS	1065	0.70	0.30	0.40	0.02	0.38	-

^a N_2 volume adsorbed at $p/p^0 = 0.95$; ^b $V_{\text{meso}} = V_{\text{total}} - V_{\alpha \text{ total}}$; ^c Activation yield.

The data concerning atenolol adsorption showed that lab-made carbons are highly efficient since removal efficiencies $\approx 90 \%$ were attained against 62 % obtained with commercial samples. The better performance of the lab-made activated carbons is most likely due to their high volume of supermicropores. The study will proceed in order to obtain kinetic and equilibrium data for atenolol and also tiamulin fumarate adsorption.

Acknowledgements

The authors thank FCT for the project UID/MULTI/00612/2013 to CQB and for fellowships to SM (SFRH/BD/91767/2012) and ASM (SFRH/BPD/86693/2012). Quimitejo and Salmon & Cia are also acknowledged for kindly supplying the carbons CP and NS, respectively.

References

1. Beek, T.; Weber, F.; Bergamn, A.; Hickmann, S.; Ebert, I.; Hein, A.; Küster, A. J. Hazard. Mat. 282 (2015) 141-149.
2. Mestre, A.S.; Tyszko, E.; Andrade, M.A.; Galhetas, M.; Freire, C.; Carvaho, A.P. RSC Adv. 5 (2015) 19696-19707.



UNIVERSIDADE DE ÉVORA



5 a 7 SETEMBRO 2016 | ÉVORA | PORTUGAL
www.40ria.uevora.pt

40ª RIA

40ª REUNIÃO IBÉRICA DE ADSORÇÃO

CERTIFICADO

Certifica-se que

Susana Marques

participou na 40ª Reunião Ibérica de Adsorção, que decorreu nos dias 5, 6 e 7 de setembro de 2016, na Universidade de Évora, e apresentou a Comunicação Oral intitulada "Preparation of activated carbons from apple tree bark for water treatment".

A Comissão Organizadora

Marta Rosta

✓

Appendix D

Publications in international
journals with scientific arbitrage



Pharmaceuticals removal by activated carbons: Role of morphology on cyclic thermal regeneration



Susana C.R. Marques^a, Jossano M. Marcuzzo^b, Mauricio R. Baldan^b, Ana S. Mestre^a, Ana P. Carvalho^{a,*}

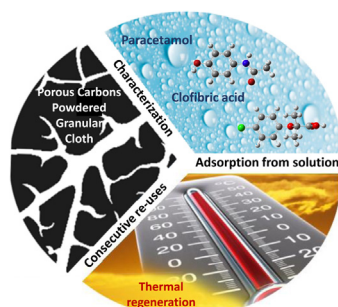
^a Centro de Química e Bioquímica, Faculdade de Ciências, Universidade de Lisboa, 1749-016 Lisboa, Portugal

^b Instituto Nacional de Pesquisas Espaciais – INPE, São José dos Campos, SP, Brazil

HIGHLIGHTS

- Cloth, granular and powder carbons were tested as adsorbents of paracetamol and clofibric acid.
- Adsorption mechanism of both compounds is ruled by the carbons' supermicropores volume.
- Higher and quicker removal of the pollutants are achieved with cloth and powder samples.
- Thermal regeneration cloth and granular carbons at 400 °C recovered high paracetamol uptake.

GRAPHICAL ABSTRACT



ARTICLE INFO

Article history:

Received 9 January 2017
Received in revised form 21 March 2017
Accepted 22 March 2017
Available online 23 March 2017

Keywords:

Activated carbon
Morphology
Paracetamol
Clofibric acid
Adsorption from solution
Thermal regeneration

ABSTRACT

This work aims to evaluate the performance of activated carbons as reusable adsorbents of pharmaceutical compounds. To achieve this objective, the behaviour of carbons with different morphologies (powdered, granular and cloth) in the adsorption of paracetamol and clofibric acid from aqueous solution was studied; as well as the thermal regeneration of paracetamol saturated activated carbons at 400 and 600 °C. For that, the properties of the carbon materials were characterized by N₂ and CO₂ adsorption, pH_{PZC}, XPS, TG, XRD and SEM. Kinetic results showed the importance of supermicropore volume for the diffusion of the probe molecules towards the adsorption active sites, and the negative effect of granular form which led to significantly lower adsorption rates. Paracetamol adsorption followed a Langmuir mechanism in almost all cases, whereas clofibric acid adsorption generally occurred through a more complex mechanism. This behaviour was explained considering the nature of the clofibric acid species present in solution. This compound was always the most adsorbed molecule, reaching a maximum adsorption capacity of ~500 mg dm⁻³ in the case of carbon cloth.

Thermal regeneration proved to be an efficient methodology to recover the porosity of the granular and cloth paracetamol exhausted activated carbons. After the second regeneration treatment at 400 °C both activated carbons retained around 57% of their initial paracetamol uptake.

The conjugation of the adsorption and regeneration results pointed out the benefits of the carbon cloth (in felt form) morphology which, being an easy handling sample, gathered the performance of the best powdered sample assayed in adsorption experiments, with the behaviour of granular carbon upon regeneration.

© 2017 Elsevier B.V. All rights reserved.

* Corresponding author.

E-mail address: ana.carvalho@fc.ul.pt (A.P. Carvalho).

1. Introduction

Pharmaceuticals are compounds with biological activity, developed to promote human health and well-being. Nevertheless, only a fraction of the pharmaceutical active compound present in, for example, a painkiller tablet, is metabolized by the organism. Therefore, a great amount of medicines is excreted, finding their way into the environment, as it is demonstrated in several monitoring studies [1–6]. For the scientific community the detection of pharmaceutical compounds in several sort of water bodies is a long time recognized problem [7], and the recent inclusion of some medicines (namely diclofenac) in the Watch List of 2015/495/EU directive reveals that this issue is now calling the attention of legislative authorities [8].

The present study is focused on paracetamol and clofibrac acid which are among the most detected pharmaceutical compounds in the aquatic environment. Paracetamol is one of the most consumed analgesic and antipyretic medicines worldwide, being a major ingredient in numerous cold and flu tablets formulation. Because of its relatively high solubility in water, it is frequently detected in the aquatic environment [9–11]. Clofibrac acid is the metabolite and active principle of several blood lipid regulators, being considered a potential endocrine disruptor; it is nowadays regarded as one of the most persistent drug residues in the environment [12,13]. The first data regarding the detection of this pollutant were reported in the 70's when it was found in raw and treated wastewater at concentrations up to $2 \mu\text{g dm}^{-3}$ [14,15]. In 1993, this chemical was detected in groundwater, in the Berlin area and, a year later, its presence was confirmed in ground, river and even in tap water [16].

Activated carbons are versatile adsorbent materials that have been employed in a large number of industrial processes, including technologies for the removal of organic pollutants from water (*i.e.*, purification of drinking water and wastewater treatment) [1,17,18]. This thematic has been explored by our research group in several studies regarding the preparation and use of biomass derived activated carbons which proved to be efficient adsorbents for the removal of various pharmaceutical compounds from aqueous solutions [19–23].

When activated carbons reach their saturation limit they fail to adsorb the targeted pollutants. The exhausted materials are, in many cases, simply disposed in a landfill or incinerated. However, aiming to a more sustainable society, and to prevent environmental contaminations, the regeneration of these materials has become an important issue both from academic and industrial perspectives, as well as from an economic point of view. In this context, companies like Cabot-Norit provide reactivation of granular activated carbons through a thermal treatment of the exhausted material [24].

Besides thermal regeneration [25–28] other regeneration procedures have been proposed in the literature, such as, desorption induced by microwave radiation [29,30], solvent extraction [31], and by chemical and catalytic decomposition [26], or microbial processes [32]. The most attractive option is the one that gathers the best compromise among the cost, the regeneration efficiency and the number of saturation-regeneration cycles that allows the recovery of a considerable degree of carbon's porosity.

Thermal treatment is the most used method for regeneration of activated carbons due to its simplicity and versatility since, as mentioned above, it consists in heating the exhausted carbon, usually under inert atmosphere, to degrade the adsorbate and so recover the largest possible fraction of the porosity. However, it must be stressed that the choice of the more adequate operational conditions to perform regeneration depends on the system formed by carbon and pollutant(s). In the literature, there are several studies in this thematic, as for example those developed by Ledesma

et al. [27], and by Sabio *et al.* [28] both focused on the regeneration of granular carbons exhausted with *p*-nitrophenol. Ledesma *et al.* [27] promoted five regeneration cycles by heating the exhausted samples at 900 °C which caused a progressive and accentuated loss of the textural properties. Sabio *et al.* [28] extended the study to more moderated temperatures (300–800 °C) promoting only a single regeneration cycle. The results showed that temperatures lower than 500 °C led to less efficient recoveries of the *p*-nitrophenol uptake. The best result was obtained with 800 °C, allowing the recovery of 75% of the initial *p*-nitrophenol uptake.

Considering the regeneration of activated carbons exhausted with pharmaceutical compounds, fewer studies are available in literature. Examples are the works developed by Ania and co-workers over carbons exhausted with salicylic acid which were submitted to 6 regeneration cycles of microwave assisted treatment [30], or thermal treatment at 850 °C [25]. In this last case the final sample retained half of the salicylic acid capacity of the fresh sample. More recently, Batista *et al.* [33] reported the regeneration of rapeseed derived carbons exhausted with caffeine through regeneration at 400, 500 and 600 °C demonstrating that after two regeneration cycles for 1 h, at the highest temperature, around 95% of the initial adsorption capacity for caffeine was recovered.

To the best of our knowledge the studies focused on the thermal regeneration process of carbons are made over only one type of morphology, generally, powder [25,33,34] or granular [27–29] carbons. However, as the regeneration of exhausted activated carbons is becoming a reality in several processes, and carbons with novel morphologies have improved performances in industrial processes, to evaluate the role of the carbons morphology on the feasibility of the regeneration process is of fundamental importance. So, in the present study the performance of activated carbons with different morphologies – granular, powdered and cloth (felt form) – for the adsorption of two pharmaceutical compounds (clofibrac acid and paracetamol) was evaluated. Consecutive re-uses of thermal regenerated paracetamol exhausted carbons were also addressed to evaluate not only the impact of the heating temperature but also to shed light on the influence of sample morphology in the regeneration process.

2. Materials and methods

2.1. Activated carbons

The lab-made activated carbon felt, herein named Activated Carbon Cloth, ACC, was prepared from 5.0dtex polyacrylonitrile (PAN) heavy tow textile fibers following the procedure detailed described in Ref. 35. Briefly, the textile fibers were submitted to a two-step air thermal oxidation process in a laboratory scale oven that operate at temperatures between 200 and 300 °C. The oxidized textile PAN fiber was converted in felt form by standard textile process. The oxidized PAN fiber in felt form was then carbonized and activated in the same electrical furnace. In the first step the material was carbonized under argon flow at 900 °C for 20 min (heating ramp $30 \text{ }^\circ\text{C min}^{-1}$). For the activation the argon gas was shifted to CO_2 and the temperature rised at $30 \text{ }^\circ\text{C min}^{-1}$ up to 1000 °C, this temperature was maintained during 50 min. In parallel with this sample three activated carbons commonly used in wastewater treatment were also assayed:

- NS, powdered carbon commercialized by Norit as SAE SUPER, with 97% (wt./wt.) of particles with dimensions $<0.15 \text{ mm}$.
- VP, powdered carbon V Plus from ChiemiVall, obtained by steam activation of pine wood. According to the technical report 90% of the particles are smaller than the $n^\circ 325$ US Standard Sieve, *i.e.*, smaller than $44 \mu\text{m}$.

– GAC, granular carbon prepared by steam activation of coal with 88% (wt./wt.) of particles with dimensions between 0.60 mm and 2.36 mm. It is commercialized by Norit as GAC830 as being particularly suitable for thermal regeneration, like it is reported in the company website [36].

2.2. Characterization of the activated carbons

The nanotexture of the carbon materials was characterized by N_2 and CO_2 adsorption at -196 and 0 °C, respectively. The N_2 adsorption assays were carried out in an automatic volumetric apparatus (ASAP 2010 from Micromeritics), and CO_2 adsorption isotherms were obtained in a conventional volumetric installation, equipped with a pressure sensor MKS-Baratron 310BHS-1000 (0–133 kPa). Before the experiments, the samples (~ 50 mg) were outgassed for 17 h at 120 °C, under vacuum better than 10^{-2} Pa.

The surface chemistry of the carbon cloth sample was characterized determining the pH of the point of zero charge, pH_{PZC} , following the procedure reported by Babić *et al.* [37]. Solutions of KNO_3 (0.01 mol dm^{-3}) with initial pH ranging from 2 to 12 were prepared mixing different volumes of KOH and HNO_3 (0.1 mol dm^{-3}) solutions. A volume of 10 cm^3 of each of the KNO_3 solutions prepared was added to 50 mg of ACC, in different vials. After introducing a magnetic stir, the vials were sealed under N_2 atmosphere and stirred at 700 rpm, for 24 h. The pH_{PZC} value of ACC was obtained from the back-extrapolation of the plateau defined in the graphic of final vs initial pH values. The surface groups were also characterized by X-ray photoelectron spectroscopy (XPS). The measurements were carried out in a Kratos Axis Ultra XPS spectrometer using a monochromatic Al-K α (1486.5 eV) X-ray radiation. The emitted photoelectrons were detected using a hemispherical analyzer and 15 μm spatial resolution. The vacuum system was maintained at approximately 10^{-7} Pa during all the experiments. Survey scans were collected from 0 to 1200 eV with 160 eV pass energy and step size of 1 eV, in order to identify the elements present on the surface, and a pass energy of 40 eV for high resolution scans on specific atomic peaks (280–300 eV and 525–543 eV). For calibration purposes C 1s band (284.6 eV) was taken as internal standard. The deconvolution of the XPS spectra was made using Casa XPS software considering a non-linear least square fitting. Before deconvolution a Shirley type background subtraction was made.

The surface morphology of ACC was analyzed by scanning electron microscopy in a NovaNanoSEM400 equipment using an accelerating voltage of 20 kV.

The ash content of the carbons was determined following the procedure described in ASTM D2866 [38]. The mineral matter obtained after total carbon matrix consumption was characterized by X-ray powder diffraction (XRD) using a Pan' Analytical PW3050/60X'Pert PRO ($\theta/2\theta$) equipped with X'Pert Data Collector detector software) using a monochromatized CuK α radiation as incident beam, 40 kV–30 mA. The diffractograms were obtained at room temperature by continuous scanning in a 2θ range of 15 – 40° with a step size of $0.017^\circ 2\theta$ and a time per step of 20 s.

2.3. Liquid phase adsorption assays

The target molecules selected for the liquid phase assays were paracetamol (Aldrich, Lot. 535764-326, purity 98%), and clofibrac acid (Alfa Aesar GmbH & Co., KG (Lot. G1266B)). All the solutions were prepared using ultra-pure water obtained from Milli-Q water purification system. The solutions were used as prepared, that is, without pH adjustment, presenting pH values around 5 and 3 units, for paracetamol and clofibrac acid, respectively.

To study the adsorption kinetics, a volume of 20 cm^3 of solution (initial concentration 120 $mg\ dm^{-3}$) was added to approximately

6 mg of adsorbent in glass vials. A magnetic stir bar was introduced, the vials sealed and placed in a thermostatic bath at 30 °C (Eurotherm 2216 L), stirring at 700 rpm in a multipoint agitation plate (Variomag Multipoint). Samples were collected between 1 min and 24 h. After filtration, the amount of adsorbate remaining in solution was determined by UV-Vis spectrophotometry (Genesys 10S) at its maximum absorbance wavelength (243 nm for paracetamol and 228 nm for clofibrac acid). The adsorbate uptake was calculated according to:

$$q_t = \frac{C_0 - C_t}{W} V \quad (1)$$

where q_t is the amount ($mg\ g^{-1}$) of compound adsorbed at time t . C_0 is the adsorbate initial concentration ($mg\ dm^{-3}$), C_t is the adsorbate concentration at time t ($mg\ dm^{-3}$), V is the volume (dm^3) of the adsorbate solution and W is the weight (g) of dried carbon.

Equilibrium adsorption studies were performed at 30 °C, varying the adsorbent dose (around 3–6 mg), solution volume (9–30 cm^3), and adsorbate initial concentration (20–180 $mg\ dm^{-3}$). After stirring overnight, the concentration of adsorbate in solution at equilibrium (C_e) was determined and the uptake was calculated, using Eq. (1).

Prior to use, the carbons were dried overnight in a ventilated oven at 100 °C, and it must also be mentioned that the assays were made, at least, in duplicate.

2.3.1. Regeneration treatment assays

Regeneration of cloth (ACC), powder (NS) and granular (GAC) carbons was performed on the exhausted samples, obtained by contact with the paracetamol solution (180 $mg\ dm^{-3}$) using the proportion of approximately 6 mg of carbon/ 30 cm^3 of solution. After equilibrium, the solids were recovered by filtration and dried at 100 °C for 24 h. To perform the thermal regeneration, the samples were placed in a ceramic boat and heated in a horizontal furnace (Thermolyne, model 21100) at 400 and 600 °C for 1 h, under N_2 flow of 5 $cm^3\ s^{-1}$ (heating rate of 10 °C min^{-1}). After cooled down to room temperature the samples were weighted and re-exhausted using the experimental conditions above mentioned.

To establish the regeneration conditions, thermogravimetric analysis of the exhausted samples was performed on a Setaram Labsys apparatus, under N_2 flow (30 $cm^3\ min^{-1}$) and at a heating rate of 15 °C min^{-1} up to 900 °C. Thermogravimetric analysis of the raw carbon materials and paracetamol were also made in the same experimental conditions.

The efficiency of each regeneration cycle was quantified by the regeneration efficiency, $RE(\%)$, defined as

$$RE(\%) = \frac{q_i}{q_0} \times 100 \quad (2)$$

where q_i is the adsorption capacity of the regenerated carbon in a given i^{th} re-use cycle, and q_0 the adsorption capacity of the fresh carbon.

The textural properties of the pristine samples heated under regeneration conditions, and after the 3^{rd} re-use were assessed by N_2 adsorption data. The fresh carbons submitted to the thermal treatment will be named according to Carbon/Regeneration Temperature (°C), and the samples regenerated after the 3^{rd} re-use cycle will be designated by Carbon exh/Regeneration Temperature (°C).

To evaluate the possible influence of the carbons GAC and NS mineral matter on their performance as adsorbents of paracetamol, the ashes obtained after total consumption of the carbon fraction were tested as adsorbents. The assays were made at 30 °C, for 24 h, using 6 mg of ashes and 30 cm^3 of 180 $mg\ dm^3$ paracetamol solution.

3. Results and discussion

3.1. Characterization of the carbon adsorbents

The N₂ adsorption-desorption isotherms at –196 °C (Fig. 1) reveal the different textural characteristics of the samples. In the case of sample ACC, the curve shows a gradual approach to the plateau which is only observed for $p/p^0 > 0.5$. According to IUPAC classification this is a type I(b) isotherm [39], revealing the presence of a broad pore size distribution in the large micropore and small mesopore range. The configuration of the isotherms obtained with the commercial carbons suggests also the presence of a micro and mesopore network, but in these cases the curves are type I + IV isotherms [39] presenting an upward deviation in the range of high relative pressure, more pronounced in the case of carbon NS denoting a more developed mesopore structure. All commercial samples present small type H4 hysteresis loops [39].

From N₂ adsorption data, the apparent surface area, A_{BET} , was determined using BET equation (in the range $0.05 < p/p^0 < 0.15$) [40]. The microporosity was analyzed applying the α_s method taking as reference the isotherm reported in Ref. 41. With this method, besides the determination total micropore volume, $V_{\alpha \text{ total}}$, the volumes of ultra (width less than 0.7 nm), $V_{\alpha \text{ ultra}}$, and supermicropores (width between 0.7 and 2 nm), $V_{\alpha \text{ super}}$, were also discriminated. The results obtained, as well as the meso, V_{meso} , and total, V_{total} , pore volumes are presented in Table 1 and S1 in Supplementary Information.

The textural parameters reveal that ACC and NS are the adsorbents with higher apparent surface areas. Nonetheless, all the adsorbents have a well-developed micropore network, with $V_{\alpha \text{ total}}$ ranging from $0.30 \text{ cm}^3 \text{ g}^{-1}$ to $0.73 \text{ cm}^3 \text{ g}^{-1}$. On the other hand, with exception of ACC, all other carbons present also relevant mesopore volumes, which in the case of carbon NS attains $0.30 \text{ cm}^3 \text{ g}^{-1}$, corresponding to 44% of the total pore volume of the sample. Regarding microporosity, all the samples have a micropore network composed mainly by supermicropores, with exception of sample VP, which presents equal volumes of narrow and wider micropores ($V_{\alpha \text{ ultra}} = V_{\alpha \text{ super}}$). In sample ACC the microporosity is only composed by supermicropores, and in NS and GAC carbons supermicropore volume corresponds to 95 and 73% of the total micropore volume, respectively.

Further characterization of the carbons' micropore structure was made by CO₂ adsorption isotherms from which micropore size distributions (Fig. 2) were obtained, using the methodology presented in Ref. 42. These results corroborate the previous discussion of the textural parameters obtained from the analysis of N₂ adsorption data, showing that the micropore network of the commercial

Table 1

Nanotextural properties and pH at the point of zero charge (pH_{PZC}) of the carbon cloth sample (ACC).

Parameter	Value
A_{BET} ($\text{m}^2 \text{ g}^{-1}$)	1136
$V_{\text{total}}^{\text{a}}$ ($\text{cm}^3 \text{ g}^{-1}$)	0.76
$V_{\text{meso}}^{\text{b}}$ ($\text{cm}^3 \text{ g}^{-1}$)	0.03
$V_{\alpha \text{ total}}^{\text{c}}$ ($\text{cm}^3 \text{ g}^{-1}$)	0.73
$V_{\alpha \text{ ultra}}^{\text{c}}$ ($\text{cm}^3 \text{ g}^{-1}$)	0.00
$V_{\alpha \text{ super}}^{\text{c}}$ ($\text{cm}^3 \text{ g}^{-1}$)	0.73
pH_{PZC}	9.0

^a N₂ volume adsorbed at $p/p^0 = 0.95$.

^b $V_{\text{meso}} = V_{\text{total}} - V_{\alpha \text{ total}}$.

^c α_s method was applied using as reference the isotherm presented in Ref. 41.

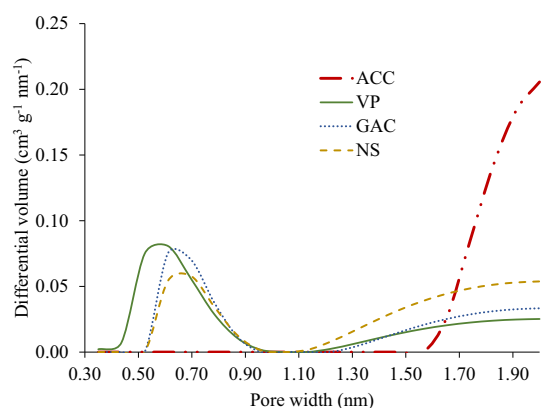


Fig. 2. Micropore size distribution of the mentioned samples obtained from the CO₂ adsorption data at 0 °C, according to the method described by Pinto *et al.* [42].

carbons present both narrow and wider micropores, *i.e.* in all the cases a broad bimodal distribution was obtained. The maximum in the region of narrow micropores is located at 0.61 nm, in the case of carbons VP and around 0.65 nm in the case of GAC and NS. In any case no pores between 0.96 and 1.13 nm are present. Sample ACC has a different micropore size distribution, revealing only the existence of micropores wider than 1.60 nm, which correspond to the highest volume assessed by the CO₂ adsorption, in line with the highest $V_{\alpha \text{ total}}$ value assessed by N₂ adsorption data.

The SEM micrographs of sample ACC reproduced in Fig. 3, show the structure typical of a carbon cloth, as it was expected for a material produced from PAN cloth. The yarns observed present a bean shape, with an average diameter of 21 μm .

Concerning surface chemistry characteristics, the carbons are basic solids with similar pH_{PZC} values (see Table S1 in Supplementary Information), allowing to discard the possibility of different interactions between the adsorbates and the carbon surface as consequence of different surface net charges.

The surface functionalities of samples ACC, NS and GAC were also characterized by XPS. The survey spectra displayed in Fig. S1 in Supplementary Information show that carbon and oxygen are the main elements detected in all the samples. Very small peaks are also noticed in the region between 100 and 200 eV, assigned to the presence of Si and Al, in trace amounts. The surface atomic percentages of carbon and oxygen obtained from the survey spectra are displayed in Table 2 showing that, as expected, carbon is the major component of the samples. Despite these three samples present pH_{PZC} values in a relatively narrow range (8.4–9.0), the amount of oxygen quantified by XPS is comprised between 5.2 and 9.0 atomic%, and the higher oxygen percentage was obtained for the more basic carbon, sample ACC, pointing out that the outer

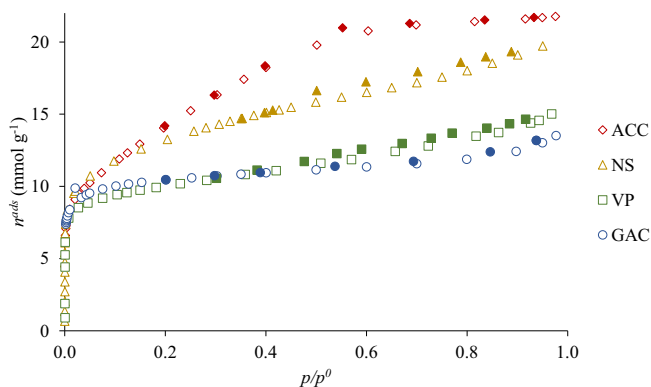


Fig. 1. Nitrogen adsorption-desorption isotherms at –196 °C of the mentioned samples (closed symbols are desorption points).

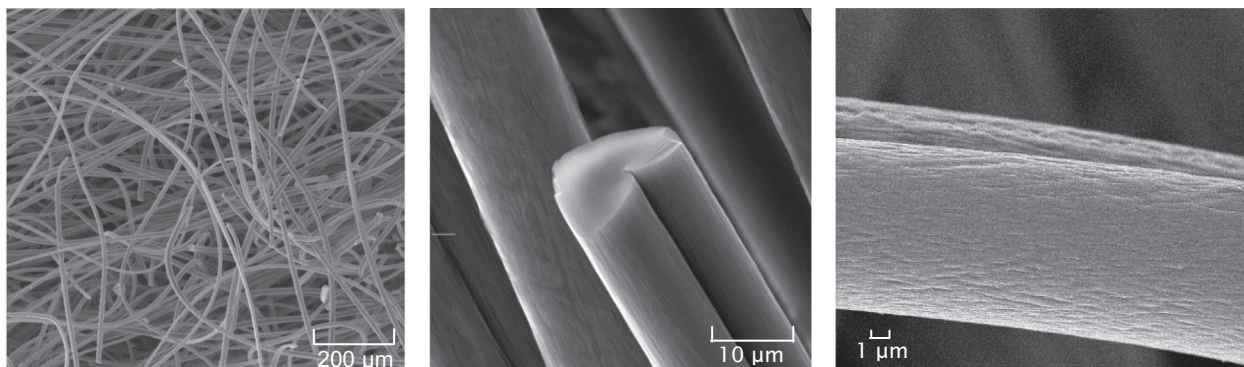


Fig. 3. SEM micrographs of carbon ACC.

Table 2
XPS atomic percentages for samples ACC, NS and GAC.

Sample	Atomic %	
	C 1s	O 1s
ACC	91.0	9.0
NS	93.2	6.8
GAC	94.8	5.2

surface of this carbon particles may present mainly oxygen basic groups.

All high-resolution C 1s spectra (Fig. 4) have asymmetric tailing for high binding energy values which is attributed to the intrinsic asymmetry of the graphitic peak, and to the contribution of oxygen surface complexes [43]. The spectra were deconvoluted considering the peaks of the carbon skeleton and of the oxygen functionalities usually reported in the literature for this type of materials at binding energies around: 284.6–285.1 eV, a main peak assigned to graphitic carbon (sp^2); 286.3–287.0 eV, attributed to alcohol or ether groups (single C–O bond); 287.5–288.1 eV assigned to carbonyl and/or quinone groups (C=O); 289.3–290.0 eV, related to carboxyl or ester groups (COO); and 291.2–292.1 eV, ascribed to shake-up satellite peaks due to π - π^* transitions in aromatic rings [43–45].

The high-resolution O 1s spectra were fitted considering three peaks which are commonly reported in the range of 530.4–530.8 eV (C=O groups), 532.4–533.1 eV (C–O bond in C–OH and/or C–O–C groups), and 534.8–535.6 eV (quimisorbed oxygen and/or water) [44].

The deconvolution of the C 1s spectra reveal differences in the chemistry of the outer surface of the carbon particles. In the spectra of carbons NS and ACC the deconvolution reflected the presence all the expected five peaks while in the case of the granular material the fitting revealed the presence of only four peaks, showing the absence of C=O related to carbonyl and/or quinone functionalities. The deconvolution of the O 1s spectra showed the presence of the three peaks attributed to C=O, C–O and quimisorbed oxygen and/or water. In line with the findings of the C 1s data for GAC sample, the amount of C=O functionalities are considerably smaller than those estimated for the other two samples.

3.2. Liquid phase adsorption

Paracetamol and clofibrac acid were the target molecules selected for the liquid phase assays. The results of the kinetic assays (Fig. 5) show that, in the experimental conditions used, the removal reached 50% in the case of paracetamol, and 80% when clofibrac acid was used.

The adsorption kinetic curves obtained for GAC show that, in comparison with the other carbons, a much slower approach to the equilibrium is observed, which is in line with the granular morphology of this sample. Actually, regardless the pollutant, equilibrium is reached after 6 h of contact time, which was confirmed by the removal after 24 h.

The adsorption onto the powdered (NS and VP) and cloth (ACC) carbons resulted in kinetic curves with similar profiles, revealing a fast adsorption process. The curves show a very marked decay in the first 5 min, after what the adsorption proceed more slowly towards equilibrium which was attained after 1 h, in the case of paracetamol, and 2 h when clofibrac acid was tested. Considering the textural characteristics of these samples, namely the fact that all have high volumes of wider micropores (see Table S1), this was the expected behaviour according to the literature. Actually, in previous studies developed in our research group [21,33,46] it was concluded that, when the samples present important volumes of supermicropores (*i.e.* pores with widths between 0.7 and 2 nm), the presence of a mesopore network does not have an impact in the diffusion of species with small critical dimensions, as is the case of paracetamol and clofibrac acid. In fact, according to the values reported in the literature, the critical dimensions of paracetamol monomer and dimer forms are 0.46 and 0.66 nm, respectively [21], and the critical dimensions of clofibrac acid is 0.70 nm [47], as illustrated in Table S2 of the Supplementary Information. Therefore, no constrains should occur to the adsorption of these molecules in the supermicropore network of the samples.

The kinetic data were fitted to the pseudo-first order kinetic model [48] but the coefficients of determination, R^2 , were very unfavorable. The pseudo-second order model [48] leads to better fittings of the experimental results, with high R^2 values and similar calculated and experimental uptake values ($q_{e \text{ calc}}$ and $q_{e \text{ exp}}$, respectively) (Table 3).

The values of initial rate, h , corroborate the analysis of the kinetic curves configuration since they show that the adsorption of both compounds is a faster process when ACC, NS and VP carbons were used. Actually, in the case of these samples the initial adsorption rate values are two orders of magnitude higher than those obtained for the granular sample (GAC).

The uptake values at equilibrium show that, with exception of carbon GAC, clofibrac acid is always more efficiently removed than paracetamol what may be explained considering the solubility of the compounds, a key factor ruling the adsorption process. The values reported in the literature [22] are 17390 mg dm^{-3} and 755 mg dm^{-3} for paracetamol and clofibrac acid, respectively. Thus, the lower affinity of clofibrac acid towards the solvent, will also favour the interaction with the carbon surface and, consequently its removal.

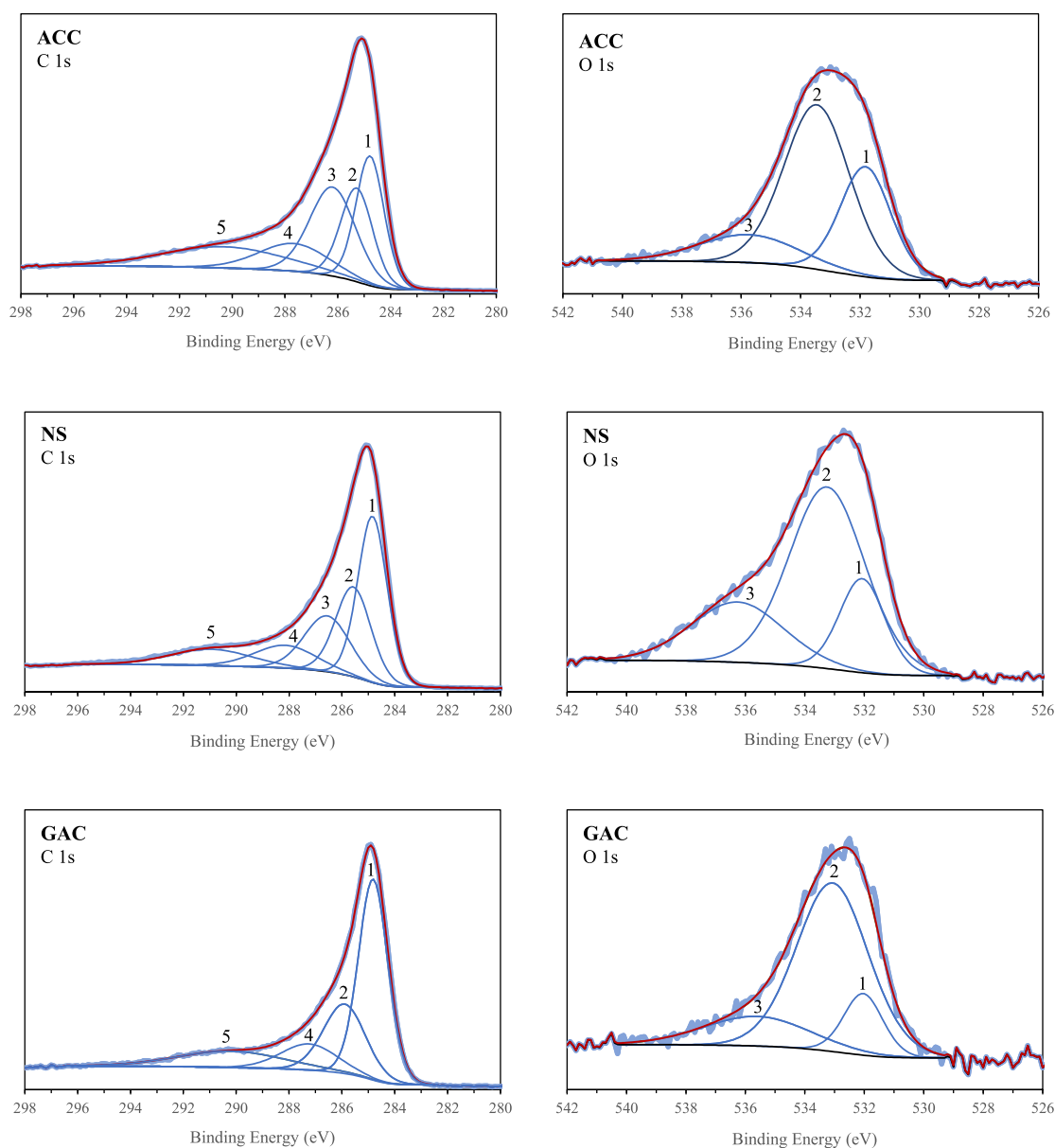


Fig. 4. Deconvoluted high-resolution C 1s (left) and O 1s (right) XPS spectra for the mentioned samples. Peaks in C 1s spectra attributed to graphitic carbon sp^2 (1), alcohols or ether groups (2), carbonyl or quinone groups (3), carboxyl or ester groups (4) and shake-up satellite peak due to π - π^* transitions in aromatic rings (5) [43–45]. Peaks in O 1s spectra attributed to C=O groups (1), C–O groups (2) and chemisorbed oxygen and/or water (3) [43–45].

The equilibrium adsorption data for both compounds at 30 °C (Fig. 6) show that, for all the carbons, clofibric acid is more efficiently adsorbed than paracetamol, most certainly due to its lower solubility that increases the adsorption potential and consequently the partition of the clofibric acid towards the adsorbed phase.

Considering the liquid phase isotherms classification for diluted solution originally proposed by Giles *et al.* [49] and further simplified by Lyklema [50], the curves obtained for paracetamol adsorption can be classified as type L, presenting a relatively well defined initial rise of the paracetamol uptake followed by a horizontal plateau for equilibrium concentrations, C_e , higher than $\sim 40 \text{ mg dm}^{-3}$. In the case of clofibric acid adsorption the isotherm classification is more difficult, since while the data obtained with carbon ACC can be classified as a type L curve, the data obtained with carbon VP is a type F isotherm, due to its less accentuated concavity towards the concentration axis. The curves obtained with samples NS and GAC seem to be a mix of L and F type isotherms. Thus, although an

important increase of the clofibric acid uptake is observed up to C_e values around $40\text{--}60 \text{ mg dm}^{-3}$ – characteristic of L-type curves – afterwards the amount of clofibric acid uptake continues to increase, but more steadily, resembling the curve to a Freundlich isotherm.

The experimental results were fitted to the linear forms of Langmuir [51] and Freundlich [52] models and the resulting parameters are presented in Table 4. The validation of the adjustments was made considering the coefficients of determination (R^2), and complemented by a chi-square test analysis (χ^2).

As it was expected from the analysis of the isotherms configuration, paracetamol equilibrium data is better described by the Langmuir model, *i.e.* higher R^2 and smaller χ^2 values in comparison with those obtained for the fitting to the Freundlich equation. Also in the case of the clofibric acid adsorption, the fitting results corroborate the discussion of the isotherms configuration, showing that the adsorption process onto ACC and VP carbons is clearly best

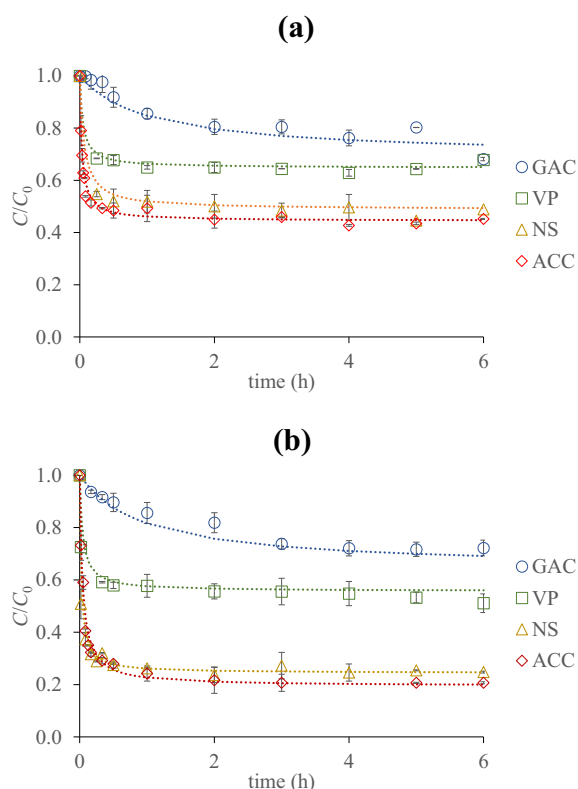


Fig. 5. Kinetic results of (a) paracetamol and (b) clofibrac acid, at 30 °C for the carbon samples (6 mg of carbon for 20 cm³ solution with $C_0 = 120 \text{ mg dm}^{-3}$). Lines show the fitting to pseudo-second order kinetic model.

described by Langmuir and Freundlich equations, respectively. For the other two carbons, NS and GAC, the fitting results indicate a good adjustment to both models, since identical R^2 and χ^2 values are obtained.

Considering the paracetamol monolayer capacity the activated carbons can be ordered $\text{ACC} > \text{NS} > \text{GAC} > \text{VP}$, which coincides with the trend of the total micropore volume of the samples. This type of correlation was observed in previous studies [21,46] and is interpreted considering the dimensions of the paracetamol species (see Table S2 in Supplementary Information) which can access both the narrow and wider micropores. However, if we take into account that the micropore volume of the carbon cloth sample, ACC, is roughly twice the values presented by the other carbons we could expect a much higher value for paracetamol monolayer capacity. This result is most probably due to the fact that the micropore network of this sample presents only pores larger than 1.7 nm (see Fig. 2) which results in an inefficient filling of the porosity, leading to the waste of some pore volume, even if we

consider that paracetamol dimer is the specie present in the monolayer.

The rationalization of the clofibrac acid results implies a different approach because for the majority of the samples the underlying mechanism of the Freundlich model cannot be disregarded. Thus, we opted to compare the carbons performance considering the amount adsorbed at C_e around 120 mg dm^{-3} . The values reveal a trend similar to the one observed for paracetamol monolayer capacities. However due to the critical dimension of this molecule (0.70 nm) we have to consider that the textural parameter ruling the clofibrac acid adsorption mechanism is the volume of the supermicropores, $V_{\alpha \text{ super}}$.

The different behaviour of clofibrac acid, reflected in the isotherms, where a steady approach to the saturation is observed (F-type isotherm), may be related to the fact that in the experimental conditions tested, *i.e.* pH 3, equal fractions of undissociated (neutral) and dissociated (negative) forms of clofibrac acid are present ($\text{p}K_a$ 3.6). At this pH the carbons have a net positively charged surface ($\text{pH} < \text{pH}_{\text{PZC}}$), so we could expect a high affinity of the deprotonated specie towards the surface. However, despite no hindrance to the access of this specie to the pore network is expected, as demonstrated in the literature [23], due to its higher solvation energy the interaction with the carbons surface is shielded. Moreover, a recent study evaluating the influence of water hardness on the adsorption of clofibrac acid onto activated carbons at pH 3 and 8 [47] reported F-type isotherms and higher adsorption capacities at pH 3. Therefore, we can admit that in the experimental conditions used in the present study the adsorption process must rely mainly on the interactions of the undissociated clofibrac molecules with the carbon surface which are of dispersive nature and may allow multilayer adsorption. The steady approach to the saturation can then be rationalized considering that the amount of species that can more effectively interact with the carbon is only a fraction of the total clofibrac acid concentration, which is dependent of the equilibrium between undissociated and dissociated clofibrac acid species. In fact, once the first undissociated species are adsorbed the equilibrium is shifted towards this specie, leading to a progressive increase of the uptake.

3.3. Regeneration by thermal treatment

The regeneration assays were made considering samples ACC, NS and GAC and paracetamol as target compound. To gather more information regarding the characteristics of these materials some complementary assays were made, as it is presented in the following. The results of the ash content determination revealed that carbon ACC is an almost ash free material since the mineral matter is only 0.2% (wt/wt). This result was expected since the XPS basically indicated C1s and O1s. The ash content is 6.9% and 14.0% (wt/wt) for GAC and NS, respectively. Further characterization of the NS and GAC ashes by X-ray diffraction (see Fig. S2 in Supplementary

Table 3

Pseudo-second order parameters for the pharmaceutical compounds adsorption onto the studied carbon samples at 30 °C: k_2 is the pseudo-second order rate constant, h is the initial adsorption rate; $t_{1/2}$ is the half-life time; $q_{e \text{ calc}}$ and $C_e \text{ calc}$ are, respectively, the pharmaceutical compounds uptake and that remaining in solution at equilibrium, both calculated by the pseudo-second order kinetic model, and $q_{e \text{ exp}}$ the experimental uptake value.

	Paracetamol				Clofibrac acid			
	ACC	NS	VP	GAC	ACC	NS	VP	GAC
$k_2 \times 10^{-4} (\text{g mg}^{-1} \text{min}^{-1})$	26	40	40	1	12	23	2	2
$h (\text{mg g}^{-1} \text{min}^{-1})$	130	179	102	2	137	222	72	3
$t_{1/2} (\text{min})$	1.7	1.2	1.7	61	2.4	1.4	2.7	39
$q_{e \text{ calc}} (\text{mg g}^{-1})$	222	217	169	132	333	313	196	115
$q_{e \text{ exp}} (\text{mg g}^{-1})$	218	225	170	143	314	304	186	113
$C_e \text{ calc} (\text{mg dm}^{-3})$	53	52	69	81	20	26	61	86
R^2	0.999	0.999	0.999	0.870	0.999	0.999	0.995	0.992

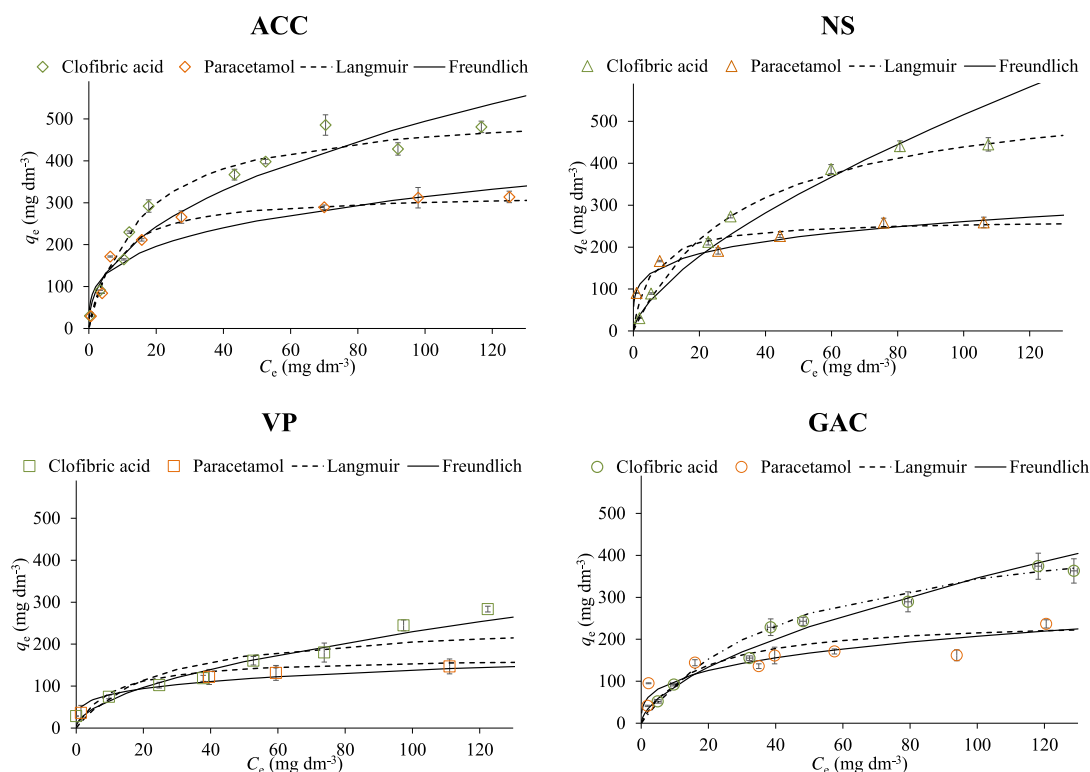


Fig. 6. Equilibrium adsorption isotherms of paracetamol and clofibric acid, at 30 °C. Points represent experimental data while lines correspond to the fitting to Langmuir and Freundlich models. The data concerning the adsorption of paracetamol onto carbons NS and VP were previously reported in Ref. 21 and clofibric acid onto VP in Ref. 47.

Table 4
Langmuir and Freundlich isotherm parameters for the adsorption of paracetamol and clofibric acid adsorption onto the mentioned carbons. Coefficients of determination, R^2 , and chi-square test analysis, χ^2 , for all the fittings. Best fitting for each system is indicated in bold.

	Paracetamol				Clofibric acid			
	ACC	NS ^a	VP ^a	GAC	ACC	NS	VP ^b	GAC
Langmuir equation								
q_m (mg g ⁻¹)	322.6	267.7	169.5	250.0	526.3	567.5	321.3	500.0
K_L (dm ³ mg ⁻¹)	0.137	0.180	0.097	0.062	0.056	0.028	0.026	0.022
R^2	0.996	0.997	0.993	0.969	0.992	0.991	0.785	0.986
χ^2	6.0	5.3	4.2	18.2	19.7	20.0	31.3	14.5
Freundlich equation								
$1/n$	0.295	0.350	0.239	0.311	0.448	0.659	0.536	0.592
K_F (mg ^{1-1/n} (dm ³) ^{1/n} g ⁻¹)	80.9	56.4	46.0	49.4	63.8	25.0	19.5	22.7
R^2	0.810	0.862	0.868	0.850	0.929	0.976	0.957	0.983
χ^2	55.6	47.0	9.3	33.8	30.3	14.0	9.3	14.6

^a Results presented in Ref. 21.

^b Results reported in Ref. 47.

Information) showed that in both cases SiO₂ is the major crystalline structure present, as demonstrated by the most intense peaks of quartz (ICCD- 33-1161) and cristobalite (ICCD- 39-1425) at around 26 and 21 °2 θ , respectively [53]. These findings are in line with the XPS survey spectra where trace amounts of Si were detected.

To disclose any possible influence of the mineral matter on the performance of the carbons as adsorbents of paracetamol from aqueous phase, the ashes obtained after total consumption of the GAC and NS carbon fractions were assayed as adsorbents. No removal was observed after 24 h of contact time, so, even though these results cannot be straightly compared with the effect of the mineral matter when distributed in the bulk, they point out that, by itself the ash has a negligible contribution to the performance of the carbons as adsorbents.

The experimental conditions for the thermal regeneration studies of the paracetamol exhausted carbons were defined after thermogravimetry studies. The thermograms (TG) displayed in Fig. 7(a) show that the raw NS and GAC materials have negligible weight loss, while carbon cloth ACC losses 10% of its weigh when heat treated under N₂ up to 900 °C. The exhausted samples present similar weight loss profiles with weight loss ranging from 14% (GACexh) to 22% (NSexh). The differential thermogravimetric (DTG) curves (Fig. 7(b)) show that the most important weight loss occurs between 300 and 500 °C, and in the case of NS and ACC carbons the maximum is centered at 375 °C and 366 °C, respectively, while for the granular sample it occurs at 411 °C. Comparing the TG profiles of the exhausted samples with those of paracetamol and raw carbons (see Fig. 7 and Fig. S3 in Supplementary Information), it is possible to attribute the weight loss of the exhausted samples

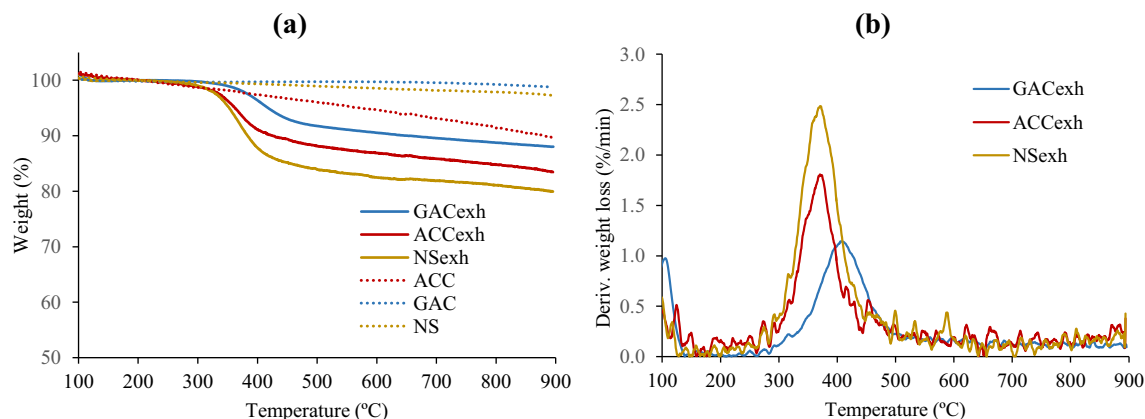


Fig. 7. (a) Thermograms of the raw and exhausted carbons and (b) corresponding DTG curves.

mainly to the removal/degradation of the adsorbed paracetamol, since the thermogram of paracetamol reveals an almost complete weight loss in the temperature range between 300 and 400 °C. The slightly higher temperature needed to remove/degrade paracetamol adsorbed onto sample GAC (411 °C versus 366 and 375 °C for ACC and NS) seems to be linked to the granular morphology of the material. In fact, in the case of granular particles heat distribution along the particles may be distinct than that occurring in materials with smaller particles sizes (NS), or fiber-like morphologies (ACC) where the microporosity is readily available. Specific interactions could also explain the higher temperature needed in the case of GAC but equilibrium adsorption data revealed the opposite trend. The adsorption affinity value (K_L , Table 4) of GAC for paracetamol is one order of magnitude lower than the values of the carbons NS and ACC indicating a weaker interaction between carbon surface and adsorbed paracetamol.

These results are similar to those reported by Ania *et al.* [25], for carbons exhausted with salicylic acid, being the presence of a single peak at around 300 °C assigned to the degradation of physically adsorbed compound. In the same study, the authors also tested phenol saturated carbons for which the DTG presented two peaks, being the one at lower temperature assigned to phenol physically adsorbed, and the one at higher temperature attributed to the degradation of chemically adsorbed specie. The study developed by Ledesma *et al.* [27] with carbons saturated with *p*-nitrophenol proved that also in this case the desorption mechanism is a two-step process. So, according to the results reported in the literature, the paracetamol adsorption onto the carbons tested in the present study seems to follow a physisorption mechanism.

The fact that, in the case of GAC sample, the most important weight loss occurs at higher temperature than that of ACC and NS carbons may be explained in terms of samples morphology, porosity and surface chemistry. Actually, in the case of GAC we can admit that the temperature distribution inside the granular particles is not uniform. So, for molecules adsorbed in the inner part of the granules a higher temperature must be applied. On the other hand, as reported in the literature [34,54], in carbons with wide pore size distributions, desorption of the adsorbate may require lower temperatures. So, the behaviour of carbon NS may be linked to its developed mesopore network, associated to a high volume of wider micropores (see Table S1). In the case of sample ACC, we can also admit that desorption is facilitated because the micropores of this carbon are connected to the surface. Additionally, the small particle size of sample NS favors the diffusion of the desorbed molecules towards the gas phase in comparison with what is expected to occur in the case of the granular sample. The surface chemistry may also justify the slightly distinct surface interactions of GAC with paracetamol since the C 1s XPS

spectra reveals that on the contrary of NS and ACC, in sample GAC no carbonyl or quinone groups were identified.

According to these results the regeneration experiments were made at 400 and 600 °C, for 1 h. To evaluate the impact of the heating regimes on the carbon texture, the samples were submitted to the experimental conditions chosen for the regeneration assays in the absence of the paracetamol. The N₂ adsorption isotherms (see Fig. S4 (left) in Supplementary Information) show that the curves of the treated samples maintain the configuration of the starting material, and only in for carbon ACC there is a decrease of the adsorption capacity, most certainly related with the 10% weight loss observed in ACC thermogravimetric profile (Fig. 7(a)). In the case of sample GAC the isotherms of the fresh and heated samples are coincident, and for NS the heating regime causes only a slightly increase in mesopore volume, especially when a higher temperature is used.

The textural parameters presented in Table 5 allow us to quantify the impact of the heating treatment on the carbon's texture. Regarding the cloth carbon, ACC, the heat treatment leads to an important loss of apparent surface area and supermicropore volume. Compared to the initial values, and regardless the temperature used, the A_{BET} decreases around 25 percentage points, and $V_{\alpha \text{ super}}$ about 32 percentage points. On the contrary, the heating has no significant impact on GAC texture, and a slight positive effect in the case of the sample NS. The results show that, regardless the temperature, the A_{BET} values of the NS treated samples are quite close to the value of the pristine carbon. The heating treatment only affects the mesopore volume that, in comparison to the value presented by NS carbon increases a maximum of 27 percentage points, when 600 °C were used.

The regeneration efficiency, $RE(\%)$, as defined previously in the experimental section, was assessed in terms of the paracetamol adsorption capacity retained by the recovered carbons, compared to the value presented by the fresh sample. The results obtained (Fig. 8) show that, as expected, the $RE(\%)$ values decrease gradually with the consecutive re-uses of the carbons, being this effect more accentuated after the 3rd re-use. On the other hand, the influence of the regeneration temperature on the carbon's performance seems to be dependent of the type of carbon used.

The results obtained with ACC sample show that the use of milder conditions (400 °C) allows to recover somewhat higher paracetamol adsorption capacities. In these conditions, it is possible to apply two saturation-regeneration cycles maintaining 56% of ACC initial paracetamol capacity. Having in mind that, as it was previously discussed, the heating temperature by itself has a significant effect on this carbon texture, the decrease of the $RE(\%)$ values may result from the combination of the temperature impact on the texture and of a partial blocking of the porosity due to

Table 5
Nanotextural properties of the fresh activated carbons, samples heated at 400 °C and 600 °C and obtained after the 3rd re-use.

Samples	A_{BET} ($\text{m}^2 \text{g}^{-1}$)	$V_{\text{total}}^{\text{a}}$ ($\text{cm}^3 \text{g}^{-1}$)	$V_{\text{meso}}^{\text{b}}$ ($\text{cm}^3 \text{g}^{-1}$)	α_s method ^c		
				$V_{\alpha \text{ total}}$ ($\text{cm}^3 \text{g}^{-1}$)	$V_{\alpha \text{ ultra}}$ ($\text{cm}^3 \text{g}^{-1}$)	$V_{\alpha \text{ super}}$ ($\text{cm}^3 \text{g}^{-1}$)
ACC	1136	0.76	0.03	0.73	0.00	0.73
ACC/400	828	0.51	0.03	0.48	0.00	0.48
ACC/600	851	0.53	0.03	0.50	0.00	0.50
ACCexh/400	435	0.29	0.02	0.27	0.00	0.27
ACCexh/600	449	0.29	0.01	0.28	0.00	0.28
GAC	838	0.47	0.13	0.34	0.09	0.25
GAC/400	848	0.51	0.17	0.34	0.09	0.25
GAC/600	840	0.50	0.16	0.34	0.08	0.26
GACexh/400	166	0.22	0.14	0.08	0.00	0.08
GACexh/600	321	0.27	0.13	0.14	0.00	0.14
NS ^d	1065	0.70	0.30	0.40	0.02	0.38
NS/400	1083	0.72	0.33	0.39	0.01	0.38
NS/600	1088	0.80	0.41	0.39	0.01	0.38
NSexh/400	185	0.20	0.12	0.08	0.00	0.08

^a N_2 volume adsorbed at $p/p^0 = 0.95$.

^b $V_{\text{meso}} = V_{\text{total}} - V_{\alpha \text{ total}}$.

^c α_s method was applied using as reference the isotherm presented in Ref. 41.

^d Values presented in Ref. 55.

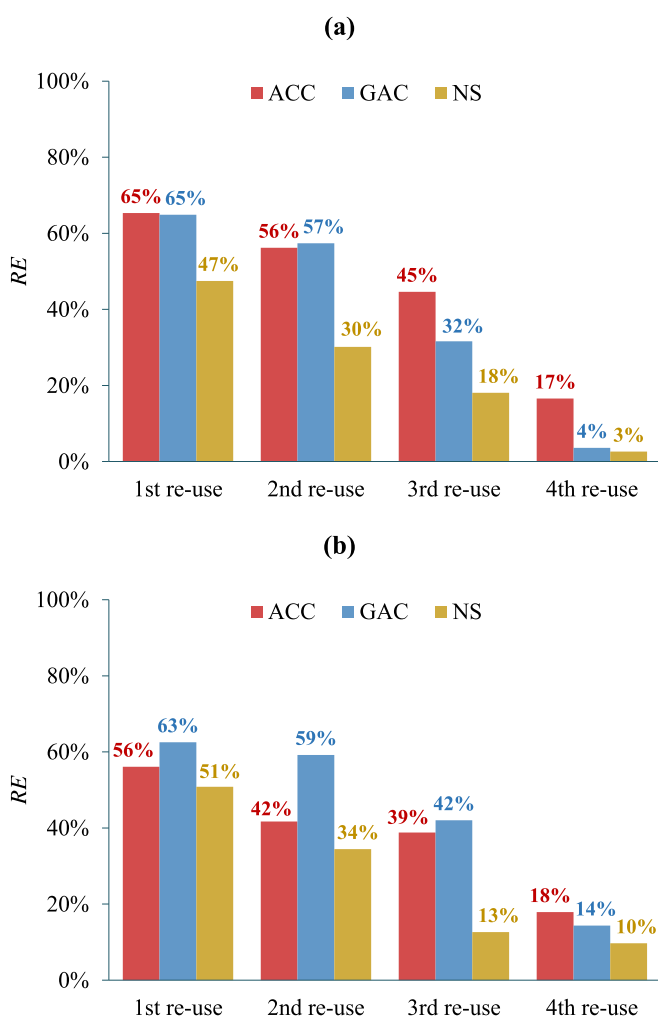


Fig. 8. Regeneration efficiency ($RE(\%)$) of samples ACC, NS and GAC, for consecutive re-uses after regeneration by thermal treatment at (a) 400 °C and (b) 600 °C for 1 h.

incomplete removal of paracetamol. The loss of ACC porosity is demonstrated by the textural parameters of the samples obtained after the 3rd re-use upon regeneration at 400 and 600 °C. The

values estimated from the analysis of the N_2 isotherms (see Fig. S4 (right) of Supplementary Information), presented in Table 5, reveal that the regenerated ACC carbon retains around 40% of the A_{BET} and $V_{\alpha \text{ super}}$ values presented by the fresh sample.

Regarding the thermal regeneration of the granular carbon, our experiments were able to restore ~58% of initial paracetamol adsorption capacity after two saturation-regeneration cycles at both temperatures. In this case, the decrease of the $RE(\%)$ may be attributed to the progressive obstruction of the porosity, since the textural characterization of samples heated at 400 and 600 °C in the absence of paracetamol did not reveal any significant loss of porosity. The N_2 adsorption results of the GAC regenerated samples (Fig. S4 (right) of Supplementary Information and Table 5) support this conclusion since there is a significant decrease of A_{BET} and micropore volume, especially in the case of the sample submitted to heat treatment at 400 °C. The relatively better results in the 3rd and 4th re-use cycles when the treatments were performed at 600 °C may be also linked to the fact that, as demonstrated by the DTG analysis, paracetamol removal from this carbon requires a higher temperature than in the case of the other samples.

The less efficient regeneration was achieved with the powdered sample NS which, according to the results obtained only presents $RE(\%)$ values around 50% after a single regeneration. Further re-uses of this carbon lead to a much accentuated decrease of paracetamol uptake. This behaviour is most likely due to the retention of paracetamol on the porosity, which as proved by the data presented in Table 5 for sample NSexh/400, obtained after 3 re-uses, leads to a drastic decrease of all the textural parameters.

4. Conclusions

The removal of paracetamol and clofibric acid by powdered, granular and cloth activated carbons was evaluated by kinetic and equilibrium assays. The kinetic results showed that, for small molecules as those tested, the diffusion towards the adsorption active sites is ruled by the volume of wider micropores. Equilibrium data revealed different underlying adsorption mechanisms for the two target molecules. Paracetamol adsorption follows a Langmuir mechanism in all the carbons, while in the case of clofibric acid a more complex mechanism seems to be involved, which was attributed to the nature of the species present in solution. At high equilibrium concentrations, clofibric acid is always adsorbed in much larger amounts.

The regeneration through thermal treatment proved to be a valid strategy to the recovery of the paracetamol exhausted samples porosity, especially at the lowest temperature tested (400 °C). The impact of the carbons' morphology was also demonstrated, differentiating positively the granular and cloth samples which could be re-used at least twice keeping adsorption capacities higher than 50%.

Lastly, the overall results show the potentialities of carbon cloth to compete with traditional morphologies since it presented adsorption performances identical, or even better, than powdered samples, and behaved equally well as granular samples when submitted to thermal regeneration. Thus aiming to a more sustainable society where the regeneration of spent carbons must become a rule, carbon cloth is an excellent option to the presently used granular morphology.

Acknowledgments

The authors thank the Fundação para a Ciência e Tecnologia (FCT), Portugal, for financial support to CQB through the project UID/MULTI/00612/2013, and FAPESP (Brazil) process 12/51087-6 for Activated carbon felt production. SCRMM thanks FCT for the PhD grant, SFRH/BD/91767/2012 and ASM thanks the financial support of FCT for the Post-doc grant SFRH/BPD/86693/2012. The authors thank Dr. C.O. Ania for the TG analysis, Quimitejo for providing carbon VP, and Salmon & Cia for the supply of carbons NS and GAC.

Appendix A. Supplementary data

Supplementary data associated with this article can be found, in the online version, at <http://dx.doi.org/10.1016/j.cej.2017.03.101>.

References

- [1] N. Bolong, A.F. Ismail, M.R. Salim, T. Matsuura, A review of the effects of emerging contaminants in wastewater and options for their removal, *Desalination* 239 (2009) 229–246.
- [2] J.O. Tijani, O.O. Fatoba, O.O. Babajide, L.F. Petrik, Pharmaceuticals, endocrine disruptors, personal care products, nanomaterials and perfluorinated pollutants: a review, *Environ. Chem. Lett.* 14 (2016) 27–49.
- [3] D. Taylor, T. Senac, Human pharmaceutical products in the environment – the “problem” in perspective, *Chemosphere* 115 (2014) 95–99.
- [4] J. Rivera-Utrilla, M. Sánchez-Polo, M.A. Ferro-García, G. Prados-Joya, R. Ocampo-Pérez, Pharmaceuticals as emerging contaminants and their removal from water. A review, *Chemosphere* 93 (2013) 1268–1287.
- [5] C.G. Daughton, Pharmaceuticals Ingredients in Drinking Water: overview of Occurrence and Significance of Human Exposure, in: *Contaminants of Emerging Concern in the Environment: Ecological and Human Health Considerations*, Am. Chem. Soc., 2010, pp. 9–68.
- [6] K.E. Murray, S.M. Thomas, A.A. Bodour, Prioritizing research for trace pollutants and emerging contaminants in the freshwater environment, *Environ. Pollut.* 158 (2010) 3462–3471.
- [7] E. Stumm-Zollinger, Biodegradation of steroid hormones, *J. Water Pollut. Fed.* 37 (1965) 1506–1510.
- [8] Directive 2015, 2015/495/EU of the European Parliament and of the Council of 20 March 2015 establishing a watch list of substances for Union-wide monitoring in the field of water policy pursuant to Directive 2008/105/EC. *Off. J. Eur. Commun.* L78/40.
- [9] A.P. Carvalho, A.S. Mestre, M. Haro, C.O. Ania, Advanced methods for the removal of acetaminophen from water, *Acetaminophen: Properties, Clinical Uses and Adverse Effects*, Nova Science Publishers Inc, 2012, pp. 57–105.
- [10] M.J. Gómez, M.J. Bueno, S. Lacorte, A.R. Fernández-Alba, A. Agüera, Pilot survey monitoring pharmaceuticals and related compounds in a sewage treatment plant located on the Mediterranean Coast, *Chemosphere* 66 (2007) 993–1002.
- [11] E. Gracia-Lor, J.V. Sancho, F. Hernández, Multi-class determination of around 50 pharmaceuticals, including 26 antibiotics, in environmental and wastewater samples by ultra-high performance liquid chromatography-tandem mass spectrometry, *J. Chromatogr. A* 1218 (2011) 2264–2275.
- [12] S.K. Khetan, T.J. Collins, Human pharmaceuticals in the aquatic environment: a challenge to green chemistry, *Chem. Rev.* 107 (2007) 2319–2364.
- [13] T. Heberer, Occurrence, fate and removal of pharmaceutical residues in the aquatic environment: a review of recent research data, *Toxicol. Lett.* 131 (2002) 5–17.
- [14] A.W. Garrison, J.D. Pope, F.R. Allen, GC/MS analysis of organic compounds in domestic wastewaters, in: C.H. Keith (Ed.), *Identification and Analysis of Organic Pollutants in Water*, Ann Arbor Science Publishers Inc., 1976, pp. 517–566.
- [15] C. Hignite, D.L. Azamoff, Drugs and drug metabolites as environmental contaminants: chlorophenoxyisobutyrate and salicylic acid in sewage treatment effluent, *Life Sci.* 20 (1977) 337–342.
- [16] H.J. Stan, T. Heberer, M. Linkerhägner, Occurrence of clofibrac acid in the aquatic system – is the use in human medical care the source of the contamination of surface, ground, and drinking water?, *Vom Wasser* 83 (1994) 57–68.
- [17] POSEIDON, Assessment of technologies for the removal of pharmaceuticals and personal care products in sewage and drinking water facilities to improve the indirect potable water reuse, Contract No. EVK1-CT-2000-0047, in: <http://www.eu-poseidon.com>, 2001–2004.
- [18] A.L. Cukierman, Development and environmental applications of activated carbon cloths, *ISRN Chem. Eng.* (2013) 1–21.
- [19] I. Cabrita, B. Ruiz, A.S. Mestre, I.M. Fonseca, A.P. Carvalho, C.O. Ania, Removal of an analgesic using activated carbons prepared from urban and industrial residues, *Chem. Eng. J.* 163 (2010) 249–255.
- [20] A.S. Mestre, A.S. Bexiga, M. Proença, M. Andrade, M.L. Pinto, I. Matos, I.M. Fonseca, A.P. Carvalho, Activated carbons from sisal waste by chemical activation with K₂CO₃ kinetics of paracetamol and ibuprofen removal from aqueous solution, *Bioresour. Technol.* 102 (2011) 8253–8260.
- [21] M. Galhetas, A.S. Mestre, M.L. Pinto, I. Gulyurtlu, H. Lopes, A.P. Carvalho, Carbon-based materials prepared from pine gasification residues for acetaminophen adsorption, *Chem. Eng. J.* 240 (2014) 344–351.
- [22] A.S. Mestre, R.A. Pires, I. Aroso, E.M. Fernandes, M.L. Pinto, R.L. Reis, M.A. Andrade, J. Pires, S.P. Silva, A.P. Carvalho, Activated carbons prepared from industrial pre-treated cork: sustainable adsorbents for pharmaceutical compounds removal, *Chem. Eng. J.* 253 (2014) 408–417.
- [23] A.S. Mestre, M.L. Pinto, J. Pires, J.M. Nogueira, A.P. Carvalho, Effect of solution pH on the removal of clofibrac acid by cork-based activated carbons, *Carbon* 48 (2010) 972–980.
- [24] <http://www.cabotcorp.com/solutions/products-plus/activated-carbon/reactivation-services>.
- [25] C.O. Ania, J.B. Parra, C. Pevida, A. Arenillas, F. Rubiera, J.J. Pis, Pyrolysis of activated carbons exhausted with organic compounds, *J. Anal. Appl. Pyrol.* 74 (2005) 518–524.
- [26] R. Berenguer, J.P. Marco-Lozar, C. Quijada, D. Cazorla-Amorós, E. Morallón, Comparison among chemical, thermal and electrochemical regeneration of phenol-saturated activated carbon, *Energy Fuels* 24 (2010) 3366–3372.
- [27] B. Ledesma, S. Román, A. Álvarez-Murillo, E. Sabio, J.F. González, Cyclic adsorption/thermal regeneration of activated carbons, *J. Anal. Appl. Pyrolysis* 106 (2014) 112–117.
- [28] E. Sabio, E. González, J.F. González, C.M. González-García, A. Ramiro, J. Gañan, Thermal regeneration of activated carbon saturated with *p*-nitrophenol, *Carbon* 42 (2004) 2285–2293.
- [29] C.O. Ania, J.A. Menéndez, J.B. Parra, J.J. Pis, Microwave-induced regeneration of activated carbons polluted with phenol. A comparison with conventional thermal regeneration, *Carbon* 42 (2004) 1383–1387.
- [30] C.O. Ania, J.B. Parra, J.A. Menéndez, J.J. Pis, Microwave-assisted regeneration of activated carbons loaded with pharmaceuticals, *Water Res.* 41 (15) (2007) 3299–3306.
- [31] D. Cooney, A. Nagerl, A. Hines, Solvent regeneration of activated carbon, *Water Res.* 17 (1983) 403–410.
- [32] K. Sodha, S. Panchani, K. Nath, Feasibility study of microbial regeneration of spent activated carbon sorbed with phenol using mixed bacteria culture, *Indian J. Chem. Technol.* 20 (2013) 33–39.
- [33] M.K. Batista, A.S. Mestre, I. Matos, I.M. Fonseca, A.P. Carvalho, Biodiesel production waste as promising biomass precursor of reusable activated carbons for caffeine removal, *RSC Adv.* 6 (2016) 45419–45427.
- [34] B. Ledesma, S. Román, A. Álvarez-Murillo, E. Sabio, C.M. González-García, Fundamental study on the thermal regeneration stages of exhausted activated carbons: kinetics, *J. Therm. Anal. Calorim.* 115 (2014) 537–543.
- [35] J.S. Marcuzzo, C. Otani, H.A. Polidoro, S. Otani, Influence of thermal treatment on porosity formation on carbon fiber from textile PAN, *Mater. Res.* 16 (2013) 137–144.
- [36] <http://www.cabotcorp.com/solutions/products-plus/activated-carbon/granulated>.
- [37] B.M. Babić, S.K. Milonjić, M.J. Polovina, B.V. Kaludierović, Point of zero charge and intrinsic equilibrium constants of activated carbon cloth, *Carbon* 37 (1999) 477–481.
- [38] ASTM D 2866, 2011. Standard test method for total ash content of activated carbons.
- [39] M. Thommes, K. Kaneko, A. Neimark, J. Olivier, F. Rodríguez-Reinoso, J. Rouquerol, K. Sing, Physisorption of gases, with special reference to the evaluation of surface area and pore size distribution (IUPAC Technical Report), *Pure Appl. Chem.* 87 (2015) 1051–1069.
- [40] F. Rouquerol, J. Rouquerol, K. Sing, *Adsorption by Powders and Porous Solids – Principles, Methodology and Applications*, Academic Press, San Diego, 1999.
- [41] F. Rodríguez-Reinoso, J.M. Martín-Martínez, A standard adsorption isotherm for the characterization of activated carbons, *J. Phys. Chem.* 91 (1987) 515–516.
- [42] M.L. Pinto, A.S. Mestre, A.P. Carvalho, J. Pires, Comparison of methods to obtain micropore size distributions of carbonaceous materials from CO₂ adsorption

- based on the Dubinin-Radushkevich isotherm, *Ind. Eng. Chem. Res.* 49 (2010) 4726–4730.
- [43] C. Moreno-Castilla, M.V. Lopez-Ramon, F. Carrasco-Marin, Changes in surface chemistry of activated carbons by wet oxidation, *Carbon* 38 (2000) 1995–2001.
- [44] S. Biniak, G. Szymanski, J. Siedlewski, A. Swiatkowski, The characterization of activated carbons with oxygen and nitrogen surface groups, *Carbon* 35 (1997) 1799–1810.
- [45] T.J. Bandosz, C.O. Ania, Surface chemistry of activated carbons and its characterization, in: T.J. Bandosz (Ed.), *Activated Carbon Surfaces in Environmental Remediation*, Elsevier, New York, 2006, pp. 159–229.
- [46] M. Galhetas, A.S. Mestre, M.L. Pinto, I. Gulyurtlu, H. Lopes, A.P. Carvalho, Chars from gasification of coal and pine activated with K_2CO_3 : acetaminophen and caffeine adsorption from aqueous solutions, *J. Colloid Interface Sci.* 433 (2014) 94–103.
- [47] A.S. Mestre, A. Nabiço, P.L. Figueiredo, M.L. Pinto, M.S.C. Santos, I.M. Fonseca, Enhanced clofibrac acid removal by activated carbons: water hardness as a key parameter, *Chem. Eng. J.* 286 (2016) 538–548.
- [48] Y.-S. Ho, Review of second-order models for adsorption systems, *J. Hazard Mater.* 136 (2006) 681–689.
- [49] C.H. Giles, D. Smith, A. Huitson, A general treatment and classification of the solute adsorption isotherm. I. Theoretical, *J. Colloid Interface Sci.* 47 (1974) 755–765.
- [50] J. Lyklema, *Fundamentals of Interface and Colloid Science, Vol II - Solid-liquid interfaces*, Academic Press, New York, 1995.
- [51] I. Langmuir, The adsorption of gases on plane surfaces of glass, mica and platinum, *J. Am. Chem. Soc.* 40 (1918) 1361–1403.
- [52] H.M.F. Freundlich, Over the adsorption in solution, *J. Phys. Chem.* 57 (1906) 385–470.
- [53] Powder Diffraction File Alphabetic Index, ICDD, International Center for Diffraction Data, Swarthmore, PA, 1988.
- [54] M.A. Ferro-García, E. Utrera-Hidalgo, J. Rivera-Utrilla, C. Moreno-Castilla, Regeneration of activated carbons exhausted with chlorophenol, *Carbon* 31 (1993) 857–863.
- [55] A.S. Mestre, S.C.R. Marques, A.P. Carvalho, Effect of cosolvent in the removal of caffeine by activated carbons, *Ind. Eng. Chem. Res.* 51 (2012) 9850–9857.

Manuscript Number:

Title: Apple tree bark derived activated carbons for the removal of beta-blocker atenolol

Article Type: Original research paper

Keywords: Biomass derived activated carbons

Atenolol

Liquid phase adsorption

Thermogravimetric analysis

Pharmaceuticals racemic mixtures

Corresponding Author: Dr. Ana P Carvalho, Ph.D.

Corresponding Author's Institution: Faculty of Sciences of Lisbon University

First Author: Susana C Marques, MSc

Order of Authors: Susana C Marques, MSc; Ana S Mestre, PhD; Miguel Machuqueiro, PhD; Andreja Z Gotvajn, PhD; Marjan Marinsek, PhD; Ana P Carvalho, Ph.D.

Abstract: This work approaches the preparation of KOH and K₂CO₃ activated carbons from apple tree bark char with preparation yields around 40 %, and apparent surface areas up to 2472 m² g⁻¹. The treatment duration had a marked impact on the micropore structure, causing the widening of the narrow micropores to supermicropores, and eventually to mesopores. The adsorption characteristics of lab-made carbons for atenolol removal from aqueous phase was assessed by kinetic and equilibrium experiments. Monolayer adsorption capacities between 346 and 556 mg g⁻¹ were achieved. The commercial atenolol, consisting in a racemic mixture, gave rise to a two-step thermal decomposition process. Thermogravimetric analysis of the exhausted samples revealed that the predominant atenolol specie adsorbed is conditioned by the carbons' surface chemistry: neutral/acidic lab-made carbons generally favoured the adsorption of the more stable specie; basic commercial samples retained predominantly the less stable one.

Suggested Reviewers: Francisco J Maldonado Hódar PhD
Full Professor, Inorganic Chemistry, University of Granada
fjmaldon@ugr.es

Prof. Maldonado has a large experience in activated carbon research. He has a large number of papers focused on the preparation and adsorption from liquid phase as well as catalysis.

Juan Matos PhD
Full Professor, Biomaterials, University of Concepcion, Chile
jmatoslale@gmail.com

Professor Matos is a recognized expert in carbon materials preparation, and their use as adsorbents and catalysts

Conchi Ania PhD

Directeur de Recherche, CEMHTI UPR 3079, CNRS, Université de Orléans
conchi.ania@cnrs-orleans.fr

Dr. Ania has a long experience in preparation and characterization of activated carbons. Her expertise on the application of carbons as adsorbents of organic compounds from liquid phase is recognized by the scientific community, as well as her expertise in the use of carbons as catalysts

Leticia F Velasco PhD

Researcher, Royal Military Academy, Brussels, Belgium
leticia.fernandez@rma.ac.be

Dr. Velasco has a large number of studies focused on the use of carbon materials as adsorbents from liquid phase and also as catalysts of organic compounds degradation. Her expertise regarding the textural characterization of carbons is recognized.



November, 23rd, 2017

Dear Prof. Ashok Pandey

The work entitled “Apple tree bark derived activated carbons for removal of the β -blocker atenolol” by Susana C. R. Marques, Ana S. Mestre, Miguel Machuqueiro, Andreja Žgajnar Gotvajn, Marjan Marinšek and Ana P. Carvalho is focused on the preparation and characterization of waste biomass derived activated carbons. The materials were tested as adsorbents of a pharmaceutical compound that due to its recalcitrant behaviour regarding the common wastewater treatment process is an ecological risk of great concern.

The novelty of the work, besides the valorisation of an abundant natural biomass residue (apple tree bark) to produce activated carbon by chemical activation with K_2CO_3 or KOH , is the detailed analysis of the thermogravimetric data of the atenolol exhausted samples. This study pointed out that when the pharmaceutical compound is present as a racemic mixture, it is important that the analysis of the adsorption data takes into account the presence of the different species, since as it was demonstrated, even carbons with the same acid-base characteristics can interact differently with the two components of the mixture. This is a different and innovative approach to the common discussion of the influence of texture and surface chemistry of activated carbons on the adsorption of pharmaceutical compounds from aqueous solution.

This work has not been published previously and it is not under consideration for publication elsewhere. Its publication is approved by all authors and tacitly or explicitly by the responsible authorities where the work was carried out, and that, if accepted, it will not be published elsewhere in the same form, in English or in any other language, including electronically without the written consent of the copyright-holder.

The subject classification selected in the EES was: Other thermo-chemical processed with the code 70.040.

For the mentioned reasons, we would like you to consider the evaluation of this work for publication in a future number of Bioresource Technology.

With our kindest regards,

Ana Paula Carvalho
(Assistant Professor)

e-mail: ana.carvalho@fc.ul.pt

Graphical abstract



Highlights

- Superactivated carbons were obtained by chemical activation of apple tree bark char
- β -blocker medicine atenolol was used as target compound for liquid phase assays
- Monolayer adsorption capacities of lab-made carbons between 345 and 556 mg g⁻¹
- Thermal decomposition of atenolol racemic mixture is a two-step process
- Adsorption of each atenolol specie is conditioned by the carbons' surface chemistry

Apple tree bark derived activated carbons for the removal of β -blocker atenolol

Susana C. R. Marques¹, Ana S. Mestre¹, Miguel Machuqueiro¹, Andreja Žgajnar Gotvajn^{2*}, Marjan Marinšek², Ana P. Carvalho^{1*}

¹ *Centro de Química e Bioquímica, Faculdade de Ciências, Universidade de Lisboa, 1749-016 Lisboa, Portugal*

² *Faculty of Chemistry and Chemical Technology, University of Ljubljana, Slovenia*

* Corresponding authors: Ana P. Carvalho (ana.carvalho@fc.ul.pt), Andreja Žgajnar Gotvajn (andreja.zgajnar@fkkt.uni-lj.si)

Abstract

This work approaches the preparation of KOH and K₂CO₃ activated carbons from apple tree bark char with preparation yields around 40 %, and apparent surface areas up to 2472 m² g⁻¹. The treatment duration had a marked impact on the micropore structure, causing the widening of the narrow micropores to supermicropores, and eventually to mesopores.

The adsorption characteristics of lab-made carbons for atenolol removal from aqueous phase was assessed by kinetic and equilibrium experiments. Monolayer adsorption capacities between 346 and 556 mg g⁻¹ were achieved.

The commercial atenolol, consisting in a racemic mixture, gave rise to a two-step thermal decomposition process. Thermogravimetric analysis of the exhausted samples revealed that the predominant atenolol specie adsorbed is conditioned by the carbons' surface chemistry: neutral/acidic lab-made carbons generally favoured the adsorption of the more stable specie; basic commercial samples retained predominantly the less stable one.

Keywords

Biomass derived activated carbons

Atenolol

Liquid phase adsorption

Thermogravimetric analysis

Pharmaceuticals racemic mixtures

1. Introduction

In the last years, the contamination of water bodies by pharmaceutically active ingredients (PhACs) and their continuous presence in treated water (even water for human consumption) has imprinted the urgency in the scientific community to find solutions to this alarming environmental problem and its potential effects on human health.

To understand how to contain, or hopefully solve, this contamination scenario, it is necessary to comprehend its causes. One of the main reasons is the fact that the development of the medical care system led to the production of increasingly effective PhACs which are present in numerous medicines, highly consumed worldwide. After administration, a large amount of these compounds is excreted by the human body partially or completely un-metabolized, resulting in their continuous release to the sewer systems, along with their metabolites (Petrovic *et al.*, 2008; Alder *et al.*, 2006). The contaminated influents reach the wastewater treatment plants (WWTPs) where the conventional water treatment processes are rather ineffective in their complete removal and/or degradation, resulting in PhACs being continuously released into the environment, reaching surface and groundwater reserves, *i.e.* drinking water sources (Daughton, 2010).

To prevent further contamination of the aquatic environment, the implementation of technologies involving the use of porous materials for the removal of trace contaminants from water has gained a lot of attention by the scientific and industrial community (Bolong *et al.*, 2009). In this context, the production of activated carbons from biomass wastes has proven to be a “green” and advantageous strategy from the economic point of view (Dias *et al.*, 2007).

Among the agricultural wastes, woody materials are relevant and challenging precursors for the development of porous materials because they exhibit textural characteristics favourable to the development of porosity (Dias *et al.*, 2007; Zhang and Zhang, 2014). In the particular case of wood bark, there are various studies in the literature showing the viability of these type of materials as activated carbon precursors. An example is the study developed by Zhang and Zhang (2014) focused

on the preparation of activated carbons from poplar wood bark stripes, which were firstly carbonized at 600 °C and then activated with steam at 700 and 800 °C. The carbons obtained presented basic surface chemistry properties, and relatively developed porosity (total pore volume around 0.50 cm³ g⁻¹ and specific surface area around 552 m² g⁻¹). Patnukao *et al.* (2008) explored the chemical activation of *Eucalyptus camaldulensis* bark with phosphoric acid. The material prepared with a weight ratio of 1:1 and submitted to heat treatment at 500 °C for 1 h, attained a BET specific surface area of 1239 m² g⁻¹ being the pore network volume formed by 88 % of micropores and 12 % of mesopores.

To consider a possible implementation of newly developed activated carbons in the water treatment process for the removal of micropollutants, as is the case of PhACs, it is crucial to gather data on their efficiency for removal of this type of compounds from aqueous solution, and also to understand the factors ruling the adsorption/desorption mechanisms involved in the phenomena.

In this context the aim of our work was to assess the feasibility of a largely available wood waste (apple tree bark) for the production activated carbons in a two-step procedure: controlled pyrolysis to obtain a biochar, which was further chemically activated with KOH and K₂CO₃. The impact of the various experimental parameters on the textural properties of the carbon materials was evaluated and selected samples were tested as adsorbents of atenolol from aqueous solution. Additionally, atenolol thermal desorption from the surface of activated carbons was also studied and described.

Atenolol belongs to the group of β-blocker medicines and is used for the treatment of disorders such as hypertension, angina and arrhythmias (Borchard, 1998). This compound was detected in various water bodies such as river water (83 ng L⁻¹) (Alder *et al.*, 2010) and sewage treatment plant effluent (2 µg L⁻¹) (Huggett *et al.*, 2003), indicating its low biodegradability as it was demonstrated in the study developed by Carucci *et al.* (2006). These authors demonstrated that although biologic treatment, *i.e.* activated sludge digestion, is able to remove up to 90 % of atenolol present in a 2 ppm

high purity water solution, in a more realistic scenario, that is, using real wastewater and the same atenolol concentration, a removal of only 36 % is attained.

These results point out the need of implementing a subsequent treatment to decrease atenolol concentration before releasing the effluent into the aquatic environment, and also show that atenolol is an interesting target compound for adsorption experiments. Even so few and very recent studies concerning atenolol adsorption by activated carbons were reported in the literature (Haro *et al.*, 2017; To *et al.*, 2017). It must be also mentioned that, as reported by Cleuvers (2005), the presence of β -blocker medicines in water sources is an ecological risk of great concern due to its potential ecotoxicity as it can affect cardiac rhythm, generate abnormalities or reduce mobility of spermatozoids of fish.

2. Materials and methods

2.1. Preparation of activated carbons

The activated carbons were prepared from apple tree branches in a multi-step procedure which started with carbonization of dried 10 cm long branches in a pyro-furnace for approximately 30 minutes. The resulting biochar (sample A) was grounded and sieved to obtain particles within size frame between 0.420 - 0.297 mm, which were subsequently chemically activated with K_2CO_3 (Aldrich, 99 %) or KOH (Panreac, 85 %). The biochar was mixed with the adequate amount of selected activating agent dissolved in *ca.* 5 cm³ of water, and stirred at room temperature for 17 h, then heated at 373 K until complete dryness. The activation with K_2CO_3 was performed using two char:activating agent weight ratios, 1:3 and 1:4, whereas the KOH activation was made using only the 1:3 proportion. The mixtures were activated in a horizontal furnace (Thermolyne 21100), under N_2 flow (5 cm³ s⁻¹), at 973 K or 1073 K (heating rate 10 K min⁻¹) and kept at selected temperature for 1 to 4 h. After cooling under N_2 flow, samples were thoroughly washed with distilled water and dried at 373 K. The final materials are named according to the expression: CA or HA (impregnation

ratio/temperature of activation (K)/duration of activation (h)), where C and H stand for K_2CO_3 or KOH activation, respectively.

For benchmarking, two activated carbons commercialized for wastewater treatment purposes, were also assayed: i) NS, powdered carbon commercialized by Norit as SAE SUPER, with 97 % (wt./wt.) of particles with dimensions under 0.15 mm; and ii) CP, powdered carbon commercialized by ChiemiVall under the designation CCP 900.

2.2. Nanotextural and chemical characterization

The nanotextural characterization of the samples was made by N_2 and CO_2 adsorption isotherms at 77 K and 273 K, respectively. The nitrogen adsorption isotherms were obtained in an automatic apparatus Micromeritics ASAP 2010, while the CO_2 adsorption experiments were made in a conventional volumetric apparatus equipped with a MKS-Baratron (310BHS-1000) pressure transducer (0-133kPa). In any case, before the isotherm measurements, the samples (~ 50 mg) were outgassed overnight at 393 K under vacuum ($p < 10^{-2}$ Pa).

The surface chemistry of the activated carbons was characterized by determination of the pH at the point of zero charge (pH_{PZC}), following the reversed mass titration procedure reported in Noh and Schwarz (1989). In brief, aqueous carbon suspensions of 2 to 10 % (wt./wt.) were prepared and pH measurements were made after 24 h of stirring, at room temperature using a Symphony SP70P pH meter. Infrared spectroscopy (FTIR) was also performed and the spectra data were recorded at room temperature on a Nicolet 6700 FTIR spectrometer (200 scans, resolution 4 cm^{-1}). The samples were analysed in the form of KBr supported pellets.

The volatile content of the samples was assessed by heating the previously dried (overnight at 373 K) activated carbons under nitrogen flow up to 1173 K (15 K min^{-1}) and maintaining the temperature for 10 min (D5832-98, 2014). The mass lost during heating allowed determination of volatile content of the samples.

The samples morphology was characterized by Scanning Electron Microscopy (SEM) photographs obtained in a field emission gun scanning electron microscope (JEOL mod. 7001F) with an X-ray energy-dispersive system (EDS), using an accelerating voltage of 25 kV.

2.3.Liquid phase adsorption

The target molecule selected for the liquid phase assays - atenolol - was supplied by Generis (Kopran Research Laboratories, India) and all the solutions were prepared using ultra-pure water obtained from Milli-Q water purification system and used as prepared (pH of atenolol solutions is 8.2).

To study the adsorption kinetics, a volume of 20 cm³ of pollutant solution (initial atenolol concentration of 120 mg dm⁻³) was added to 6.0 ± 0.2 mg of adsorbent in glass vials. The vials were sealed, placed in a thermostatic bath at 304 K (Eurotherm 2216L), and stirred magnetically at 700 rpm in a multipoint agitation plate (Variomag Multipoint). Samples were collected between 5 min and

24 h. After filtration, the amount of adsorbate remaining in solution was determined by UV-Vis spectrophotometry (Genesys 10S) at its maximum absorbance wavelength (225 nm). The adsorbate uptake was calculated according to:

$$q_t = \frac{C_0 - C_t}{W} V \quad \text{Eq. 1}$$

where q_t is the amount (mg g⁻¹) of atenolol adsorbed at desired time t . C_0 and C_t are concentrations (mg dm⁻³), initial and at time t , respectively, V is the volume (dm³) of the atenolol solution and W is the weight (g) of dried carbon adsorbent.

Equilibrium adsorption studies were performed at 303 K, varying the adsorbent dose (around 3-6 mg), solution volume (9-30 cm³) and adsorbate initial concentration (20-180 mg dm⁻³). After stirring overnight, the concentration of adsorbate remaining in solution at equilibrium (C_e) was determined

and the uptake was calculated. Prior to use, the adsorbents were dried overnight in a ventilated oven at 373 K.

Thermogravimetric studies of atenolol desorption and decomposition were performed using ~50 mg of the sample and a NETZSCH STA 449 F3 set-up with a microbalance having a sensitivity of ± 0.1 g coupled with QMS 403 C system. The experiments were conducted in a constant Ar flow ($50 \text{ cm}^3 \text{ min}^{-1}$) with heating rates, β , of 5, 10 and $20 \text{ }^\circ\text{C min}^{-1}$ up to $900 \text{ }^\circ\text{C}$.

2. Results and discussion

2.1. Nanotextural and chemical characterization of the carbons

The N_2 adsorption-desorption isotherms, at 77 K presented in **Fig. 1** and in the Supplementary Information (**Fig. S1**), show that all carbons present type I isotherms according to IUPAC classification (Thommes *et al.*, 2015), characteristic of essentially microporous structures. At low relative pressure values, less pronounced rectangular character is observed, suggesting a wide micropore size distribution. The broadening of the initial knee is evident for all samples prepared with KOH, and also for samples activated with K_2CO_3 with longer periods of activation time. For higher relative pressures a plateau is observed and hysteresis loops are absent in all cases, demonstrating that no significant mesopore network or external surface area is present.

Fig. 1

From the adsorption data, apparent surface area, A_{BET} , was evaluated through BET equation (Rouquerol *et al.*, 1999). The range of p/p^0 used for this determination was chosen according to the methodology reported in ISO-9277 (2012). The microporosity was analysed applying the α_s method taking as reference the isotherm reported in Rodriguez-Reinoso and Martin-Martinez (1987). With this method, besides the determination of the total micropore volume, $V_{\alpha \text{ total}}$, the specific volumes of ultra (width less than 0.7 nm), $V_{\alpha \text{ ultra}}$, and supermicropores (width between 0.7 and 2 nm), $V_{\alpha \text{ super}}$,

were also assessed. The results obtained, as well as the meso, V_{meso} , and total, V_{total} , pore volumes, pH_{PZC} and preparation yield, η , are presented in **Table 1**.

Table 1

The values obtained show that the activation with KOH produces carbons with very high values of A_{BET} , attaining up to $2472 \text{ m}^2 \text{ g}^{-1}$. The use of K_2CO_3 results in somewhat lower values of A_{BET} reaching $1963 \text{ m}^2 \text{ g}^{-1}$. On the other hand, the textural parameters reveal that, in both cases, the more pronounced porosity development occurs for activation times up to 3 h, and that the micropore volume ($V_{\alpha\text{total}}$) of the samples corresponds to 91 – 98 % of the total pore volume, confirming the microporous nature of the samples.

A more detailed analysis of the textural parameters of the KOH activated carbons suggests that the duration of the treatment has a noticeable impact on the composition of the micropore network, leading to the progressive widening of the pores. In fact, the increase of the treatment duration from 1 to 2 h leads to practically zero $V_{\alpha\text{ultra}}$, and an increase of $V_{\alpha\text{super}}$ from 0.76 to $1.02 \text{ cm}^3 \text{ g}^{-1}$, pointing out the conversion of ultramicropores into supermicropores. Longer treatments result in further enlargement of the supermicropores leading to the development of mesoporosity which, in the case of sample HA(1:3/1073/4), attains the highest value of V_{meso} for the set of samples prepared in this study.

In the case of K_2CO_3 activation, besides the influence of the chemical agent amount and duration of treatment, the effect of temperature was also evaluated. Confronting the characteristics of samples CA(1:3/973/2) and CA(1:3/1073/2), it is noticeable that the higher temperature, 1073 K, leads to a more pronounced development of porosity (higher A_{BET} and $V_{\alpha\text{total}}$). The increase of treatment temperature also results in a different micropore network composition since in sample CA(1:3/973/2) the narrow microporosity corresponds to 67 % of the total micropore volume, while for sample CA(1:3/1073/2) this percentage reaches only 23 %.

The influence of the treatment duration was evaluated considering char:K₂CO₃ ratios of 1:3 and 1:4. In any case, longer calcinations favoured the porosity development associated to micropore broadening. However, on the contrary of what was observed for KOH activated samples, the use of K₂CO₃ always resulted in the presence of some ultramicropores, even though under the conditions used to prepare sample CA(1:3/1073/4) the relative amount of $V_{\alpha \text{ ultra}}$ decreases down to 6 % of the total micropore volume. This is the expected behaviour considering the different mechanism of KOH and K₂CO₃ activation, that according to the literature (Wang and Kaskel, 2012) start between 673 and 873 K for KOH while for K₂CO₃ reactions with the carbon matrix begin at temperatures around 973 - 1073 K.

Somewhat unexpected, the use of a larger amount of K₂CO₃ did not enhanced porosity development. This result may be explained considering that when larger amount of K₂CO₃ is used homogeneous dispersion of K₂CO₃ within the char matrix is prevented, which will result in the formation of clusters. This hypothesis explains higher preparation yields observed for the carbons prepared with 1:4 char: K₂CO₃ ratio, since a fraction of the activating agent is not in direct contact with the char matrix and then it cannot react to create porosity. The matrix consumption would then be prevented, resulting in higher preparation yields.

The two commercial carbons, used as benchmark for the liquid phase assays, present less developed porosity than the lab-made carbons, with lower A_{BET} values and pore volumes. These samples differ in terms of meso and microporosity being CP an essentially microporous carbon, with similar volumes of ultra and supermicropores, whereas NS has a significant mesopore volume (0.30 cm³ g⁻¹) and a microporous network composed mainly by wider micropores.

The microporosity of the commercial carbons and lab-made samples assayed in the liquid phase tests was further characterized through CO₂ adsorption data, which were used to obtain the micropore size distributions according to the method described by Pinto *et al.* (2012). The results (**Fig. 2**) reveal that all the samples exhibit bimodal micropore distribution. Such observation is in accordance with the

N₂ adsorption data that revealed the presence of both narrow and wider micropores. The maximum in the region of narrow micropores is centred at 0.52 nm and 0.60 nm for KOH and K₂CO₃ activated samples, respectively. In the case of carbons CP and NS the maximum is centered at 0.60 and 0.70 nm, respectively.

Fig. 2

The pH_{PZC} values of the lab-made samples (**Table 1**) seem to indicate that the choice of activating agent have impact on the surface chemistry properties of the carbons. KOH activation leads to neutral or slightly acid carbons whereas samples activated with K₂CO₃ present more acidic nature with pH_{PZC} values around 5.5. Both commercial carbons are basic, with pH_{PZC} values of 10.3 and 8.4 for CP and NS, respectively.

As expected the chemical activation had a strong impact on the volatile content of the samples. The values determined show that the very high volatile content of the char (49 %) decreases to around 16 and 13 %, for samples activated with KOH and K₂CO₃, respectively.

The high amount of volatile matter in the char justifies the interesting results obtained with apple tree bark char in comparison with the values reported in the literature for samples activated under similar conditions. In fact, the textural parameters reported in Mestre *et al.*, (2015) for carbons prepared from glucose hydrochars by KOH and K₂CO₃ activation, using a 1:4 proportion, and treated at 1073 K for 1 h, are close to that of the samples obtained using similar conditions but with 1:3 proportion of either KOH or K₂CO₃.

The morphology of the biochar used as precursor, and also of samples CA(1:3/1073/1) and HA(1:3/1073/1) was studied by scanning electron microscopy (SEM) (**Fig. 3**).

Figure 3

The biochar micrographs reveal characteristic features of a wood-derived material (Zhang and Zhang, 2014), *i.e.* elongated fibrous shaped particles, with a capillary structure and pores which are observed in more detail in the higher magnification micrographs (right images). As expected, the

K_2CO_3 activation allowed maintaining some of the morphological characteristics of the precursor, which are especially evident in the larger particles. From the lower magnification image of sample CA(1:3/1073/1) it is also possible to conclude the activation process results in formation of a polydisperse system. Activation with KOH caused a much more extensive destruction of the biochar particles structure, leading to a more homogeneous particle size distribution of the activated carbon material. The particles have rounded shape and sponge-like structure, thus presenting a completely different topography in comparison to the precursor. The EDS analysis (not shown) revealed that no potassium remaining from the activation procedure is detected in the carbons since only C and O could be quantified.

2.2. Adsorption characteristics of produced carbons

As a proof of concept four lab-made samples were tested as adsorbents of a pharmaceutical compound - atenolol - through kinetic and equilibrium assays. For comparison purposes, commercial carbons CP and NS were studied in parallel.

The kinetic curves obtained (**Fig. 4**) show that the concentration of atenolol in solution presents a marked decay in the first 30 min of contact time, after which the adsorption continues slowly until equilibrium is attained, for all the samples, at 6 h, what was confirmed by the experimental points corresponding to 24 h of contact time (data not shown).

The kinetic data were fitted to the pseudo-first and pseudo-second order kinetic models (Ho, 2006). The pseudo-second order model leads to better fittings of the experimental results, as demonstrated by the high R^2 values quoted in **Table 2**. The good adjust of the data to this model is also confirmed comparing the calculated and experimental uptake values ($q_{e \text{ calc}}$ and $q_{e \text{ exp}}$, respectively). The initial adsorption rate, h , and half-life time, $t_{1/2}$, values quoted in **Table 2** show that the performance of the lab-made carbons compares favourably with that of the best commercial sample tested, that is, carbon NS.

Fig. 4

Table 2

Considering the textural characteristics of the samples we have to conclude that in the case of atenolol, and as we have already observed for other small PhACs molecules (Galhetas *et al.*, 2014a, 2014b; Batista *et al.*, 2016), the presence of a developed mesoporosity is not the determinant factor that controls the adsorption kinetics. Actually, the behaviour of carbon NS, the only sample in this set presenting a significant mesopore volume ($V_{\text{meso}} = 0.30 \text{ g cm}^{-3}$), is not different from other carbons that have much smaller, or even almost absent, mesopore network. In previous studies, this behaviour is justified considering that once the materials have a considerable volume of larger micropores, the diffusion of, for example caffeine that has a critical dimension of 0.45 nm (Galhetas *et al.*, 2014b), towards an active site for adsorption is ruled by this wide microporosity. To verify if this hypothesis is also correct in the case of atenolol, the molecular dimensions of this compound were estimated by building atenolol initial structure in Avogadro software package (<http://avogadro.cc>) and optimizing the geometries with GAUSSIAN 09 software package (Frisch *et al.*, 2009) using the B3LYP functional (Becke, 1993; Lee *et al.*, 1988) and the 6-31+G** basis set. All calculations were done using a SMD water model (Marenich *et al.*, 2009). Frequency calculations were performed to confirm the absence of imaginary frequencies for the obtained minima. The torsions around the rotatable bonds were explored without success to identify alternatives to the most extended conformations. The results are presented in **Table 3** showing that the critical dimension of atenolol is 0.7 nm thus, no hindrance for its diffusion in the larger microporosity (supermicropores) is likely to occur.

In the conditions used for the kinetic assays all the prepared carbons attain adsorption efficiencies $\geq 57 \%$. However it must be noted that relatively higher removals were obtained with the synthesized samples that, with the exception of sample CA(1:3/1073/1), reached values around 90 %.

Table 3

The equilibrium adsorption isotherms of atenolol, displayed in **Fig. 5**, show a very steep initial rise up to adsorbed amounts ranging from 100 to 300 mg dm⁻³. These features reveal a high affinity of atenolol molecule towards the surface of the carbons, and allow to classify the isotherms as L-type curves (Giles *et al.*, 1974; Lyklema, 1995). In the majority of the cases the initial knee is followed by a horizontal plateau for C_e values higher than 40 – 60 mg dm⁻³. In the case of samples activated with KOH this plateau is less defined, and this part of the curves resembles a Freundlich isotherm.

The equilibrium data was fitted to the linear forms of Langmuir (Langmuir, 1918) and Freundlich (Freundlich, 1906) models and the resulting parameters, as well as the corresponding determination coefficients, R^2 , and non-linear chi-square analysis, χ^2 , are presented in **Table 4**.

Fig. 5

In line with the analysis of the isotherms configuration, better fittings of Langmuir model were obtained with higher values of the determination coefficient, R^2 , and smaller or identical χ^2 values obtained for the adjust of Freundlich equation. As expected, the highest χ^2 values are obtained for the KOH activated carbons regardless the isotherm model applied since, in this case, the initial part of the isotherms is a Langmuir curve but no horizontal plateau is clearly defined for higher equilibrium concentrations.

The values of the monolayer adsorption capacities, q_m , follow the trend HA(1:3/1073/2) > HA(1:3/1073/1) > CA(1:3/1073/2) > CA(1:3/1073/1) > NS > CP. Considering that the critical dimension of atenolol (0.7 nm) prevents its access to the narrow microporosity it can only be retained in the supermicropores. In fact, the values of $V_{\alpha \text{ super}}$, assessed from N₂ adsorption, present practically the same tendency. The exception is sample CA(1:3/1073/1) that, according to the $V_{\alpha \text{ super}}$ value (0.25 cm³ g⁻¹) should present a lower monolayer capacity than sample NS with a $V_{\alpha \text{ super}}$ of 0.38 cm³ g⁻¹, what points out that texture by itself does not explain all the results obtained. Thus, the surface chemistry must have an impact on atenolol adsorption process as well.

Actually, in solution, atenolol molecule (pK_a 9.6) will have a positive charge due to the protonation of the amine group, resulting in the increase of OH^- species in solution, causing the solution pH to be basic (pH 8.2). Thus, having NS a pH_{PZC} of 8.4, its net surface charge will be neutral, but CA(1:3/1073/1), with a pH_{PZC} of 5.5, will present a negative net surface charge. Therefore, in the case of NS the texture should be a key factor ruling the adsorption process, whereas in sample CA(1:3/1073/1) the relatively high density of surface negative charge will also favour the interaction with the positive atenolol specie. The contribution of the carbon's surface chemistry to the adsorptive properties of the materials is highlighted when considering that CA(1:3/1073/2) has a comparable adsorptive performance to the KOH-activated carbons with more than double of its $V_{\alpha \text{ super}}$. These results support the conclusion that, even though the surface chemistry of the KOH-activated samples favours the electrostatic interaction with atenolol, their higher pH_{PZC} (between 6 and 7), seems to be enough to affect their adsorption capacity. This observation is further validated by the similar results obtained with KOH-activated samples, with different supermicropore volumes.

Table 4

2.3. Thermal desorption of atenolol

Thermal desorption of atenolol was studied by thermogravimetric analysis of the exhausted carbons. To assess the desorption activation energy, the studies were performed using three heating rates (5, 10 and 20 K min^{-1}). Thermal degradation of atenolol and of the pristine materials was also assessed, at 20 K min^{-1} .

Considering the known polymorphism of several pharmaceutical compounds in the solid state (Lee, 2014), the atenolol sample used in the present study was characterized by X-ray diffraction. The pattern obtained (**Fig. S2**) presented the same features as that reported by de Castro *et al.* (2007) confirming the presence of a racemic mixture. In fact, the results (see **Fig. S3** and **Table S1**) show that atenolol is easily thermally degraded (loss of 85 % of its initial mass) and two DTG marked decomposition peaks at 601.4 K and 645.9 K, which support the existence of two forms of atenolol,

in the solid state. The predominant form seems to be the most thermally stable, as pointed out by a higher mass loss at 645.9 K.

The fresh carbons present low thermal degradation, retaining between 72 and 93 % of their initial mass. The samples less tolerant to thermal treatment are the K_2CO_3 -activated, since they present acidic surface properties (pH_{PZC} around 5).

As expected, in comparison with the pristine materials, the exhausted samples exhibit higher mass losses (more 20 to 35 percentage points) during thermal treatment (**Table 5**). In accordance with the classical temperature programmed desorption theory (Redhead, 1962; Cvetanovic and Amenomiya, 1967), an increase of the heating rate causes higher mass losses and a shift of the DTG peaks to higher temperatures. This peak shift is due to the fact that the heat transfer at higher heating rates is not as effective as it is when lower heating rates are used. For this reason, the DTG profiles of the spent carbons were analysed considering the curves obtained at the intermediate heating rate of 10 K min^{-1} , with lower limitations of heat transfer inside the samples and adequate definition for the interpretation of the results.

Table 5

In all the samples, accentuated mass losses occur in three temperature ranges, 529 – 556 K, 591-606 K and 641-655 K, presented in **Table 5** as peak I, II and III, respectively. The DTG curves (**Fig. 6**) confirm these findings showing an initial subtle peak followed by two more prominent mass losses at higher temperature.

Fig. 6

The first mass loss peak, in the lowest temperature range and less distinctive, can be caused by desorption of atenolol molecules weakly adsorbed onto the surface of the activated carbon materials. The two other peaks can be attributed to atenolol thermal decomposition. When atenolol is adsorbed onto activated carbon surface its thermal decomposition, in some cases, occurs at temperatures slightly higher in comparison to pure atenolol thermal decomposition. Such effect is partially

explained with slower heat transfer toward active sites of adsorption (*i.e.* inside pores) of the activated carbons. In the case of the lab-made carbons atenolol's decomposition profile seems to be maintained, whereas when the basic commercial samples are used, an inverted profile is observed. It seems that, with exception of sample CA(1:3/1073/1), in the lab-made materials (with acidic and neutral pH_{PZC} values) the adsorption of the more stable form of atenolol is favoured, whereas in CP and NS (basic carbons) is the less stable form that is predominantly adsorbed. Sample CA(1:3/1073/1) has a clearly different DTG profile, which demonstrates that it has distinct surface adsorption properties allowing it to interact with both atenolol species which may explain the unexpected high adsorption capacity presented by this sample, as discussed in the previous section. These findings clearly demonstrate that the surface chemistry of the carbons interacts differently with the two forms of atenolol and, consequently determines which of the two possible species will be predominantly adsorbed.

The desorption activation energy, E_{des} , and the pre-exponential Arrhenius factor, A , may be calculated from the DTG maximum peak temperature, T , at a heating rate β , according to a first-order desorption process given by the linear equation:

$$\ln\left(\frac{T^2}{\beta}\right) = \frac{E_{des}}{R} \left(\frac{1}{T}\right) + \ln\left(\frac{E_{des}}{AR}\right) \quad (1)$$

From the first-order atenolol desorption parameters, given in **Table 6**, relatively low E_{des} and A values are calculated for peak I desorption process. These E_{des} and A values are similar for all investigated materials, supporting the conclusion that, at this temperature range, the release of weakly adsorbed atenolol species occurs. Contrary, E_{des} and A values determined for peaks II and III clearly distinguish the materials. As expected, stronger interactions of atenolol with the acidic K_2CO_3 -activated carbons are demonstrated through higher E_{des} and A values, compared to the neutral KOH-activated materials and the basic commercial solids.

Table 6

3. Conclusions

Activated carbons with high apparent surface areas were prepared by chemical activation of apple tree bark char. The potential of lab-made samples for atenolol removal from aqueous phase was assessed by kinetic and equilibrium experiments, showing that atenolol is mainly adsorbed on the supermicropores.

The commercial atenolol, consisting in a racemic mixture, gave rise to a two-step thermal decomposition process. Thermogravimetric analysis of the exhausted samples revealed that the predominant atenolol specie adsorbed is conditioned by the carbons' surface chemistry.

Finally, this work points out that the racemic nature of PhACs must be considered in the analysis of adsorption results.

4. Acknowledgments

The authors thank the Fundação para a Ciência e Tecnologia (FCT), Portugal, for financial support to CQB through the project UID/MULTI/00612/2013. SCRIM thanks FCT for the PhD grant, SFRH/BD/91767/2012 ASM thanks the financial support of FCT for the Post-doc grant SFRH/BPD/86693/2012. The authors thank Salmon & Cia and Quimitejo for the supply of carbons NS and CP, respectively.

References

Alder, A.C., Bruchet, A., Carballa, M., Clara, M., Joss, A., Löttler, D., McArdell, C.S., Miksch, K., Omil, F., Tuhkanen, T., Ternes, T.A., 2006. Consumption and Occurrence, in: Ternes, T.A., Joss, A. (Eds.), Human Pharmaceuticals, Hormones and Fragrances. The challenge of Micropollutants in Urban Water Management, IWA Publishing, London, pp. 15-24.

Alder, A.C., Schaffner, C., Majewsky, M., Fenner, K., 2010. Fate of β -blocker human pharmaceuticals in surface water: Comparison of measured and simulated concentration in the Glatt Valley Watershed, Switzerland. *Water Res.* 44, 936-948.

Batista, M.K., Mestre, A.S., Matos, I., Fonseca, I.M., Carvalho, A.P., 2016. Biodiesel production waste as promising biomass precursor of reusable activated carbons for caffeine removal. *RSC Adv.* 6, 45419-45427.

Becke, A.D., 1993. Density-functional thermochemistry. III. The role of exact exchange. *J. Chem. Phys.* 98, 5648-5652.

Bolong, N., Ismail, A.F., Salim, M.R., Matsuura, T., 2009. A review of the effects of emerging contaminants in wastewater and options for their removal. *Desalination* 239, 229-246.

Borchard, U., 1998. Pharmaceutical properties of beta adrenoceptor blocking drugs. *J. Clin. Basic Cardiol.* 1, 5-9.

Carucci, A., Cappai, G., Piredda, M., 2006. Biodegradability and toxicity of pharmaceuticals in biological wastewater treatment plants. *J. Environ. Sci. Health A. Tox. Hazard. Subst. Environ. Eng.* 41, 1831-1842.

Cleuvers, M., 2005. Initial rise assessment for three β -blockers found in the aquatic environment. *Chemosphere* 59, 199-205.

Cvetanovic, R.J., Amenomiya, Y., 1967. Application of a temperature-programmed desorption technique to catalyst studies, in: Eley, D.D., Pines, H., Weisz, P.B. (Eds.), *Advances in Catalysis*. Academic Press, New York 17, 103-149.

Daughton, C. G., 2010. Pharmaceutical Ingredients in Drinking Water: Overview of Occurrence and Significance of Human Exposure, in: Halden, R. (Ed.), *Contaminants of Emerging Concern in the Environment: Ecological and Human Health Considerations*, ACS, Washington DC, pp. 9-68.

Dias, J.M., Alvim-Ferraz, M.C., Almeida, M.F., Rivera-Utrilla, J., Sánchez-Polo, M., 2007. Waste materials for activated carbon preparation and its use in aqueous-phase treatment: A review. *J. Environ. Manage.* 85, 833-846.

D5832 – 98, 2014. Standard Test Method for Volatile Matter Content of Activated Carbon Samples.

de Castro, R.A.E., Canotilho, J., Barbosa, R.M., Silva, M.R., Beja, A.M., Paixa, J.A., Redinha, J.S.E., 2007. Conformational isomorphism of organic crystals: Racemic and homochiral atenolol, *Cryst. Growth Des.* 7, 496-500.

Freundlich, H.M.F., 1906. Over the adsorption in solution. *J. Phys. Chem.* 57, 385-470.

Frisch, M.J., Trucks, G.W., Schlegel, H.B., Scuseria, G.E., Robb, M.A., Cheeseman, J.R., Scalmani, G., Barone, V., Mennucci, B., Petersson, G.A., Nakatsuji, H., Caricato, M., Li, X., Hratchian, H.P., Izmaylov, A.F., Bloino, J., Zheng, G., Sonnenberg, J.L., Hada, M., Ehara, M., Toyota, K., Fukuda, R., Hasegawa, J., Ishida, M., Nakajima, T., Honda, Y., Kitao, O., Nakai, H., Vreven, T., Montgomery Jr., J.A., Peralta, J.E., Ogliaro, F., Bearpark, M., Heyd, J.J., Brothers, E., Kudin, K.N., Staroverov, V.N., Kobayashi, R., Normand, J., Raghavachari, K., Rendell, A., Burant, J.C., Iyengar, S.S., Tomasi, J., Cossi, M., Rega, N., Millam, J.M., Klene, M., Knox, J.E., Cross, J.B., Bakken, V.,

Adamo, C., Jaramillo, J., Gomperts, R., Stratmann, R.E., Yazyev, O., Austin, A.J., Cammi, R., Pomelli, C., Ochterski, J.W., Martin, R.L., Morokuma, K., Zakrzewski, V.G., Voth, G.A., Salvador, P., Dannenberg, J.J., Dapprich, S., Daniels, A.D., Farkas, Ö., Foresman, J.B., Ortiz, J.V., Cioslowski, J., Fox, D.J., 2009. Gaussian 09. Gaussian, Inc., Wallingford CT.

Galhetas, M., Mestre, A.S., Pinto, M.L., Gulyurtlu, I., Lopes, H., Carvalho, A.P., 2014a. Carbon-based materials prepared from pine gasification residues for acetaminophen adsorption. *Chem. Eng. J.* 240, 344-351.

Galhetas, M., Mestre, A.S., Pinto, M.L., Gulyurtlu, I., Lopes, H., Carvalho, A.P., 2014b. Chars from gasification of coal and pine activated with K_2CO_3 : acetaminophen and caffeine adsorption from aqueous solutions. *J. Colloid Interface Sci.* 433, 94-103.

Giles, C.H., Smith, D., Huitson, A., 1974. A general treatment and classification of the solute adsorption isotherm. I. Theoretical. *J. Colloid Interface Sci.* 47, 755-765.

Haro, N.K., Vecchio, P.D., Marcilio, N.R., Féris, L.A., 2017. Removal of atenolol by adsorption – Study of kinetics and equilibrium. *J. Clean Prod.* 154, 214-219.

Ho, Y.-S., 2006. Review of second-order models for adsorption systems. *J. Hazard Mater.* 136, 681-689.

Huggett, D.B., Khan, L.A., Foran, C.M., 2003. Determination of beta-adrenergic receptor blocking pharmaceuticals in United States wastewater effluent. *Environ. Pollut.* 121, 199-205.

ISO 9277-2010, 2012. Determination of the specific surface area of solids by gas adsorption – BET method.

Langmuir, I., 1918. The adsorption of gases on plane surfaces of glass, mica and platinum. *J. Am. Chem. Soc.* 40, 1361-1403.

Lee, C., Yang, W., Parr, R.G., 1988. Development of the Colle-Salvetti correlation-energy formula into a functional of the electron density. *Phys. Rev. B* 37, 785-789.

Lee, E.H., 2014. A practical guide to pharmaceutical polymorph screening & selection, *Asian J. Pharm. Sci.* 9, 163-175.

Lyklema, J., 1995. *Fundamentals of Interface and Colloid Science, Vol II – Solid-Liquid interfaces.* Academic Press, New York.

Marenich, A.V., Cramer, C.J., Truhlar, D.G., 2009. Universal solvation model based on solute electron density and a continuum model of the solvent defined by the bulk dielectric constant and atomic surface tensions. *J. Phys. Chem. B* 113, 6378-96.

Mestre, A.S., Tyszko, E., Andrade, M.A., Galhetas, M., Freire, C., Carvalho, A.P., 2015. Sustainable activated carbons prepared from a sucrose-derived hydrochar: remarkable adsorbents for pharmaceutical compounds. *RSC Advances* 5, 19696-19707.

Noh, J.S., Schwarz, J.A., 1989. Estimation of the point of zero charge of simple oxides by mass titration. *J. Colloid Interface Sci.* 130, 157-164.

Patnukao, P., Kongsuwan, A., Pavasant, P., 2008. Batch studies of adsorption of copper and lead on activated carbon from *Eucalyptus camaldulensis* dehn. Bark. *J. Environ. Sci.* 20, 1028-1034.

Petrovic, M., Radjenovic, J., Postigo, C., Kuster, M., Farre, M., de Alda, M.L., Barceló, D., 2008. Emerging contaminants in waste waters: Sources and occurrences, in: Barceló, D., Petrovic, M. (Eds.), *Emerging Contaminants from Industrial and Municipal Waste*. Springer, Berlin, pp. 1-36.

Pinto, M.L., Mestre, A.S., Carvalho, A.P., Pires, J., 2010. Comparison of methods to obtain micropore size distributions of carbonaceous materials from CO₂ adsorption based on the Dubinin-Radushkevich isotherm. *Ind. Eng. Chem. Res.* 49, 4726-4730.

Redhead, P.A., 1962. Thermal desorption of gases. *Vacuum* 12, 203-211.

Rodriguez-Reinoso, F., Martin-Martinez, J.M., 1987. A standard adsorption isotherm for the characterization of activated carbons. *J. Phys. Chem. – US* 91, 515-516.

Rouquerol, F., Rouquerol, J., Sing, K., 1999. *Adsorption by Powders and Porous Solids – Principles, Methodology and Applications*. Academic Press, New York.

Thommes, M., Kaneko, K., Neimark, A., Olivier, J., Rodriguez-Reinoso, F., Rouquerol, J., Sing, K., 2015. Physisorption of gases, with special reference to the evaluation of surface area and pore size distribution (IUPAC Technical Report). *Pure Appl. Chem.* 87, 1051-1069.

To, M.-H., Hadi, P., Hui, C.-W., Lin, C.S.K., McKay, G., 2017. Mechanistic study of atenolol, acebutolol and carbamazepine adsorption on waste biomass derived activated carbon. *J. Mol. Liq.* 241, 386-398.

Wang, J., Kaskel, S., 2012. KOH activation of carbon-based materials for energy storage 22, 23710 – 23725.

Zhang, J., Zhang, W., 2014. Preparation and Characteristics of Activated Carbons from Wood Bark and Its Use for Adsorption of Cu(II). *Mat. Sci.* 20, 474-478.

Figure captions

Figure 1. Nitrogen adsorption-desorption isotherms at 77 K of the mentioned lab-made samples. Adsorption and desorption points are represented by open and closed symbols, respectively.

Figure 2. Micropore size distribution obtained from the CO₂ adsorption data, according to the method described by Pinto *et al.* (2010).

Figure 3. SEM micrographs of the biochar and of the activated carbons mentioned, with amplifications of $\times 150$ (left) and $\times 500$ (right).

Figure 4. Kinetic results of atenolol adsorption onto the mentioned carbons, at 303 K. Symbols correspond to the experimental data, whereas lines represent the fitting to the pseudo-second order kinetic equation (6 mg carbon / 20 cm³ of pollutant solution with 120 mg dm⁻³). Error bars are included.

Figure 5. Atenolol adsorption isotherms of the mentioned carbons, at 303 K. Symbols correspond to the experimental data, whereas lines represent the fitting to Langmuir model. Error bars are included.

Figure 6. DTG profiles of the pristine and atenolol-exhausted carbons at heating rates of 5, 10 and 20 K min⁻¹.

Figure

[Click here to download Figure: S Marques et al _Figures.docx](#)

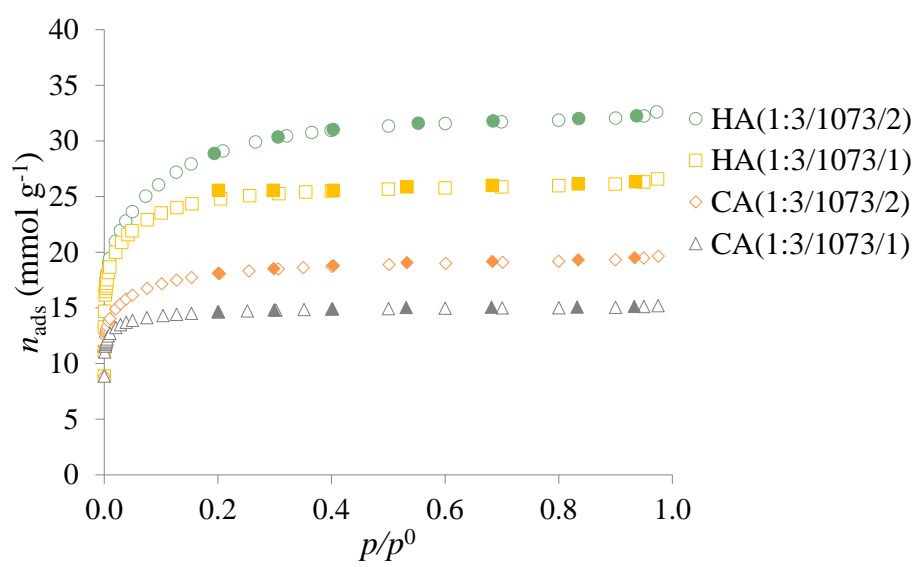


Figure 1

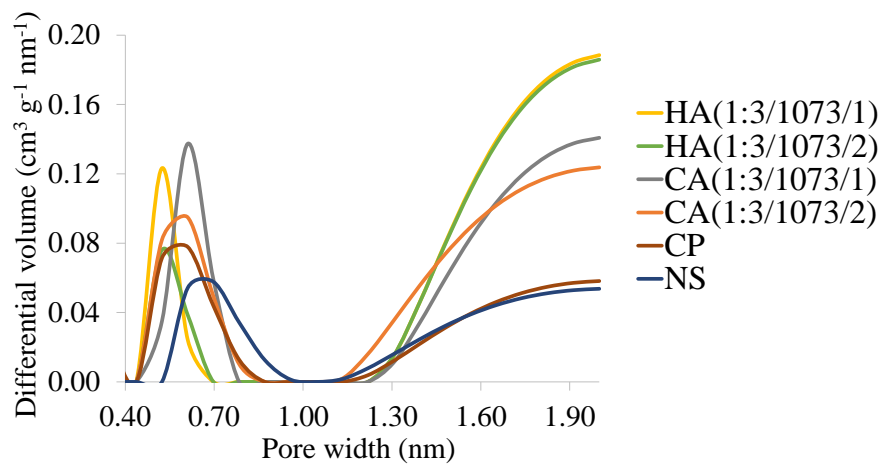


Figure 2

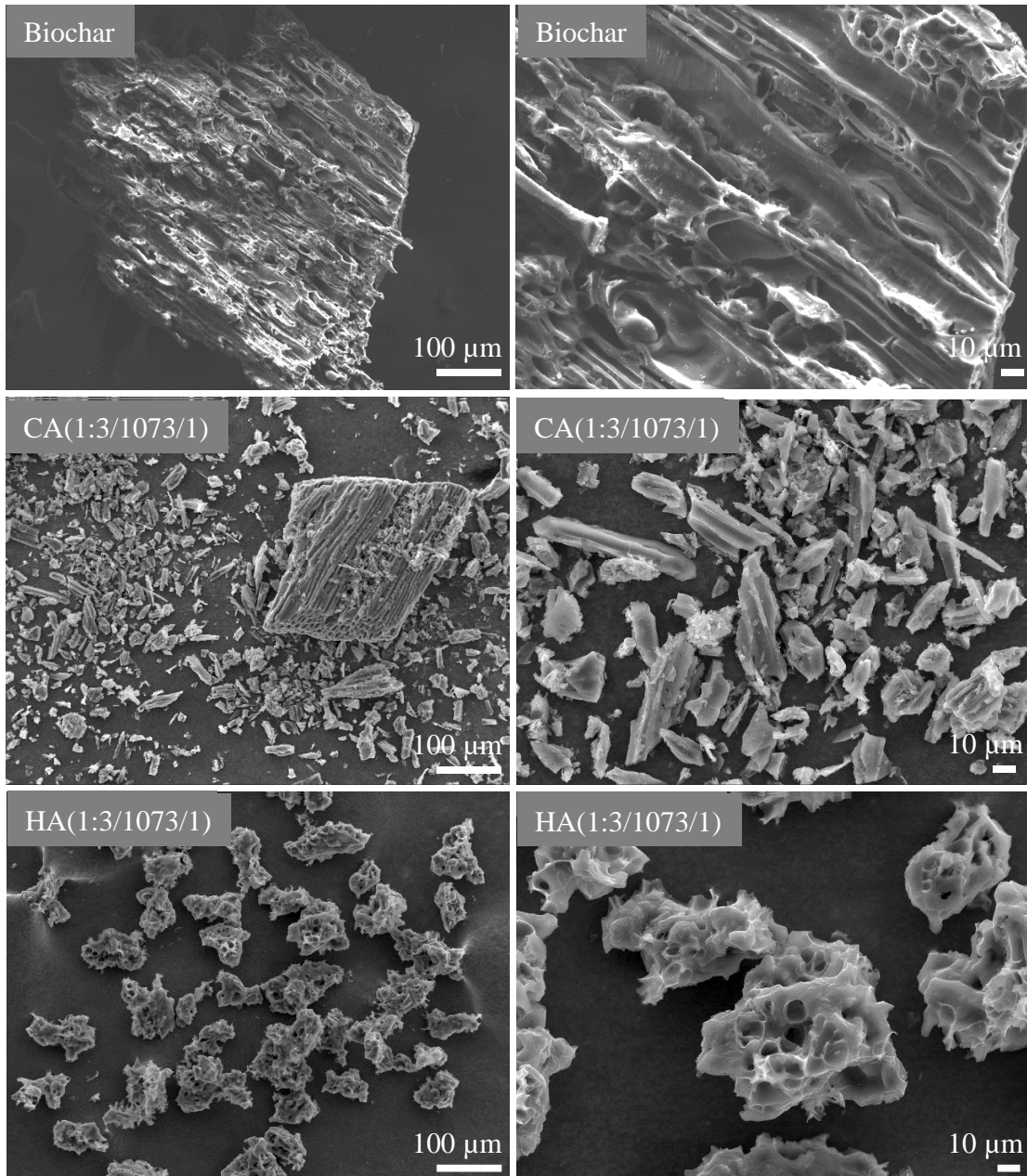


Figure 3

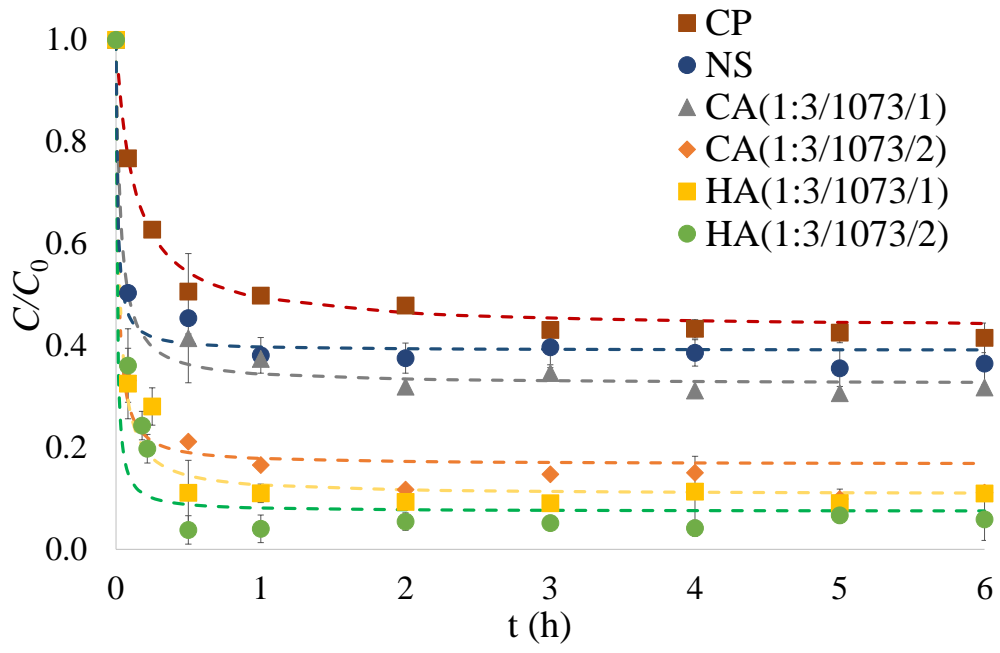


Figure 4

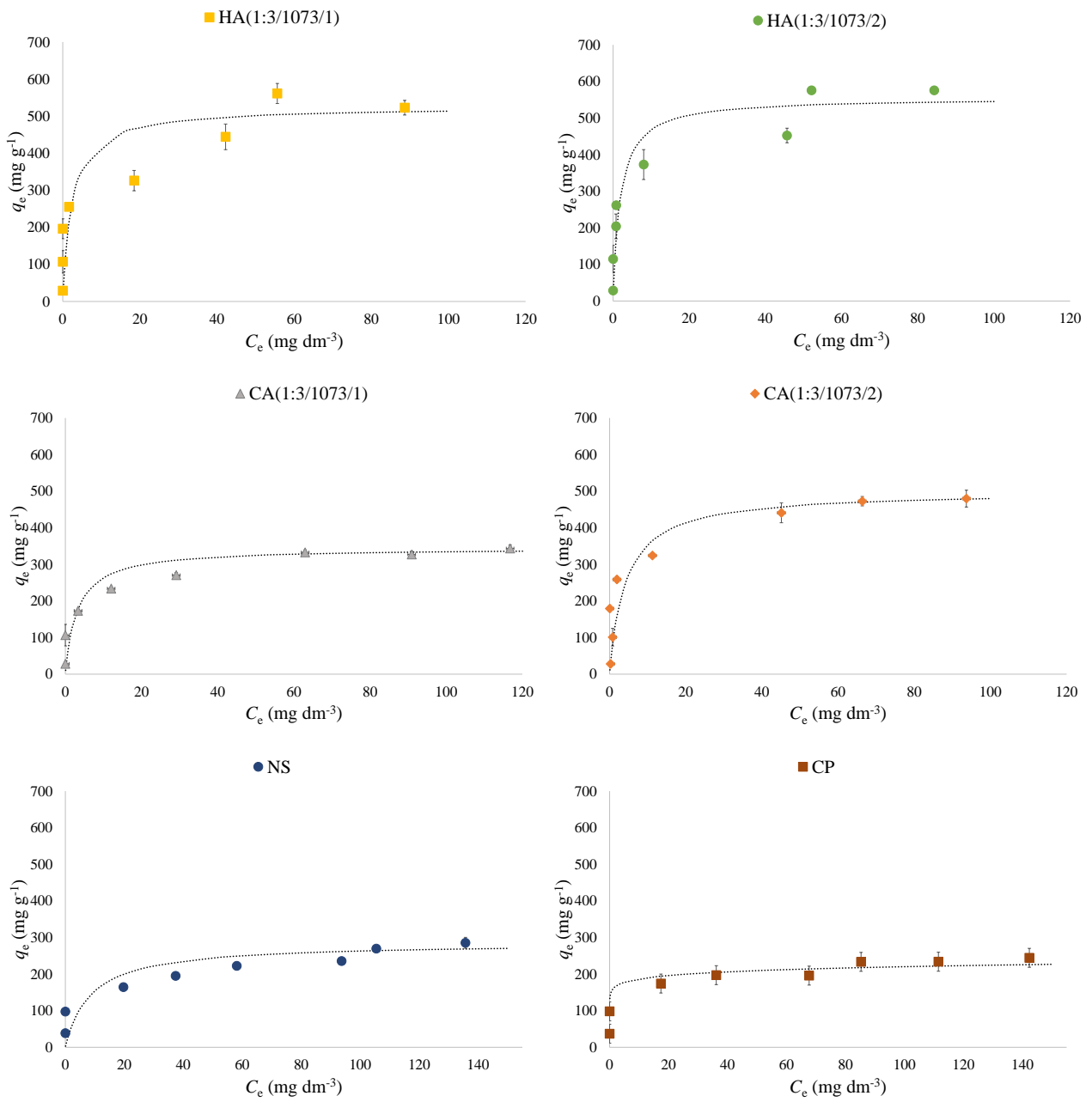


Figure 5

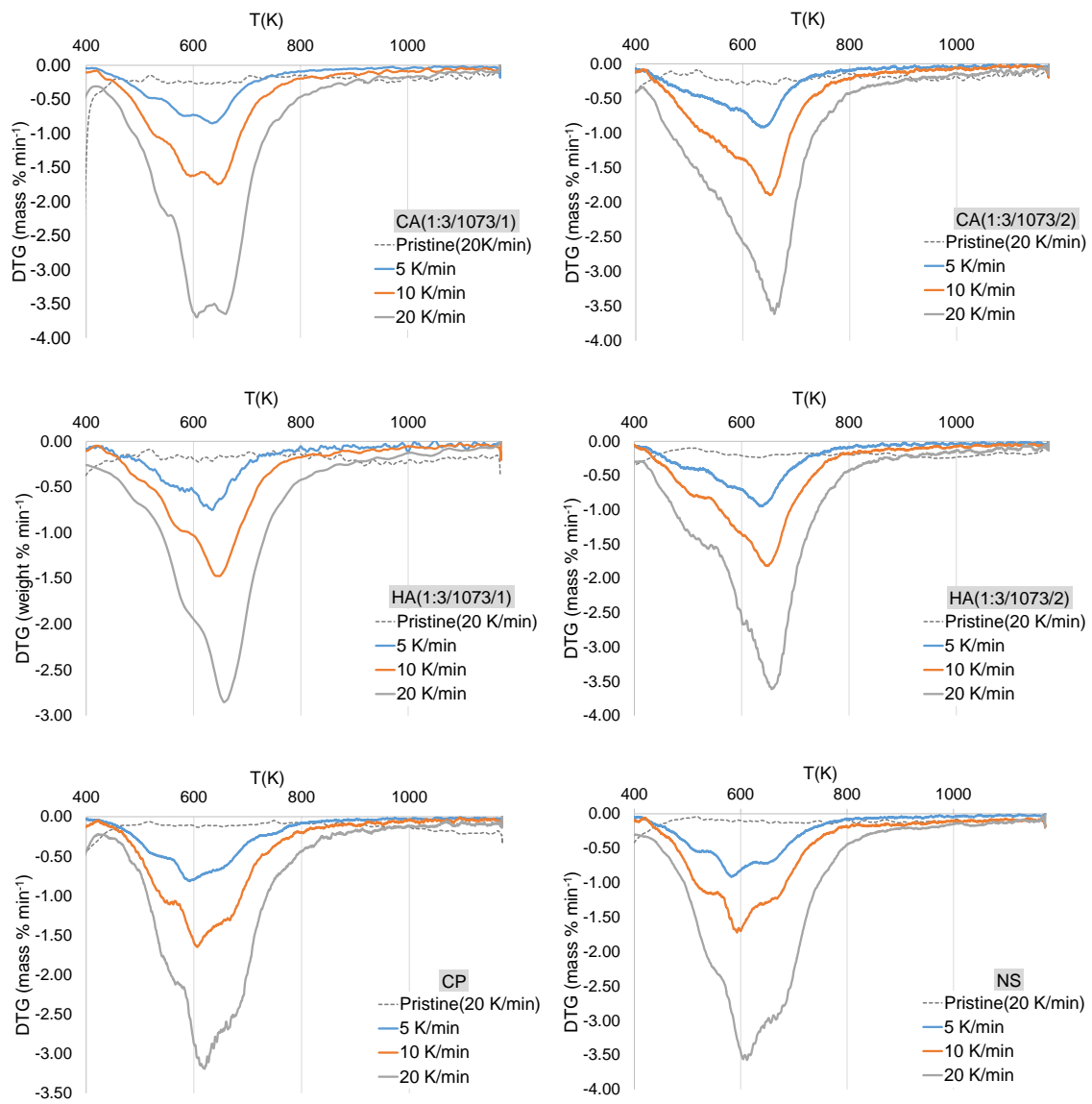


Figure 6

Table 1. Nanotextural properties of the lab-made carbons, preparation yield, and pH_{PZC} values.

Samples	η^a (%)	A_{BET} ($\text{m}^2 \text{g}^{-1}$)	V_{total}^b ($\text{cm}^3 \text{g}^{-1}$)	V_{meso}^c ($\text{cm}^3 \text{g}^{-1}$)	α_s method ^d			pH _{PZC}
					$V_{\alpha \text{ total}}$ ($\text{cm}^3 \text{g}^{-1}$)	$V_{\alpha \text{ ultra}}$ ($\text{cm}^3 \text{g}^{-1}$)	$V_{\alpha \text{ super}}$ ($\text{cm}^3 \text{g}^{-1}$)	
Lab-made								
KOH								
HA(1:3/1073/1)	46	2114	0.93	0.05	0.88	0.12	0.76	6.0
HA(1:3/1073/2)	38	2371	1.14	0.08	1.06	0.04	1.02	7.2
HA(1:3/1073/3)	22	2472	1.24	0.08	1.16	0.00	1.16	7.0
HA(1:3/1073/4)	22	2367	1.27	0.18	1.19	0.00	1.19	-
K ₂ CO ₃								
CA(1:3/973/2)	51	1119	0.48	0.02	0.46	0.31	0.15	-
CA(1:3/1073/1)	44	1302	0.53	0.01	0.52	0.27	0.25	5.4
CA(1:3/1073/2)	42	1539	0.69	0.06	0.64	0.15	0.49	5.5
CA(1:3/1073/3)	38	1959	0.91	0.08	0.83	0.09	0.74	5.6
CA(1:3/1073/4)	30	1963	0.95	0.09	0.86	0.05	0.81	5.6
CA(1:4/1073/1)	49	1330	0.54	0.01	0.53	0.27	0.26	5.0
CA(1:4/1073/2)	49	1569	0.66	0.03	0.63	0.28	0.35	4.5
CA(1:4/1073/4)	42	1705	0.82	0.05	0.77	0.06	0.71	-
Commercial								
CP ^e	-	907	0.43	0.03	0.40	0.16	0.24	10.3
NS ^e	-	1065	0.70	0.30	0.40	0.02	0.38	8.4

^aPreparation yield is defined as: g of activated carbon per 1 g of apple tree bark char; ^bN₂ volume adsorbed at $p/p^0 =$

0.95; ^c $V_{\text{meso}} = V_{\text{total}} - V_{\alpha \text{ total}}$; ^d α_s method was applied using as reference the isotherm presented in Rodríguez-Reinoso and

Martin--Martinez (1987), ^e values presented in Mestre *et al.* (2015).

Table 2. Pseudo-second order parameters for atenolol adsorption onto the studied carbon samples at 30 °C: k_2 is the pseudo-second order rate constant; h is the initial adsorption rate; $t_{1/2}$ is the half-life time; $q_{e \text{ calc}}$, $q_{e \text{ exp}}$ and $C_{e \text{ calc}}$ are, respectively, the pharmaceutical compounds uptake and that remaining in solution at equilibrium, both calculated by the pseudo-second order kinetic model.

	$k_2 \times 10^{-4}$ ($\text{g mg}^{-1}\text{min}^{-1}$)	h ($\text{mg g}^{-1}\text{min}^{-1}$)	$t_{1/2}$ (min)	$q_{e \text{ calc}}$ (mg g^{-1})	$q_{e \text{ exp}}$ (mg g^{-1})	$C_{e \text{ calc}}$ (mg dm^{-3})	Re(%)	R^2
HA(1:3/1073/1)	21	270	1.3	357	363	13	89	0.999
HA(1:3/1073/2)	61	833	0.4	370	374	9	93	0.999
CA(1:3/1073/1)	20	149	1.8	271	272	39	68	0.991
CA(1:3/1073/2)	35	385	0.9	350	375	20	83	0.999
CP	5	26	9	227	237	52	57	0.996
NS	60	357	0.7	244	251	47	61	0.999

Table 3. Atenolol molecular structure, weight and dimensions, and pK_a . The critical dimension of the most stable specie is highlighted in bold.

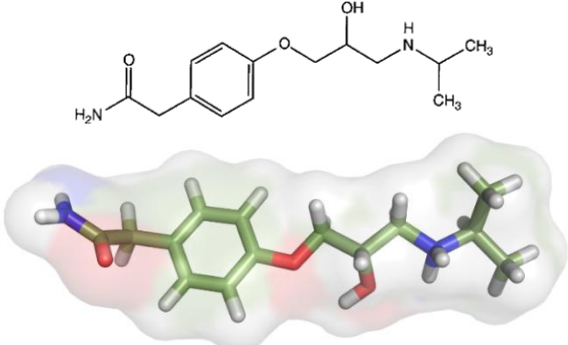
Pharmaceutical compound	Molecular structure and critical dimensions	Molecular weight and pK_a
Atenolol		266.3 g mol ⁻¹ pK_a 9.6
0.7 nm (length) × 1.8 nm (width) × 0.7 nm (thickness)		

Table 4. Fitting parameters of atenolol equilibrium data to the Langmuir and Freundlich models, coefficient of determination, R^2 , and chi-square test analysis, χ^2 . Langmuir parameters: q_m – monolayer adsorption capacity, K_L – Langmuir constant. Freundlich parameters: n – Freundlich exponent, K_F – Freundlich constant. Higher R^2 and lower χ^2 values are highlighted in bold.

Samples	Langmuir				Freundlich			
	q_m (mg g ⁻¹)	K_L (dm ³ mg ⁻¹)	R^2	χ^2	$1/n$	K_F (mg ^{1-1/n} (dm ³) ^{1/n} g ⁻¹)	R^2	χ^2
HA(1:3/1073/1)	526.3	0.404	0.979	63.2	0.077	324.4	0.719	76.8
HA(1:3/1073/2)	555.6	0.529	0.984	41.1	0.125	290.6	0.859	52.4
CA(1:3/1073/1)	344.8	0.319	0.996	11.5	0.077	212.3	0.813	30.3
CA(1:3/1073/2)	500.0	0.238	0.998	10.7	0.176	208.4	0.692	55.8
CP	243.9	0.202	0.988	7.41	0.073	157.8	0.842	7.2
NS	285.7	0.116	0.973	18.4	0.076	165.9	0.843	13.2

Table 5. Percentage of final weight (W_{final}) of atenolol-exhausted carbons and correspondent DTG peaks. Heating rates (β) of DTGs are 5, 10 and 20 K min⁻¹.

Atenolol exhausted carbons	β (K/min)	W_{final} (%)	T(K)		
			Peak I	Peak II	Peak III
CA(1:3/1073/1)	5	63.5	525.0	585.2	635.8
	10	62.1	539.4	596.5	645.1
	20	58.2	550.2	609.2	659.6
CA(1:3/1073/2)	5	62.2	520.4	583.4	635.4
	10	62.3	529.0	596.7	649.6
	20	61.9	545.5	607.2	658.8
HA(1:3/1073/1)	5	69.4	514.0	582.5	632.2
	10	71.7	529.4	591.7	645.6
	20	71.7	537.2	608.0	657.7
HA(1:3/1073/2)	5	61.4	516.1	584.0	634.4
	10	63.3	530.1	602.1	647.5
	20	62.8	541.2	611.2	658.9
CP	5	66.2	541.3	592.7	639.5
	10	66.1	556.5	606.3	655.4
	20	65.8	568.2	623.2	665.2
NS	5	61.5	530.6	584.8	630.5
	10	62.6	546.2	596.4	641.2
	20	60.9	557.6	613.2	654.0

Table 6. Desorption activation energy (E_{ads}) and pre-exponential factor (A) for the various peaks and corresponding correlation coefficients.

Samples	E_{des} (kJ mol ⁻¹)	A (s ⁻¹)	R^2
CA(1:3/1073/1)			
Peak I	121.9	3.5×10^8	0.9889
Peak II	161.3	7.1×10^{10}	0.9996
Peak III	189.2	1.0×10^{12}	0.9857
CA(1:3/1073/2)			
Peak I	118.2	2.1×10^8	0.9683
Peak II	161.0	7.1×10^{10}	0.9927
Peak III	192.2	1.0×10^{12}	0.9800
HA(1:3/1073/1)			
Peak I	123.4	9.2×10^8	0.9551
Peak II	147.0	4.3×10^9	0.9751
Peak III	177.0	1.2×10^{11}	0.9880
HA(1:3/1073/2)			
Peak I	118.6	2.6×10^8	0.9931
Peak II	135.7	3.1×10^8	0.9548
Peak III	185.2	4.8×10^{11}	0.9974
CP			
Peak I	121.6	1.3×10^8	0.9909
Peak II	129.2	5.4×10^7	0.9973
Peak III	175.9	5.8×10^{10}	0.9759
NS			
Peak I	116.0	6.2×10^7	0.9878
Peak II	134.4	2.5×10^8	0.9901
Peak III	191.3	2.1×10^{12}	0.9981

Electronic Annex

[Click here to download Electronic Annex: S Marques et al _Supplementary information.docx](#)